

AFRL-WS-WP-TR-2007-9002

JASPO-V-4-04-001

**EVALUATION OF SKIN-SPAR JOINT
RESISTANCE TO HYDRODYNAMIC RAM**

Greg Czarneck and Michele Maxson

780th Test Squadron (780 TS/OL-AC)

46th Test Wing (46 OG/OGM/OL-AC)

Aerospace Survivability and Safety Flight Division

Air Armament Center, Air Force Materiel Command

Wright-Patterson Air Force Base, OH 45433-7605

J. Sawdy and M. Miller

Wyle Laboratories

2700 Indian Ripple Rd.

Dayton, OH 45440-3638

R. Hinrichsen

RHAMM Technologies

332 Skyland Dr.

Bellbrook, OH 45305



MARCH 2006

Final Report for 01 October 2003 – 30 November 2005

Approved for public release; distribution is unlimited.

STINFO COPY

AEROSPACE SURVIVABILITY AND SAFETY FLIGHT

AIR ARMAMENT CENTER

AIR FORCE MATERIEL COMMAND

WRIGHT-PATTERSON AIR FORCE BASE, OH 45433-7605

NOTICE AND SIGNATURE PAGE

Using Government drawings, specifications, or other data included in this document for any purpose other than Government procurement does not in any way obligate the U.S. Government. The fact that the Government formulated or supplied the drawings, specifications, or other data does not license the holder or any other person or corporation; or convey any rights or permission to manufacture, use, or sell any patented invention that may relate to them.

This report was cleared for public release by the Air Force Materiel Command (AFMC) Public Affairs Office and is available to the general public, including foreign nationals. Copies may be obtained from the Defense Technical Information Center (DTIC) (<http://www.dtic.mil>).

AFRL-WS-WP-TR-2007-9002 HAS BEEN REVIEWED AND IS APPROVED FOR PUBLICATION IN ACCORDANCE WITH ASSIGNED DISTRIBUTION STATEMENT.

*//Signature//

Gregory J. Czarnecki, Program Mgr.
USAF, 780th Test Squadron
Aerospace Survivability & Safety Flight

//Signature//

John J. Murphy Jr, Technical Director
USAF, 780th Test Squadron
Aerospace Survivability & Safety Flight

//Signature//

Paul C. Ulrich, Flight Chief
USAF, 780th Test Squadron
Aerospace Survivability & Safety Flight

This report is published in the interest of scientific and technical information exchange, and its publication does not constitute the Government's approval or disapproval of its ideas or findings.

*Disseminated copies will show “//Signature//” stamped or typed above the signature blocks.

REPORT DOCUMENTATION PAGE				<i>Form Approved</i> OMB No. 0704-0188	
The public reporting burden for this collection of information is estimated to average 1 hour per response, including the time for reviewing instructions, searching existing data sources, gathering and maintaining the data needed, and completing and reviewing the collection of information. Send comments regarding this burden estimate or any other aspect of this collection of information, including suggestions for reducing this burden, to Department of Defense, Washington Headquarters Services, Directorate for Information Operations and Reports (0704-0188), 1215 Jefferson Davis Highway, Suite 1204, Arlington, VA 22202-4302. Respondents should be aware that notwithstanding any other provision of law, no person shall be subject to any penalty for failing to comply with a collection of information if it does not display a currently valid OMB control number. PLEASE DO NOT RETURN YOUR FORM TO THE ABOVE ADDRESS.					
1. REPORT DATE (DD-MM-YY) March 2006		2. REPORT TYPE Final		3. DATES COVERED (From - To) 10/01/2003 – 11/30/2005	
4. TITLE AND SUBTITLE EVALUATION OF SKIN-SPAR JOINT RESISTANCE TO HYDRODYNAMIC RAM				5a. CONTRACT NUMBER In-house3	
				5b. GRANT NUMBER	
				5c. PROGRAM ELEMENT NUMBER N/A	
6. AUTHOR(S) Greg Czarneck and Michele Maxson (780 th TS/OL-AC) J. Sawdy and M. Miller (Wyle Laboratories) R. Hinrichsen (RHAMM Technologies)				5d. PROJECT NUMBER JZZE	
				5e. TASK NUMBER 00	
				5f. WORK UNIT NUMBER 43	
7. PERFORMING ORGANIZATION NAME(S) AND ADDRESS(ES) 780 th Test Squadron (780th TS/OL-AC) 46th Test Wing (46 OG/OGM/OL-AC) Aerospace Survivability and Safety Flight Division Air Armament Center Air Force Materiel Command Wright-Patterson Air Force Base, OH 45433-7605				8. PERFORMING ORGANIZATION REPORT NUMBER OL-AC-DPR-07-08	
9. SPONSORING/MONITORING AGENCY NAME(S) AND ADDRESS(ES) 780th Test Squadron (780 TS/OL-AC) 46th Test Wing (46 OG/OGM/OL-AC) Aerospace Survivability and Safety Flight Division Air Armament Center, Air Force Materiel Command Wright-Patterson Air Force Base, OH 45433-7605				10. SPONSORING/MONITORING AGENCY ACRONYM(S) AFRL-WS-WP	
				11. SPONSORING/MONITORING AGENCY REPORT NUMBER(S) AFRL-WS-WP-TR-2007-9002 JASPO-V-4-04-001	
12. DISTRIBUTION/AVAILABILITY STATEMENT Approved for public release; distribution is unlimited.					
13. SUPPLEMENTARY NOTES PAO case number: AFMC 06-076; Date cleared: 22 Feb 2006. Report contains color.					
14. ABSTRACT <p>Projectile-induced hydrodynamic ram can generate fuel-tank pressures in excess of 10,000 psi. This event is potentially catastrophic for aircraft fuel tanks designed to survive sustained pressures of little more than 50 psi. While the magnitude of ram pressure is dictated by a combination of fuel-level and projectile threat, skin-spar joint design is the primary means by which damage can otherwise be controlled. Damage resistant joints restrict the spread of damage and assist aircraft survival.</p> <p>Joint resistance to ram is conventionally evaluated using a combination of two methods: a) T-joint pull-off tests and b) ballistically-tested wingboxes. While T-joint tests are a low-cost method of ranking skin-spar joints according to their load at failure, realism is traded away in favor of an economical and easily understood test. T-joint pull-off tests are symmetrically performed quasi-statically at a strain rate of less than 0.01 in/in-sec, whereas projectile-generated ram events involve asymmetric high-rate loading conditions on the order of 100 in/in-sec. Contrary to T-joint pull-off tests, wingbox ram tests with actual threat projectiles are fully realistic, but these tests come with a price tag in excess of \$250,000 (inclusive of tooling, structural materials, test costs, and labor). This is too expensive for wholesale evaluation of competing joint concepts.</p> <p style="text-align: right;"><i>Continued on back page</i></p>					
15. SUBJECT TERMS RamGun, ram, hydrodynamic ram, high, strain, rate, failure, load, skin, spar, joint, resistance, composite, aluminum, failure criteria, static, dynamic, damage, test					
16. SECURITY CLASSIFICATION OF:			17. LIMITATION OF ABSTRACT: SAR	18. NUMBER OF PAGES 360	19a. NAME OF RESPONSIBLE PERSON (Monitor) Greg Czarnecki 19b. TELEPHONE NUMBER (Include Area Code) (937) 255-6302 x203
a. REPORT Unclassified	b. ABSTRACT Unclassified	c. THIS PAGE Unclassified			

14. ABSTRACT (concluded)

When attempting to model high-strain rate events associated with ram, conventional static failure criteria has proven inadequate. The required dynamic failure criterion is typically 2-4 times that of the static case. The present test program applies a new RamGun test methodology to dynamically load T-joints at a rate coincident with projectile induced hydrodynamic ram. The effort is sponsored by the Joint Aircraft Survivability Program Office and directed by the 46th Test Wing (46 TW) at Wright-Patterson AFB, OH.

Objectives of the present effort are two-fold:

- Evaluate the ability of aircraft skin-spar joints to withstand hydrodynamic ram forces.
- Lay the foundation for establishing a dynamic (high-strain rate) failure criteria as a function of joint design.

Static and dynamic tests are performed on a wide variety of skin-spar joint designs. Failure strains are compared.

Table of Contents

1	BACKGROUND AND OBJECTIVES.....	1
1.1	BACKGROUND.....	1
1.2	OBJECTIVES.....	2
2	PLAN OF ACTION.....	3
3	INSTRUMENTATION.....	6
3.1	COMMON INSTRUMENTATION (T-JOINT SPECIMENS).....	6
3.2	COMMON INSTRUMENTATION (J-JOINT SPECIMENS).....	8
3.3	STATIC TEST INSTRUMENTATION.....	10
3.4	DYNAMIC TEST INSTRUMENTATION.....	10
4	TEST SETUP.....	13
4.1	STATIC TEST SETUP.....	13
4.2	DYNAMIC TEST SETUP.....	14
4.3	ADJUSTMENTS TO THE DYNAMIC TEST SETUP.....	14
5	DYNAMIC DATA ANALYSIS TECHNIQUE.....	17
5.1	IDENTIFICATION OF THE LOAD INTERVAL OF INTEREST AND VERIFICATION OF LOAD SYMMETRY.....	17
5.2	DETERMINATION OF PULL-OFF SYMMETRY.....	17
5.3	ASSESSMENT OF STRAIN AT FAILURE.....	21
5.4	EXAMPLE COMPARISON OF DYNAMIC VS. STATIC FAILURE DATA.....	22
6	SYNOPSIS OF TEST RESULTS.....	23
6.1	SPECIMEN SET 1: COBONDED (STITCHED).....	23
6.1.1	Dynamically Tested Specimens 1a, 1b, 1c, 1d (Tests #01, 02, 03, 25).....	26
6.1.2	Statically Tested Specimens 1e, 1f, 1g, 1h.....	28
6.1.3	Specimen Set 1: Dynamic vs. Static Comparisons.....	31
6.2	SPECIMEN SET 2: BOLTED.....	32
6.2.1	Dynamically Tested Specimens 2a, 2b, 2c, 2d, 2e (Tests #04, 05, 06, 26, 27).....	35
6.2.2	Statically Tested Specimens 2f, 2g, 2h, 2i.....	37
6.2.3	Specimen Set 2: Dynamic vs. Static Comparisons.....	40
6.3	SPECIMEN SET 3: TUFTED CARBON.....	40
6.3.1	Dynamically Tested Specimens 3a, 3b, 3c, 3d, 3e (Tests #07, 08, 09, 36, 37).....	44
6.3.2	Statically Tested Specimens 3f, 3g, 3h, 3i, 3j.....	47
6.3.3	Specimen Set 3: Dynamic vs. Static Comparisons.....	51
6.4	SPECIMEN SET 4: TUFTED ARAMIDE.....	51
6.4.1	Dynamically Tested Specimens 4a, 4b, 4c, 4d, 4e (Tests #10, 11, 12, 31, 32).....	54
6.4.2	Statically Tested Specimens 4f, 4g, 4h, 4i, 4j.....	57
6.4.3	Specimen Set 4: Dynamic vs. Static Comparisons.....	59
6.5	SPECIMEN SET 5: COBONDED PREPREG.....	60
6.5.1	Dynamically Tested Specimens 5a, 5b, 5c, 5d, 5e (Tests #13, 14, 15, 30, 33).....	63
6.5.2	Statically Tested Specimens 5f, 5g, 5h, 5i, 5j.....	66
6.5.3	Specimen Set 5: Dynamic vs. Static Comparisons.....	68
6.6	SPECIMEN SET 6: ONE SHOT INFILTRATION.....	69
6.6.1	Dynamically Tested Specimens 6a, 6b, 6c, 6d, 6e (Tests #16, 17, 18, 28, 29).....	72
6.6.2	Statically Tested Specimens 6f, 6g, 6h, 6i, 6j.....	75
6.6.3	Specimen Set 6: Dynamic vs. Static Comparisons.....	77
6.7	SPECIMEN SET 7: COBONDED.....	78
6.7.1	Dynamically Tested Specimens 7a, 7b, 7c, 7d, 7e (Tests #19, 20, 21, 34, 35).....	81
6.7.2	Statically Tested Specimens 7f, 7g, 7h, 7i, 7j.....	83
6.7.3	Specimen Set 7: Dynamic vs. Static Comparisons.....	86
6.8	SPECIMEN SET 8: WELDED ALUMINUM.....	87
6.8.1	Dynamically Tested Specimens 8a, 8b, 8c, 8d, 8e (Tests #22, 23, 24, 38, 39).....	90

6.8.2	Statically Tested Specimens 8f, 8g, 8h, 8i, 8j	92
6.8.3	Specimen Set 8: Dynamic vs. Static Comparisons	96
6.9	SPECIMEN SET 9: BONDED.....	97
6.9.1	Dynamically Tested Specimens 9a, 9b, 9c, 9d, 9e (Tests #40, 41, 42, 43, 44)	100
6.9.2	Statically Tested Specimens 9f, 9g, 9h, 9i	102
6.9.3	Specimen Set 9: Dynamic vs. Static Comparisons	105
6.10	SPECIMEN SET 10: BONDED (HONEYCOMB CORE)	105
6.10.1	Dynamically Tested Specimens 10a, 10b, 10c (Tests #50, 51, 52).....	108
6.10.2	Statically Tested Specimens 10d, 10e, 10f, 10g, 10h, 10i, 10j, 10k.....	109
6.10.3	Specimen Set 10: Dynamic vs. Static Comparisons.....	114
6.11	SPECIMEN SET 11: PI BONDED.....	115
6.11.1	Dynamically Tested Specimens 11a, 11b, 11c, 11d.....	116
6.11.2	Statically Tested Specimens 11e, 11f.....	120
6.11.3	Specimen Set 11: Dynamic vs. Static Comparisons.....	122
6.12	SYNOPSIS OF JOINT-FAILURE MEASURES	123
7	FINDINGS AND CONCLUSIONS	130
7.1	RAMGUN PERFORMANCE	130
7.2	JOINT PERFORMANCE	131
8	SUMMARY	132
9	REFERENCES.....	133
	APPENDIX A: INSTRUMENTATION AND TEST PARAMETERS.....	134
	APPENDIX B: EVALUATION OF DIAPHRAGM RUPTURE RESISTANCE ON RAM PRESSURE	139
	APPENDIX C: DATA ANALYSIS FOR DYNAMICALLY-TESTED SPECIMENS.....	142
C.1	SPECIMEN SET 1: COBONDED (STITCHED).....	143
C.1.1	DYNAMIC TESTS OF SPECIMEN SET 1	143
	Specimen 1a, Test 01	143
	Specimen 1b, Test 02	147
	Specimen 1c, Test 03	151
	Specimen 1d, Test 25	155
C.2	SPECIMEN SET 2: BOLTED	160
C.2.1	DYNAMIC TESTS OF SPECIMEN SET 2	160
	Specimen 2a, Test 04	160
	Specimen 2b, Test 05	160
	Specimen 2c, Test 06	163
	Specimen 2d, Test 26	166
	Specimen 2e, Test 27	169
C.3	SPECIMEN SET 3: TUFTED CARBON	174
C.3.1	DYNAMIC TESTS OF SPECIMEN SET 3	174
	Specimen 3a, Test 07	174
	Specimen 3b, Test 08.....	177
	Specimen 3c, Test 09	181
	Specimen 3d, Test 36.....	184
	Specimen 3e, Test 37	188
C.4	SPECIMEN SET 4: TUFTED ARAMIDE.....	193
C.4.1	DYNAMIC TESTS OF SPECIMEN SET 4	193
	Specimen 4a, Test 10	193
	Specimen 4b, Test 11	196
	Specimen 4c, Test 12	200

Specimen 4d, Test 31	203
Specimen 4e, Test 32	207
C.5 SPECIMEN SET 5: COBONDED PREPREG.....	212
C.5.1 DYNAMIC TESTS OF SPECIMEN SET 5	212
Specimen 5a, Test 13	212
Specimen 5b, Test 14.....	215
Specimen 5c, Test 15	219
Specimen 5d, Test 30.....	223
Specimen 5e, Test 33	227
C.6 SPECIMEN SET 6: ONE SHOT INFILTRATION	232
C.6.1 DYNAMIC TESTS OF SPECIMEN SET 6.....	232
Specimen 6a, Test 16	232
Specimen 6b, Test 17	235
Specimen 6c, Test 18	239
Specimen 6d, Test 28.....	243
Specimen 6e, Test 29	247
C.7 SPECIMEN SET 7: COBONDED	252
C.7.1 DYNAMIC TESTS OF SPECIMEN SET 7	252
Specimen 7a, Test 19	252
Specimen 7b, Test 20.....	255
Specimen 7c, Test 21	259
Specimen 7d, Test 34.....	263
Specimen 7e, Test 35	267
C.8 SPECIMEN SET 8: WELDED ALUMINUM.....	272
C.8.1 DYNAMIC TESTS OF SPECIMEN SET 8	272
Specimen 8a, Test 22	272
Specimen 8b, Test 23	275
Specimen 8c, Test 24	279
Specimen 8d, Test 38.....	283
Specimen 8e, Test 39	287
C.9 SPECIMEN SET 9: BONDED	292
C.9.1 DYNAMIC TESTS OF SPECIMEN SET 9	292
Specimen 9a, Test 40	292
Specimen 9b, Test 41	296
Specimen 9c, Test 42	300
Specimen 9d, Test 43.....	304
Specimen 9e, Test 44	308
C.10 SPECIMEN SET 10: BONDED (HONEYCOMB CORE)	313
C.10.1 DYNAMIC TESTS OF SPECIMEN SET 10	313
Specimen 10a, Test 50	313
Specimen 10b, Test 51	317
Specimen 10c, Test 52	321
C.11 SPECIMEN SET 11: PI BONDED	325
C.11.1 DYNAMIC TESTS OF SPECIMEN SET 11	325
Specimen 11a, Test 53	325
Specimen 11b, Test 59	329
Specimen 11c, Test 60	333
Specimen 11d, Test 61	337

Table of Figures

Figure 1.1.1: T-joint and J-Joint components	2
Figure 2.1: Joint dimension requirements.....	4
Figure 2.2: Example single spar T-joint	5
Figure 3.1.1: Strain gage locations for T-joint specimens	6
Figure 3.1.2: Layout of instrumentation on T-joint (looking down from above).....	7
Figure 3.1.3: Layout of instrumentation on T-joint (looking into test chamber from barrel).....	7
Figure 3.2.1: Strain gage locations for J-joint specimens	8
Figure 3.2.3: Layout of instrumentation on J-joint (looking into test chamber from barrel)	9
Figure 3.4.1: Three section cuts through the FEM	11
Figure 3.4.2: Load vs. time at the three section cuts.....	12
Figure 4.1.1: Static test fixture.....	13
Figure 4.2.1: Schematic drawing of RamGun test apparatus.....	15
Figure 4.2.2: RamGun test apparatus, end view.	15
Figure 5.1: Example specimen failure as a result of dynamic test.....	17
Figure 5.1.1: Ram pressure vs. time (example).	18
Figure 5.2.1: Example of SG 1 & 4 symmetry	19
Figure 5.2.2: Example of SG 1 & 4 asymmetry	19
Figure 5.2.3: Example of SG 2 & 3 symmetry	20
Figure 5.2.4: Example of SG 2 & 3 asymmetry	20
Figure 5.3.1: Average spar-strain vs. time (example).....	21
Figure 6.1.1: Specimen dimension coding.....	23
Figure 6.1.2: Example image of joint from Specimen Set 1 (pretest)	25
Figure 6.1.3: Example cross section of joint from Specimen Set 1 (pretest).....	25
Figure 6.1.1.1: Specimen 1a after dynamic test.....	26
Figure 6.1.1.2: Specimen 1b after dynamic test.....	27
Figure 6.1.1.3: Specimen 1c after dynamic test.....	27
Figure 6.1.1.4: Specimen 1d after dynamic test.....	28
Figure 6.1.2.1: Specimen 1e after static test.	29
Figure 6.1.2.2: Specimen 1f after static test.....	29
Figure 6.1.2.3: Specimen 1g after static test.....	30
Figure 6.1.2.4: Specimen 1h after static test.....	31
Figure 6.2.1: Specimen dimension coding.....	32
Figure 6.2.2: Example image of joint from Specimen Set 2 (pretest)	34
Figure 6.2.3: Example cross section of joint from Specimen Set 2 (pretest).....	34
Figure 6.2.1.1: Specimen 2a after dynamic test.....	35
Figure 6.2.1.2: Specimen 2b after dynamic test.....	36
Figure 6.2.1.3: Specimen 2c after dynamic test.....	36
Figure 6.2.1.4: Specimen 2d after dynamic test.....	37
Figure 6.2.1.5: Specimen 2e after dynamic test.....	37
Figure 6.2.2.1: Specimen 2f after static test.....	38
Figure 6.2.2.2: Specimen 2g after static test.....	38
Figure 6.2.2.3: Specimen 2h after static test.....	39
Figure 6.2.2.4: Specimen 2i after static test.....	39
Figure 6.3.1: Specimen dimension coding.....	41
Figure 6.3.2: Example image of joint from Specimen Set 3 (pretest)	43

Figure 6.3.3: Example cross section of joint from Specimen Set 3 (pretest).....	44
Figure 6.3.1.1: Specimen 3a after dynamic test.....	45
Figure 6.3.1.2: Specimen 3b after dynamic test.....	45
Figure 6.3.1.3: Specimen 3c after dynamic test.....	46
Figure 6.3.1.4: Specimen 3d after dynamic test.....	47
Figure 6.3.1.5: Specimen 3e after dynamic test.....	47
Figure 6.3.2.1: Specimen 3f after static test.....	48
Figure 6.3.2.2: Specimen 3g after static test.....	49
Figure 6.3.2.3: Specimen 3h after static test.....	49
Figure 6.3.2.4: Specimen 3i after static test.....	50
Figure 6.3.2.5: Specimen 3j after static test.....	50
Figure 6.4.1: Specimen dimension coding.....	52
Table 6.4.1: Dimensions of Specimen Set 4.....	52
Figure 6.4.2: Example image of joint from Specimen Set 4 (pretest)	53
Figure 6.4.3: Example cross section of joint from Specimen Set 4 (pretest).....	53
Figure 6.4.1.1: Specimen 4a after dynamic test.....	54
Figure 6.4.1.2: Specimen 4b after dynamic test.....	55
Figure 6.4.1.3: Specimen 4c after dynamic test.....	55
Figure 6.4.1.4: Specimen 4d after dynamic test.....	56
Figure 6.4.1.5: Specimen 4e after dynamic test.....	56
Figure 6.4.2.1: Specimen 4f after static test.....	57
Figure 6.4.2.2: Specimen 4g after static test.....	58
Figure 6.4.2.3: Specimen 4h after static test.....	58
Figure 6.4.2.4: Specimen 4i after static test.....	59
Figure 6.4.2.5: Specimen 4j after static test.....	59
Figure 6.5.1: Specimen dimension coding.....	61
Figure 6.5.2: Example image of joint from Specimen Set 5 (pretest)	62
Figure 6.5.3: Example cross section of joint from Specimen Set 5 (pretest).....	63
Figure 6.5.1.1: Specimen 5a after dynamic test.....	63
Figure 6.5.1.2: Specimen 5b after dynamic test.....	64
Figure 6.5.1.3: Specimen 5c after dynamic test.....	64
Figure 6.5.1.4: Specimen 5d after dynamic test.....	65
Figure 6.5.1.5: Specimen 5e after dynamic test.....	66
Figure 6.5.2.1: Specimen 5f after static test.....	66
Figure 6.5.2.2: Specimen 5g after static test.....	67
Figure 6.5.2.3: Specimen 5h after static test.....	67
Figure 6.5.2.4: Specimen 5i after static test.....	68
Figure 6.5.2.5: Specimen 5j after static test.....	68
Figure 6.6.1: Specimen dimension coding.....	70
Figure 6.6.2: Example image of joint from Specimen Set 6 (pretest)	71
Figure 6.6.3: Example cross section of joint from Specimen Set 6 (pretest).....	72
Figure 6.6.1.1: Specimen 6a after dynamic test.....	72
Figure 6.6.1.2: Specimen 6b after dynamic test.....	73
Figure 6.6.1.3: Specimen 6c after dynamic test.....	73
Figure 6.6.1.4: Specimen 6d after dynamic test.....	74
Figure 6.6.1.5: Specimen 6e after dynamic test.....	74

Figure 6.6.2.1: Specimen 6f after static test.....	75
Figure 6.6.2.2: Specimen 6g after static test.....	75
Figure 6.6.2.3: Specimen 6h after static test.....	76
Figure 6.6.2.4: Specimen 6i after static test.....	76
Figure 6.6.2.5: Specimen 6j after static test.....	77
Figure 6.7.1: Specimen dimension coding.....	79
Figure 6.7.2: Example image of joint from Specimen Set 7 (pretest)	80
Figure 6.7.3: Example cross section of joint from Specimen Set 7 (pretest).....	80
Figure 6.7.1.1: Specimen 7a after dynamic test.....	81
Figure 6.7.1.2: Specimen 7b after dynamic test.....	82
Figure 6.7.1.3: Specimen 7c after dynamic test.....	82
Figure 6.7.1.4: Specimen 7d after dynamic test.....	83
Figure 6.7.1.5: Specimen 7e after dynamic test.....	83
Figure 6.7.2.1: Specimen 7f after static test.....	84
Figure 6.7.2.2: Specimen 7g after static test.....	84
Figure 6.7.2.3: Specimen 7h after static test.....	85
Figure 6.7.2.4: Specimen 7i after static test.....	85
Figure 6.7.2.5: Specimen 7j after static test.....	86
Figure 6.8.1: Specimen dimension coding.....	88
Table 6.8.1: Dimensions of Specimen Set 8.....	88
Figure 6.8.2: Example image of joint from Specimen Set 8 (pretest)	89
Figure 6.8.3: Example cross section of joint from Specimen Set 8 (pretest).....	89
Figure 6.8.1.1: Specimen 8a after dynamic test.....	90
Figure 6.8.1.2: Specimen 8b after dynamic test.....	91
Figure 6.8.1.3: Specimen 8c after dynamic test.....	91
Figure 6.8.1.4: Specimen 8d after dynamic test.....	92
Figure 6.8.1.5: Specimen 8e after dynamic test.....	92
Figure 6.8.2.1: Specimen 8f after static test.....	93
Figure 6.8.2.2: Specimen 8g after static test.....	93
Figure 6.8.2.3: Specimen 8h after static test.....	94
Figure 6.8.2.4: Specimen 8i after static test.....	95
Figure 6.8.2.5: Specimen 8j after static test.....	96
Figure 6.9.1: Specimen dimension coding.....	98
Figure 6.9.2: Example image of joint from Specimen Set 9 (pretest)	99
Figure 6.9.3: Example cross section of joint from Specimen Set 9 (pretest).....	99
Figure 6.9.1.1: Specimen 9a after dynamic test.....	100
Figure 6.9.1.2: Specimen 9b after dynamic test.....	101
Figure 6.9.1.3: Specimen 9c after dynamic test.....	101
Figure 6.9.1.4: Specimen 9d after dynamic test.....	102
Figure 6.9.1.5: Specimen 9e after dynamic test.....	102
Figure 6.9.2.1: Specimen 9f after static test.....	103
Figure 6.9.2.2: Specimen 9g after static test.....	103
Figure 6.9.2.3: Specimen 9h after static test.....	104
Figure 6.9.2.4: Specimen 9i after static test.....	104
Figure 6.10.1: Specimen dimension coding.....	106
Figure 6.10.2: Example image of joint from Specimen Set 10 (pretest)	107

Figure 6.10.3: Example cross section of joint from Specimen Set 10 (pretest).....	107
Figure 6.10.1.1: Specimen 10a after dynamic test.....	108
Figure 6.10.1.2: Specimen 10b after dynamic test.....	109
Figure 6.10.1.3: Specimen 10c after dynamic test.....	109
Figure 6.10.2.1: Specimen 10d after static test.....	110
Figure 6.10.2.2: Specimen 10e after static test.....	110
Figure 6.10.2.3: Specimen 10f after static test.....	111
Figure 6.10.2.4: Specimen 10g after static test.....	111
Figure 6.10.2.5: Specimen 10h after static test.....	112
Figure 6.10.2.6: Specimen 10i after static test.....	112
Figure 6.10.2.7: Specimen 10j after static test.....	113
Figure 6.11.1: Specimen dimension coding.....	115
Figure 6.11.1: Example image of joint from Specimen Set 11 (pretest)	116
Figure 6.11.1.1: Specimen 11a after dynamic test.....	117
Figure 6.11.1.2: Specimen 11b after dynamic test.....	118
Figure 6.11.1.3: Specimen 11c after dynamic test.....	119
Figure 6.11.1.4: Specimen 11d after dynamic test.....	120
Figure 6.11.2.1: Specimen 11e after static test.....	121
Figure 6.11.2.2: Specimen 11f after static test.....	122
Figure B.1: Typical failure of an aluminum diaphragm.	140
Figure B.2: Typical failure of a UHMWPE diaphragm (0.015 thick).	141
Figure C.1a.1: Kistler pressure vs. time (Specimen 1a)	144
Figure C.1a.2: SG1 & SG4 skin strain vs. time (Specimen 1a).....	145
Figure C.1a.3: SG2 & SG3 spar strain vs. time (Specimen 1a).....	146
Figure C.1a.4: SG2 & SG3 average spar strain vs. time (Specimen 1a)	147
Figure C.1b.1: Kistler pressure vs. time (Specimen 1b).....	148
Figure C.1b.2: SG1 & SG4 skin strain vs. time (Specimen 1b)	149
Figure C.1b.3: SG2 & SG3 spar strain vs. time (Specimen 1b)	150
Figure C.1b.4: SG2 & SG3 average spar strain vs. time (Specimen 1b).....	151
Figure C.1c.1: Kistler pressure vs. time (Specimen 1c)	152
Figure C.1c.2: SG1 & SG4 skin strain vs. time (Specimen 1c).....	153
Figure C.1c.4: SG2 & SG3 average spar strain vs. time (Specimen 1c)	155
Figure C.1d.1: Kistler pressure vs. time (Specimen 1d).....	156
Figure C.1d.2: SG1 & SG4 skin strain vs. time (Specimen 1d)	157
Figure C.1d.3: SG2 & SG3 spar strain vs. time (Specimen 1d)	158
Figure C.1d.4: SG2 & SG3 average spar strain vs. time (Specimen 1d).....	159
Figure C.2b.1: Kistler pressure vs. time (Specimen 2b).....	161
Figure C.2b.2: SG1 & SG4 skin strain vs. time (Specimen 2b)	162
Figure C.2b.3: SG2 & SG3 spar strain vs. time (Specimen 2b)	162
Figure C.2b.4: SG2 & SG3 average spar strain vs. time (Specimen 2b).....	163
Figure C.2c.1: Kistler pressure vs. time (Specimen 2c)	163
Figure C.2c.2: SG1 & SG4 skin strain vs. time (Specimen 2c).....	164
Figure C.2c.4: SG2 & SG3 average spar strain vs. time (Specimen 2c)	166
Figure C.2d.1: Kistler pressure vs. time (Specimen 2d).....	167
Figure C.2d.2: SG1 & SG4 skin strain vs. time (Specimen 2d)	168
Figure C.2d.3: SG2 & SG3 spar strain vs. time (Specimen 2d)	169

Figure CA.2e.1: Kistler pressure vs. time (Specimen 2e).....	170
Figure C.2e.2: SG1 & SG4 skin strain vs. time (Specimen 2e).....	171
Figure C.2e.3: SG2 & SG3 spar strain vs. time (Specimen 2e).....	172
Figure C.2e.4: SG2 & SG3 average spar strain vs. time (Specimen 2e)	173
Figure C.3a.1: Kistler pressure vs. time (Specimen 3a)	174
Figure C.3a.2: SG1 & SG4 skin strain vs. time (Specimen 3a).....	175
Figure C.3a.3: SG2 & SG3 spar strain vs. time (Specimen 3a).....	176
Figure C.3a.4: SG2 & SG3 average spar strain vs. time (Specimen 3a)	177
Figure C.3b.1: Kistler pressure vs. time (Specimen 3b).....	178
Figure C.3b.2: SG1 & SG4 skin strain vs. time (Specimen 3b)	179
Figure C.3b.3: SG2 & SG3 spar strain vs. time (Specimen 3b)	180
Figure C.3b.4: SG2 & SG3 average spar strain vs. time (Specimen 3b).....	181
Figure C.3c.1: Kistler pressure vs. time (Specimen 3c)	181
Figure C.3c.2: SG1 & SG4 skin strain vs. time (Specimen 3c).....	182
Figure C.3c.4: SG2 & SG3 average spar strain vs. time (Specimen 3c)	184
Figure C.3d.1: Kistler pressure vs. time (Specimen 3d).....	185
Figure C.3d.2: SG1 & SG4 skin strain vs. time (Specimen 3d)	186
Figure C.3d.3: SG2 & SG3 spar strain vs. time (Specimen 3d)	187
Figure C.3d.4: SG2 & SG3 average spar strain vs. time (Specimen 3d).....	188
Figure C.3e.1: Kistler pressure vs. time (Specimen 3e)	189
Figure C.3e.2: SG1 & SG4 skin strain vs. time (Specimen 3e).....	190
Figure C.3e.3: SG2 & SG3 spar strain vs. time (Specimen 3e).....	191
Figure C.3e.4: SG2 & SG3 average spar strain vs. time (Specimen 3e)	192
Figure C.4a.1: Kistler pressure vs. time (Specimen 4a)	193
Figure C.4a.2: SG1 & SG4 skin strain vs. time (Specimen 4a).....	194
Figure C.4a.3: SG2 & SG3 spar strain vs. time (Specimen 4a).....	195
Figure C.4a.4: SG2 & SG3 average spar strain vs. time (Specimen 4a)	196
Figure C.4b.1: Kistler pressure vs. time (Specimen 4b).....	197
Figure C.4b.2: SG1 & SG4 skin strain vs. time (Specimen 4b)	198
Figure C.4b.3: SG2 & SG3 spar strain vs. time (Specimen 4b)	199
Figure C.4b.4: SG2 & SG3 average spar strain vs. time (Specimen 4b).....	199
Figure C.4c.1: Kistler pressure vs. time (Specimen 4c)	200
Figure C.4c.2: SG1 & SG4 skin strain vs. time (Specimen 4c).....	201
Figure C.4c.4: SG2 & SG3 average spar strain vs. time (Specimen 4c)	203
Figure C.4d.1: Kistler pressure vs. time (Specimen 4d).....	204
Figure C.4d.2: SG1 & SG4 skin strain vs. time (Specimen 4d)	205
Figure C.4d.3: SG2 & SG3 spar strain vs. time (Specimen 4d)	206
Figure C.4d.4: SG2 & SG3 average spar strain vs. time (Specimen 4d).....	207
Figure C.4e.1: Kistler pressure vs. time (Specimen 4e)	208
Figure C.4e.2: SG1 & SG4 skin strain vs. time (Specimen 4e).....	209
Figure C.4e.3: SG2 & SG3 spar strain vs. time (Specimen 4e).....	210
Figure C.4e.4: SG2 & SG3 average spar strain vs. time (Specimen 4e)	211
Figure C.5a.1: Kistler pressure vs. time (Specimen 5a)	212
Figure C.5a.2: SG1 & SG4 skin strain vs. time (Specimen 5a).....	213
Figure C.5a.3: SG2 & SG3 spar strain vs. time (Specimen 5a).....	214
Figure C.5a.4: SG2 & SG3 average spar strain vs. time (Specimen 5a)	215

Figure C.5b.1: Kistler pressure vs. time (Specimen 5b)	216
Figure C.5b.2: SG1 & SG4 skin strain vs. time (Specimen 5b)	217
Figure C.5b.3: SG2 & SG3 spar strain vs. time (Specimen 5b)	218
Figure C.5b.4: SG2 & SG3 average spar strain vs. time (Specimen 5b)	219
Figure C.5c.1: Kistler pressure vs. time (Specimen 5c)	220
Figure C.5c.2: SG1 & SG4 skin strain vs. time (Specimen 5c)	221
Figure C.5c.4: SG2 & SG3 average spar strain vs. time (Specimen 5c)	223
Figure C.5d.1: Kistler pressure vs. time (Specimen 5d)	224
Figure C.5d.2: SG1 & SG4 skin strain vs. time (Specimen 5d)	225
Figure C.5d.3: SG2 & SG3 spar strain vs. time (Specimen 5d)	226
Figure C.5d.4: SG2 & SG3 average spar strain vs. time (Specimen 5d)	227
Figure C.5e.1: Kistler pressure vs. time (Specimen 5e)	228
Figure C.5e.2: SG1 & SG4 skin strain vs. time (Specimen 5e)	229
Figure C.5e.3: SG2 & SG3 spar strain vs. time (Specimen 5e)	230
Figure C.5e.4: SG2 & SG3 average spar strain vs. time (Specimen 5e)	231
Figure C.6a.1: Kistler pressure vs. time (Specimen 6a)	233
Figure C.6a.2: SG1 & SG4 skin strain vs. time (Specimen 6a)	233
Figure C.6a.3: SG2 & SG3 spar strain vs. time (Specimen 6a)	234
Figure C.6a.4: SG2 & SG3 average spar strain vs. time (Specimen 6a)	235
Figure C.6b.1: Kistler pressure vs. time (Specimen 6b)	236
Figure C.6b.2: SG1 & SG4 skin strain vs. time (Specimen 6b)	237
Figure C.6b.3: SG2 & SG3 spar strain vs. time (Specimen 6b)	238
Figure C.6b.4: SG2 & SG3 average spar strain vs. time (Specimen 6b)	239
Figure C.6c.1: Kistler pressure vs. time (Specimen 6c)	240
Figure C.6c.2: SG1 & SG4 skin strain vs. time (Specimen 6c)	241
Figure C.6c.4: SG2 & SG3 average spar strain vs. time (Specimen 6c)	243
Figure C.6d.1: Kistler pressure vs. time (Specimen 6d)	244
Figure C.6d.2: SG1 & SG4 skin strain vs. time (Specimen 6d)	245
Figure C.6d.3: SG2 & SG3 spar strain vs. time (Specimen 6d)	246
Figure C.6d.4: SG2 & SG3 average spar strain vs. time (Specimen 6d)	247
Figure C.6e.1: Kistler pressure vs. time (Specimen 6e)	248
Figure C.6e.2: SG1 & SG4 skin strain vs. time (Specimen 6e)	249
Figure C.6e.3: SG2 & SG3 spar strain vs. time (Specimen 6e)	250
Figure C.6e.4: SG2 & SG3 average spar strain vs. time (Specimen 6e)	251
Figure C.7a.1: Kistler pressure vs. time (Specimen 7a)	253
Figure C.7a.2: SG1 & SG4 skin strain vs. time (Specimen 7a)	253
Figure C.7a.3: SG2 & SG3 spar strain vs. time (Specimen 7a)	254
Figure C.7a.4: SG2 & SG3 average spar strain vs. time (Specimen 7a)	255
Figure C.7b.1: Kistler pressure vs. time (Specimen 7b)	256
Figure C.7b.2: SG1 & SG4 skin strain vs. time (Specimen 7b)	257
Figure C.7b.3: SG2 & SG3 spar strain vs. time (Specimen 7b)	258
Figure C.7b.4: SG2 & SG3 average spar strain vs. time (Specimen 7b)	259
Figure C.7c.1: Kistler pressure vs. time (Specimen 7c)	260
Figure C.7c.2: SG1 & SG4 skin strain vs. time (Specimen 7c)	261
Figure C.7c.4: SG2 & SG3 average spar strain vs. time (Specimen 7c)	263
Figure C.7d.1: Kistler pressure vs. time (Specimen 7d)	264

Figure C.7d.2: SG1 & SG4 skin strain vs. time (Specimen 7d)	265
Figure C.7d.3: SG2 & SG3 spar strain vs. time (Specimen 7d)	266
Figure C.7d.4: SG2 & SG3 average spar strain vs. time (Specimen 7d)	267
Figure C.7e.1: Kistler pressure vs. time (Specimen 7e)	268
Figure C.7e.2: SG1 & SG4 skin strain vs. time (Specimen 7e)	269
Figure C.7e.3: SG2 & SG3 spar strain vs. time (Specimen 7e)	270
Figure C.7e.4: SG2 & SG3 average spar strain vs. time (Specimen 7e)	271
Figure C.8a.1: Kistler pressure vs. time (Specimen 8a)	273
Figure C.8a.2: SG1 & SG4 skin strain vs. time (Specimen 8a)	273
Figure C.8a.3: SG2 & SG3 spar strain vs. time (Specimen 8a)	274
Figure C.8a.4: SG2 & SG3 average spar strain vs. time (Specimen 8a)	275
Figure C.8b.1: Kistler pressure vs. time (Specimen 8b)	276
Figure C.8b.2: SG1 & SG4 skin strain vs. time (Specimen 8b)	277
Figure C.8b.3: SG2 & SG3 spar strain vs. time (Specimen 8b)	278
Figure C.8b.4: SG2 & SG3 average spar strain vs. time (Specimen 8b)	279
Figure C.8c.1: Kistler pressure vs. time (Specimen 8c)	280
Figure C.8c.2: SG1 & SG4 skin strain vs. time (Specimen 8c)	281
Figure C.8c.4: SG2 & SG3 average spar strain vs. time (Specimen 8c)	283
Figure C.8d.1: Kistler pressure vs. time (Specimen 8d)	284
Figure C.8d.2: SG1 & SG4 skin strain vs. time (Specimen 8d)	285
Figure C.8d.3: SG2 & SG3 spar strain vs. time (Specimen 8d)	286
Figure C.8d.4: SG2 & SG3 average spar strain vs. time (Specimen 8d)	287
Figure C.8e.1: Kistler pressure vs. time (Specimen 8e)	288
Figure C.8e.2: SG1 & SG4 skin strain vs. time (Specimen 8e)	289
Figure C.8e.3: SG2 & SG3 spar strain vs. time (Specimen 8e)	290
Figure C.8e.4: SG2 & SG3 average spar strain vs. time (Specimen 8e)	291
Figure C.9a.1: Kistler pressure vs. time (Specimen 9a)	293
Figure C.9a.2: SG1 & SG4 skin strain vs. time (Specimen 9a)	294
Figure C.9a.3: SG2 & SG3 spar strain vs. time (Specimen 9a)	295
Figure C.9a.4: SG2 & SG3 average spar strain vs. time (Specimen 9a)	296
Figure C.9b.1: Kistler pressure vs. time (Specimen 9b)	297
Figure C.9b.2: SG1 & SG4 skin strain vs. time (Specimen 9b)	298
Figure C.9b.3: SG2 & SG3 spar strain vs. time (Specimen 9b)	299
Figure C.9b.4: SG2 & SG3 average spar strain vs. time (Specimen 9b)	300
Figure C.9c.1: Kistler pressure vs. time (Specimen 9c)	301
Figure C.9c.2: SG1 & SG4 skin strain vs. time (Specimen 9c)	302
Figure C.9c.4: SG2 & SG3 average spar strain vs. time (Specimen 9c)	304
Figure C.9d.1: Kistler pressure vs. time (Specimen 9d)	305
Figure C.9d.2: SG1 & SG4 skin strain vs. time (Specimen 9d)	306
Figure C.9d.3: SG2 & SG3 spar strain vs. time (Specimen 9d)	307
Figure C.9d.4: SG2 & SG3 average spar strain vs. time (Specimen 9d)	308
Figure C.9e.1: Kistler pressure vs. time (Specimen 9e)	309
Figure C.9e.2: SG1 & SG4 skin strain vs. time (Specimen 9e)	310
Figure C.9e.3: SG2 & SG3 spar strain vs. time (Specimen 9e)	311
Figure C.9e.4: SG2 & SG3 average spar strain vs. time (Specimen 9e)	312
Figure C.10a.1: Kistler pressure vs. time (Specimen 10a)	314

Figure C.10a.2: SG1 & SG4 skin strain vs. time (Specimen 10a).....	315
Figure C.10a.3: SG2 & SG3 spar strain vs. time (Specimen 10a).....	316
Figure C.10a.4: SG2 & SG3 average spar strain vs. time (Specimen 10a)	317
Figure C.10b.1: Kistler pressure vs. time (Specimen 10b).....	318
Figure C.10b.2: SG1 & SG4 skin strain vs. time (Specimen 10b)	319
Figure C.10b.3: SG2 & SG3 spar strain vs. time (Specimen 10b)	320
Figure C.10b.4: SG2 & SG3 average spar strain vs. time (Specimen 10b).....	321
Figure C.10c.1: Kistler pressure vs. time (Specimen 10c)	322
Figure C.10c.2: SG1 & SG4 skin strain vs. time (Specimen 10c).....	323
Figure C.10c.4: SG2 & SG3 average spar strain vs. time (Specimen 10c)	325
Figure C.11a.1: Kistler pressure vs. time (Specimen 11a)	326
Figure C.11a.2: SG2 & SG4 skin strain vs. time (Specimen 11a).....	327
Figure C.11a.3: SG5 & SG6 spar strain vs. time (Specimen 11a).....	328
Figure C.11a.4: SG5 & SG6 average spar strain vs. time (Specimen 11a)	329
Figure C.11b.1: Kistler pressure vs. time (Specimen 11b).....	330
Figure C.11b.2: SG2 & SG4 skin strain vs. time (Specimen 11b)	331
Figure C.11b.3: SG5 & SG6 spar strain vs. time (Specimen 11b)	332
Figure C.11b.4: SG5 & SG6 average spar strain vs. time (Specimen 11b).....	333
Figure C.11c.1: Kistler pressure vs. time (Specimen 11c)	334
Figure C.11c.2: SG2 & SG4 skin strain vs. time (Specimen 11c).....	335
Figure C.11c.4: SG5 & SG6 average spar strain vs. time (Specimen 11c)	337
Figure C.11d.1: Kistler pressure vs. time (Specimen 11d).....	338
Figure C.11d.2: SG2 & SG4 skin strain vs. time (Specimen 11d)	339
Figure C.11d.4: SG5 & SG6 average spar strain vs. time (Specimen 11d).....	341

Table of Tables

Table 5.4.1: Example Load and Strain-at-Failure Data	22
Table 6.1.1: Dimensions of Specimen Set 1	24
Table 6.1.2.1: Load and Strain at Failure for Specimen Set 1	31
Table 6.1.2.2: Summary of Results for Specimen Set 1	32
Table 6.2.1: Dimensions of Specimen Set 2	33
Table 6.2.2.1: Load and Strain at Failure for Specimen Set 2	40
Table 6.2.2.2: Summary of Results for Specimen Set 2	40
Table 6.3.1: Dimensions of Specimen Set 3	42
Table 6.3.2.1: Load and Strain at Failure for Specimen Set 3	51
Table 6.3.2.2: Summary of Results for Specimen Set 3	51
Table 6.4.2.1: Load and Strain at Failure for Specimen Set 4	60
Table 6.4.2.2: Summary of Results for Specimen Set 4	60
Table 6.5.1: Dimensions of Specimen Set 5	61
Table 6.5.2.1: Load and Strain at Failure for Specimen Set 5	69
Table 6.5.2.2: Summary of Results for Specimen Set 5	69
Table 6.6.1: Dimensions of Specimen Set 6	70
Table 6.6.2.1: Load and Strain at Failure for Specimen Set 6	78
Table 6.6.2.2: Summary of Results for Specimen Set 6	78
Table 6.7.1: Dimensions of Specimen Set 7	79
Table 6.7.2.1: Load and Strain at Failure for Specimen Set 7	87
Table 6.7.2.2: Summary of Results for Specimen Set 7	87
Table 6.8.2.1: Load and Strain at Failure for Specimen Set 8	97
Table 6.8.2.2: Summary of Results for Specimen Set 8	97
Table 6.9.1: Dimensions of Specimen Set 9	98
Table 6.9.2.1: Load and Strain at Failure for Specimen Set 9	105
Table 6.9.2.2: Summary of Results for Specimen Set 9	105
Table 6.10.1: Dimensions of Specimen Set 10	106
Table 6.10.2.1: Load and Strain at Failure for Specimen Set 10	114
Table 6.10.2.2: Summary of Results for Specimen Set 10	114
Table 6.11.3.1: Load and Strain at Failure for Specimen Set 11	123
Table 6.11.3.2: Summary of Results for Specimen Set 11	123
Table 6.12.1: Summary of Joint Failure Symmetry, Loads, and Strains	124
Table 6.12.1 (continued): Summary of Joint Failure Symmetry, Loads, and Strains.....	125
Table 6.12.1 (continued): Summary of Joint Failure Symmetry, Loads, and Strains.....	126
Table 6.12.2: Static Joint Performance Based on Failure Load.....	127
Table 6.12.3: Static Joint Performance Based on Failure Strain	127
Table 6.12.4: Dynamic Joint Performance Based on Failure Strain.....	128
Table A.1: Kistler Pressure Sensor Parameters	134
Table A.2: Recorded Test Parameters	135
Table A.2: Recorded Test Parameters (continued).....	136
Table A.2: Recorded Test Parameters (continued).....	137
Table B.1: Diaphragm Rupture Evaluation	139

1 BACKGROUND AND OBJECTIVES

1.1 Background

Projectile-induced hydrodynamic ram can generate fuel-tank pressures in excess of 10,000 psi. This event is potentially catastrophic for aircraft fuel tanks designed to survive sustained pressures of little more than 50 psi. While the magnitude of ram pressure is dictated by a combination of fuel-level and projectile threat, skin-spar joint design is the primary means by which damage can otherwise be controlled. Damage resistant joints restrict the spread of damage and assist aircraft survival.

Joint resistance to ram is conventionally evaluated using a combination of two methods: a) T-joint pull-off tests and b) ballistically-tested wingboxes. While T-joint tests are a low-cost method of ranking skin-spar joints according to their load at failure, realism is traded away in favor of an economical and easily understood test. T-joint pull-off tests are symmetrically performed quasi-statically at a strain rate of less than 0.01 in/in-sec, whereas projectile-generated ram events involve asymmetric high-rate loading conditions on the order of 100 in/in-sec. Contrary to T-joint pull-off tests, wingbox ram tests with actual threat projectiles are fully realistic, but these tests come with a price tag in excess of \$250,000 (inclusive of tooling, structural materials, test costs, and labor). This is too expensive for wholesale evaluation of competing joint concepts.

When attempting to model high-strain rate events associated with ram, conventional static failure criteria has proven inadequate. The required dynamic failure criterion is believed on the order of 2-4 times that of the static case. The present test program applies a new RamGun test methodology¹ to dynamically load T-joints and J-joints at a rate coincident with projectile induced hydrodynamic ram. The effort is sponsored by the Joint Aircraft Survivability Program Office and directed by the 46th Test Wing (46 TW) at Wright-Patterson AFB, OH.

Figure 1.1.1 is a diagram that standardizes notation of the T-joint and J-joint described throughout this report.

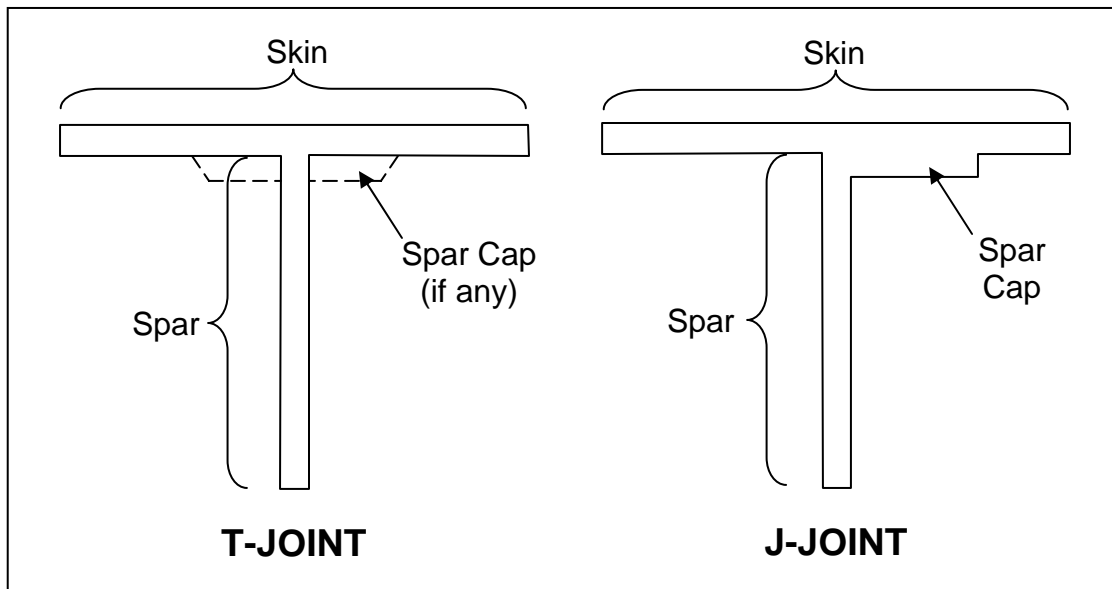


Figure 1.1.1: T-joint and J-Joint components

1.2 Objectives

Objectives of the present effort are two-fold:

- Evaluate the ability of aircraft skin-spar joints to withstand hydrodynamic ram forces.
- Lay the foundation for establishing a dynamic (high-strain rate) failure criteria as a function of joint design.

Overall, the program goal is to evaluate as many different joint designs as possible and to quantify inherent differences between quasi-static and high strain rate failure modes and properties.

2 PLAN OF ACTION

An established RamGun (hydrodynamic ram simulator) test technique¹ is used to investigate the ram-resistance of aircraft skin-spar joints. While the RamGun is capable of delivering ram-like pressures to single and double T-joint and J-joint specimens, only single joints are evaluated in this test series in order to remain consistent with the geometry used to evaluate joints statically.

The focus on stated program objectives (as opposed to development of damage resistant joint design and fabrication techniques), allowed evaluation of a representative cross section of aircraft joint designs voluntarily donated by both U.S. and international industry sources. At the program's on-set, an announcement to industry was issued whereby potential participants were encouraged to submit for evaluation any/all joint designs of interest to their organization. The requirement was that ten identical joint-specimens be tendered for each particular joint design, allowing a side-by-side evaluation of quasi-static and dynamic failure properties. The goal was to evaluate as many different joint designs as possible and to quantify inherent differences between quasi-static and high strain rate properties. In return, all participating organizations would share, first hand, in data generated.

Figure 2.1 lists joint dimension requirements that were provided to industry participants, where $A = 5.00''$ ($\pm 0.25''$), $B = 4.00''$ ($+0.00''$, $-0.05''$), and $C = 2.00''$ ($+0.00''$, $-0.05''$). *Note: An adjustment to dimension C (to 1.00'') was allowed only for Specimen Set 9 based on limited material availability. Doing so required that the RamGun's Window End Plate be replaced with one accepting the 1'' specimen dimension.*

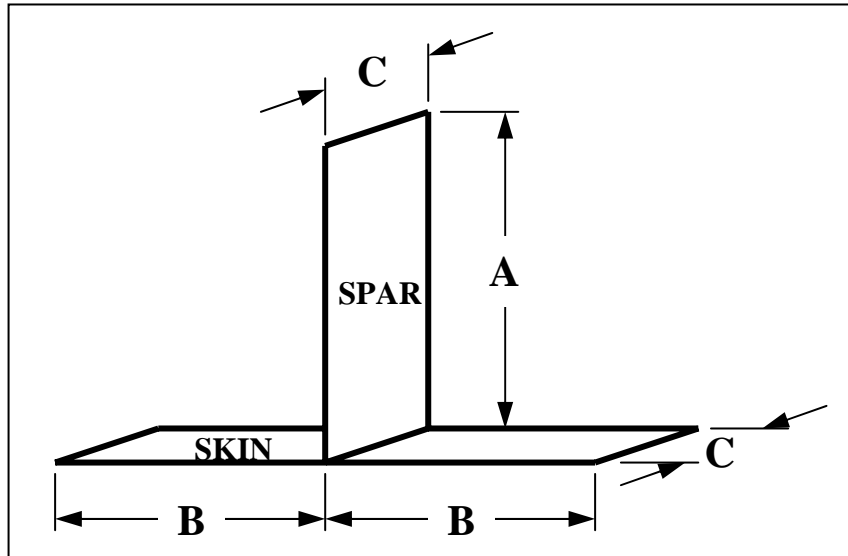


Figure 2.1: Joint dimension requirements

A sample of a single joint (representing one of ten designs submitted for evaluation) is shown in Figure 2.2. For each joint design, five symmetric T pull-off tests were conducted by the Air Force Research Laboratory (AFRL) using a conventional quasi-static loading method. Load and strain-to-failure were recorded. Similarly, for each joint design, five symmetric T pull-off tests were conducted by the 46 TW using the new high-strain rate (dynamic) loading method. Strain-to-failure values were recorded.

In addition to the ten joint designs submitted for AFRL and 46 TW evaluation, one additional joint set is evaluated herein. Although details associated with this final joint set is reported under separate cover², the joint conforms dimensionally to Figure 2.1, instrumentation was similar to the aforementioned ten joint sets, and the joint was subjected to a combination of static and dynamic (RamGun) testing. Based on test similarities, a synopsis of failure load and failure strain results for this eleventh joint is presented herein.



Figure 2.2: Example single spar T-joint

3 INSTRUMENTATION

3.1 Common Instrumentation (T-Joint Specimens)

Test specimen instrumentation consisted of four single-axis strain gages (Micro Measurement Division type CEA-06125UN350 with a gage factor of 2.1) uniformly installed by the 46 TW. Strain gage placement on the skin was according to dimension D in Figure 3.1.1 (where $D = 2.50''$) such that each gage is centered on dimension C of Figure 2.1 and axially aligned with dimension B. Skin strain gages monitored flexural symmetry. Back-to-back gage placement on the spar-web was also according to dimension D in Figure 3.1.1, such that each gage is centered on dimension C of Figure 2.1 and axially aligned with dimension A. Spar-web gages monitored bending and recorded the strain rate and pull-off strain-to-failure.

Test instrumentation on specimen set 11 differs slightly. (As discussed in Section 2, these specimen sets were fabricated and tested in support of a separate effort.²) Skin strain gages in specimen set 11 were positioned according to dimension D in Figure 3.1.1 at 2.50". Web gages were positioned according to dimension D in Figure 3.1.1 at 2.00".

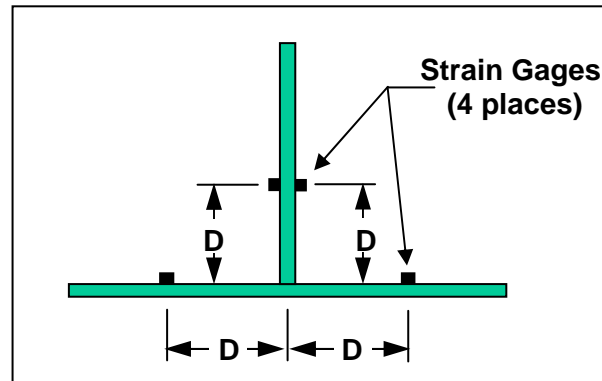


Figure 3.1.1: Strain gage locations for T-joint specimens

Figures 3.1.2 and 3.1.3 show side and end-view sensor layouts on and around the test specimen. The exception is for specimen set 11 where positions of skin and spar gages are noted in the above paragraph.

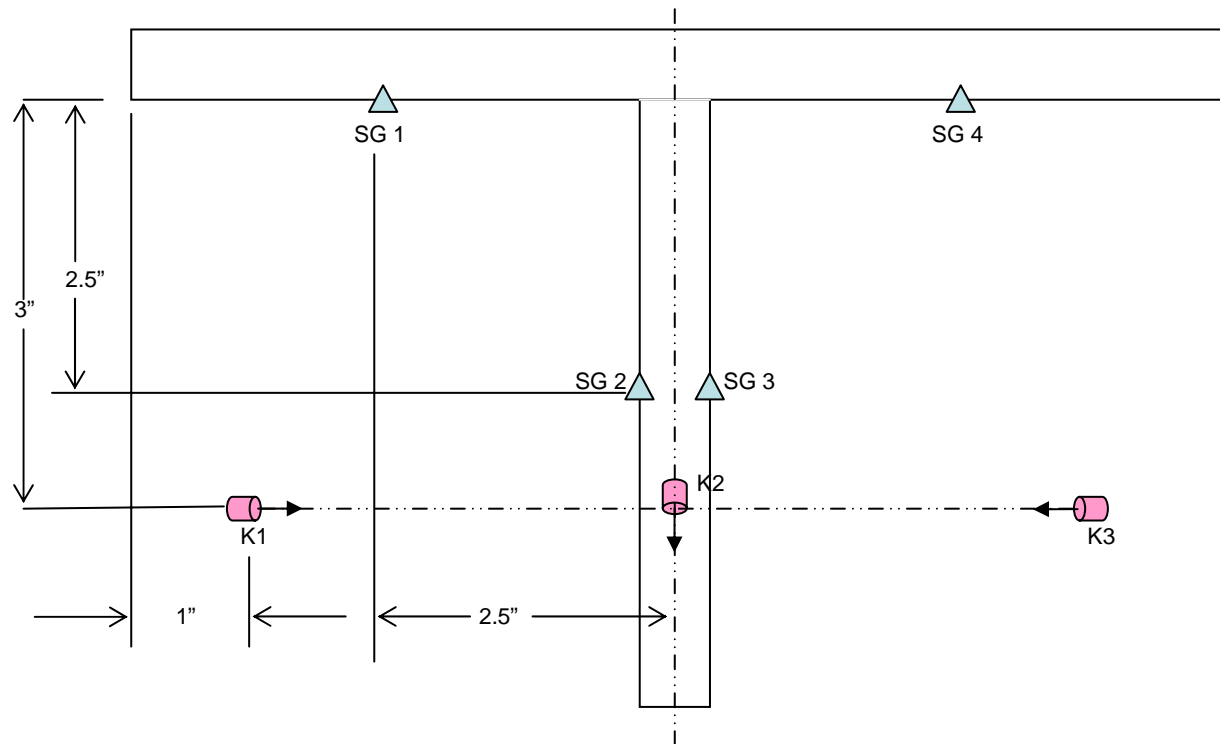


Figure 3.1.2: Layout of instrumentation on T-joint (looking down from above)

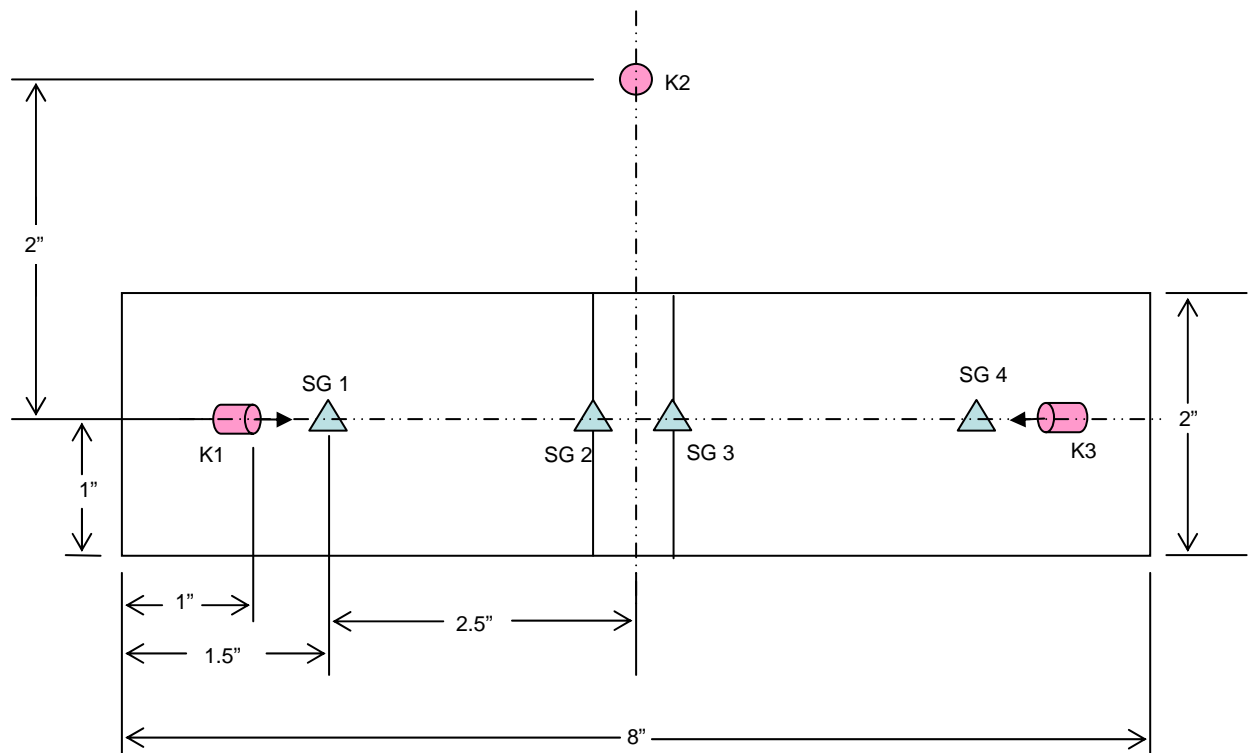


Figure 3.1.3: Layout of instrumentation on T-joint (looking into test chamber from barrel)

3.2 Common Instrumentation (J-Joint Specimens)

The length of the spar cap on the J-joint specimens forced relocation of one of the skin gages to the right side as shown in Figure 3.2.1. Test specimen instrumentation consists of four single-axis strain gages (Micro Measurement Division type CEA-06125UN350 with a gage factor of 2.1) uniformly installed by the 46 TW. Strain gage placement on the skin is according to dimension D (where $D = 2.50''$). Back-to-back gages are centered on dimension C of Figure 2.1 and axially aligned with dimension B. The side-by-side gage pair is spaced by 1 inch with the center of the pair centered on dimension C of Figure 2.1 and axially aligned with dimension B. Because skin gages are side-by-side, the skin's flexural symmetry cannot be evaluated. Back-to-back gage placement on the spar-web was also according to dimension D in Figure 3.2.1, such that each gage is centered on dimension C of Figure 2.1 and axially aligned with dimension A. Spar-web gages monitored bending and recorded the strain rate and pull-off strain-to-failure.

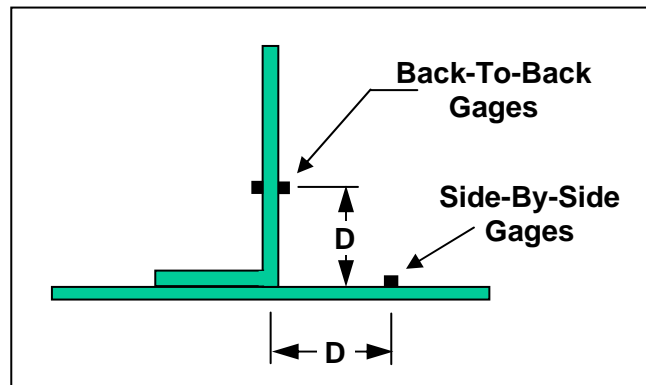


Figure 3.2.1: Strain gage locations for J-joint specimens

Figures 3.2.2 and 3.2.3 show side and end-view sensor layouts on and around the test specimen. Instrumentation details can be found in Appendix A.

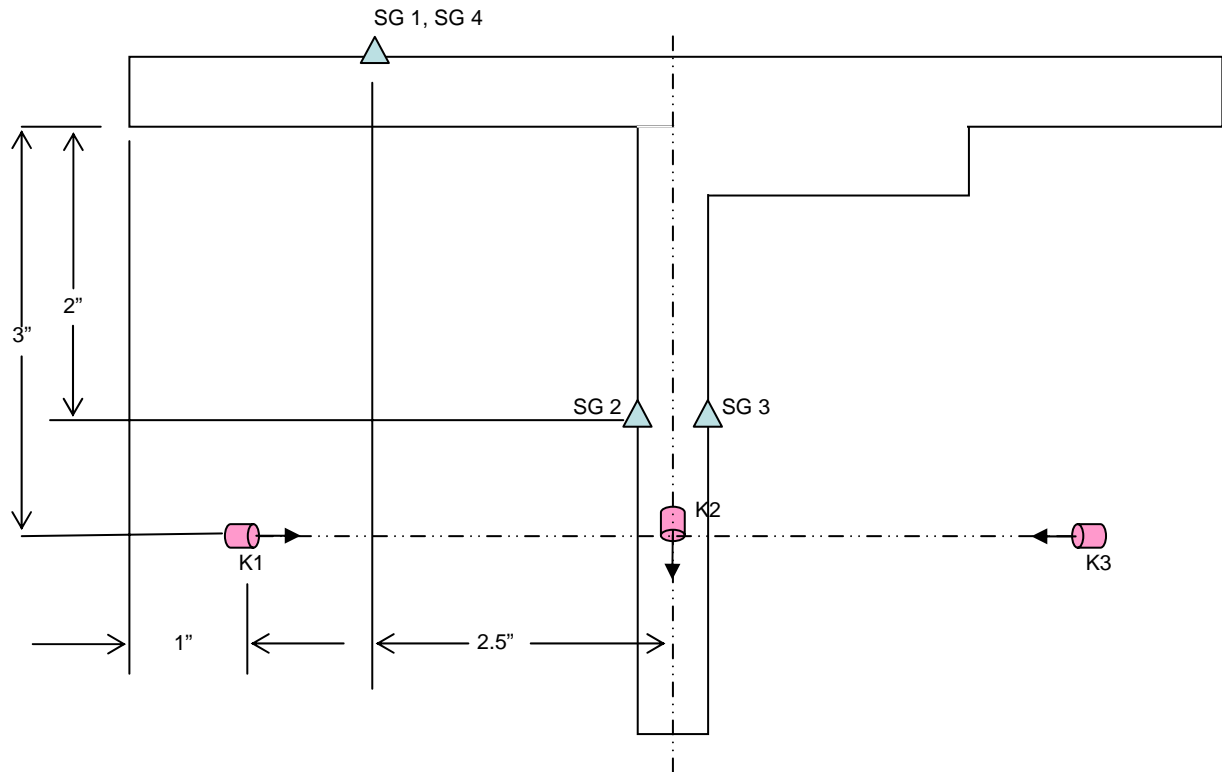


Figure 3.2.2: Layout of instrumentation on J-joint (looking down from above)

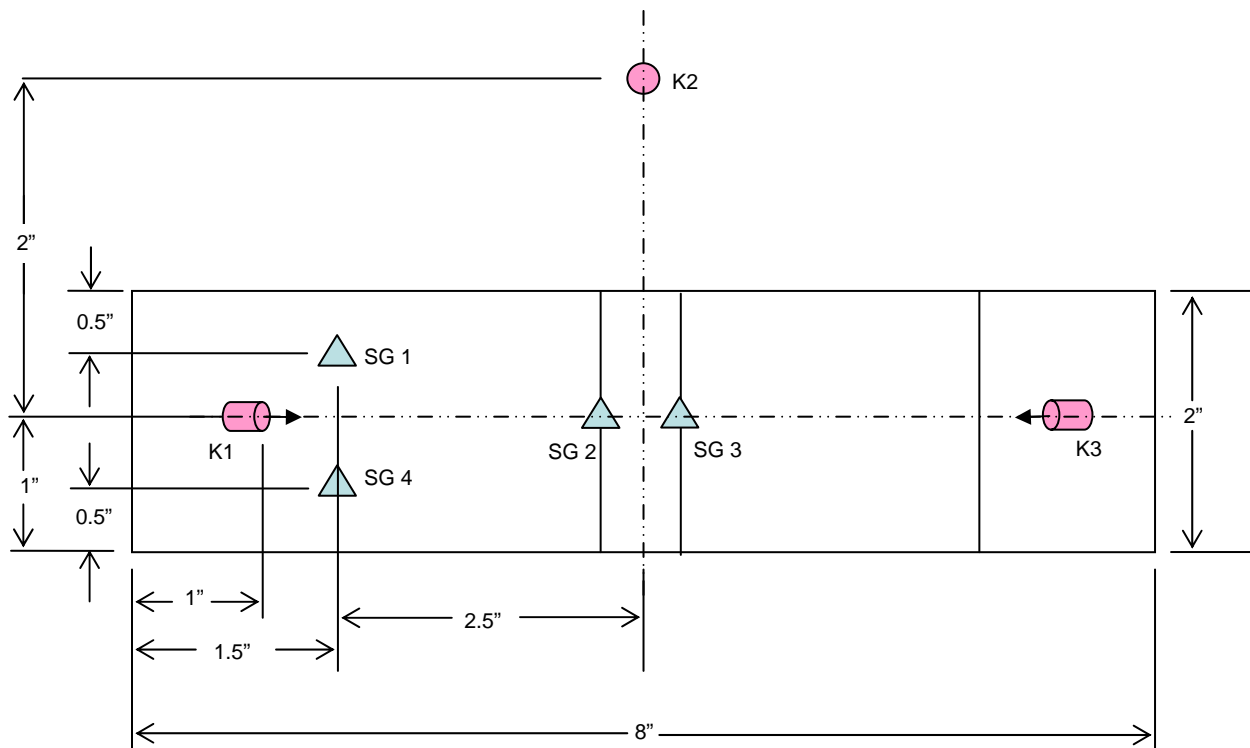


Figure 3.2.3: Layout of instrumentation on J-joint (looking into test chamber from barrel)

3.3 Static Test Instrumentation

Strain gage instrumentation consisted of a 3-wire configuration (identical to those of the dynamic tests). AFRL used a National Instruments SCXI chassis with bridge completion and excitation (which multiplexes the data) and Labview software to acquire strain, load, and displacement data as a function of time. Strain and load-displacement data were acquired at 10Hz (10 samples per second) during quasi-static testing.

3.4 Dynamic Test Instrumentation

Test fixture instrumentation included Kistler pressure transducers in the RamGun's fluid chamber (to assess ram pressures). The Kistlers consisted of type 211B1 with a range of 0-5,000 psi and type 211B2 with a range of 0-10,000 psi.^a Other test fixture instrumentation included pressure gages within the gas gun's pressure chamber (to indirectly control RamGun projectile velocities and, in-turn, control ram pressures) and break-wires (to record projectile velocity). Strain and pressure data were acquired at 1MHz (one million samples per second) during dynamic testing.

Early in the test effort, instrumentation also included a pair of calibrated strain gages on the spar grip-rod (in an attempt to provide load-to-failure information). It quickly became apparent that these gages were not capable of providing the desired information due to mass and inertia of attached structure downstream of the grip. Once this material was put into motion due to applied pressure load, the material's inertia continued to register load at the remote gage location even though failure occurred. To a limited extent, this same phenomenon occurred with back-to-back gages on the spar-web, however these gages were much nearer the failure site (minimizing downstream mass).

In order to better understand this phenomenon, we performed a modeling study in which a finite element model (FEM) of the holding fixture and sample joint specimen was subjected to the measured pressure pulse. The model was sectioned at various locations, and the loads at those sections were observed as a function of time.

^a See Appendix A.

Figure 3.4.1 shows the finite element model of the setup and three section cuts through the model at different locations. Section 1 is located where joint failure is most likely to occur. Section 5 is on the joint's web, near web strain gages 2 and 3. Section 9 is at an assumed strain gage location on the T-Joint Fixture (positioned within the RamGun's Test Article Chamber).

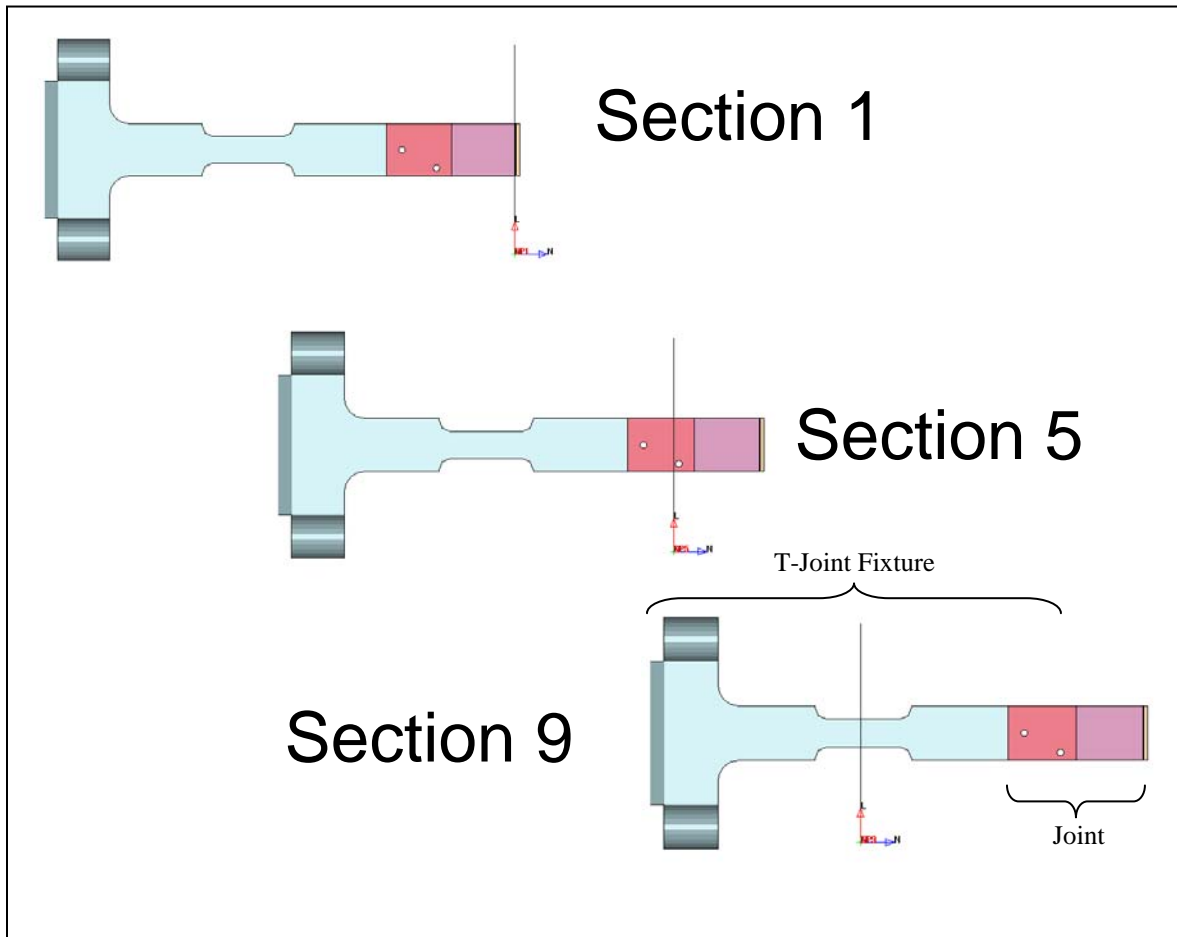


Figure 3.4.1: Three section cuts through the FEM

Figure 3.4.2 shows a plot of the loads occurring in the model at each of the three section cuts. By observing the comparison of these curves, one can see the effects of the mass/inertia of the structures downstream of the section cuts. In the figure, curve A represents the load at the expected failure location (Section 1), curve B represents the load on the joint's web (Section 5), and curve C represents the load that would be measured on the T-Joint Fixture. The failure load at Section 1 is 3,000 pounds at 0.12 msec. The failure load at Section 5 is 3,800 pounds at 0.14 msec. And the failure load at Section 9 is 4,000 pounds at 0.17 msec. Stated differently, the load that causes joint failure is actually 3000 pounds. As the distance from the specimen skin increases, the apparent load increases (due to fixture-mass acceleration) to much higher values that have little real meaning. Because dynamic failure loads can be misleading, the authors opt for strain as a preferred metric describing dynamic failure.

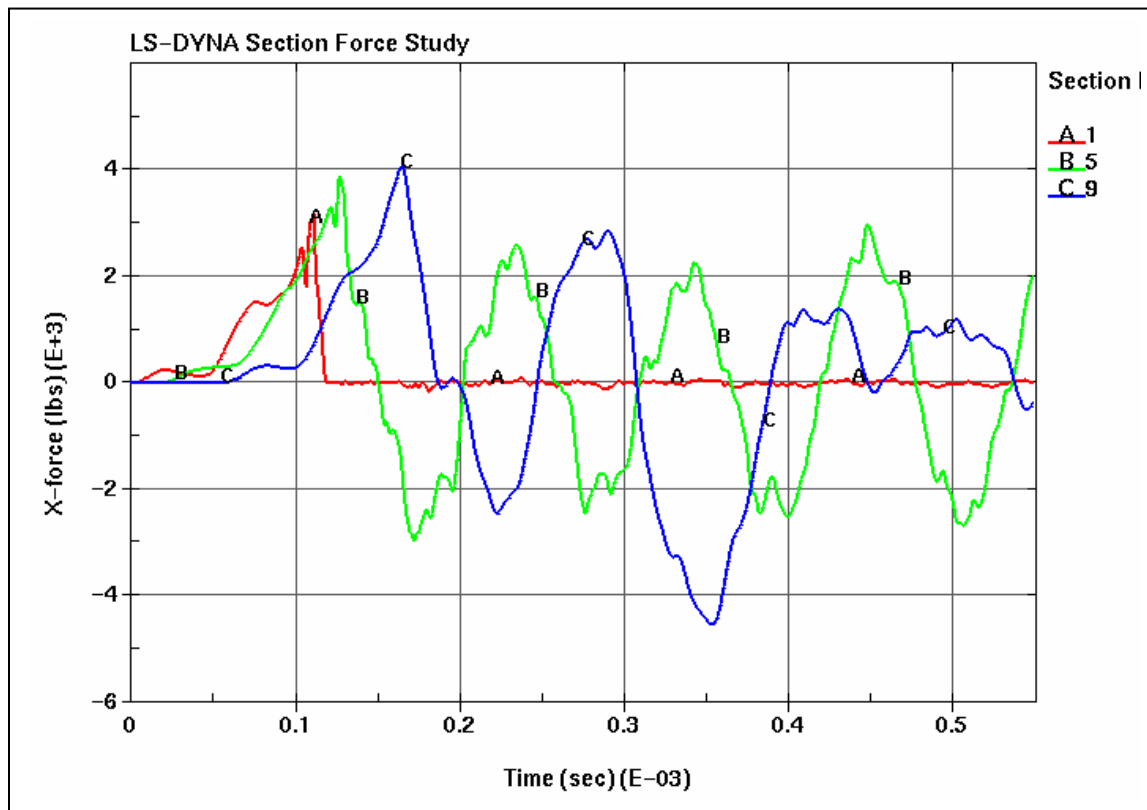


Figure 3.4.2: Load vs. time at the three section cuts

4 TEST SETUP

4.1 Static Test Setup

The following static test setup is unique to specimen sets 1 – 10. Static testing of specimen set 11 was performed independently.²

Fiberglass tabs were epoxied to the spar-web end of each specimen to assist with load distribution. The test specimen's skin was then supported in the test fixture at a 6" span as shown in Figure 4.1.1. The only exceptions to the span were Specimens 1g and 1h, which utilized a 3" span.

All specimens were tested on a 50,000 pound MTS Servohydraulic Test Machine with 3" wide hydraulic wedge grips attached to the fixture. A preload of 100-300 pounds force (lbf) was applied to seat each specimen. Following preload, specimens were unloaded to 10-15 lbf to maintain specimen and fixture alignment. Each displacement-control test was conducted at a rate of 0.4 to 0.5 in/min with a data acquisition rate of 10Hz.

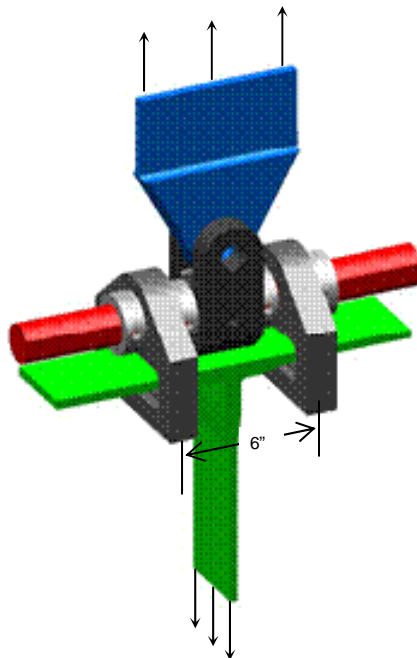


Figure 4.1.1: Static test fixture

4.2 Dynamic Test Setup

To replicate projectile-generated ram conditions, a pressure pulse, with requisite peak and impulse characteristics, had to be created. This was achieved using a hydrodynamic ram simulator, called the RamGun, as shown in Figures 4.2.1 through 4.2.3. The RamGun is a large-diameter gas gun designed to launch a 379.5g cylindrical polymer (Delrin) puck against a steel impact that caps a fluid column. Impact creates a pressure wave that traverses down the fluid column to later interact with a T-joint test specimen at the far-end. Pressure wave interaction with the T-joint occurs in a manner consistent with projectile-generated hydrodynamic ram within an aircraft fuel tank.¹

The RamGun is composed of several major elements as follows:

Impact Plate – 11 gage (0.1196” thick) steel plate that separates the gas gun and the water reservoir.

Water Reservoir – houses the water column.

Transition Cone – flared cone that connects water reservoir to test article chamber.

Test Article Chamber – houses the T-joint test specimen.

T-Joint Fixture – grips the spar and holds the joint stationary.

T-Joint – skin-spar joint test specimen.

Blow-Out Panel – diaphragm seals the tail of the RamGun’s fluid column until specimen failure.

Window Spacer and Window End Plate – clamp to either side of the blow-out panel to keep panel stationary and seal the tail of the RamGun. *Note: During all tests outlined in this report, the Window End Plate was horizontal (as shown in Figures 4.2.1 and 4.2.2). Doing so assists in maintaining pressure load symmetry should the Test Article Chamber contain any measure of entrained air.*

4.3 Adjustments to the Dynamic Test Setup

The first four specimens were tested with a 0.015” thick high-density polyethylene (HDPE) diaphragm (blow-out panel). Observed variation in ram pressures (despite consistent projectile impact velocities) were a cause for concern that lead to replacing the diaphragm with a corner-etched piece of 0.015” thick ultra-high molecular weight polyethylene (UHMWPE). Etching, to

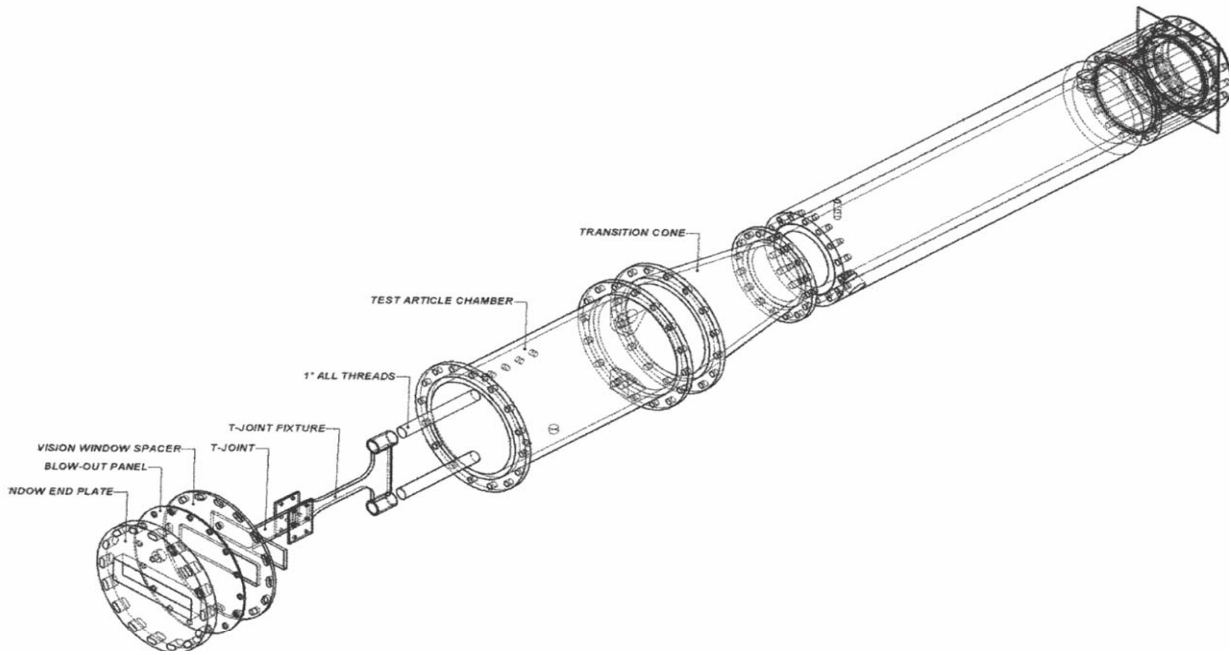


Figure 4.2.1: Schematic drawing of RamGun test apparatus

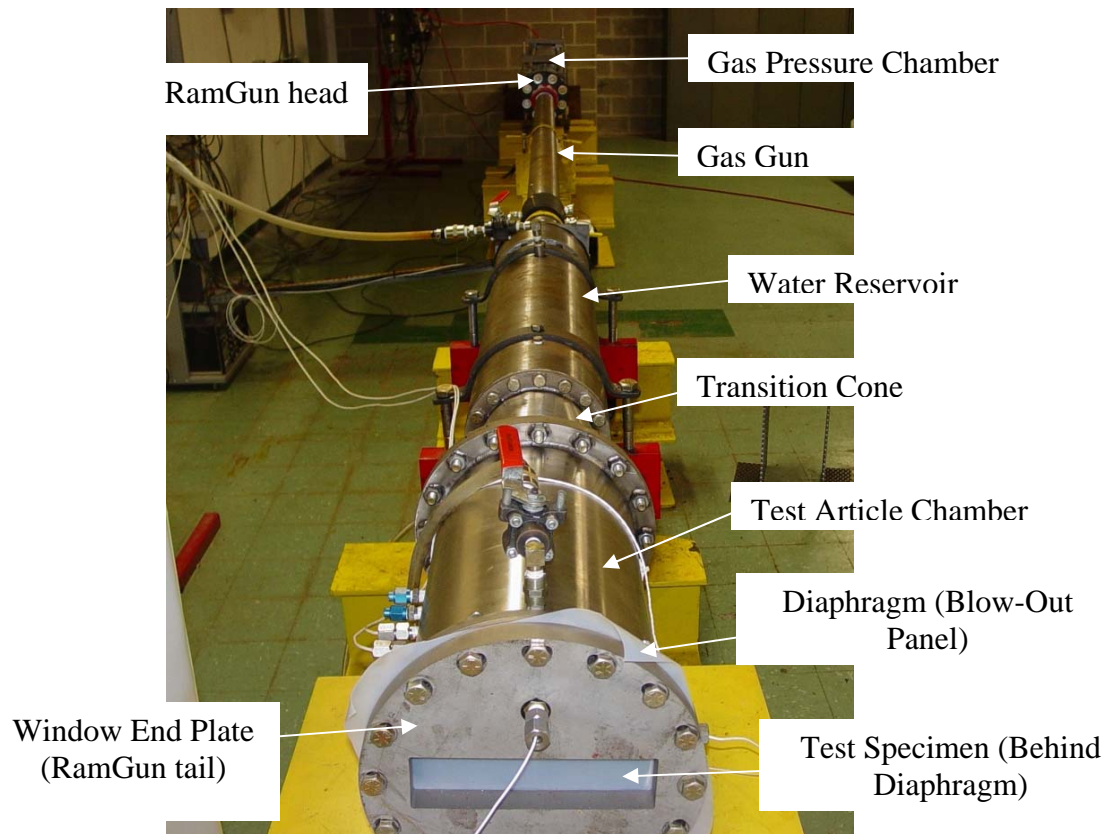


Figure 4.2.2: RamGun test apparatus, end view.

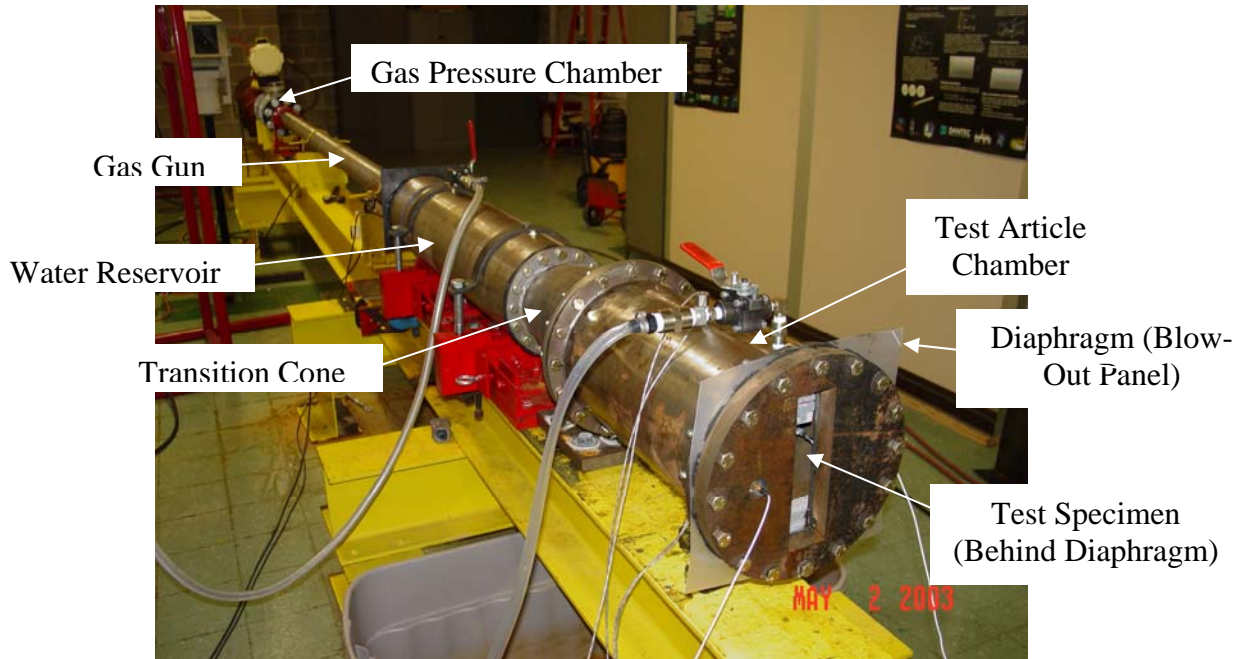


Figure 4.2.3: RamGun test apparatus, side view.

encourage rupture, was applied with a pen-knife. This UHMWPE diaphragm was then used for tests 5-24. Continued variations in ram pressure, combined with observation that etched UHMWPE remained resistant to tearing, forced a reevaluation of diaphragm materials. Reevaluation consisted of a brief series of RamGun tests using three candidate diaphragm materials (0.015" thick and 0.125" thick UHMWPE, and 0.003" thick 1100 aluminum alloy sheet). Each was independently evaluated without a T-joint in place. (See Appendix B for test results.) Results demonstrated that, for the diaphragm materials tested, the inherent resistance to rupture did not influence ram pressure amplitude. As such, measured differences in ram pressure amplitude are assumed to be caused by a combination of projectile-impact conditions (projectile alignment, projectile fracture, and plate deformation) and an absence of entrained air in the fluid column. Because pressure amplitudes proved more than adequate to fail all T-joint test specimens, the fact that pressures (during some tests) continued to rise higher did not seem to influence the specimen's failure strain. Based on preferred aluminum-diaphragm failure properties (observed shear with little stretching), 0.003" thick aluminum foil was installed as a diaphragm for all remaining tests, 25-63.

5 DYNAMIC DATA ANALYSIS TECHNIQUE

This section prescribes the method by which dynamic RamGun data are analyzed. The discussion refers to an example T-joint (Figure 5.1) that was subjected to RamGun testing.^b Four example graphs are presented to display and analyze the test outcome.



Figure 5.1: Example specimen failure as a result of dynamic test.

5.1 Identification of the Load Interval of Interest and Verification of Load Symmetry

The first graph is pressure vs. time (reference Figure 5.1.1).^c This graph identifies the load interval (dotted red lines denoting the beginning and ending of the primary pressure pulse) which is equated to the time interval where specimen failure most probably occurred. In this example, the load interval of interest falls roughly between 1.17 and 1.50 ms. Pressure amplitude is between 2,150 and 2,400 psi. Also in this example, we note that symmetrically-positioned pressure sensors K1 and K3 are in close agreement and verify that the pressure load is uniformly applied side-to-side on the joint.

5.2 Determination of Pull-Off Symmetry

The second graph in the data analysis process is used to assess skin pull-off symmetry and identifies strain vs. time for skin strain gages 1 and 4, or SG1 and SG4, respectively. In this strain graph, we examine only the load time interval of interest obtained the pressure curve. If

^b A synopsis of test results is presented in Section 6. For a complete data analyses of all T-joints, refer to Appendix C.

^c All of the data that reads as “smoothed” used a moving average technique with 5 points before and 5 points after for a total of 11 points averaged for each smoothed point plotted.

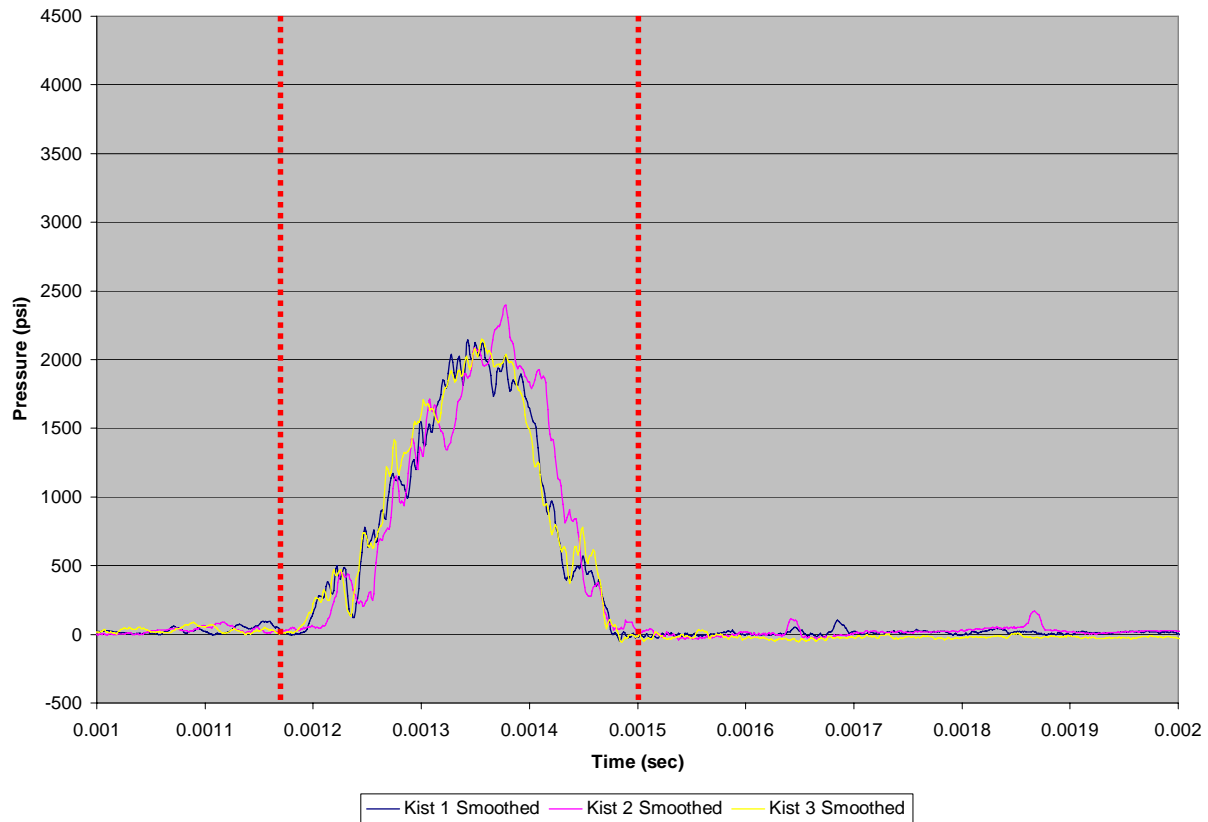


Figure 5.1.1: Ram pressure vs. time (example).

SG1 is in-phase with SG4 during this time interval and strains are of similar amplitude, it is assumed that the pull-off was symmetric. If SG1 is out-of-phase with SG4, we assume the pull-off is asymmetric. An example of pull-off symmetry (indicated by SG1 and SG4 during the time interval of interest) is shown in Figure 5.2.1. An example of pull-off asymmetry (indicated by SG1 and SG4 during the time interval of interest) is shown in Figure 5.2.2.

The third graph in the data analysis process is used to assess spar bending and compares strain vs. time for spar strain gages 2 and 3, or SG2 and SG3, respectively. When SG1 and SG4 show that the pull-off is symmetric, SG2 and SG3 should be in-phase (having strains of similar amplitude) indicating a symmetric pull-off. Likewise, if SG1 and SG4 show that the pull-off is asymmetric then SG2 and SG3 should be out-of-phase (or exhibiting strains of dissimilar amplitude) indicating that the pull-off is asymmetric. Should these two strain graphs not correlate, there will be further discussion in the accompanying text. An example of pull-off

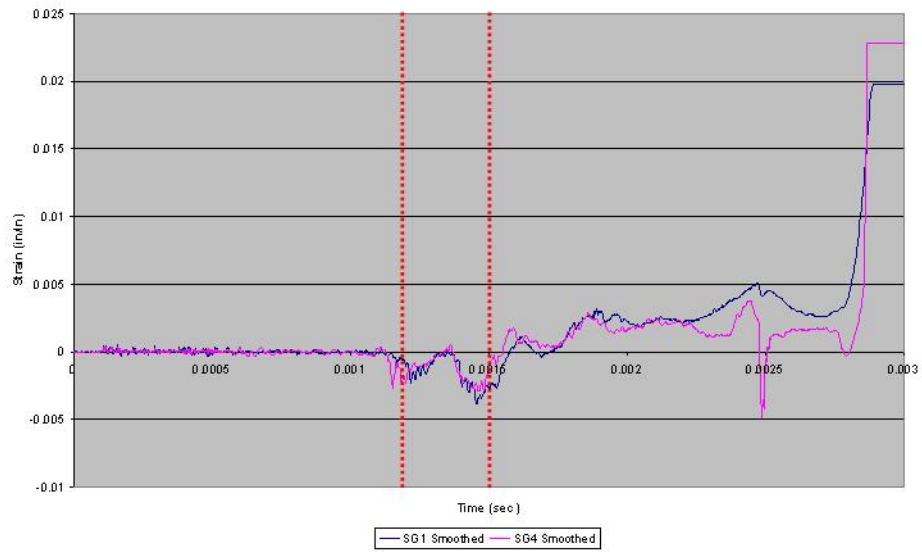


Figure 5.2.1: Example of SG 1 & 4 symmetry

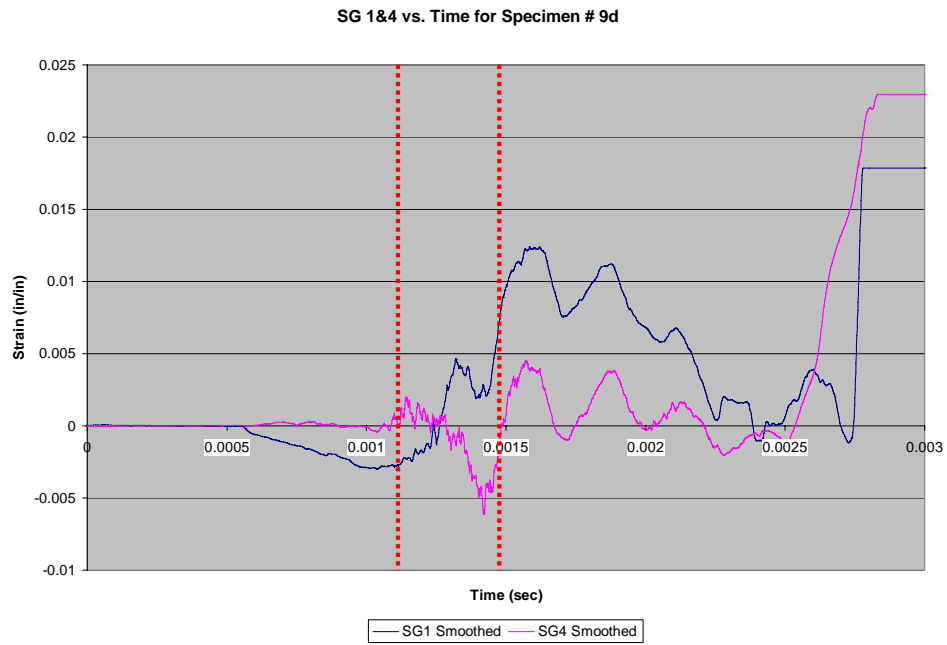


Figure 5.2.2: Example of SG 1 & 4 asymmetry

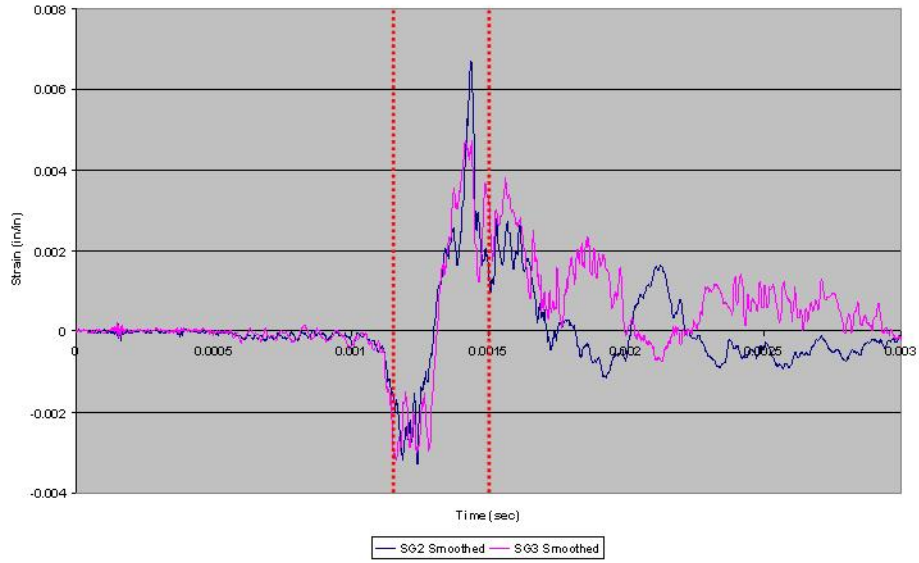


Figure 5.2.3: Example of SG 2 & 3 symmetry

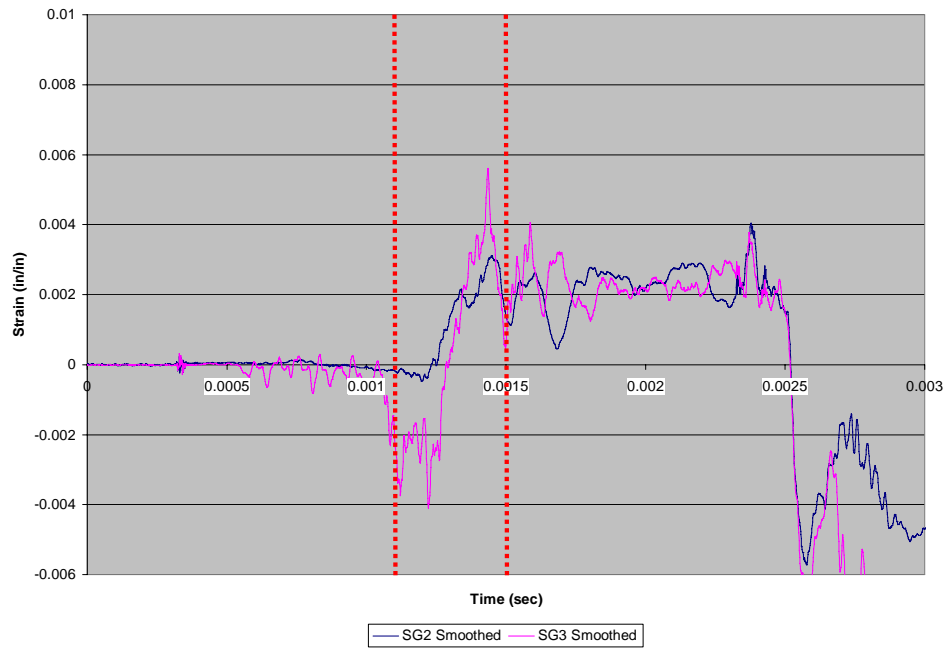


Figure 5.2.4: Example of SG 2 & 3 asymmetry

symmetry (indicated by SG2 and SG3 during the time interval of interest) is shown in Figure 5.2.3. An example of pull-off asymmetry (indicated by SG2 and SG3 during the time interval of interest) is shown in Figure 5.2.4.

While the above determination of failure symmetry is not critical to the analysis, the assessment of failure symmetry offers feedback to the joint fabrication process. Assuming that a uniformly distributed pressure wave loads the joint, symmetric failure is expected. Asymmetric failure of a joint that has a symmetric cross section can be an indicator of a non-uniform fabrication process. One may also expect to see a lower recorded strains-at-failure on joints that fail asymmetrically. In this report, with only four to five dynamic-test replications for each joint design, the statistical variance between symmetric and asymmetric failure strains is not attempted.

5.3 Assessment of Strain at Failure

The fourth and final graph in the data analysis process is used to assess failure metrics. The graph shows average strain (for spar gages SG2 and SG3) versus time (reference Figure 5.3.1).

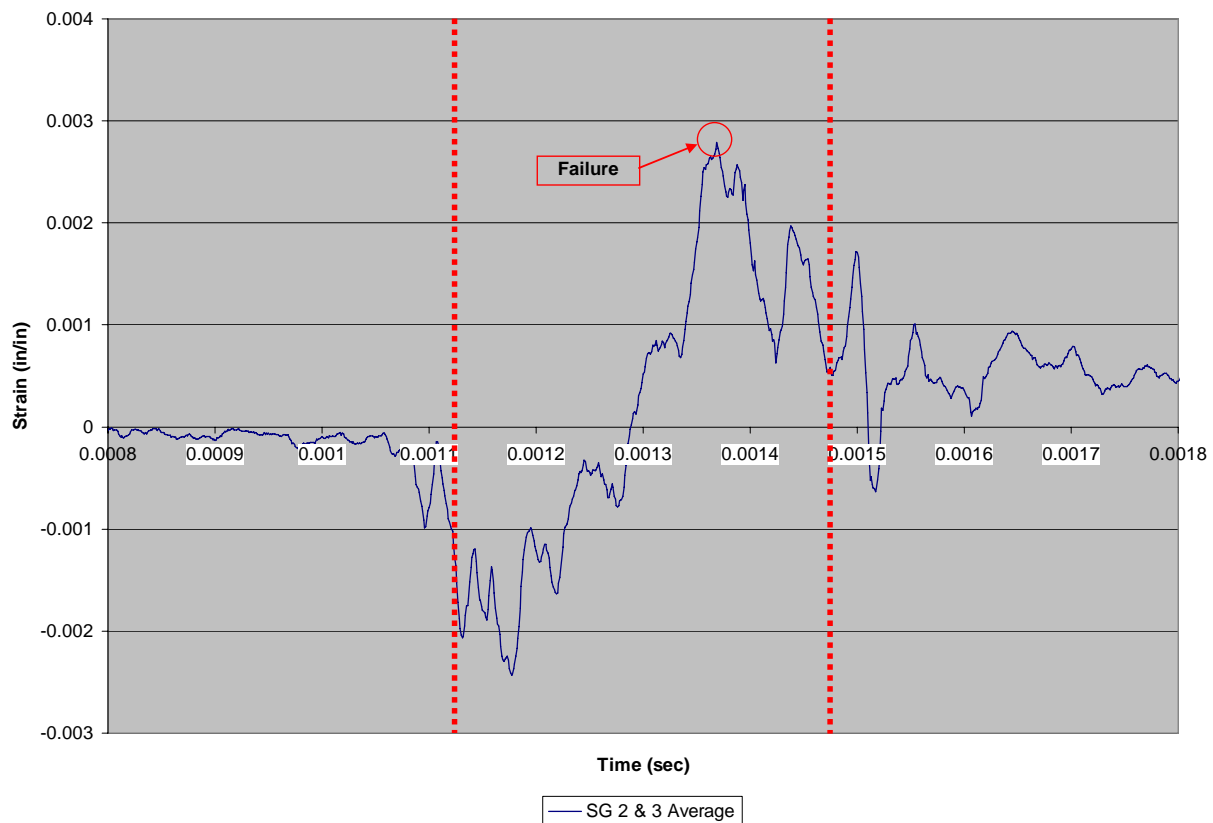


Figure 5.3.1: Average spar-strain vs. time (example)

In this graph, the peak tensile strain (maximum pull-off strain) is assumed to correspond with the time of failure. By taking the average, bending effects (due to load asymmetries) are eliminated from consideration. In this example, the dynamic strain at failure is 2.8×10^{-3} in/in.

This dynamic strain-at-failure is the easily-understood and critical metric which we seek. While it can be compared 1:1 with its quasi-statically obtained counterpart, dynamic strain-at-failure (as produced by the RamGun) is a structural mechanical property that relates directly and realistically to projectile-induced ram loading conditions. Dynamic strain-at-failure can either be used to rank a series of candidate joint designs for inherent resistance to hydrodynamic ram, or as a joint failure criterion within finite element codes.

5.4 Example Comparison of Dynamic vs. Static Failure Data

Table 5.4.1 shows an example of strain-at-failure data where dynamic data was assessed based on the above methodology, and quasi-static data assessed using standard methods. This particular dataset is based on T-joint test Specimen Set #4. The average dynamic failure strain was 3.79 in/in. Conversely, the quasi-static failure strain was 0.99 in/in. Thus, for this case, the apparent dynamic strain at failure was 3.83 times greater than the static strain at failure.

Table 5.4.1: Example Load and Strain-at-Failure Data

	Specimen	Load at Failure (lbf)	Strain at Failure ($\times 10^{-3}$ in/in)
Dynamic	4a	-	4.375
Dynamic	4b	-	3.877
Dynamic	4c	-	2.988
Dynamic	4d	-	4.062
Dynamic	4e	-	3.663
Static	4f	1092	1.032
Static	4g	1061	0.965
Static	4h	1040	0.886
Static	4i	1164	1.055
Static	4j	1100	1.02

6 SYNOPSIS OF TEST RESULTS

6.1 Specimen Set 1: Cobonded (Stitched)

Specimen Set 1 consists of bonded skin-spar joints salvaged from an Air Force “Battle Damage Tolerant Composite Wing Structure” (BDT-CWS) test program³. The specific material is toughened graphite/epoxy (IM6/8551). The bonding adhesive is MMS 350, Type I. Stitching is Kevlar. Figure 6.1.1 and Table 6.1.1 show measured and average joint dimensions for Specimen Set 1.^d

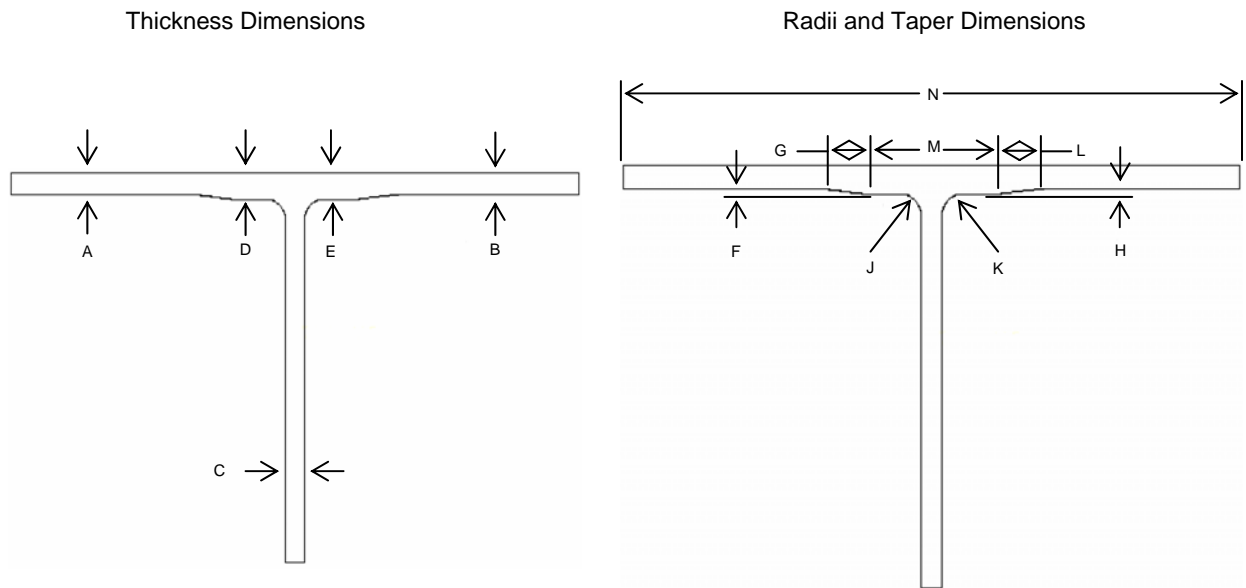


Figure 6.1.1: Specimen dimension coding

^d A complete set of measured dimensions was not obtained. Values for dimensions F, G, J, and K are nominal.

Table 6.1.1: Dimensions of Specimen Set 1

		Dimension Label													
	Test #	Specimen #	A (inch)	B (inch)	C (inch)	D (inch)	E (inch)	F (inch)	G (inch)	H (inch)	J (inch)	K (inch)	L (inch)	M (inch)	N (inch)
Dynamic	1	1a	0.155	0.155	0.14	0.21	0.21	0.060	0.313		0.021	0.034			
	2	1b	0.159	0.16	0.16	0.214	0.255								
	3	1c	0.159	0.16	0.158	0.218	0.215								
	25	1d	0.157	0.155	0.158	0.212	0.219								
Static	-	1e			0.141										
	-	1f			0.138										
	-	1g			0.139										
	-	1h	0.16	0.16	0.155	0.218	0.212								
Averages			0.158	0.158	0.149	0.214	0.222	0.060	0.313		0.021	0.034			

All specimens are 2" width.

Figures 6.1.2 and 6.1.3 are representative of Specimen Set 1 construction. These images were collected prior to testing and show strain gage instrumentation.

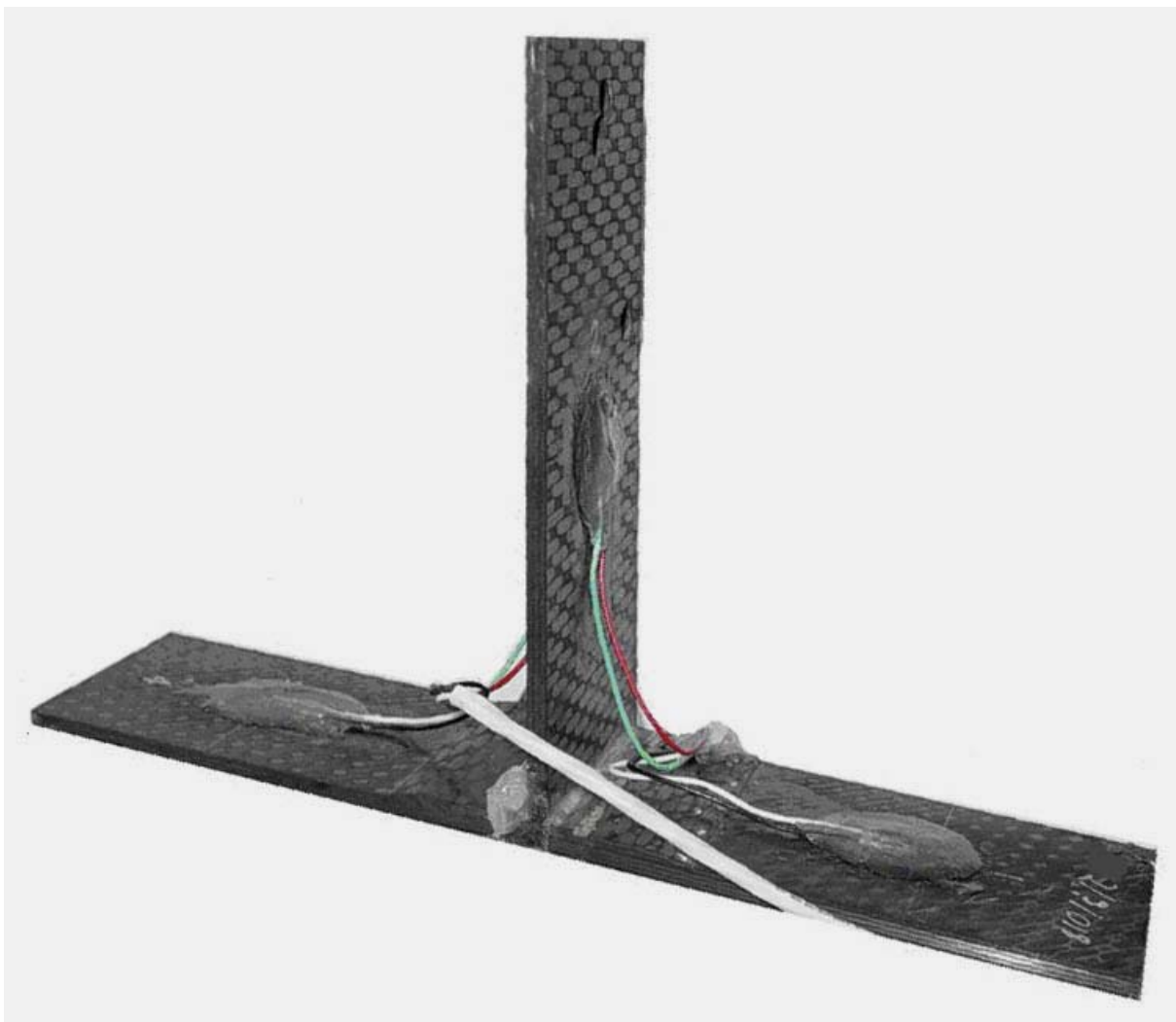


Figure 6.1.2: Example image of joint from Specimen Set 1 (pretest)



Figure 6.1.3: Example cross section of joint from Specimen Set 1 (pretest)

6.1.1 Dynamically Tested Specimens 1a, 1b, 1c, 1d (Tests #01, 02, 03, 25)

This section includes post-test cross section images of all dynamically tested joints associated with Specimen Set 1. *Note: Because these joints were salvaged from a completed contractual effort, only four joints were available for RamGun testing.*

Specimen 1a, Test 01

Figure 6.1.1.1 shows a complete and somewhat asymmetric failure of joint Specimen 1a. Fracture occurred mostly along the spar cap to skin interface, although a portion of the spar cap on the right side became severed at the stitch-line and remained attached to the skin. Without considering visual aspects of the failure, the strain data analysis (presented in Appendix C, Section C.1) revealed that failure was asymmetric.



Figure 6.1.1.1: Specimen 1a after dynamic test

Specimen 1b, Test 02

Figure 6.1.1.2 shows an asymmetric and incomplete (skin remained attached) fracture of joint Specimen 1b. Severe skin fracture occurred just to the left of the spar web. Delamination ran down the center of the web. Without considering visual aspects of the failure, the strain data analysis (presented in Appendix C, Section C.1) revealed that failure symmetry was inconclusive.



Figure 6.1.1.2: Specimen 1b after dynamic test

Specimen 1c, Test 03

Figure 6.1.1.3 shows a complete and symmetric failure of joint Specimen 1c. Spar cap fracture occurred along the stitch-lines. Without considering visual aspects of the failure, the strain data analysis (presented in Appendix C, Section C.1) revealed that failure was asymmetric.



Figure 6.1.1.3: Specimen 1c after dynamic test

Specimen 1d, Test 25

Figure 6.1.1.4 shows that joint Specimen 1d did not fail at the joint. (It pulled out of the grip and through the bolt hole at the end of the spar.) Strain data obtained prior to grip pull-out (presented in Appendix C, Section C.1) revealed that initial aspects of the failure were asymmetric. Failure

initiated at the noodle, with spar-cap cracks stopping at the stitching and another crack running down the center of the spar.



Figure 6.1.1.4: Specimen 1d after dynamic test.

6.1.2 Statically Tested Specimens 1e, 1f, 1g, 1h

This section includes post-test cross section images of all statically tested joints associated with Specimen Set 1. *Note: Because these joints were salvaged from a completed contractual effort, only four joints were available for static testing.*

Specimen 1e

Figure 6.1.2.1 shows a somewhat symmetric and incomplete fracture of joint Specimen 1e. Joint failure consisted of a skin fracture immediately to the left of the spar web, delamination that extends for a short distance along the spar cap interface with the skin, and delamination that extends down the center of the spar web.

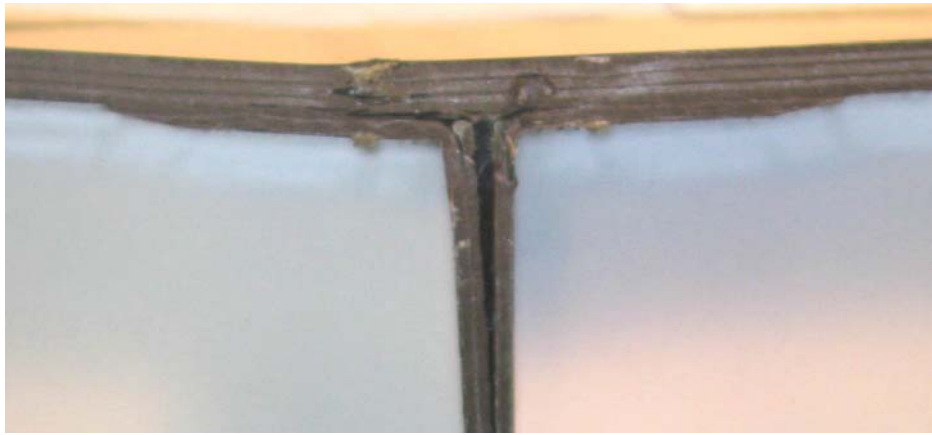


Figure 6.1.2.1: Specimen 1e after static test.

Specimen 1f

Figure 6.1.2.2 shows a symmetric and incomplete fracture of joint Specimen 1f. Joint failure consisted of a skin fracture directly above the spar web, delamination that extends for a short distance along the spar cap interface with the skin, and delamination that extends down the center of the spar web.



Figure 6.1.2.2: Specimen 1f after static test.

Specimen 1g

Figure 6.1.2.3 shows a somewhat symmetric and incomplete fracture of joint Specimen 1g. Joint failure consisted of a skin fracture immediately to the right of the spar web and delamination that extends down the center of the spar web.

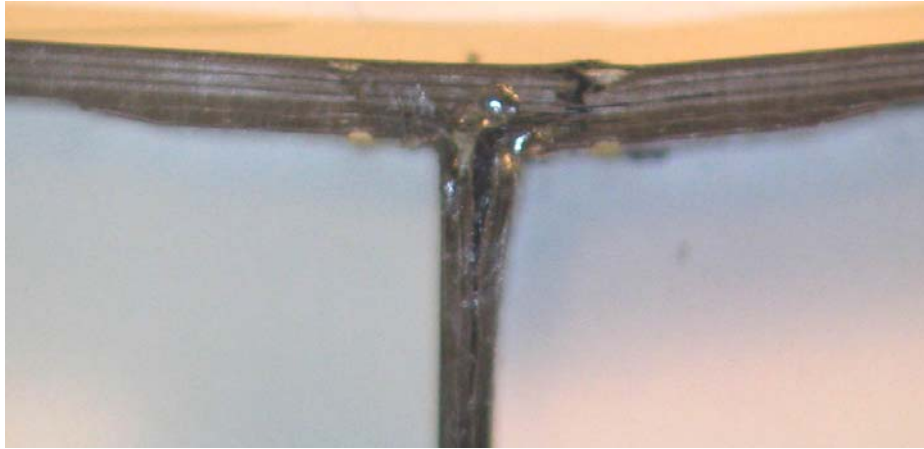


Figure 6.1.2.3: Specimen 1g after static test.

Specimen 1h

Figure 6.1.2.4 shows a mostly symmetric and incomplete fracture of joint Specimen 1h. Joint failure consisted of a skin fracture immediately to the right of the spar web, delamination that extends for a short distance along the spar cap interface with the skin, and delamination that extends down the center of the spar web.

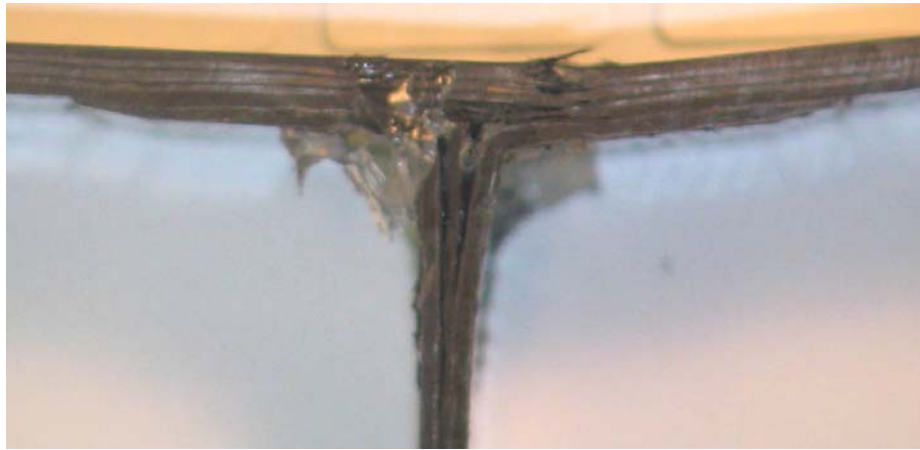


Figure 6.1.2.4: Specimen 1h after static test.

6.1.3 Specimen Set 1: Dynamic vs. Static Comparisons

Tables 6.1.3.1 and 6.1.3.2 list loads and strains at failure for joints from Specimen Set 1. Specimens 1a thru 1d were tested dynamically and specimens 1e thru 1h were tested statically. Dynamically tested specimens had nearly three times the strain at failure than specimens that were tested statically (see Tables 6.1.2.1 and 6.1.2.2). A more detailed data analysis is found in Appendix C, Section C.1.

Table 6.1.3.1: Load and Strain at Failure for Specimen Set 1

		Load at Failure (lbf)	Strain at Failure ($\times 10^{-3}$ in/in)	Notes
Dynamic	1a	-	1.899	
	1b	-	3.550	Specimen did not completely fail. Spar remained attached to skin.
	1c	-	2.507	
	1d	-	5.103	Specimen pulled out of the grip
Static	1e	488	1.051	
	1f	465	1.065	
	1g	456	0.853	
	1h	948	1.063	

Table 6.1.3.2: Summary of Results for Specimen Set 1

	Load at Failure (lbf)		Strain at Failure ($\times 10^{-3}$ in/in)	
	Average	Standard Deviation	Average	Standard Deviation
Dynamic	-	-	3.265	1.402
Static	589	240	1.008	0.104

6.2 Specimen Set 2: Bolted

Specimen Set 2 consists of bolted skin-spar joints. Figure 6.2.1 and Table 6.2.1 show measured and average joint dimensions for Specimen Set 2.^e

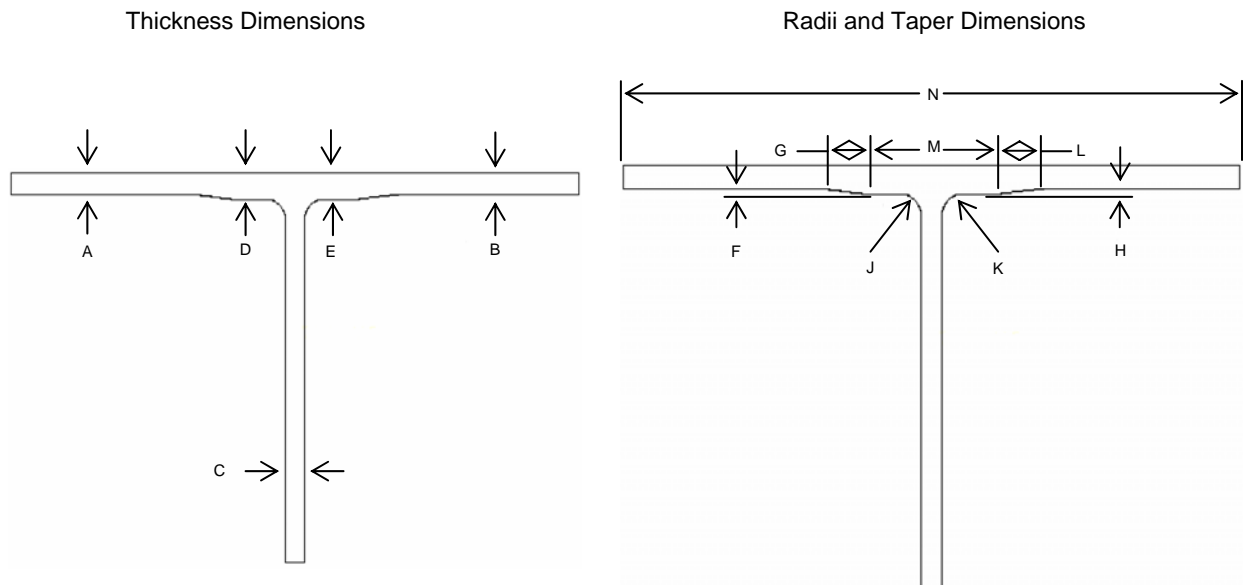


Figure 6.2.1: Specimen dimension coding

^e A complete set of measured dimensions was not obtained. Values for dimensions F through M are nominal.

Table 6.2.1: Dimensions of Specimen Set 2

			Dimension Label											
	Test #	Specimen #	A (inch)	B (inch)	C (inch)	D (inch)	E(inch)	F (inch)	G (inch)	H (inch)	J (inch)	K (inch)	L (inch)	M (inch)
Dynamic	4	2a	0.248	0.245	0.310	0.414	0.410							
	5	2b	0.247	0.251	0.220	0.399	0.405							
	6	2c	0.242	0.242	0.160	0.395	0.396							
	26	2d	0.243	0.235	0.185	0.400	0.395							
	27	2e	0.250	0.250	0.222	0.412	0.418							
Static	-	2f			0.188									
	-	2g			0.181									
	-	2h			0.168									
	-	2i			0.181									
	Averages		0.246	0.245	0.202	0.404	0.405	0.184	0.000	0.180	0.215	0.124	0.000	3.338

All specimens are 2" width.

Figures 6.2.2 and 6.2.3 are representative of Specimen Set 2 constructions. These images were collected prior to testing and show strain gage instrumentation. (Nylon wire tie-downs were removed after specimen installation in the test fixture.)



Figure 6.2.2: Example image of joint from Specimen Set 2 (pretest)

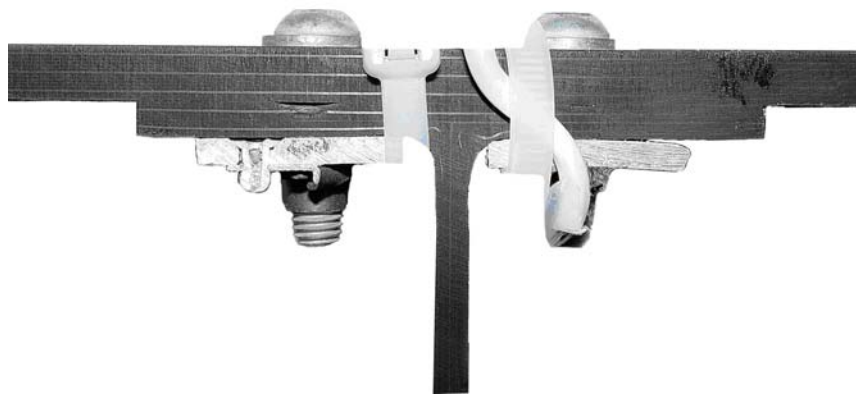


Figure 6.2.3: Example cross section of joint from Specimen Set 2 (pretest)

6.2.1 Dynamically Tested Specimens 2a, 2b, 2c, 2d, 2e (Tests #04, 05, 06, 26, 27)

This section includes post-test cross section images of all dynamically tested joints associated with Specimen Set 2.

Specimen 2a, Test 04

Figure 6.2.1.1 shows a complete and symmetric failure of joint Specimen 2a. The spar web detached from the spar cap, with separation localized between the nut-plates. Without considering visual aspects of the failure, the strain data analysis (presented in Appendix C, Section C.2) revealed that failure symmetry was inconclusive.

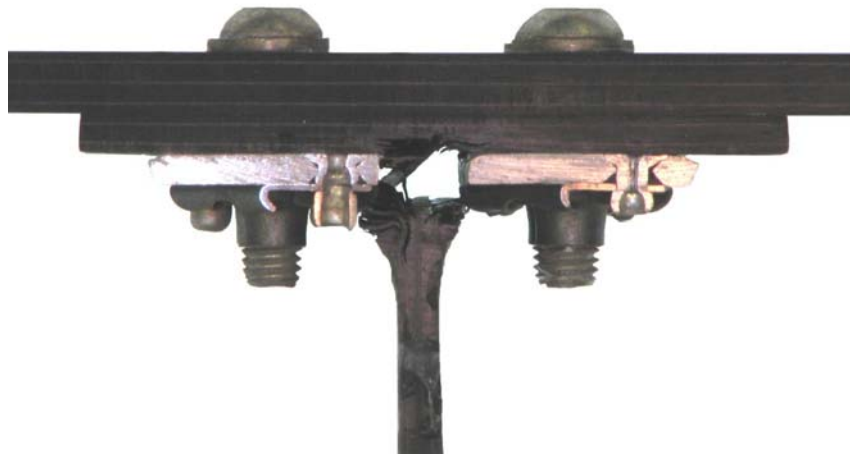


Figure 6.2.1.1: Specimen 2a after dynamic test

Specimen 2b, Test 05

Figure 6.2.1.2 shows a symmetric and complete fracture of joint Specimen 2b. The spar web detached from the spar cap, with separation localized between the nut-plates. Without considering visual aspects of the failure, the strain data analysis (presented in Appendix C, Section C.2) revealed that the failure was symmetric.

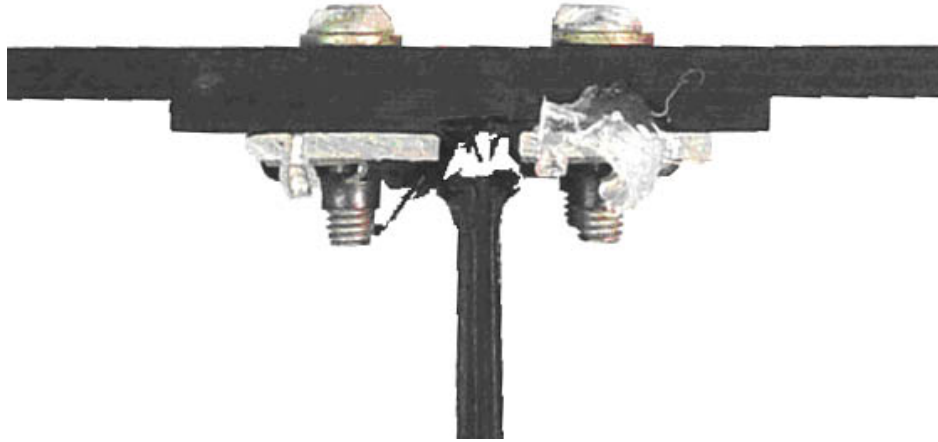


Figure 6.2.1.2: Specimen 2b after dynamic test

Specimen 2c, Test 06

Figure 6.2.1.3 shows an incomplete and asymmetric failure of joint Specimen 2c. There is delamination at the spar web-cap interface. Skin fracture occurred along the right bolt-line. Without considering visual aspects of the failure, the strain data analysis (presented in Appendix C, Section C.2) revealed that failure symmetry was inconclusive.



Figure 6.2.1.3: Specimen 2c after dynamic test

Specimen 2d, Test 26

Figure 6.2.1.4 shows a complete and symmetric failure of joint Specimen 2d. The spar web detached from the spar cap, with separation localized between the nut-plates. Without considering visual aspects of the failure, the strain data analysis (presented in Appendix C, Section C.2) revealed that failure symmetry was inconclusive.



Figure 6.2.1.4: Specimen 2d after dynamic test.

Specimen 2e, Test 27

Figure 6.2.1.5 shows a complete and symmetric failure of joint Specimen 2e. The spar web detached from the spar cap, with separation localized between the nut-plates. Without considering visual aspects of the failure, the strain data analysis (presented in Appendix C, Section C.2) revealed that failure was symmetric.



Figure 6.2.1.5: Specimen 2e after dynamic test.

6.2.2 Statically Tested Specimens 2f, 2g, 2h, 2i

This section includes post-test cross section images of all statically tested joints associated with Specimen Set 2.

Specimen 2f

Figure 6.2.2.1 shows an asymmetric and incomplete fracture of joint Specimen 2f. Joint failure consisted of a skin fracture along the left bolt line and some delamination extending from the noodle.

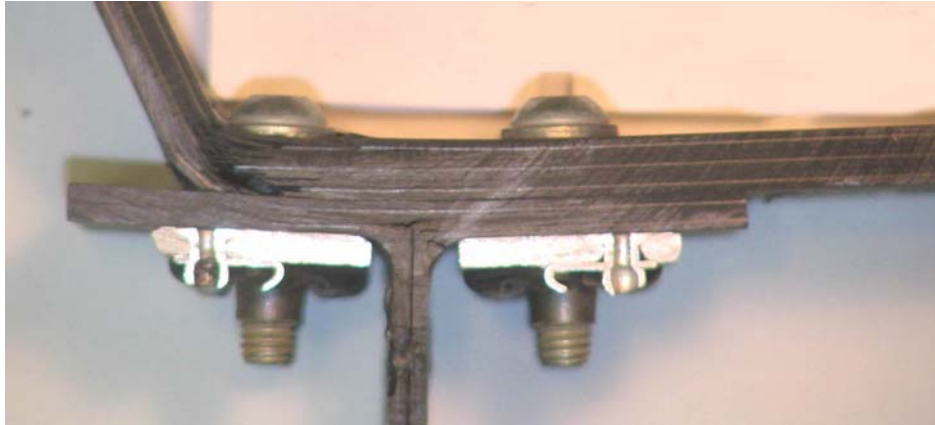


Figure 6.2.2.1: Specimen 2f after static test.

Specimen 2g

Figure 6.2.2.2 shows an asymmetric and incomplete fracture of joint Specimen 2g. Joint failure consisted of a skin fracture along the right bolt line.

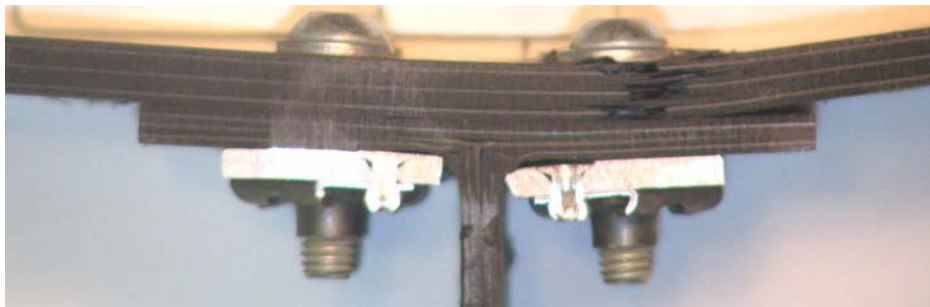


Figure 6.2.2.2: Specimen 2g after static test.

Specimen 2h

Figure 6.2.2.3 shows an asymmetric and complete fracture of joint Specimen 2h. Joint failure consisted of a skin fracture along the left bolt line.

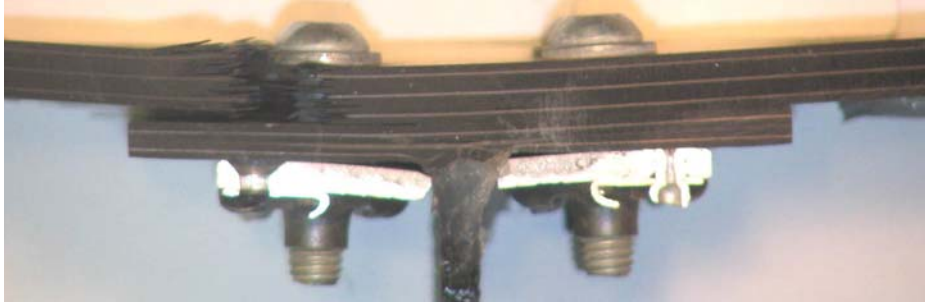


Figure 6.2.2.3: Specimen 2h after static test.

Specimen 2i

Figure 6.2.2.4 shows an asymmetric and complete fracture of joint Specimen 2i. Joint failure consisted of a skin fracture along the left bolt line.

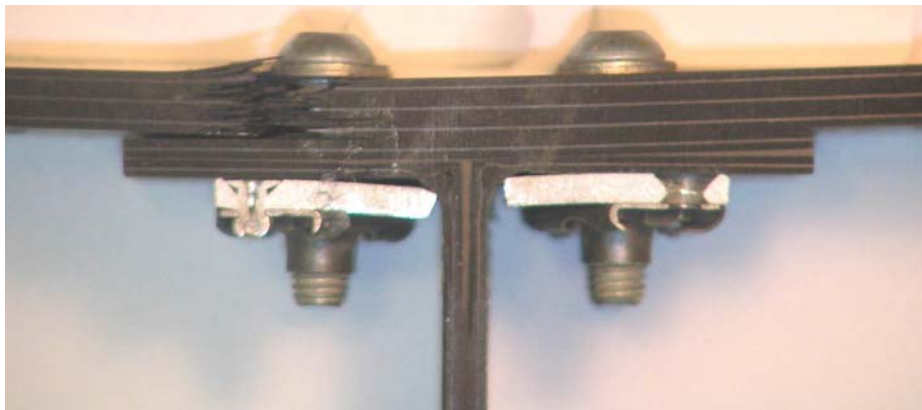


Figure 6.2.2.4: Specimen 2i after static test.

6.2.3 Specimen Set 2: Dynamic vs. Static Comparisons

Below is a table of loads and strains at failure for joints from Specimen Set 2. Specimens 2a thru 2d were tested dynamically and 2e thru 2h were tested statically. Dynamically tested specimens had nearly twice the strain at failure than specimens that were tested statically (see Tables 6.2.3.1 and 6.2.3.2). A more detailed data analysis is found in Appendix C, Section C.2.

Table 6.2.3.1: Load and Strain at Failure for Specimen Set 2

		Load at Failure (lbf)	Strain at Failure ($\times 10^{-3}$ in/in)	Notes
Dynamic	2a	-	-	Time window on Nicolet was not set correctly; no data collected.
	2b	-	2.663	
	2c	-	2.745	
	2d	-	1.820	SG 2 had bad reading during test.
	2e		1.654	
Static	2f	1102	1.117	
	2g	1046	0.955	
	2h	1036	0.866	
	2i	964	1.013	

Table 6.2.3.2: Summary of Results for Specimen Set 2

	Load at Failure (lbf)		Strain at Failure ($\times 10^{-3}$ in/in)	
	Average	Standard Deviation	Average	Standard Deviation
Dynamic	-	-	2.221	0.563
Static	1037	57	0.988	0.105

6.3 Specimen Set 3: Tufted Carbon

Specimen Set 3 consists of tufted carbon skin-spar joints. The basic material is non-criped fabric using a standard modulus fiber. The noodle is braided carbon fiber. The layup was fixed by binder to form a textile perform. The whole perform was infiltrated with RTM 6 Epoxy resin in

an autoclave process. In addition, a through-thickness reinforcement was implemented for the skin-to-cap connection by means of tufting with carbon fibers. Tufting involves a special stitching process where the needle places a fiber loop in the material and by friction, the fiber remains in place as the needle is retracted. The stitch pattern was 4x10mm under 0° and one line at 4mm and 45° into the noodle from each side of the cap. Figure 6.3.1 and Table 6.3.1 show measured and average joint dimensions for Specimen Set 3.^f

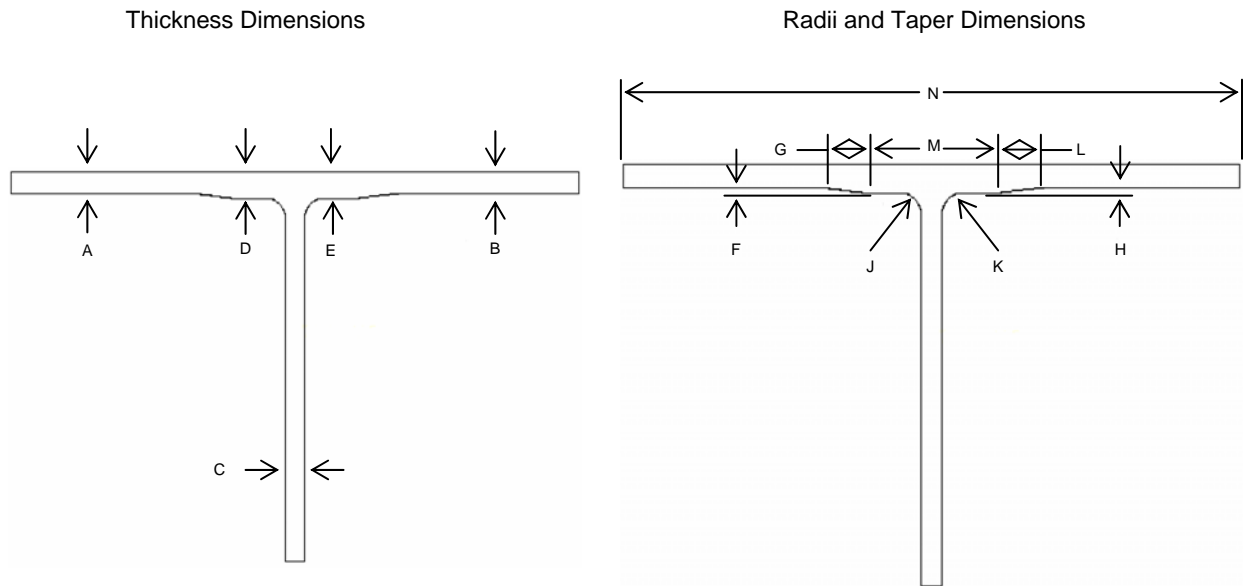


Figure 6.3.1: Specimen dimension coding

^f A complete set of measured dimensions was not obtained. Values for dimensions F through N are nominal.

Table 6.3.1: Dimensions of Specimen Set 3

		Dimension Label													
	Test #	Specimen #	A (inch)	B (inch)	C (inch)	D (inch)	E (inch)	F (inch)	G (inch)	H (inch)	J (inch)	K (inch)	L (inch)	M (inch)	N (inch)
Dynamic	7	3a	0.315	0.313	0.185	0.390	0.383								
	8	3b	0.307	0.313	0.187	0.393	0.385								
	9	3c	0.306	0.312	0.185	0.390	0.385								
	36	3d	0.320	0.323	0.190	0.395	0.385								
	37	3e	0.301	0.312	0.188	0.389	0.380								
Static	-	3f	0.311	0.318	0.197	0.397	0.387								
	-	3g	0.307	0.315	0.190	0.395	0.385								
	-	3h	0.310	0.315	0.198	0.395	0.388								
	-	3i	0.310	0.316	0.193	0.393	0.385								
	-	3j	0.315	0.308	0.193	0.384	0.397								
	Averages		0.3098	0.315	0.190	0.391	0.384	0.077	0.151	0.069	0.105	0.085	0.142	1.943	7.987

All specimens are 2" width.

Figures 6.3.2 and 6.3.3 are representative of Specimen Set 3 construction.



Figure 6.3.2: Example image of joint from Specimen Set 3 (pretest)



Figure 6.3.3: Example cross section of joint from Specimen Set 3 (pretest)

6.3.1 Dynamically Tested Specimens 3a, 3b, 3c, 3d, 3e (Tests #07, 08, 09, 36, 37)

This section includes post-test cross section images of all dynamically tested joints associated with Specimen Set 3.

Specimen 3a, Test 07

Figure 6.3.1.1 shows a complete and largely symmetric failure of joint Specimen 3a. Joint debonding and carbon tuft failure occurred at the spar-cap to skin interface. Delamination extended down the center of the spar web. Without considering visual aspects of the failure, the strain data analysis (presented in Appendix C, Section C.3) revealed that failure was symmetric.



Figure 6.3.1.1: Specimen 3a after dynamic test

Specimen 3b, Test 08

Figure 6.3.1.2 shows a complete and largely symmetric fracture of joint Specimen 3b. Joint debonding and carbon tuft failure occurred several plies into the skin. Delamination extended down the center of the spar web. Without considering visual aspects of the failure, the strain data analysis (presented in Appendix C, Section C.3) revealed that failure symmetry was inconclusive.



Figure 6.3.1.2: Specimen 3b after dynamic test

Specimen 3c, Test 09

Figure 6.3.1.3 shows a complete and asymmetric failure of joint Specimen 3c. Joint debonding and carbon tuft failure occurred at the spar-cap to skin interface (extending into the skin on the right). Delamination extended down the center of the spar web. Without considering visual aspects of the failure, the strain data analysis (presented in Appendix C, Section C.3) revealed that failure was symmetric.



Figure 6.3.1.3: Specimen 3c after dynamic test

Specimen 3d, Test 36

Figure 6.3.1.4 shows a complete and symmetric failure of joint Specimen 3d. Joint debonding and carbon tuft failure occurred at the spar-cap to skin interface. Delamination extended down the center of the spar web. Without considering visual aspects of the failure, the strain data analysis (presented in Appendix C, Section C.3) revealed that failure symmetry was inconclusive.

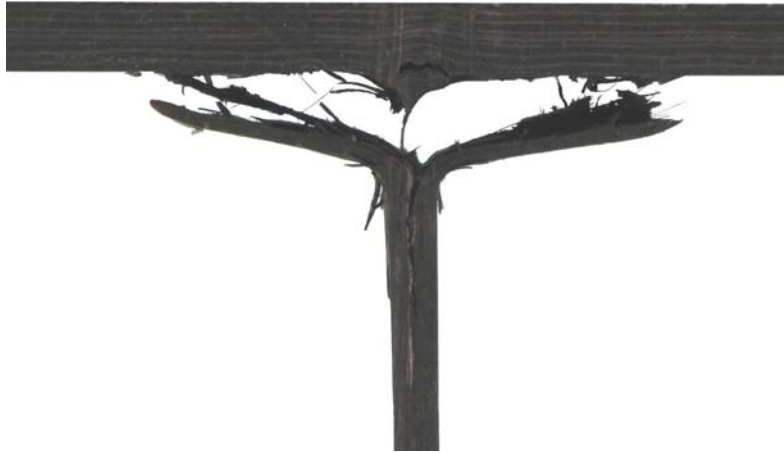


Figure 6.3.1.4: Specimen 3d after dynamic test.

Specimen 3e, Test 37

Figure 6.3.1.5 shows a complete and symmetric failure of joint Specimen 3e. Joint debonding and carbon tuft failure occurred at the spar-cap to skin interface. Delamination extended down the center of the spar web. Without considering visual aspects of the failure, the strain data analysis (presented in Appendix C, Section C.3) revealed that failure was symmetric.



Figure 6.3.1.5: Specimen 3e after dynamic test.

6.3.2 Statically Tested Specimens 3f, 3g, 3h, 3i, 3j

This section includes post-test cross section images of all statically tested joints associated with Specimen Set 3.

Specimen 3f

Figure 6.3.2.1 shows a symmetric and incomplete fracture of joint Specimen 3f. Joint failure consisted of a skin fracture immediately above the spar web and delamination that extends down the center of the spar web.

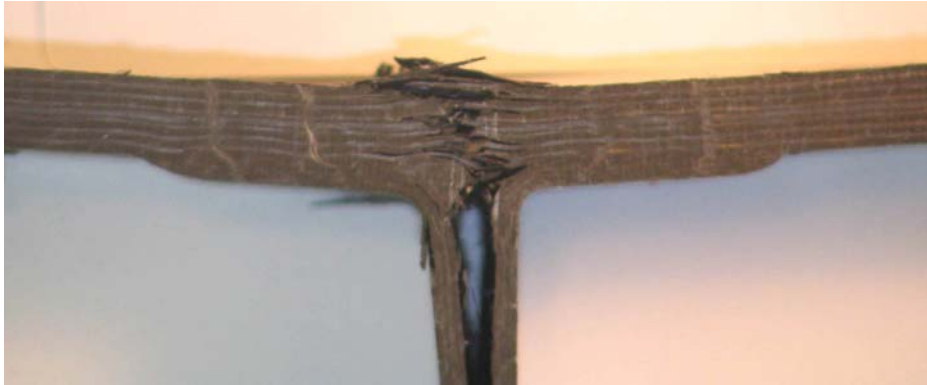


Figure 6.3.2.1: Specimen 3f after static test.

Specimen 3g

Figure 6.3.2.2 shows a symmetric and incomplete fracture of joint Specimen 3g. Joint failure consisted of a skin fracture immediately above the spar web and delamination that extends down the center of the spar web.

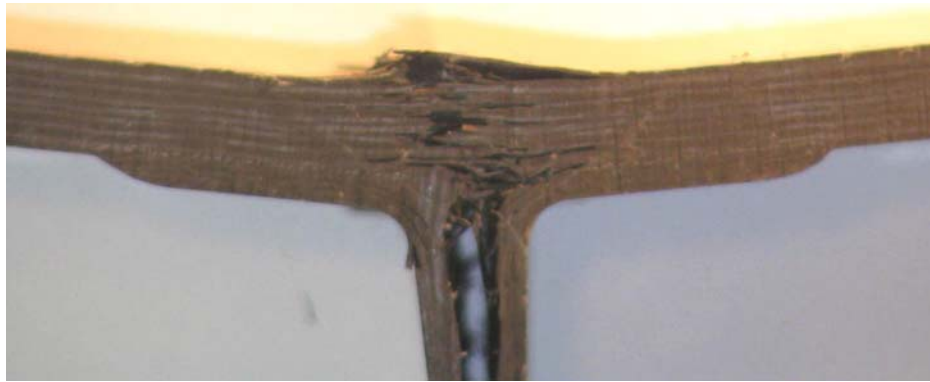


Figure 6.3.2.2: Specimen 3g after static test.

Specimen 3h

Figure 6.3.2.3 shows a symmetric and incomplete fracture of joint Specimen 3h. Joint failure consisted of a skin fracture immediately above the spar web and delamination that extends down the center of the spar web.



Figure 6.3.2.3: Specimen 3h after static test.

Specimen 3i

Figure 6.3.2.4 shows a symmetric and complete fracture of joint Specimen 3i. Joint failure consisted of debonding and tufted fiber fracture along the spar cap to skin interface. In addition, delamination extends a short distance down the center of the spar web.



Figure 6.3.2.4: Specimen 3i after static test.

Specimen 3j

Figure 6.3.2.5 shows a symmetric and incomplete fracture of joint Specimen 3j. Joint failure consisted of a skin fracture immediately above the spar web and delamination that extends down the center of the spar web.



Figure 6.3.2.5: Specimen 3j after static test.

6.3.3 Specimen Set 3: Dynamic vs. Static Comparisons

Tables 6.3.3.1 and 6.3.3.2 list loads and strains at failure for joints from Specimen Set 3. Specimens 3a thru 3e were tested dynamically and 3f thru 3j were tested statically. Dynamically tested specimens had nearly four times the strain at failure than specimens that were tested statically. A more detailed data analysis is found in Appendix C, Section C.3.

Table 6.3.3.1: Load and Strain at Failure for Specimen Set 3

		Load at Failure (lbs)	Strain at Failure ($\times 10^{-3}$ in/in)	Comments
Dynamic	3a	-	5.699	
	3b	-	3.840	
	3c	-	3.410	Event 1 didn't break
	3d	-	5.063	
	3e	-	3.986	
Static	3f	1094	0.997	
	3g	1178	1.066	
	3h	956	0.898	
	3i	1253	1.385	
	3j	1228	1.144	

Table 6.3.3.2: Summary of Results for Specimen Set 3

	Load at Failure (lbs)		Strain at Failure ($\times 10^{-3}$ in/in)	
	Average	Standard Deviation	Average	Standard Deviation
Dynamic	-	-	4.400	0.948
Static	1142	120	1.098	0.184

6.4 Specimen Set 4: Tufted Aramide

Specimen Set 4 consists of tufted Aramide skin-spar joints. The basic material is non-criped fabric using a standard modulus fiber. The noodle is braided carbon fiber. The layup was fixed by binder to form a textile perform. The whole perform was infiltrated with RTM 6 Epoxy resin in an autoclave process. In addition, a through-thickness reinforcement was implemented for the skin-to-cap connection by means of tufting with Aramide fibers. The stitch pattern was 4x10mm under 0° and one line at 4mm and 45° into the noodle from each side of the cap. Figure 6.4.1 and Table 6.4.1 show measured and average joint dimensions for Specimen Set 4.

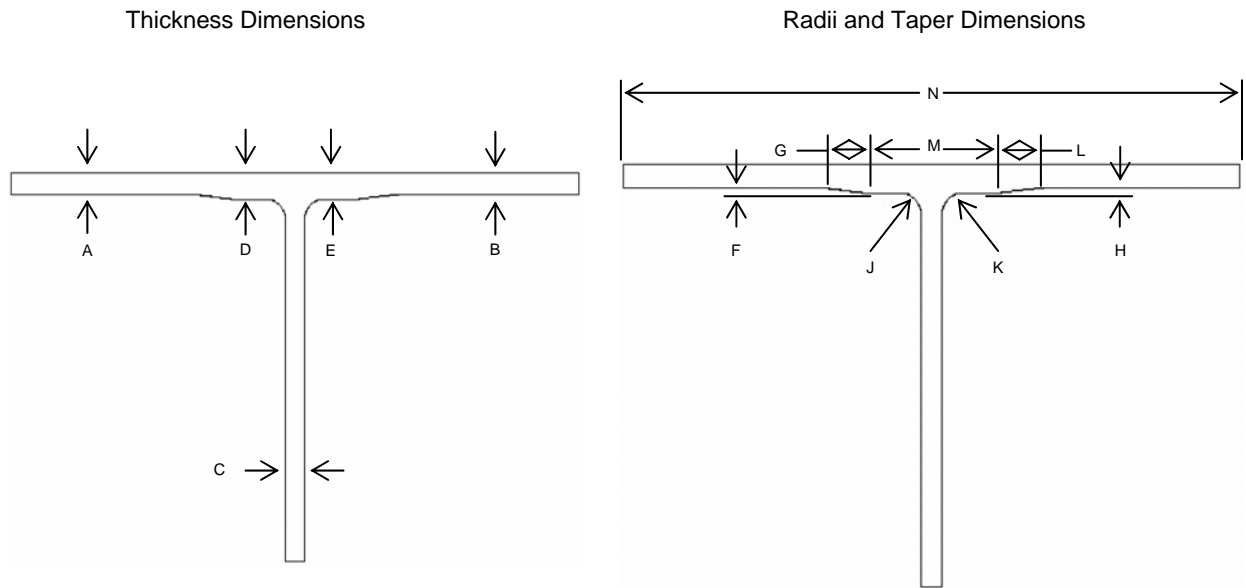


Figure 6.4.1: Specimen dimension coding

Table 6.4.1: Dimensions of Specimen Set 4

		Dimension Label													
	Test #	Specimen #	A (inch)	B (inch)	C (inch)	D (inch)	E (inch)	F (inch)	G (inch)	H (inch)	J (inch)	K (inch)	L (inch)	M (inch)	N (inch)
Dynamic	10	4a	0.306	0.298	0.173	0.385	0.382								
	11	4b	0.304	0.298	0.177	0.388	0.385								
	12	4c	0.307	0.300	0.180	0.389	0.385								
	31	4d	0.303	0.297	0.178	0.381	0.380								
	32	4e	0.305	0.300	0.180	0.390	0.388								
Static	-	4f	0.312	0.305	0.186	0.394	0.392								
	-	4g	0.301	0.299	0.173	0.385	0.383								
	-	4h	0.313	0.305	0.199	0.395	0.387								
	-	4j	0.313	0.305	0.190	0.390	0.387								
	Averages		0.305	0.301	0.183	0.389	0.389	0.082	0.145	0.098	0.108	0.132	0.235	2.575	7.984

All specimens are 2" width.

Figures 6.4.2 and 6.4.3 are representative of Specimen Set 4 construction.



Figure 6.4.2: Example image of joint from Specimen Set 4 (pretest)



Figure 6.4.3: Example cross section of joint from Specimen Set 4 (pretest)

6.4.1 Dynamically Tested Specimens 4a, 4b, 4c, 4d, 4e (Tests #10, 11, 12, 31, 32)

This section includes post-test cross section images of all dynamically tested joints associated with Specimen Set 4.

Specimen 4a, Test 10

Figure 6.4.1.1 shows a complete and largely symmetric failure of joint Specimen 4a. Joint failure consisted of debonding and Aramide fiber fracture at the spar-cap to skin interface. Delamination extended down the center of the spar web. Without considering visual aspects of the failure, the strain data analysis (presented in Appendix C, Section C.4) revealed that failure symmetry was inconclusive.



Figure 6.4.1.1: Specimen 4a after dynamic test

Specimen 4b, Test 11

Figure 6.4.1.2 shows a symmetric and complete fracture of joint Specimen 4b. Joint failure consisted of debonding and Aramide fiber fracture at the spar-cap to skin interface. Delamination extended down the center of the spar web. Without considering visual aspects of the failure, the strain data analysis (presented in Appendix C, Section C.4) revealed that failure was symmetric.



Figure 6.4.1.2: Specimen 4b after dynamic test

Specimen 4c, Test 12

Figure 6.4.1.3 shows a complete and symmetric failure of joint Specimen 4c. Joint failure consisted of debonding and Aramide fiber fracture at the spar-cap to skin interface. Delamination extended down the center of the spar web. Without considering visual aspects of the failure, the strain data analysis (presented in Appendix C, Section C.4) revealed that failure was symmetric.



Figure 6.4.1.3: Specimen 4c after dynamic test

Specimen 4d, Test 31

Figure 6.4.1.4 shows a complete and symmetric failure of joint Specimen 4d. Joint failure consisted of debonding and Aramide fiber fracture at the spar-cap to skin interface. Delamination extended down the center of the spar web. Without considering visual aspects of

the failure, the strain data analysis (presented in Appendix C, Section C.4) revealed that failure was symmetric.



Figure 6.4.1.4: Specimen 4d after dynamic test.

Specimen 4e, Test 32

Figure 6.4.1.5 shows a complete and symmetric failure of joint Specimen 4e. Joint failure consisted of debonding and Aramide fiber fracture at the spar-cap to skin interface. Delamination was extensive throughout the spar cap and extended down the center of the spar web. Without considering visual aspects of the failure, the strain data analysis (presented in Appendix C, Section C.4) revealed that failure was symmetric.



Figure 6.4.1.5: Specimen 4e after dynamic test.

6.4.2 Statically Tested Specimens 4f, 4g, 4h, 4i, 4j

This section includes post-test cross section images of all statically tested joints associated with Specimen Set 4.

Specimen 4f

Figure 6.4.2.1 shows a mostly symmetric and complete fracture of joint Specimen 4f. Joint failure consisted of debonding and Aramide fiber fracture along the spar cap to skin interface. In addition, delamination extends a short distance down the center of the spar web.



Figure 6.4.2.1: Specimen 4f after static test.

Specimen 4g

Figure 6.4.2.2 shows a symmetric and complete fracture of joint Specimen 4g. Joint failure consisted of debonding and Aramide fiber fracture along the spar cap to skin interface. In addition, delamination extends a short distance down the center of the spar web.

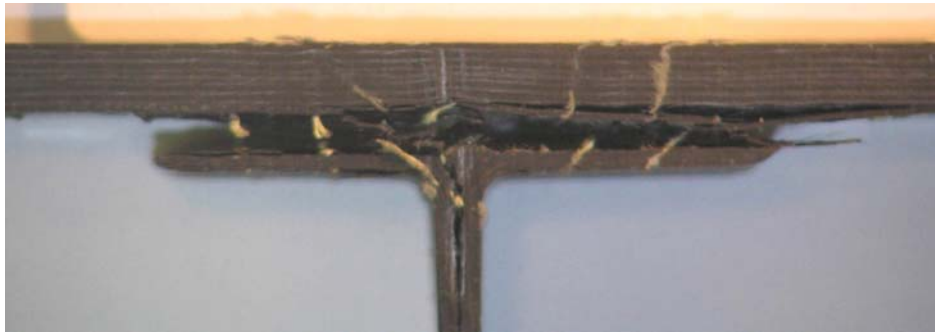


Figure 6.4.2.2: Specimen 4g after static test.

Specimen 4h

Figure 6.4.2.3 shows a symmetric and complete fracture of joint Specimen 4h. Joint failure consisted of debonding and Aramide fiber fracture along the spar cap to skin interface. In addition, delamination extends a short distance down the center of the spar web.



Figure 6.4.2.3: Specimen 4h after static test.

Specimen 4i

Figure 6.4.2.4 shows a mostly symmetric and complete fracture of joint Specimen 4i. Joint failure consisted of debonding and Aramide fiber fracture along the spar cap to skin interface. In addition, delamination extends a short distance down the center of the spar web.

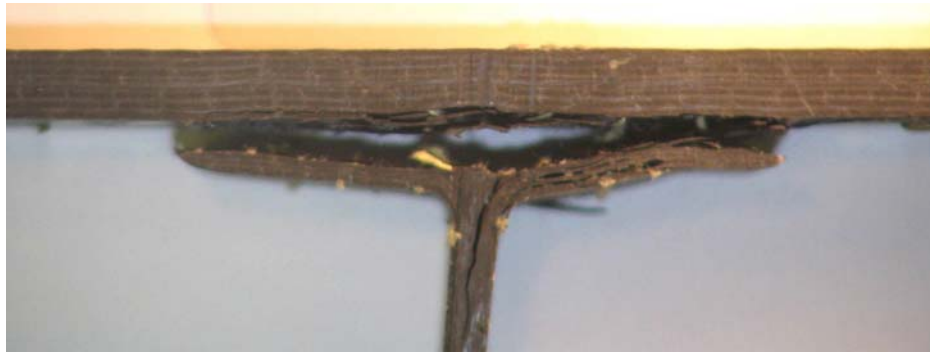


Figure 6.4.2.4: Specimen 4i after static test.

Specimen 4j

Figure 6.4.2.5 shows an asymmetric and incomplete fracture of joint Specimen 4j. Joint failure consisted of debonding and Aramide fiber fracture along the spar cap to skin interface. In addition, delamination extends down the center of the spar web.



Figure 6.4.2.5: Specimen 4j after static test.

6.4.3 Specimen Set 4: Dynamic vs. Static Comparisons

Tables 6.4.3.1 and 6.4.3.2 list loads and strains at failure for joints from Specimen Set 4. Specimens 4a thru 4e were tested dynamically and specimens 4f thru 4j were tested statically. Dynamically tested specimens had more than three times the strain at failure than specimens that were tested statically. A more detailed data analysis is found in Appendix C, Section C.4.

Table 6.4.3.1: Load and Strain at Failure for Specimen Set 4

		Load at Failure (lbs)	Strain at Failure ($\times 10^{-3}$ in/in)	Comments
Dynamic	4a	-	4.375	
	4b	-	3.877	
	4c	-	2.988	Kistler 2 pressure approximated because it grounded during the test causing it to re-zero
	4d	-	4.062	
	4e	-	3.663	
Static	4f	1092	1.032	
	4g	1061	0.965	
	4h	1040	0.886	
	4i	1164	1.055	
	4j	1100	1.020	

Table 6.4.3.2: Summary of Results for Specimen Set 4

	Load at Failure (lbf)		Strain at Failure ($\times 10^{-3}$ in/in)	
	Average	Standard Deviation	Average	Standard Deviation
Dynamic	-	-	3.793	0.520
Static	1091	47	0.992	0.068

6.5 Specimen Set 5: Cobonded Prepreg

Specimen Set 5 consists of cobonded prepreg skin-spar joints. Basic material is Hexcel prepreg IM7/8552. The noodle is also from this prepreg material. Figure 6.5.1 and Table 6.5.1 show measured and average joint dimensions for Specimen Set 5.^g

^g A complete set of measured dimensions was not obtained. Values for dimensions F through N are nominal.

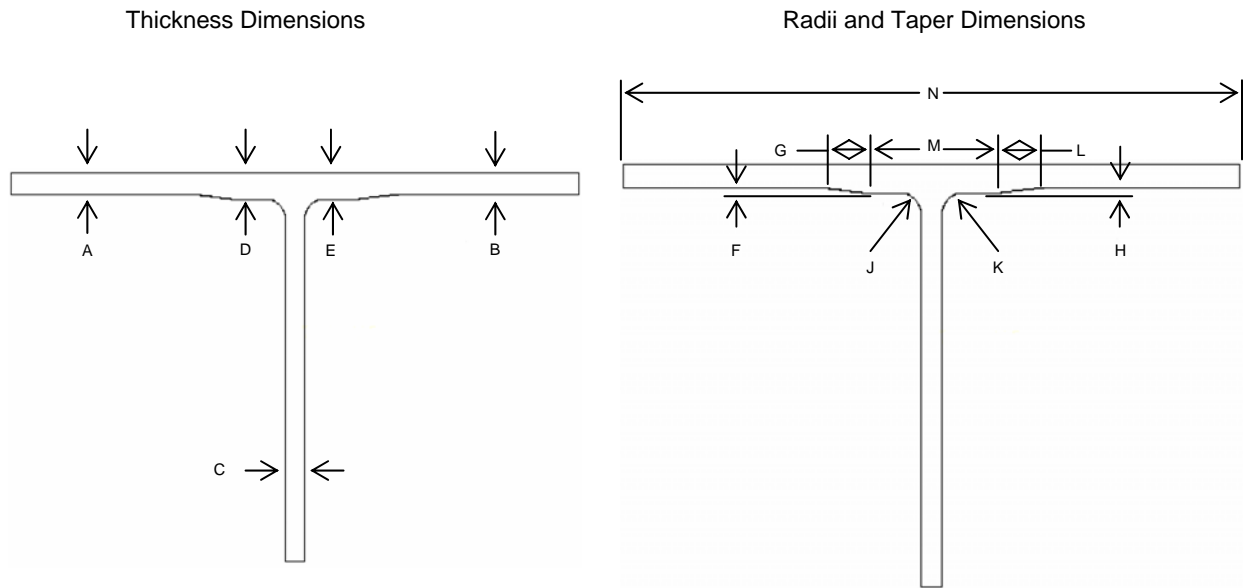


Figure 6.5.1: Specimen dimension coding

Table 6.5.1: Dimensions of Specimen Set 5

			Dimension Label												
	Test #	Specimen #	A (inch)	B (inch)	C (inch)	D (inch)	E (inch)	F (inch)	G (inch)	H (inch)	J (inch)	K (inch)	L (inch)	M (inch)	N (inch)
Dynamic	10	5a	0.286	0.285	0.170	0.400	0.405								
	11	5b	0.284	0.284	0.175	0.410	0.404								
	12	5c	0.285	0.283	0.175	0.409	0.406								
	31	5d	0.285	0.285	0.175	0.409	0.405								
	32	5e	0.287	0.284	0.180	0.405	0.406								
Static	-	5f	0.285	0.283	0.173	0.408	0.405								
	-	5g	0.285	0.286	0.173	0.405	0.411								
	-	5h	0.291	0.280	0.168	0.413	0.401								
	-	5i	0.282	0.282	0.175	0.411	0.406								
	Averages		0.285	0.285	0.176	0.408	0.404	0.142	0.471	0.110	0.315	0.303	0.406	2.225	7.994

All specimens are 2" width.

Figures 6.5.2 and 6.5.3 are representative of Specimen Set 5 construction.



Figure 6.5.2: Example image of joint from Specimen Set 5 (pretest)



Figure 6.5.3: Example cross section of joint from Specimen Set 5 (pretest)

6.5.1 Dynamically Tested Specimens 5a, 5b, 5c, 5d, 5e (Tests #13, 14, 15, 30, 33)

This section includes post-test cross section images of all dynamically tested joints associated with Specimen Set 5.

Specimen 5a, Test 13

Figure 6.5.1.1 shows a complete and largely symmetric failure of joint Specimen 5a. Joint failure consisted of debonding and fracture along the spar-cap to skin interface. Without considering visual aspects of the failure, the strain data analysis (presented in Appendix C, Section C.5) revealed that failure was symmetric.



Figure 6.5.1.1: Specimen 5a after dynamic test

Specimen 5b, Test 14

Figure 6.5.1.2 shows a complete and largely symmetric failure of joint Specimen 5b. Joint failure consisted of debonding and fracture along the spar-cap to skin interface. Without considering visual aspects of the failure, the strain data analysis (presented in Appendix C, Section C.5) revealed that failure symmetry was inconclusive.



Figure 6.5.1.2: Specimen 5b after dynamic test

Specimen 5c, Test 15

Figure 6.5.1.3 shows a complete and symmetric failure of joint Specimen 5c. Joint failure consisted of debonding and fracture along the spar-cap to skin interface. Without considering visual aspects of the failure, the strain data analysis (presented in Appendix C, Section C.5) revealed that failure was symmetric.



Figure 6.5.1.3: Specimen 5c after dynamic test

Specimen 5d, Test 30

Figure 6.5.1.4 shows a complete and mostly symmetric failure of joint Specimen 5d. Joint failure consisted of debonding and fracture along the spar-cap to skin interface. The noodle remained attached to the skin. Delamination extended down the center of the spar web. Without considering visual aspects of the failure, the strain data analysis (presented in Appendix C, Section C.5) revealed that failure was symmetric.



Figure 6.5.1.4: Specimen 5d after dynamic test.

Specimen 5e, Test 33

Figure 6.5.1.5 shows a complete and symmetric failure of joint Specimen 5e. Joint failure consisted of debonding and fracture along the spar-cap to skin interface. The noodle remained attached to the skin. Delamination extended down the center of the spar web. Without considering visual aspects of the failure, the strain data analysis (presented in Appendix C, Section C.5) revealed that failure was symmetric.



Figure 6.5.1.5: Specimen 5e after dynamic test.

6.5.2 Statically Tested Specimens 5f, 5g, 5h, 5i, 5j

This section includes post-test cross section images of all statically tested joints associated with Specimen Set 5.

Specimen 5f

Figure 6.5.2.1 shows a symmetric and complete fracture of joint Specimen 5f. Joint failure consisted of debonding along the spar cap to skin interface.

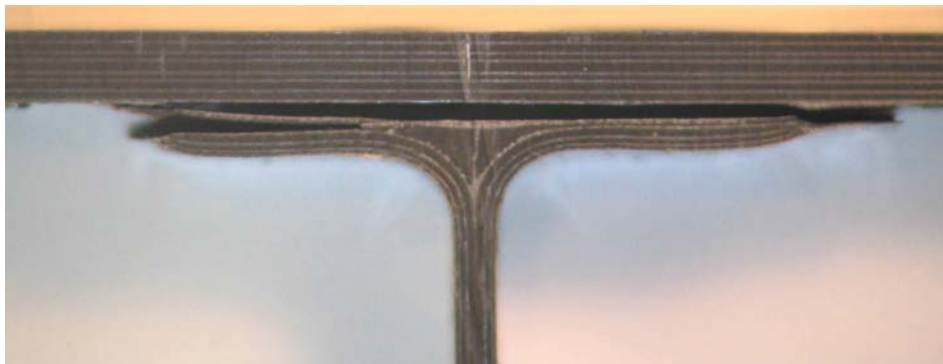


Figure 6.5.2.1: Specimen 5f after static test.

Specimen 5g

Figure 6.5.2.2 shows a symmetric and complete fracture of joint Specimen 5g. Joint failure consisted of debonding along the spar cap to skin interface.

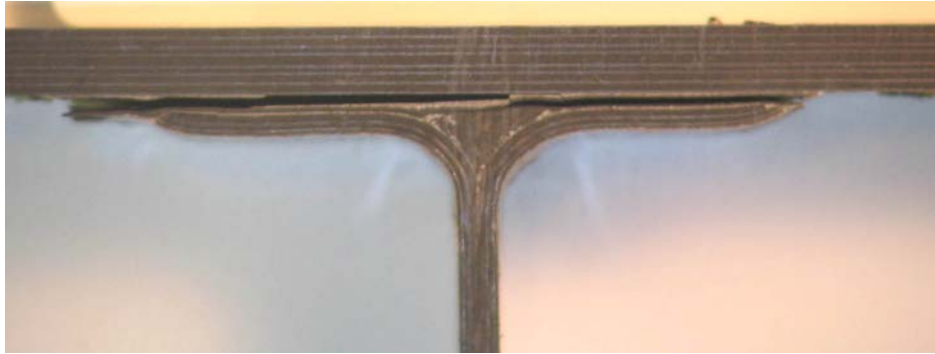


Figure 6.5.2.2: Specimen 5g after static test.

Specimen 5h

Figure 6.5.2.3 shows an asymmetric and incomplete fracture of joint Specimen 5h. Joint failure consisted of debonding along the spar cap to skin interface.

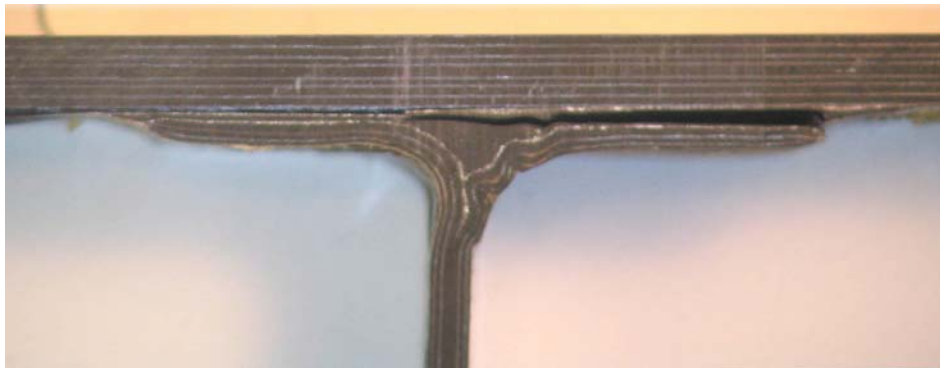


Figure 6.5.2.3: Specimen 5h after static test.

Specimen 5i

Figure 6.5.2.4 shows a symmetric and complete fracture of joint Specimen 5i. Joint failure consisted of debonding along the spar cap to skin interface.

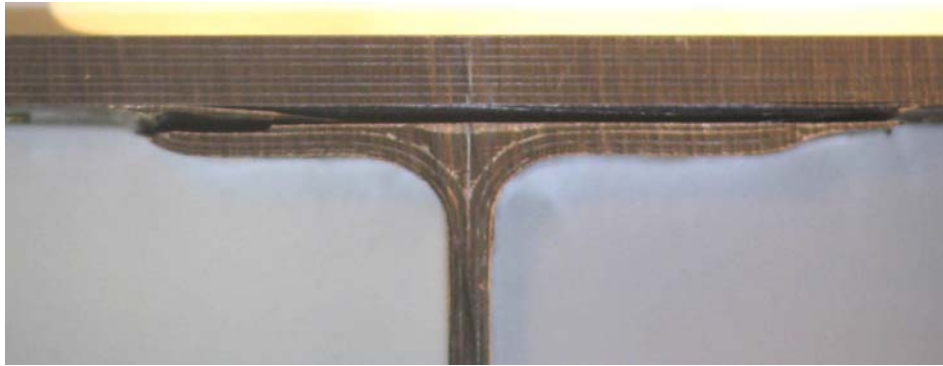


Figure 6.5.2.4: Specimen 5i after static test.

Specimen 5j

Figure 6.5.2.5 shows a symmetric and complete fracture of joint Specimen 5j. Joint failure consisted of debonding along the spar cap to skin interface.

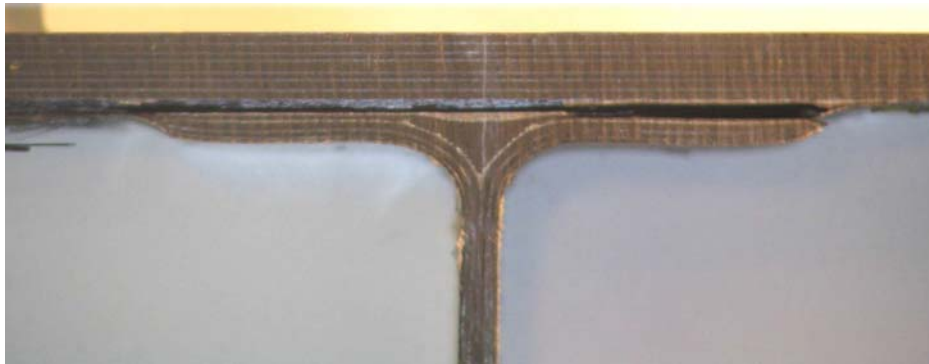


Figure 6.5.2.5: Specimen 5j after static test.

6.5.3 Specimen Set 5: Dynamic vs. Static Comparisons

Tables 6.5.3.1 and 6.5.3.2 list loads and strains at failure for joints from Specimen Set 5. Specimens 5a thru 5e were tested dynamically and specimens 5f thru 5j were tested statically. Dynamically tested specimens had nearly four times the strain at failure than specimens that were tested statically. A more detailed data analysis is found in Appendix C, Section C.5.

Table 6.5.3.1: Load and Strain at Failure for Specimen Set 5

		Load at Failure (lbf)	Strain at Failure ($\times 10^{-3}$ in/in)	Notes
Dynamic	5a	-	1.687	
	5b	-	2.351	SG 3 had a bad reading during test
	5c	-	1.07	
	5d	-	2.788	Specimen pulled thru after failure; Kistler 2 did not get a good reading
	5e	-	2.429	
Static	5f	1371	0.498	
	5g	1248	0.478	
	5h	1239	0.480	
	5i	1472	0.540	
	5j	1489	0.599	

Table 6.5.3.2: Summary of Results for Specimen Set 5

	Load at Failure (lbf)		Strain at Failure ($\times 10^{-3}$ in/in)	
	Average	Standard Deviation	Average	Standard Deviation
Dynamic	-	-	2.065	0.684
Static	1364	119	0.519	0.051

6.6 Specimen Set 6: One Shot Infiltration

Specimen Set 6 consists of one shot infiltration skin-spar joints. Figure 6.6.1 and Table 6.6.1 show measured and average joint dimensions for Specimen Set 6.^h

^h A complete set of measured dimensions was not obtained. Values for dimensions F through N are nominal.

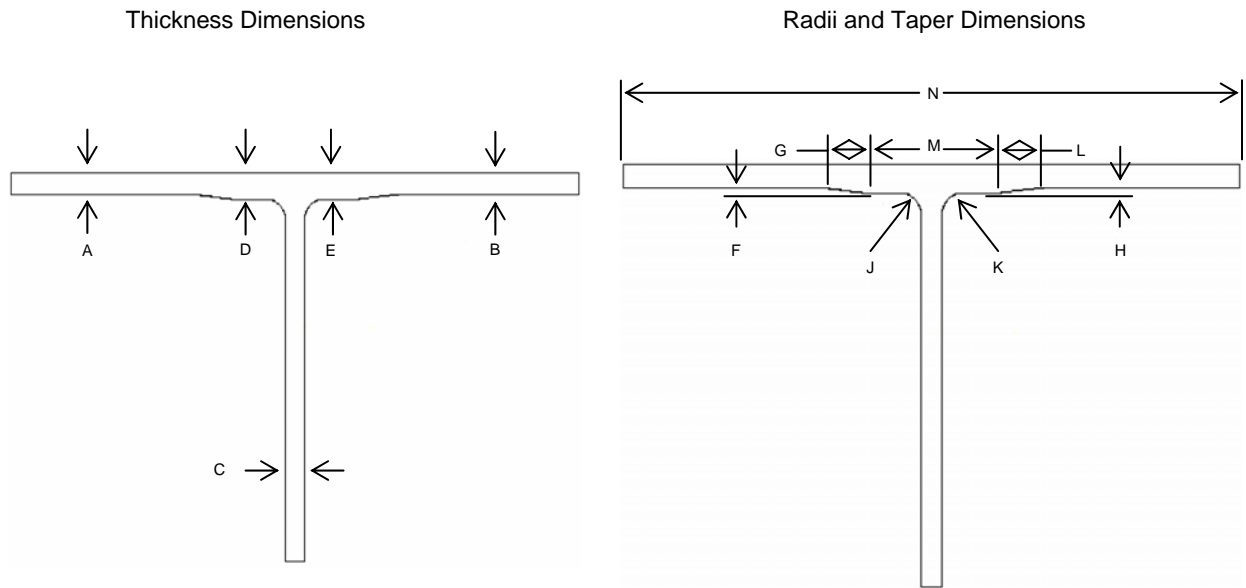


Figure 6.6.1: Specimen dimension coding

Table 6.6.1: Dimensions of Specimen Set 6

			Dimension Label																				
	Test #	Specimen #	A (inch)	B (inch)	C (inch)	D (inch)	E (inch)	F (inch)	G (inch)	H (inch)	J (inch)	K (inch)	L (inch)	M (inch)	N (inch)								
Dynamic	16	6a	0.300	0.300	0.185	0.381	0.378																
	17	6b	0.307	0.302	0.185	0.381	0.383																
	18	6c	0.307	0.301	0.185	0.384	0.382																
	28	6d	0.305	0.301	0.190	0.380	0.384																
	29	6e	0.305	0.302	0.185	0.395	0.380																
Static	-	6f	0.311	0.305	0.179	0.379	0.381																
	-	6g	0.313	0.310	0.193	0.389	0.398																
	-	6h	0.311	0.316	0.190	0.386	0.389																
	-	6i	0.300	0.298	0.186	0.375	0.379																
	-	6j	0.314	0.315	0.195	0.395	0.389																
	Averages		0.307	0.305	0.187	0.385	0.384	0.078	0.237	0.079	0.134	0.133	0.205	2.236	7.996								

All specimens are 2" width.

Figures 6.6.2 and 6.6.3 are representative of Specimen Set 6 construction. Basic material is non-criped fabric, standard modulus carbon fiber. The noodle is braided carbon fiber. The lay-up was fixed by binder to form a textile preform. The whole preform was infiltrated with RTM 6 Epoxy resin in an autoclave process.



Figure 6.6.2: Example image of joint from Specimen Set 6 (pretest)



Figure 6.6.3: Example cross section of joint from Specimen Set 6 (pretest)

6.6.1 Dynamically Tested Specimens 6a, 6b, 6c, 6d, 6e (Tests #16, 17, 18, 28, 29)

This section includes post-test cross section images of all dynamically tested joints associated with Specimen Set 6.

Specimen 6a, Test 16

Figure 6.6.1.1 shows a complete and symmetric failure of joint Specimen 6a. Joint failure consisted of debonding and fracture along the spar-cap to skin interface. Some delamination extended into the skin (to the right) and for a short distance down the center of the spar web. Without considering visual aspects of the failure, the strain data analysis (presented in Appendix C, Section C.6) revealed that failure was symmetric.



Figure 6.6.1.1: Specimen 6a after dynamic test

Specimen 6b, Test 17

Figure 6.6.1.2 shows a symmetric and complete fracture of joint Specimen 6b. Joint failure consisted of debonding and fracture along the spar-cap to skin interface. Delamination extended into lower skin plies on either side of the joint and down the center of the spar web. Without considering visual aspects of the failure, the strain data analysis (presented in Appendix C, Section C.6) revealed that failure was asymmetric.

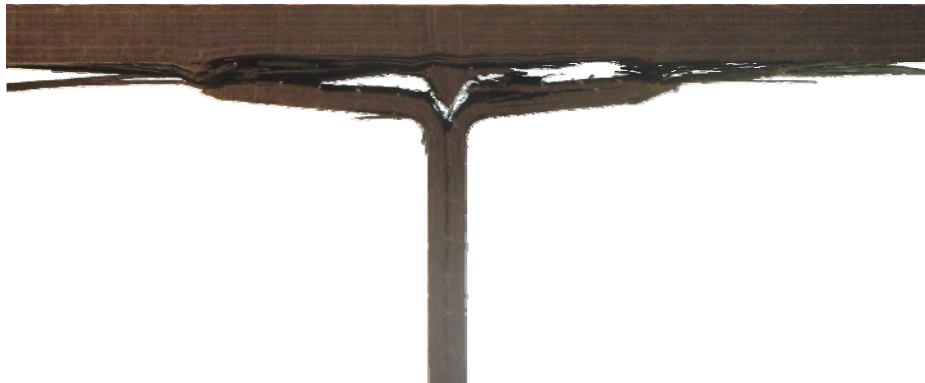


Figure 6.6.1.2: Specimen 6b after dynamic test

Specimen 6c, Test 18

Figure 6.6.1.3 shows a complete and symmetric failure of joint Specimen 6c. Joint failure consisted of debonding and fracture along the spar-cap to skin interface. Without considering visual aspects of the failure, the strain data analysis (presented in Appendix C, Section C.6) revealed that failure was symmetric.



Figure 6.6.1.3: Specimen 6c after dynamic test

Specimen 6d, Test 28

Figure 6.6.1.4 shows a complete and symmetric failure of joint Specimen 6d. Joint failure consisted of debonding and fracture along the spar-cap to skin interface. Delamination extended a short distance down the center of the spar web. Without considering visual aspects of the failure, the strain data analysis (presented in Appendix C, Section C.6) revealed that failure was symmetric.



Figure 6.6.1.4: Specimen 6d after dynamic test.

Specimen 6e, Test 29

Figure 6.6.1.5 shows a complete and symmetric failure of joint Specimen 6e. Joint failure consisted of debonding and fracture along the spar-cap to skin interface. Delamination extended a short distance down the center of the spar web. Without considering visual aspects of the failure, the strain data analysis (presented in Appendix C, Section C.6) revealed that failure was symmetric.



Figure 6.6.1.5: Specimen 6e after dynamic test.

6.6.2 Statically Tested Specimens 6f, 6g, 6h, 6i, 6j

This section includes post-test cross section images of all statically tested joints associated with Specimen Set 6.

Specimen 6f

Figure 6.6.2.1 shows a symmetric and complete fracture of joint Specimen 6f. Joint failure consisted of debonding and fiber fracture along the spar cap to skin interface.

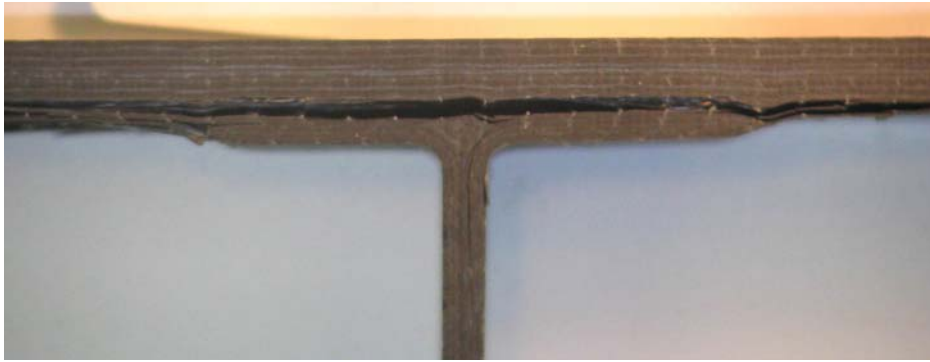


Figure 6.6.2.1: Specimen 6f after static test.

Specimen 6g

Figure 6.6.2.2 shows a symmetric and complete fracture of joint Specimen 6g. Joint failure consisted of debonding and fiber fracture along the spar cap to skin interface.



Figure 6.6.2.2: Specimen 6g after static test.

Specimen 6h

Figure 6.6.2.3 shows a symmetric and complete fracture of joint Specimen 6h. Joint failure consisted of debonding and fiber fracture along the spar cap to skin interface. In addition, delamination ran down the center of the spar web.

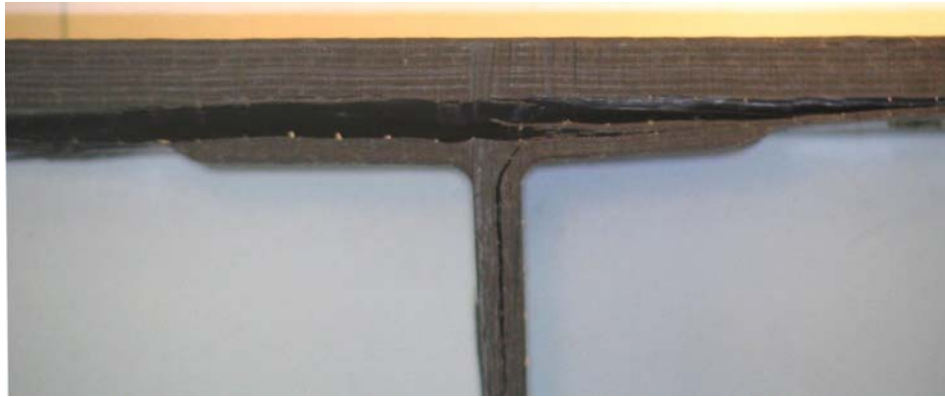


Figure 6.6.2.3: Specimen 6h after static test.

Specimen 6i

Figure 6.6.2.4 shows mostly symmetric and complete fracture of joint Specimen 6i. Joint failure consisted of debonding and fiber fracture along the spar cap to skin interface. In addition, delamination ran down the center of the spar web.

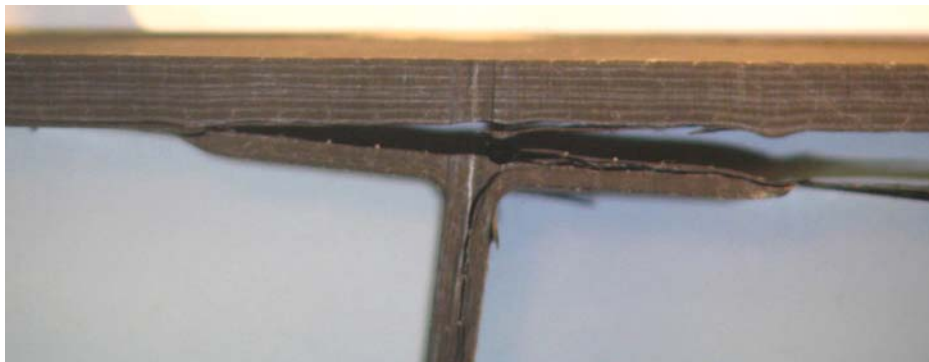


Figure 6.6.2.4: Specimen 6i after static test.

Specimen 6j

Figure 6.6.2.5 shows a mostly symmetric and complete fracture of joint Specimen 6j. Joint failure consisted of debonding and fiber fracture along the spar cap to skin interface. In addition, delamination ran down the center of the spar web.



Figure 6.6.2.5: Specimen 6j after static test.

6.6.3 Specimen Set 6: Dynamic vs. Static Comparisons

Tables 6.6.3.1 and 6.6.3.2 list loads and strains at failure for joints from Specimen Set 6. Specimens 6a thru 6e were tested dynamically and specimens 6f thru 6j were tested statically. Dynamically tested specimens had roughly five times the strain at failure than specimens that were tested statically. A more detailed data analysis is found in Appendix C, Section C.6.

Table 6.6.3.1: Load and Strain at Failure for Specimen Set 6

		Load at Failure (lbf)	Strain at Failure ($\times 10^{-3}$ in/in)	Notes
Dynamic	6a	-	3.05	
	6b	-	3.05	Event 1 didn't break; Velocity estimated
	6c	-	3.063	
	6d	-	4.825	
	6e	-	3.542	
Static	6f	748	0.709	
	6g	763	0.681	
	6h	757	0.683	
	6i	734	0.643	
	6j	662	0.656	

Table 6.6.3.2: Summary of Results for Specimen Set 6

		Load at Failure (lbf)		Strain at Failure ($\times 10^{-3}$ in/in)	
		Average	Standard Deviation	Average	Standard Deviation
Dynamic		-	-	3.506	0.767
Static		733.032	40.941	0.674	0.026

6.7 Specimen Set 7: Cobonded

Specimen Set 7 consists of cobonded skin-spar joints. Figure 6.7.1 and Table 6.7.1 show measured and average joint dimensions for Specimen Set 7.

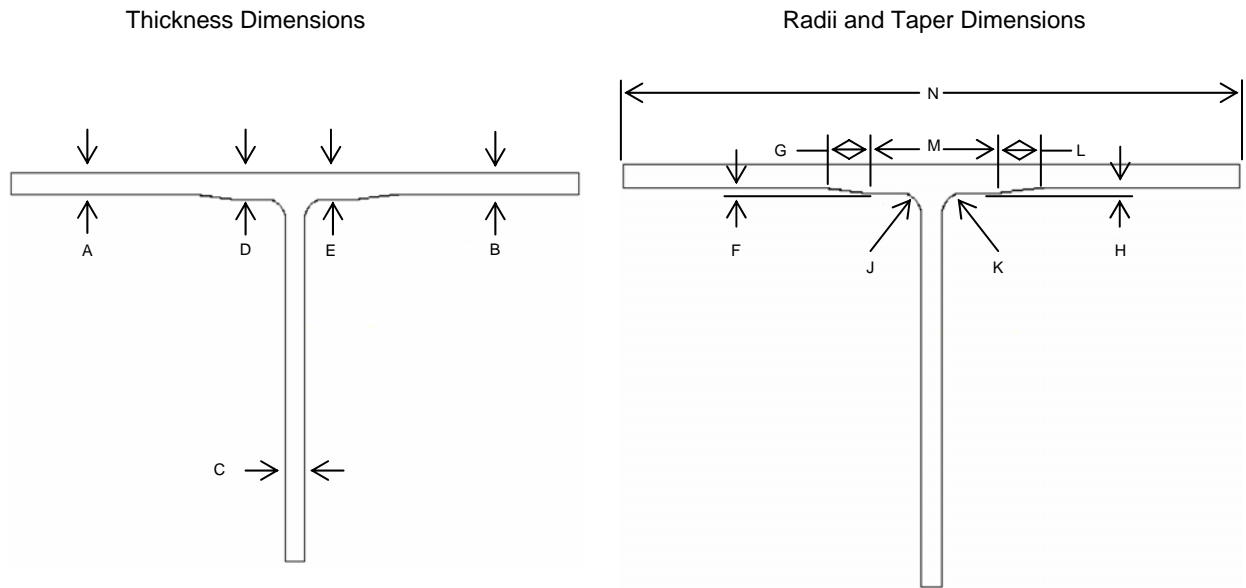


Figure 6.7.1: Specimen dimension coding

Table 6.7.1: Dimensions of Specimen Set 7

		Dimension Label												
Test #	Specimen #	A (inch)	B (inch)	C (inch)	D (inch)	E (inch)	F (inch)	G (inch)	H (inch)	J (inch)	K (inch)	L (inch)	M (inch)	N (inch)
Dynamic	19	7a	0.174	0.170	0.070	0.164	0.168							
	20	7b	0.180	0.175	0.083	0.165	0.195							
	21	7c	0.180	0.174	0.074	0.162	0.191							
	34	7d	0.179	0.174	0.073	0.1587	0.187							
	35	7e	0.170	0.178	0.075	0.195	0.195							
Static	-	7f												
	-	7g												
	-	7h												
	-	7i												
	-	7j												
Averages			0.177	0.174	0.075	0.169	0.187							

All specimens are 2" width.

Figures 6.7.2 and 6.7.3 are representative of Specimen Set 7 construction.



Figure 6.7.2: Example image of joint from Specimen Set 7 (pretest)



Figure 6.7.3: Example cross section of joint from Specimen Set 7 (pretest)

6.7.1 Dynamically Tested Specimens 7a, 7b, 7c, 7d, 7e (Tests #19, 20, 21, 34, 35)

This section includes post-test cross section images of all dynamically tested joints associated with Specimen Set 7.

Specimen 7a, Test 19

Figure 6.7.1.1 shows an incomplete failure of joint Specimen 7a. The joint pulled through the grip at the end of the spar. Still, some delamination is noted directly above the noodle. Without considering visual aspects of the failure, the strain data analysis (presented in Appendix C, Section C.7) revealed that initial failure remained symmetric.



Figure 6.7.1.1: Specimen 7a after dynamic test

Specimen 7b, Test 20

Figure 6.7.1.2 shows a complete and symmetric failure of joint Specimen 7b. Joint failure consisted of debonding along the wrap-around spar cap to skin interface. Delamination extended down the center of the spar web. Without considering visual aspects of the failure, the strain data analysis (presented in Appendix C, Section C.7) revealed that failure was asymmetric.



Figure 6.7.1.2: Specimen 7b after dynamic test

Specimen 7c, Test 21

Figure 6.7.1.3 shows a complete and asymmetric failure of joint Specimen 7c. Joint failure on the left side consisted of debonding along the wrap-around spar cap to skin interface. Failure on the right side has fiber fracture at the noodle. Delamination extended down the center of the spar web. Without considering visual aspects of the failure, the strain data analysis (presented in Appendix C, Section C.7) revealed that failure was asymmetric.



Figure 6.7.1.3: Specimen 7c after dynamic test

Specimen 7d, Test 34

Figure 6.7.1.4 shows a complete and symmetric failure of joint Specimen 7d. Joint failure consisted of debonding along the wrap-around spar cap to skin interface. Delamination extended down the center of the spar web. Without considering visual aspects of the failure, the strain

data analysis (presented in Appendix C, Section C.7) revealed that failure symmetry was inconclusive.



Figure 6.7.1.4: Specimen 7d after dynamic test.

Specimen 7e, Test 35

Figure 6.7.1.5 shows a complete and asymmetric failure of joint Specimen 7e. Joint failure on the left consisted of debonding along the wrap-around spar cap to skin interface. Failure on the right included fiber fracture at the noodle. Delamination extended a short distance down the center of the spar web. Without considering visual aspects of the failure, the strain data analysis (presented in Appendix C, Section C.7) revealed that failure was asymmetric.



Figure 6.7.1.5: Specimen 7e after dynamic test.

6.7.2 Statically Tested Specimens 7f, 7g, 7h, 7i, 7j

This section includes post-test cross section images of all statically tested joints associated with Specimen Set 7.

Specimen 7f

Figure 6.7.2.1 shows a symmetric and incomplete fracture of joint Specimen 7f. Joint failure consisted of debonding along the spar cap to skin interface.



Figure 6.7.2.1: Specimen 7f after static test.

Specimen 7g

Figure 6.7.2.2 shows a symmetric and incomplete fracture of joint Specimen 7g. Joint failure consisted of debonding along the spar cap to skin interface.



Figure 6.7.2.2: Specimen 7g after static test.

Specimen 7h

Figure 6.7.2.3 shows a symmetric and incomplete fracture of joint Specimen 7h. Joint failure consisted of debonding along the spar cap to skin interface.



Figure 6.7.2.3: Specimen 7h after static test.

Specimen 7i

Figure 6.7.2.4 shows a symmetric and incomplete fracture of joint Specimen 7i. Joint failure consisted of debonding along the spar cap to skin interface. In addition, delamination ran down the center of the spar web.



Figure 6.7.2.4: Specimen 7i after static test.

Specimen 7j

Figure 6.7.2.5 shows a symmetric and incomplete fracture of joint Specimen 7j. Joint failure consisted of debonding along the spar cap to skin interface. In addition, delamination ran down the center of the spar web.



Figure 6.7.2.5: Specimen 7j after static test.

6.7.3 Specimen Set 7: Dynamic vs. Static Comparisons

Tables 6.7.3.1 and 6.7.3.2 list loads and strains at failure for joints from Specimen Set 7. Specimens 7a thru 7e were tested dynamically and specimens 7f thru 7j were tested statically. Static test data was lost during a computer malfunction. A more detailed data analysis of dynamically tested specimens is found in Appendix C, Section C.7.

Table 6.7.3.1: Load and Strain at Failure for Specimen Set 7

		Load at Failure (lbf)	Strain at Failure ($\times 10^{-3}$ in/in)	Notes
Dynamic	7a	-	1.788	Specimen pulled thru at bolt hole and didn't fail.
	7b	-	2.637	
	7c	-	4.290	
	7d	-	3.586	
	7e	-	5.938	
Static	7f			Data lost (computer malfunction)
	7g			Data lost (computer malfunction)
	7h			Data lost (computer malfunction)
	7i			Data lost (computer malfunction)
	7j			Data lost (computer malfunction)

Table 6.7.3.2: Summary of Results for Specimen Set 7

		Load at Failure (lbf)		Strain at Failure ($\times 10^{-3}$ in/in)	
		Average	Standard Deviation	Average	Standard Deviation
Dynamic		-	-	3.648	1.592
Static		NA		NA	

6.8 Specimen Set 8: Welded Aluminum

Specimen Set 8 consists of laser beam welded aluminum skin-spar joints. These samples are made from aluminum alloy 6056 sheet of 3 mm thickness for both skin and spar. The two parts were clamped together and welded by a Nd YAG laser beam in two runs, one side of the joint at a time. The welding filler wire was AlSi12 (12% Si). Samples were checked by the manufacturer via penetrant testing and were assessed to be free of cracks. Figure 6.8.1 and Table 6.8.1 show average joint dimensions for Specimen Set 8.

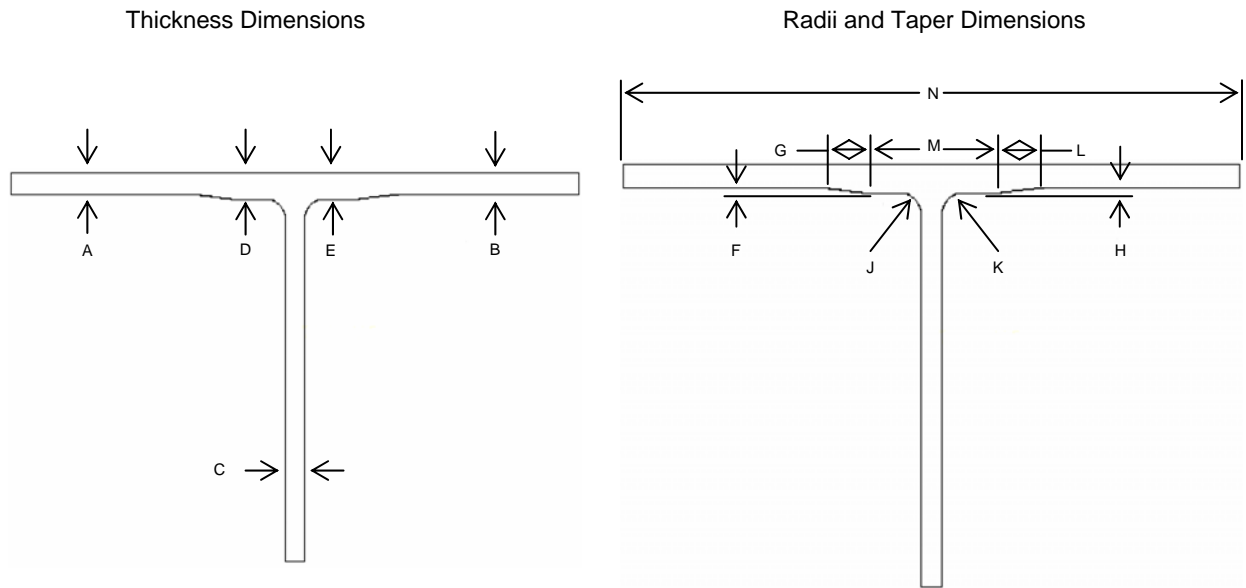


Figure 6.8.1: Specimen dimension coding

Table 6.8.1: Dimensions of Specimen Set 8

		Dimension Label												
Test #	Specimen #	A (inch)	B (inch)	C (inch)	D (inch)	E (inch)	F (inch)	G (inch)	H (inch)	J (inch)	K (inch)	L (inch)	M (inch)	N (inch)
Dynamic	22 8a													
	23 8b													
	24 8c													
	38 8d													
	39 8e													
Static	- 8f													
	- 8g													
	- 8h													
	- 8i													
	- 8j													
Averages		0.121	0.121	0.121										

All specimens are 2" width.

Figures 6.8.2 and 6.8.3 are representative of Specimen Set 8 construction.



Figure 6.8.2: Example image of joint from Specimen Set 8 (pretest)



Figure 6.8.3: Example cross section of joint from Specimen Set 8 (pretest)

6.8.1 Dynamically Tested Specimens 8a, 8b, 8c, 8d, 8e (Tests #22, 23, 24, 38, 39)

This section includes post-test cross section images of all dynamically tested joints associated with Specimen Set 8.

Specimen 8a, Test 22

Figure 6.8.1.1 shows a complete and symmetric failure of joint Specimen 8a. Joint failure consisted of a three-way fracture at the weld. Without considering visual aspects of the failure, the strain data analysis (presented in Appendix C, Section C.8) revealed that failure was symmetric.



Figure 6.8.1.1: Specimen 8a after dynamic test

Specimen 8b, Test 23

Figure 6.8.1.2 shows a complete and symmetric fracture of joint Specimen 8b. Joint failure consisted of a three-way fracture at the weld. Without considering visual aspects of the failure, the strain data analysis (presented in Appendix C, Section C.8) revealed that failure symmetry was inconclusive.



Figure 6.8.1.2: Specimen 8b after dynamic test

Specimen 8c, Test 24

Figure 6.8.1.3 shows a complete and symmetric failure of joint Specimen 8c. Joint failure consisted of a three-way fracture at the weld. Without considering visual aspects of the failure, the strain data analysis (presented in Appendix C, Section C.8) revealed that failure symmetry was inconclusive.



Figure 6.8.1.3: Specimen 8c after dynamic test

Specimen 8d, Test 38

Figure 6.8.1.4 shows a complete and symmetric failure of joint Specimen 8d. Joint failure consisted of a three-way fracture at the weld. Without considering visual aspects of the failure, the strain data analysis (presented in Appendix C, Section C.8) revealed that failure symmetry was inconclusive.



Figure 6.8.1.4: Specimen 8d after dynamic test.

Specimen 8e, Test 39

Figure 6.8.1.5 shows a complete and symmetric failure of joint Specimen 8e. Joint failure consisted of a three-way fracture at the weld. Without considering visual aspects of the failure, the strain data analysis (presented in Appendix C, Section C.8) revealed that failure symmetry was inconclusive.

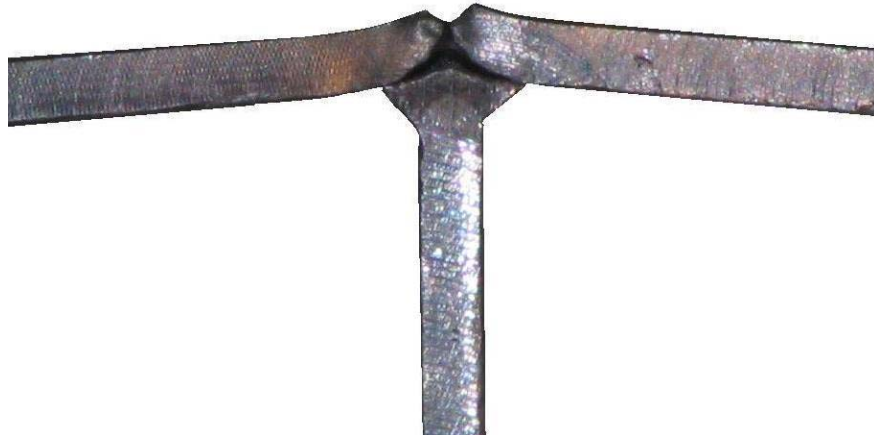


Figure 6.8.1.5: Specimen 8e after dynamic test.

6.8.2 Statically Tested Specimens 8f, 8g, 8h, 8i, 8j

This section includes post-test cross section images of all statically tested joints associated with Specimen Set 8.

Specimen 8f

Figure 6.8.2.1 shows a symmetric and complete fracture of joint Specimen 8f. Joint failure consisted of excessive skin deformation and a weld fracture at the skin-spar interface.



Figure 6.8.2.1: Specimen 8f after static test.

Specimen 8g

Figure 6.8.2.2 shows a symmetric and incomplete fracture of joint Specimen 8g. Joint failure consisted of excessive skin deformation and a weld fracture at the skin-spar interface.



Figure 6.8.2.2: Specimen 8g after static test.

Specimen 8h

Figure 6.8.2.3 shows a symmetric and incomplete fracture of joint Specimen 8h. Joint failure consisted of excessive skin deformation and a weld fracture at the skin-spar interface.

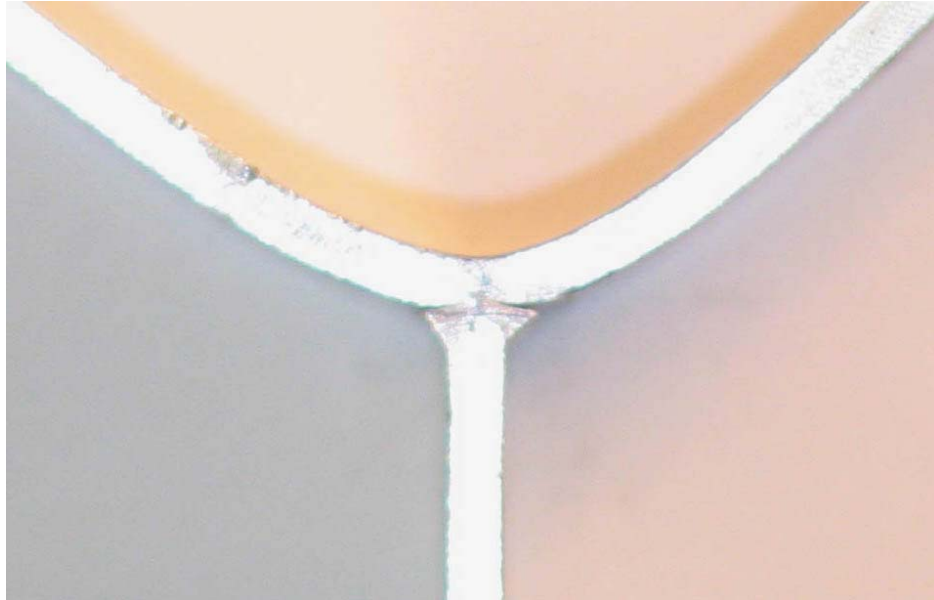


Figure 6.8.2.3: Specimen 8h after static test.

Specimen 8i

Figure 6.8.2.4 shows a symmetric and incomplete fracture of joint Specimen 8i. Joint failure consisted of excessive skin deformation and a weld fracture at the skin-spar interface.

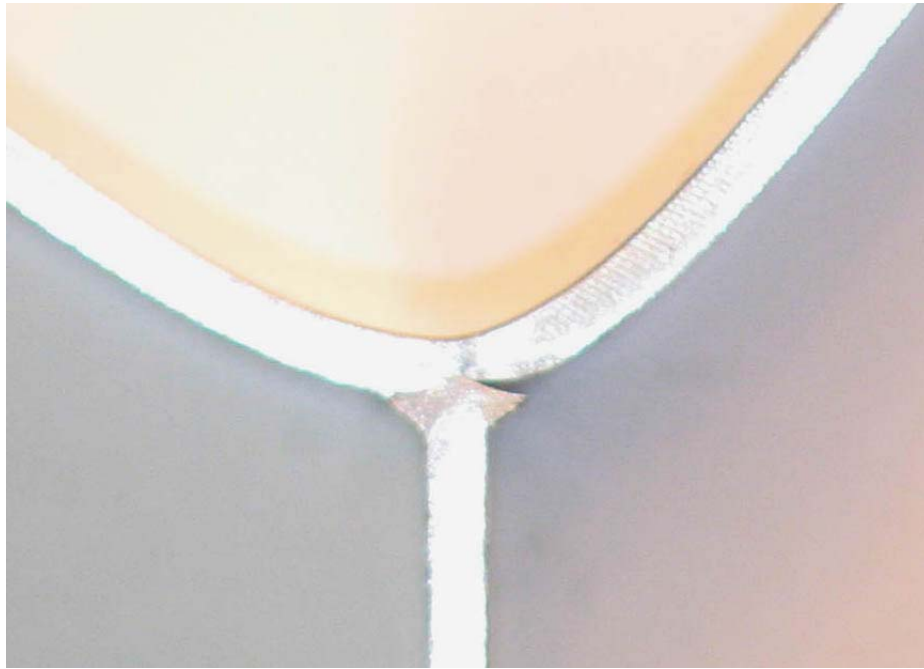


Figure 6.8.2.4: Specimen 8i after static test.

Specimen 8j

Figure 6.8.2.5 shows a symmetric and incomplete fracture of joint Specimen 8j. Joint failure consisted of excessive skin deformation and a weld fracture at the skin-spar interface.

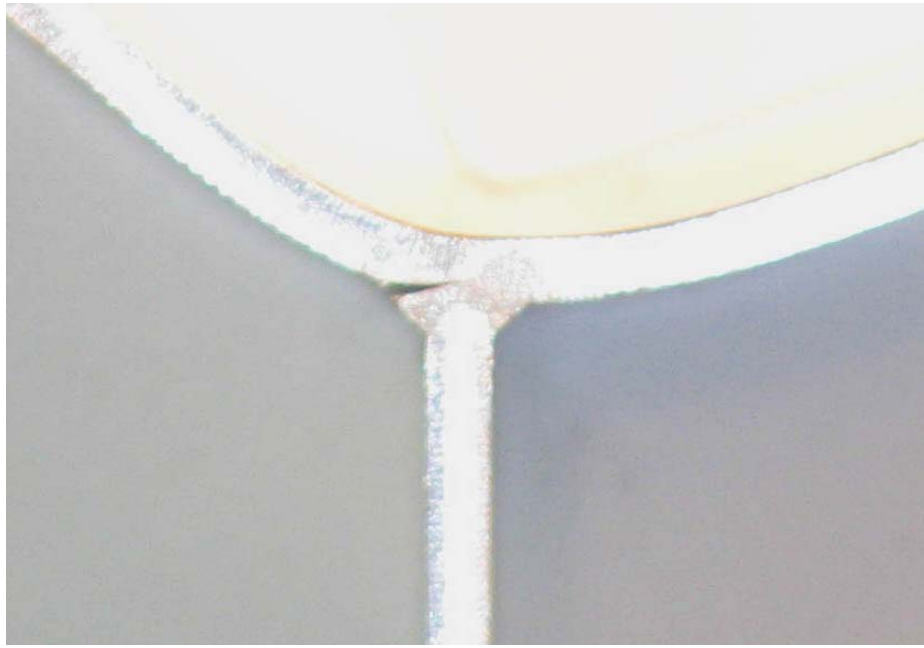


Figure 6.8.2.5: Specimen 8j after static test.

6.8.3 Specimen Set 8: Dynamic vs. Static Comparisons

Tables 6.8.3.1 and 6.8.3.2 list loads and strains at failure for joints from Specimen Set 8. Specimens 8a thru 8e were tested dynamically and specimens 8f thru 8j were tested statically. Dynamically tested specimens had several times the strain at failure than specimens that were tested statically. A more detailed data analysis is found in Appendix C, Section C.8.

Table 6.8.3.1: Load and Strain at Failure for Specimen Set 8

		Load at Failure (lbf)	Strain at Failure ($\times 10^{-3}$ in/in)	Notes
Dynamic	8a	-	1.566	
	8b	-	1.857	Kistler 3 pressure approximated and Kistler 2 pressure is high. Velocity is inaccurate because events were switched
	8c	-	2.620	First event didn't have a clear signal
	8d	-	2.978	
	8e	-	2.006	
Static	8f	263	0.095*	Joint 078
	8g	250	0.098	Joint 079
	8h	535	0.247	
	8i	-	-	Data lost (computer malfunction)
	8j	-	-	Data lost (computer malfunction)

*Specimen 8f was loaded initially (sustaining only minor plastic strain). The load was then removed and strain gages re-zeroed (negating plastic strain) before loading to failure.

Table 6.8.3.2: Summary of Results for Specimen Set 8

		Load at Failure (lbf)		Strain at Failure ($\times 10^{-3}$ in/in)	
		Average	Standard Deviation	Average	Standard Deviation
Dynamic		-	-	2.205	0.579
Static		349	161	0.147	0.087

6.9 Specimen Set 9: Bonded

Specimen Set 9 consists of bonded skin-spar joints. Figure 6.9.1 and Table 6.9.1 show measured and average joint dimensions for Specimen Set 9.ⁱ

ⁱ A complete set of measured dimensions was not obtained. Values for dimensions F through M are nominal.

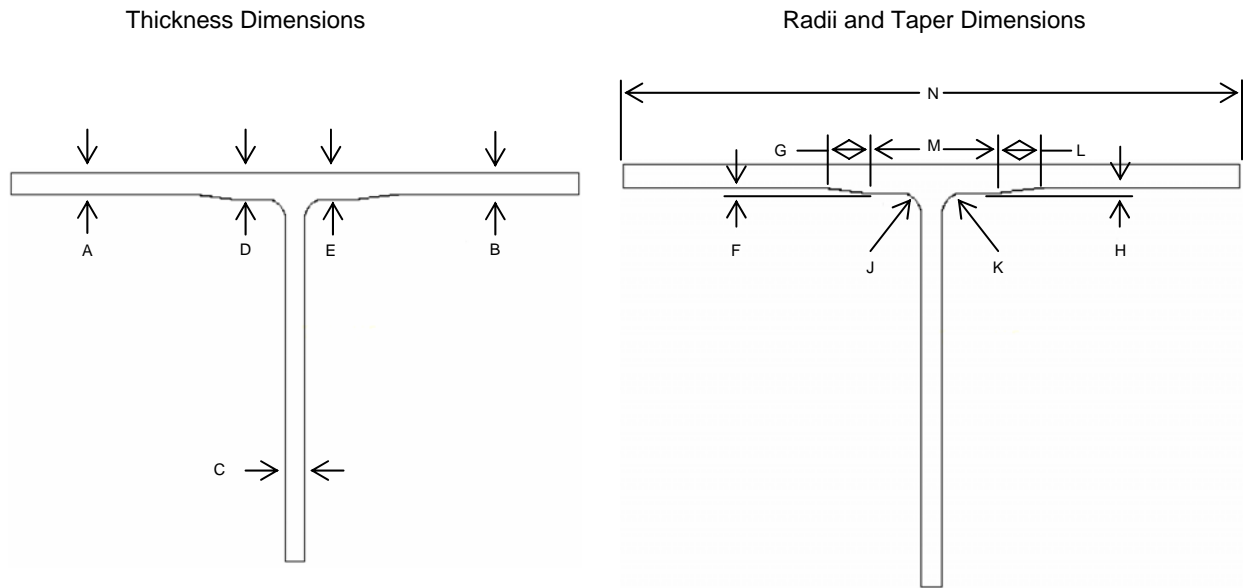


Figure 6.9.1: Specimen dimension coding

Table 6.9.1: Dimensions of Specimen Set 9

			Dimension Label												
	Test #	Specimen #	A (inch)	B (inch)	C (inch)	D (inch)	E (inch)	F (inch)	G (inch)	H (inch)	J (inch)	K (inch)	L (inch)	M (inch)	N (inch)
Dynamic	40	9a	0.25	0.261	0.19	0.336	0.348								
	41	9b	0.25	0.25	0.22	0.358	0.365								
	42	9c	0.253	0.251	0.169	0.355	0.391								
	43	9d	0.26	0.249	0.195	0.335	0.345								
	44	9e	0.25	0.249	0.202	0.335	0.336								
Static	-	9f			0.18										
	-	9g			0.178										
	-	9h			0.192										
	-	9i			0.17										
	Averages		0.2526	0.252	0.188	0.344	0.357	0.152	0.226	0.113	0.219	0.291	0.176	3.334	

All specimens are 1" width.

Figures 6.9.2 and 6.9.3 are representative of Specimen Set 9 construction. These images were collected prior to testing and show strain gage instrumentation.



Figure 6.9.2: Example image of joint from Specimen Set 9 (pretest)



Figure 6.9.3: Example cross section of joint from Specimen Set 9 (pretest)

6.9.1 Dynamically Tested Specimens 9a, 9b, 9c, 9d, 9e (Tests #40, 41, 42, 43, 44)

This section includes post-test cross section images of all dynamically tested joints associated with Specimen Set 9.

Specimen 9a, Test 40

Figure 6.9.1.1 shows a complete and asymmetric failure of joint Specimen 9a. Joint failure on the left side consists of a severed and debonded spar cap. The cap on the right side has fiber-fracture at the spar web intersection and is detached from the skin. Delamination extended a short distance down the center of the spar web. Without considering visual aspects of the failure, the strain data analysis (presented in Appendix C, Section C.9) revealed that failure symmetry was inconclusive.



Figure 6.9.1.1: Specimen 9a after dynamic test

Specimen 9b, Test 41

Figure 6.9.1.2 shows a complete and largely symmetric fracture of joint Specimen 9b. Joint failure occurred along the length of the spar cap, much of which avoided the actual bond line. The upper half of the left cap and a portion of the right cap remained bonded to the skin. Delamination extended a short distance down the center of the spar web. Without considering visual aspects of the failure, the strain data analysis (presented in Appendix C, Section C.9) revealed that failure was asymmetric.



Figure 6.9.1.2: Specimen 9b after dynamic test

Specimen 9c, Test 42

Figure 6.9.1.3 shows a complete and symmetric failure of joint Specimen 9c. Joint failure occurred along the length of the spar cap, much of which avoided the actual bond line. A couple plies of the upper spar cap remain bonded to the skin. Delamination extended a short distance down the center of the spar web. Without considering visual aspects of the failure, the strain data analysis (presented in Appendix C, Section C.9) revealed that failure was asymmetric.



Figure 6.9.1.3: Specimen 9c after dynamic test

Specimen 9d, Test 43

Figure 6.9.1.4 shows a complete and somewhat asymmetric failure of joint Specimen 9d. Joint failure occurred along the length of the spar cap, much of which avoided the actual bond line. A portion of left and right spar caps remain bonded to the skin. Without considering visual aspects

of the failure, the strain data analysis (presented in Appendix C, Section C.9) revealed that failure was asymmetric.



Figure 6.9.1.4: Specimen 9d after dynamic test.

Specimen 9e, Test 44

Figure 6.9.1.5 shows a complete and asymmetric failure of joint Specimen 9e. Joint failure occurred along the length of the left spar cap, much of which avoided the actual bond line. The upper half of the left cap and the entire right cap remained bonded to the skin. Without considering visual aspects of the failure, the strain data analysis (presented in Appendix C, Section C.9) revealed that failure symmetry was inconclusive.



Figure 6.9.1.5: Specimen 9e after dynamic test.

6.9.2 Statically Tested Specimens 9f, 9g, 9h, 9i

This section includes post-test cross section images of all statically tested joints associated with Specimen Set 9.

Specimen 9f

Figure 6.9.2.1 shows a symmetric and complete fracture of joint Specimen 9f. Joint failure consisted of debonding along the spar cap to skin interface.

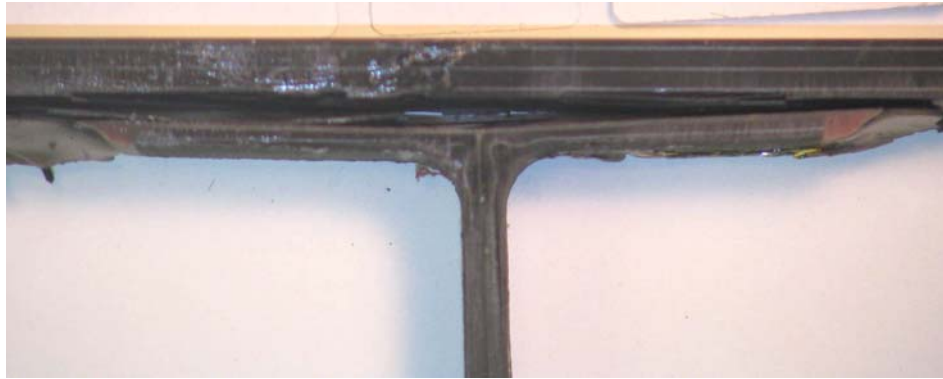


Figure 6.9.2.1: Specimen 9f after static test.

Specimen 9g

Figure 6.9.2.2 shows a symmetric and complete fracture of joint Specimen 9g. Joint failure consisted of debonding along the spar cap to skin interface. In addition, delamination ran down the center of the spar web.



Figure 6.9.2.2: Specimen 9g after static test.

Specimen 9h

Figure 6.9.2.3 shows a symmetric and complete fracture of joint Specimen 9h. Joint failure consisted of debonding along the spar cap to skin interface. In addition, delamination ran down the center of the spar web.

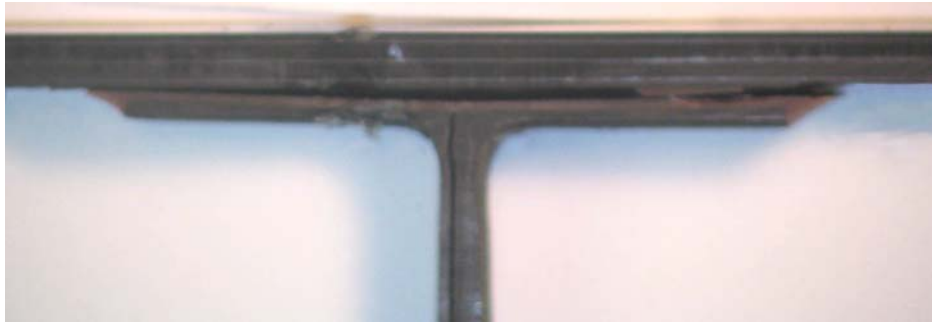


Figure 6.9.2.3: Specimen 9h after static test.

Specimen 9i

Figure 6.9.2.4 shows a symmetric and complete fracture of joint Specimen 9i. Joint failure consisted of debonding along the spar cap to skin interface.



Figure 6.9.2.4: Specimen 9i after static test.

6.9.3 Specimen Set 9: Dynamic vs. Static Comparisons

Tables 6.9.3.1 and 6.9.3.2 lists loads and strains at failure for joints from Specimen Set 9. Specimens 9a thru 9e were tested dynamically and specimens 9f thru 9i were tested statically. Dynamically tested specimens had more than four times the strain at failure than specimens that were tested statically. A more detailed data analysis is found in Appendix C, Section C.9.

Table 6.9.3.1: Load and Strain at Failure for Specimen Set 9

		Load at Failure (lbf)	Strain at Failure ($\times 10^{-3}$ in/in)	Notes
Dynamic	9a	-	4.206	
	9b	-	3.707	
	9c	-	3.736	
	9d	-	2.771	
	9e	-	2.085	
Static	9f	400	0.831	
	9g	399	0.818	
	9h	207	0.437	
	9i	442	0.670	

Table 6.9.3.2: Summary of Results for Specimen Set 9

	Load at Failure (lbf)		Strain at Failure ($\times 10^{-3}$ in/in)	
	Average	Standard Deviation	Average	Standard Deviation
Dynamic	-	-	3.301	0.856
Static	362	105	0.689	0.183

6.10 Specimen Set 10: Bonded (Honeycomb Core)

Specimen Set 10 consists of bonded (honeycomb core) skin-spar joints. Figure 6.10.1 and Table 6.10.1 show measured dimensions taken from a typical joint in Specimen Set 10.

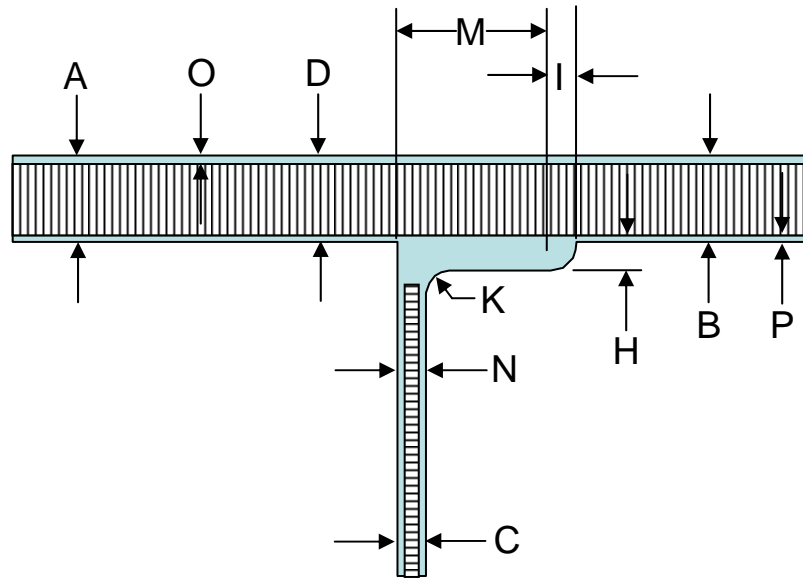


Figure 6.10.1: Specimen dimension coding

Table 6.10.1: Dimensions of Specimen Set 10

Dimension Label											
A (inch)	B (inch)	C (inch)	D (inch)	E (inch)	H (inch)	I (inch)	K (inch)	M (inch)	N (inch)	O (inch)	P (inch)
0.555	0.553	0.232	0.556	0.882	0.308	0.201	0.965	1.794	0.233	0.0125	0.05

All specimens are 2" width.

Figures 6.10.2 and 6.10.3 are representative of Specimen Set 10 construction.

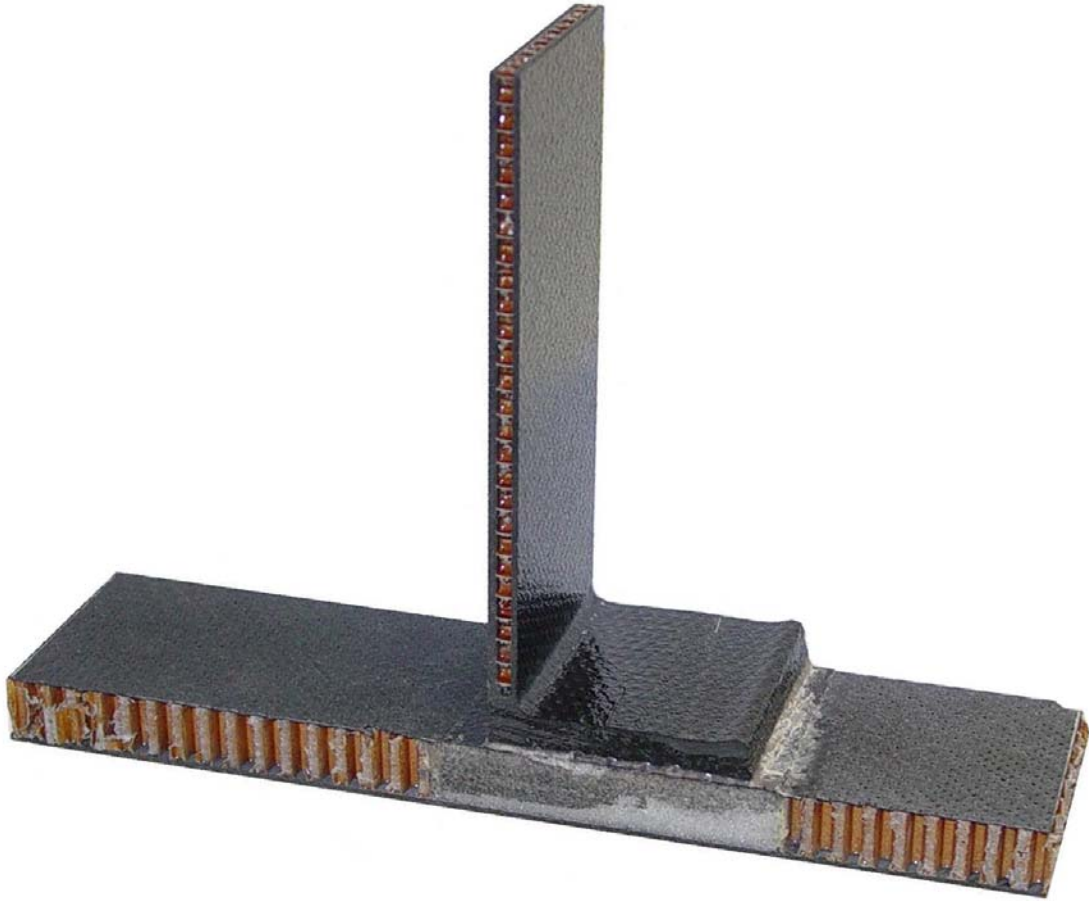


Figure 6.10.2: Example image of joint from Specimen Set 10 (pretest)



Figure 6.10.3: Example cross section of joint from Specimen Set 10 (pretest)

6.10.1 Dynamically Tested Specimens 10a, 10b, 10c (Tests #50, 51, 52)

This section includes post-test cross section images of all dynamically tested joints associated with Specimen Set 10. Only three specimens were tested dynamically.

Specimen 10a, Test 50

Figure 6.10.1.1 shows a complete and asymmetric failure of joint Specimen 10a. Joint failure occurred along bond-line and core interfaces, extending to the right (in the direction of the J). Without considering visual aspects of the failure, the strain data analysis (presented in Appendix C, Section C.10) revealed that failure symmetry was inconclusive.



Figure 6.10.1.1: Specimen 10a after dynamic test

Specimen 10b, Test 51

Figure 6.10.1.2 shows a complete and asymmetric fracture of joint Specimen 10b. Joint failure occurred along bond-line and core interfaces, extending to the right (in the direction of the J). Without considering visual aspects of the failure, the strain data analysis (presented in Appendix C, Section C.10) revealed that failure symmetry was inconclusive.



Figure 6.10.1.2: Specimen 10b after dynamic test

Specimen 10c, Test 52

Figure 6.10.1.3 shows a complete and asymmetric failure of joint Specimen 10c. Joint failure occurred along bond-line and core interfaces, extending to the right (in the direction of the J). Without considering visual aspects of the failure, the strain data analysis (presented in Appendix C, Section C.10) revealed that failure was asymmetric.



Figure 6.10.1.3: Specimen 10c after dynamic test

6.10.2 Statically Tested Specimens 10d, 10e, 10f, 10g, 10h, 10i, 10j, 10k

This section includes post-test cross section images of all statically tested joints associated with Specimen Set 10.

Specimen 10d

Figure 6.10.2.1 shows an asymmetric and incomplete fracture of joint Specimen 10d. Joint failure occurred through a combination of core disbonding and spar cap separation from the inner skin plies.



Figure 6.10.2.1: Specimen 10d after static test.

Specimen 10e

Figure 6.10.2.2 shows an asymmetric and complete fracture of joint Specimen 10e. Joint failure occurred through a combination of core fracture and spar cap separation from the inner skin ply.



Figure 6.10.2.2: Specimen 10e after static test.

Specimen 10f

Figure 6.10.2.3 shows an asymmetric and complete fracture of joint Specimen 10f. Joint failure occurred through core and spar cap disbonding from the inner skin plies.



Figure 6.10.2.3: Specimen 10f after static test.

Specimen 10g

Figure 6.10.2.4 shows an asymmetric and incomplete fracture of joint Specimen 10g. Joint failure occurred through core shear and skin fracture on the left. Early failure on the left caused joint rotation in the fixture, creating a bending condition in the spar web (placing SG2 in compression and SG3 in tension). The average web strain is therefore lower than expected.



Figure 6.10.2.4: Specimen 10g after static test.

Specimen 10h

Figure 6.10.2.5 shows an asymmetric and incomplete fracture of joint Specimen 10h. The test truncated prematurely when a displacement limit of 1” was reached. The limit should have been set to 2” as was the case in all other tests.



Figure 6.10.2.5: Specimen 10h after static test.

Specimen 10i

Figure 6.10.2.6 shows an asymmetric and incomplete fracture of joint Specimen 10i. Joint failure occurred through core shear and skin fracture on the left. Early failure on the left caused joint rotation in the fixture, creating a bending condition in the spar web (placing SG2 in compression and SG3 in tension). The average web strain is therefore lower than expected.



Figure 6.10.2.6: Specimen 10i after static test.

Specimen 10j

Figure 6.10.2.7 shows an asymmetric and complete fracture of joint Specimen 10j. Joint failure occurred through core fracture and spar cap disbonding from the inner skin plies.



Figure 6.10.2.7: Specimen 10j after static test.

Specimen 10k

Figure 6.10.2.8 shows an asymmetric and incomplete fracture of joint Specimen 10k. Joint failure occurred through core shear on the left. Early failure on the left caused joint rotation in the fixture, creating a bending condition in the spar web (placing SG2 in compression and SG3 in tension). The average web strain is therefore lower than expected.



Figure 6.10.2.8: Specimen 10k after static test.

6.10.3 Specimen Set 10: Dynamic vs. Static Comparisons

Tables 6.10.3.1 and 6.10.3.2 list loads and strains at failure for joints from Specimen Set 10. Specimens 10a thru 10c were tested dynamically and specimens 10d thru 10g were tested statically. Dynamically tested specimens had nearly 50 times the strain at failure than specimens that were tested statically. A more detailed data analysis is found in Appendix C, Section C.10.

Table 6.10.3.1: Load and Strain at Failure for Specimen Set 10

		Load at Failure (lbf)	Strain at Failure (x10 ⁻³ in/in)	Notes
Dynamic	10a	-	4.51	
	10b	-	6.03	
	10c	-	3.48	
Static	10d	-	-	Data lost (computer malfunction)
	10e	-	-	Data lost (computer malfunction)
	10f	-	-	Data lost (computer malfunction)
	10g	214	0.065	Joint 103
	10h	175*	0.098	Joint 104
	10i	216	0.050	Joint 105
	10j	208	0.119	Joint 106
	10k	207	0.143	Joint 107

*Load terminated prematurely when an incorrectly-set displacement limit was reached.

Table 6.10.3.2: Summary of Results for Specimen Set 10

	Load at Failure (lbf)		Strain at Failure (x10 ⁻³ in/in)	
	Average	Standard Deviation	Average	Standard Deviation
Dynamic	-	-	4.673	1.283
Static*	211	4.4	0.094	0.044

*Omits data from Specimen 10h due to a prematurely terminated load.

6.11 Specimen Set 11: Pi Bonded

Specimen Set 11 consists of Pi bonded skin-spar joints that were fabricated and tested in support of a separate effort.² A synopsis of results is presented herein. Figure 6.11.1 and Table 6.11.1 show measured and average joint dimensions for Specimen Set 11.^j

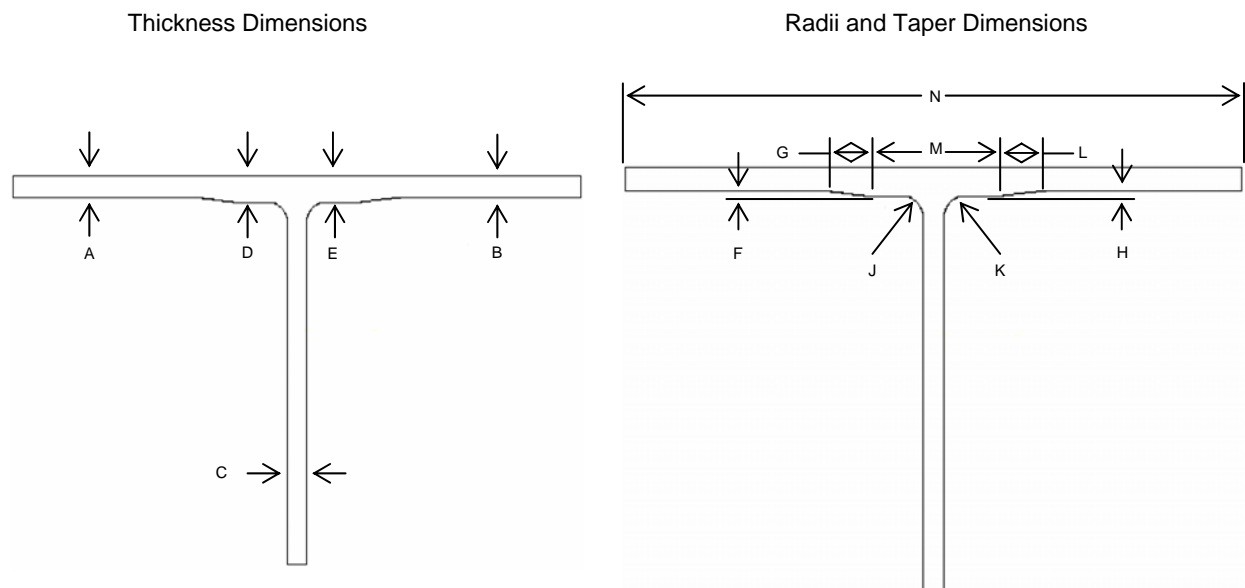


Figure 6.11.1: Specimen dimension coding

Table 6.11.1: Dimensions of Specimen Set 11

		Dimension Label								
	Test #	Specimen #	A (inch)	B (inch)	C (inch)	D (inch)	E (inch)	F (inch)	H (inch)	N (inch)
Dynamic										
Static										
Averages		11	0.2065	0.2065	0.185	0.325	0.325	0.1185	0.1185	8

All specimens are 2" width.

Figure 6.11.1 is representative of Specimen Set 11 construction.

^j A complete set of measured dimensions was not obtained. Values shown are nominal.

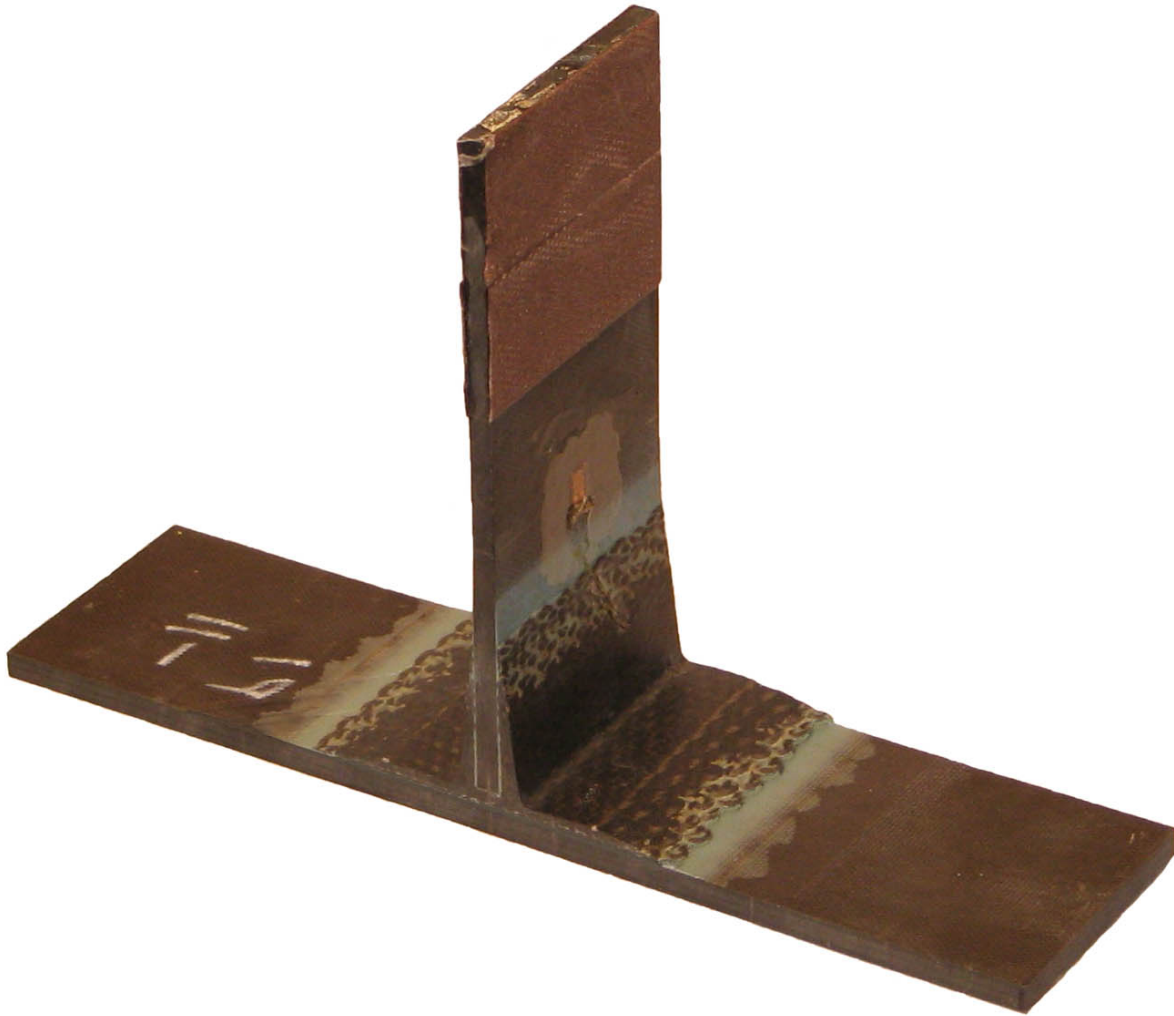


Figure 6.11.1: Example image of joint from Specimen Set 11 (pretest)

6.11.1 Dynamically Tested Specimens 11a, 11b, 11c, 11d

This section includes post-test cross section images of all dynamically tested joints associated with Specimen Set 11.

Specimen 11a

Figure 6.11.1.1 shows a complete and symmetric failure of joint Specimen 11a. Joint failure consists of a debonded spar cap. Delamination is also present within skin layers. Without considering visual aspects of the failure, the strain data analysis (presented in Appendix C, Section C.11) revealed that failure symmetry was inconclusive.

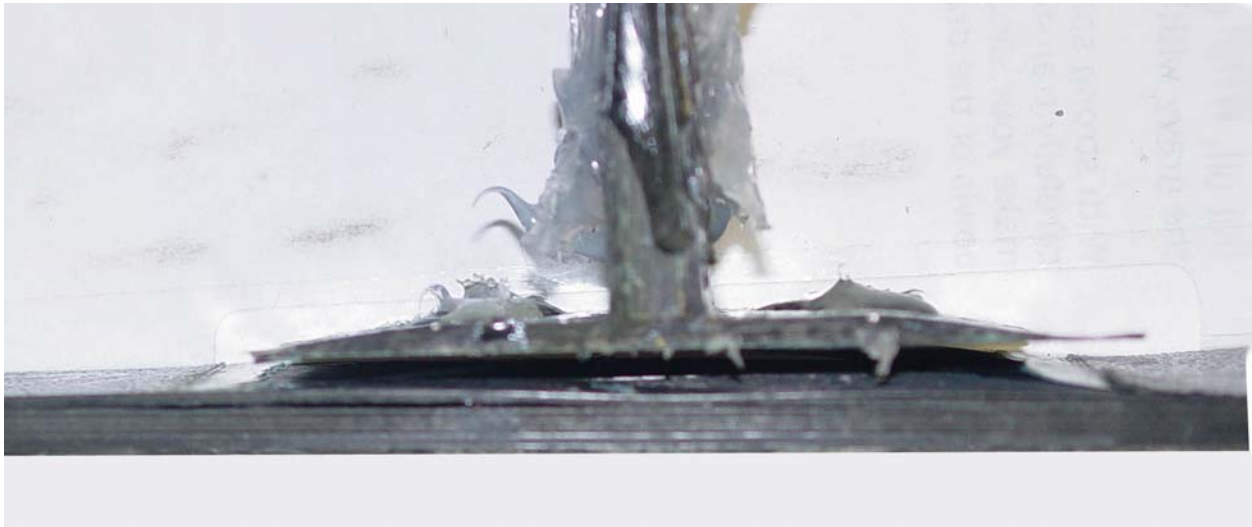


Figure 6.11.1.1: Specimen 11a after dynamic test

Specimen 11b

Figure 6.11.1.2 shows a complete and symmetric fracture of joint Specimen 11b. Joint failure occurred at the web's intersection with the spar cap. (The web is completely severed from the cap.) Without considering visual aspects of the failure, the strain data analysis (presented in Appendix C, Section C.11) revealed that failure symmetry was inconclusive.

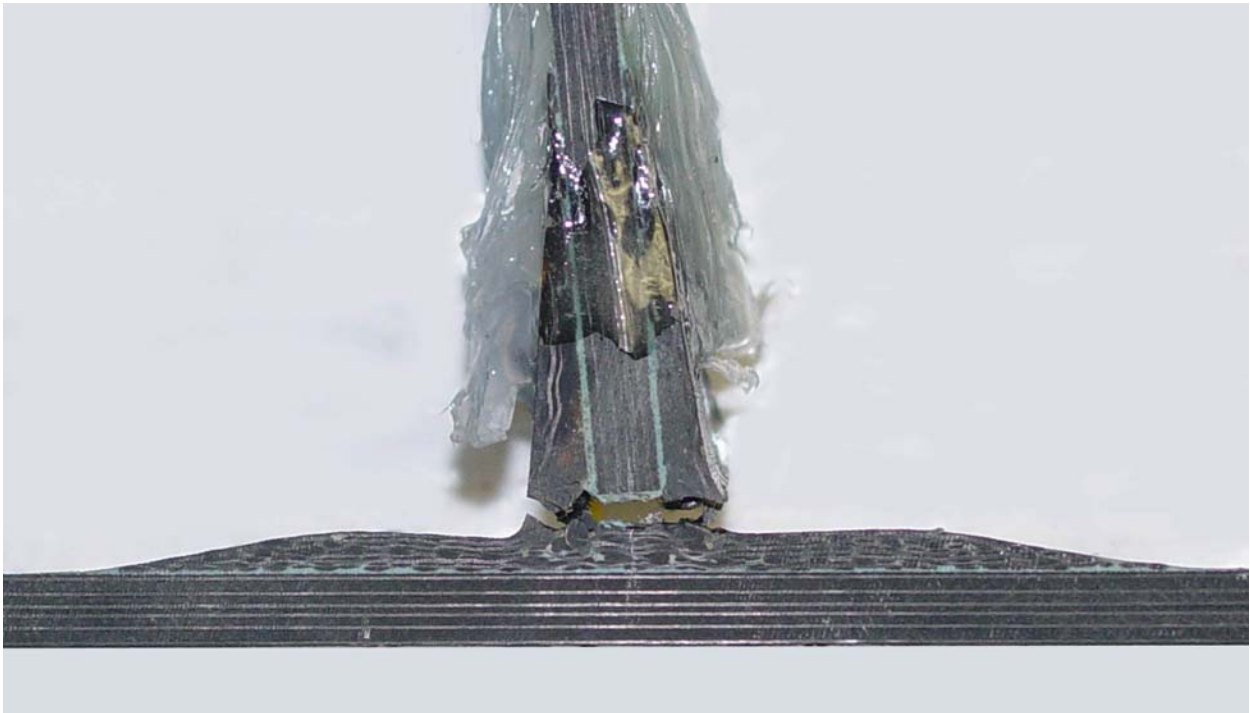


Figure 6.11.1.2: Specimen 11b after dynamic test

Specimen 11c

Figure 6.11.1.3 shows a complete and somewhat asymmetric failure of joint Specimen 11c. Joint failure occurred along the length of the spar cap, but one or two plies deep within the skin. Extensive through-thickness skin delamination is present. There is also a complete separation of the web from the spar cap. Without considering visual aspects of the failure, the strain data analysis (presented in Appendix C, Section C.11) revealed that failure was symmetric.

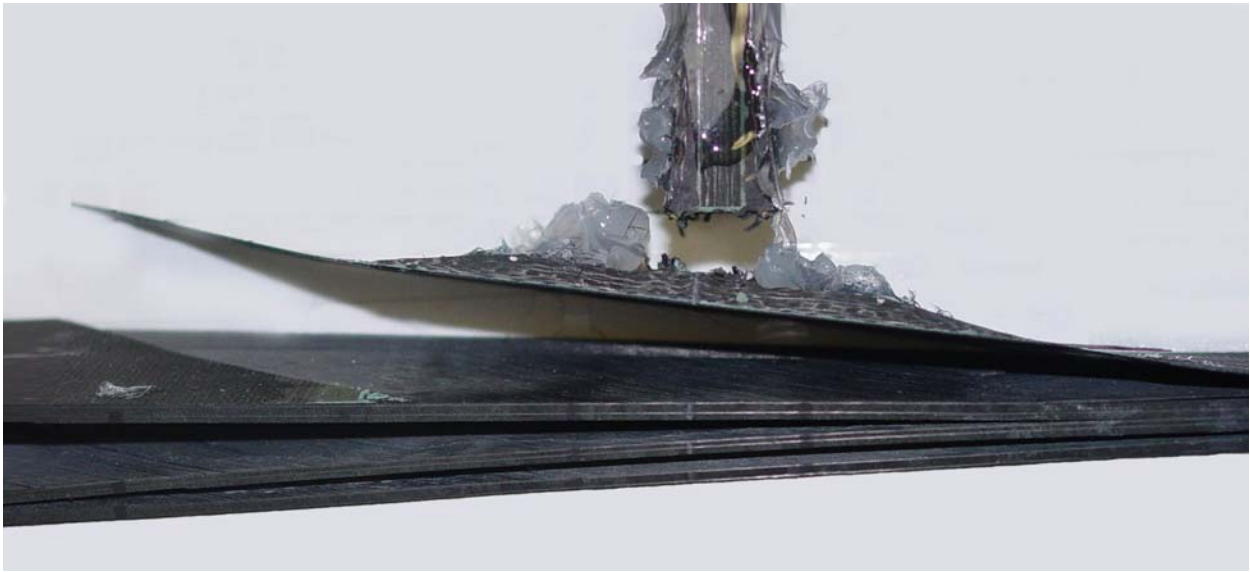


Figure 6.11.1.3: Specimen 11c after dynamic test

Specimen 11d

Figure 6.11.1.4 shows a complete and somewhat asymmetric failure of joint Specimen 11d. Joint failure occurred along the length of the spar cap, but one or two plies deep within the skin. Through the thickness skin delamination is also present on the right side of the specimen. In addition, the web is severed from the spar cap. Without considering visual aspects of the failure, the strain data analysis (presented in Appendix C, Section C.11) revealed that failure symmetry was inconclusive.

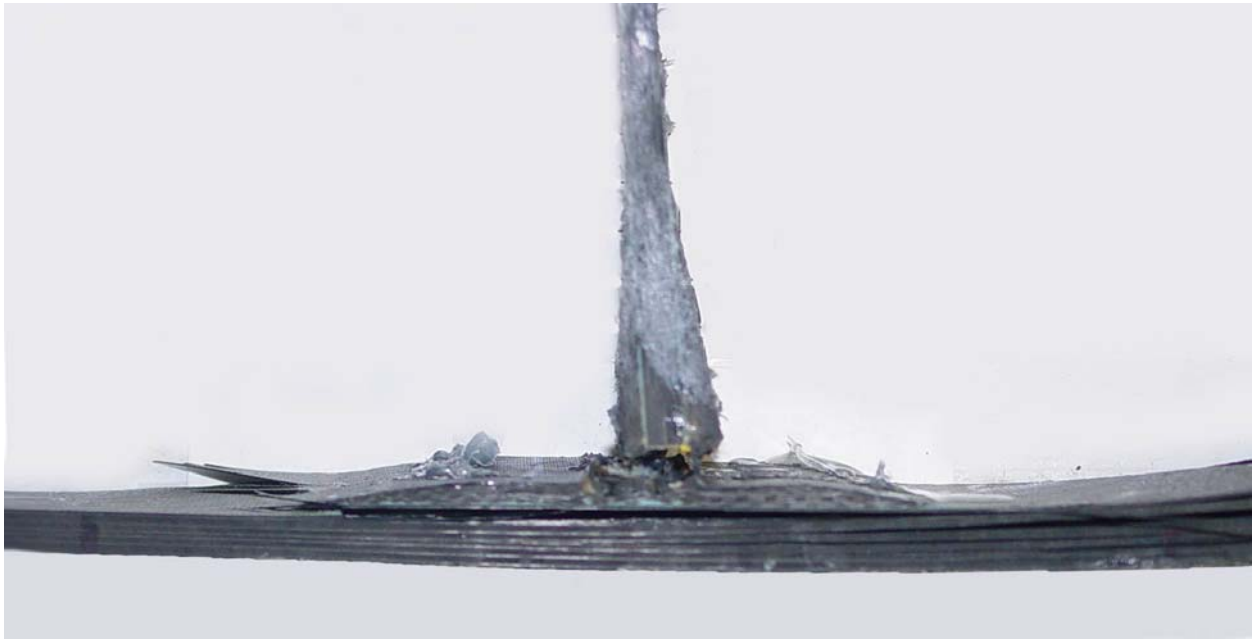


Figure 6.11.1.4: Specimen 11d after dynamic test.

6.11.2 Statically Tested Specimens 11e, 11f

This section includes post-test cross section images of all statically tested joints associated with Specimen Set 11.

Specimen 11e

Figure 6.11.2.1 shows a symmetric and complete fracture of joint Specimen 11e. Joint failure consisted of debonding along the spar cap to skin interface.

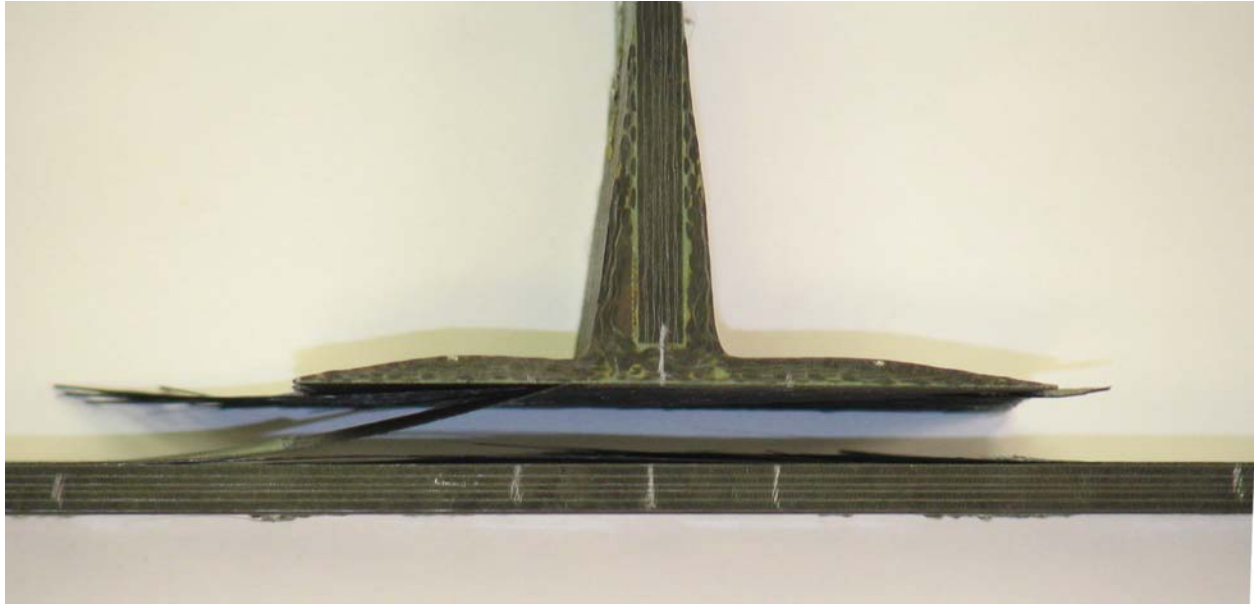


Figure 6.11.2.1: Specimen 11e after static test.

Specimen 11f

Figure 6.11.2.2 shows a symmetric and complete fracture of joint Specimen 11f. Joint failure consisted of debonding along the spar cap to skin interface.

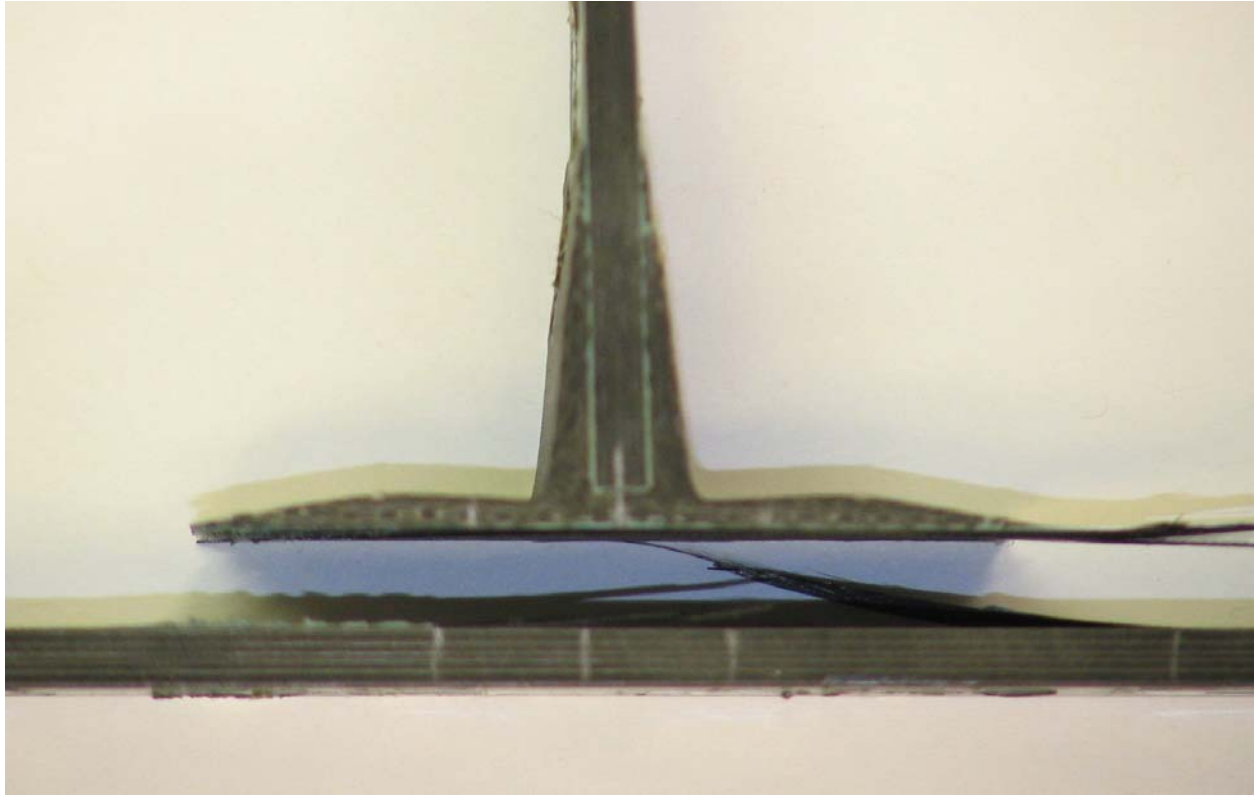


Figure 6.11.2.2: Specimen 11f after static test.

6.11.3 Specimen Set 11: Dynamic vs. Static Comparisons

Tables 6.11.3.1 and 6.11.3.2 list loads and strains at failure for joints from Specimen Set 11. Specimens 11a thru 11d were tested dynamically and specimens 11e and 11f were tested statically. Dynamically tested specimens had more than three times the strain at failure than specimens that were tested statically. A more detailed data analysis is found in Appendix C, Section C.11.

Table 6.11.3.1: Load and Strain at Failure for Specimen Set 11

		Load at Failure (lbf)	Strain at Failure ($\times 10^{-3}$ in/in)	Notes
Dynamic	11a	-	1.063	Test B6 in ref. 2
	11b	-	3.241	Test B12 in ref. 2
	11c	-	2.798	Test B13 in ref. 2
	11d	-	2.898	Test B14 in ref. 2
Static	11e	Avg only*	Avg only*	
	11f	Avg only*	Avg only*	

* Static loads and strains at failure were not retained on individual specimens. Average values are reported in Table 6.11.3.2.

Table 6.11.3.2: Summary of Results for Specimen Set 11

		Load at Failure (lbf)		Strain at Failure ($\times 10^{-3}$ in/in)	
		Average	Standard Deviation	Average	Standard Deviation
Dynamic		-	-	2.500	0.977
Static		1350	-	0.688	-

6.12 Synopsis of Joint-Failure Measures

This subsection summarizes test outcomes and then provides a top-level overview of how joint designs compared to one another based on static failure load, static failure strain, dynamic failure strain, and dynamic/static failure strain ratio metrics.

First, a summary of individual joint test specimen loads and strains at failure are presented in Table 6.12.1. Included in the table are somewhat-subjective metrics concerning dynamic failure symmetry. Visual observations of failure symmetry are compared to those of strain measurements.

Table 6.12.1: Summary of Joint Failure Symmetry, Loads, and Strains

Specimen #	Test #	Test Type	Visual Failure Symmetry	Strain Failure Symmetry	Load at Failure (lbf)	Strain at Failure ($\times 10^3$ in/in)
1a	1	Dynamic	No	No		1.899
1b	2	Dynamic	No	?		3.550
1c	3	Dynamic	Yes	No		2.507
1d	25	Dynamic	-	No		5.103
1e		Static	Yes		488	1.051
1f		Static	Yes		465	1.065
1g		Static	Yes		456	0.853
1h		Static	Yes		948	1.063
2a	4	Dynamic	Yes	?		-
2b	5	Dynamic	Yes	Yes		2.663
2c	6	Dynamic	No	?		2.745
2d	26	Dynamic	Yes	?		1.820
2e	27	Dynamic	Yes	Yes		1.654
2f		Static	No		1102	1.117
2g		Static	No		1046	0.955
2h		Static	No		1036	0.866
2i		Static	No		964	1.013
3a	7	Dynamic	Yes	Yes		5.699
3b	8	Dynamic	Yes	?		3.840
3c	9	Dynamic	No	Yes		3.410
3d	36	Dynamic	Yes	?		5.063
3e	37	Dynamic	Yes	Yes		3.986
3f		Static	Yes		1094	0.997
3g		Static	Yes		1178	1.066
3h		Static	Yes		956	0.898
3i		Static	Yes		1253	1.385
3j		Static	Yes		1228	1.144
4a	10	Dynamic	Yes	?		4.375
4b	11	Dynamic	Yes	Yes		3.877
4c	12	Dynamic	Yes	Yes		2.988
4d	31	Dynamic	Yes	Yes		4.062
4e	32	Dynamic	Yes	Yes		3.663
4f		Static	Yes		1092	1.032
4g		Static	Yes		1061	0.965
4h		Static	Yes		1040	0.886
4i		Static	Yes		1164	1.055
4j		Static	No		1100	1.020

Table 6.12.1 (continued): Summary of Joint Failure Symmetry, Loads, and Strains

Specimen #	Test #	Test Type	Visual Failure Symmetry	Strain Failure Symmetry	Load at Failure (lbf)	Strain at Failure ($\times 10^3$ in/in)
5a	13	Dynamic	Yes	Yes		1.687
5b	14	Dynamic	Yes	?		2.351
5c	15	Dynamic	Yes	Yes		1.070
5d	30	Dynamic	Yes	Yes		2.788
5e	33	Dynamic	Yes	Yes		2.429
5f		Static	Yes		1371	0.498
5g		Static	Yes		1248	0.478
5h		Static	No		1239	0.480
5i		Static	Yes		1472	0.540
5j		Static	Yes		1489	0.599
6a	16	Dynamic	Yes	Yes		3.050
6b	17	Dynamic	Yes	No		3.050
6c	18	Dynamic	Yes	Yes		3.063
6d	28	Dynamic	Yes	Yes		4.825
6e	29	Dynamic	Yes	Yes		3.542
6f		Static	Yes		748	0.709
6g		Static	Yes		763	0.681
6h		Static	Yes		757	0.683
6i		Static	Yes		734	0.643
6j		Static	Yes		662	0.656
7a	19	Dynamic	-	Yes		1.788
7b	20	Dynamic	Yes	No		2.637
7c	21	Dynamic	No	No		4.290
7d	34	Dynamic	Yes	?		3.586
7e	35	Dynamic	No	No		5.938
7f		Static	Yes		-	-
7g		Static	Yes		-	-
7h		Static	Yes		-	-
7i		Static	Yes		-	-
7j		Static	Yes		-	-
8a	22	Dynamic	Yes	Yes		1.566
8b	23	Dynamic	Yes	?		1.857
8c	24	Dynamic	Yes	?		2.620
8d	38	Dynamic	Yes	?		2.978
8e	39	Dynamic	Yes	?		2.006
8f		Static	Yes		263	0.095
8g		Static	Yes		250	0.098
8h		Static	Yes		535	0.247
8i		Static	Yes		-	-
8j		Static	Yes		-	-

*Specimen 8f was loaded initially (sustaining only minor plastic strain). The load was then removed and strain gages re-zeroed (negating plastic strain) before loading to failure.

Table 6.12.1 (continued): Summary of Joint Failure Symmetry, Loads, and Strains

Specimen #	Test #	Test Type	Visual Failure Symmetry	Strain Failure Symmetry	Load at Failure (lbf)	Strain at Failure ($\times 10^3$ in/in)
9a	40	Dynamic	No	?		4.206
9b	41	Dynamic	Yes	No		3.707
9c	42	Dynamic	Yes	No		3.736
9d	43	Dynamic	No	No		2.771
9e	44	Dynamic	No	?		2.085
9f		Static	Yes		400	0.831
9g		Static	Yes		399	0.818
9h		Static	Yes		207	0.437
9i		Static	Yes		442	0.670
10a	50	Dynamic	No	?		4.510
10b	51	Dynamic	No	?		6.030
10c	52	Dynamic	No	No		3.480
10d		Static	No		-	-
10e		Static	No		-	-
10f		Static	No		-	-
10g		Static	No		214	0.065
10h		Static	No		175*	0.098
10i		Static	No		216	0.050
10j		Static	No		208	0.119
10k		Static	No		207	0.143
11a	53	Dynamic	Yes	?		1.063
11b	59	Dynamic	Yes	?		3.241
11c	60	Dynamic	No	Yes		2.798
11d	61	Dynamic	No	?		2.898
11e		Static	Yes		1350	0.688
11f		Static	Yes		1350	0.688

*Load on Specimen 10h was terminated prematurely when an incorrectly-set displacement limit was reached.

Table 6.12.2 compares joints in terms of static failure load. Joints containing transverse reinforcements (stitching or pinning) tended to perform better than joints that were simply bonded. Nevertheless, two of the better-performing joints contained no transverse reinforcement.

Table 6.12.2: Static Joint Performance Based on Failure Load

Order	Joint Specimen Set	Joint Specimen Description	Average Static Failure Load (lbs)
1	5	Cobonded Prepreg	1364
2	11	Pi Bonded	1350
3	3	Tufted Carbon	1142
4	4	Tufted Aramide	1091
5	2	Bolted	1037
6	6	One Shot Infiltration	733
7	1	Cobonded (Stitched)	589
8	9	Bonded	362
9	8	Welded Aluminum	349
10	10	Bonded (Honeycomb)	211

Note: Specimen set 7 was not included

Table 6.12.3 compares joints in terms of static failure strain. Joints containing transverse reinforcements clearly perform better than those without reinforcement.

Table 6.12.3: Static Joint Performance Based on Failure Strain

Order	Joint Specimen Set	Joint Specimen Description	Average Static Failure Strain (x10E-3)
1	3	Tufted Carbon	1.098
2	1	Cobonded (Stitched)	1.008
3	4	Tufted Aramide	0.992
4	2	Bolted	0.988
5	9	Bonded	0.689
6	11	Pi Bonded	0.688
7	6	One Shot Infiltration	0.674
8	5	Cobonded Prepreg	0.519
9	8	Welded Aluminum	0.147
10	10	Bonded (Honeycomb)	0.094

Note: Specimen set 7 was not included

Table 6.12.4 compares joints in terms of dynamic failure strain. The presence/absence of transverse reinforcements does not appear to have a strong influence on joint performance. Joint weight does not correlate with the joint's dynamic performance.

Table 6.12.4: Dynamic Joint Performance Based on Failure Strain

Order	Joint Specimen Set	Joint Specimen Description	Average Dynamic Failure Strain (x10E-3)	Average Specimen Weight (grams)
1	10	Bonded (Honeycomb)	4.673	123.3
2	3	Tufted Carbon	4.400	178.2
3	4	Tufted Aramide	3.793	170.6
4	7	Cobonded	3.648	104.0
5	6	One Shot Infiltration	3.506	170.3
6	9	Bonded	3.301	86.9
7	1	Cobonded (Stitched)	3.265	108.0
8	11	Pi Bonded	2.500	158.4
9	2	Bolted	2.221	219.9
10	8	Welded Aluminum	2.205	144.8
11	5	Cobonded Prepreg	2.065	184.1

Table 6.12.5 compares joints in terms of their dynamic/static failure strain ratios. The presence/absence of transverse reinforcements does not appear to have a strong influence on joint performance. Joint weight does not correlate with the joint's dynamic performance.

Table 6.12.5: Joint Performance Based on Dynamic/Static Failure Strain Ratio

Order	Joint Specimen Set	Joint Specimen Description	Dynamic/Static Failure Strain Ratio	Average Specimen Weight (grams)
1	10	Bonded (Honeycomb)	49.71	123.3
2	8	Welded Aluminum	15.00	144.8
3	6	One Shot Infiltration	5.20	170.3
4	9	Bonded	4.79	86.9
5	3	Tufted Carbon	4.01	178.2
6	5	Cobonded Prepreg	3.98	184.1
7	4	Tufted Aramide	3.82	170.6
8	11	Pi Bonded	3.63	158.4
9	1	Cobonded (Stitched)	3.24	108.0
10	2	Bolted	2.25	219.9

Note: Specimen set 7 was not included

7 FINDINGS AND CONCLUSIONS

7.1 RamGun Performance

While Delrin-projectile impact velocities were tightly controlled, and deformations of the impact plate (at the head of the fluid column) were uniform, recorded ram pressures varied widely from test to test. Some variation seemed to dampen out as the test series progressed, indicating ram pressure variations may have been driven by uncontrolled test-process variations early-on. An example of an uncontrolled element is entrained air in the fluid column. Although care was taken (from the onset of testing) to insure the fluid column was void of air, the fluid column could not be examined for verification of air removal. Still, test-to-test variations in ram pressure did not appear to influence failure strain magnitudes. This suggests there was ample ram to insure failure, and test-to-test consistency of the load rate.

As evidenced throughout the test series, symmetrically-positioned pressure sensors K1 and K3 verified that pressure loads were being uniformly applied (side-to-side) to the joint's skin.

Early concerns over the RamGun diaphragm's resistance to rupture (potentially influencing ram pressure accumulation in the test chamber) proved unfounded. A special series of tests were performed to independently evaluate diaphragm performance. Ram pressures did not correlate with diaphragm toughness. Nevertheless, an aluminum foil diaphragm was used in follow-on tests to prevent any resistance (however slight) to joint failure.

As the distance from the specimen skin increases, the apparent load increases (due to fixture-mass acceleration) to much higher values that have little real meaning. Because dynamic failure loads can be misleading, the authors opt for strain as a preferred metric describing dynamic failure.

Test results demonstrate that joint mass does not correlate with the joint's dynamic performance. For example, neither dynamic failure loads nor the dynamic/static failure ratios correlated with specimen mass for measurements collected close to the failure location. As such, concerns over

specimen mass-acceleration (and whether the test outcome will be affected by mass-acceleration) are largely put to rest.

7.2 Joint Performance

When joints were compared based on static failure loads, joints containing transverse reinforcements (stitching or pinning) tended to perform better than joints that were simply bonded. Nevertheless, two of the better-performing joints contained no transverse reinforcements.

When joints were compared based on static failure strains, joints containing transverse reinforcements clearly performed better than those without reinforcement.

When joints were compared based on dynamic failure strains, the presence/absence of transverse reinforcements did not appear to have a strong influence on joint performance.

When joints were compared based on dynamic/static failure strain ratios, the presence/absence of transverse reinforcements did not appear to have a strong influence on joint performance.

As evidenced by skin and spar strain gage pairs, the symmetry of joint failure varied. Some joints (having symmetric geometries) exhibited consistent visual and strain-based symmetries of failure. Other joint designs appeared prone to some measure of asymmetric failure.

For many joint designs, there was considerable test-to-test variation in the dynamic failure strain. Other joint designs exhibited data sets with smaller standard deviations, indicative of joint-to-joint uniformity.

Recorded static and dynamic strains at failure varied as a function of joint design, with dynamic failure strains typically having a comparatively large standard deviation. Dynamic strains at failure ranged (on average) from two to five times greater than static failure strains. Exceptions were the bonded honeycomb and welded aluminum joints where failure strain ratios were much higher.

8 SUMMARY

This paper presents the application of a new dynamic joint loading methodology that uses a RamGun device. The RamGun provides a one of a kind capability for economically evaluating high-strain rate failure properties of single and double T-joint and J-joint specimens under realistic boundary conditions similar to those encountered during a projectile-generated hydrodynamic ram events on aircraft fuel tank structure.

A variety of composite and metallic joints are tested quasi-statically and dynamically, yielding critical strain-at-failure metrics. Where quasi-static failure strain is conveniently obtained, dynamic failure strain (as produced by the RamGun) is a structural mechanical property that relates directly and realistically to projectile-induced ram loading conditions. Dynamic failure strain is a meaningful metric that can either be applied, together with static failure loads and strains, to compare a series of candidate joint designs. Dynamic failure strain is a unique property that relates more-directly to a joint's inherent resistance to hydrodynamic ram. Once obtained, dynamic failure strain can be applied as a user-defined joint failure criterion within finite element codes for prediction of dynamic failure events.

The RamGun test method is an easily-understood test that yields a dynamic strain-at-failure metric that can be compared 1:1 with quasi-statically obtained values. Dynamic failure strains recorded (using the RamGun) range from two to five times greater than static failure strains, with the difference being a function of the joint design. Dynamic failure properties produced by the RamGun are representative of real-world conditions and are generated at approximately 1% the cost and a fraction of the time of ballistically-tested wingboxes. This test series demonstrated that the RamGun can be used with confidence to perform comparative testing, design down-selection, and failure metrics for competing joint concepts.

9 REFERENCES

1. Hinrichsen, R., Dynamic Loading Methodologies, JASPO-V-1-05-0001, 1995.
2. Soni, S.R., Strain Rate Effects in Ballistic Analyses of Bonded and Co-Cured Composite Structures, AFRL-ML-WP-TR-2005-4195, October 2005.
3. Salvatore, L., Battle Damage Tolerant Composite Wing Structure, JTCG/AS-96-V-004, 1996.

APPENDIX A: Instrumentation and Test Parameters

Kistler pressure-sensor parameters (used in each test) and a review of recorded test parameters are presented in Tables A.1 and A.2, respectively.

Table A.1: Kistler Pressure Sensor Parameters

		Kistler Info								
		Location	Type	S/N	Range	Sensitivity mV/psi	Cal'ed	Temp degC		Sensitivity psi/V
P-V tests	Tests 1&2	Inside Kistler	211B2	C115892	5K	1.013	5/28/04 CWL	-55 - 120	<± 1% FSO	987.17
		End Kistler	211B2	C115889	5K	1.068	5/28/04 CWL	-55 - 120	<± 1% FSO	936.33
	Tests 3	Inside Kistler	211B1	59459	10K	0.557	8/17/04 HK			1795.33
		End Kistler	211B1	53805	10K	0.505	8/17/04 HK			1980.20
	Tests 4-10	Inside Kistler	211B2	C115889	5K	1.068	5/28/04 CWL	-55 - 120	<± 1% FSO	936.33
		End Kistler	211B2	C59503	5K	1.052	5/26/04 CWL	-55 - 120	<± 1% FSO	950.57
Actual Specimen tests	Test 1	Inside Kistler	211B2	C115889	5K	1.068	5/28/04 CWL	-55 - 120	<± 1% FSO	936.33
		End Kistler	211B2	C59503	5K	1.052	5/26/04 CWL	-55 - 120	<± 1% FSO	950.57
	Tests 2&3	Kistler 1	211B2	C3117	5K	1.036	5/28/04 CWL	-55 - 120	<± 1% FSO	965.25
		Kistler 2	211B1	59459	10K	0.557	8/17/04 HK			1795.33
		Kistler 3	211B2	C59503	5K	1.052	5/26/04 CWL	-55 - 120	<± 1% FSO	950.57
	Tests 4-31	Kistler 1	211B2	C117152	5K	1.061	9/28/04 HK	-55 - 120	<± 1% FSO	942.51
		Kistler 2	211B1	59459	10K	0.557	8/17/04 HK			1795.33
		Kistler 3	211B2	C59503	5K	1.052	5/26/04 CWL	-55 - 120	<± 1% FSO	950.57
	Tests 32-44	Kistler 1	211B2	C117152	5K	1.061	9/28/04 HK	-55 - 120	<± 1% FSO	942.51
		Kistler 2	211B2	C9031	5K	1.04	9/28/04 HK	-55 - 120	<± 1% FSO	961.54
		Kistler 3	211B2	C59503	5K	1.052	5/26/04 CWL	-55 - 120	<± 1% FSO	950.57
	Plastic Tests 1-10	Kistler 1	211B2	C117152	5K	1.061	9/28/04 HK	-55 - 120	<± 1% FSO	942.51
		Kistler 2	211B1	59459	10K	0.557	8/17/04 HK			1795.33
		Kistler 3	211B2	C59503	5K	1.052	5/26/04 CWL	-55 - 120	<± 1% FSO	950.57

Table A.2: Recorded Test Parameters

Test #	Code #	Test Date	Valve Pressure (psi)	Puck Vel. (fps)	Ram Pressure Kistler 1 (psi)	Time of Peak, Kistler 1 (msec)	Ram Pressure Kistler 2 (psi)	Time of Peak, Kistler 2 (msec)	Ram Pressure Kistler 3 (psi)	Time of Peak, Kistler 3 (msec)	Specimen Weights (grams)	Gas Type	Avg Peak Press. (psi)	Blow-out Mat'l	Comments on specimen
1	1a	9-Sep-04	225						-		108	He		Poly	Velocity is inaccurate; Zero time estimated using speed of sound in water from side kistler
2	1b	20-Sep-04	228	1012	1079	1.192	555	1.302	1108	1.188	113	He	718	Poly	Specimen did not completely fail. T-section was still attached to center piece.
3	1c	22-Sep-04	226	923	3202	1.189	3612	1.215	3468	1.231	105	He	3471	Poly	
4	2a	12-Oct-04	225		-		-		-		221	He		Poly	Timebase on Nicolet was not set correctly; Data collected was not accurate.
5	2b	13-Oct-04	226	1006	2729	1.32	3098	1.326	2959	1.32	218	He	2814	Poly	
6	2c	13-Oct-04	226	1000	3509	1.299	3649	1.29	3429	1.299	215.5	He	3322	Poly	
7	3a	13-Oct-04	225	1039	2447	1.325	2987	1.343	2575	1.326	170.5	He	2551	Poly	
8	3b	14-Oct-04	227	984	2119	1.356	2403	1.362	2175	1.335	175	He	2130	Poly	
9	3c	14-Oct-04	227		1838	1.315	2237	1.32	1928	1.333	173.5	He	1865	Poly	Event 1 didn't break
10	4a	15-Oct-04	225	974	3266	1.289	3472	1.293	3165	1.287	167.5	He	3239	Poly	
11	4b	18-Oct-04	226	986	2278	1.345	2526	1.359	2276	1.339	171.5	He	2286	Poly	
12	4c	19-Oct-04	225	986	2965	1.277	3325	1.32	2965	1.284	171.5	He	2931	Poly	Kistler 2 pressure is approximated b/c it grounded during the test causing it to rezero
13	5a	20-Oct-04	225	1204	2764	1.36	2832	1.344	2791	1.357	181.5	He	2648	Poly	
14	5b	20-Oct-04	225	994	2395	1.32	2558	1.339	2233	1.339	182.5	He	2231	Poly	SG3 had a bad reading during test
15	5c	20-Oct-04	225	648	1043	1.343	1220	1.349	1110	1.364	182.5	He	1047	Poly	Specimen did not completely fail. T-section was still attached to center piece.

Table A.2: Recorded Test Parameters (continued)

Test #	Code #	Test Date	Valve Pressure (psi)	Puck Vel. (fps)	Ram Pressure Kistler 1 (psi)	Time of Peak, Kistler 1 (msec)	Ram Pressure Kistler 2 (psi)	Time of Peak, Kistler 2 (msec)	Ram Pressure Kistler 3 (psi)	Time of Peak, Kistler 3 (msec)	Specimen Weights (grams)	Gas Type	Avg Peak Press. (psi)	Blow-out Mat'l	Comments on specimen
16	6a	21-Oct-04	226	1012	2206	1.351	2219	1.34	2573	1.364	171	He	2259	Poly	Kistler 2 pressure is approximated b/c it grounded during the test causing it to rezero
17	6b	21-Oct-04	226	906	2065	1.281	2363	1.318	2276	1.285	170	He	1980	Poly	Event 1 didn't break; Velocity estimated
18	6c	22-Oct-04	226	990	2143	1.343	2400	1.378	2148	1.356	172	He	2150	Poly	
19	7a	22-Oct-04	226	1122	2266	1.384	1455	1.4	2361	1.389	104	He	1954	Poly	Specimen pulled thru at bolt hole and didn't fail.
20	7b	27-Oct-04	227	994	1567	1.38	1709	1.399	1430	1.406	103.5	He	1507	Poly	
21	7c	27-Oct-04	225	980	2769	1.332	1550	1.34	2765	1.33	106	He	2283	Poly	
22	8a	28-Oct-04	227	1000	3293	1.322	3642	1.315	3324	1.312	144.5	He	3352	Poly	
23	8b	28-Oct-04	224	411	2378	1.608	3885	1.601	2382	1.58	141.5	He	3084	Poly	Kistler 3 press is approximated b/c it grounded during test; Kist 2 press is high; Velocity inaccurate - Events were switched
24	8c	29-Oct-04	227	990	3225	1.281	3323	1.26	3390	1.285	141.5	He	3108	Poly	First event didn't have a clear signal
25	1d	9-Nov-04	225	1060	2645	1.395	2660	1.415	2447	1.38	106	He	2457	AL	Specimen pulled thru at bolt hole and didn't fail.
26	2d	10-Nov-04	224	852	2236	1.231	2327	1.275	1973	1.246	218	He	1974	AL	SG2 had a bad reading during test
27	2e	12-Nov-04	224	1612	1471	1.299	1581	1.297	1539	1.295	227	He	1504	AL	Velocity is inaccurate; Zero time estimated using speed of sound in water from side kistler
28	6d	12-Nov-04	227	1095	2467	1.34	2451	1.338	2577	1.271	170.5	He	2070	AL	Kistler 2 pressure is approximated b/c it grounded during the test causing it to rezero

Table A.2: Recorded Test Parameters (continued)

Test #	Code #	Test Date	Valve Pressure (psi)	Puck Vel. (fps)	Ram Pressure Kistler 1 (psi)	Time of Peak, Kistler 1 (msec)	Ram Pressure Kistler 2 (psi)	Time of Peak, Kistler 2 (msec)	Ram Pressure Kistler 3 (psi)	Time of Peak, Kistler 3 (msec)	Specimen Weights (grams)	Gas Type	Avg Peak Press (psi)	Blow-out Mat'l	Comments on specimen
29	6e	12-Nov-04	225	1051	2162	1.394	2347	1.422	-	-	168	He	2161	AL	Kist 2 pressure is approximated b/c it grounded during the test causing it to rezero; Kist 3 went out of range
30	5d	15-Nov-04	227	1022	2765	1.282	-	-	2796	1.342	181.5	He	3303	AL	Specimen pulled thru after failure; Kistler 2 did not get a good reading
31	4d	15-Nov-04	224	978	3619	1.289	-	-	3598	1.28	169.5	He	3544	AL	Kistler 2 did not get a good reading
32	4e	15-Nov-04	226	952	3080	1.281	3431	1.277	3218	1.268	173	He	3073	AL	
33	5e	15-Nov-04	227	930	2949	1.262	3265	1.279	3129	1.272	192.5	He	3069	AL	Specimen pulled thru after failure
34	7d	16-Nov-04	225	966	2031	1.349	1988	1.394	1808	1.375	104.5	He	1695	AL	
35	7e	16-Nov-04	224	1020	2676	1.337	2686	1.375	2764	1.353	102	He	2576	AL	
36	3d	22-Nov-04	224	898	2802	1.221	2964	1.238	2796	1.254	187	He	2756	AL	
37	3e	22-Nov-04	226	1071	2021	1.404	2373	1.409	1986	1.454	185	He	2070	AL	
38	8d	22-Nov-04	225	1044	2135	1.378	2567	1.358	2234	1.38	153.5	He	2167	AL	Kistler 2 pressure is approximated b/c it grounded during the test causing it to rezero
39	8e	22-Nov-04	226	968	2378	1.337	2518	1.317	2365	1.291	143	He	2312	AL	
40	9a	24-Nov-04	226	856	2394	1.312	2610	1.333	2498	1.296	85.5	N ₂	2207	AL	
41	9b	24-Nov-04	228	893	1382	1.393	1572	1.419	1483	1.422	85	N ₂	1416	AL	
42	9c	24-Nov-04	224	764	1524	1.336	2168	1.377	1610	1.327	88	N ₂	1512	AL	
43	9d	24-Nov-04	251	906	2246	1.297	3384	1.331	2455	1.334	90	N ₂	2560	AL	
44	9e	24-Nov-04	274	941	1703	1.381	2274	1.387	1648	1.429	86	N ₂	1697	AL	
50	10a	21-Dec-04	300	930	1766	1.317	1659	1.354	1799	1.314	123.5	N ₂	1581	AL	
51	10b	21-Dec-04	300	1024	1896	1.374	1764	1.382	1822	1.368	116.5	N ₂	1735	AL	
52	10c	27-Dec-04	301	937	2464	1.299	2526	1.332	2320	1.318	130	N ₂	2290	AL	

Table A.2: Recorded Test Parameters (continued)

Test #	Code #	Test Date	Valve Pressure (psi)	Puck Vel. (fps)	Ram Pressure Kistler 1 (psi)	Time of Peak, Kistler 1 (msec)	Ram Pressure Kistler 2 (psi)	Time of Peak, Kistler 2 (msec)	Ram Pressure Kistler 3 (psi)	Time of Peak, Kistler 3 (msec)	Specimen Weights (grams)	Gas Type	Avg Peak Press. (psi)	Blow-out Mat'l	Comments on specimen
53	11a	25-Jan-05	182	770	1599	1.346	1673	1.366	1541	1.360	158.4	N ₂	1552	AL	SG1 and 7 bad
59	11b	11-Feb-05	451	1161	3293	1.306	3340	1.305	3452	1.288	158.4	N ₂	3237	AL	SG7 bad
60	11c	22-Feb-05	450	1170	3433	1.342	3372	1.355	3528	1.330	158.4	N ₂	3270	AL	SG7 bad
61	11d	23-Feb-05	450	1222	3558	1.304	3624	1.320	3491	1.310	158.4	N ₂	3383	AL	SG7 and 8 bad

Appendix B: Evaluation of Diaphragm Rupture Resistance on Ram Pressure

In a special study, the effect of diaphragm rupture-resistance on ram pressure accumulation was evaluated. Table B.1 presents a review of test results where aluminum and two thicknesses of UHMWPE diaphragms were evaluated. Conclusions are that, for the diaphragm materials and thicknesses tested, diaphragm rupture-resistance had little effect on overall ram pressure accumulations. These diaphragms also had little influence on ram pressure variance from test to test. Aluminum was the preferred material due to its good mechanical-shear properties. UHMWPE tended to plastically deform and seemingly resist joint-skin flexure and separation from the spar. Figures B.1 and B.2 show typical aluminum and UHMWPE diaphragm failures.

Table B.1: Diaphragm Rupture Evaluation

Test #	Material	Date	Valve Pressure (psi)	Velocity (fps)	Ram Pressure (psi)	Comments on specimen
2	Aluminum Foil	2-Nov-04	226	972	2435	
7	Aluminum Foil	4-Nov-04	226	974	1745	
8	Aluminum Foil	4-Nov-04	224	1087	2979	
9	Aluminum Foil	5-Nov-04	226	1022	2785	
10	Aluminum Foil	5-Nov-04	226	984	3515	AVG=2692
1	UHMWPE .015 thk	2-Nov-04	226	976	3312	
3	UHMWPE .015 thk	2-Nov-04	226	1020	2935	
4	UHMWPE .015 thk	2-Nov-04	226	1556	3374	Velocity seems very high and inaccurate
5	UHMWPE .015 thk	3-Nov-04	226	1006	2905	
6	UHMWPE .015 thk	4-Nov-04	226	992	1935	AVG=2892
11	UHMWPE .125 thk	8-Nov-04	226	1004	3035	
12	UHMWPE .125 thk	8-Nov-04	225	1125	3009	
13	UHMWPE .125 thk	8-Nov-04	226	1055	2856	
14	UHMWPE .125 thk	8-Nov-04	225	984	2139	
15	UHMWPE .125 thk	8-Nov-04	224	980	2945	AVG=2797

AVG 1049 2794

Note: AVG pressure (using joint specimens) was 2575 psi.
AVG velocity (using joint specimens) was 998 f/s.



Figure B.1: Typical failure of an aluminum diaphragm.



Figure B.2: Typical failure of a UHMWPE diaphragm (0.015 thick).

APPENDIX C: Data Analysis for Dynamically-Tested Specimens

This appendix contains the data analysis of each dynamic test conducted. Included for each dynamically-tested specimen are four graphs and an accompanying discussion of the data interpretation. As stated in Section 5, data associated with each specimen is analyzed as follows:

- 1) A pressure vs. time graph is presented to identify the load time interval during which failure most probably occurred. Pressure load uniformity is verified through observation that pressure sensors K1 and K3 are in agreement.
- 2) The SG1 & SG4 vs. time and SG2 & SG3 vs. time graphs are examined during the load time interval as to decide if the pull-off was symmetric or asymmetric.
- 3) The SG2 & SG3 average strain vs. time graph is used to identify the maximum strain (failure strain) attained during the load time interval.

Data results are summarized within the tables of Section 6.

C.1 Specimen Set 1: Cobonded (Stitched)

C.1.1 Dynamic Tests of Specimen Set 1

Specimen 1a, Test 01

The impact velocity reading for test Specimen 1a was inaccurate. Zero time is estimated using the speed of sound in water as derived from Kistler 1. The load interval (and therefore the strain vs. time interval of interest) is approximately 1.15ms to 1.45ms as seen in Figure C.1a.1.

As observed in Figure C.1a.2, during the load time interval of interest, SG1 and SG4 are mostly out of phase (indicative of asymmetric strains on the skin). T-joint failure for Specimen 1a is therefore assumed to be asymmetric.

Similarly, Figure C.1a.3 shows that SG2 and SG3 recordings of spar strains are also out of phase. This supports our assumption of asymmetric failure. Maximum strains (and corresponding times) recorded by SG2 and SG3 are also denoted in Figure C.1a.3.

Figure C.1a.4 shows the averaged SG2 and SG3 strain and time of failure. The maximum average strain for SG2 and SG3 is equated to the joint's failure strain which occurs at 1.263ms with a maximum strain of 0.00190 in/in.

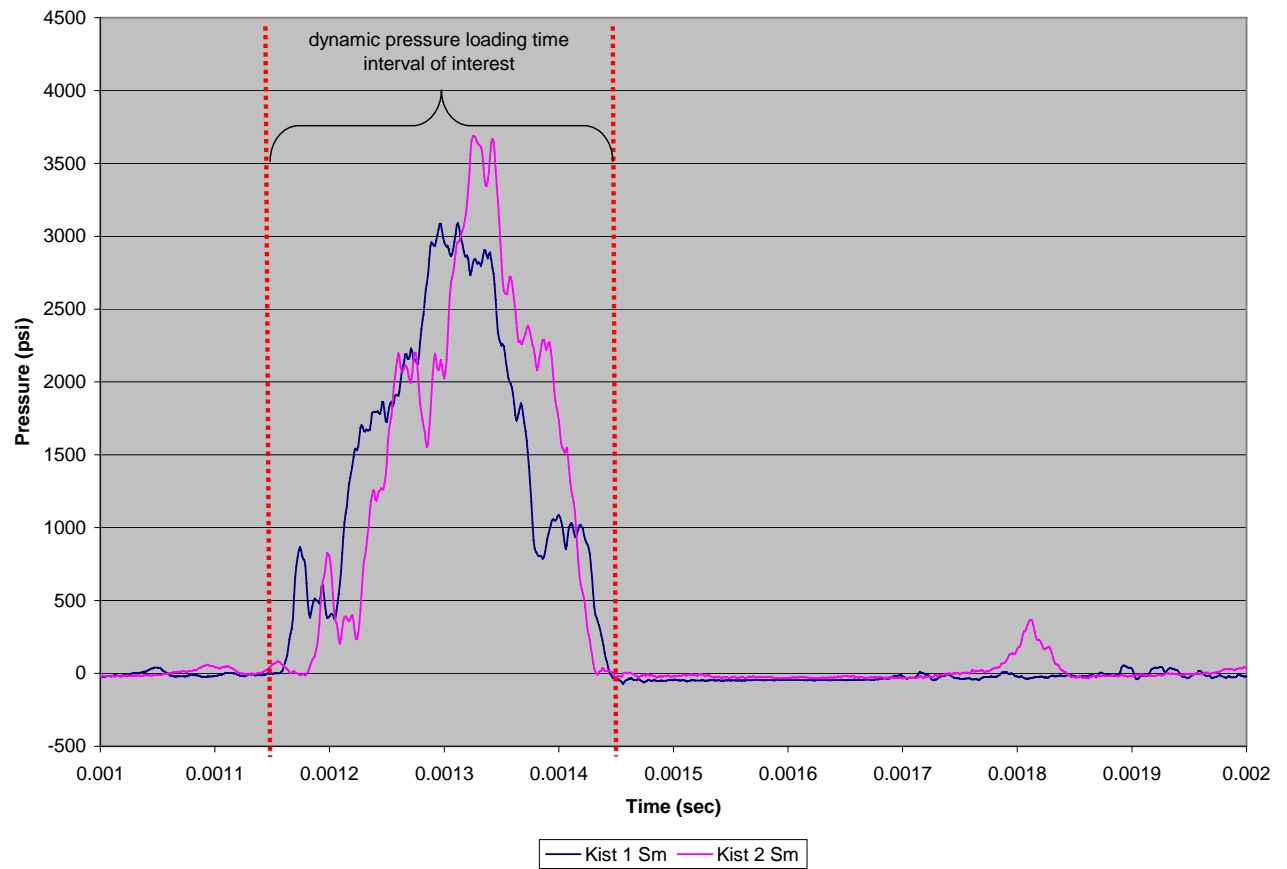


Figure C.1a.1: Kistler pressure vs. time (Specimen 1a)

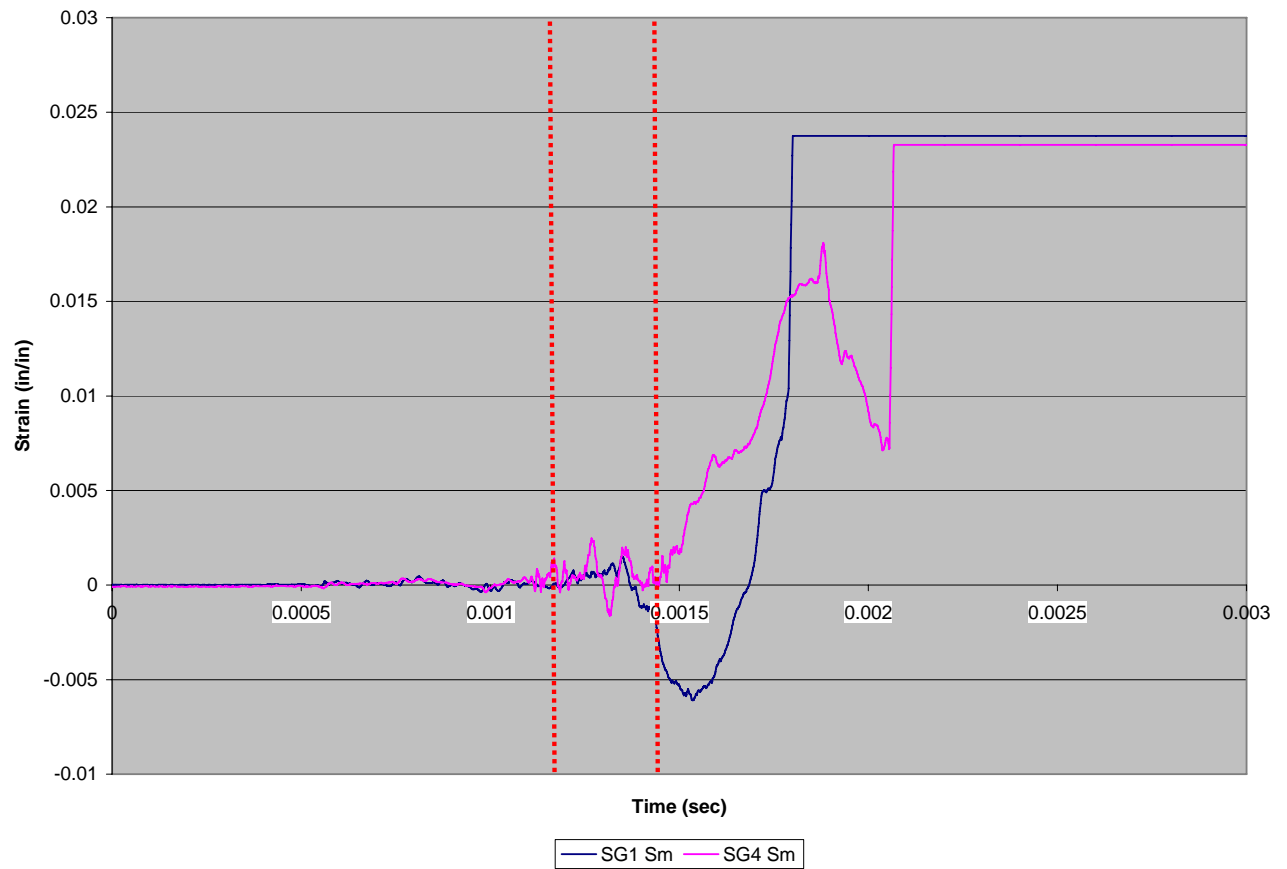


Figure C.1a.2: SG1 & SG4 skin strain vs. time (Specimen 1a)

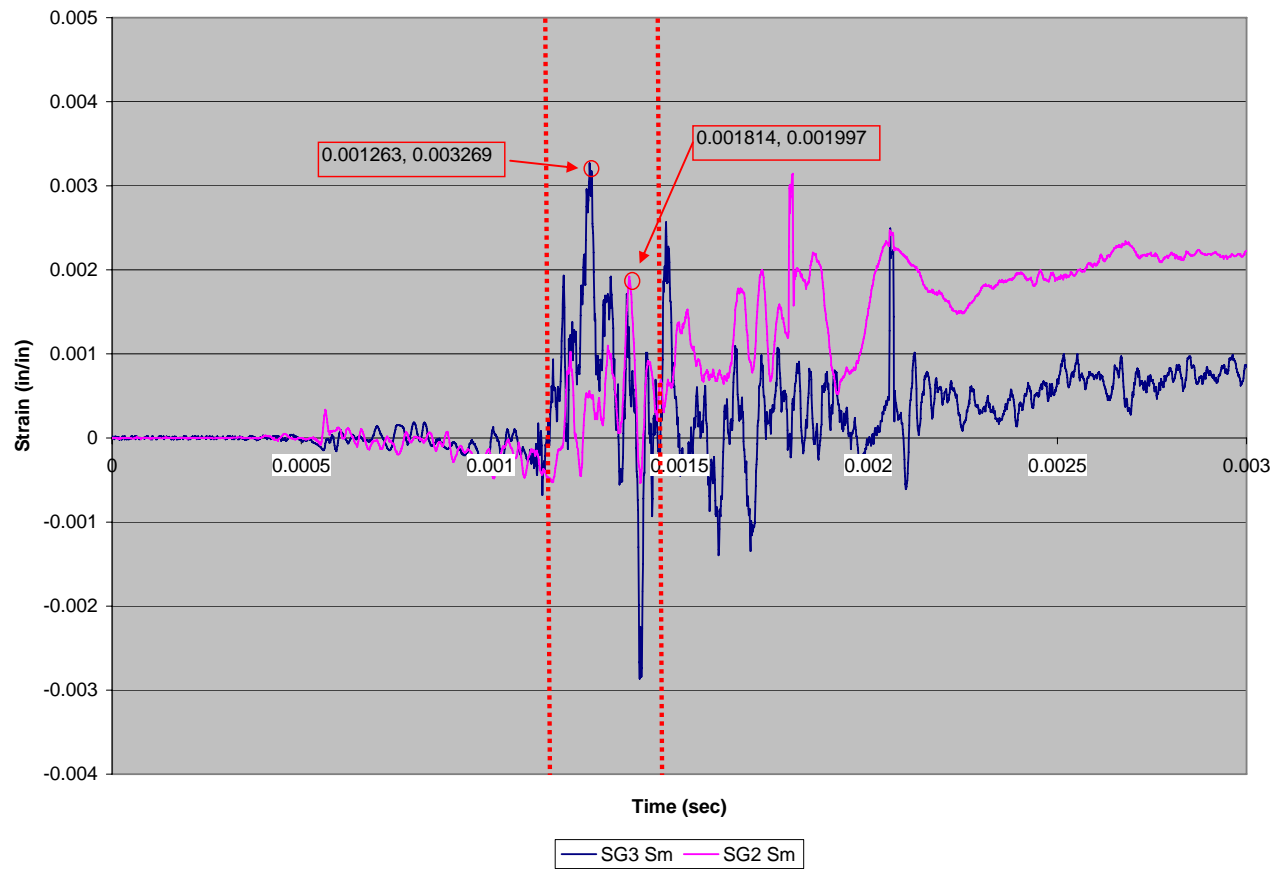


Figure C.1a.3: SG2 & SG3 spar strain vs. time (Specimen 1a)

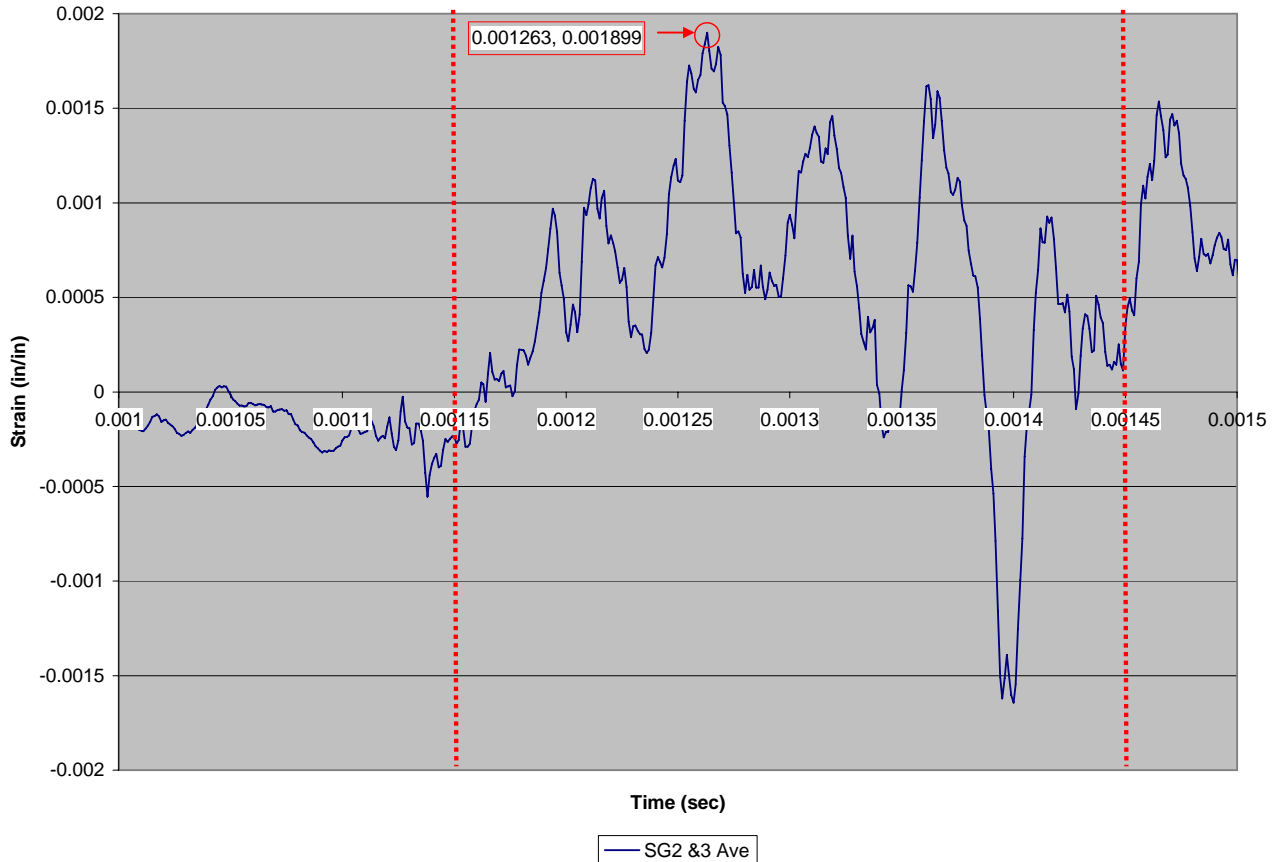


Figure C.1a.4: SG2 & SG3 average spar strain vs. time (Specimen 1a)

Specimen 1b, Test 02

For Specimen 1b, the load interval (and therefore the strain vs. time interval of interest) is approximately 1.10ms - 1.40ms as seen in Figure C.1b.1. As desired, pressure sensors K1 and K3 are largely in agreement, indicating side-to-side uniformity of load on the test specimen. During the load interval, Figure C.1b.2 shows that SG1 and SG4 tend to stay in phase, indicating the skin pulled away from the spar in a symmetric fashion. Conversely SG2 and SG3 appear to be out of phase (as seen in Figure C.1b.3) implying that the spar underwent bending during testing. While either SG2 or SG3 may be in error, evidence of asymmetric failure remains inconclusive. Failure metrics for Specimen 1b is obtained from Figure C.1b.4. Failure strain occurred at 1.117ms with a maximum strain of 0.00355 in/in.

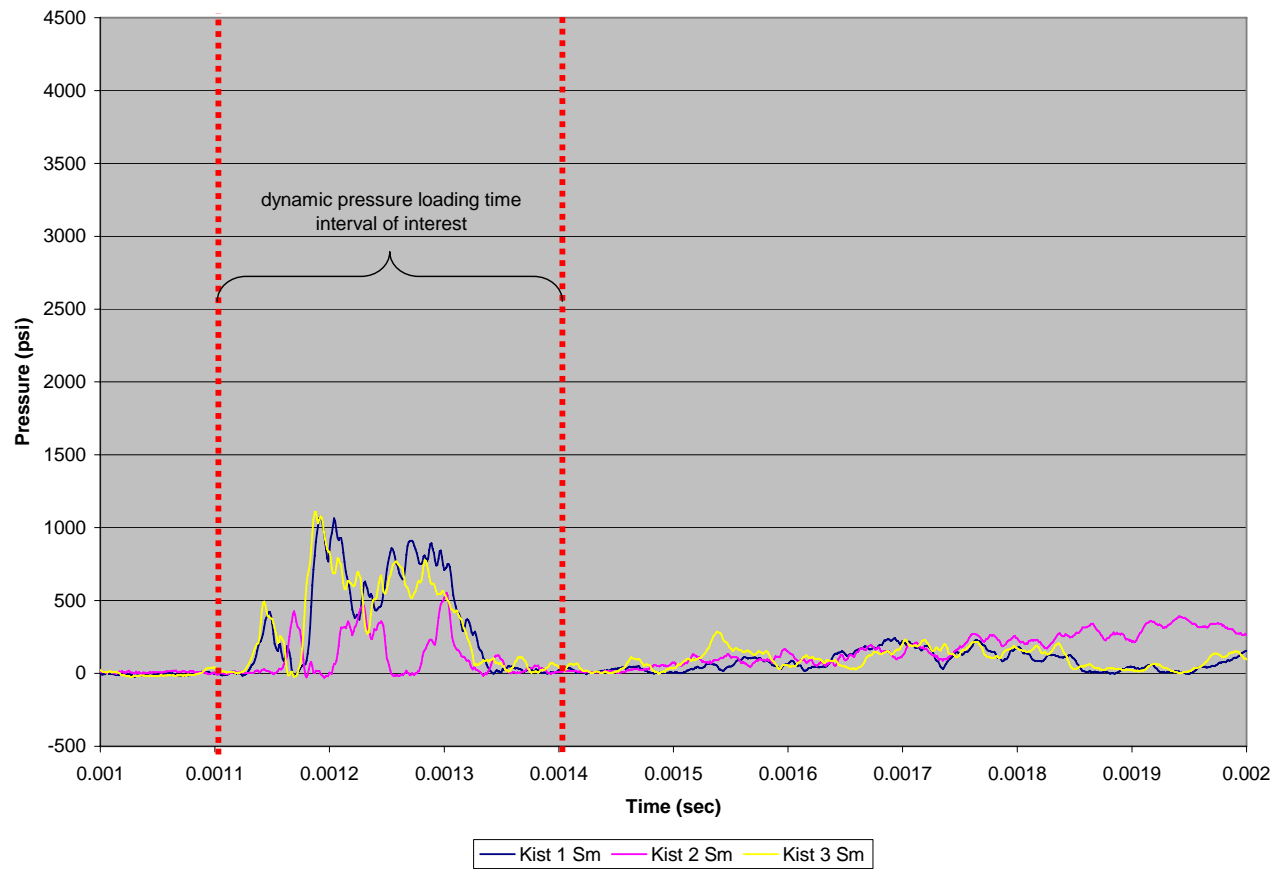


Figure C.1b.1: Kistler pressure vs. time (Specimen 1b)

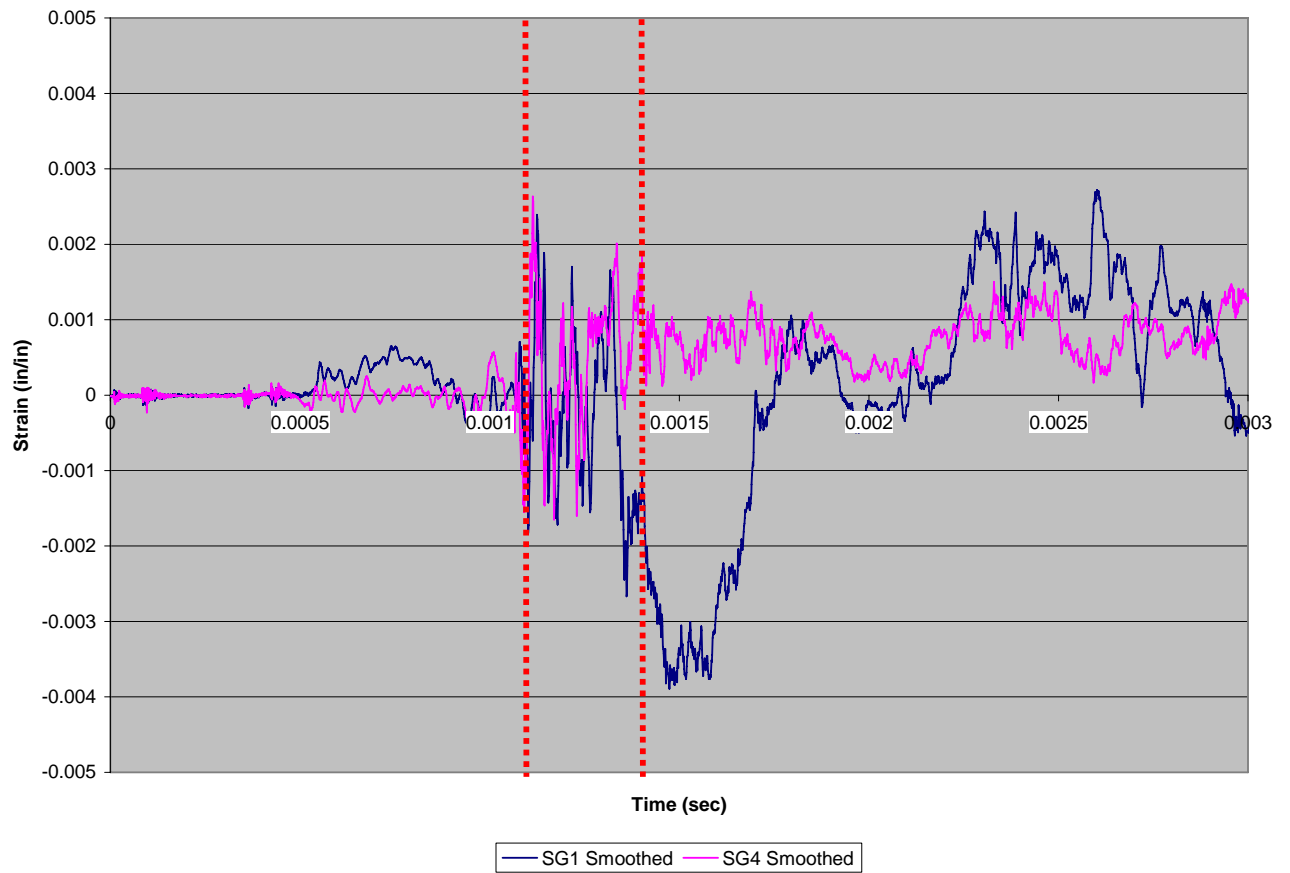


Figure C.1b.2: SG1 & SG4 skin strain vs. time (Specimen 1b)

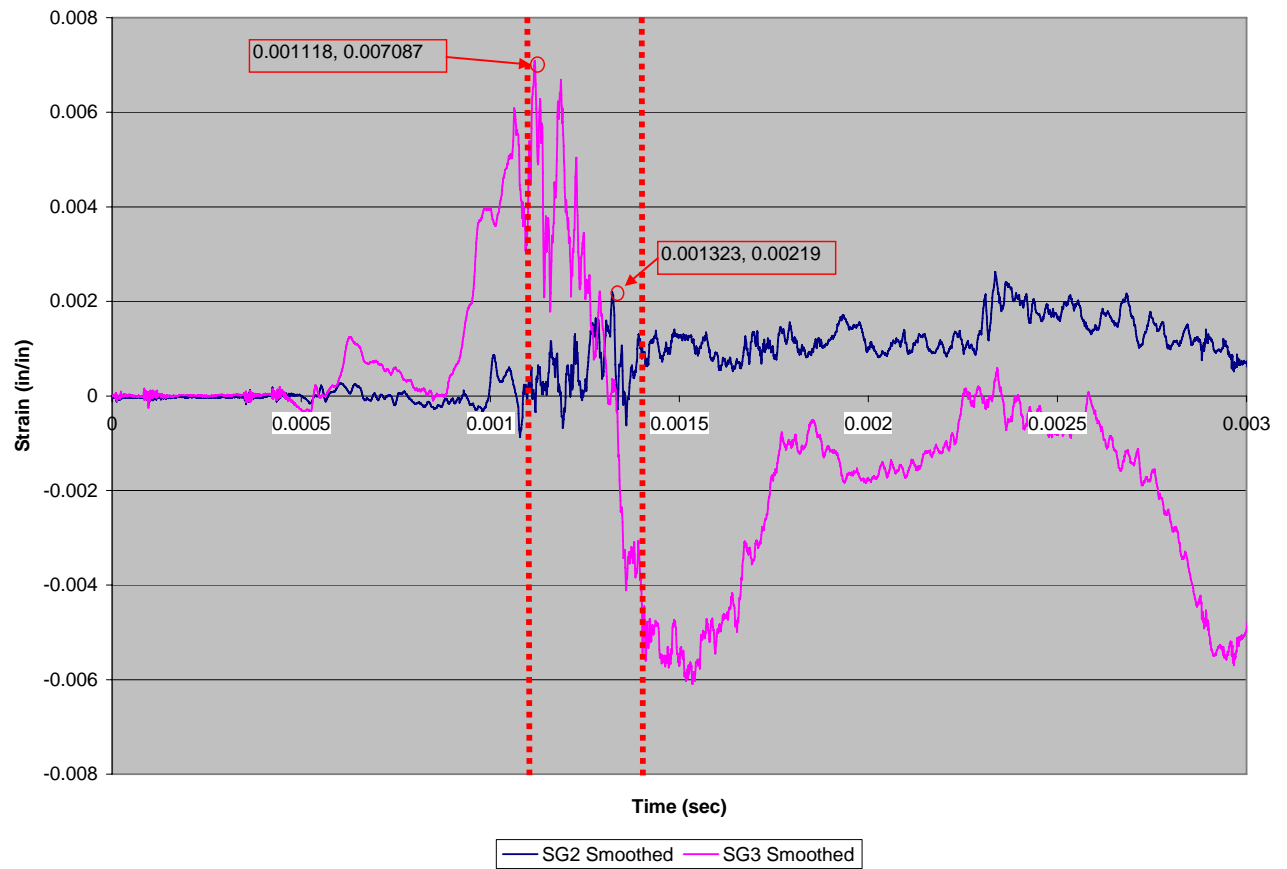


Figure C.1b.3: SG2 & SG3 spar strain vs. time (Specimen 1b)

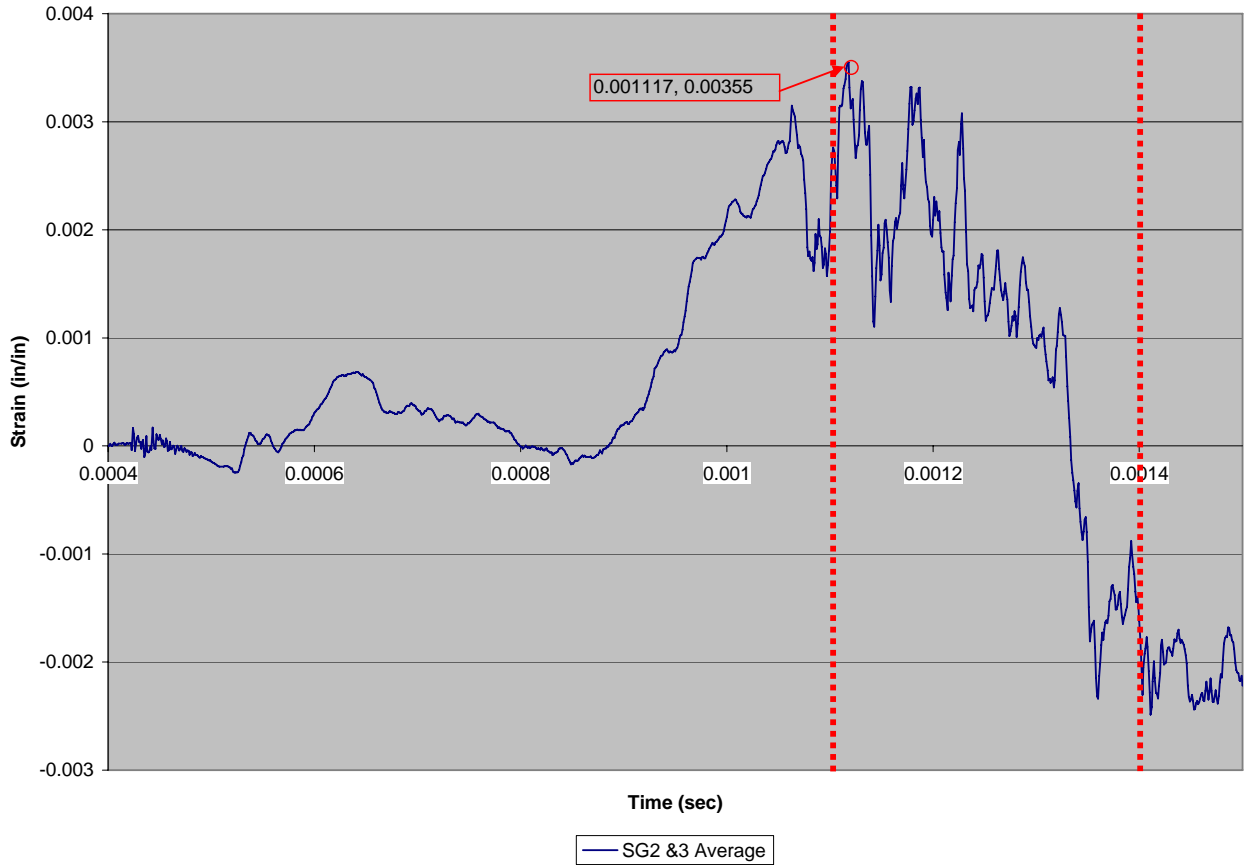


Figure C.1b.4: SG2 & SG3 average spar strain vs. time (Specimen 1b)

Specimen 1c, Test 03

For Specimen 1c, the load interval (and therefore the strain vs. time interval of interest) is approximately 1.05 ms to 1.35ms as shown in Figure C.1c.1. While pressure sensor K1 behaved erratically at times, K1 and K3 are largely in agreement, indicating side-to-side uniformity of load on the test specimen. During the load interval, Figure C.1c.2 shows that SG1 and SG4 are out of phase, indicating the skin pulled away from the spar in an asymmetric fashion. SG2 and SG3 on the spar also appear to be out of phase as seen in Figure C.1c.3. This implies that the spar underwent bending during testing. Failure metrics for Specimen 1c are derived from Figure C.1c.4. Failure strain occurred at 1.169ms with a maximum strain of 0.002507 in/in.

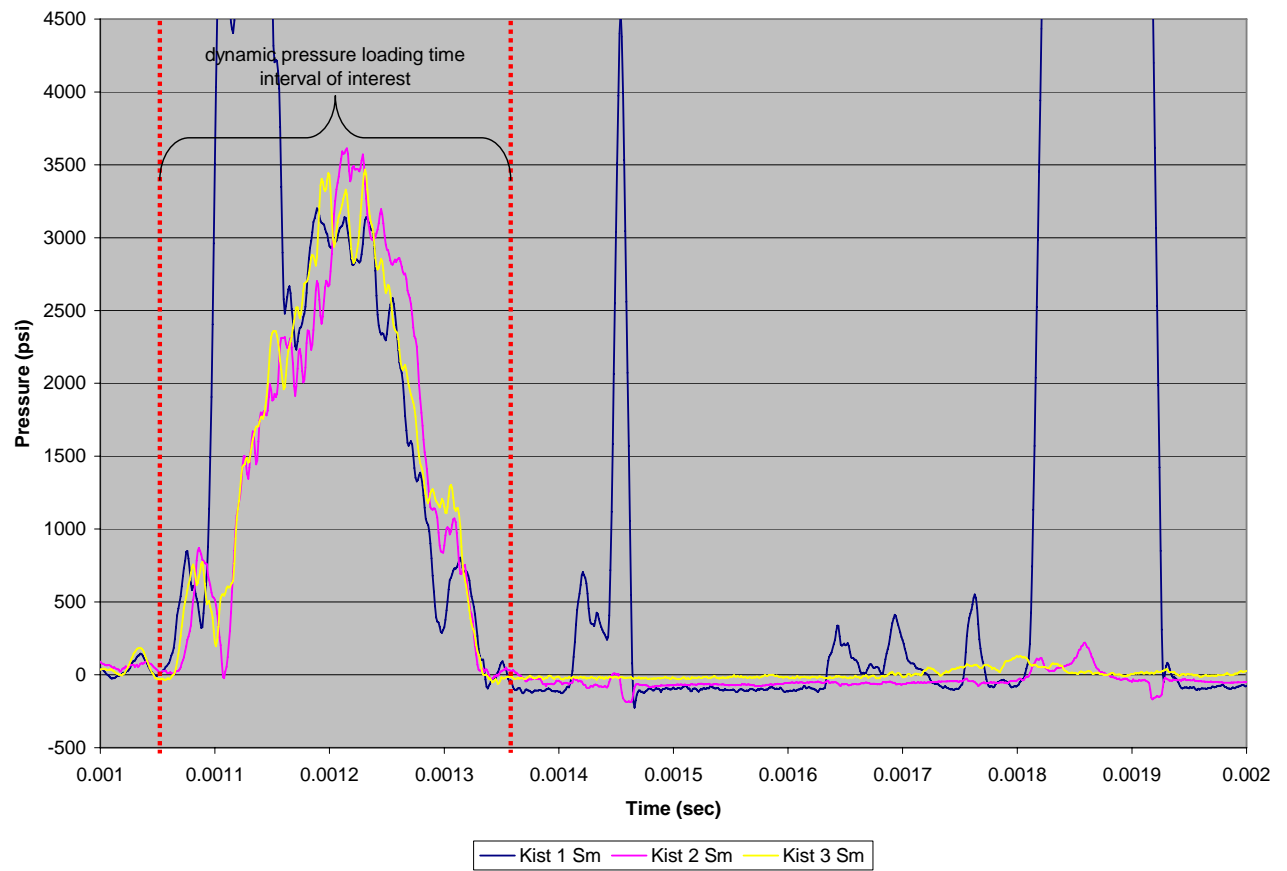


Figure C.1c.1: Kistler pressure vs. time (Specimen 1c)

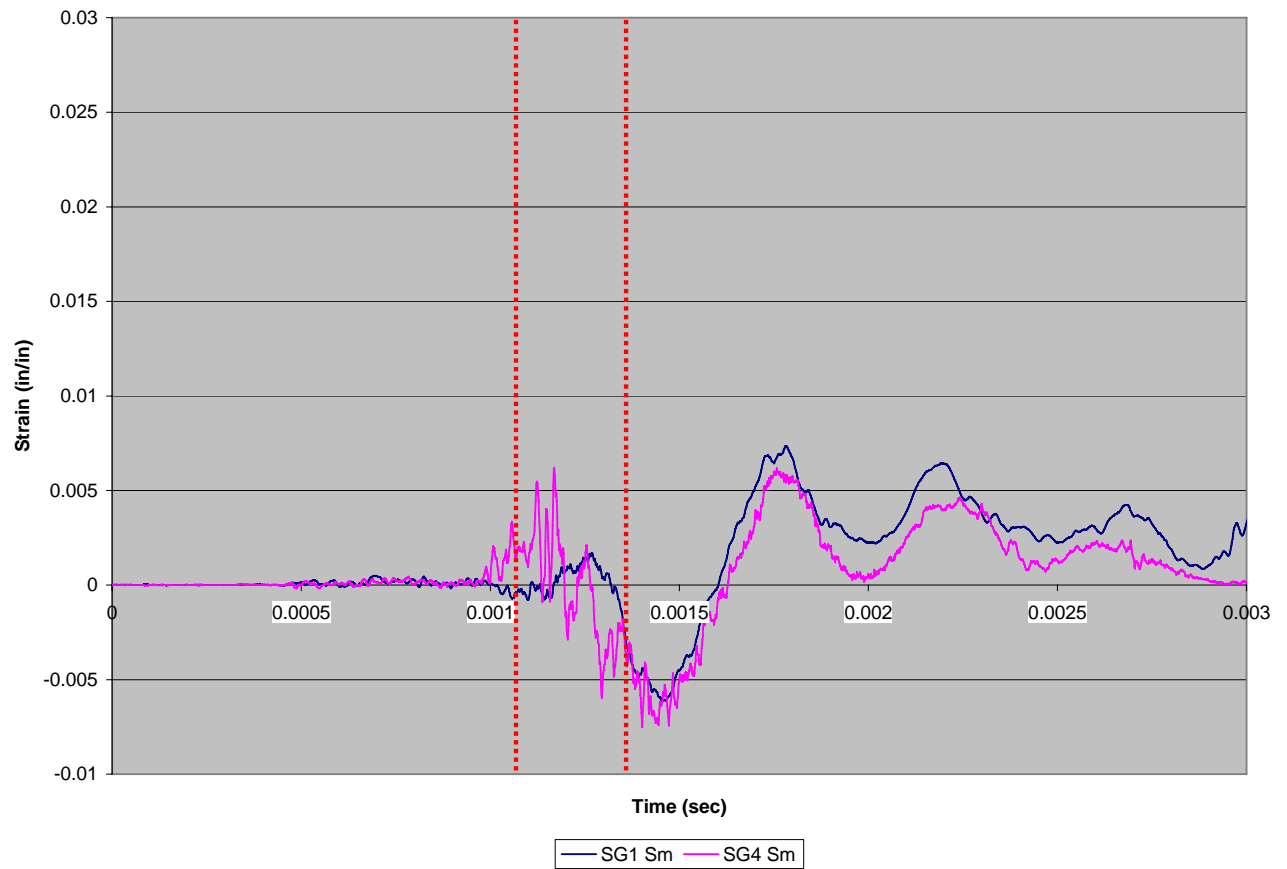


Figure C.1c.2: SG1 & SG4 skin strain vs. time (Specimen 1c)

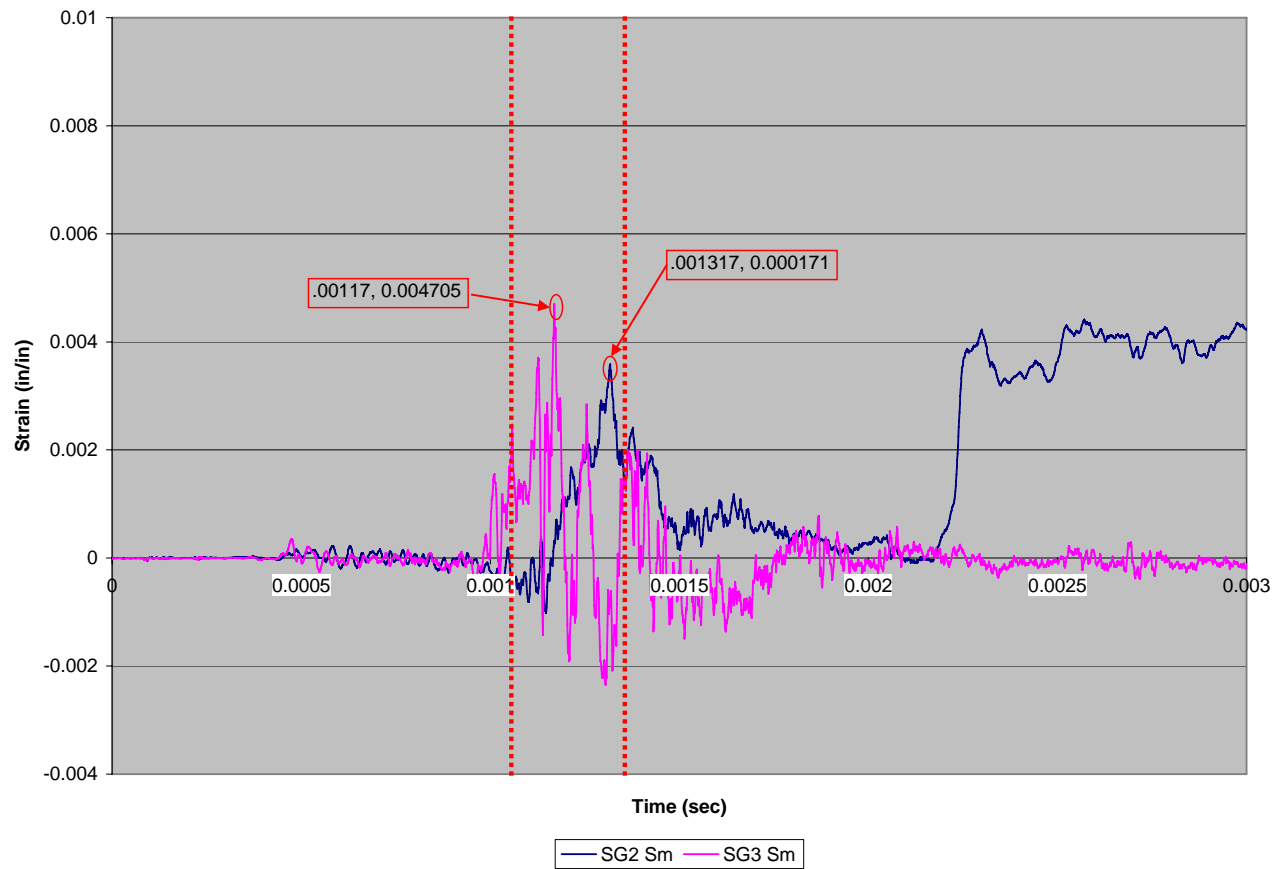


Figure C.1c.3: SG2 & SG3 spar strain vs. time (Specimen 1c)

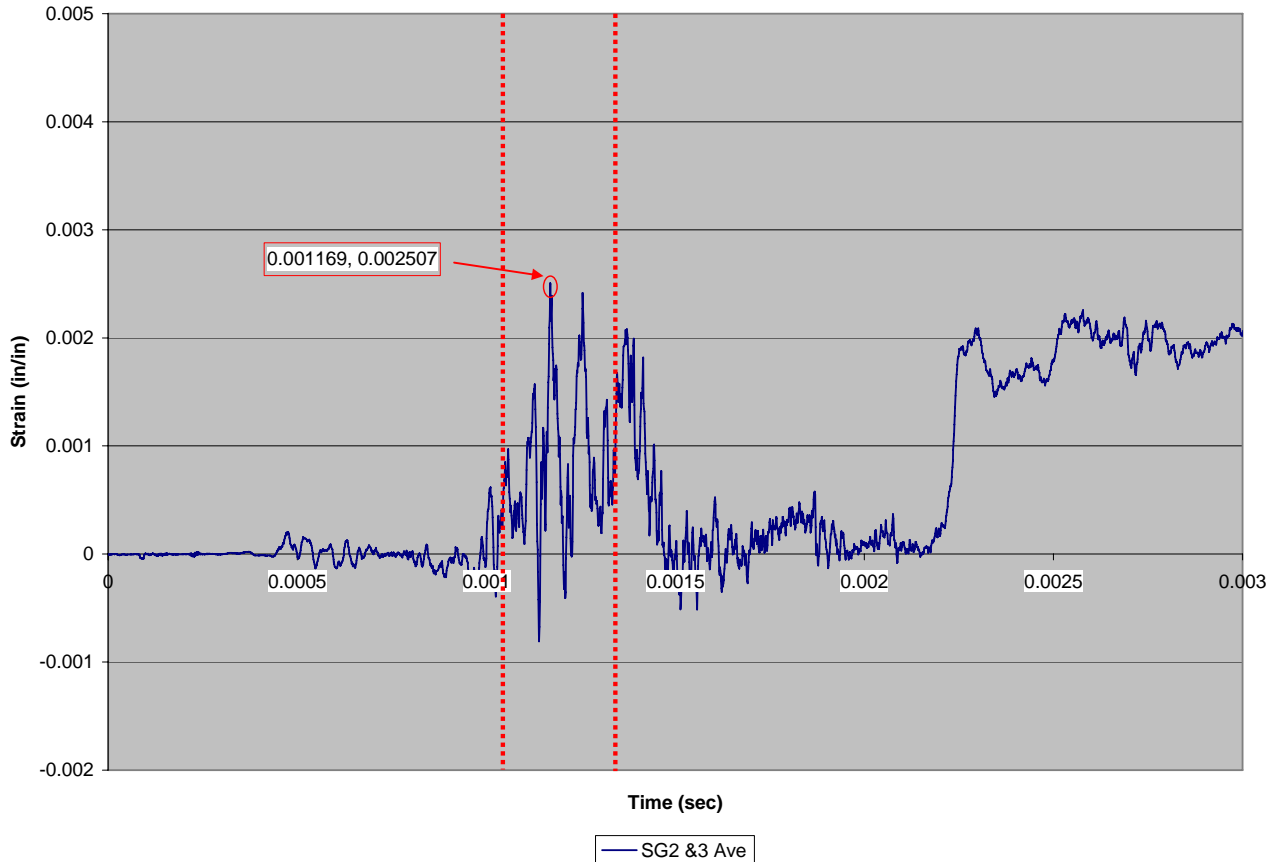


Figure C.1c.4: SG2 & SG3 average spar strain vs. time (Specimen 1c)

Specimen 1d, Test 25

For Specimen 1d, the load interval (and therefore the strain vs. time interval of interest) is approximately 1.20ms-1.60ms as shown in Figure C.1d.1. As desired, pressure sensors K1 and K3 are largely in agreement, indicating side-to-side uniformity of load on the test specimen. During the load interval, Figure C.1d.2 shows that SG1 and SG4 are in phase, but with significantly different amplitudes, through 1.45ms. Similarly, SG2 and SG3 on the spar also appear in phase until 1.45ms, again with significant amplitude differences (as seen in Figure C.1d.3). Although strain recordings are in phase, the significant amplitude differences are indicative of asymmetric failure. Failure metrics for Specimen 1d are derived from Figure C.1d.4. Failure strain occurred at 1.494ms with a maximum strain of 0.005103 in/in.

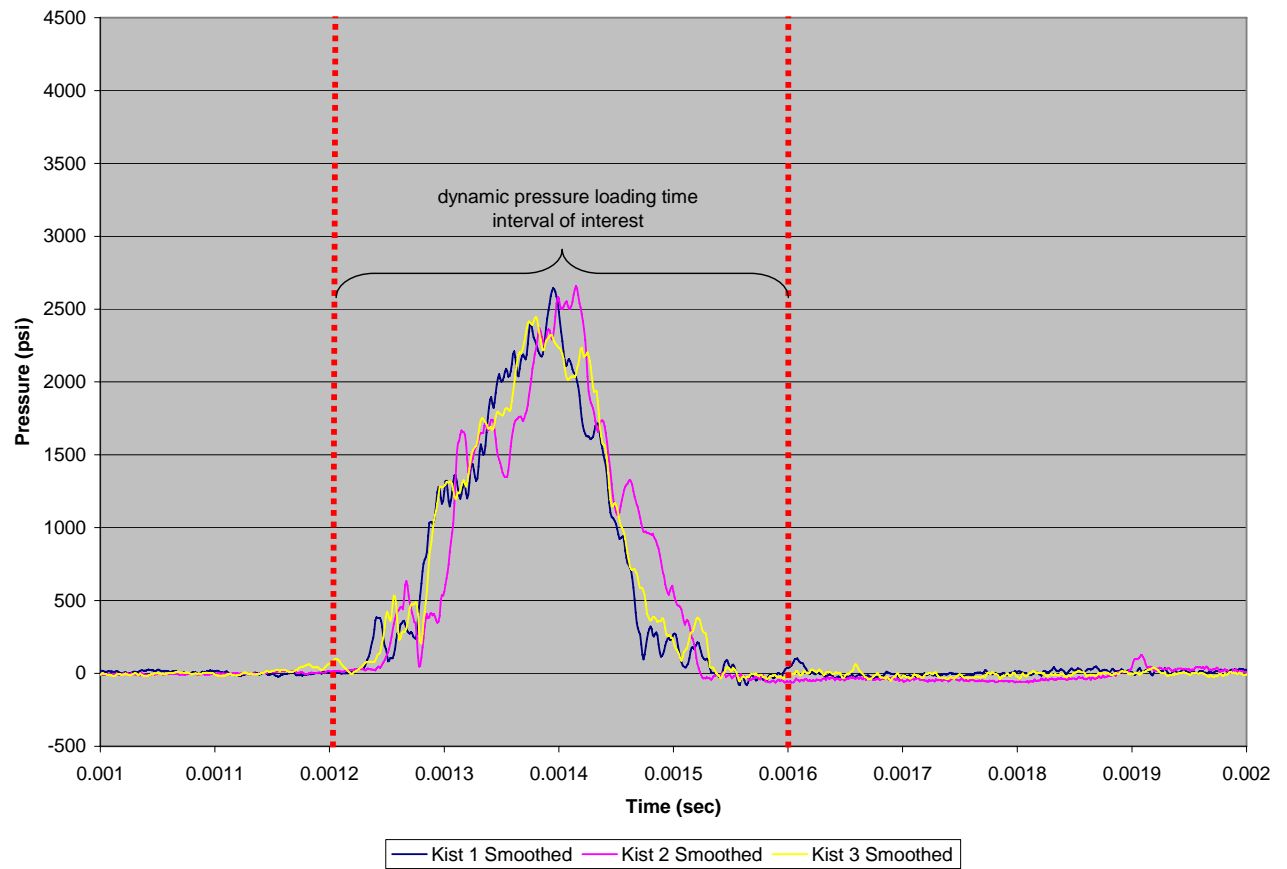


Figure C.1d.1: Kistler pressure vs. time (Specimen 1d)

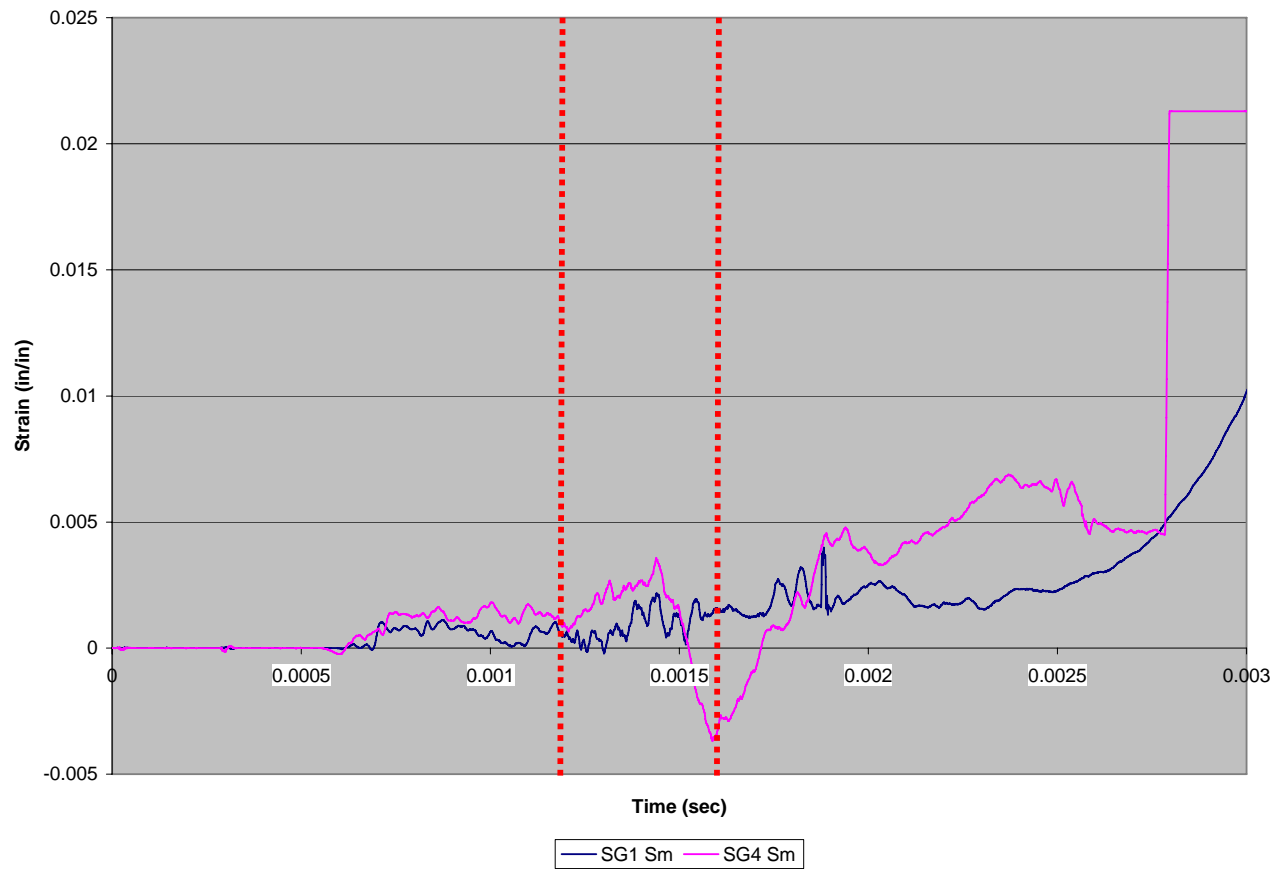


Figure C.1d.2: SG1 & SG4 skin strain vs. time (Specimen 1d)

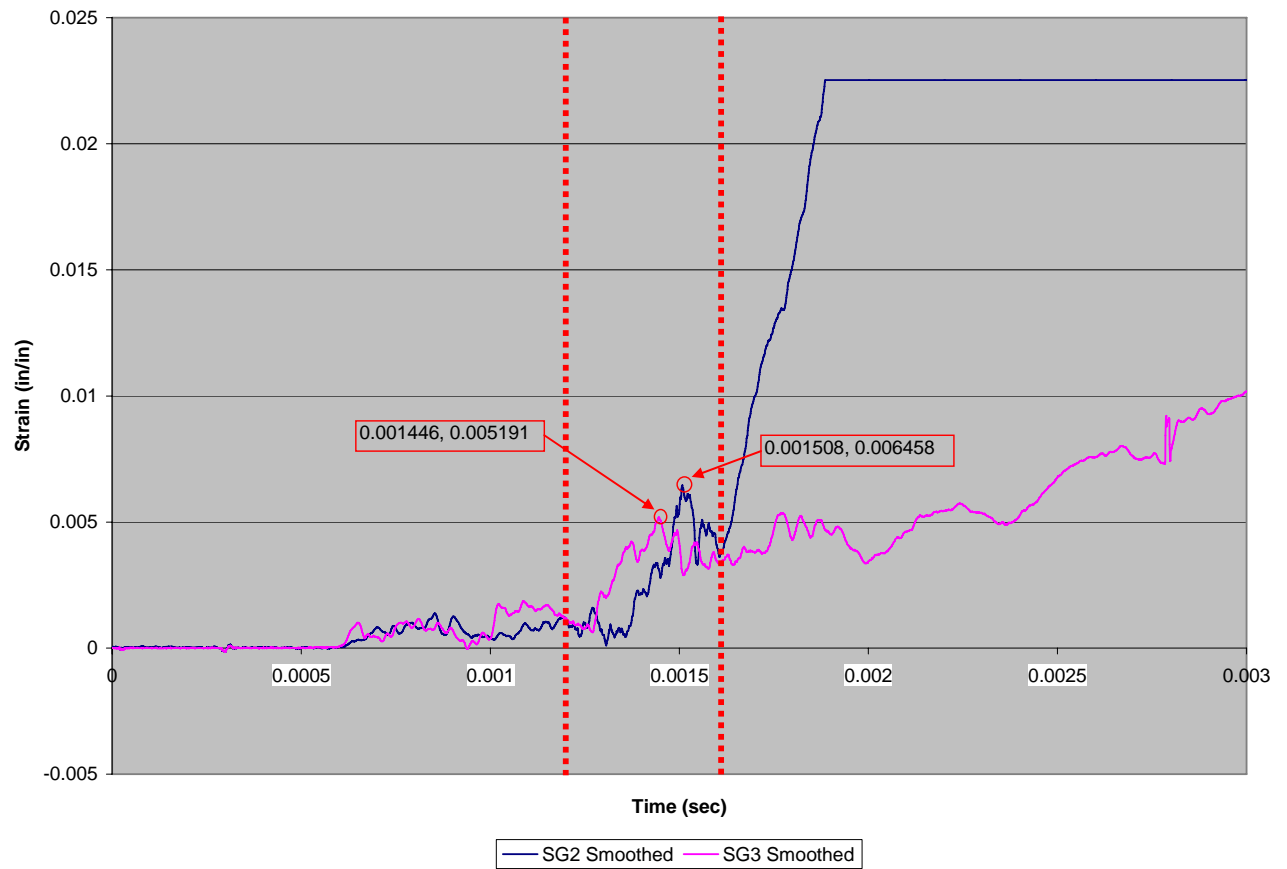


Figure C.1d.3: SG2 & SG3 spar strain vs. time (Specimen 1d)

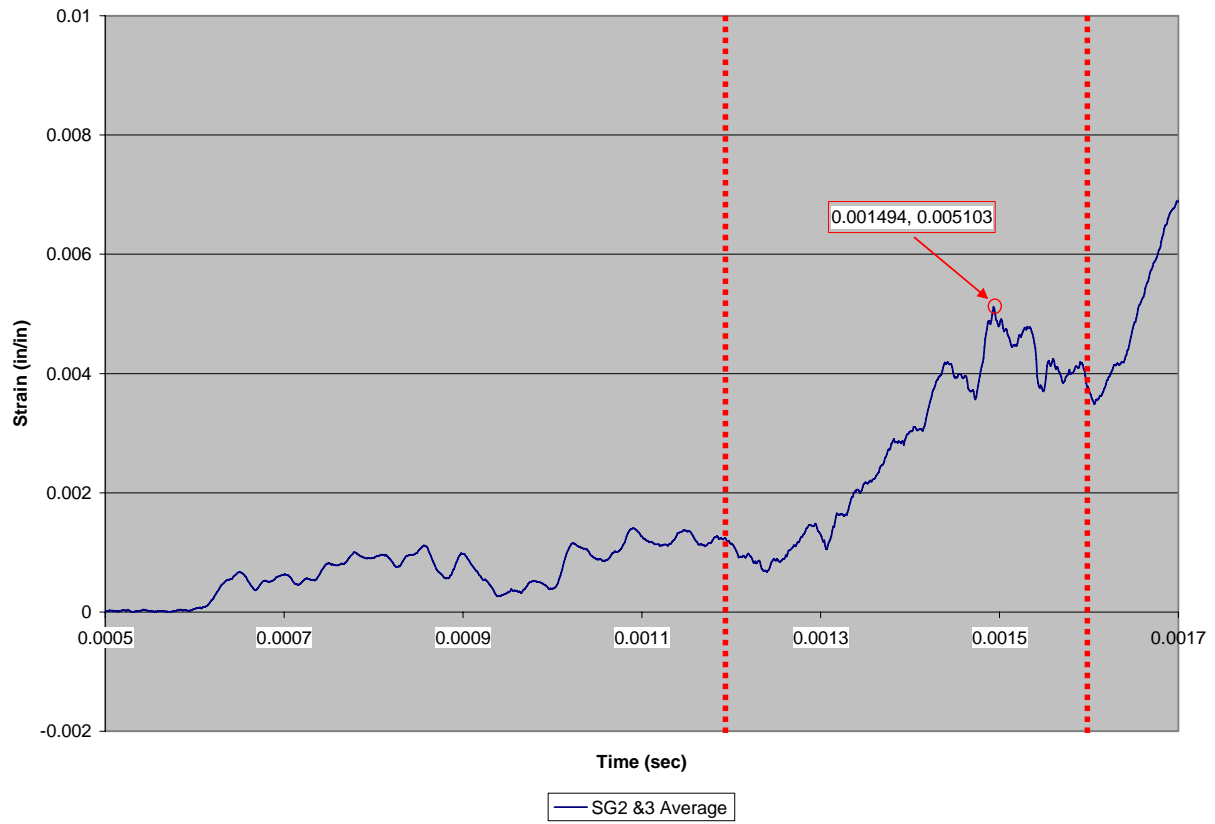


Figure C.1d.4: SG2 & SG3 average spar strain vs. time (Specimen 1d)

C.2 Specimen Set 2: Bolted

C.2.1 Dynamic Tests of Specimen Set 2

Specimen 2a, Test 04

During the conduct of Test 04 (Specimen 2a), the data acquisition system was set-up incorrectly and no data was obtained.

Specimen 2b, Test 05

For Specimen 2b, the load interval (and therefore the strain vs. time interval of interest) is approximately 1.10ms - 1.47ms as seen in Figure C.2b.1. As desired, pressure sensors K1 and K3 are largely in agreement, indicating side-to-side uniformity of load on the test specimen. During this time interval of interest, Figure C.2b.2 shows that SG1 and SG4 tend to stay in phase and of similar amplitude (particularly later in the load cycle) indicating the skin pulled away from the spar in a symmetric fashion. Similarly, SG2 and SG3 appear to be in phase and of similar amplitude (as seen in Figure C.2b.3) implying symmetric failure. Failure metrics for Specimen 2b are derived from Figure C.2b.4. Failure strain occurs at 1.291ms with a maximum strain of 0.00266 in/in.

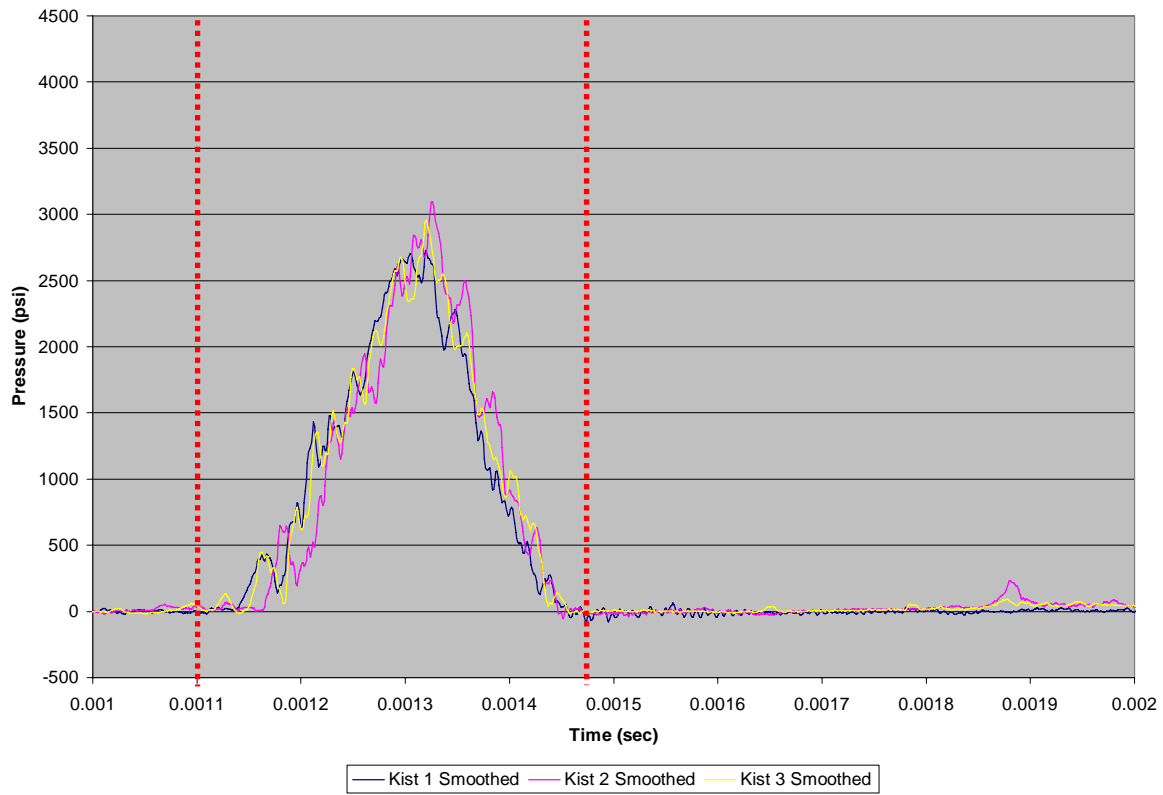


Figure C.2b.1: Kistler pressure vs. time (Specimen 2b)

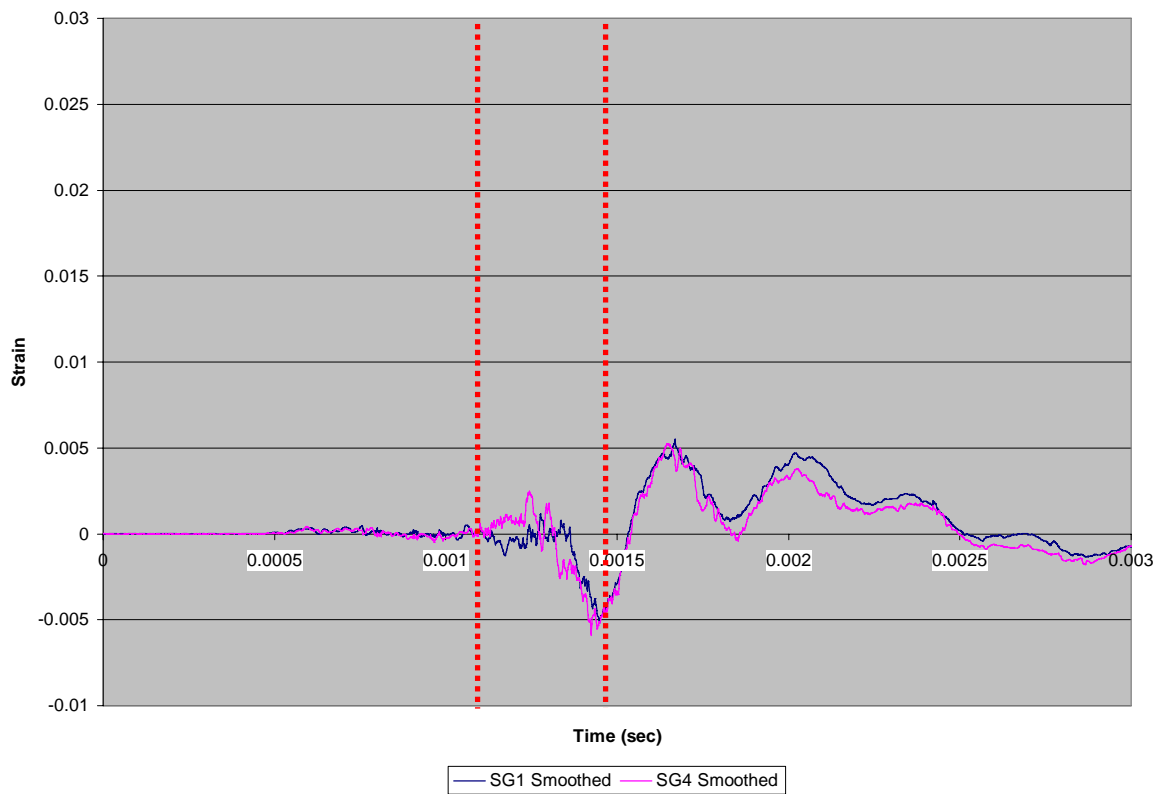


Figure C.2b.2: SG1 & SG4 skin strain vs. time (Specimen 2b)

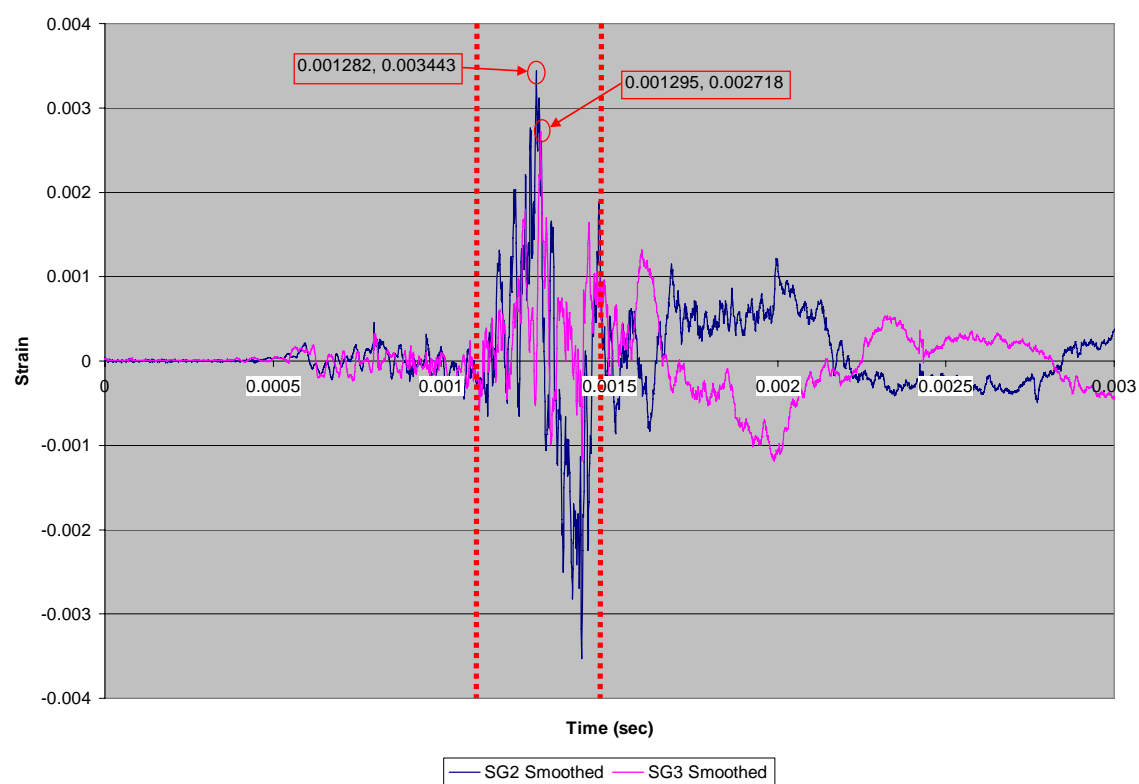


Figure C.2b.3: SG2 & SG3 spar strain vs. time (Specimen 2b)

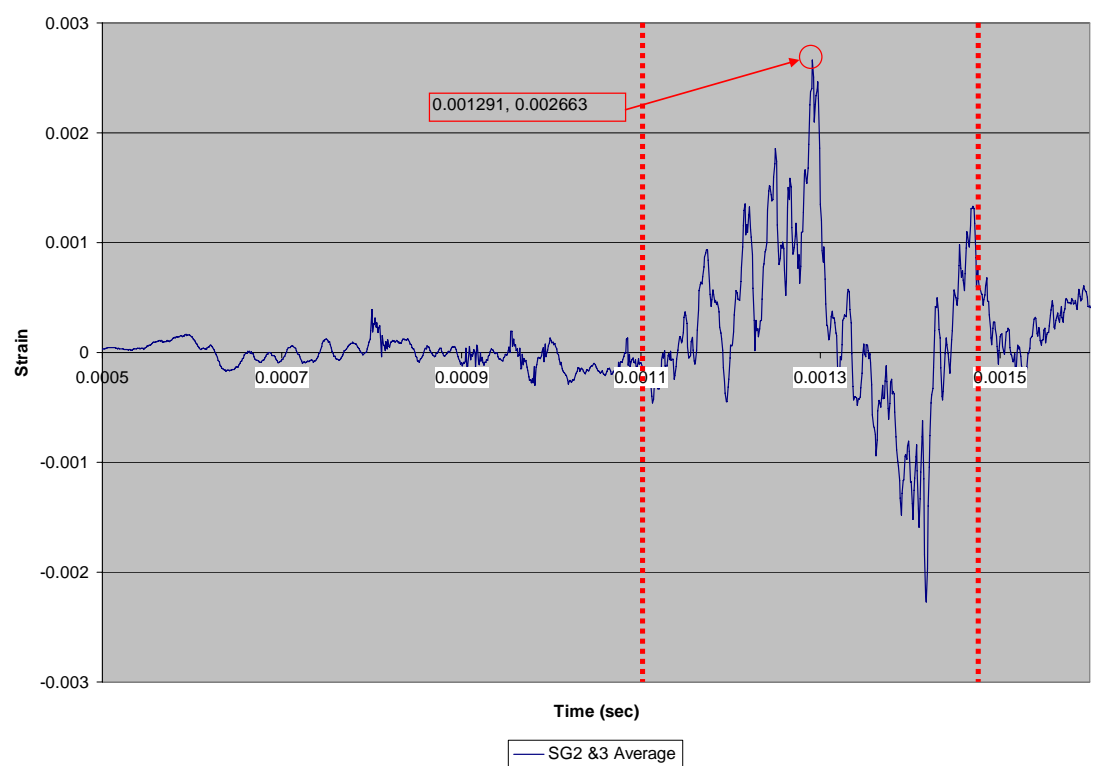


Figure C.2b.4: SG2 & SG3 average spar strain vs. time (Specimen 2b)

Specimen 2c, Test 06

For Specimen 2c, the load interval (and therefore the strain vs. time interval of interest) is approximately 1.10 ms to 1.45ms as shown in Figure C.2c.1. As desired, pressure sensors K1 and K3 are largely in agreement, indicating side-to-side uniformity of load on the test specimen. During this time interval of interest, Figure C.2c.2 shows that SG1 and SG4 are in phase, indicating the skin pulled away from the spar in a symmetric fashion. Conversely, SG2 and SG3 on the spar appear to be out of phase (as seen in Figure C.2c.3). The lack of agreement between strain gage pairs SG1/SG4 and SG2/SG3 suggests that failure symmetry is inconclusive. Failure metrics for Specimen 2c are derived from Figure C.2c.4. Failure strain occurred at 1.272ms with a maximum strain of 0.002745 in/in.

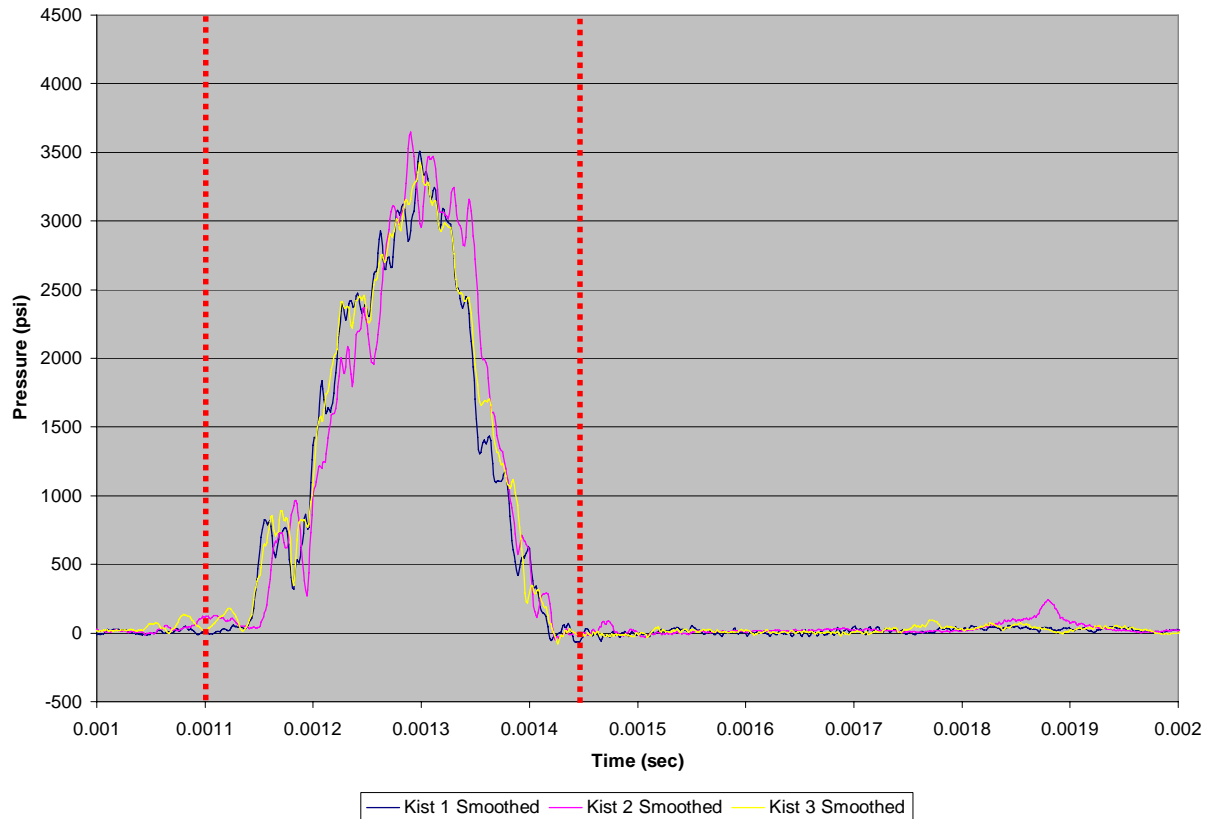


Figure C.2c.1: Kistler pressure vs. time (Specimen 2c)

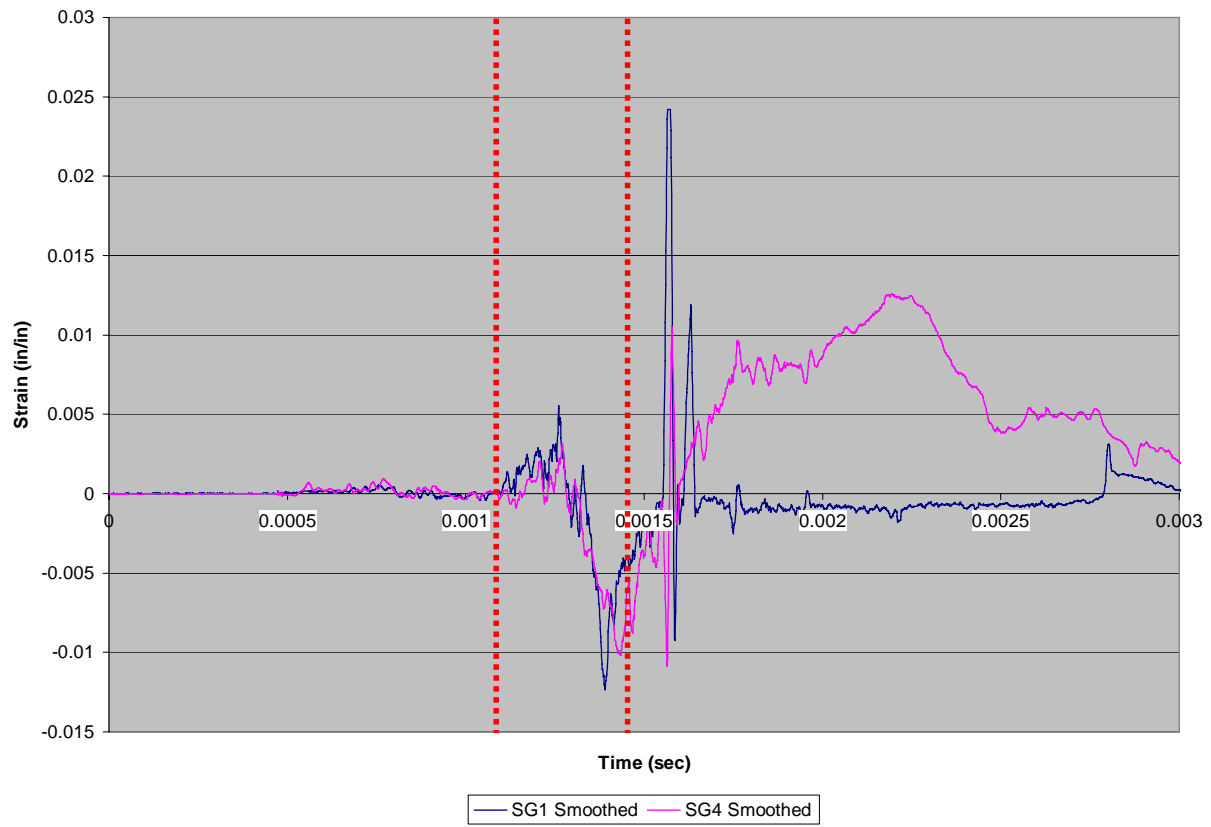


Figure C.2c.2: SG1 & SG4 skin strain vs. time (Specimen 2c)

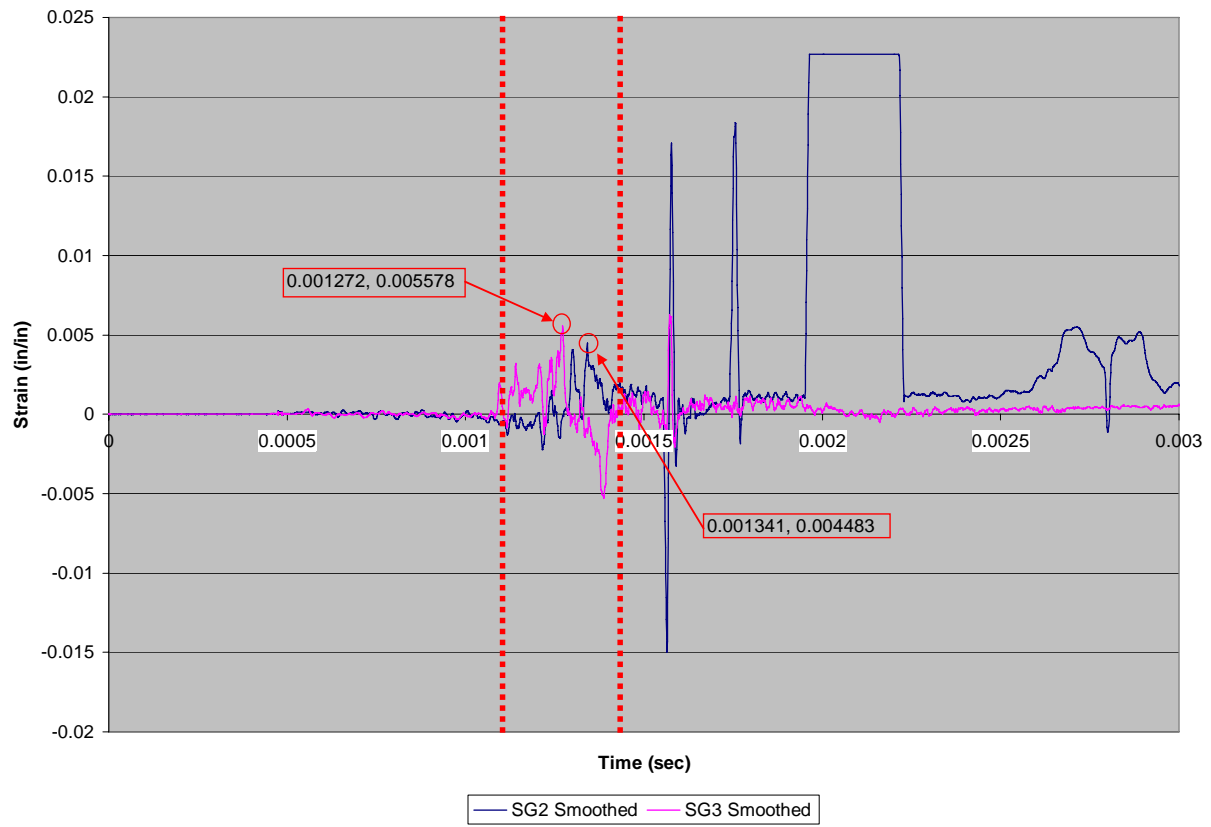


Figure C.2c.3: SG2 & SG3 spar strain vs. time (Specimen 2c)

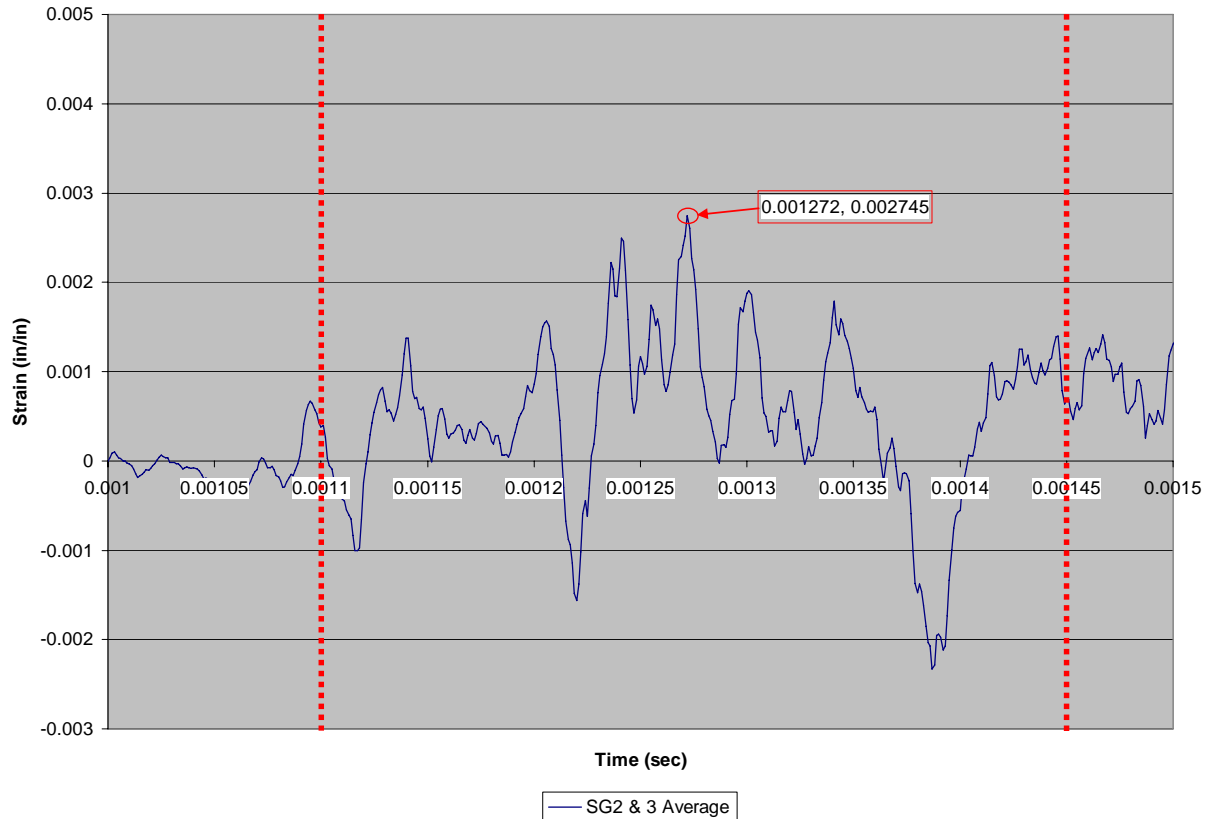


Figure C.2c.4: SG2 & SG3 average spar strain vs. time (Specimen 2c)

Specimen 2d, Test 26

For Specimen 2d, the load interval (and therefore the strain vs. time interval of interest) is approximately 1.09ms-1.40ms as shown in Figure C.2d 1. As desired, pressure sensors K1 and K3 are largely in agreement, indicating side-to-side uniformity of load on the test specimen. During the load interval, Figure C.2d.2 shows that SG1 and SG4 remain roughly in phase until 1.40ms. Afterward, the skin strains appear asymmetric. While SG3 produced good data, SG2 was inoperative (Figure C.2d.3). As such, substantiation of symmetric behavior cannot be made. Furthermore, strains recorded by the SG2/SG3 pair cannot be meaningfully averaged to indicate a fully-reliable failure strain. Based solely on SG3, we therefore estimate that failure strain occurred at 1.215ms with a maximum strain of 0.001818 in/in.

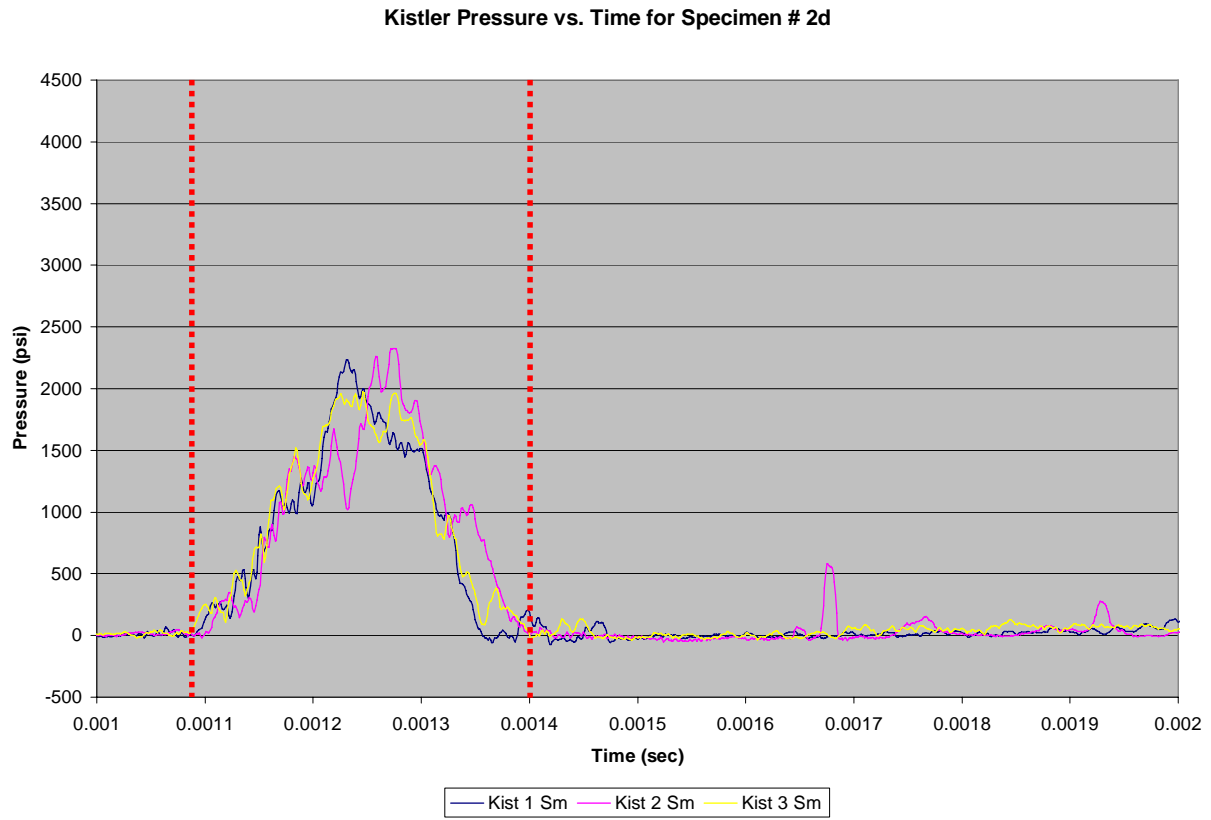


Figure C.2d.1: Kistler pressure vs. time (Specimen 2d)

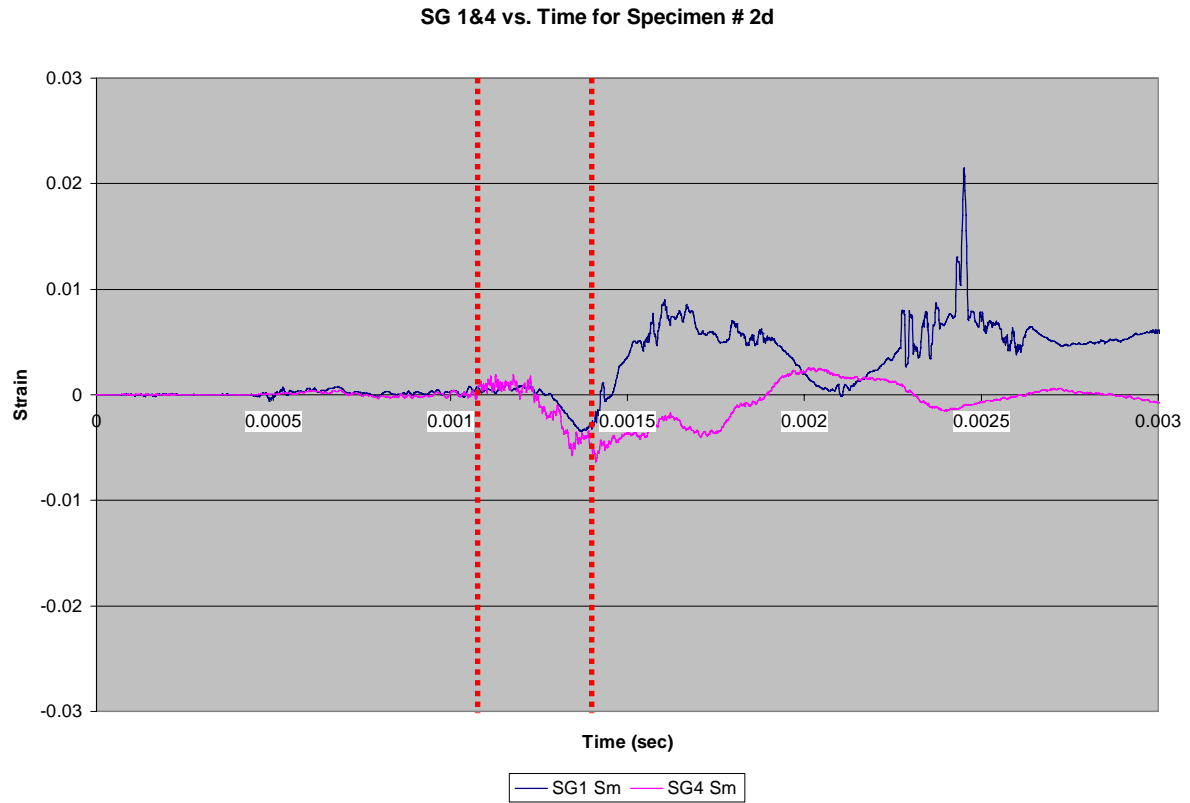


Figure C.2d.2: SG1 & SG4 skin strain vs. time (Specimen 2d)

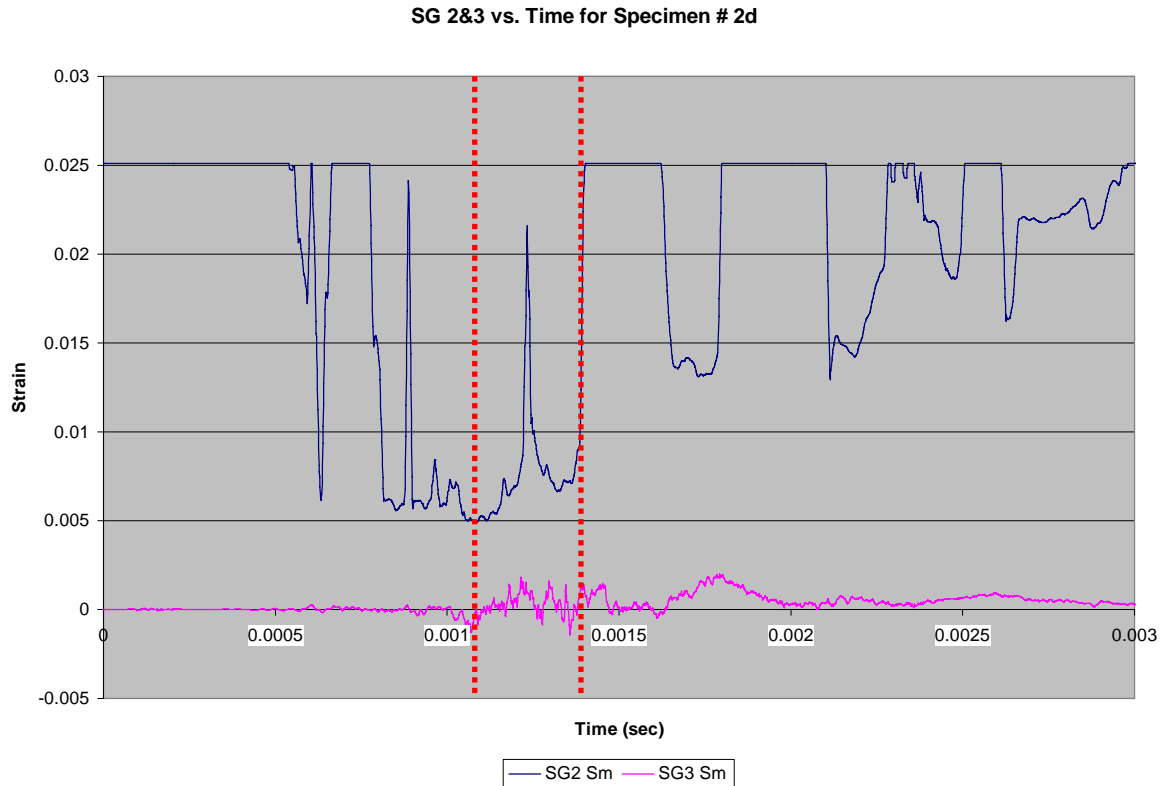


Figure C.2d.3: SG2 & SG3 spar strain vs. time (Specimen 2d)

Specimen 2e, Test 27

For Specimen 2e, the load interval (and therefore the strain vs. time interval of interest) is approximately 1.10ms-1.50ms as shown in Figure C.2e.1. As desired, pressure sensors K1 and K3 are largely in agreement, indicating side-to-side uniformity of load on the test specimen. During the load interval, Figure C.2e.2 shows that SG1 and SG4 remain roughly in phase and of similar amplitude. Similarly, SG2 and SG3 on the spar also appear to remain roughly in phase and of similar amplitude (as seen in Figure C.2e.3) indicating a symmetric failure. Failure metrics for Specimen 2e are derived from Figure C.2e.4. Failure strain occurred at 1.437ms with a maximum strain of 0.001654 in/in.

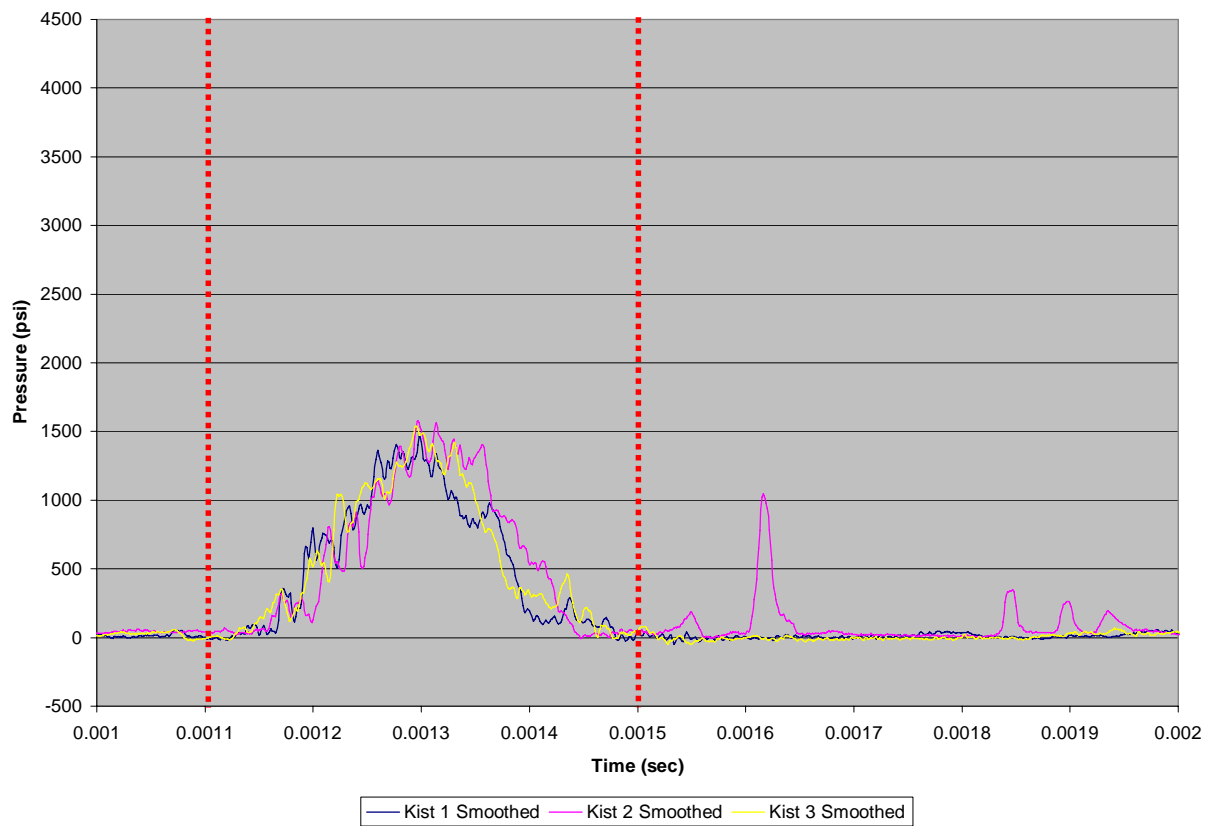


Figure CA.2e.1: Kistler pressure vs. time (Specimen 2e)

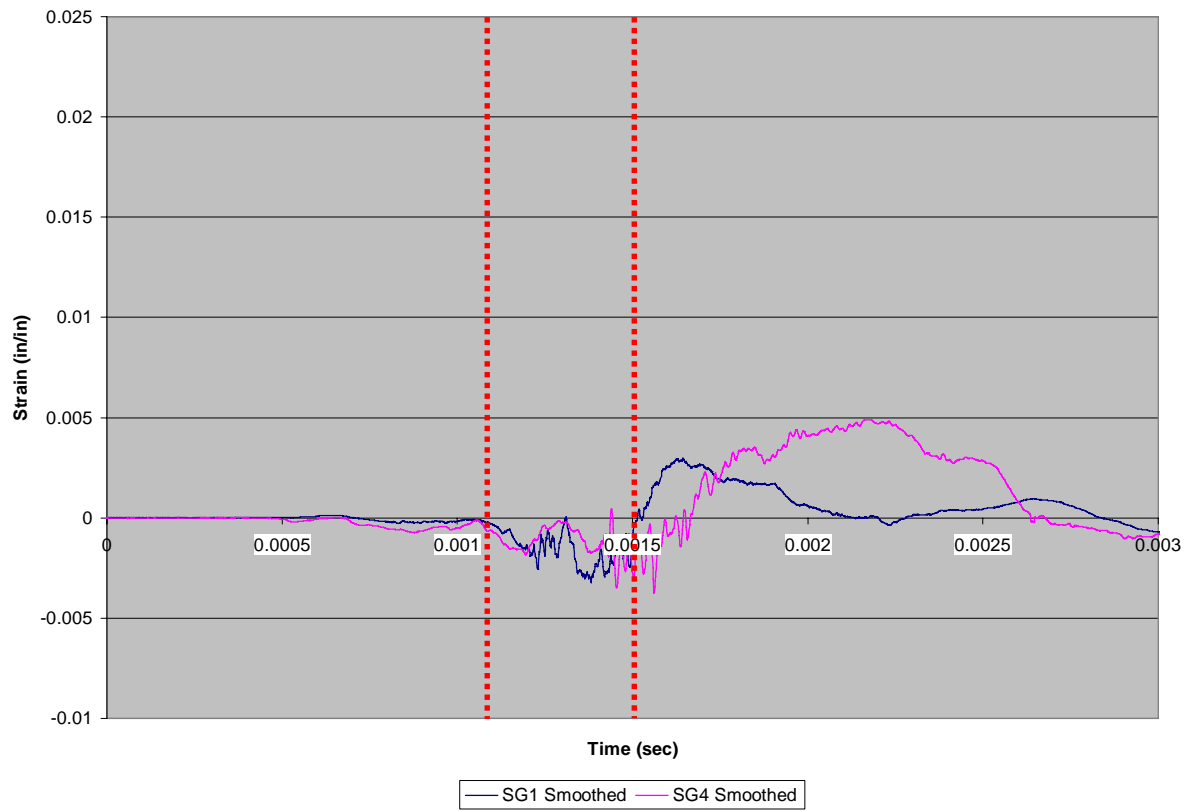


Figure C.2e.2: SG1 & SG4 skin strain vs. time (Specimen 2e)

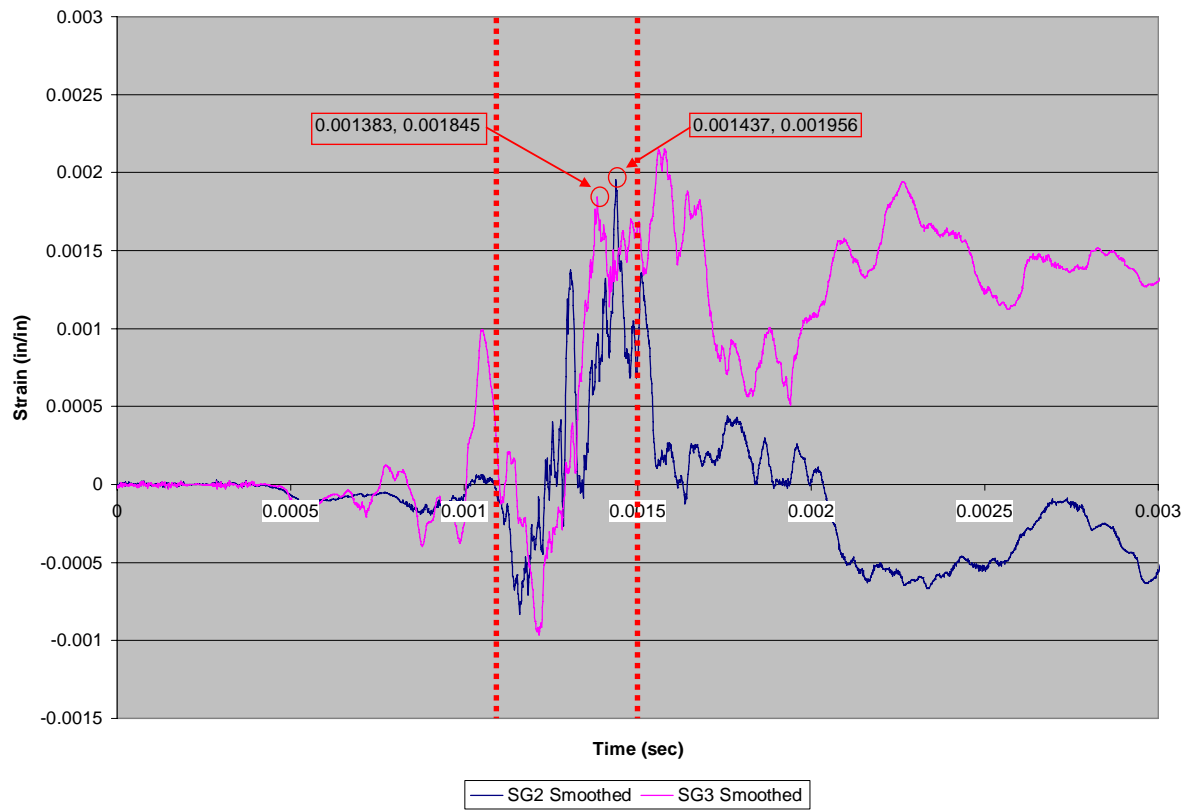


Figure C.2e.3: SG2 & SG3 spar strain vs. time (Specimen 2e)

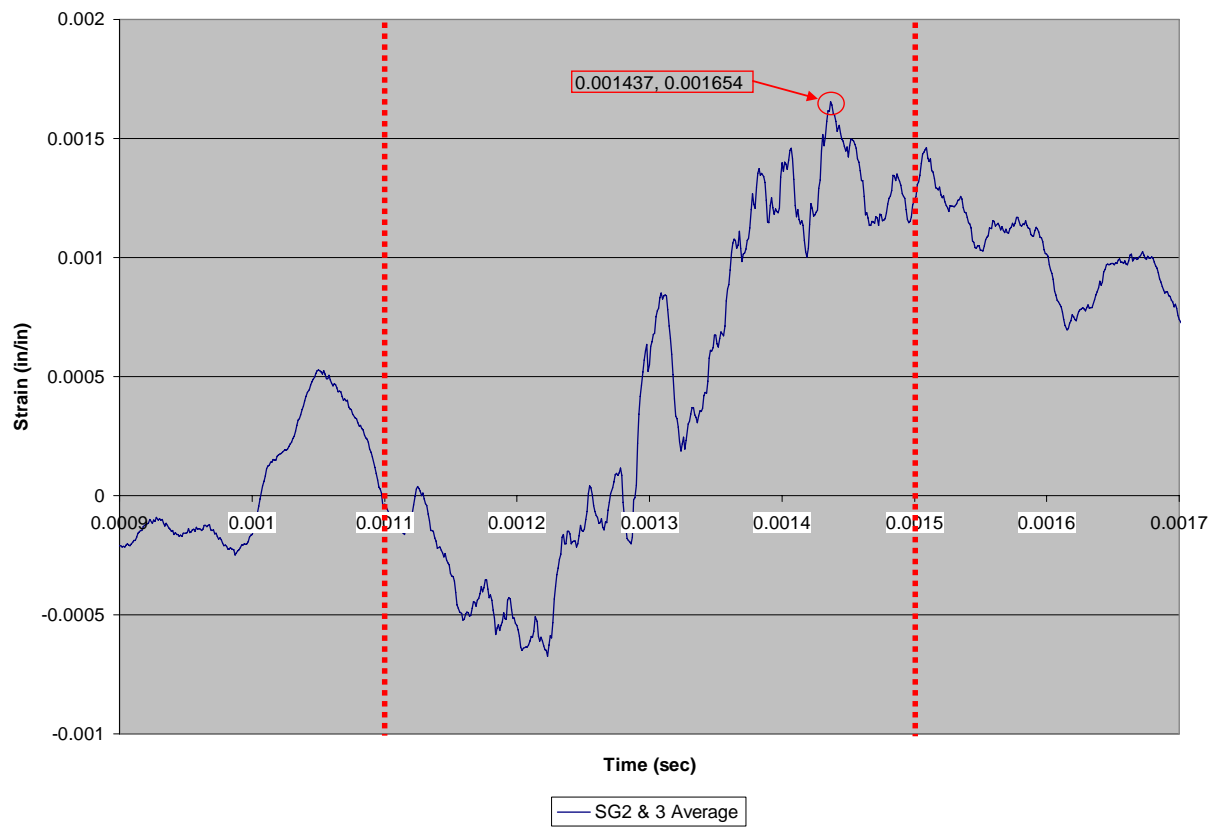


Figure C.2e.4: SG2 & SG3 average spar strain vs. time (Specimen 2e)

C.3 Specimen Set 3: Tufted Carbon

C.3.1 Dynamic Tests of Specimen Set 3

Specimen 3a, Test 07

For Specimen 3a, the load interval (and therefore the strain vs. time interval of interest) is approximately 1.15ms - 1.50ms as seen in Figure C.3a.1. As desired, pressure sensors K1 and K3 are largely in agreement, indicating side-to-side uniformity of load on the test specimen. During the load interval, Figure C.3a.2 shows that SG1 and SG4 tend to stay in phase and of similar amplitude indicating the skin pulled away from the spar in a symmetric fashion. Similarly, SG2 and SG3 are in phase and of similar amplitude (as seen in Figure C.3a.3) substantiating symmetric failure. Failure metrics for Specimen 3a are derived from Figure C.3a.4. Failure strain occurred at 1.438ms with a maximum strain of 0.00570 in/in.

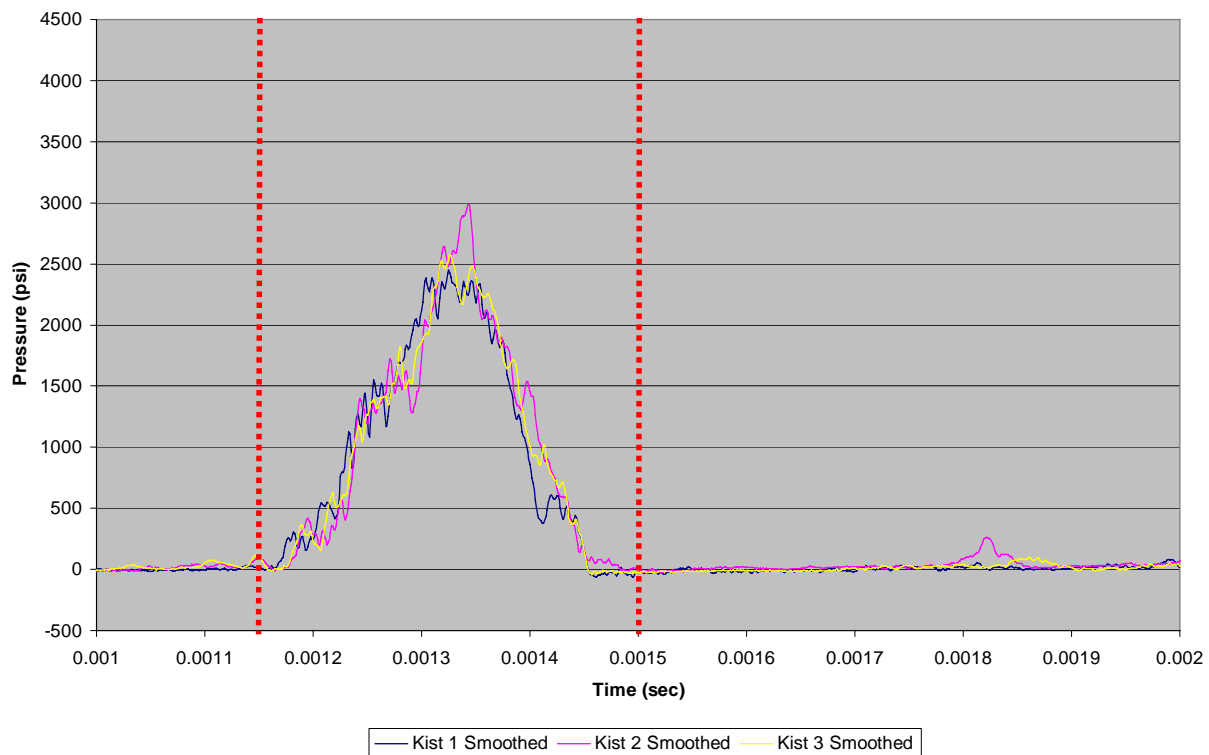


Figure C.3a.1: Kistler pressure vs. time (Specimen 3a)

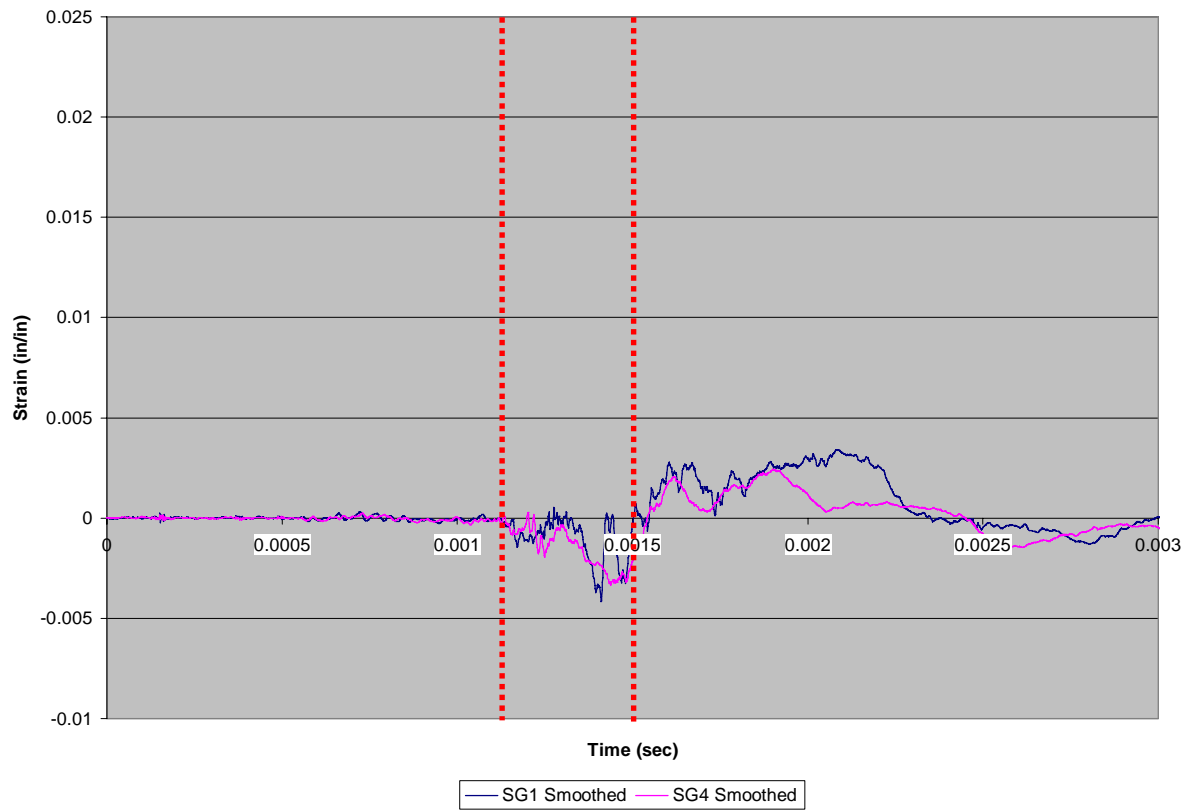


Figure C.3a.2: SG1 & SG4 skin strain vs. time (Specimen 3a)

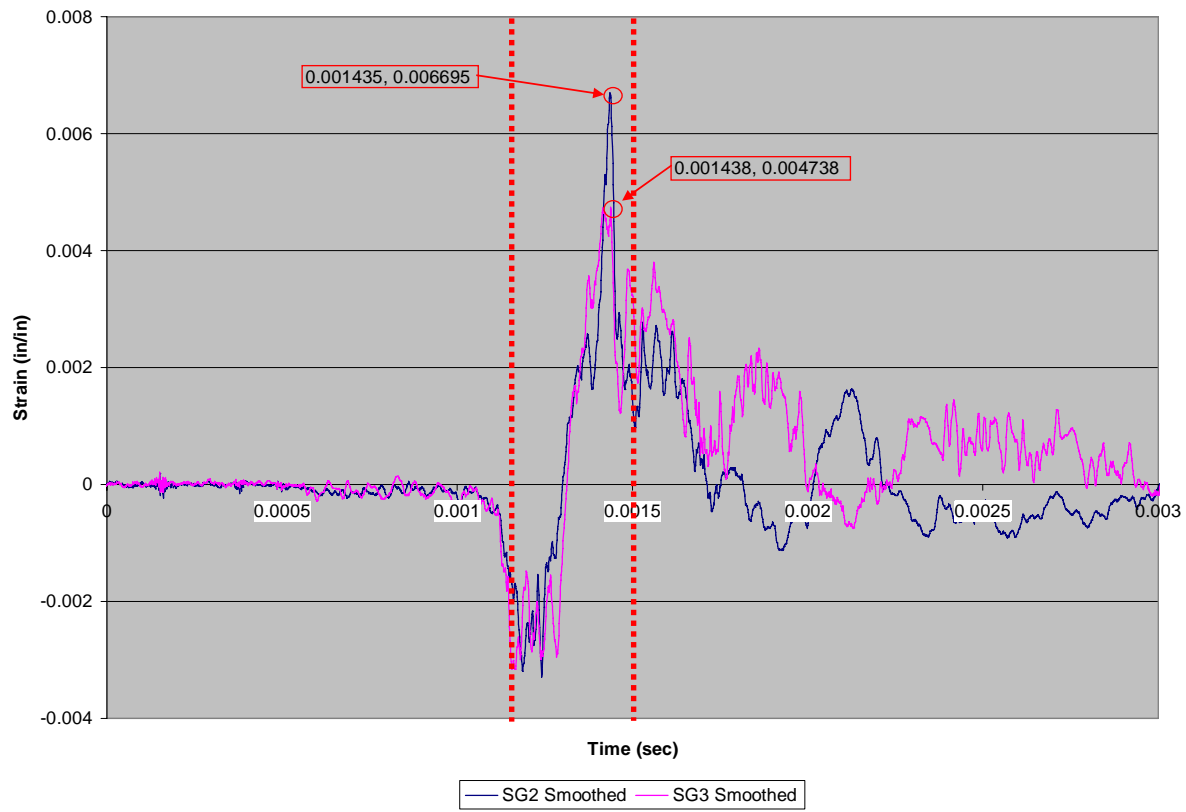


Figure C.3a.3: SG2 & SG3 spar strain vs. time (Specimen 3a)

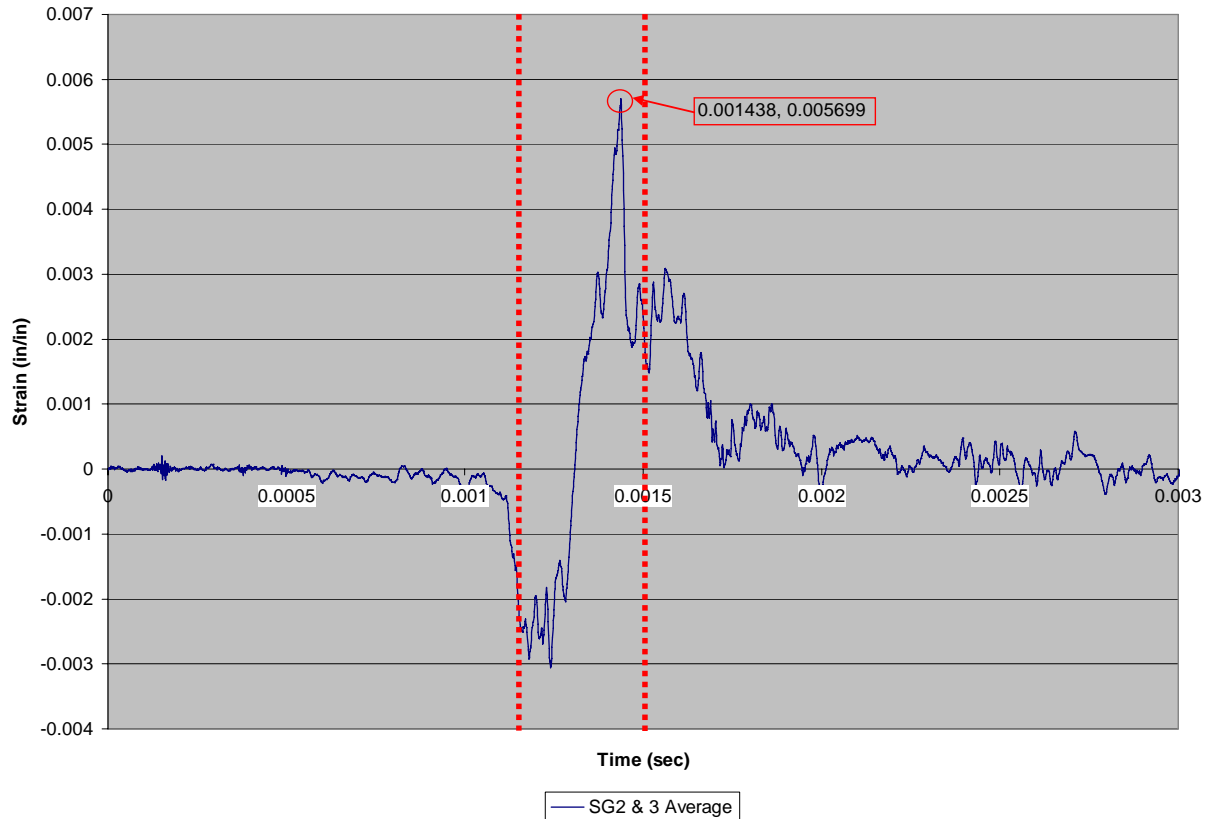


Figure C.3a.4: SG2 & SG3 average spar strain vs. time (Specimen 3a)

Specimen 3b, Test 08

For Specimen 3b, the load interval (and therefore the strain vs. time interval of interest) is approximately 1.17ms - 1.50ms as seen in Figure C.3b.1. As desired, pressure sensors K1 and K3 are largely in agreement, indicating side-to-side uniformity of load on the test specimen. During them load interval, Figure C.3b.2 shows that SG1 and SG4 are in phase indicating the skin pulled away from the spar in a symmetric fashion. While SG2 and SG3 are in phase (as seen in Figure C.3b.3), there are strain amplitude variances. This suggests a measure of asymmetry. Failure metrics for Specimen 3b are derived from Figure C.3b.4. Failure strain occurred at 1.483ms with a maximum strain of 0.00384 in/in.

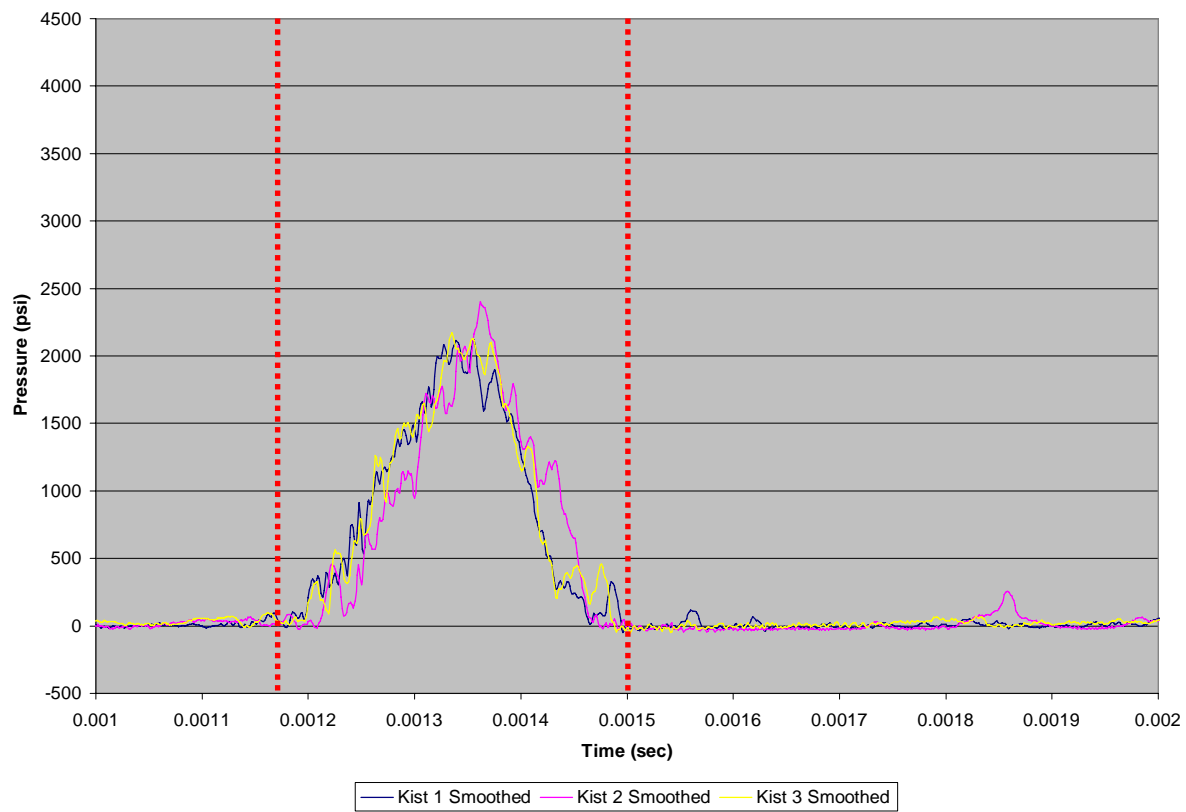


Figure C.3b.1: Kistler pressure vs. time (Specimen 3b)

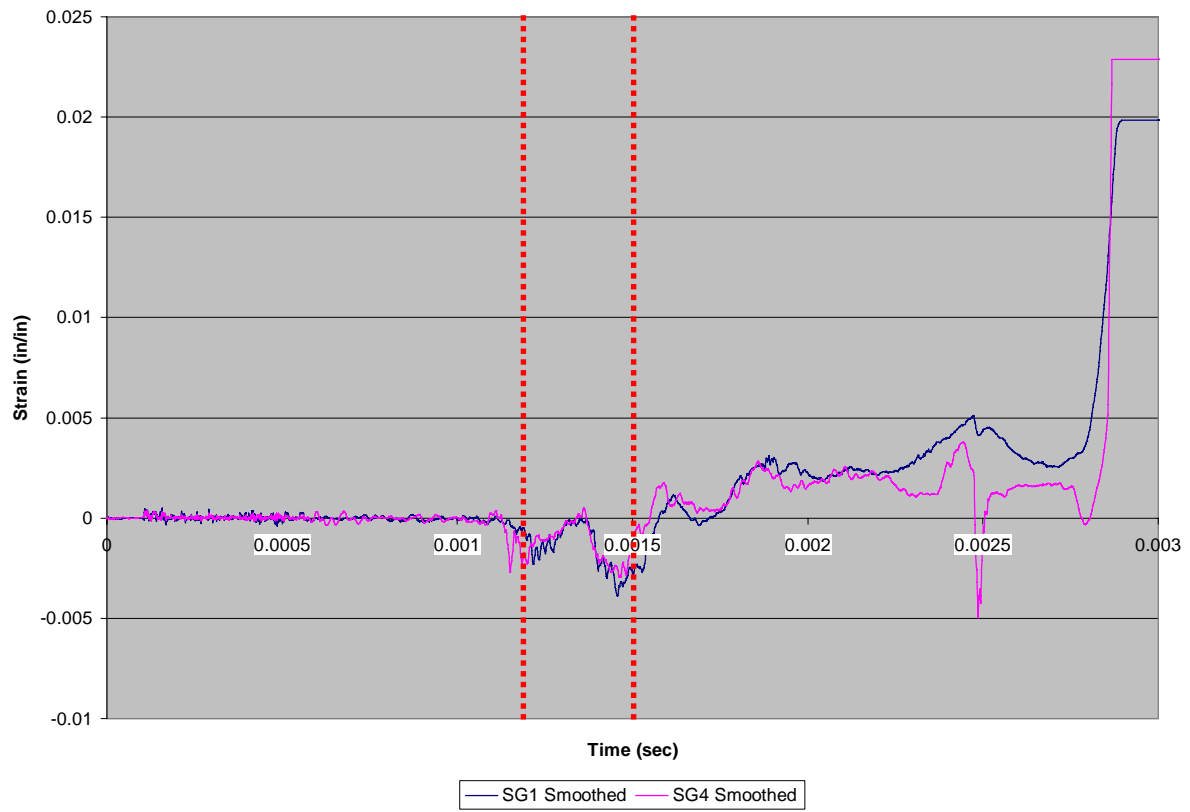


Figure C.3b.2: SG1 & SG4 skin strain vs. time (Specimen 3b)

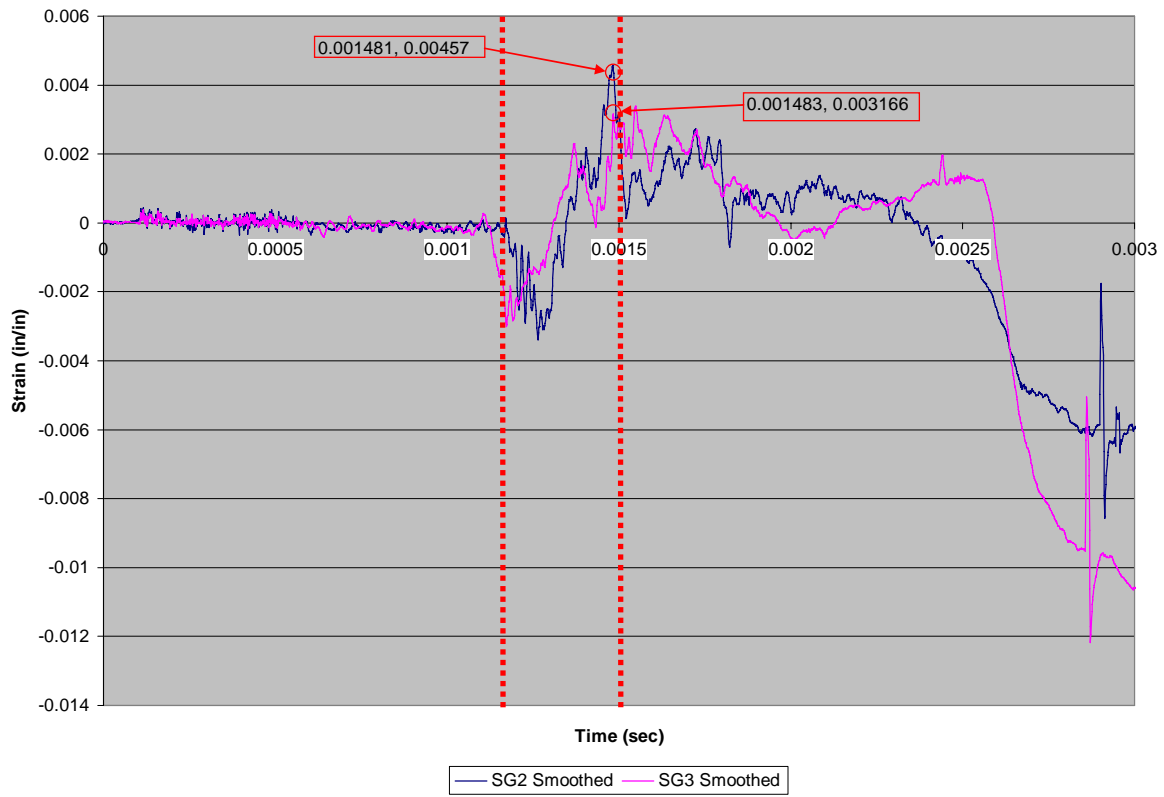


Figure C.3b.3: SG2 & SG3 spar strain vs. time (Specimen 3b)

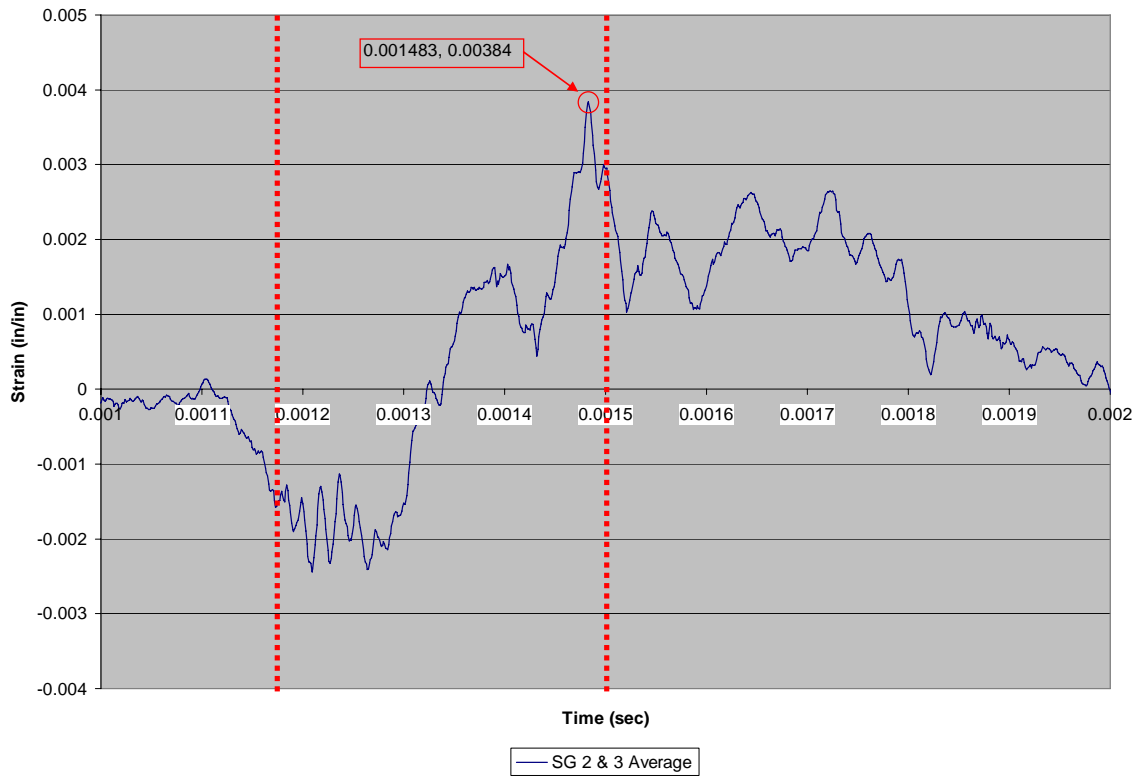


Figure C.3b.4: SG2 & SG3 average spar strain vs. time (Specimen 3b)

Specimen 3c, Test 09

For Specimen 3c, the load interval (and therefore the strain vs. time interval of interest) is approximately 1.15 ms to 1.45ms as shown in Figure C.3c.1. As desired, pressure sensors K1 and K3 are largely in agreement, indicating side-to-side uniformity of load on the test specimen. During the load interval, Figure C.3c.2 shows that SG1 and SG4 are in phase and of similar amplitude, indicating the skin pulled away from the spar in a symmetric fashion. SG2 and SG3 on the spar also appear in phase and of similar amplitude (as seen in Figure C.3c.3), implying symmetric failure. Failure metrics for Specimen 3c are derived from Figure C.3c.4. Failure strain occurred at 1.434ms with a maximum strain of 0.00336 in/in.

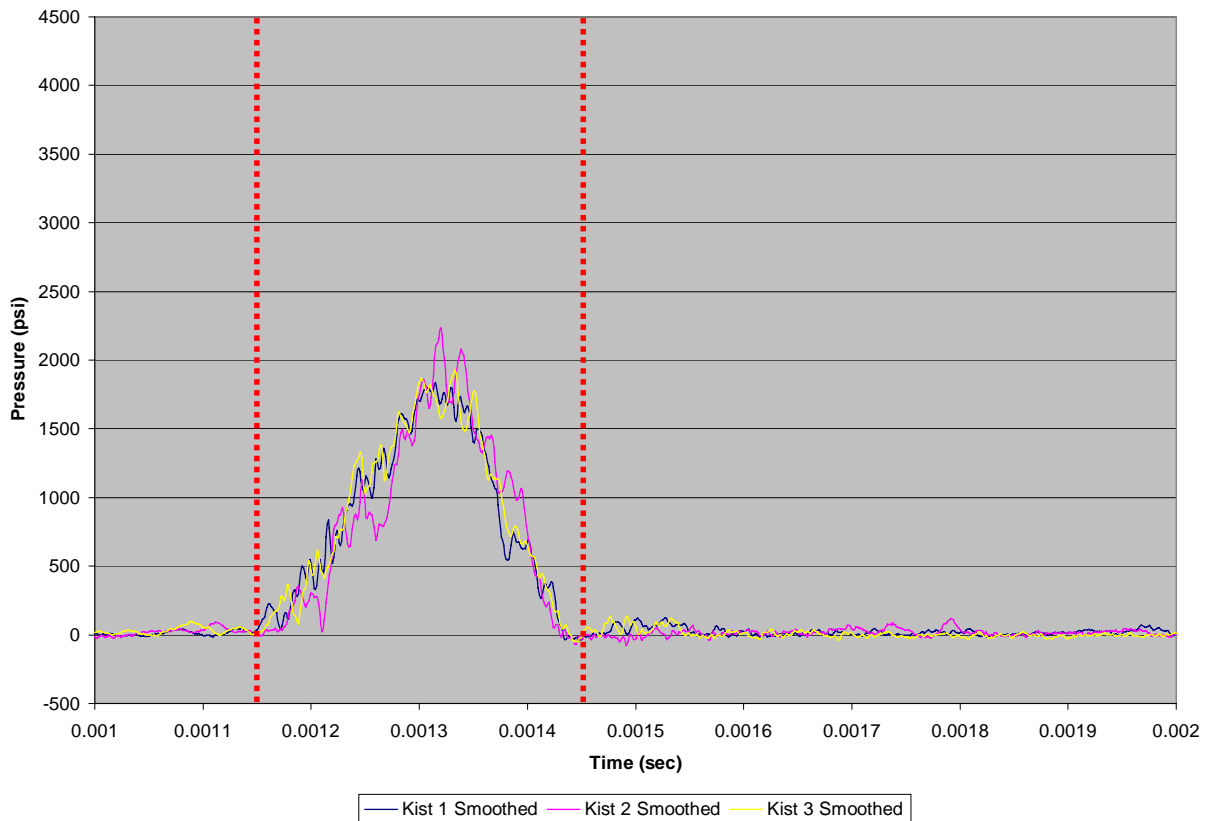


Figure C.3c.1: Kistler pressure vs. time (Specimen 3c)

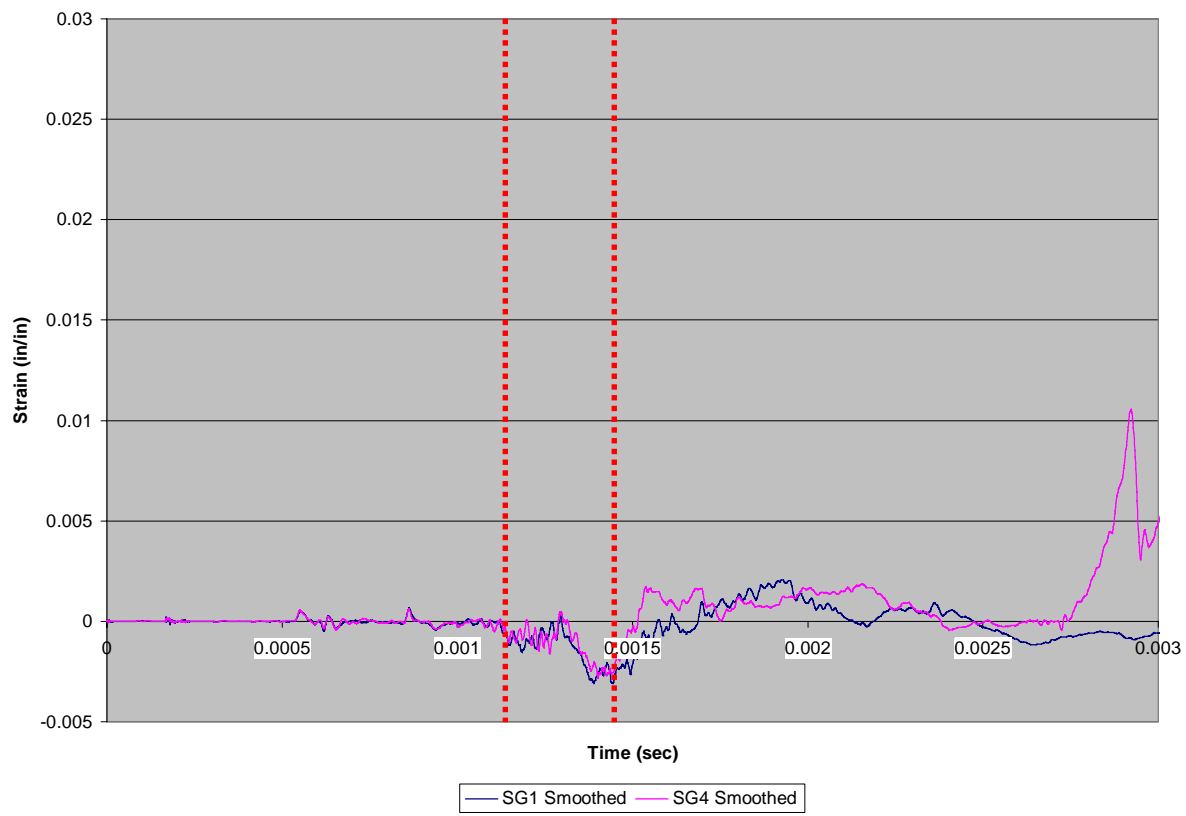


Figure C.3c.2: SG1 & SG4 skin strain vs. time (Specimen 3c)

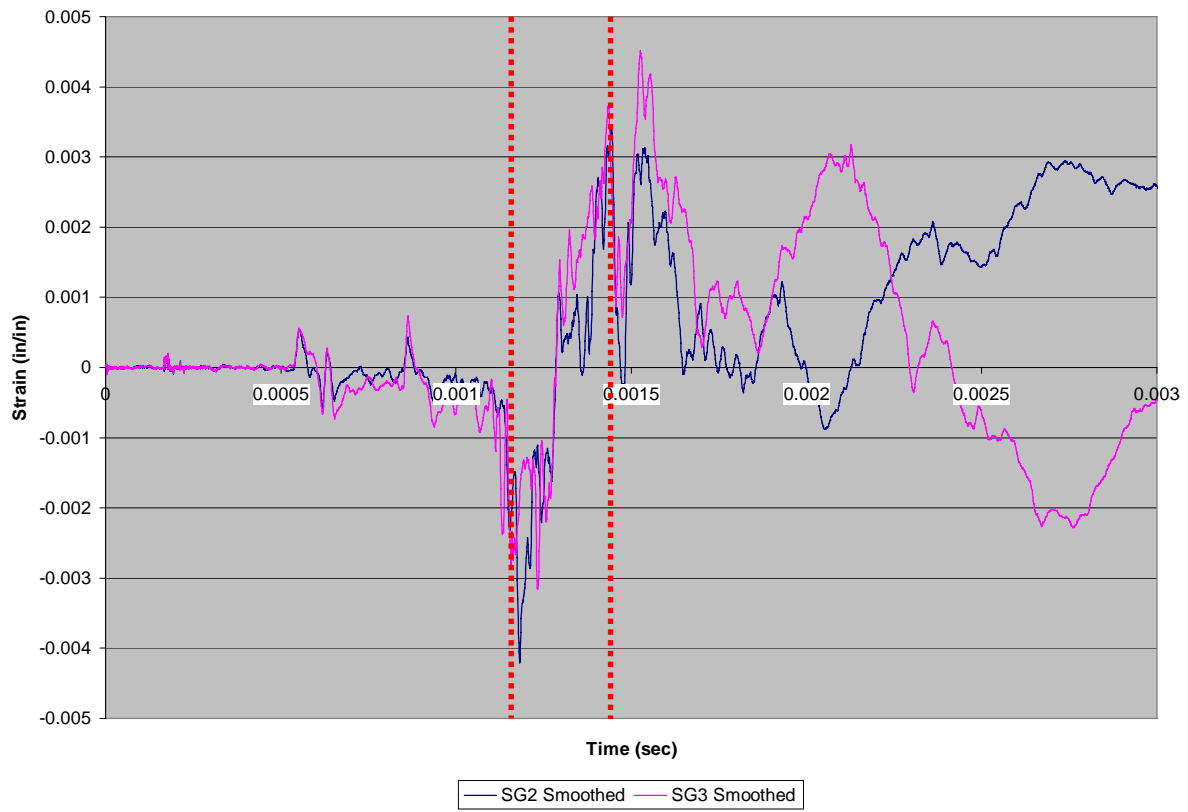


Figure C.3c.3: SG2 & SG3 spar strain vs. time (Specimen 3c)

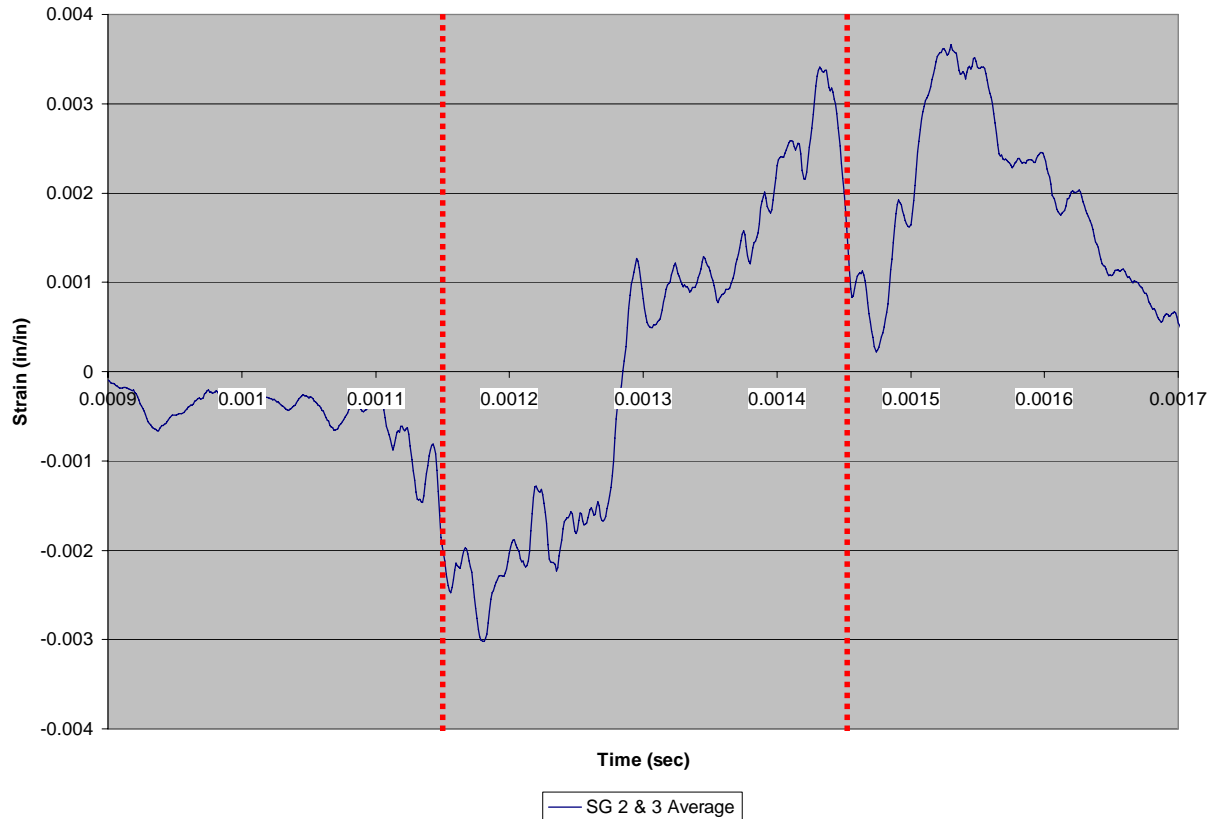


Figure C.3c.4: SG2 & SG3 average spar strain vs. time (Specimen 3c)

Specimen 3d, Test 36

For Specimen 3d, the load interval (and therefore the strain vs. time interval of interest) is approximately 1.02ms-1.40ms as shown in Figure C.3d.1. As desired, pressure sensors K1 and K3 are largely in agreement, indicating side-to-side uniformity of load on the test specimen. During the load interval, Figure C.3d.2 shows that SG1 and SG4 remain in phase and are of similar amplitude. SG2 and SG3 on the spar are in phase but, at the moment of failure, are of different amplitude (as seen in Figure C.3d.3). The difference in strain amplitudes implies asymmetric failure. Failure metrics for Specimen 3d are derived from Figure C.3d.4. Failure strain occurred at 1.245ms with a maximum strain of 0.005063 in/in.

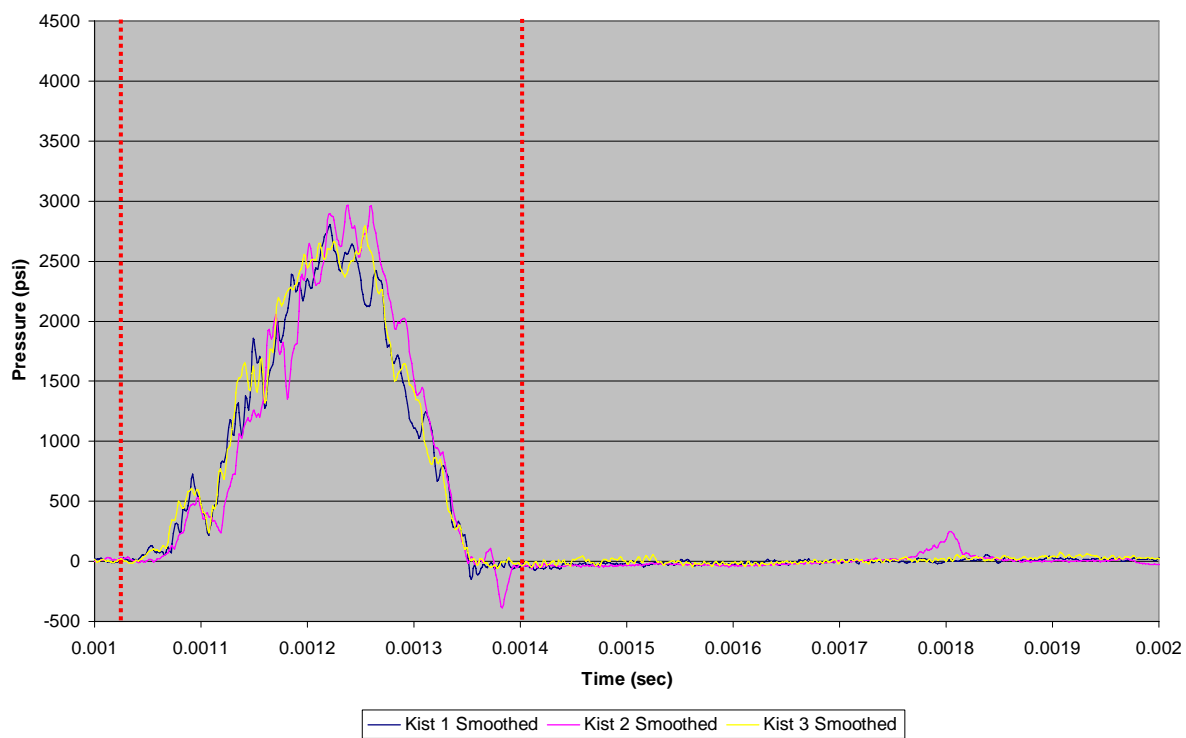


Figure C.3d.1: Kistler pressure vs. time (Specimen 3d)

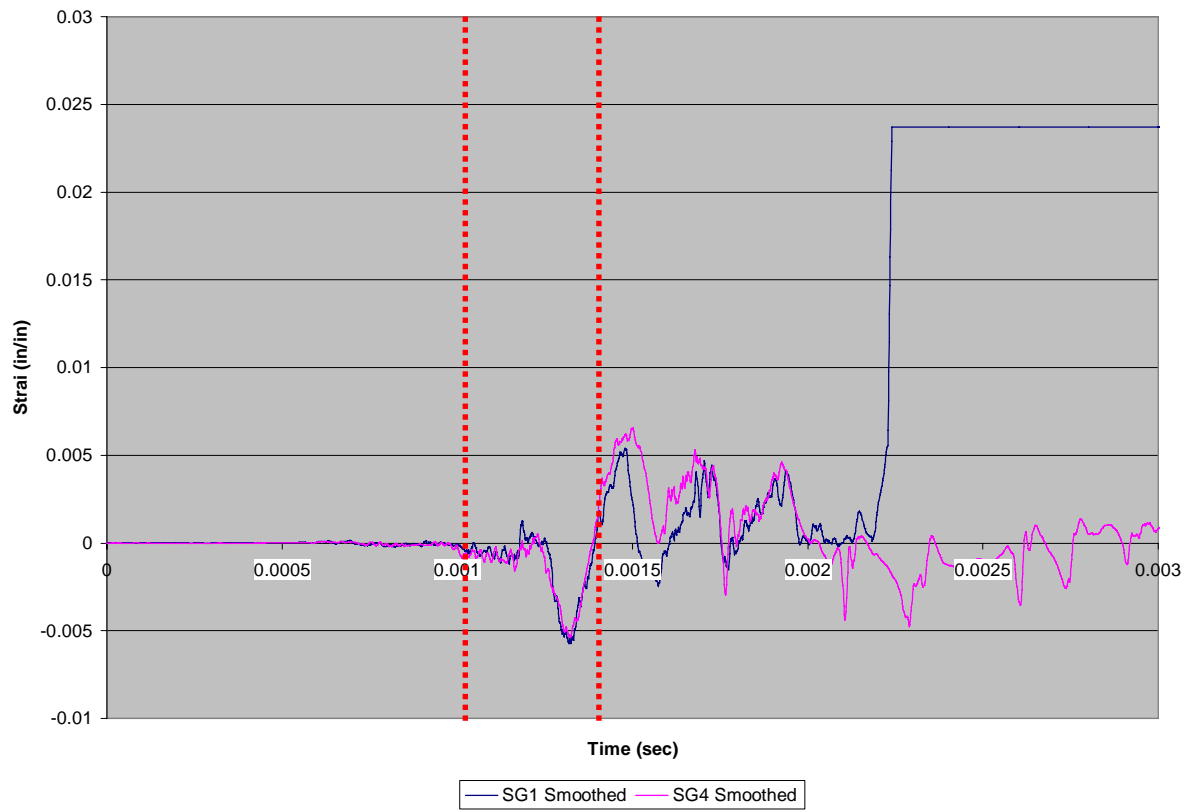


Figure C.3d.2: SG1 & SG4 skin strain vs. time (Specimen 3d)

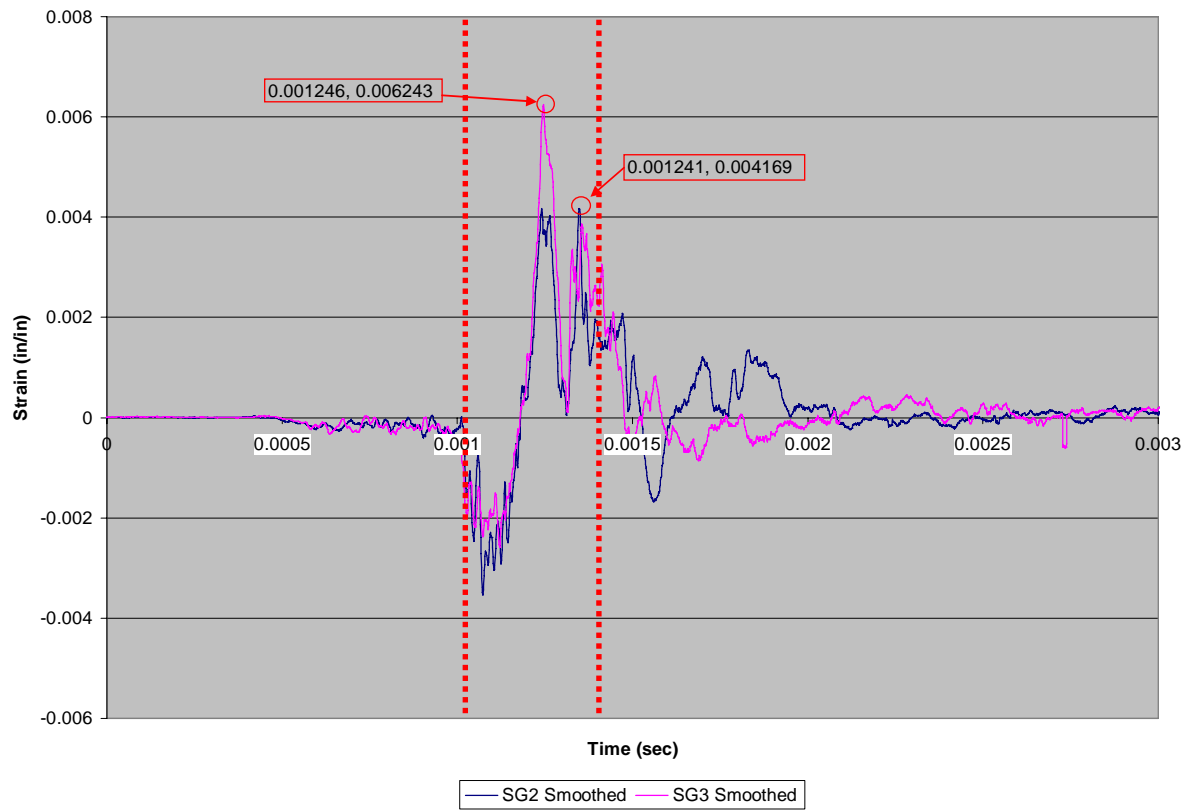


Figure C.3d.3: SG2 & SG3 spar strain vs. time (Specimen 3d)

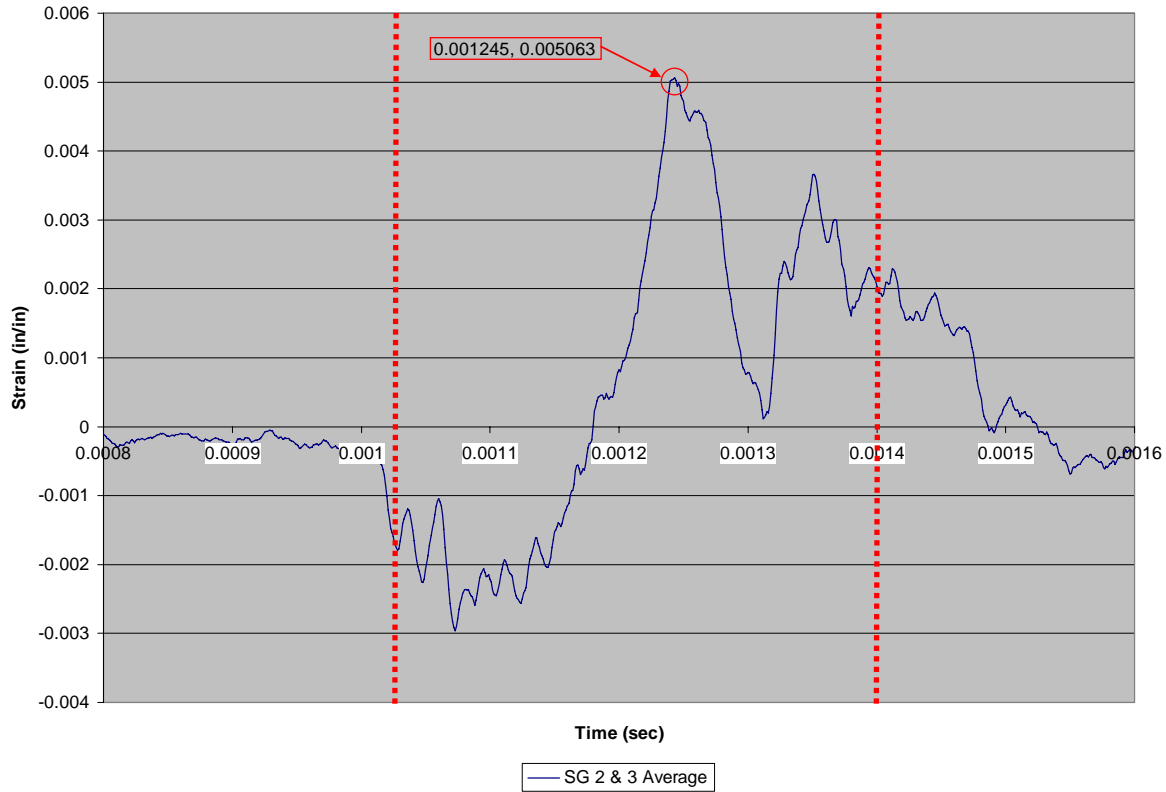


Figure C.3d.4: SG2 & SG3 average spar strain vs. time (Specimen 3d)

Specimen 3e, Test 37

For Specimen 3e, the load interval (and therefore the strain vs. time interval of interest) is approximately 1.24ms-1.55ms as shown in Figure C.3e.1. As desired, pressure sensors K1 and K3 are largely in agreement, indicating side-to-side uniformity of load on the test specimen. During the load interval, Figure C.3e.2 shows that SG1 and SG4 remain in phase and are of similar amplitude. SG2 and SG3 are initially somewhat out of phase (as seen in Figure C.3e.3), but come in phase and are of similar amplitude prior to failure. As such, failure is deemed symmetric. Failure metrics for Specimen 3e are derived from Figure C.3e.4. Failure strain occurred at 1.450ms with a maximum strain of 0.003985 in/in.

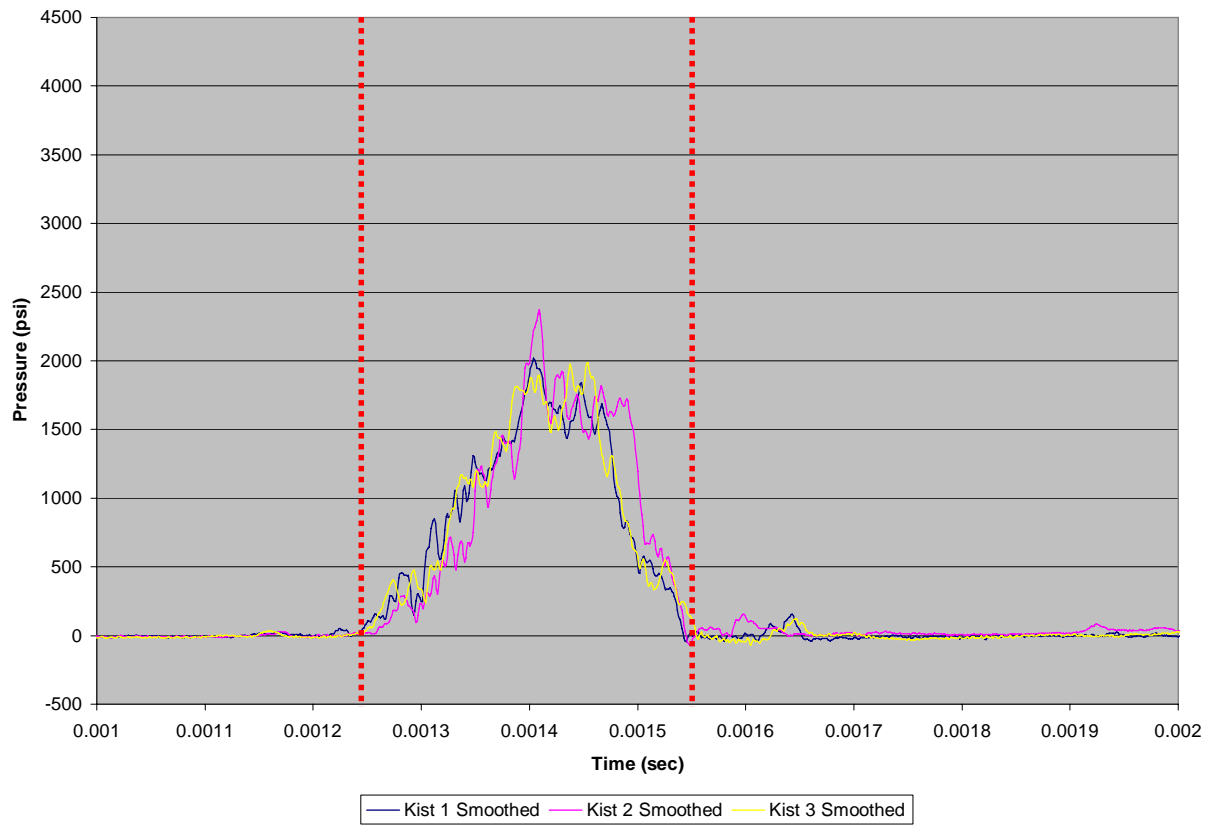


Figure C.3e.1: Kistler pressure vs. time (Specimen 3e)

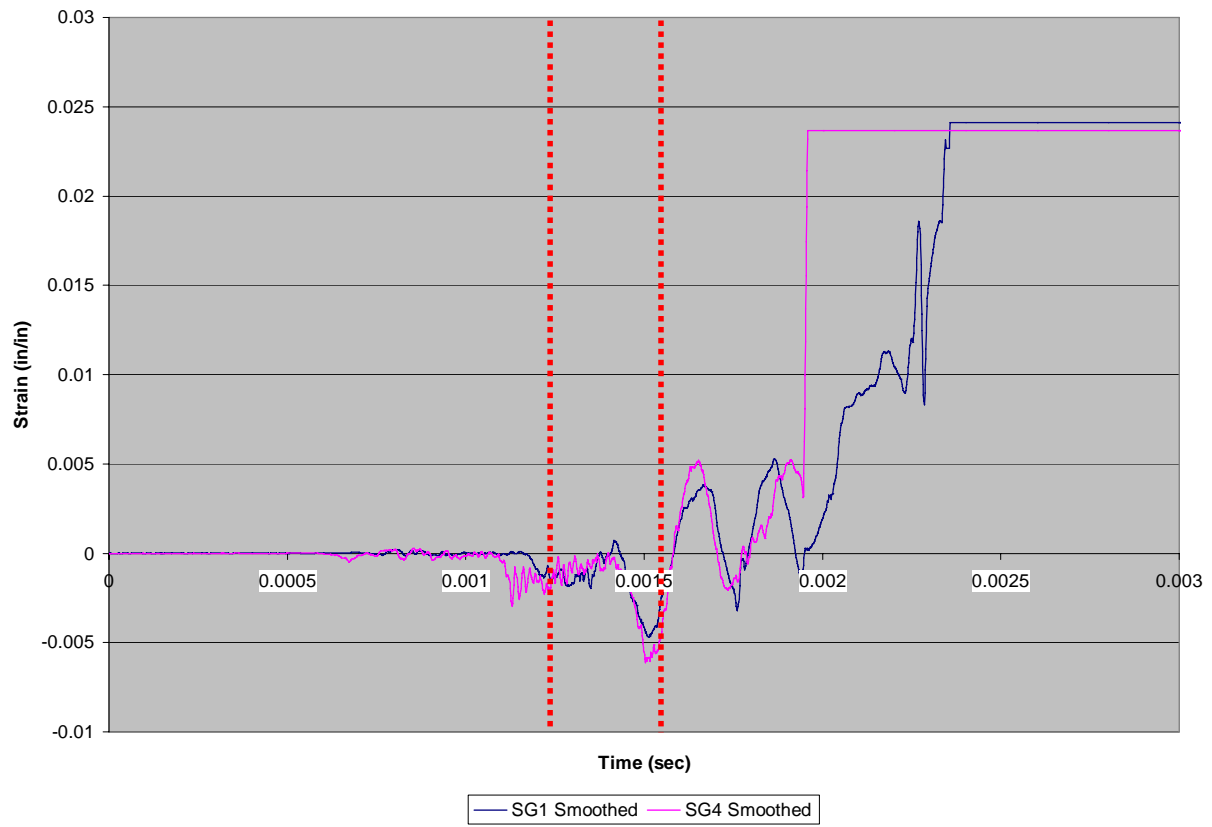


Figure C.3e.2: SG1 & SG4 skin strain vs. time (Specimen 3e)

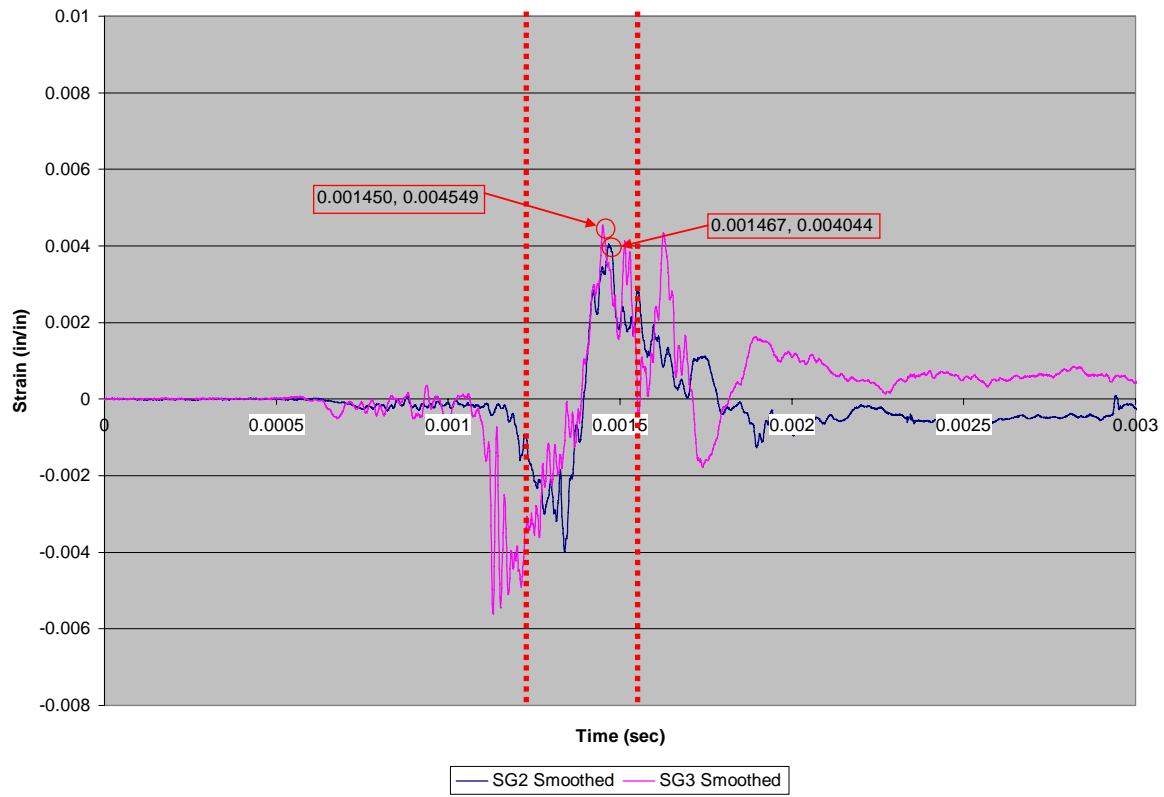


Figure C.3e.3: SG2 & SG3 spar strain vs. time (Specimen 3e)

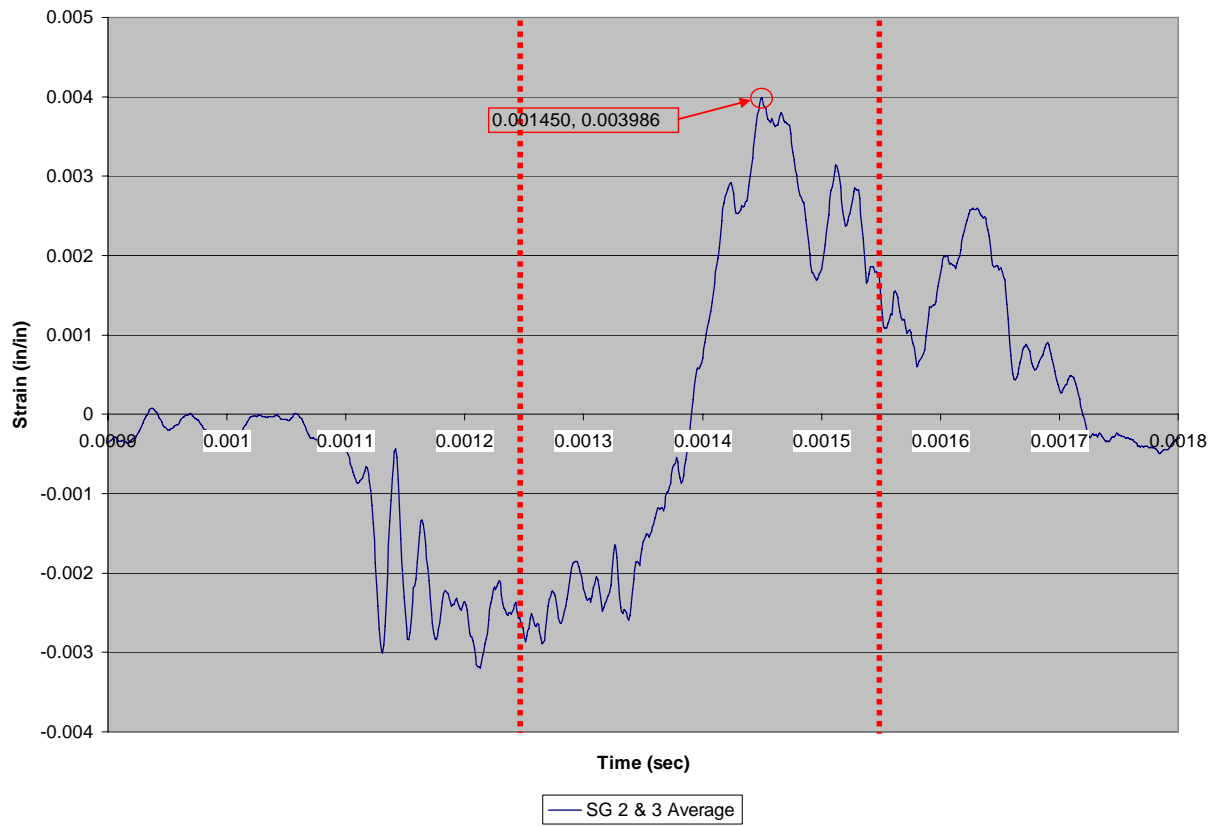


Figure C.3e.4: SG2 & SG3 average spar strain vs. time (Specimen 3e)

C.4 Specimen Set 4: Tufted Aramide

C.4.1 Dynamic Tests of Specimen Set 4

Specimen 4a, Test 10

For Specimen 4a, the load interval (and therefore the strain vs. time interval of interest) is approximately 1.10ms - 1.42ms as seen in Figure C.4a.1. As desired, pressure sensors K1 and K3 are largely in agreement, indicating side-to-side uniformity of load on the test specimen. During the load interval, Figure C.4a.2 shows that SG1 and SG4 stay in phase and are of similar amplitude, indicating the skin pulled away from the spar in a symmetric fashion. While SG2 and SG3 are in phase (as seen in Figure C.4a.3), their amplitudes differ, implying asymmetric failure. Failure metrics for Specimen 4a are derived from Figure C.4a.4. Failure strain occurred at 1.412ms with a maximum strain of 0.00438 in/in.

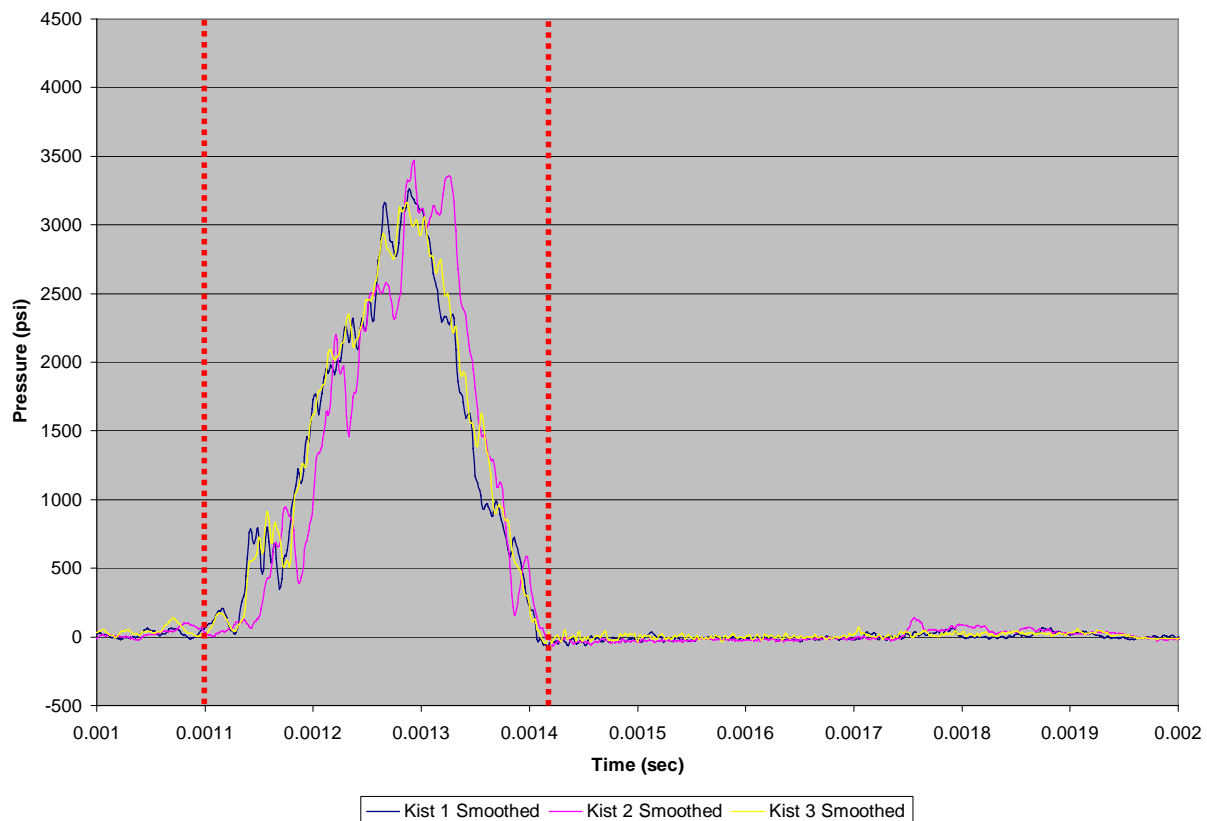


Figure C.4a.1: Kistler pressure vs. time (Specimen 4a)

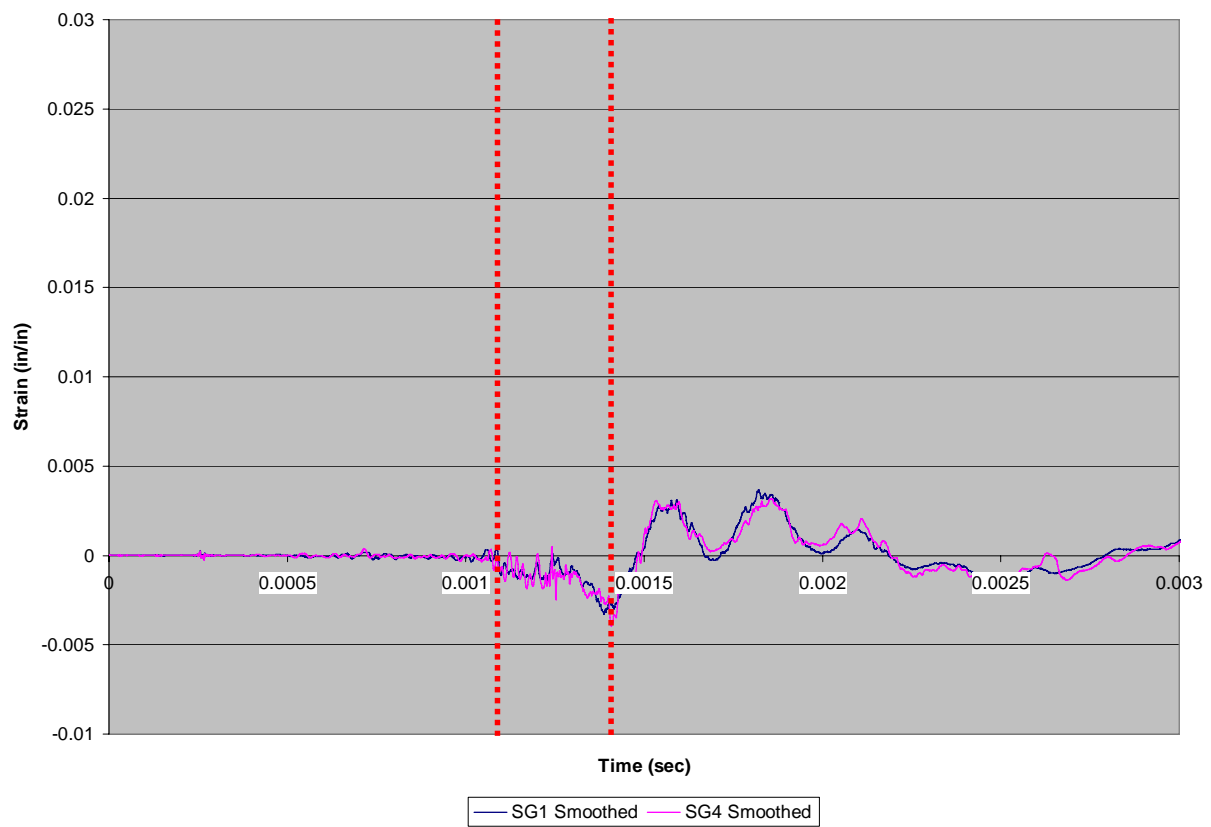


Figure C.4a.2: SG1 & SG4 skin strain vs. time (Specimen 4a)

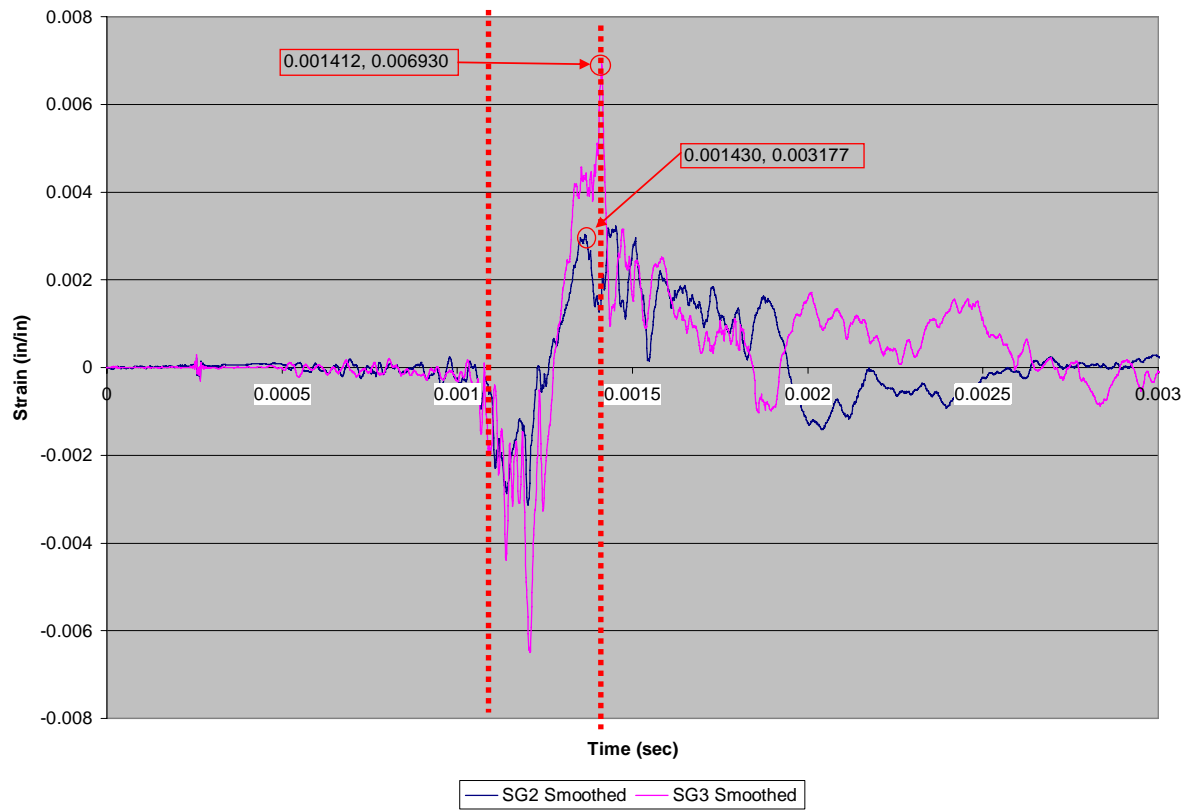


Figure C.4a.3: SG2 & SG3 spar strain vs. time (Specimen 4a)

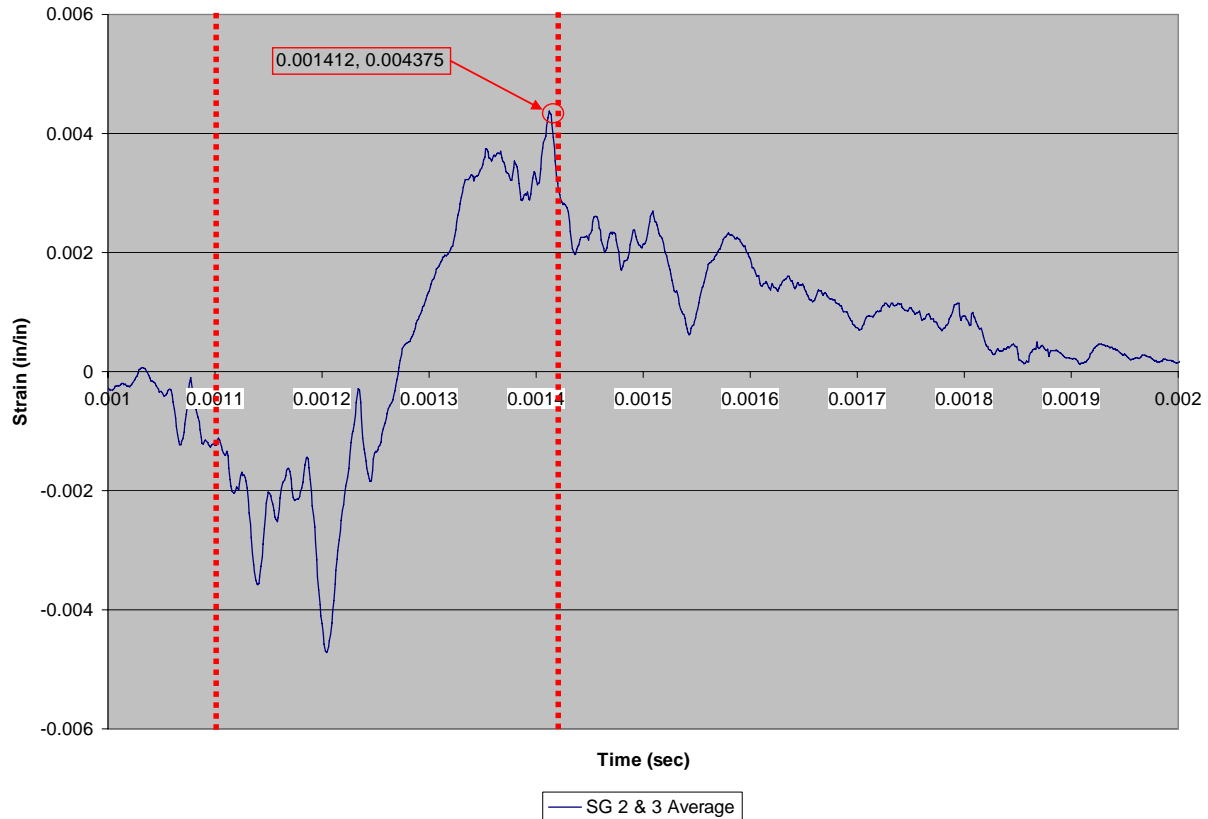


Figure C.4a.4: SG2 & SG3 average spar strain vs. time (Specimen 4a)

Specimen 4b, Test 11

For Specimen 4b, the load interval (and therefore the strain vs. time interval of interest) is approximately 1.20ms - 1.50ms as seen in Figure C.4b.1. As desired, pressure sensors K1 and K3 are largely in agreement, indicating side-to-side uniformity of load on the test specimen. During the load interval, Figure C.4b.2 shows that SG1 and SG4 are clearly in phase indicating the skin pulled away from the spar in a symmetric fashion. Similarly, SG2 and SG3 are in phase (as seen in Figure C.4b.3) implying symmetric failure. Failure metrics for Specimen 4b are derived from Figure C.4b.4. Failure strain occurred at 1.451ms with a maximum strain of 0.00388 in/in.

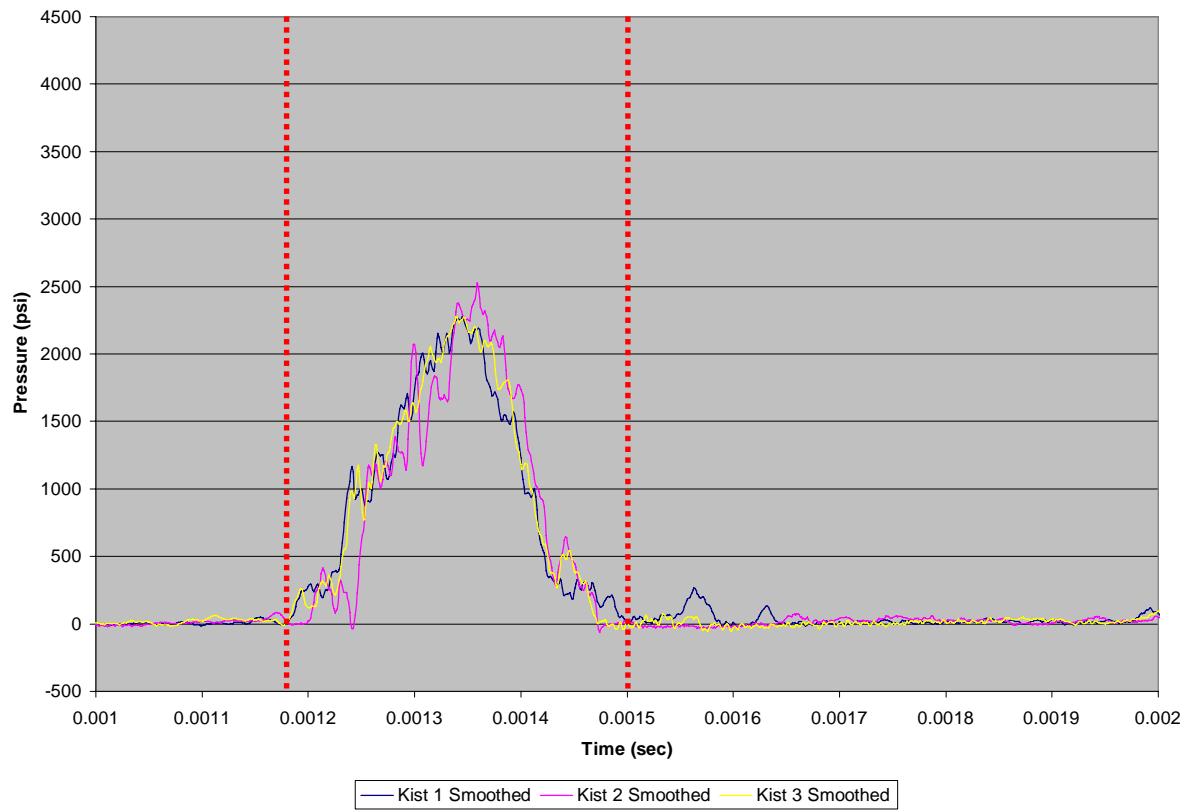


Figure C.4b.1: Kistler pressure vs. time (Specimen 4b)

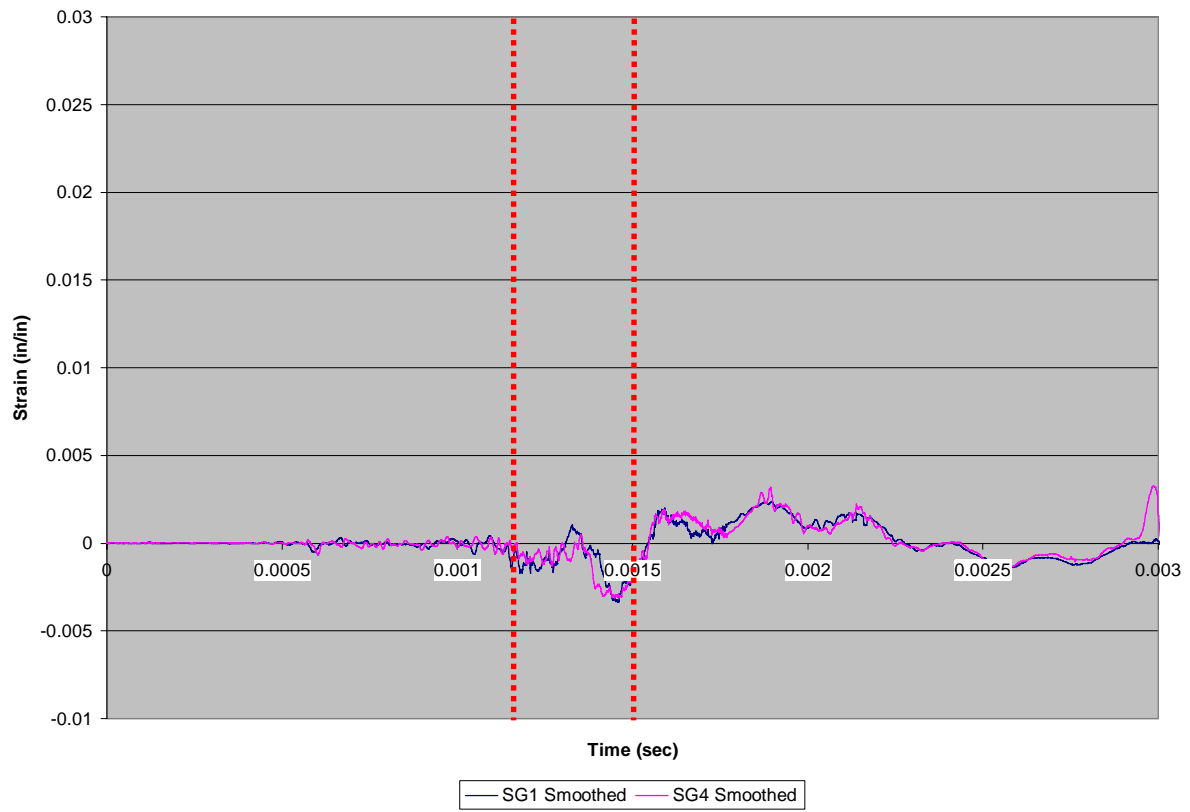


Figure C.4b.2: SG1 & SG4 skin strain vs. time (Specimen 4b)

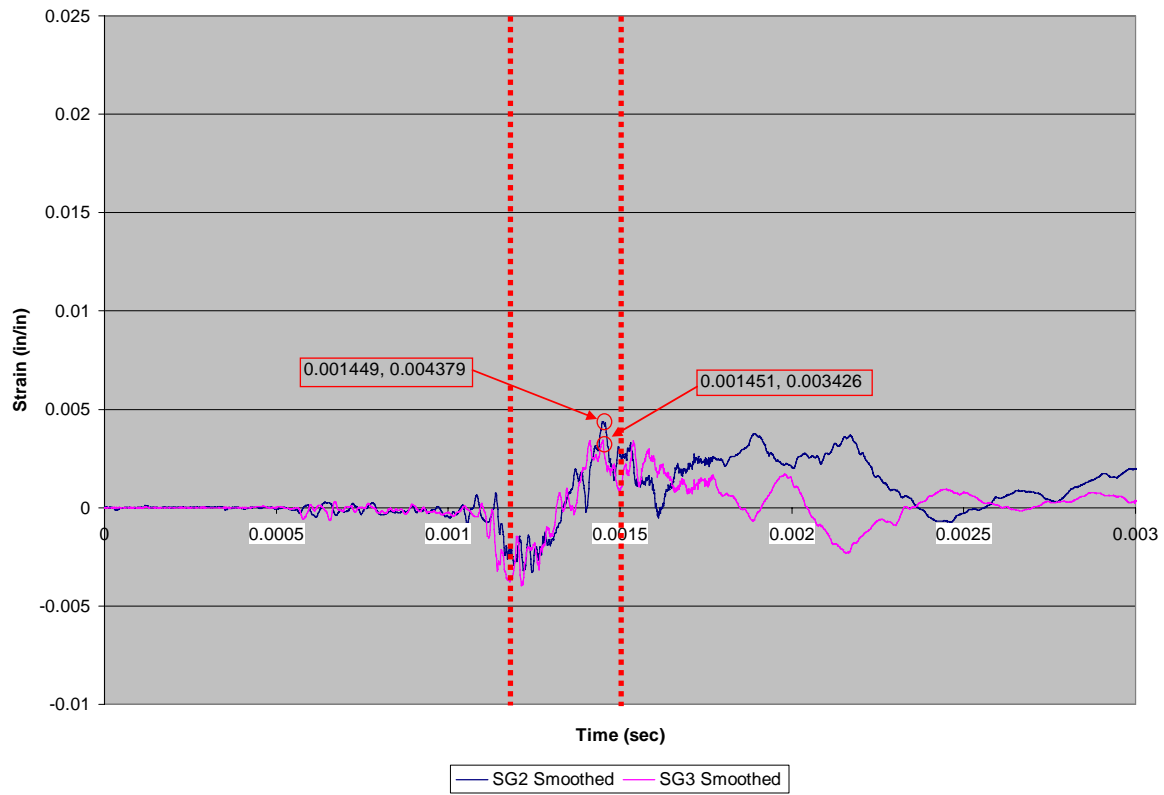


Figure C.4b.3: SG2 & SG3 spar strain vs. time (Specimen 4b)

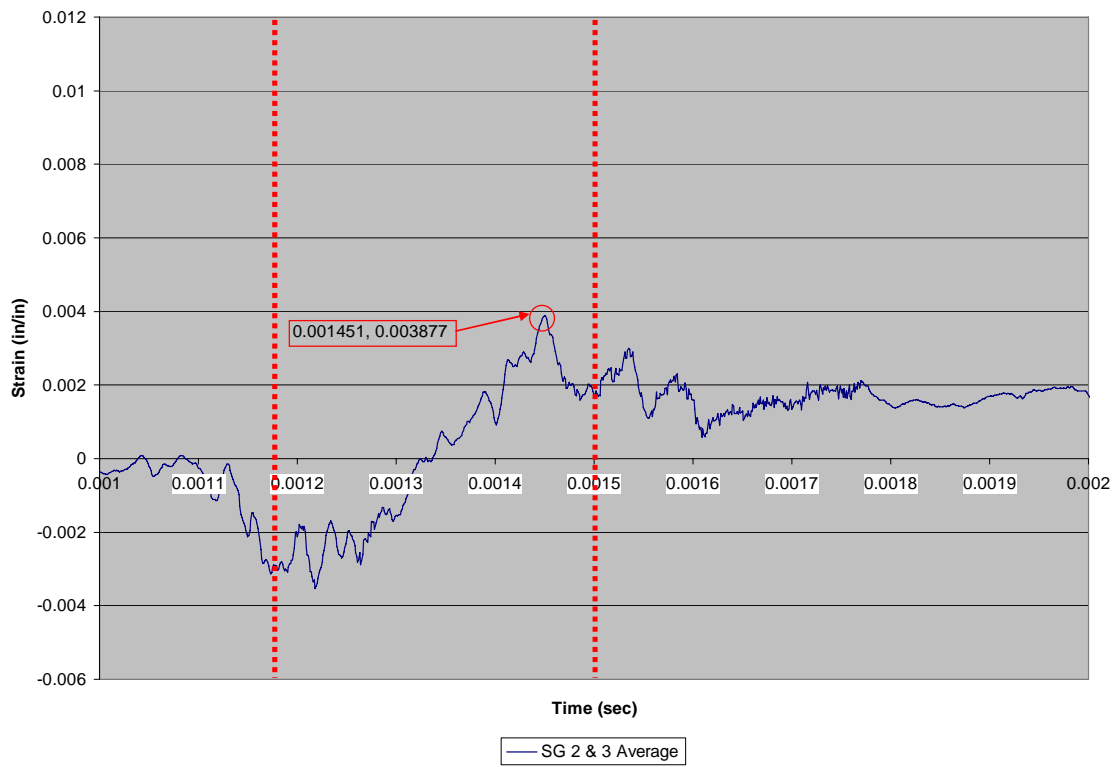


Figure C.4b.4: SG2 & SG3 average spar strain vs. time (Specimen 4b)

Specimen 4c, Test 12

For Specimen 4c, the load interval (and therefore the strain vs. time interval of interest) is approximately 1.10 ms to 1.45ms as shown in Figure C.4c.1. As desired, pressure sensors K1 and K3 are largely in agreement, indicating side-to-side uniformity of load on the test specimen. K2 (not critical to the test) failed shortly after pressure wave arrival. During the load interval, Figure C.4c.2 shows that SG1 and SG4 are clearly in phase and of similar amplitude, indicating the skin pulled away from the spar in a symmetric fashion. SG2 and SG3 on the spar are also largely in phase (as seen in Figure C.4c.3) and of similar amplitude (particularly at the moment of failure) implying symmetric failure. Failure metrics for Specimen 4c are derived from Figure C.4c.4. Failure strain occurred at 1.397ms with a maximum strain of 0.002988 in/in.

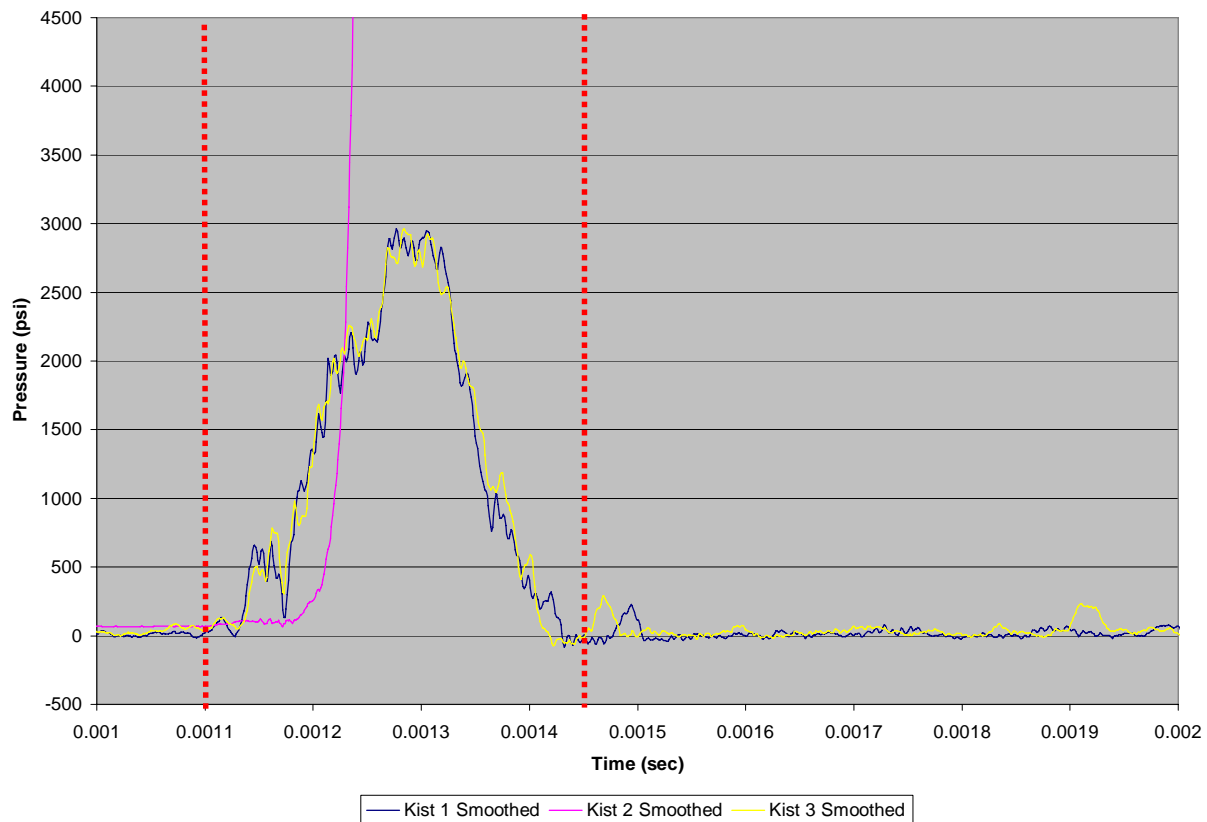


Figure C.4c.1: Kistler pressure vs. time (Specimen 4c)

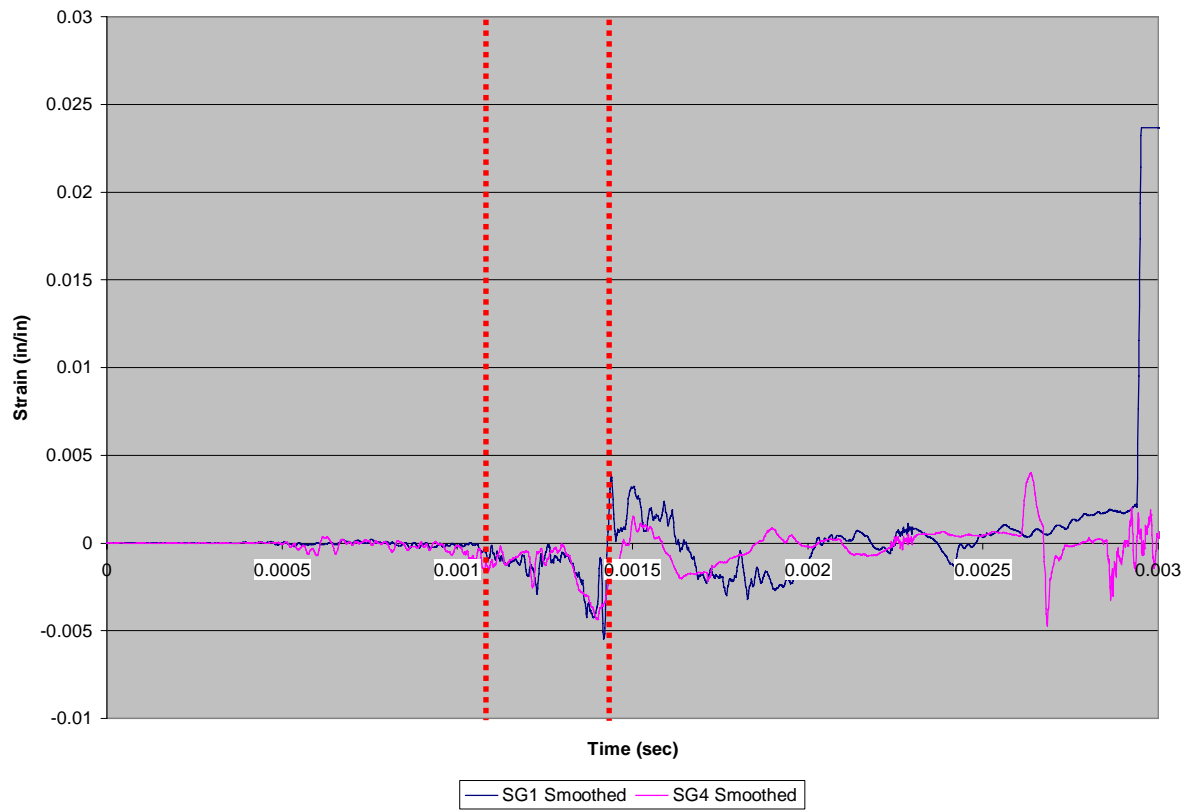


Figure C.4c.2: SG1 & SG4 skin strain vs. time (Specimen 4c)

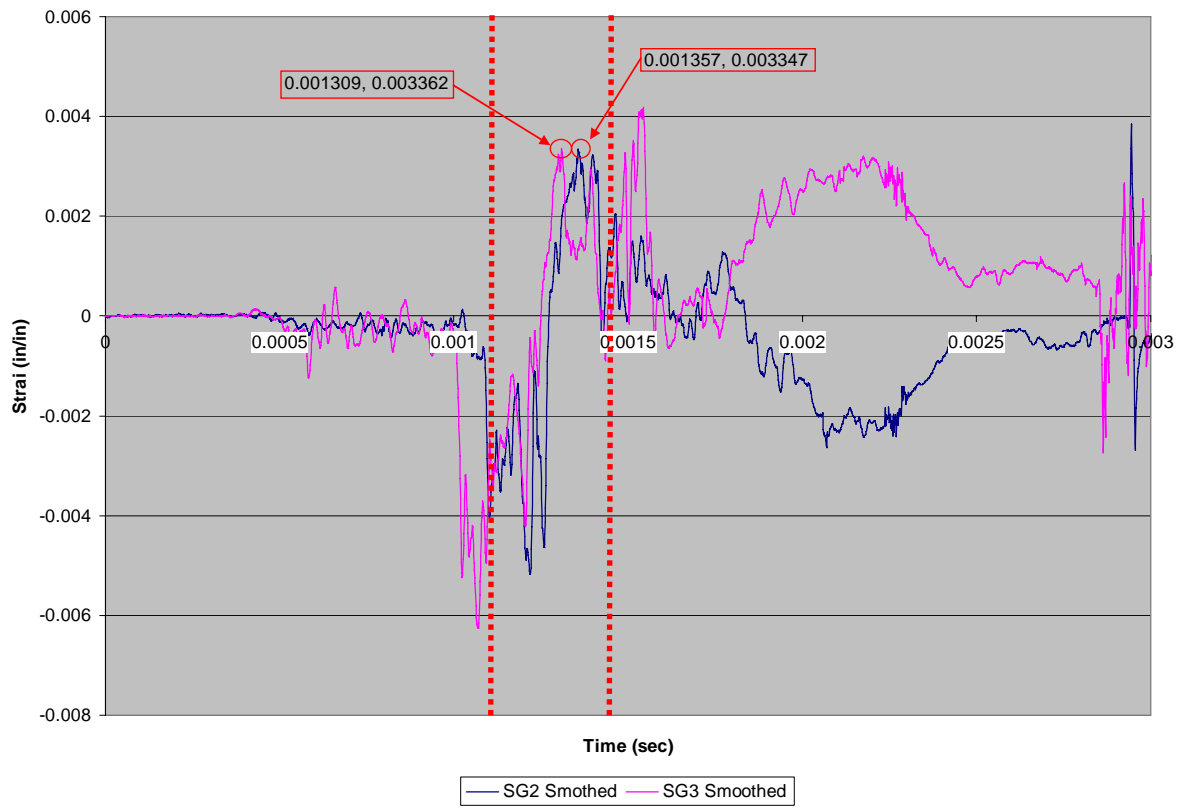


Figure C.4c.3: SG2 & SG3 spar strain vs. time (Specimen 4c)

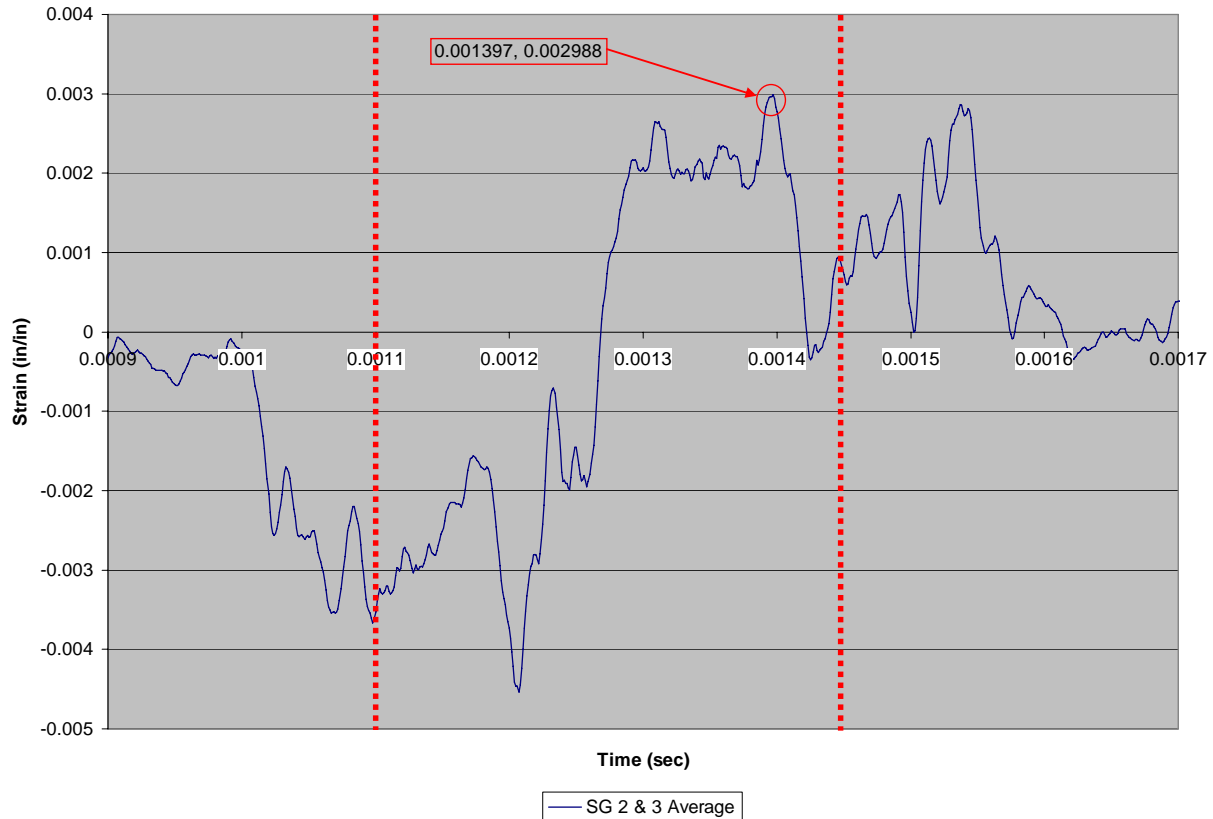


Figure C.4c.4: SG2 & SG3 average spar strain vs. time (Specimen 4c)

Specimen 4d, Test 31

For Specimen 4d, the load interval (and therefore the strain vs. time interval of interest) is approximately 1.12ms-1.43ms as shown in Figure C.4d.1. As desired, pressure sensors K1 and K3 are largely in agreement, indicating side-to-side uniformity of load on the test specimen. During the load interval, Figure C.4d.2 shows that SG1 and SG4 are in phase and of similar amplitude. Similarly, SG2 and SG3 remain in phase (as seen in Figure C.4d.3) and are of similar amplitude, implying symmetric failure. Failure metrics for Specimen 4d are derived from Figure C.4d.4. Failure strain occurred at 1.295ms with a maximum strain of 0.004062 in/in.

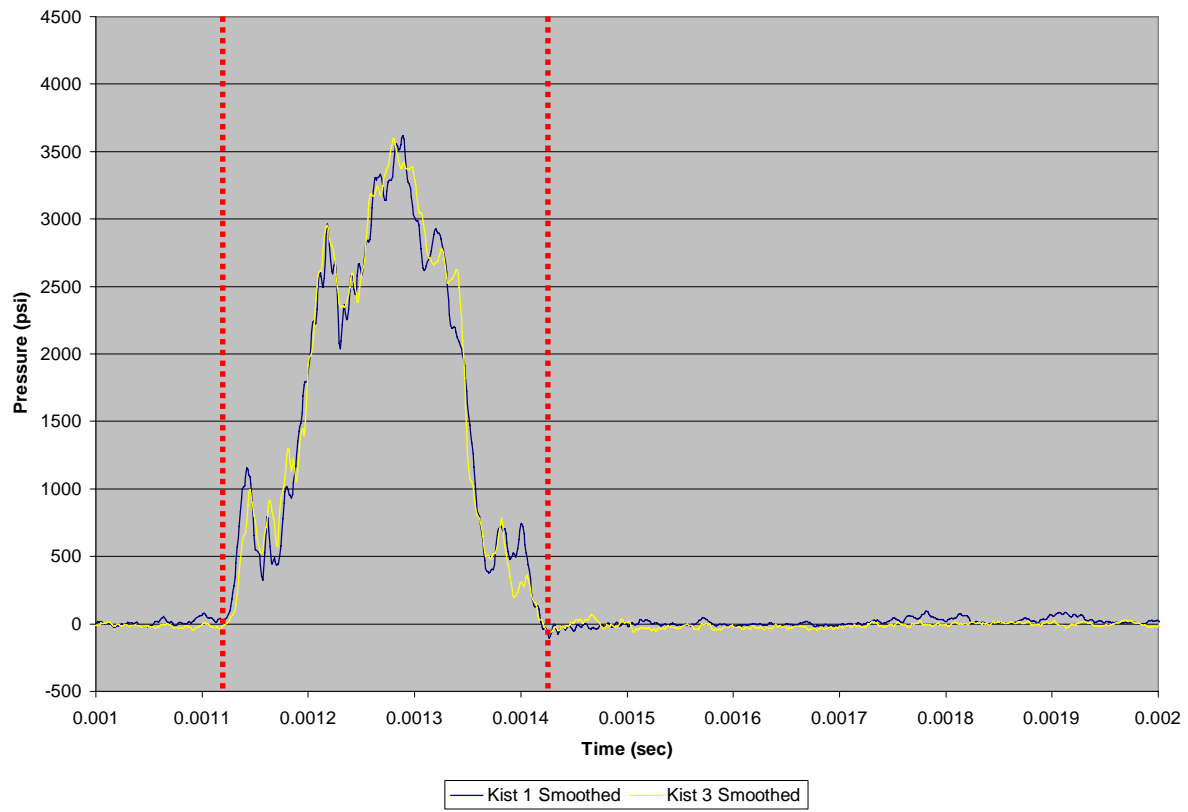


Figure C.4d.1: Kistler pressure vs. time (Specimen 4d)

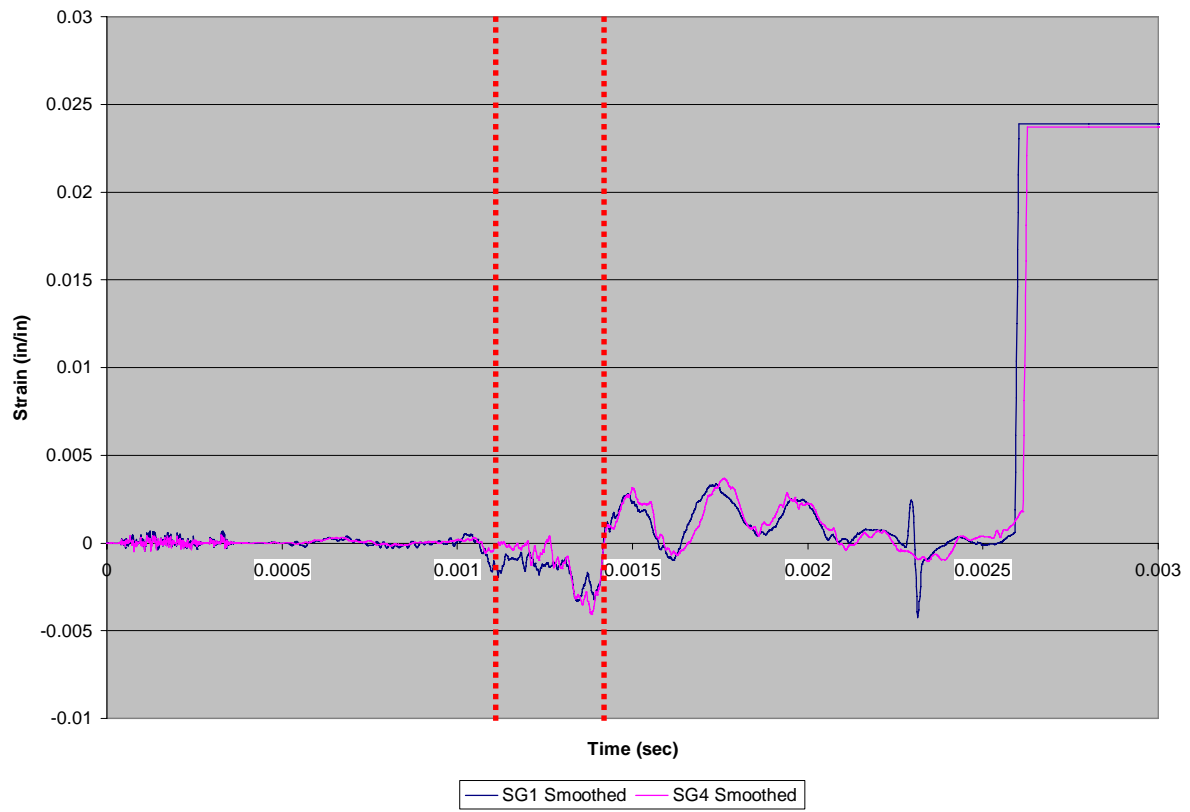


Figure C.4d.2: SG1 & SG4 skin strain vs. time (Specimen 4d)

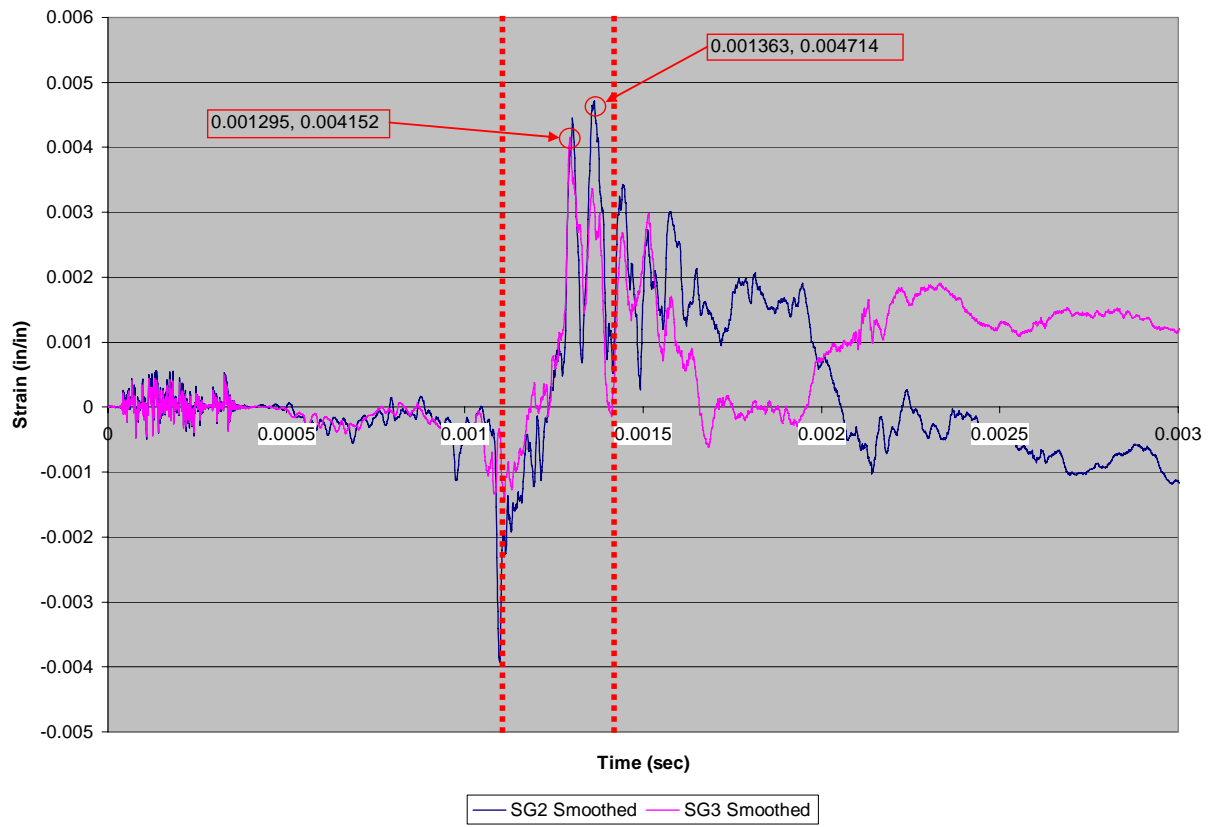


Figure C.4d.3: SG2 & SG3 spar strain vs. time (Specimen 4d)

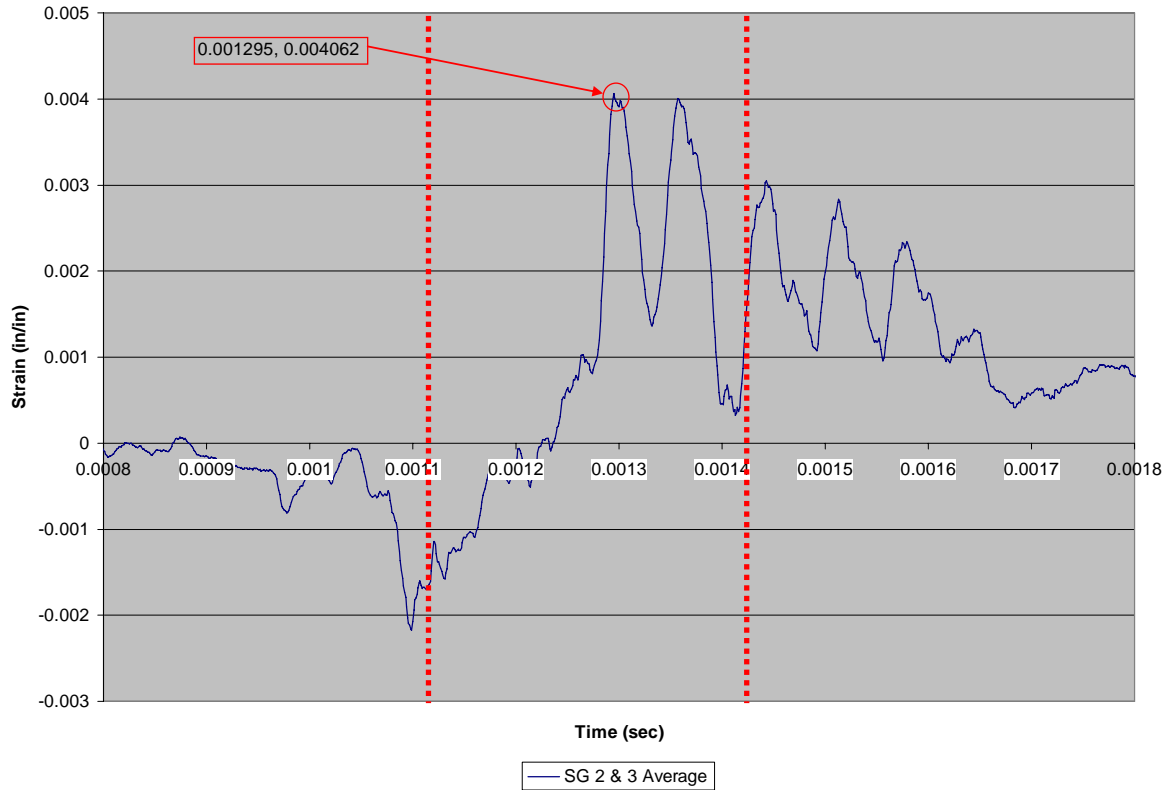


Figure C.4d.4: SG2 & SG3 average spar strain vs. time (Specimen 4d)

Specimen 4e, Test 32

For Specimen 4e, the load interval (and therefore the strain vs. time interval of interest) is approximately 1.10ms-1.45ms as shown in Figure C.4e.1. As desired, pressure sensors K1 and K3 are largely in agreement, indicating side-to-side uniformity of load on the test specimen. During the load interval, Figure C.4e.2 shows that SG1 and SG4 are in phase and of similar amplitude. Similarly, SG2 and SG3 are in phase (as seen in Figure C.4e.3), and are of similar amplitude, implying symmetric failure. Failure metrics for Specimen 4e are derived from Figure C.4e.4. Failure strain occurred at 1.352ms with a maximum strain of 0.003663 in/in. As such, it appears that the specimen strained in a symmetric manner up to the time of failure.

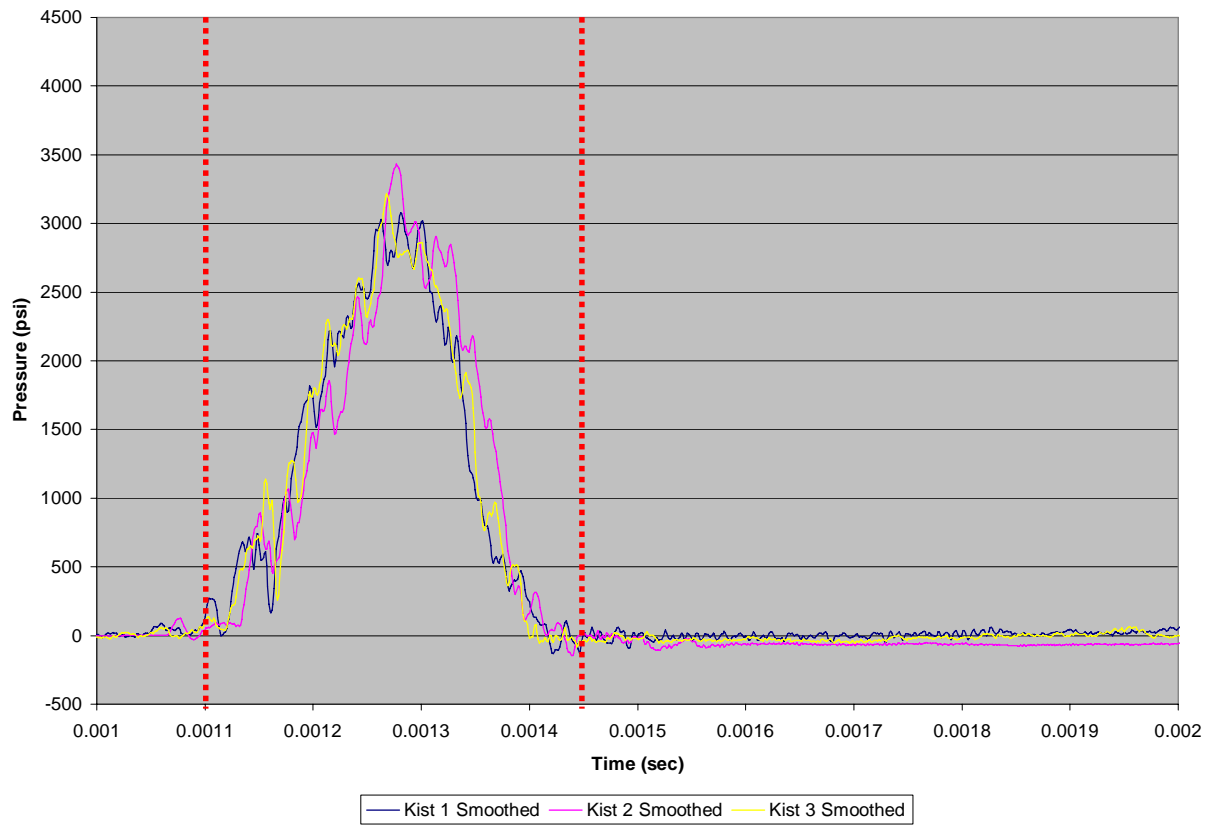


Figure C.4e.1: Kistler pressure vs. time (Specimen 4e)

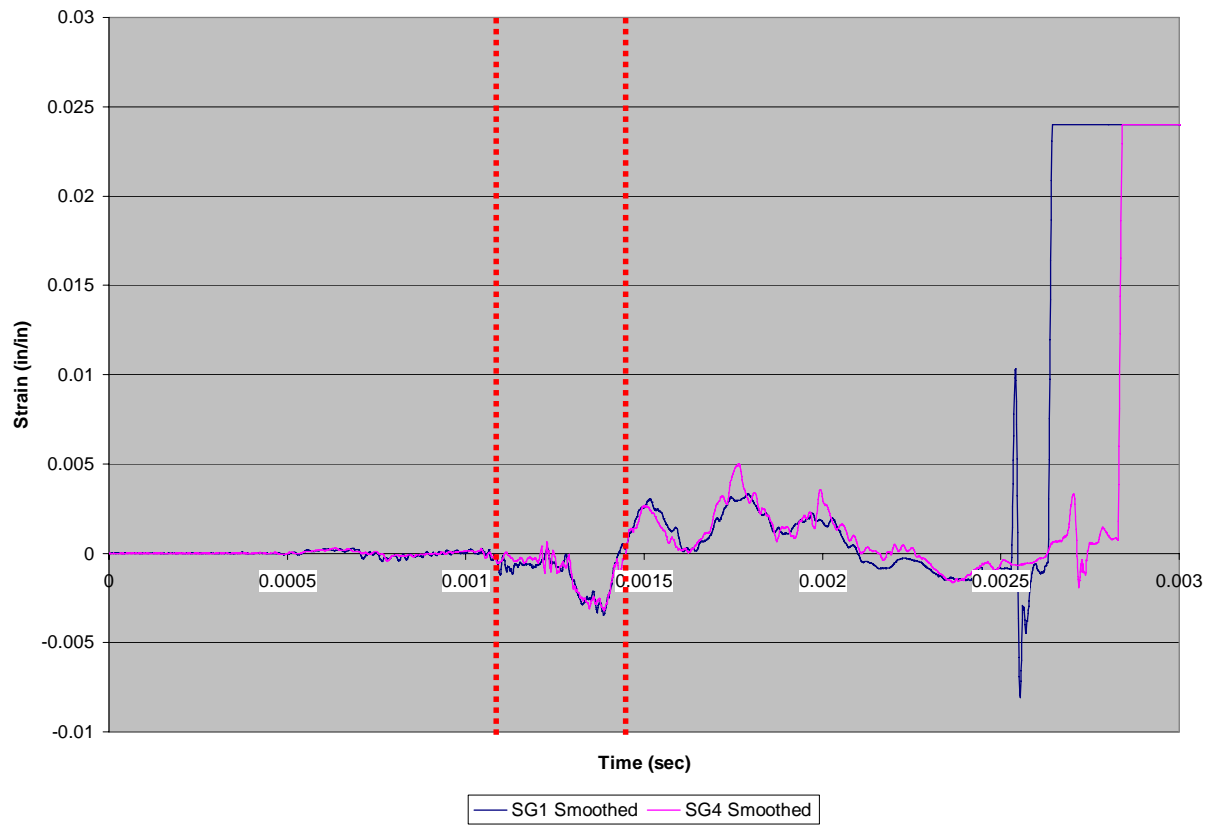


Figure C.4e.2: SG1 & SG4 skin strain vs. time (Specimen 4e)

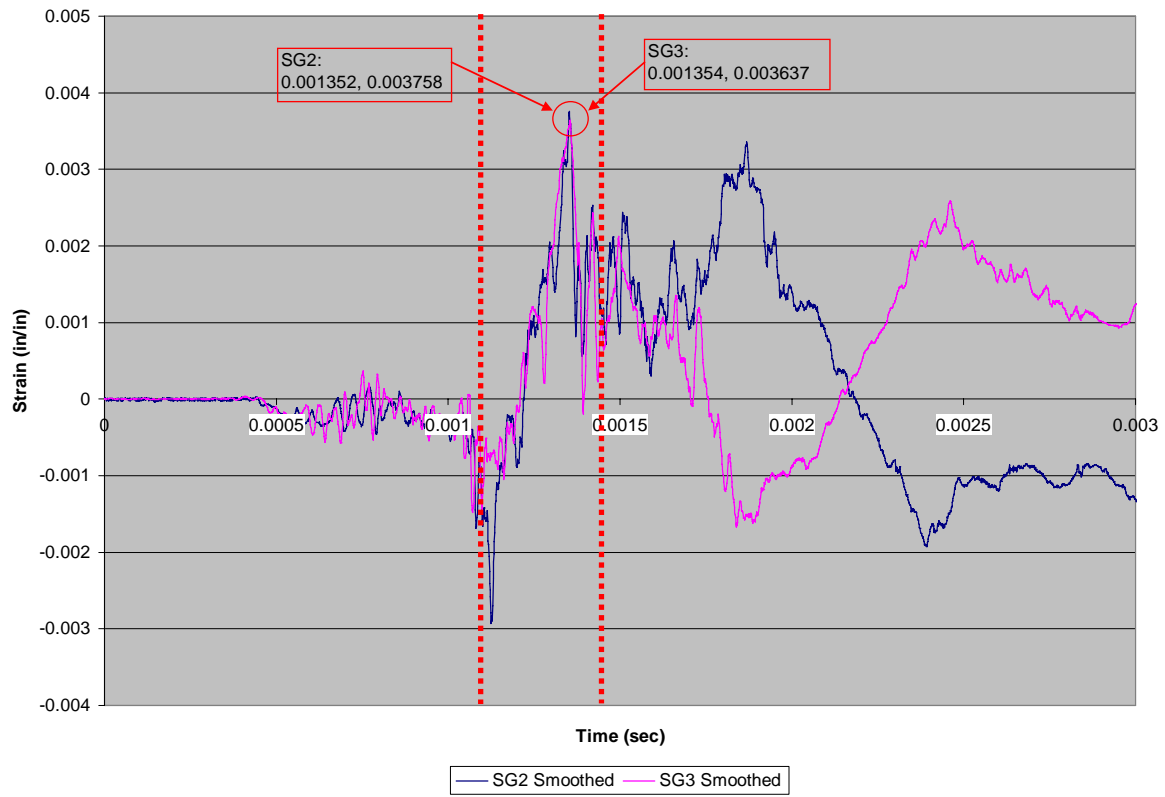


Figure C.4e.3: SG2 & SG3 spar strain vs. time (Specimen 4e)

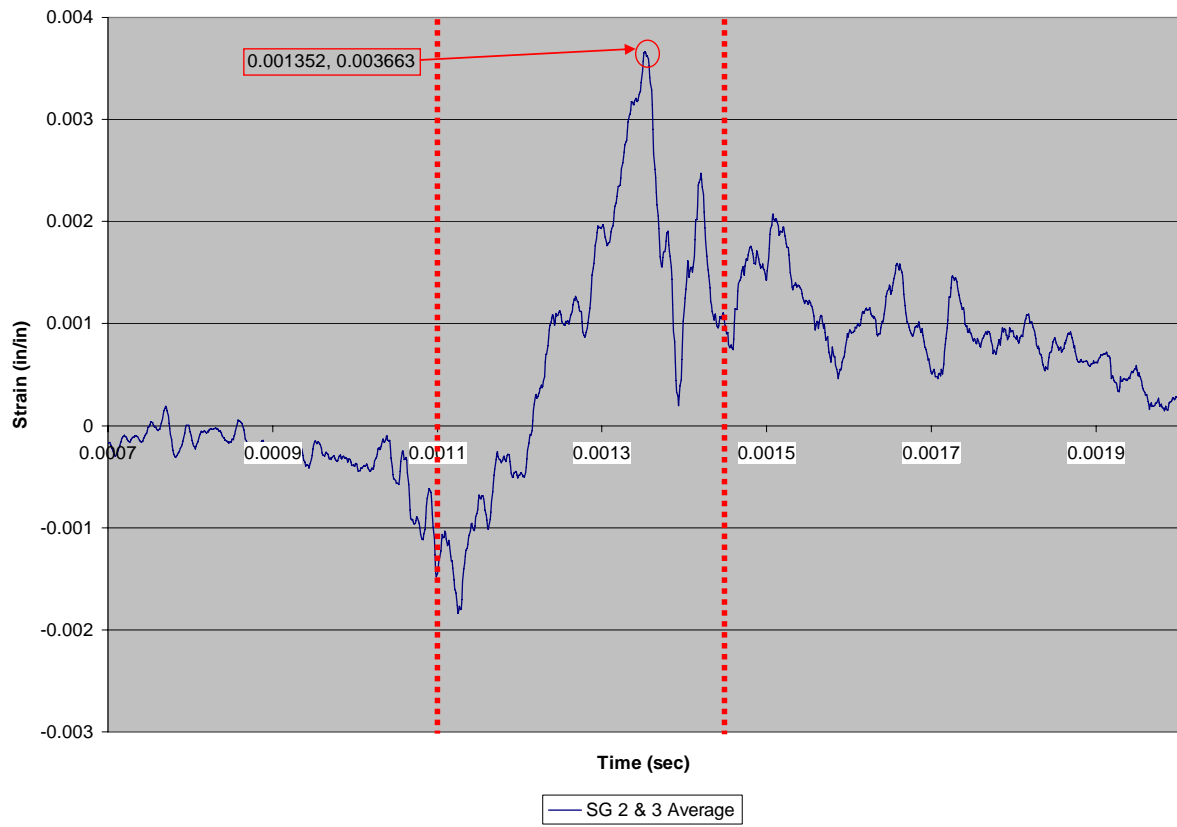


Figure C.4e.4: SG2 & SG3 average spar strain vs. time (Specimen 4e)

C.5 Specimen Set 5: Cobonded Prepreg

C.5.1 Dynamic Tests of Specimen Set 5

Specimen 5a, Test 13

For Specimen 5a, the load interval (and therefore the strain vs. time interval of interest) is approximately 1.15ms - 1.50ms as seen in Figure C.5a.1. As desired, pressure sensors K1 and K3 are largely in agreement, indicating side-to-side uniformity of load on the test specimen. During the load interval, Figure C.5a.2 shows that SG1 and SG4 are in phase and of similar amplitude, indicating the skin pulled away from the spar in a symmetric fashion. Similarly, SG2 and SG3 remain in phase and of similar amplitude (as seen in Figure C.5a.3) implying symmetric failure. Failure metrics for Specimen 5a are derived from Figure C.5a.4. Failure strain occurred at 1.432ms with a maximum strain of 0.001687 in/in.

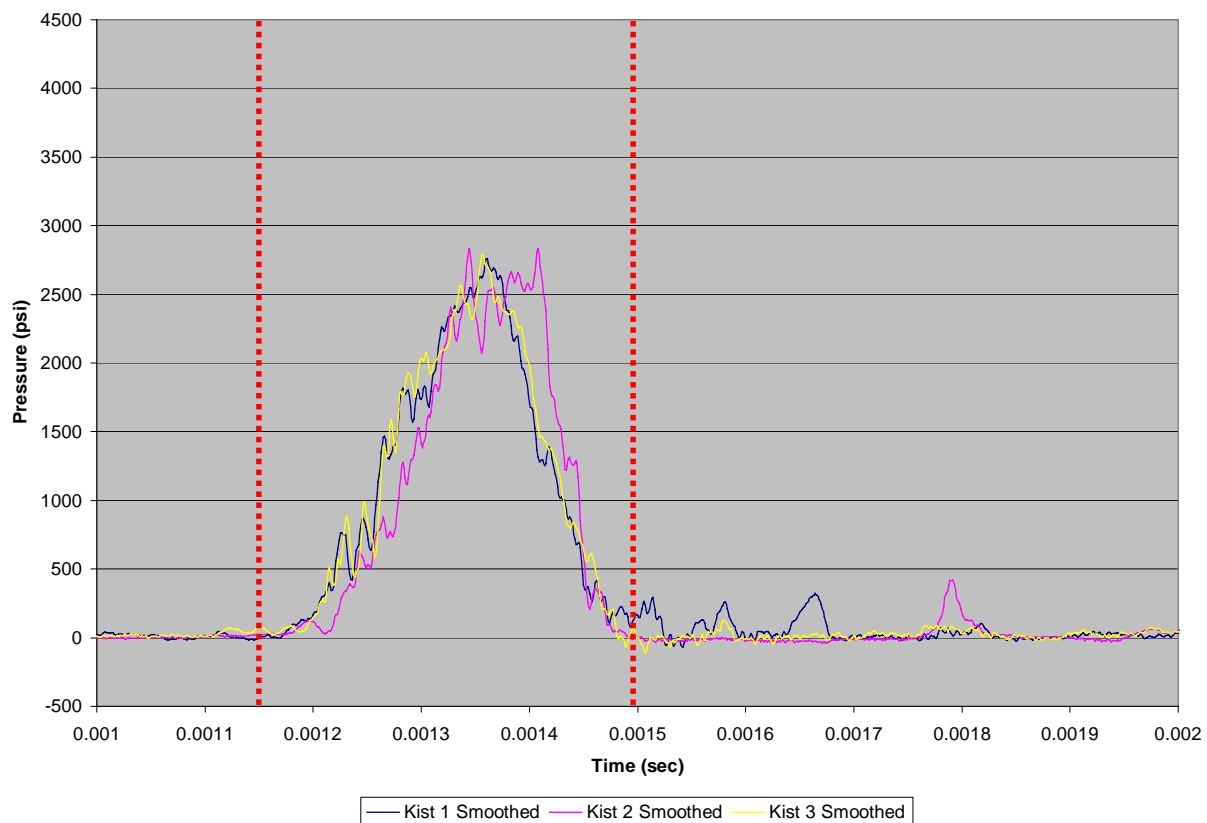


Figure C.5a.1: Kistler pressure vs. time (Specimen 5a)

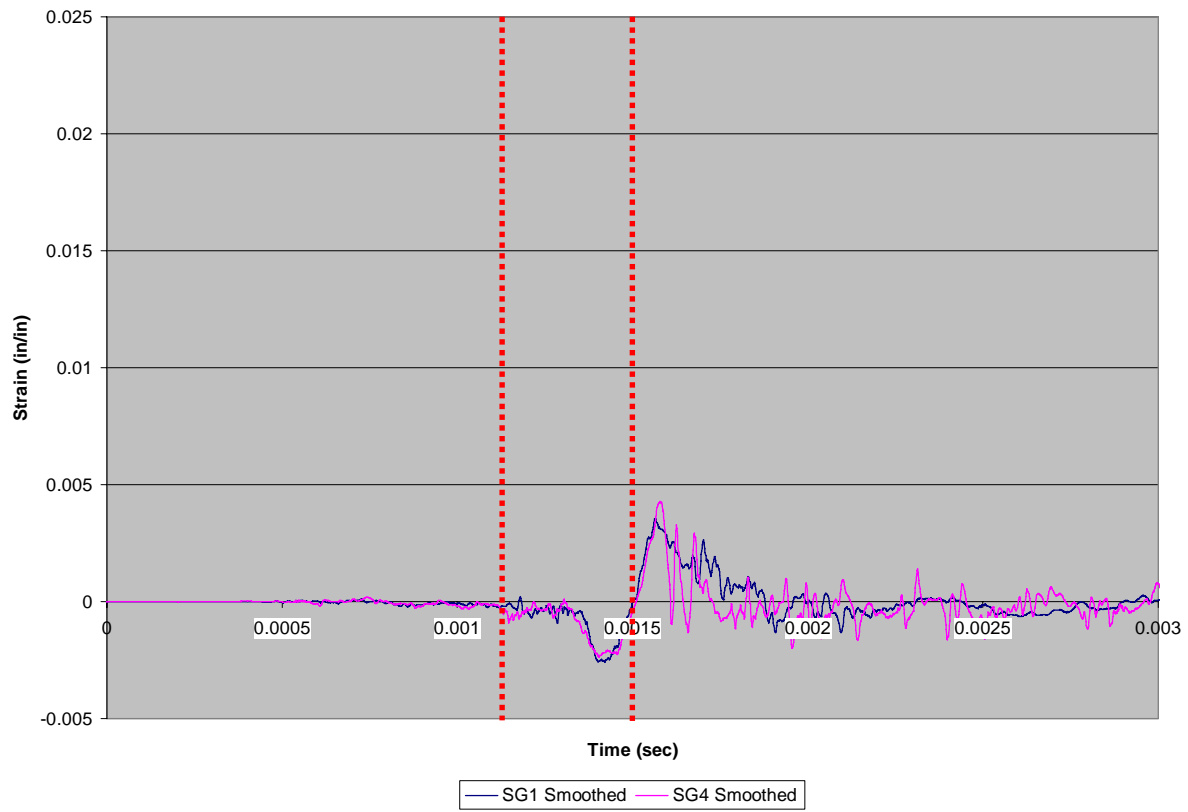


Figure C.5a.2: SG1 & SG4 skin strain vs. time (Specimen 5a)

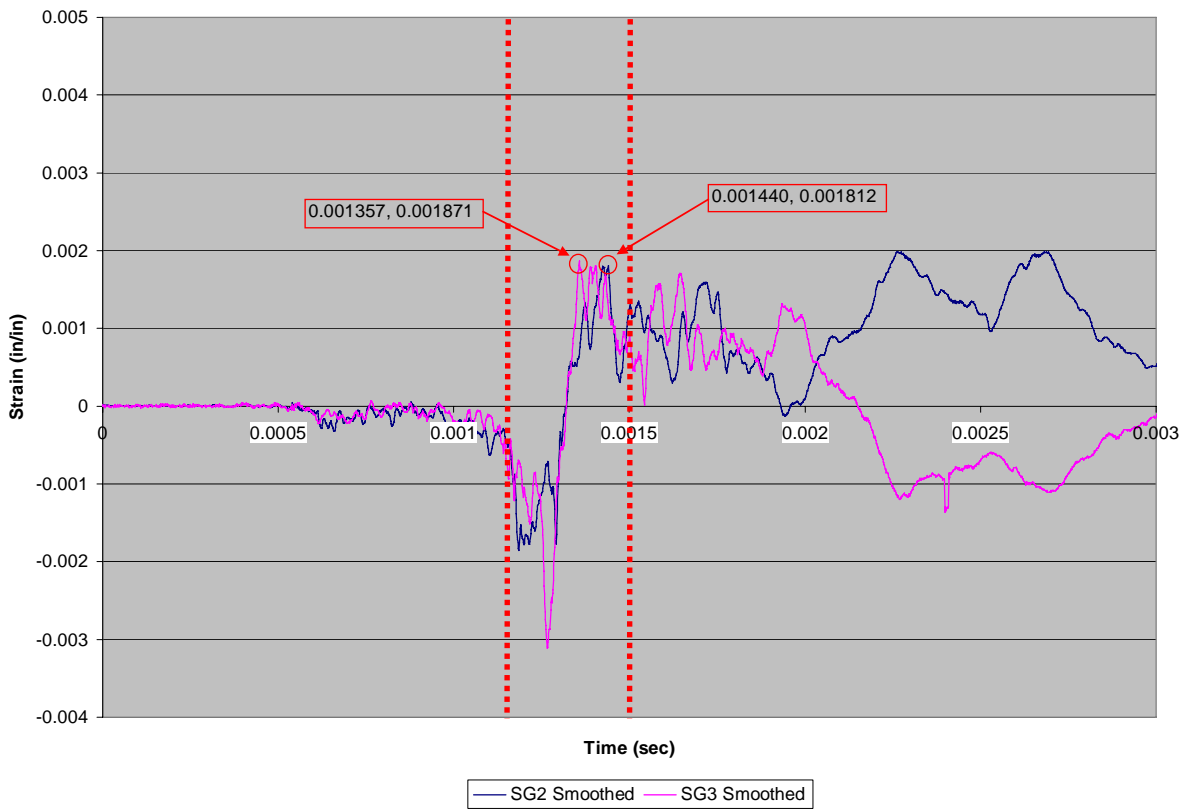


Figure C.5a.3: SG2 & SG3 spar strain vs. time (Specimen 5a)

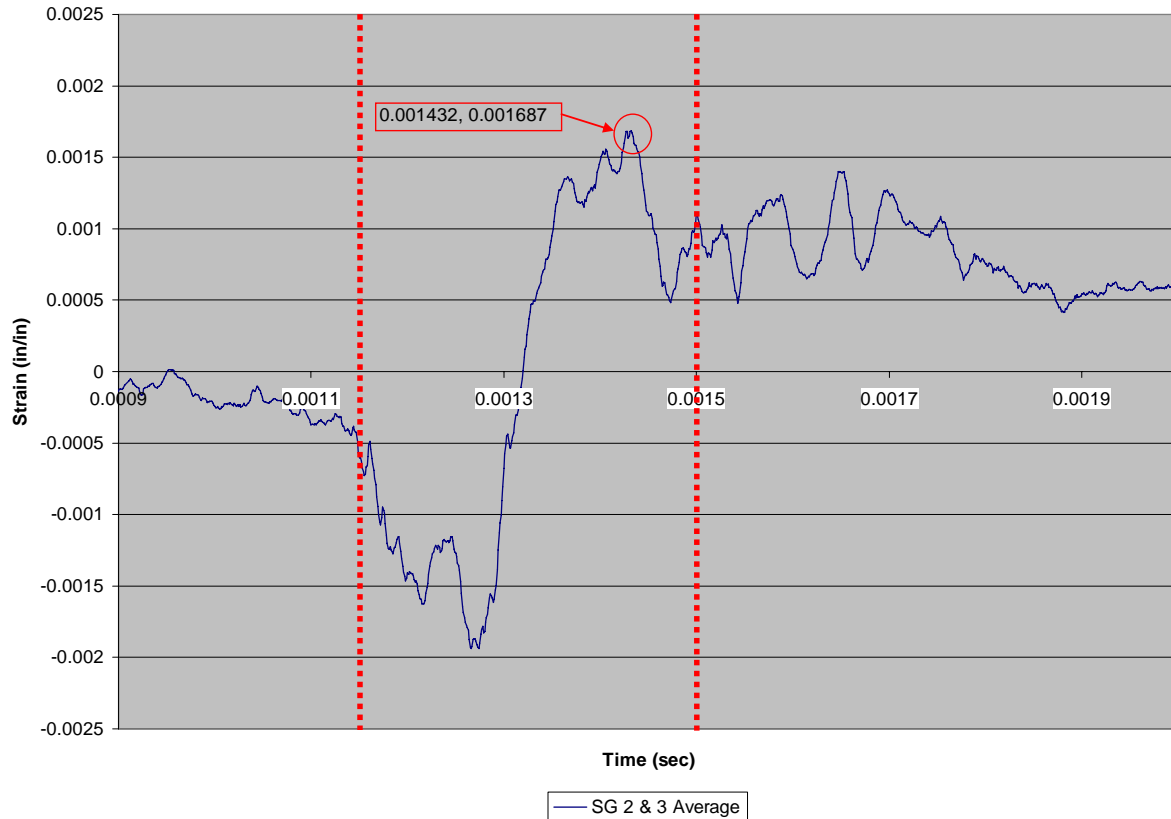


Figure C.5a.4: SG2 & SG3 average spar strain vs. time (Specimen 5a)

Specimen 5b, Test 14

For Specimen 5b, the load interval (and therefore the strain vs. time interval of interest) is approximately 1.13ms - 1.42ms as seen in Figure C.5b.1. As desired, pressure sensors K1 and K3 are largely in agreement, indicating side-to-side uniformity of load on the test specimen. During the load interval, Figure C.5b.2 shows that SG1 and SG4 are in phase and of similar amplitude, indicating the skin pulled away from the spar in a symmetric fashion. Similarly, SG2 and SG3 appear mostly in phase (as seen in Figure C.5b.3), but strains differ in amplitude, implying asymmetric failure. Failure metrics for Specimen 5b are derived from Figure C.5b.4. Failure strain occurred at 1.340ms with a maximum strain of 0.00235 in/in.

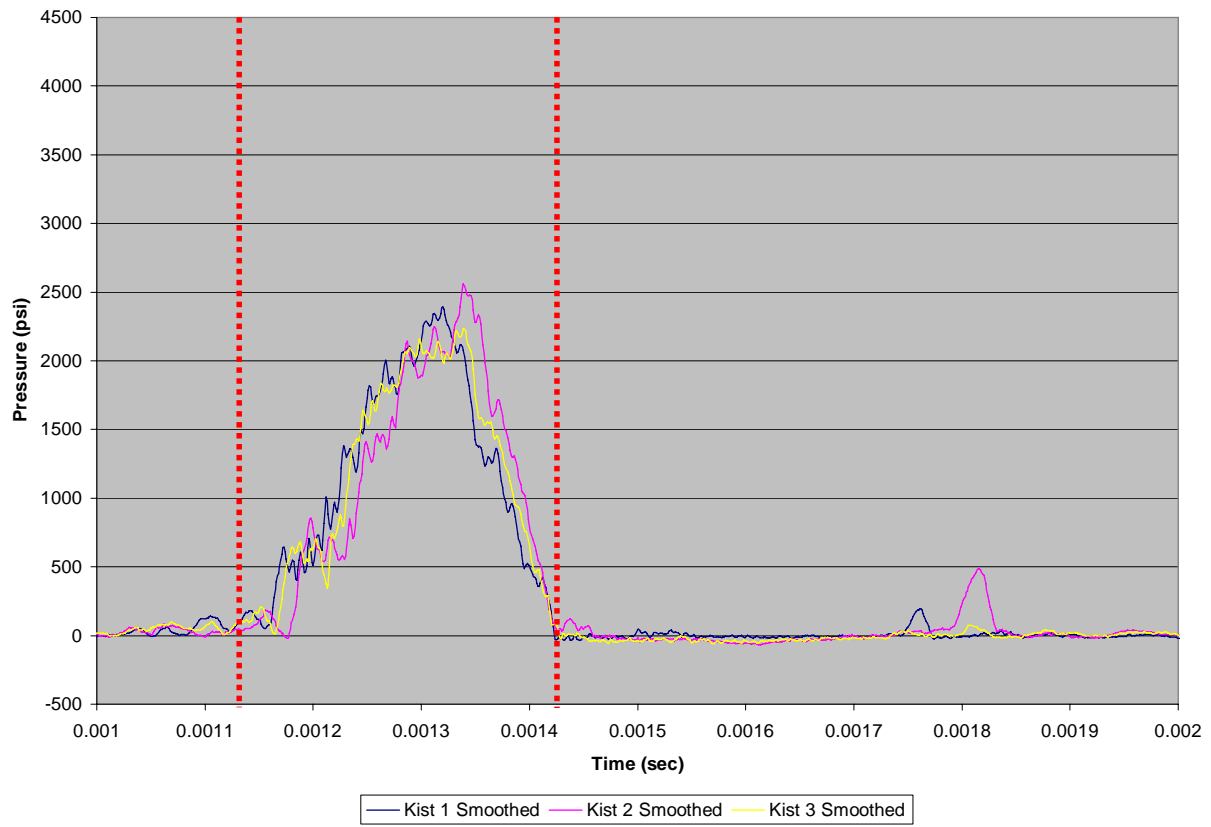


Figure C.5b.1: Kistler pressure vs. time (Specimen 5b)

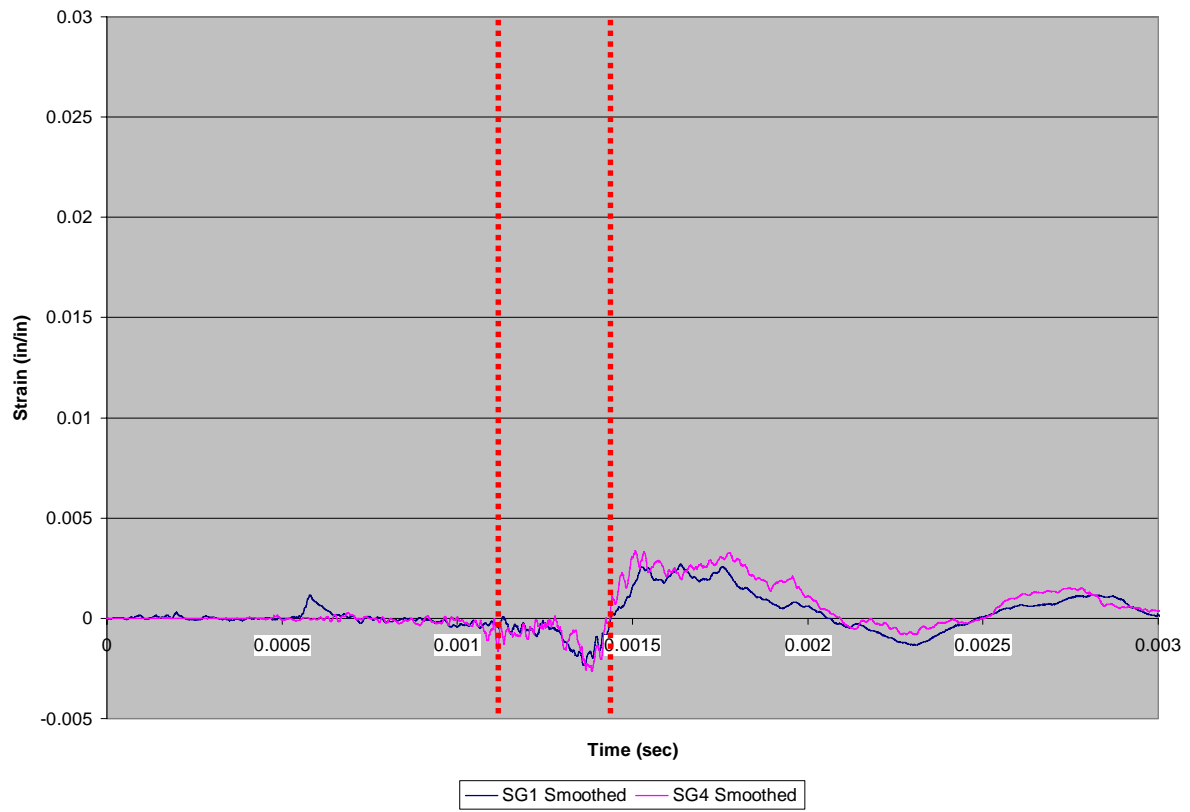


Figure C.5b.2: SG1 & SG4 skin strain vs. time (Specimen 5b)

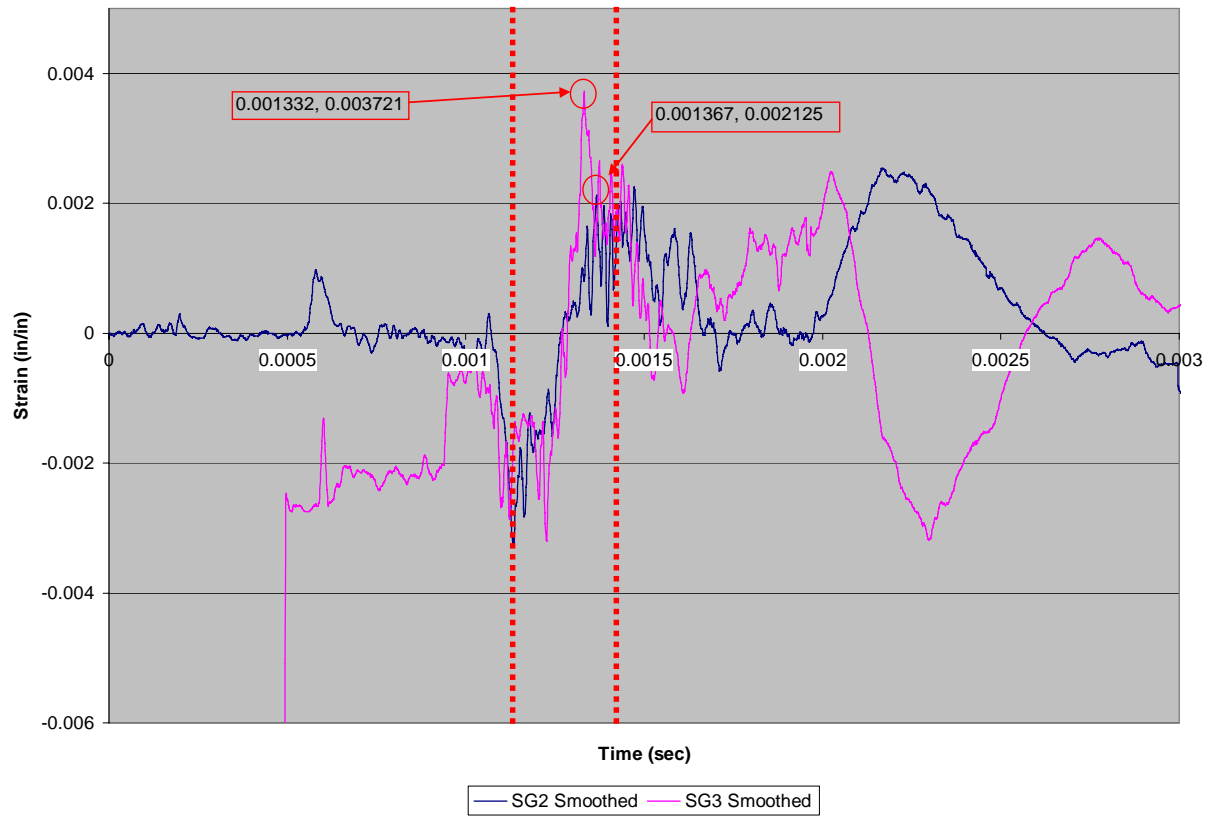


Figure C.5b.3: SG2 & SG3 spar strain vs. time (Specimen 5b)

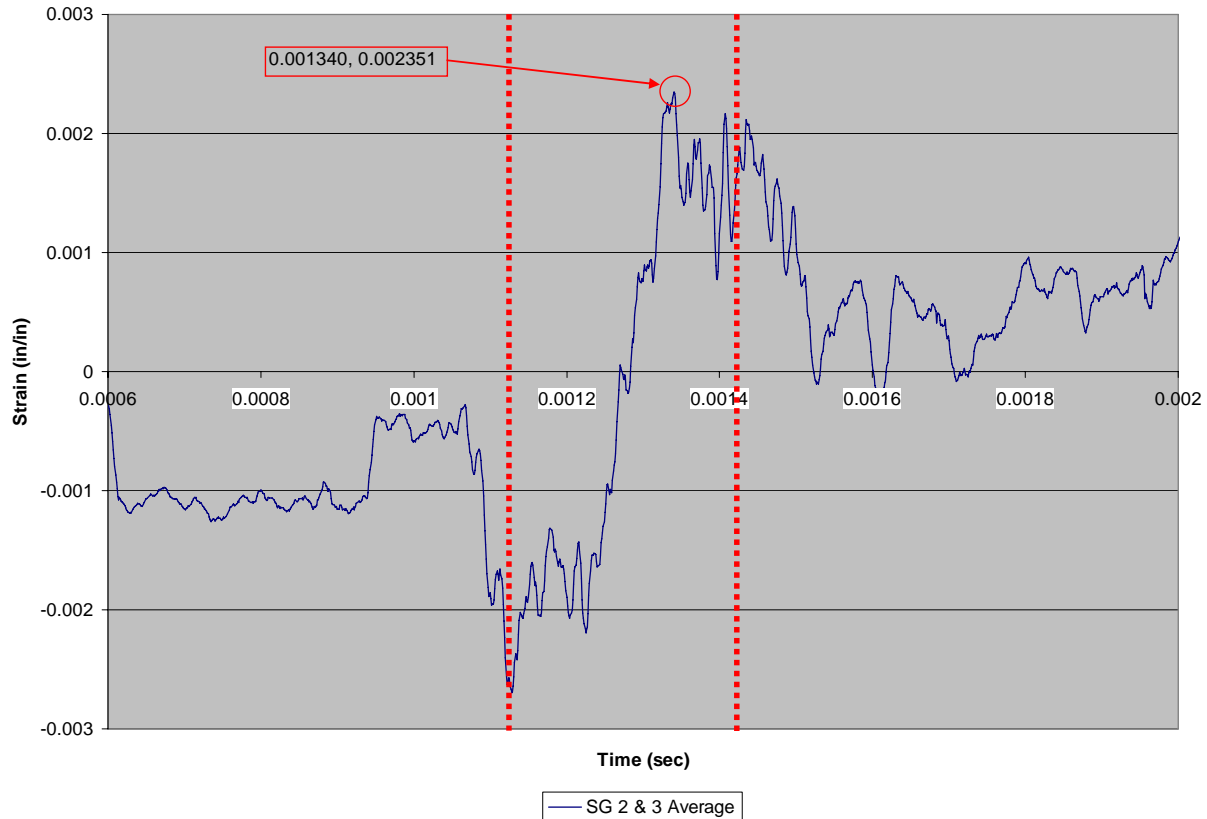


Figure C.5b.4: SG2 & SG3 average spar strain vs. time (Specimen 5b)

Specimen 5c, Test 15

For Specimen 5c, the load interval (and therefore the strain vs. time interval of interest) is approximately 1.15 ms to 1.50ms as shown in Figure C.5c.1. As desired, pressure sensors K1 and K3 are largely in agreement, indicating side-to-side uniformity of load on the test specimen. During the load interval, Figure C.5c.2 shows that SG1 and SG4 are mostly in phase (particularly late in the load profile) and are of similar amplitude at the moment of failure, indicating the skin pulled away from the spar in a symmetric fashion. SG2 and SG3 on the spar also appear mostly in phase (and of similar amplitude at the moment of failure) except for a brief spike on SG3 at 1.372ms (Figure C.5c.3). Failure metrics for Specimen 5c are derived from Figure C.5c.4 and occurs upon conclusion of the load pulse. Failure strain occurred at 1.520ms with a maximum strain of 0.001068 in/in.

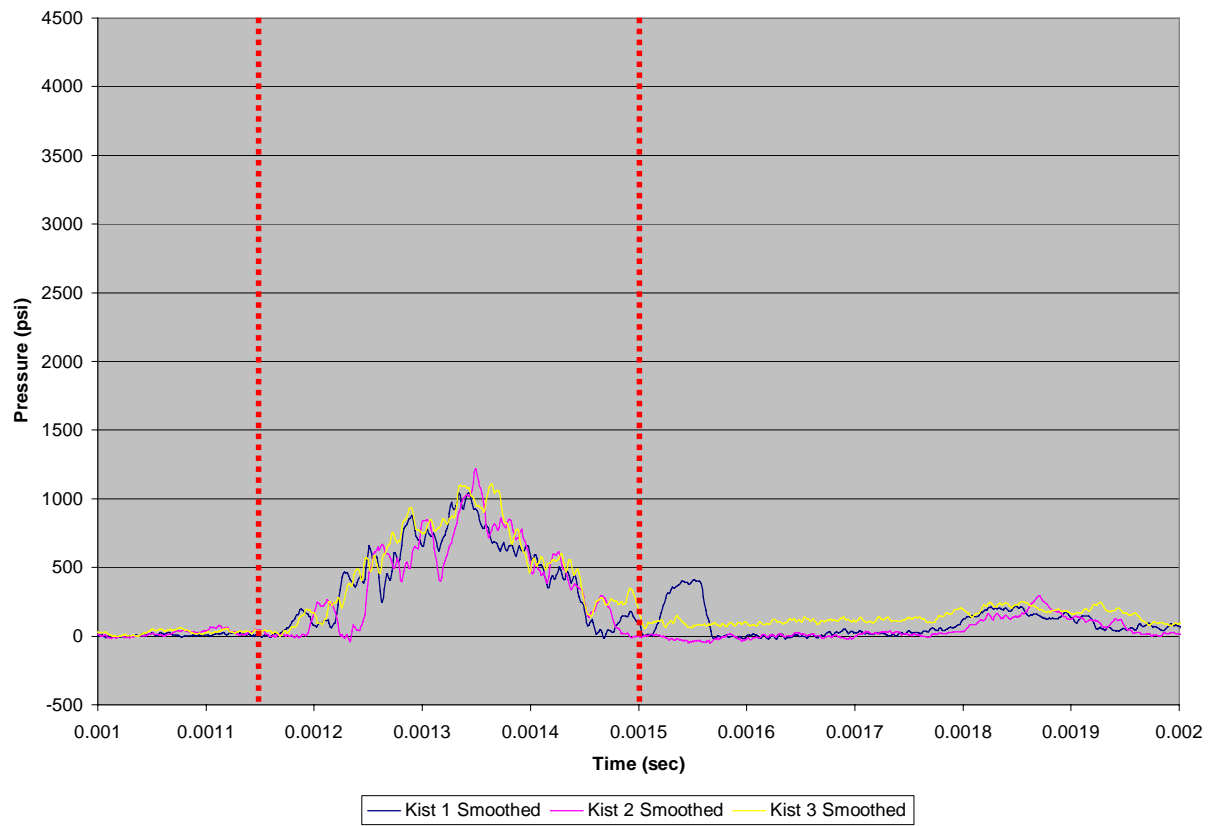


Figure C.5c.1: Kistler pressure vs. time (Specimen 5c)

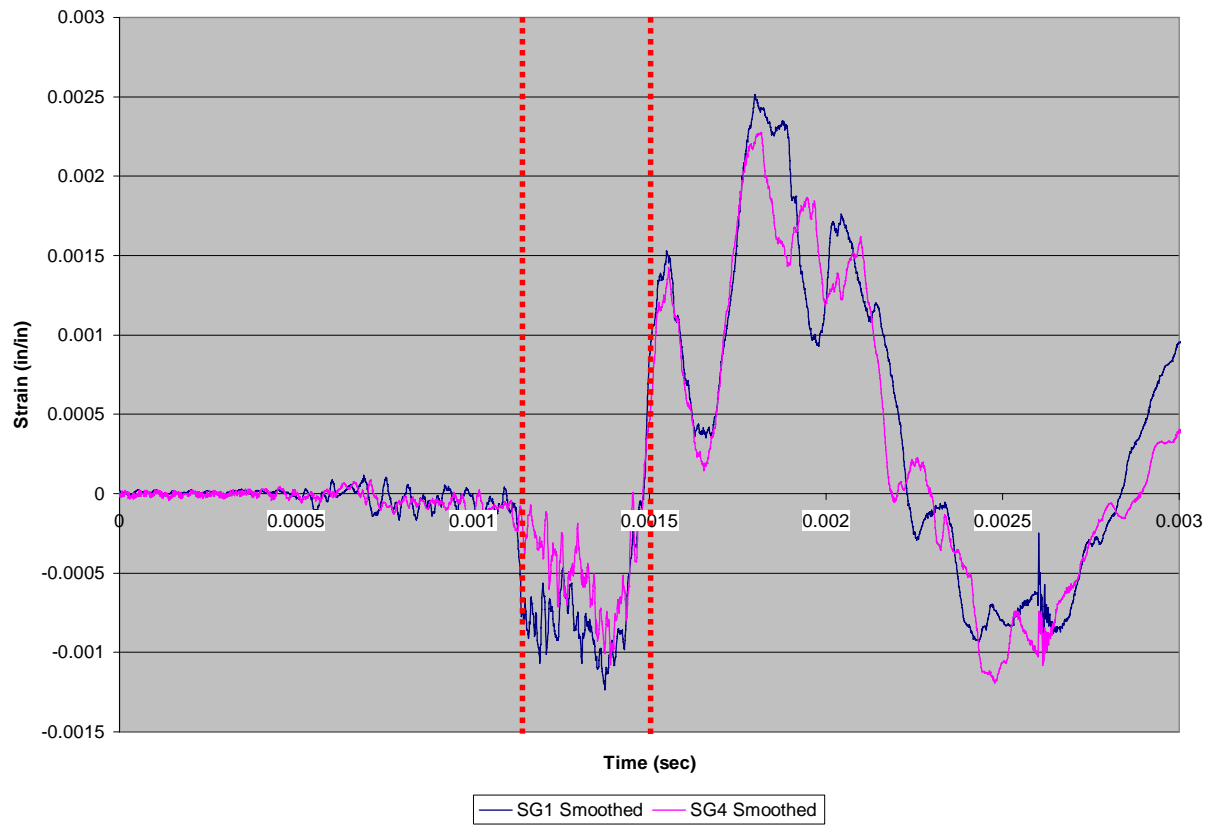


Figure C.5c.2: SG1 & SG4 skin strain vs. time (Specimen 5c)

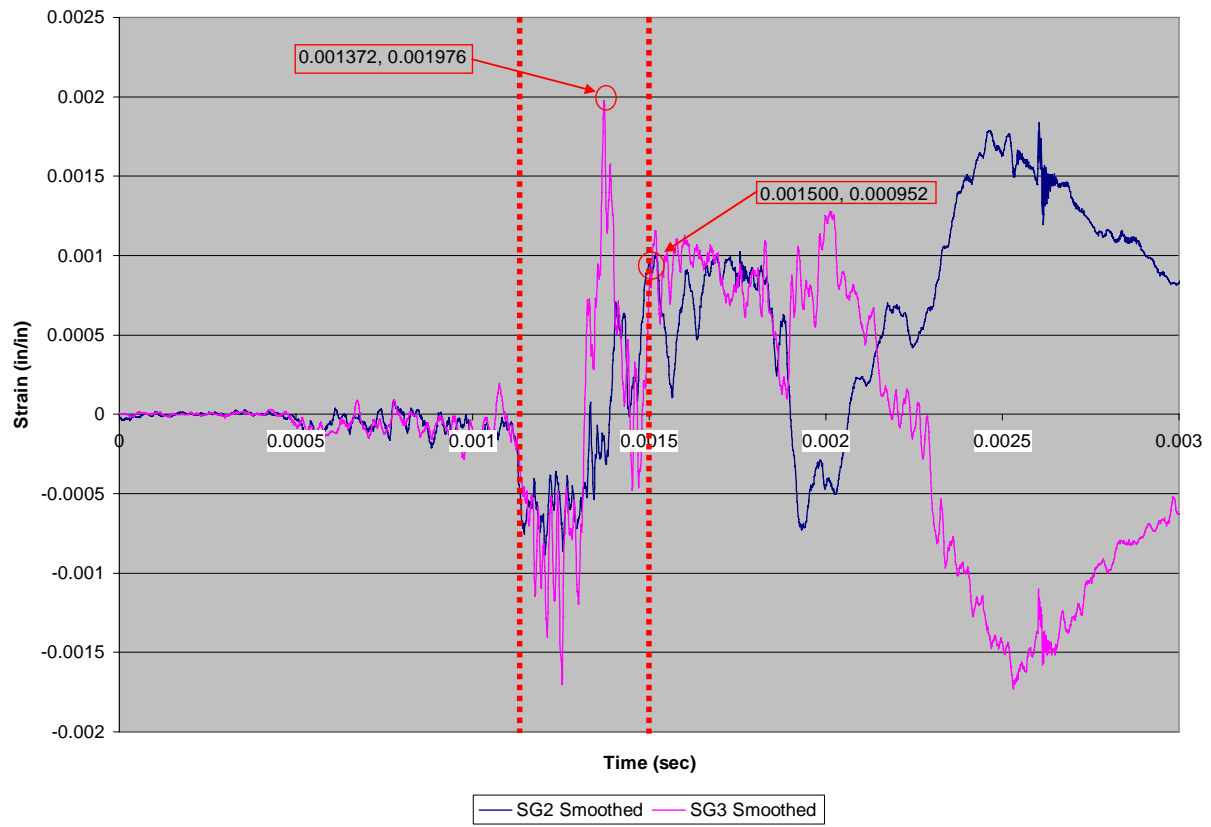


Figure C.5c.3: SG2 & SG3 spar strain vs. time (Specimen 5c)

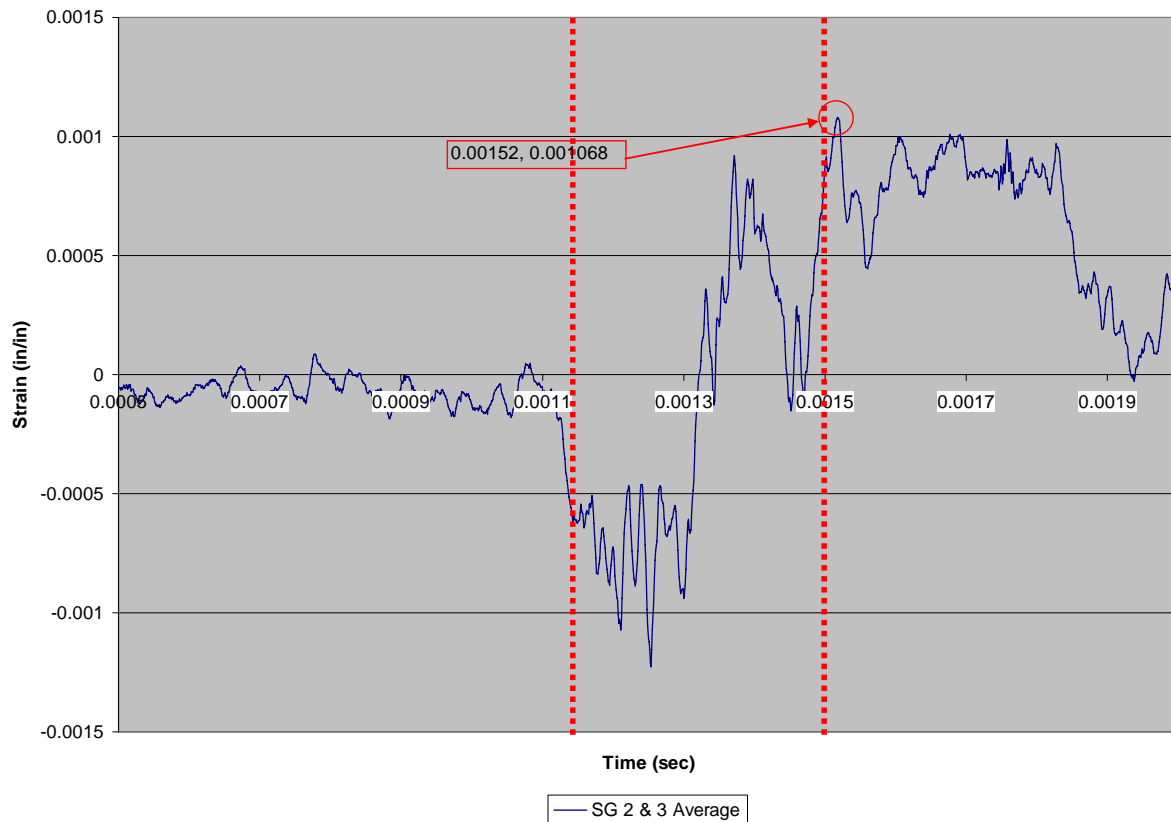


Figure C.5c.4: SG2 & SG3 average spar strain vs. time (Specimen 5c)

Specimen 5d, Test 30

For Specimen 5d, the load interval (and therefore the strain vs. time interval of interest) is approximately 1.12ms-1.46ms as shown in Figure C.5d.1. As desired, pressure sensors K1 and K3 are largely in agreement, indicating side-to-side uniformity of load on the test specimen. During the load interval, Figure C.5d.2 shows that SG1 and SG4 remain in phase and of similar amplitude. Similarly, SG2 and SG3 on the spar remain in phase and of similar amplitude (as seen in Figure C.5d.3) implying symmetric failure. Failure metrics for Specimen 5d are derived from Figure C.5d.4. Failure strain occurred at 1.369ms with a maximum strain of 0.002788 in/in.

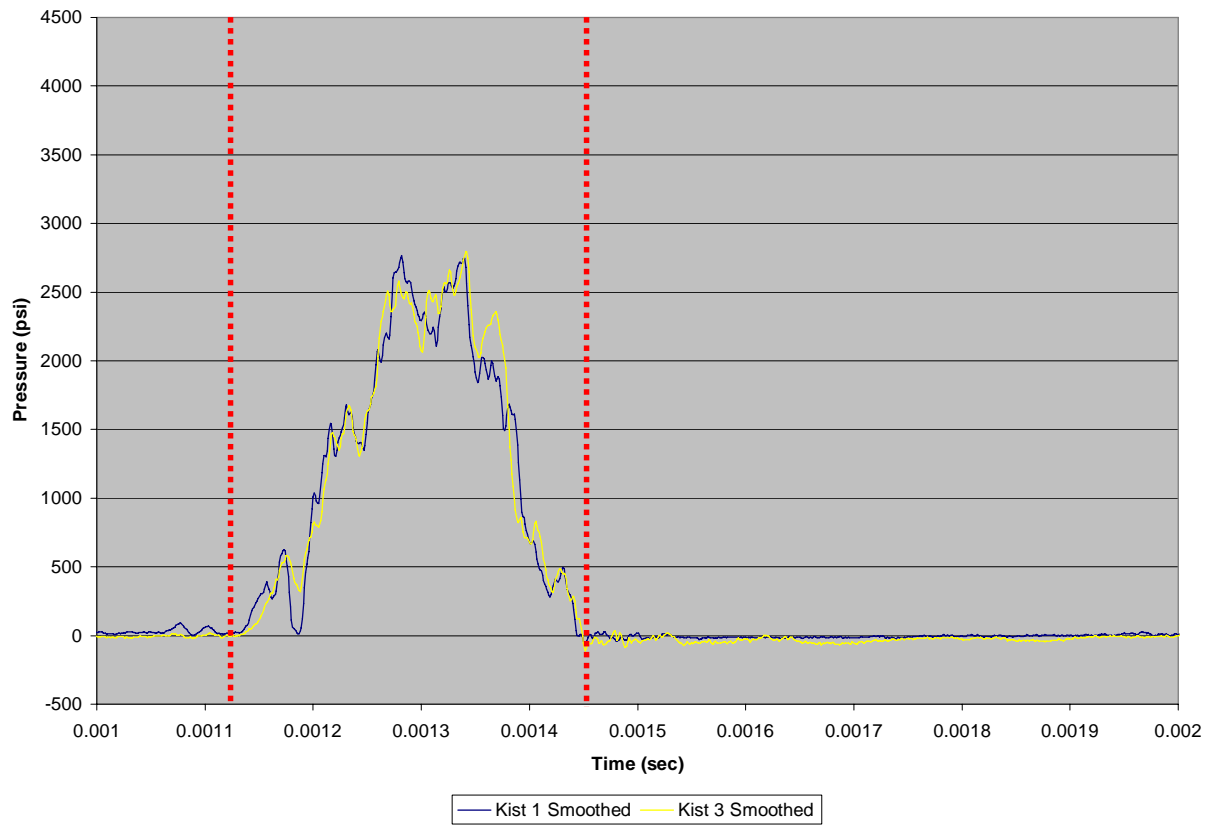


Figure C.5d.1: Kistler pressure vs. time (Specimen 5d)

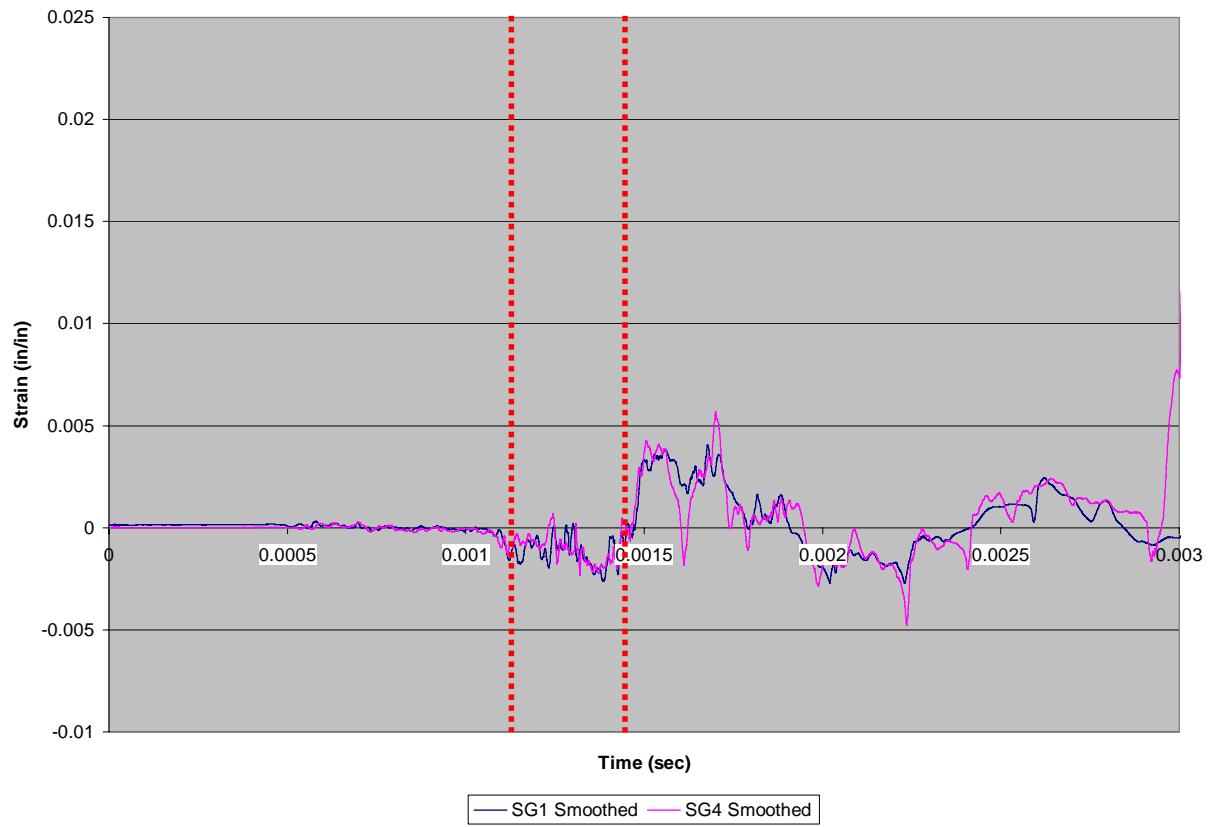


Figure C.5d.2: SG1 & SG4 skin strain vs. time (Specimen 5d)

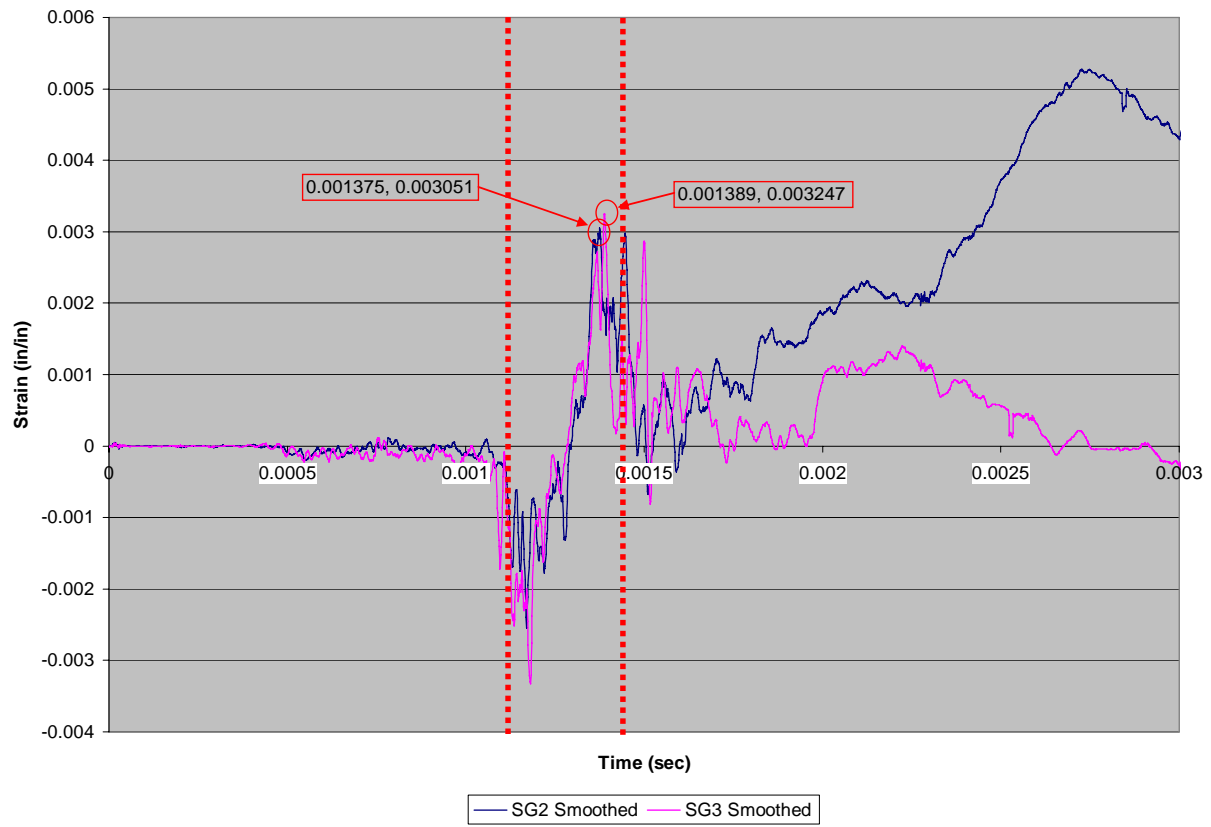


Figure C.5d.3: SG2 & SG3 spar strain vs. time (Specimen 5d)

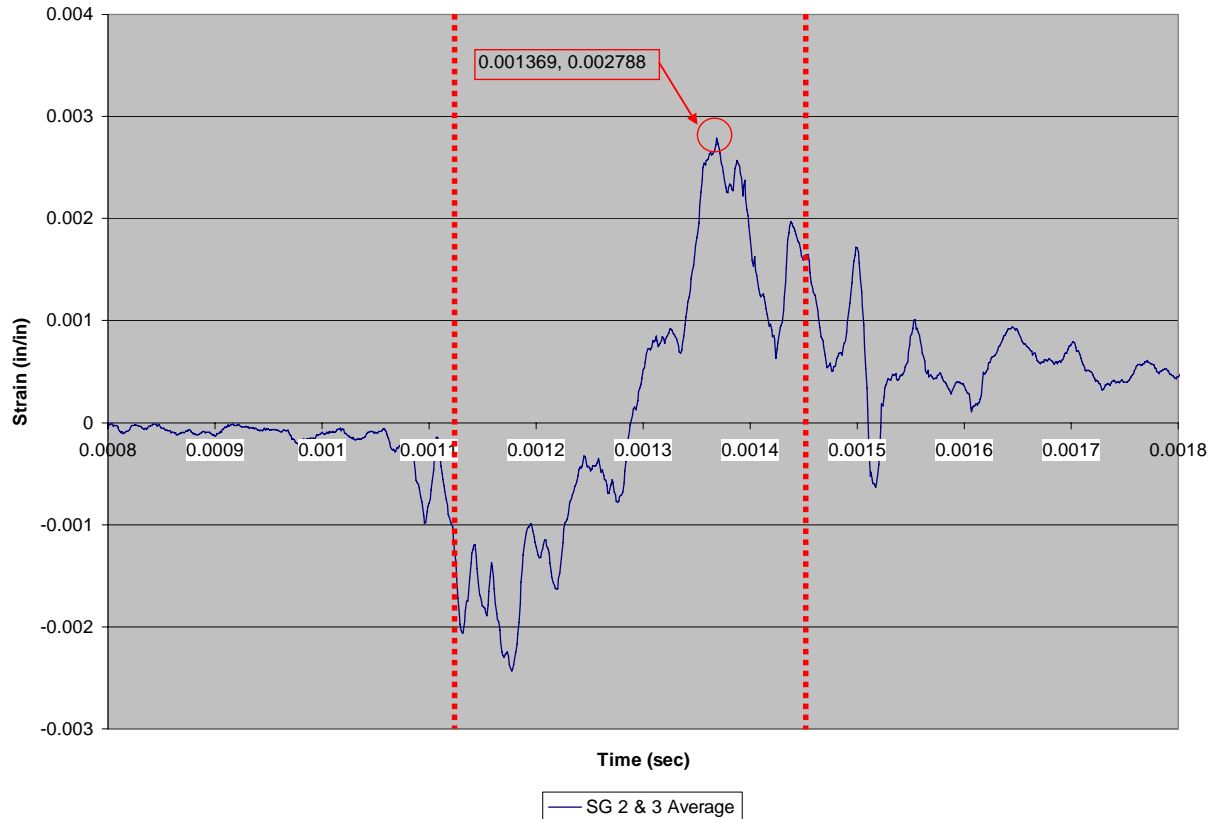


Figure C.5d.4: SG2 & SG3 average spar strain vs. time (Specimen 5d)

Specimen 5e, Test 33

For Specimen 5e, the load interval (and therefore the strain vs. time interval of interest) is approximately 1.07ms-1.40ms as shown in Figure C.5e.1. As desired, pressure sensors K1 and K3 are largely in agreement, indicating side-to-side uniformity of load on the test specimen. During this time interval of interest, Figure C.5e.2 shows that SG1 and SG4 remain in phase and of similar amplitude. Similarly, SG2 and SG3 on the spar remain in phase and of similar amplitude (as seen in Figure C.5e.3) implying symmetric failure. Failure metrics for Specimen 5e are derived from Figure C.5e.4. Failure strain occurred at 1.335ms with a maximum strain of 0.002429 in/in.

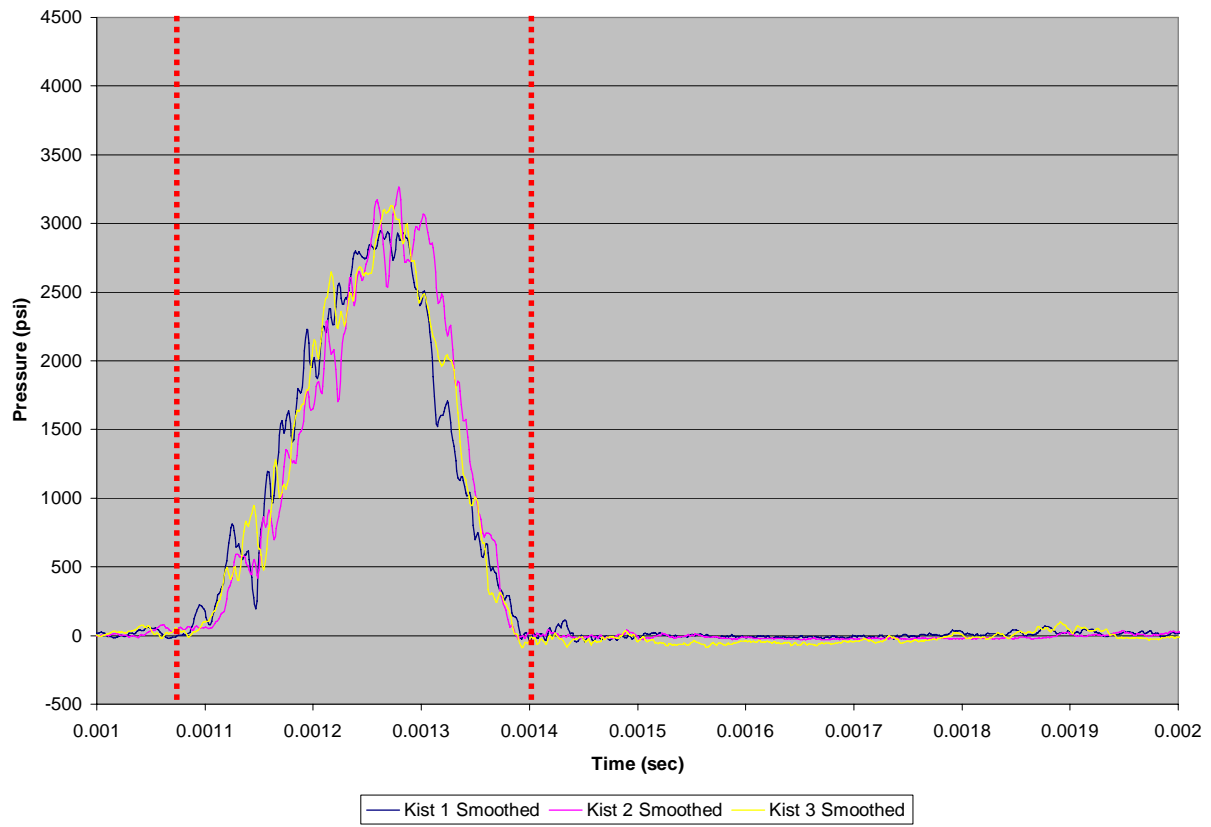


Figure C.5e.1: Kistler pressure vs. time (Specimen 5e)

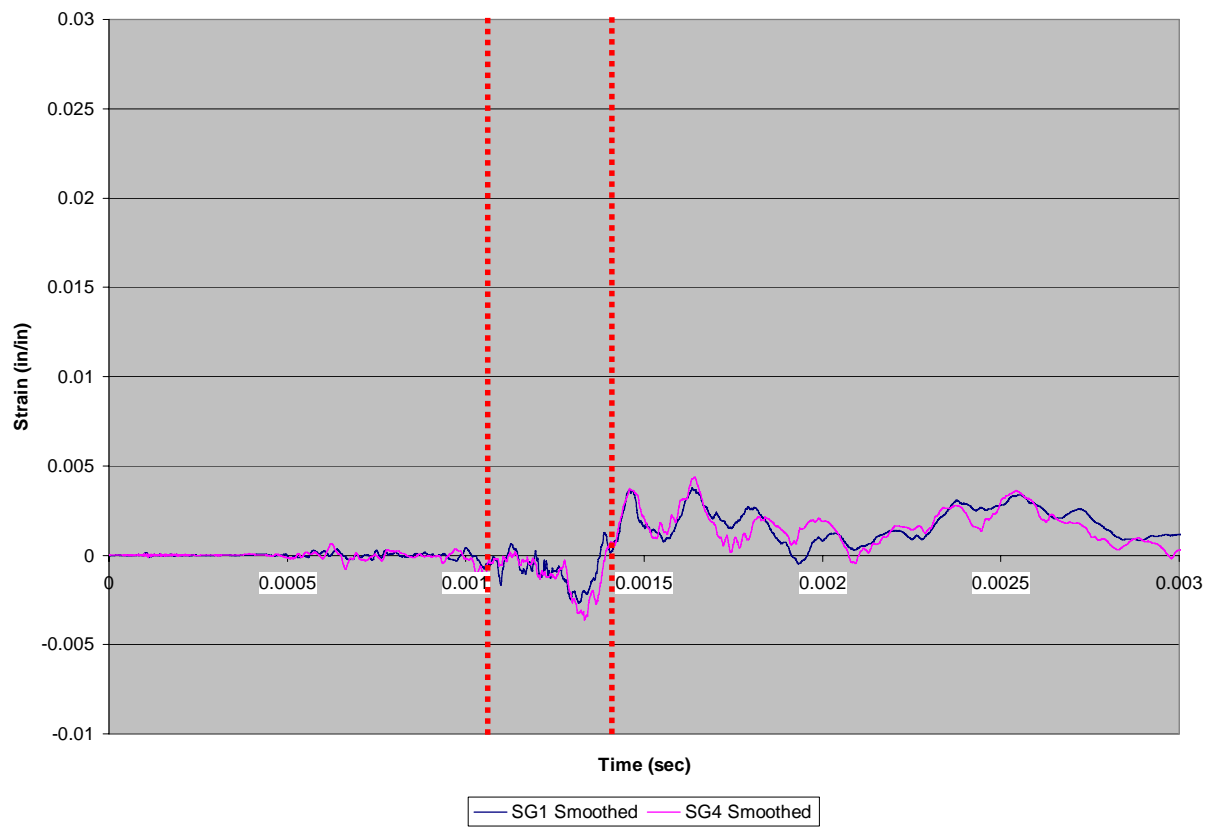


Figure C.5e.2: SG1 & SG4 skin strain vs. time (Specimen 5e)

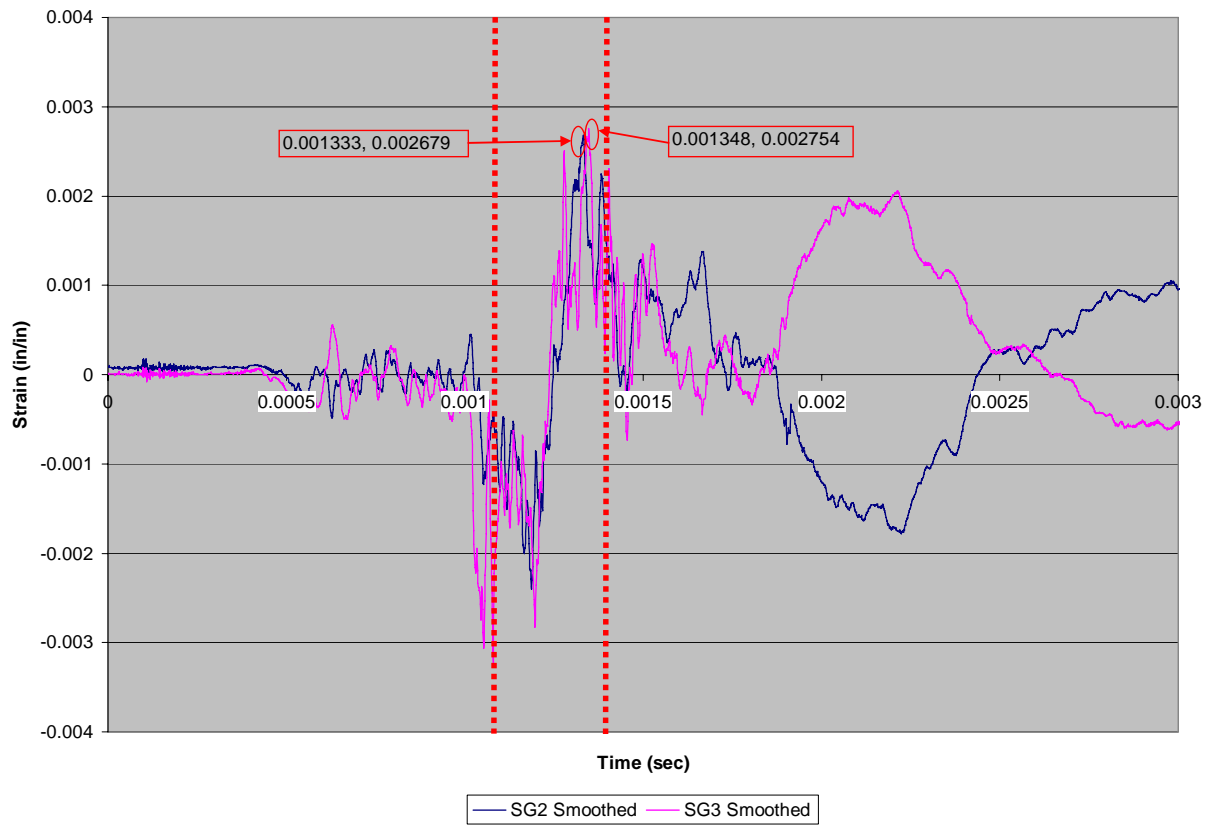


Figure C.5e.3: SG2 & SG3 spar strain vs. time (Specimen 5e)

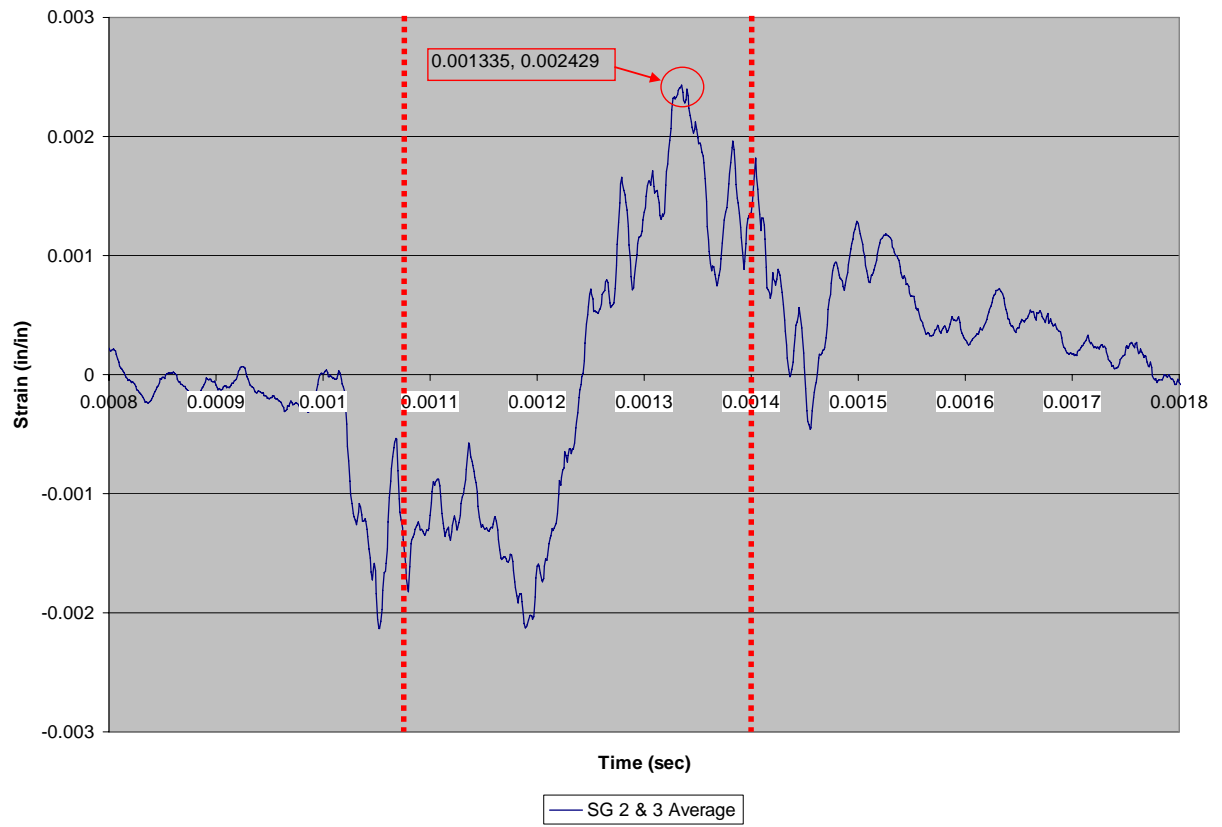


Figure C.5e.4: SG2 & SG3 average spar strain vs. time (Specimen 5e)

C.6 Specimen Set 6: One Shot Infiltration

C.6.1 Dynamic Tests of Specimen Set 6

Specimen 6a, Test 16

For Specimen 6a, the load interval (and therefore the strain vs. time interval of interest) is approximately 1.17ms - 1.53ms as seen in Figure C.6a.1. Pressure sensor K3 was inoperative during the test, so side-to-side load uniformity cannot be verified. During the load interval, Figure C.6a.2 shows that SG1 and SG4 tend to stay in phase and of similar amplitude (particularly late in the load cycle) indicating the skin pulled away from the spar in a symmetric fashion. Similarly, SG2 and SG3 also remain largely in phase and of similar amplitude (as seen in Figure C.6a.3) implying symmetric failure. Failure metrics for Specimen 6a are derived from Figure C.6a.4. Failure strain occurred at 1.441ms with a maximum strain of 0.00305 in/in.

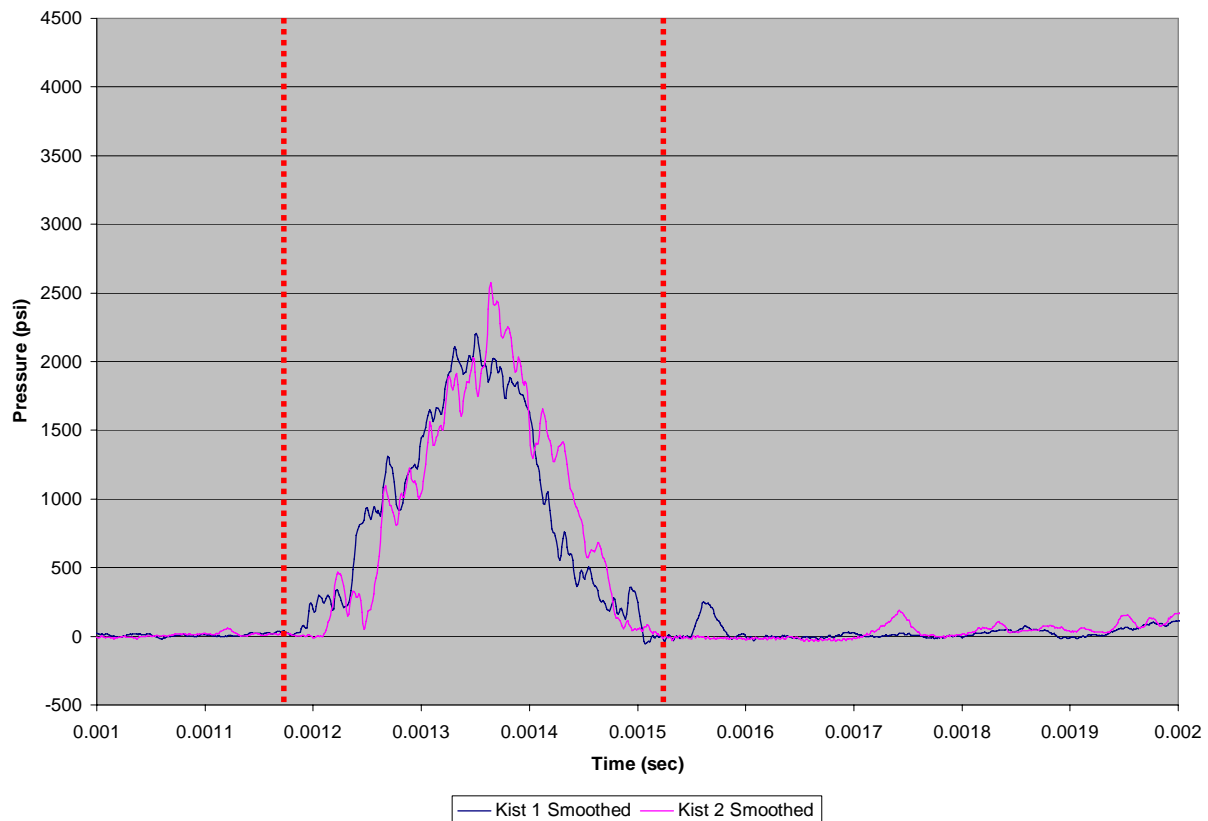


Figure C.6a.1: Kistler pressure vs. time (Specimen 6a)

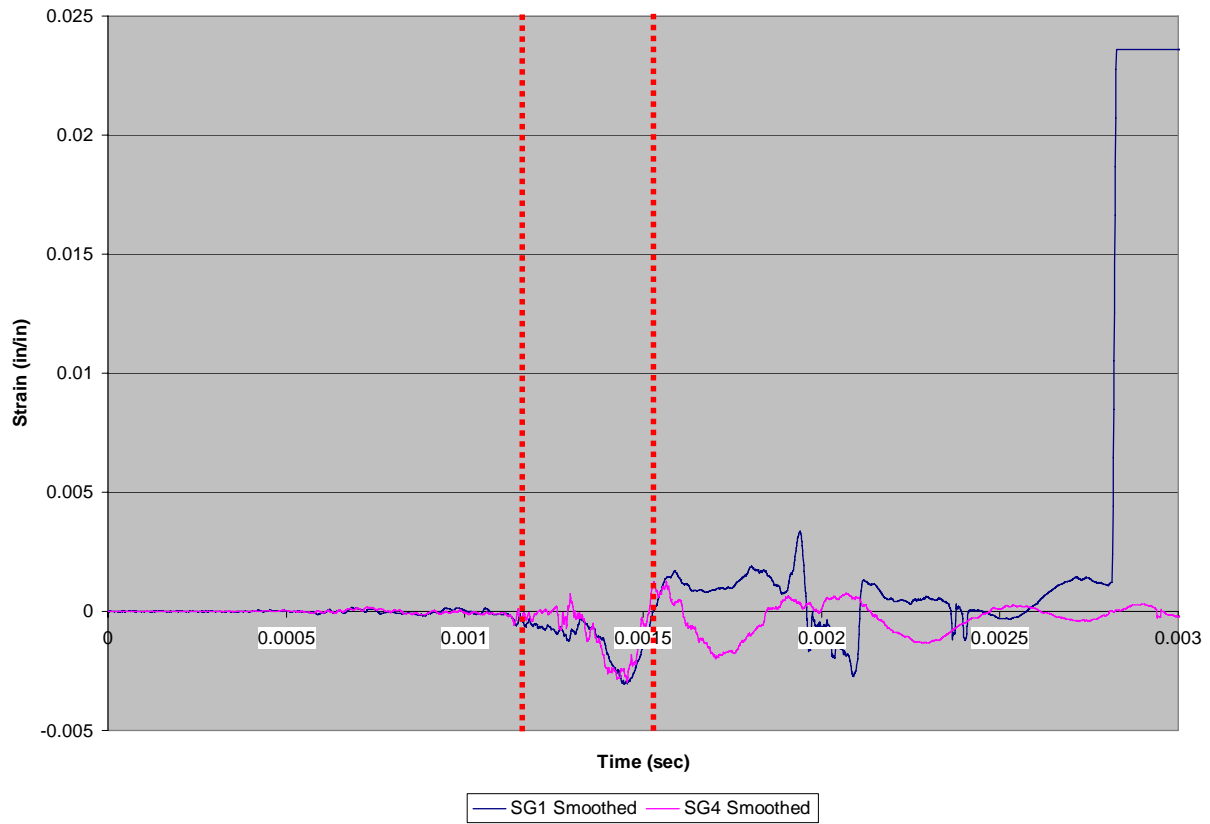


Figure C.6a.2: SG1 & SG4 skin strain vs. time (Specimen 6a)

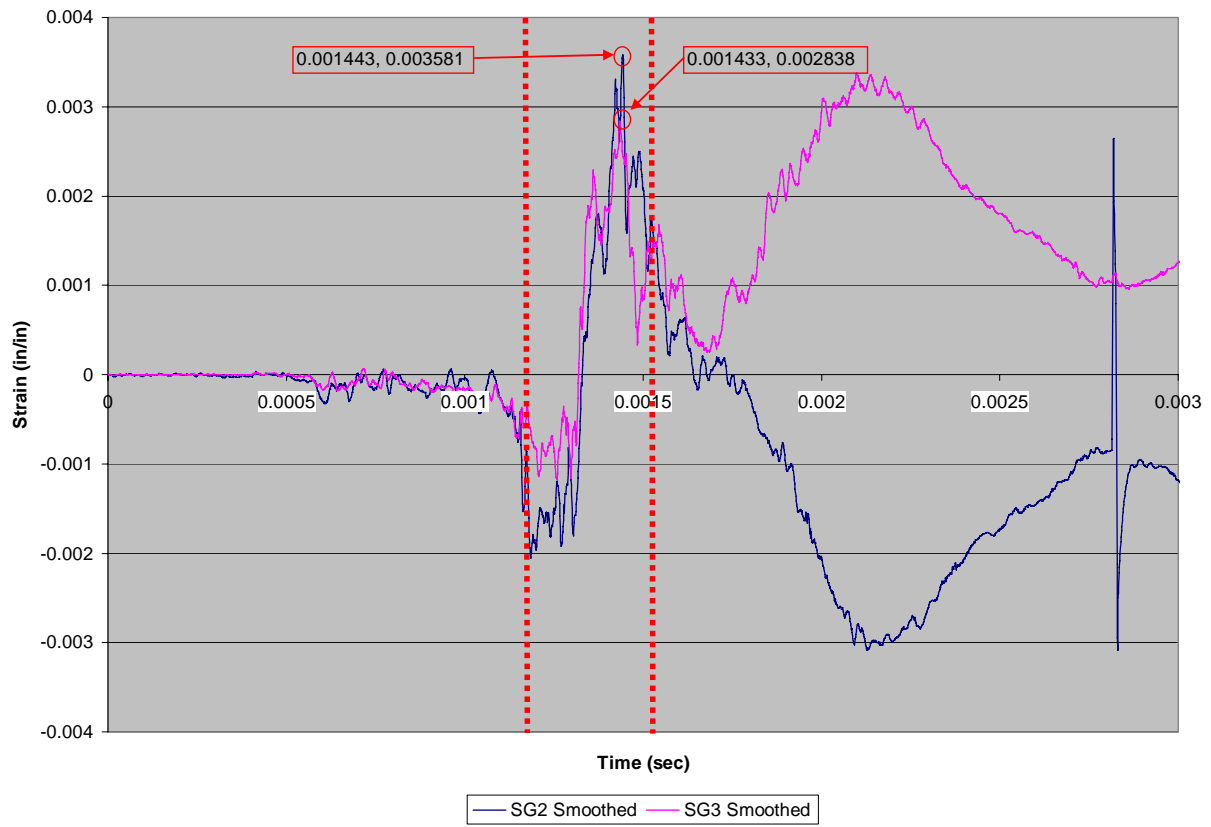


Figure C.6a.3: SG2 & SG3 spar strain vs. time (Specimen 6a)

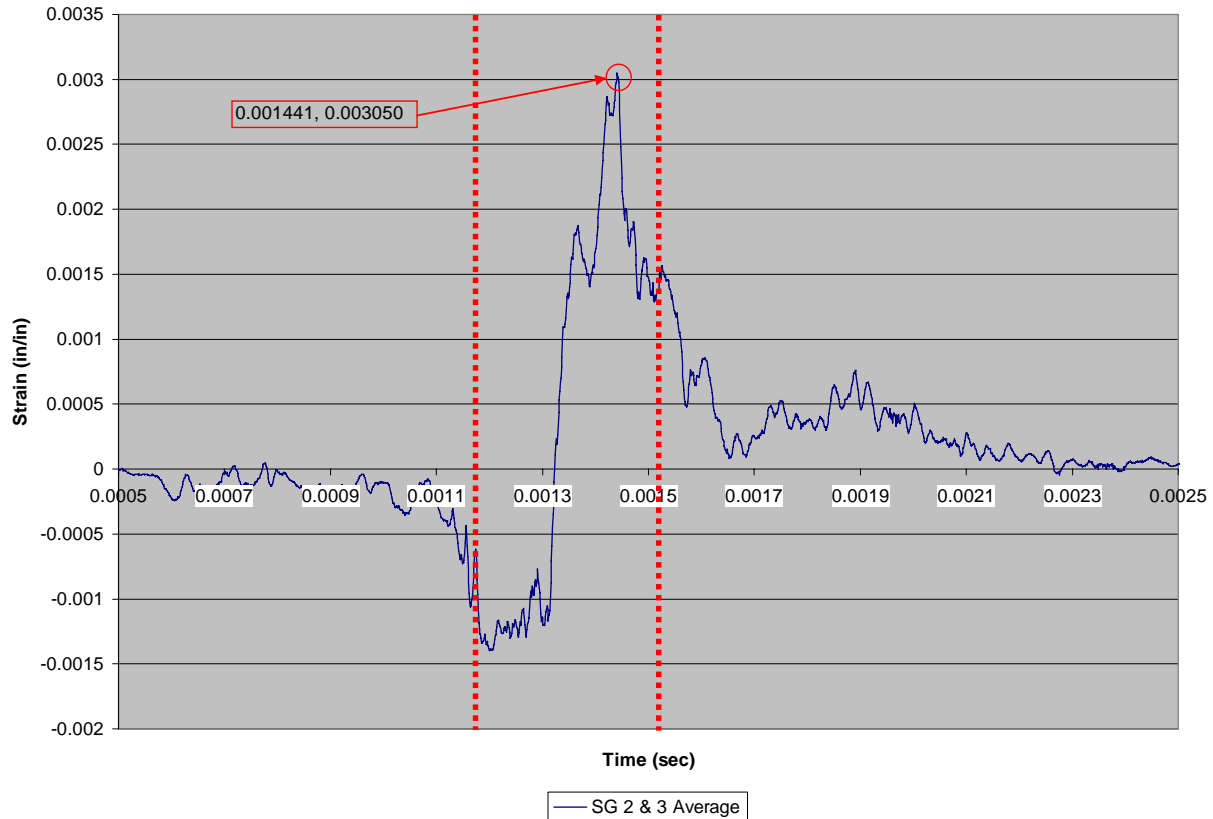


Figure C.6a.4: SG2 & SG3 average spar strain vs. time (Specimen 6a)

Specimen 6b, Test 17

For Specimen 6b, the load interval (and therefore the strain vs. time interval of interest) is approximately 1.13ms - 1.47ms as seen in Figure C.6b.1. As desired, pressure sensors K1 and K3 are largely in agreement, indicating side-to-side uniformity of load on the test specimen. During the load interval, Figure C.6b.2 shows that SG1 and SG4 remain in phase (however of different amplitude) indicating the skin pulled away from the spar in an asymmetric fashion. Similarly, SG2 and SG3 remain in phase (but of different amplitude) as seen in Figure C.6b.3 implying asymmetric failure. Failure metrics for Specimen 6b are derived from Figure C.6b.4. Failure strain occurred at 1.391ms with a maximum strain of 0.00305 in/in.

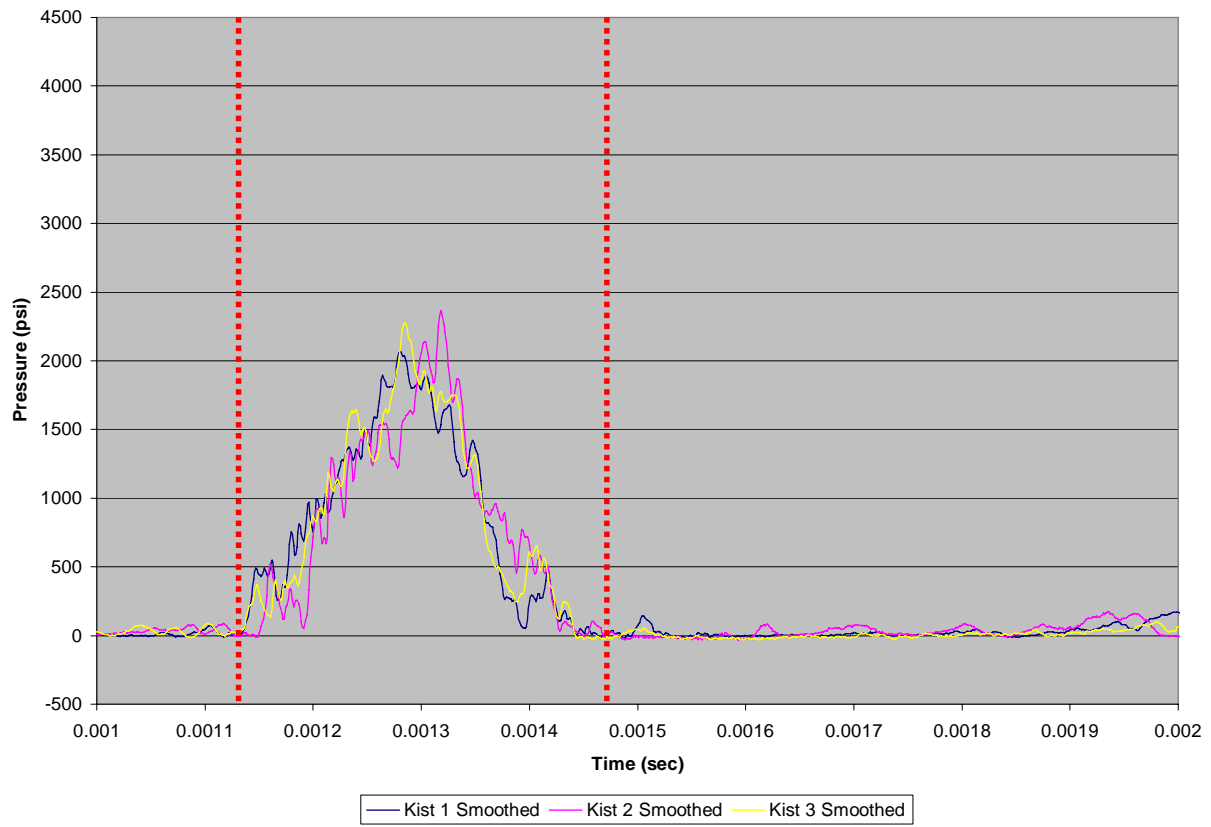


Figure C.6b.1: Kistler pressure vs. time (Specimen 6b)

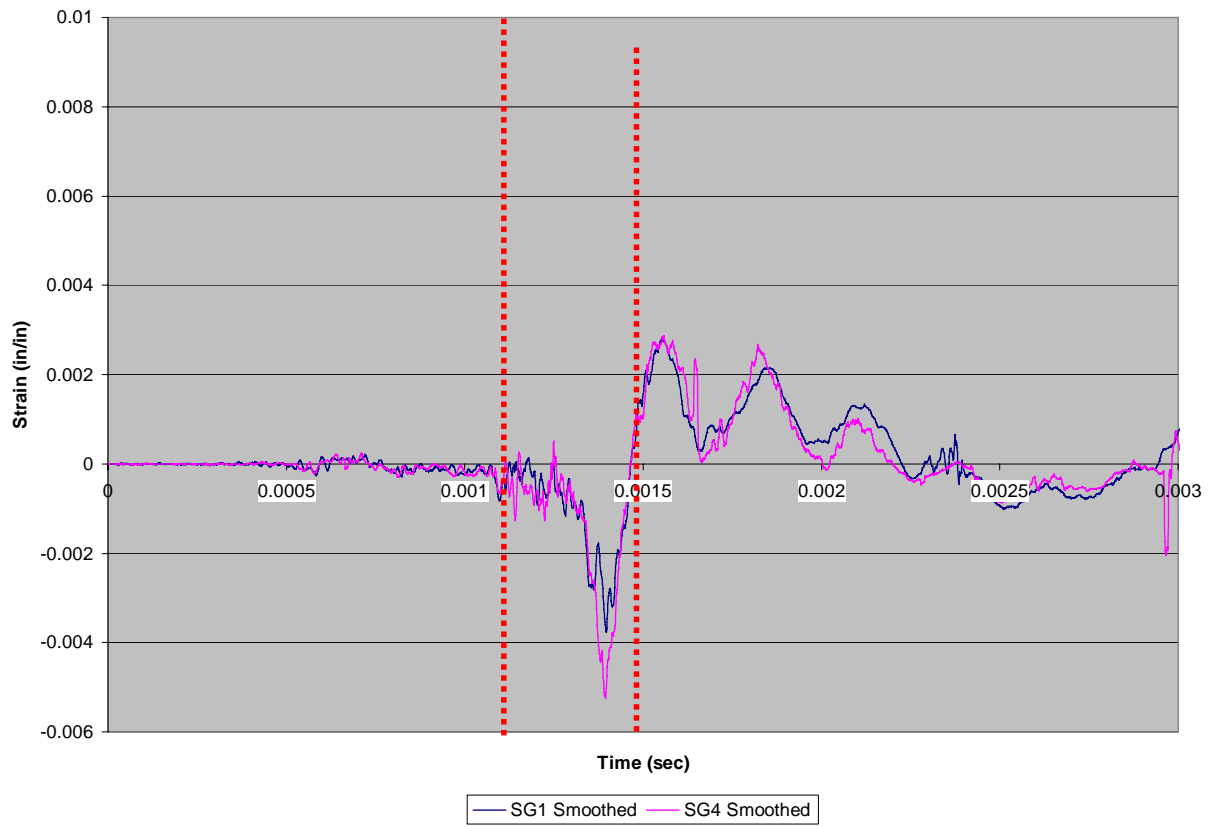


Figure C.6b.2: SG1 & SG4 skin strain vs. time (Specimen 6b)

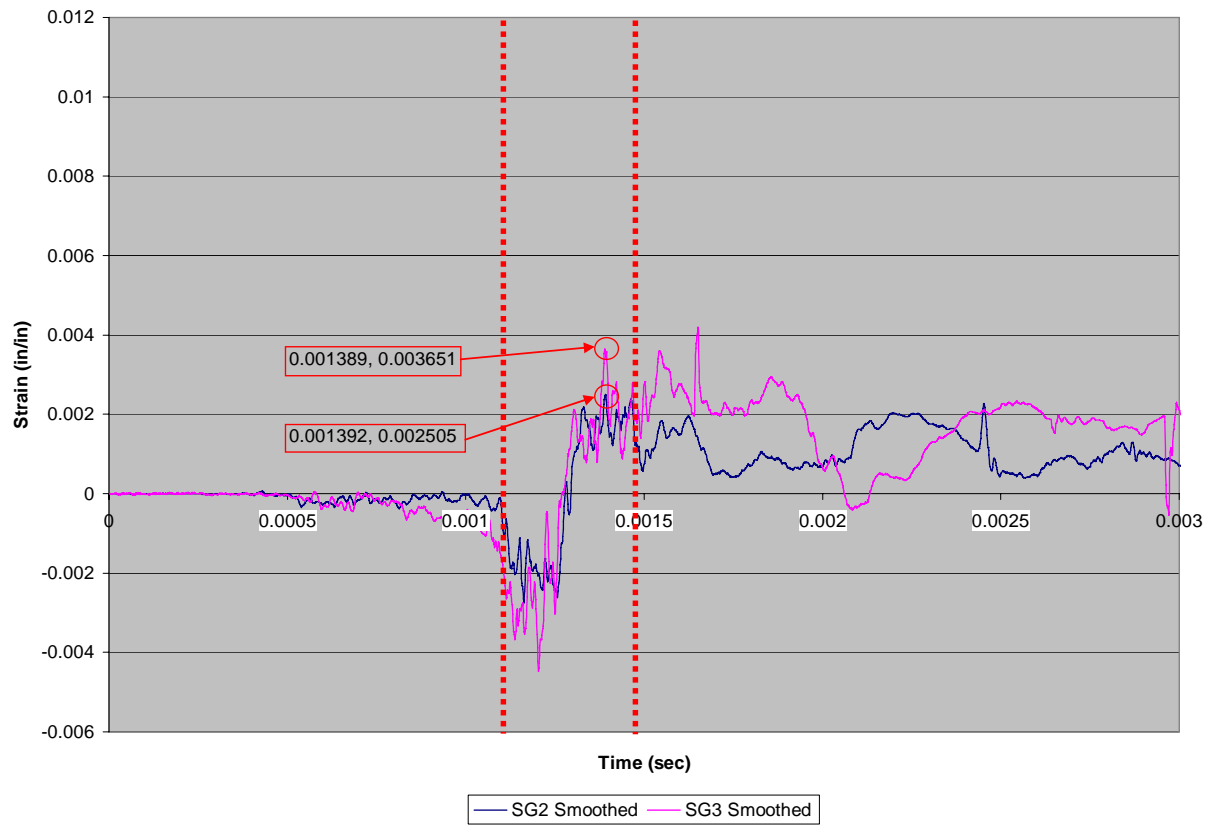


Figure C.6b.3: SG2 & SG3 spar strain vs. time (Specimen 6b)

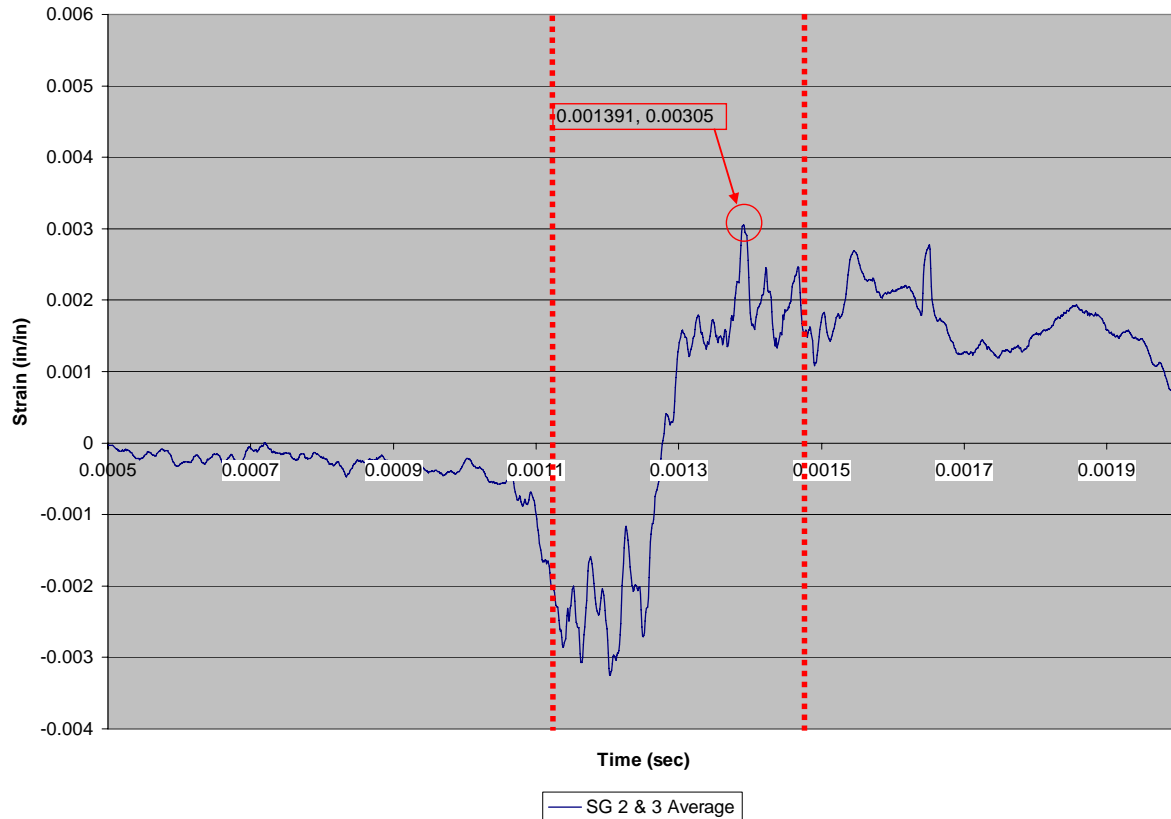


Figure C.6b.4: SG2 & SG3 average spar strain vs. time (Specimen 6b)

Specimen 6c, Test 18

For Specimen 6c, the load interval (and therefore the strain vs. time interval of interest) is approximately 1.17 ms to 1.50ms as shown in Figure C.6c.1. As desired, pressure sensors K1 and K3 are largely in agreement, indicating side-to-side uniformity of load on the test specimen. During the load interval, Figure C.6c.2 shows that SG1 and SG4 are in phase and of similar amplitude, indicating the skin pulled away from the spar in a symmetric fashion. SG2 and SG3 on the spar are initially out of phase, but go in phase and are of similar amplitude prior to failure (as seen in Figure C.6c.3). Correlation of skin and spar gages substantiate that failure was symmetric. Failure metrics for Specimen 6c are derived from Figure C.6c.4. Failure strain occurred at 1.434ms with a maximum strain of 0.003063 in/in.

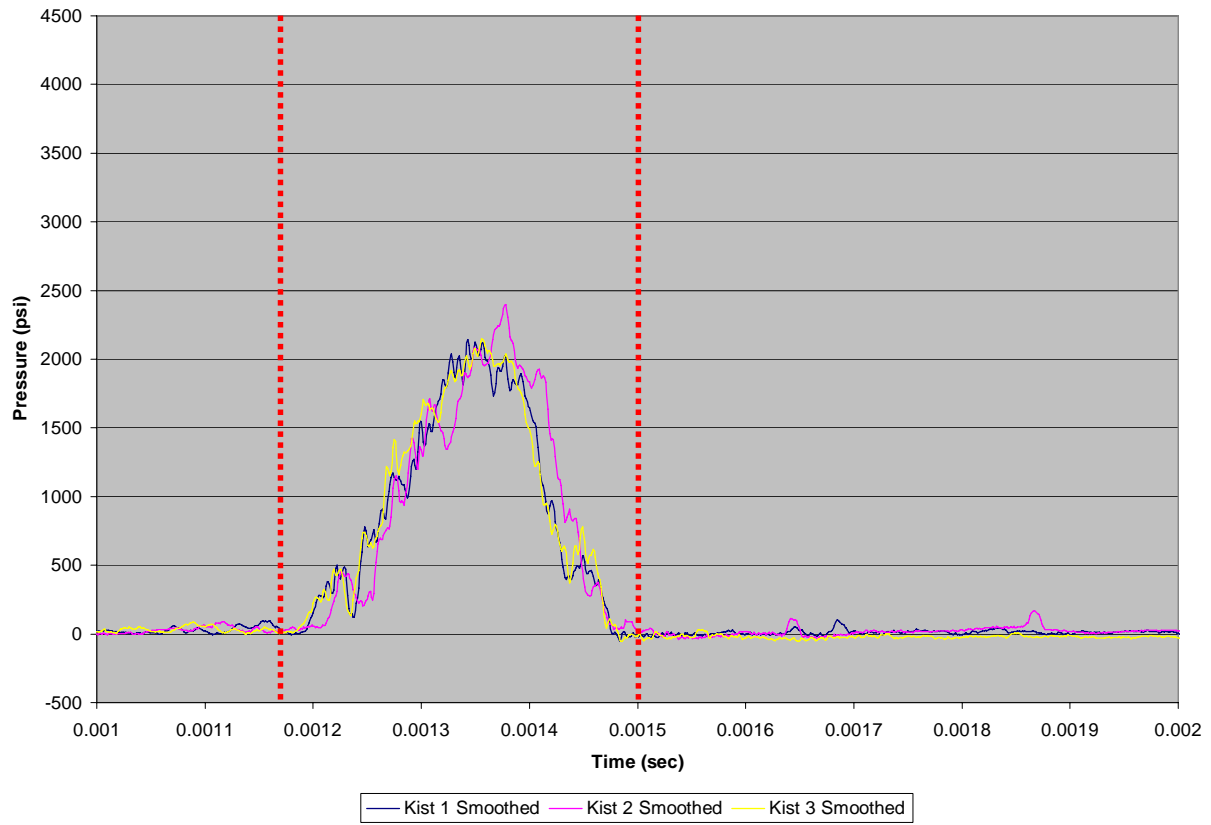


Figure C.6c.1: Kistler pressure vs. time (Specimen 6c)

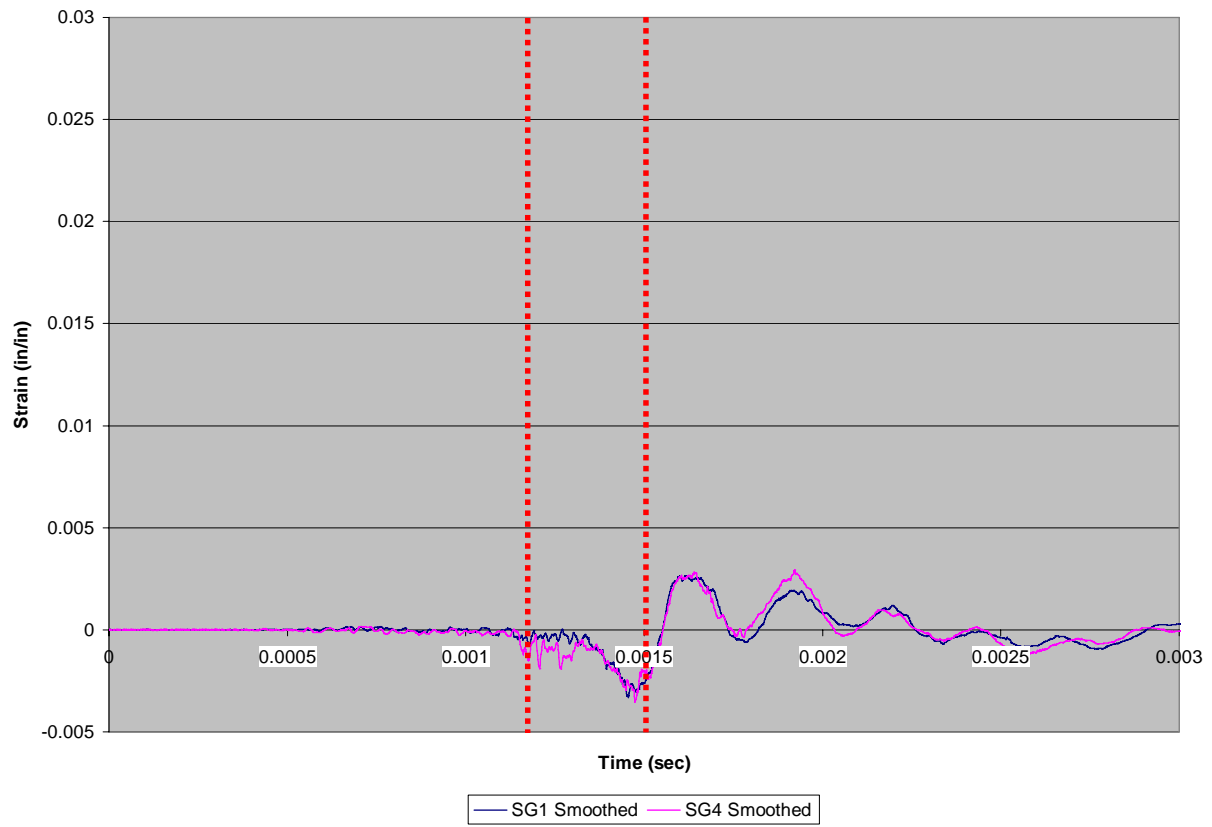


Figure C.6c.2: SG1 & SG4 skin strain vs. time (Specimen 6c)

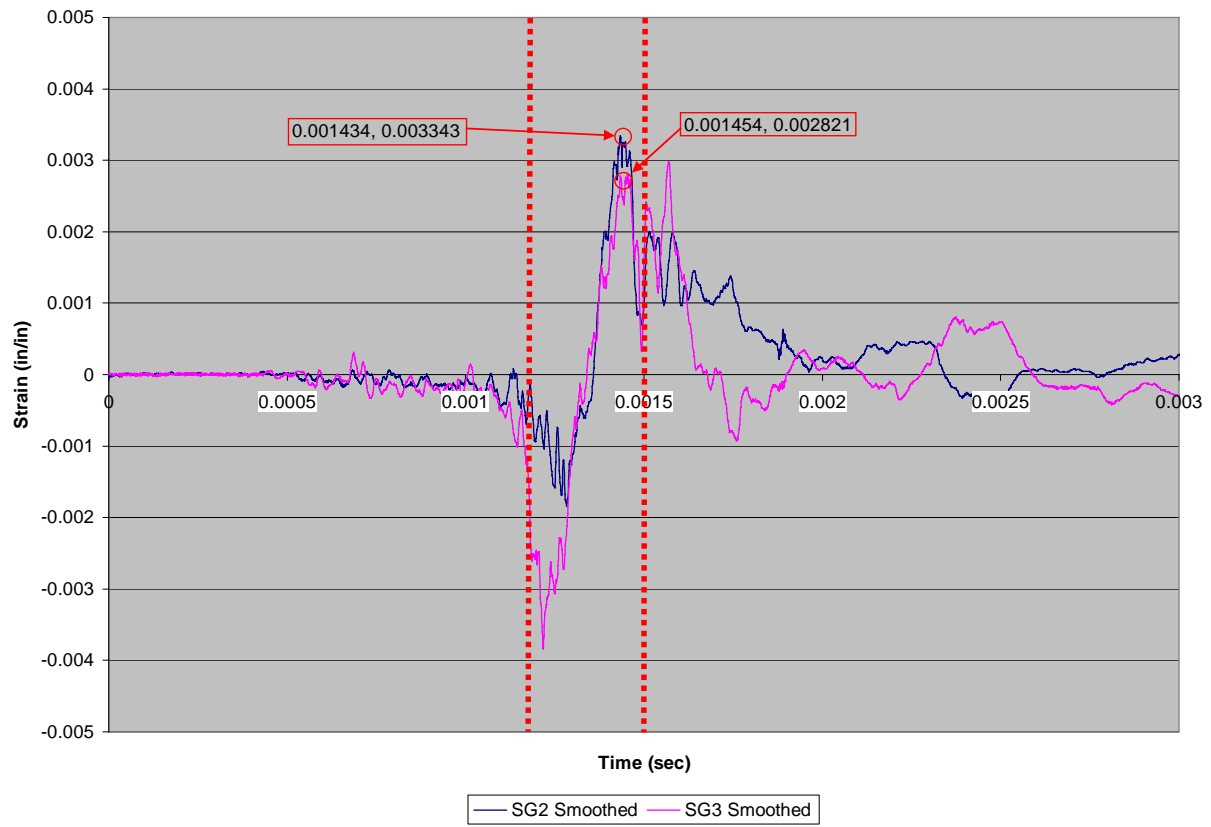


Figure C.6c.3: SG2 & SG3 spar strain vs. time (Specimen 6c)

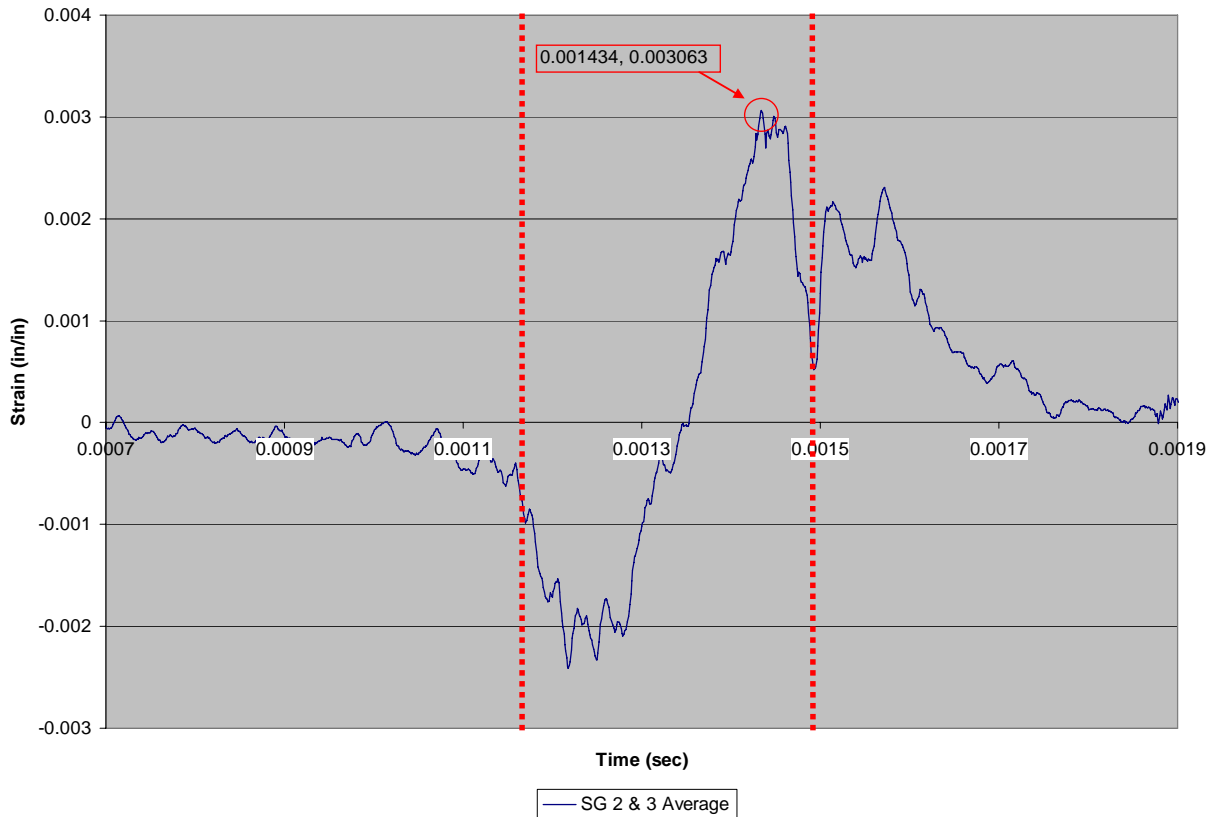


Figure C.6c.4: SG2 & SG3 average spar strain vs. time (Specimen 6c)

Specimen 6d, Test 28

For Specimen 6d, the load interval (and therefore the strain vs. time interval of interest) is approximately 1.20ms-1.50ms as shown in Figure C.6d.1. Pressure sensor K3 was inoperative during the test. As such, side-to-side uniformity of the pressure load cannot be verified. During the load interval, Figure C.6d.2 shows that SG1 and SG4 remain in phase and are of similar amplitude. Similarly, SG2 and SG3 on the spar remain in phase and of similar amplitude (as seen in Figure C.6d.3) implying symmetric failure. Failure metrics for Specimen 6d are derived from Figure C.6d.4. Failure strain occurred at 1.459ms with a maximum strain of 0.004825 in/in.

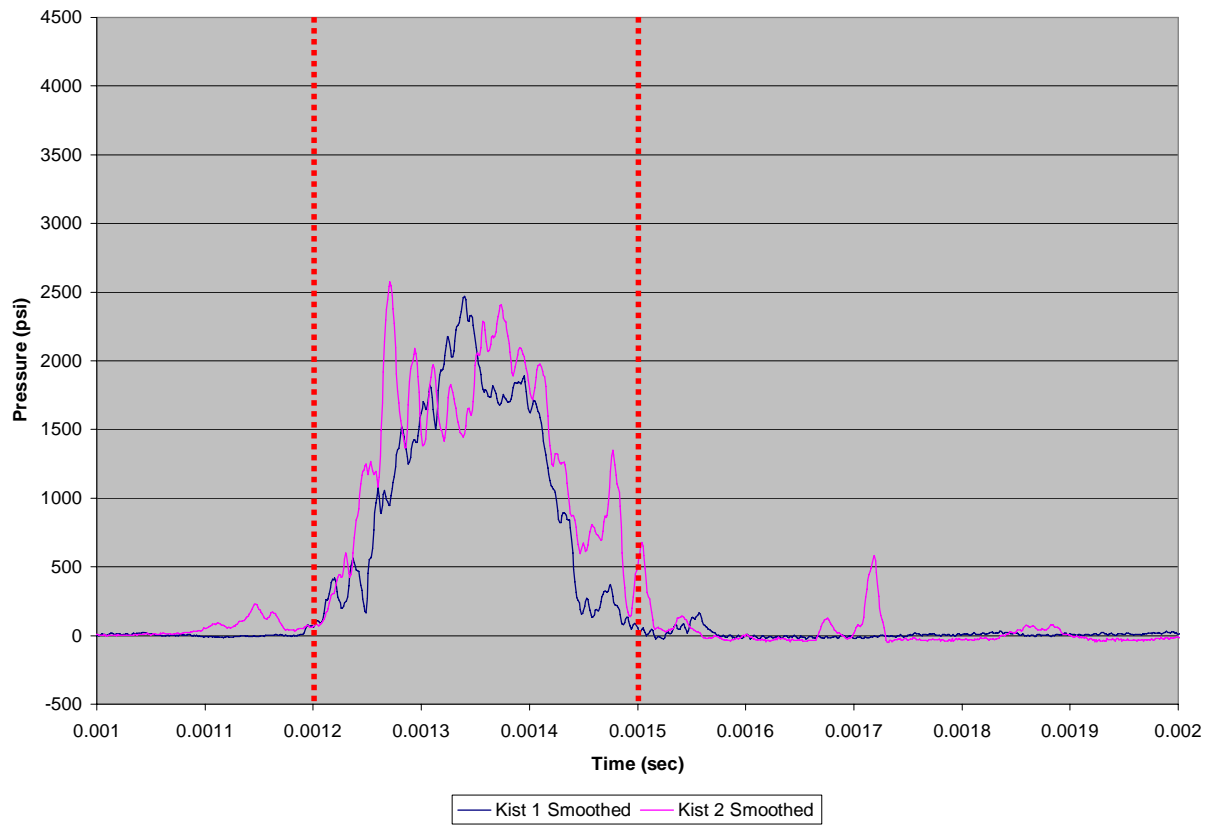


Figure C.6d.1: Kistler pressure vs. time (Specimen 6d)

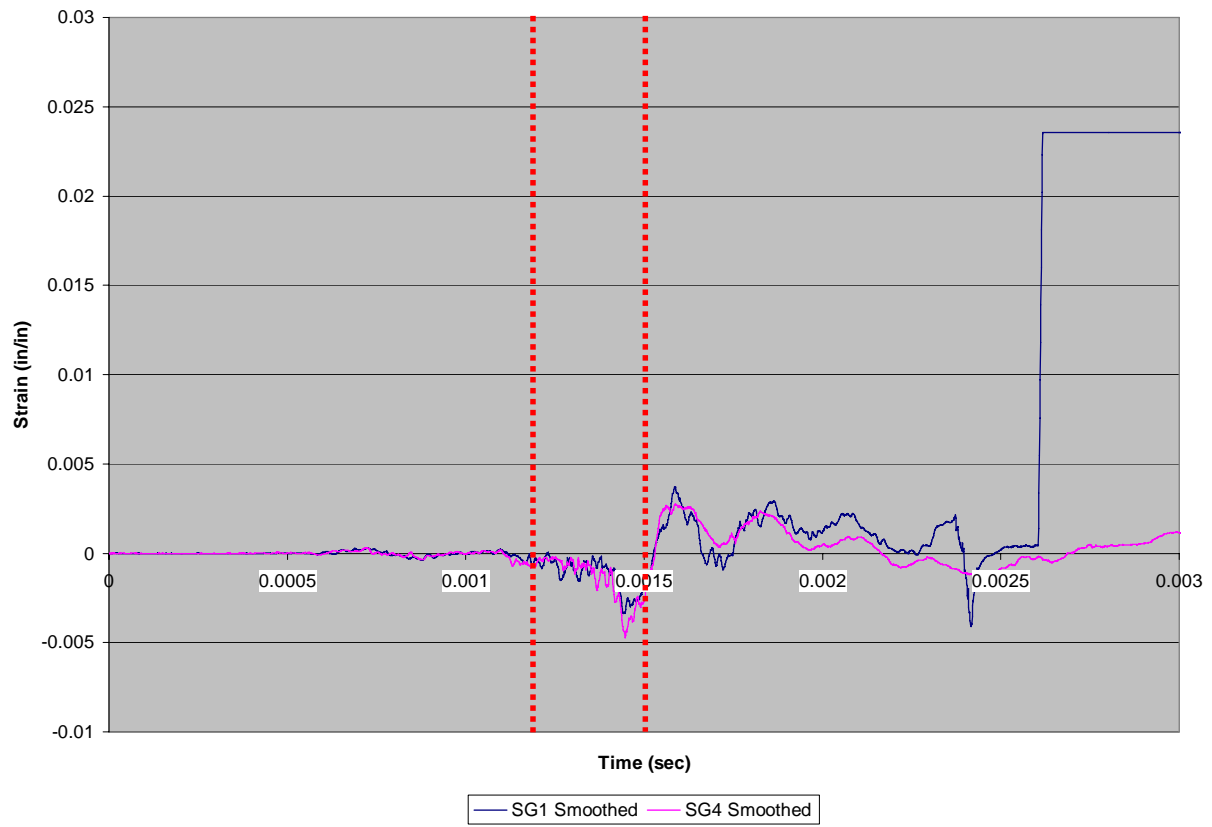


Figure C.6d.2: SG1 & SG4 skin strain vs. time (Specimen 6d)

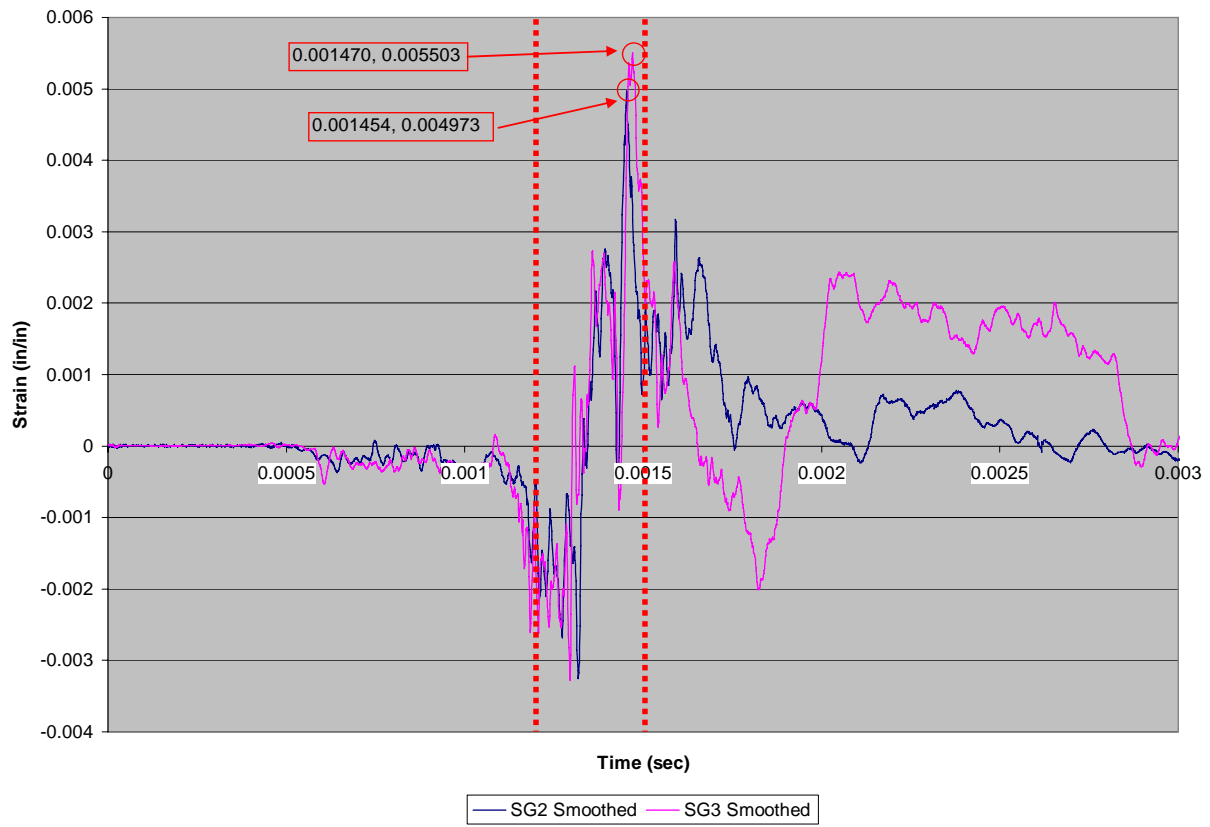


Figure C.6d.3: SG2 & SG3 spar strain vs. time (Specimen 6d)

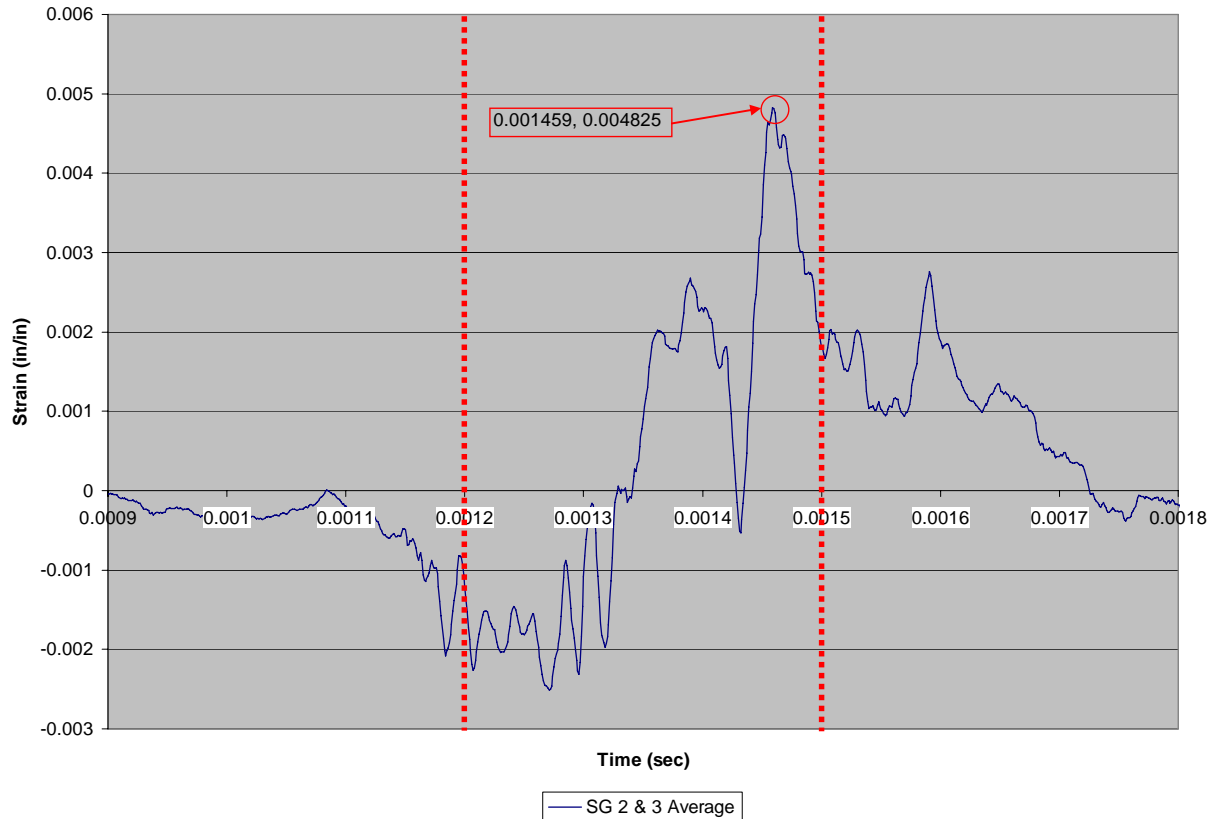


Figure C.6d.4: SG2 & SG3 average spar strain vs. time (Specimen 6d)

Specimen 6e, Test 29

For Specimen 6e, the load interval (and therefore the strain vs. time interval of interest) is approximately 1.22ms-1.60ms as shown in Figure C.6e.1. Pressure sensors K2 and K3 were inoperative during the test. As such, side-to-side uniformity of the pressure load cannot be verified. During the load interval, Figure C.6e. shows that SG1 and SG4 remain in phase and of similar amplitude. Similarly, SG2 and SG3 on the spar are strongly in phase and are of similar amplitude during the latter half of the load pulse (as seen in Figure C.6e.3). Correlation between skin and spar gages implies symmetric failure. Failure metrics for Specimen 6e are derived from Figure C.6e.4. Failure strain occurred at 1.496ms with a maximum strain of 0.003542 in/in.

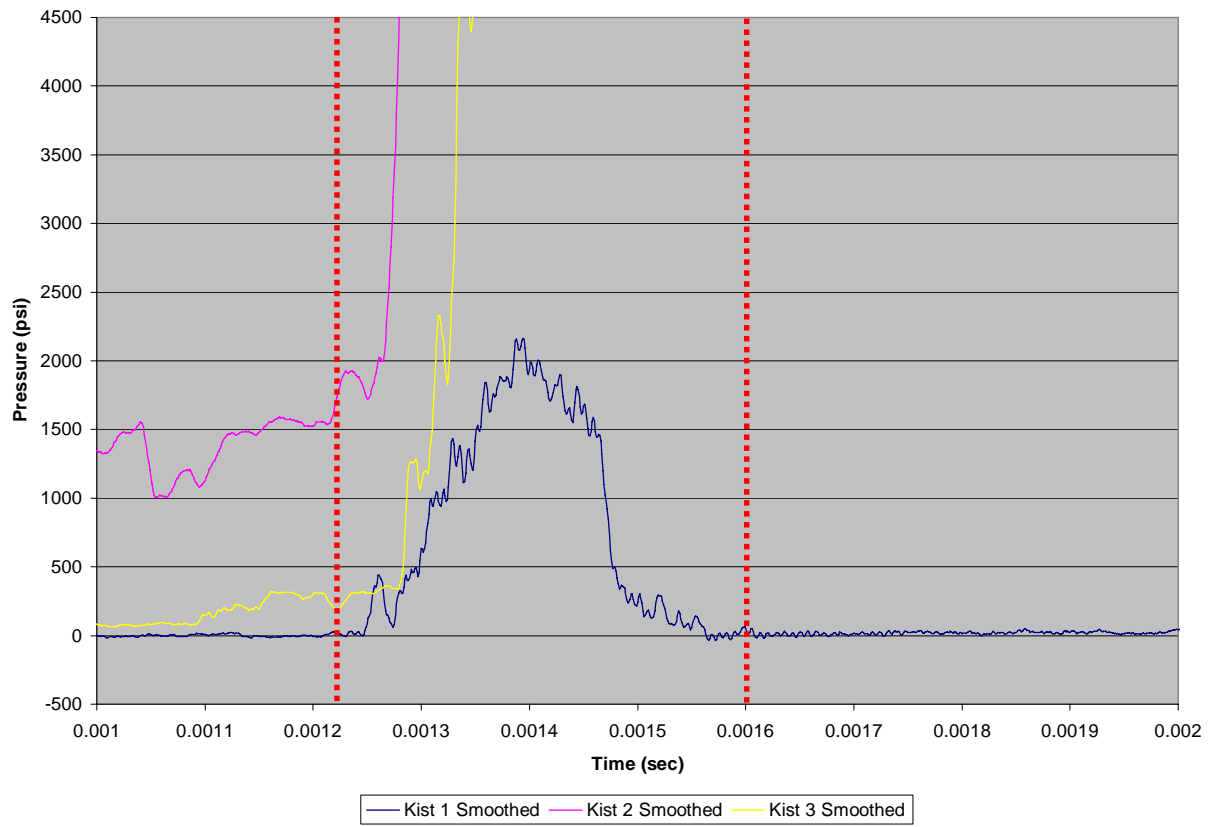


Figure C.6e.1: Kistler pressure vs. time (Specimen 6e)

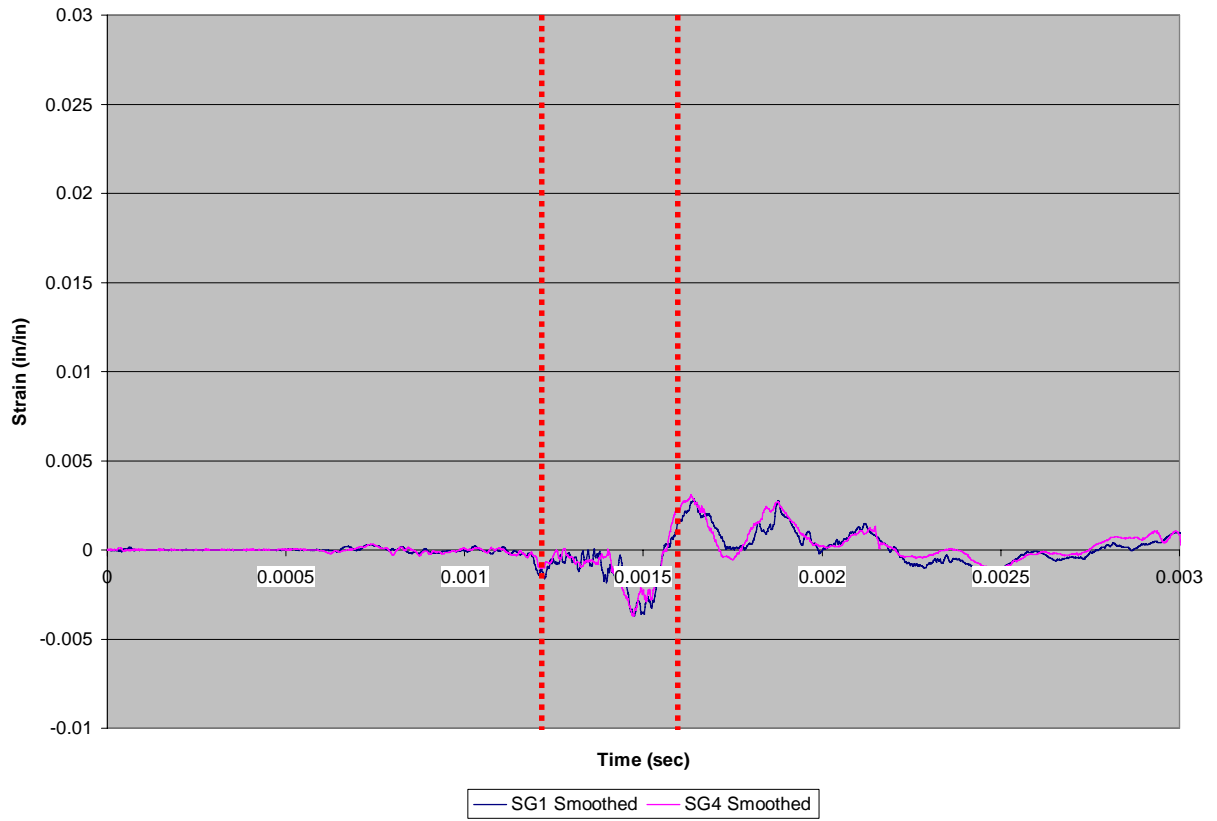


Figure C.6e.2: SG1 & SG4 skin strain vs. time (Specimen 6e)

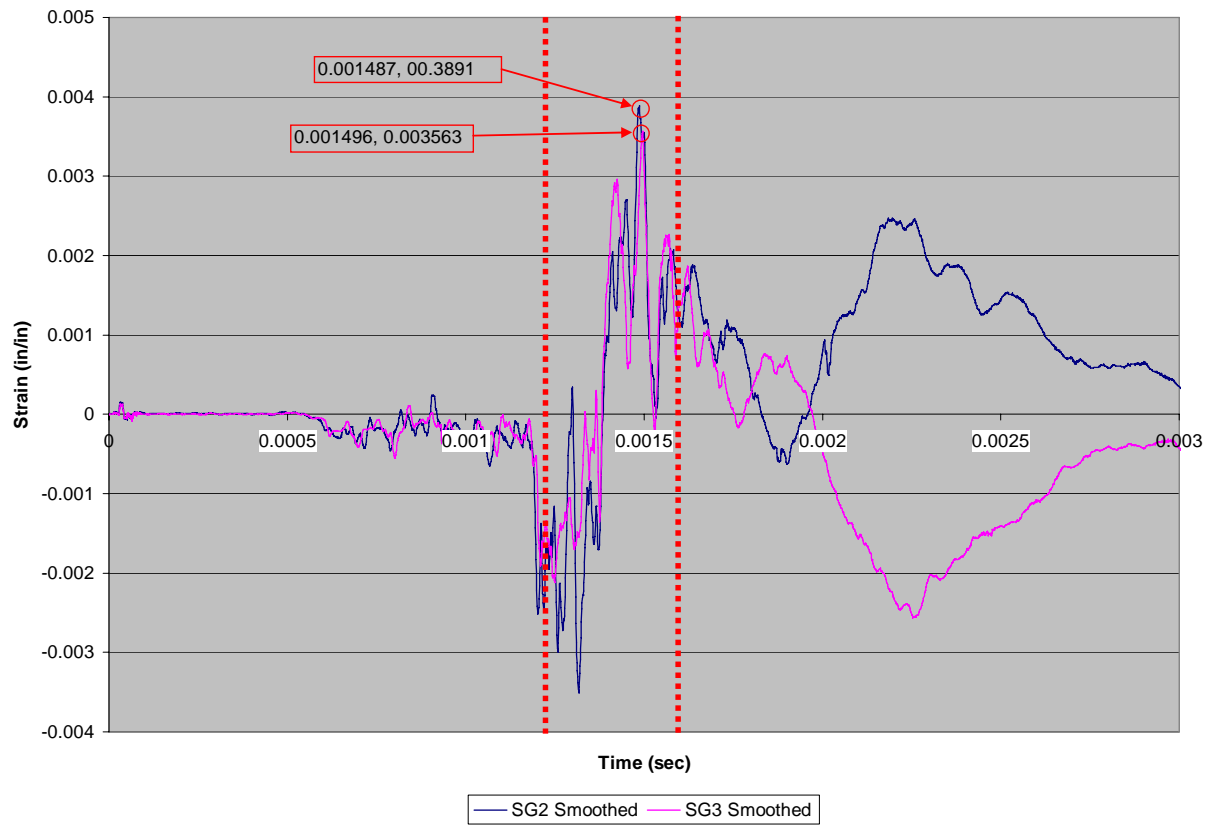


Figure C.6e.3: SG2 & SG3 spar strain vs. time (Specimen 6e)

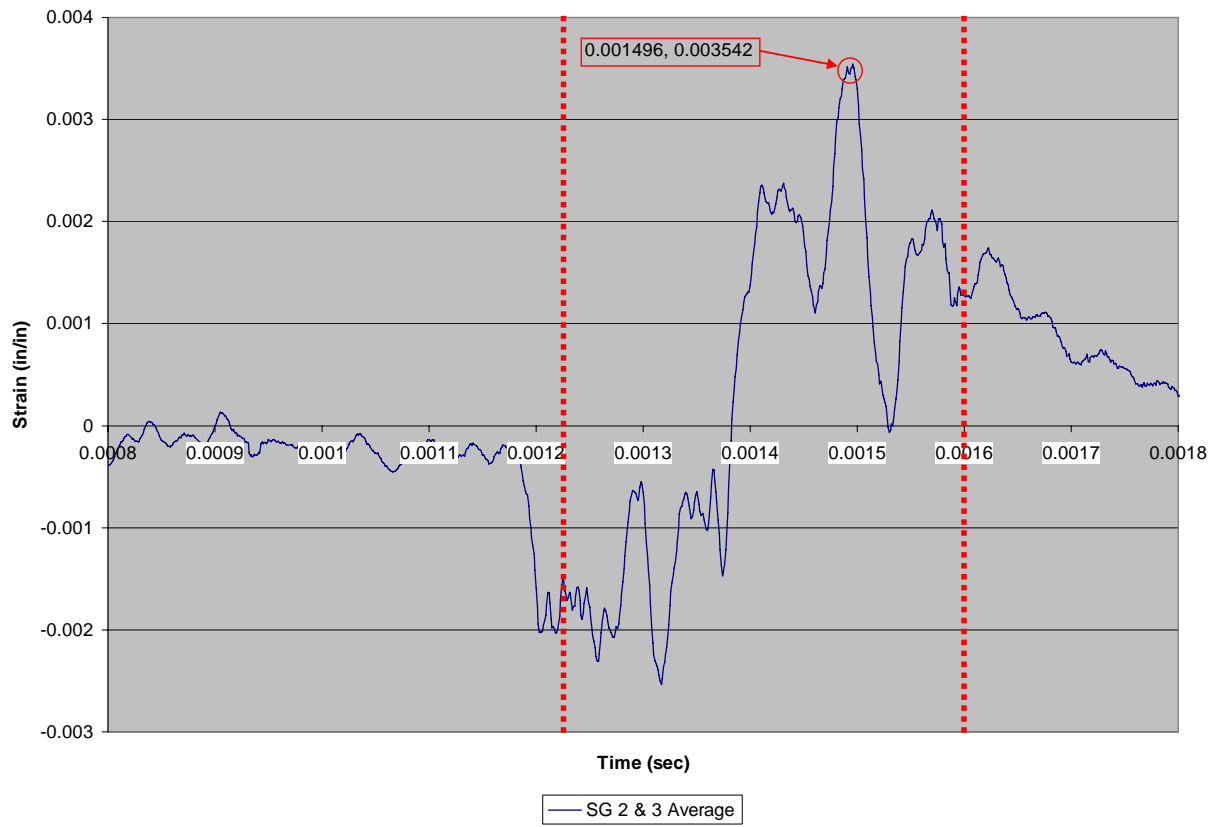


Figure C.6e.4: SG2 & SG3 average spar strain vs. time (Specimen 6e)

C.7 Specimen Set 7: Cobonded

C.7.1 Dynamic Tests of Specimen Set 7

Specimen 7a, Test 19

For Specimen 7a, the load interval (and therefore the strain vs. time interval of interest) is approximately 1.22ms - 1.53ms as seen in Figure C.7a.1. As desired, pressure sensors K1 and K3 are largely in agreement, indicating side-to-side uniformity of load on the test specimen. During the load interval, Figure C.7a.2 shows that SG1 and SG4 are in phase and of similar amplitude, indicating the skin pulled away from the spar in a symmetric fashion. Similarly, SG2 and SG3 are in phase and of similar amplitude (as seen in Figure C.7a.3), implying symmetric failure. Failure metrics for Specimen 7a was derived from Figure C.7a.4. Failure strain occurred at 1.464ms with a maximum strain of 0.001788 in/in.

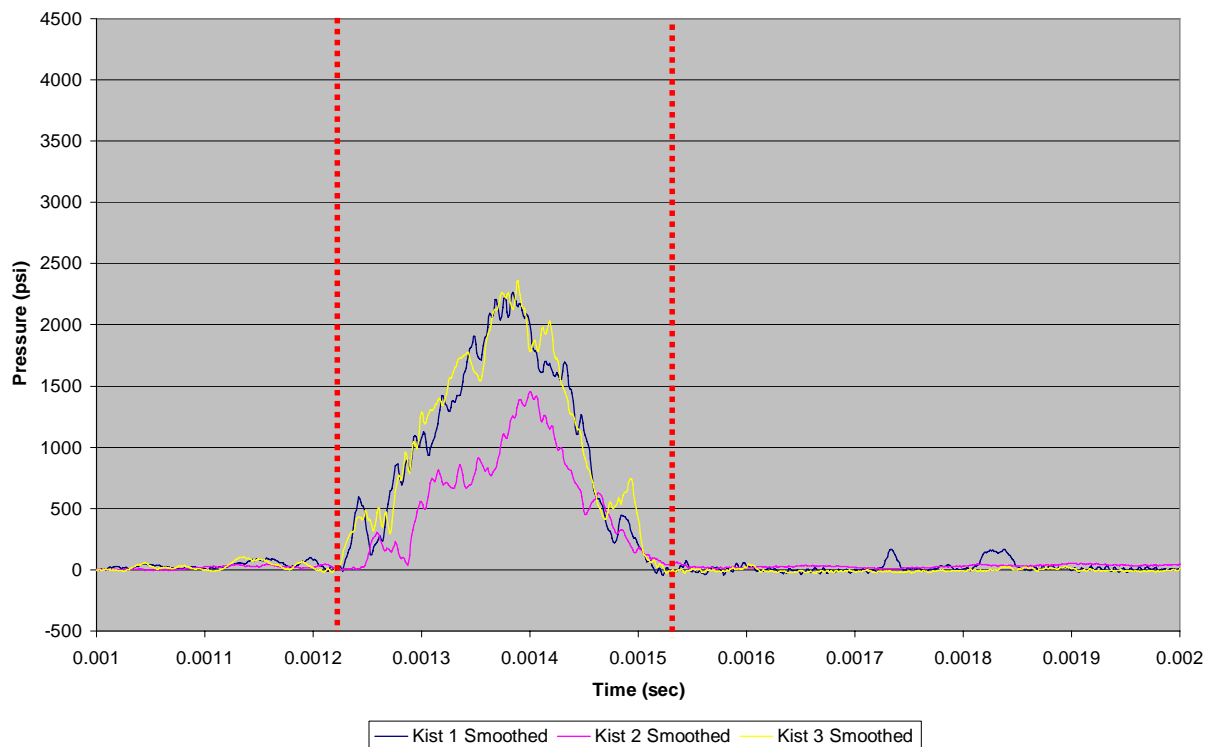


Figure C.7a.1: Kistler pressure vs. time (Specimen 7a)

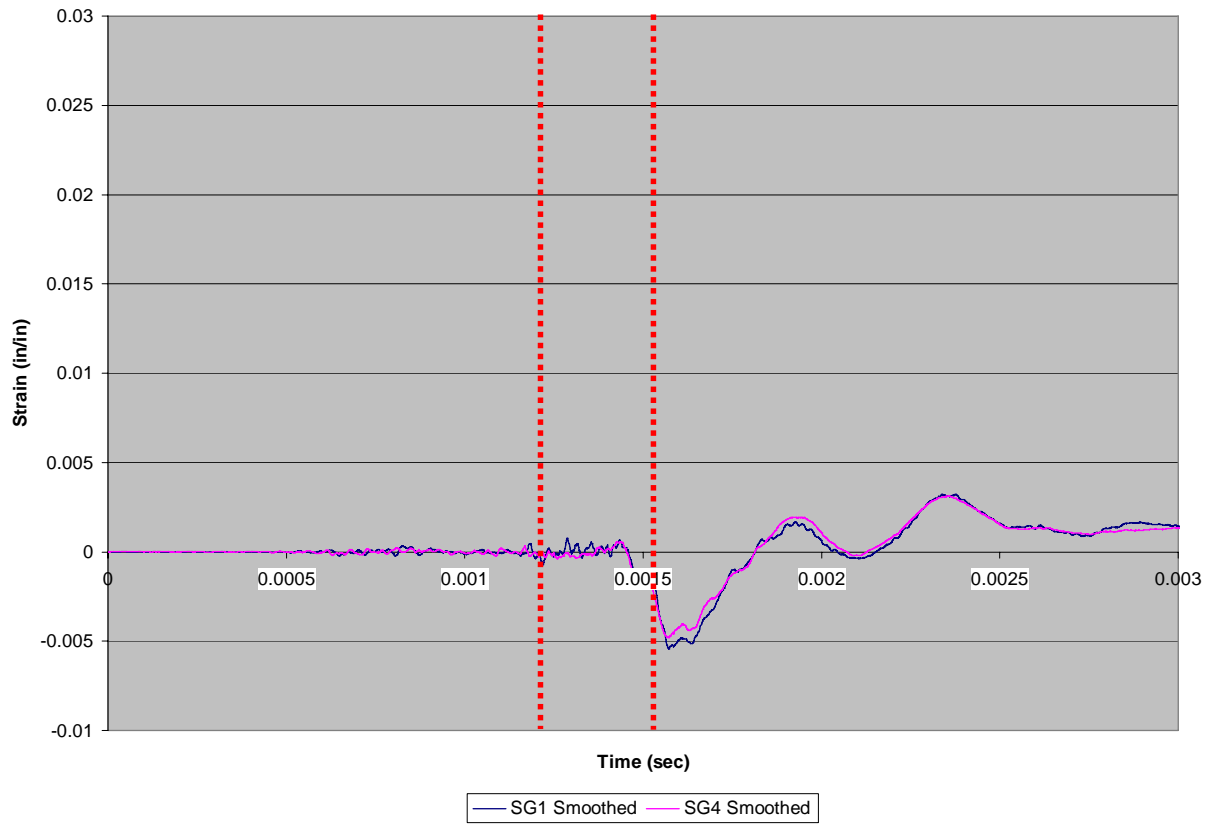


Figure C.7a.2: SG1 & SG4 skin strain vs. time (Specimen 7a)

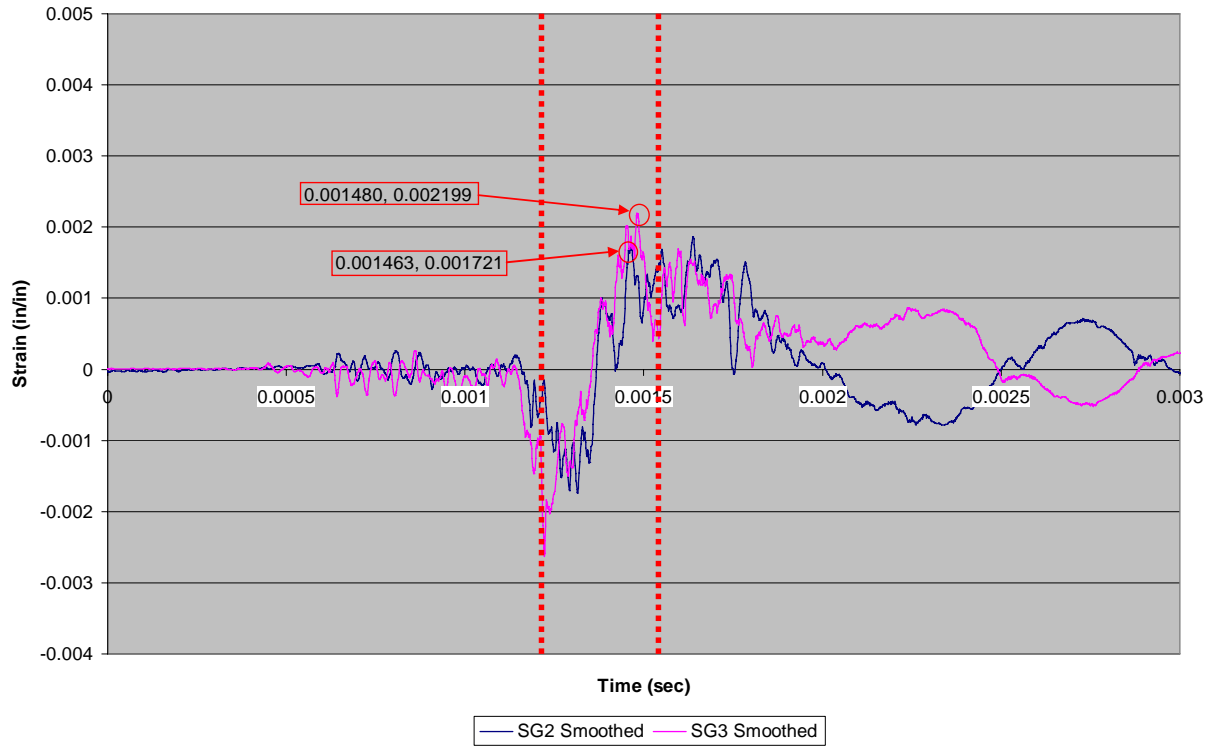


Figure C.7a.3: SG2 & SG3 spar strain vs. time (Specimen 7a)

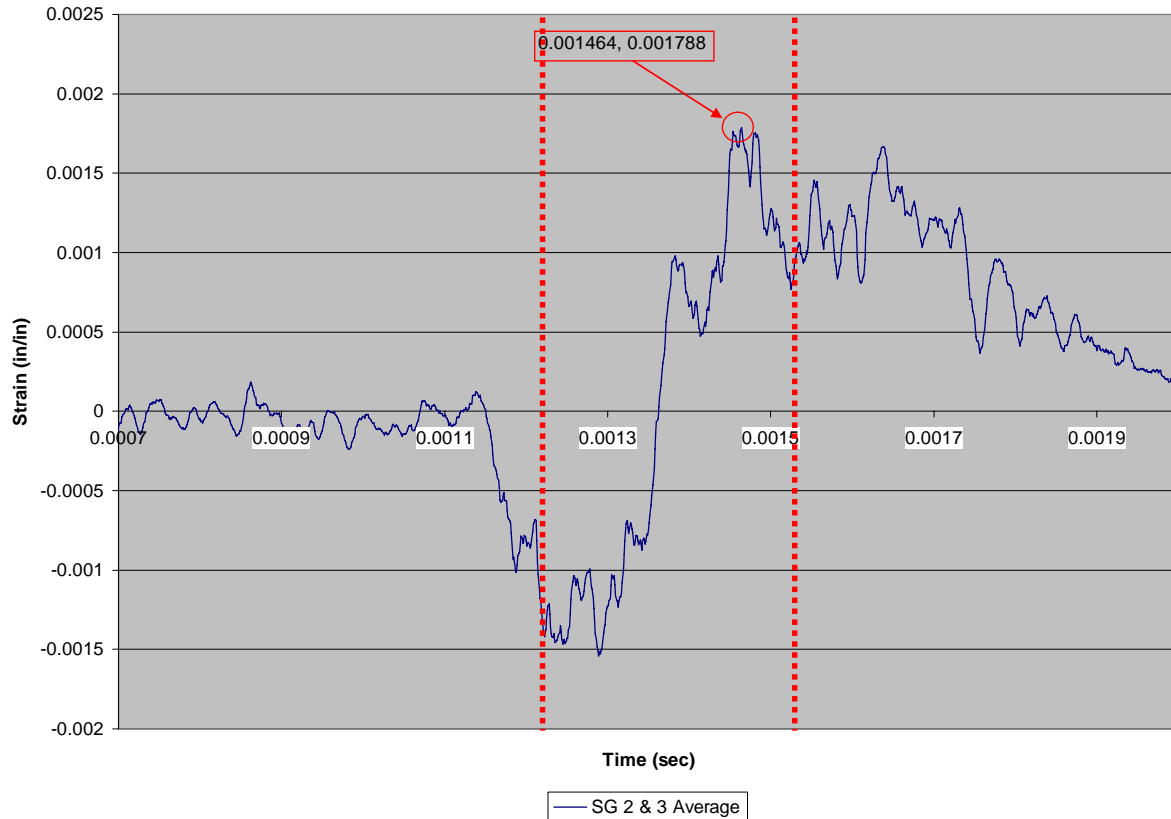


Figure C.7a.4: SG2 & SG3 average spar strain vs. time (Specimen 7a)

Specimen 7b, Test 20

For Specimen 7b, the load interval (and therefore the strain vs. time interval of interest) is approximately 1.23ms - 1.54ms as seen in Figure C.7b.1. As desired, pressure sensors K1 and K3 are largely in agreement, indicating side-to-side uniformity of load on the test specimen. During the load interval, Figure C.7b.2 shows that SG1 and SG4 tend to stay in phase (but with different amplitudes) indicating the skin pulled away from the spar in an asymmetric fashion. Similarly, SG2 and SG3 are in phase, but with different amplitudes (as seen in Figure C.7b.3) implying asymmetric failure. Failure metrics for Specimen 7b was derived from Figure C.7b.4. Failure strain occurred at 1.496ms with a maximum strain of 0.002637 in/in.

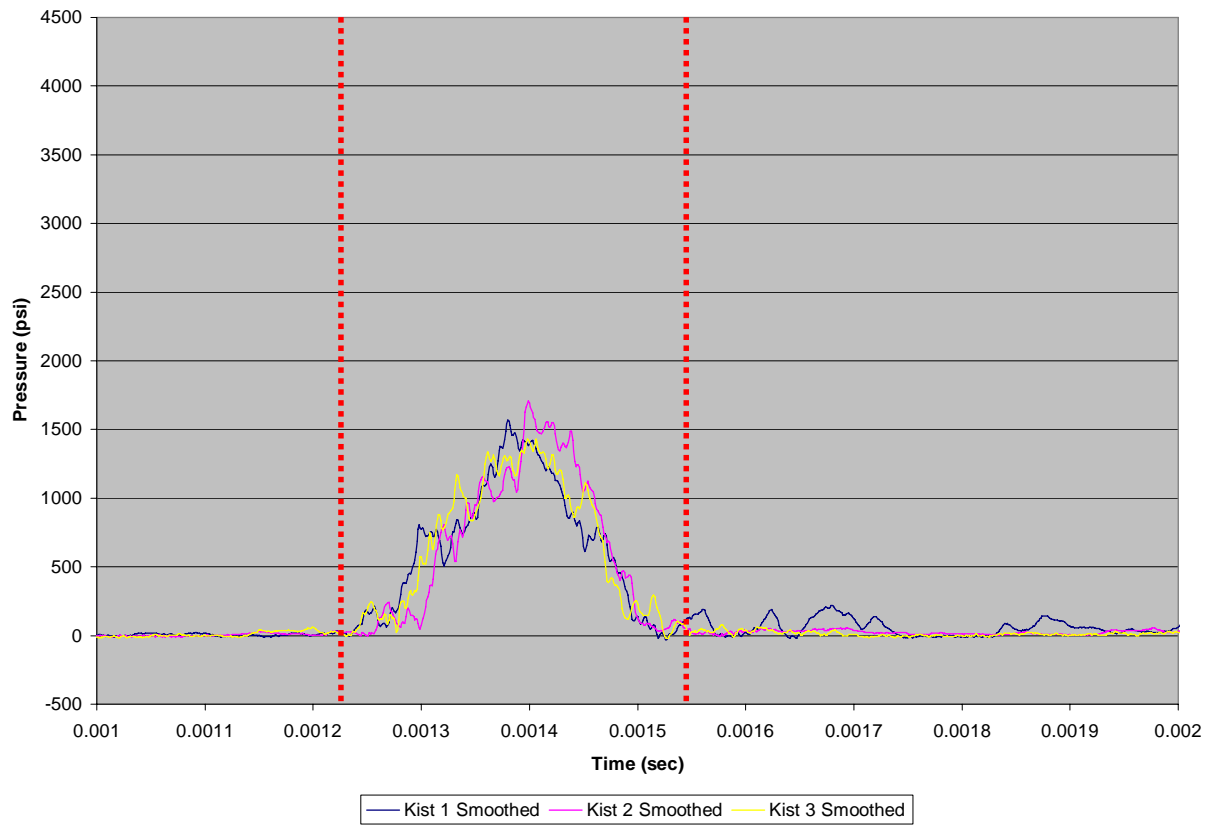


Figure C.7b.1: Kistler pressure vs. time (Specimen 7b)

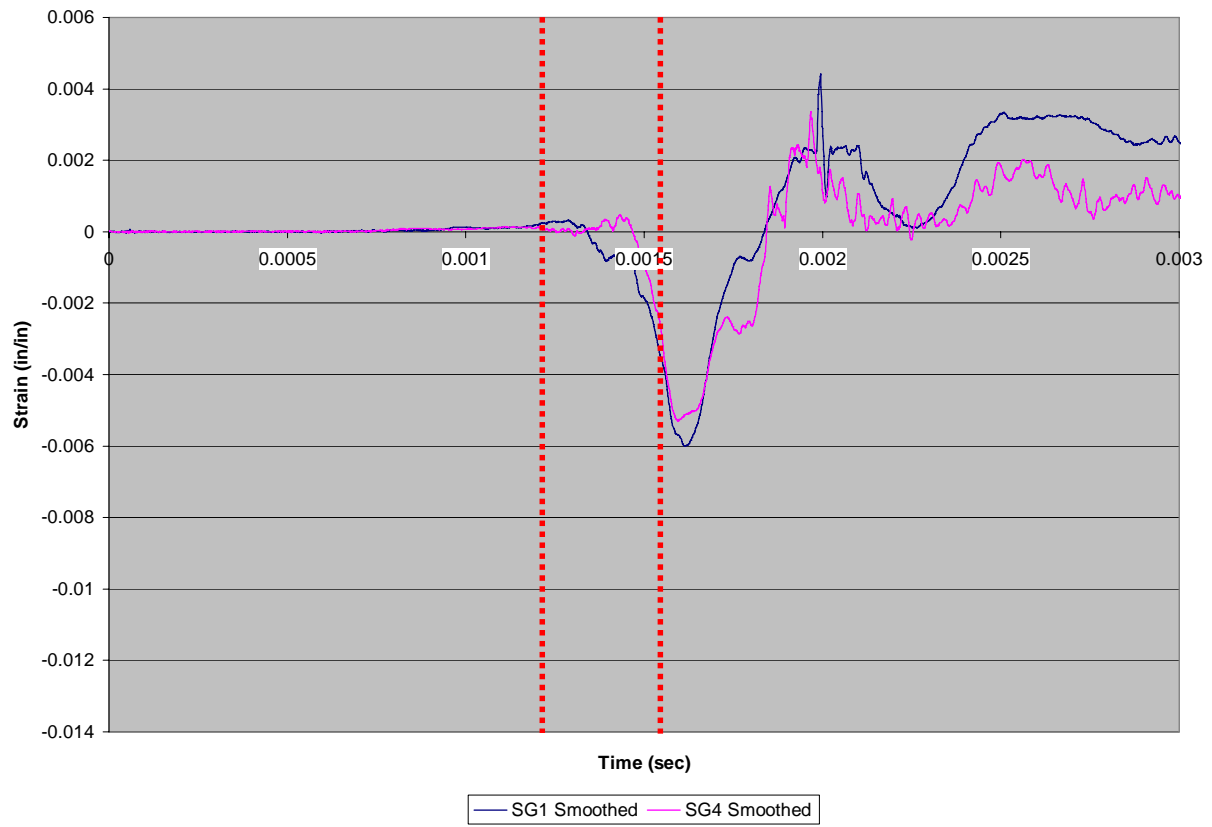


Figure C.7b.2: SG1 & SG4 skin strain vs. time (Specimen 7b)

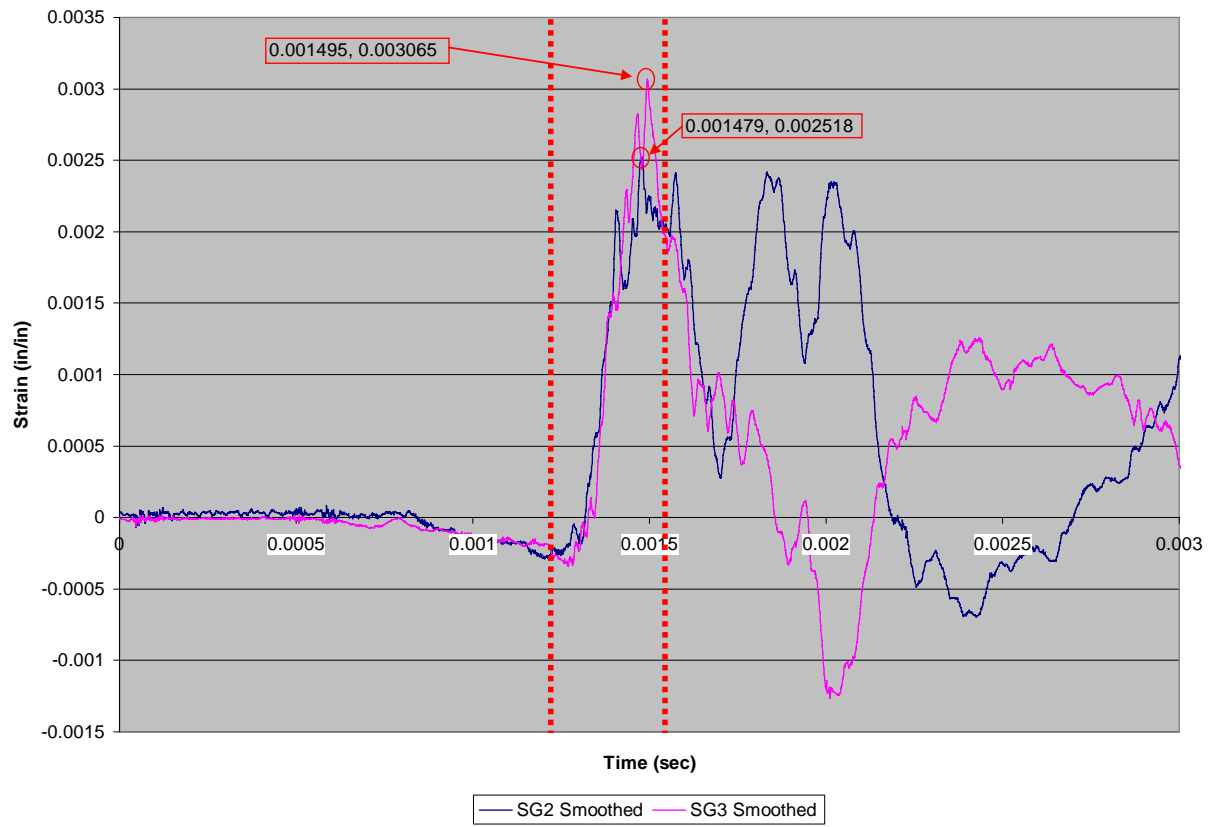


Figure C.7b.3: SG2 & SG3 spar strain vs. time (Specimen 7b)

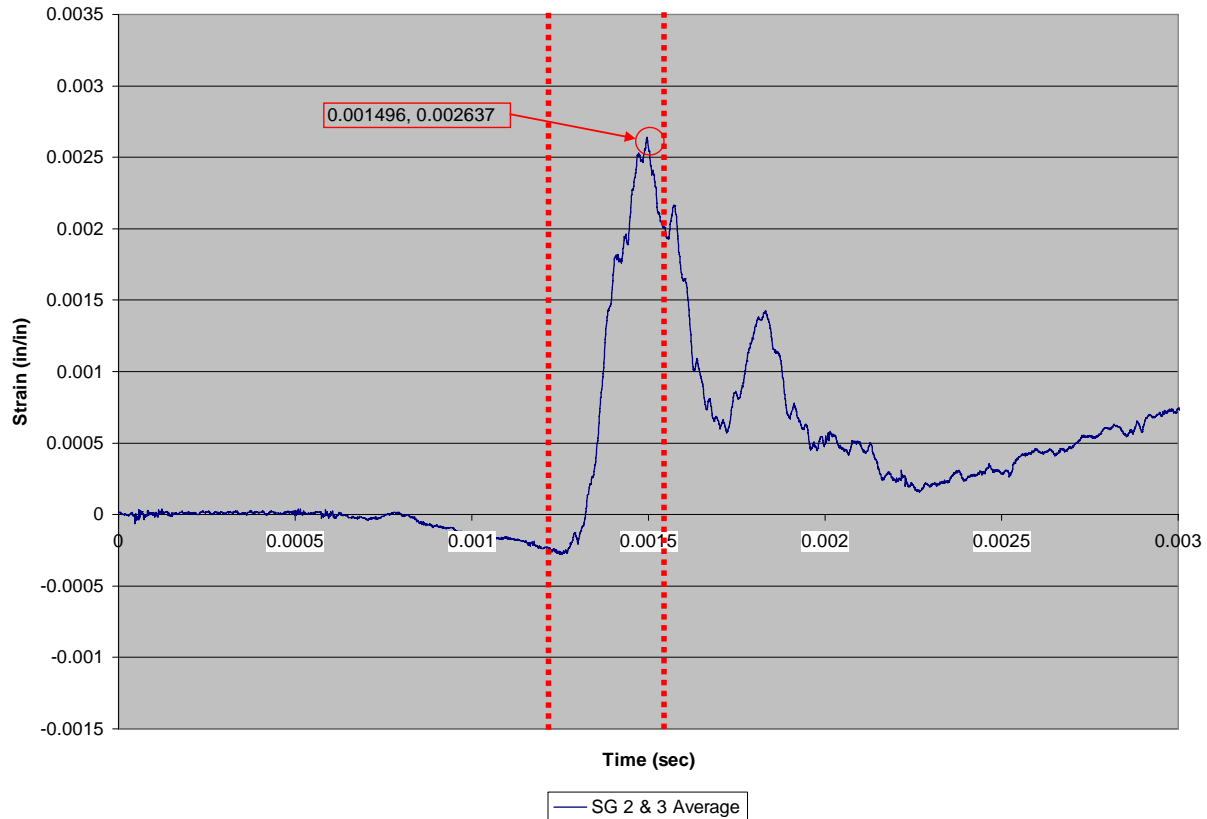


Figure C.7b.4: SG2 & SG3 average spar strain vs. time (Specimen 7b)

Specimen 7c, Test 21

For Specimen 7c, the load interval (and therefore the strain vs. time interval of interest) is approximately 1.10 ms to 1.48ms as shown in Figure C.7c.1. As desired, pressure sensors K1 and K3 are largely in agreement, indicating side-to-side uniformity of load on the test specimen. During the load interval, Figure C.7c.2 shows that SG1 and SG4 remain out of phase until late in the load cycle, indicating the skin pulled away from the spar in an asymmetric fashion. SG2 and SG3 on the spar also appear to be out of phase (as seen in Figure C.7c.3) indicating asymmetric failure. Failure metrics for Specimen 7c are derived from Figure C.7c.4. Failure strain occurred at 1.436ms with a maximum strain of 0.00429 in/in.

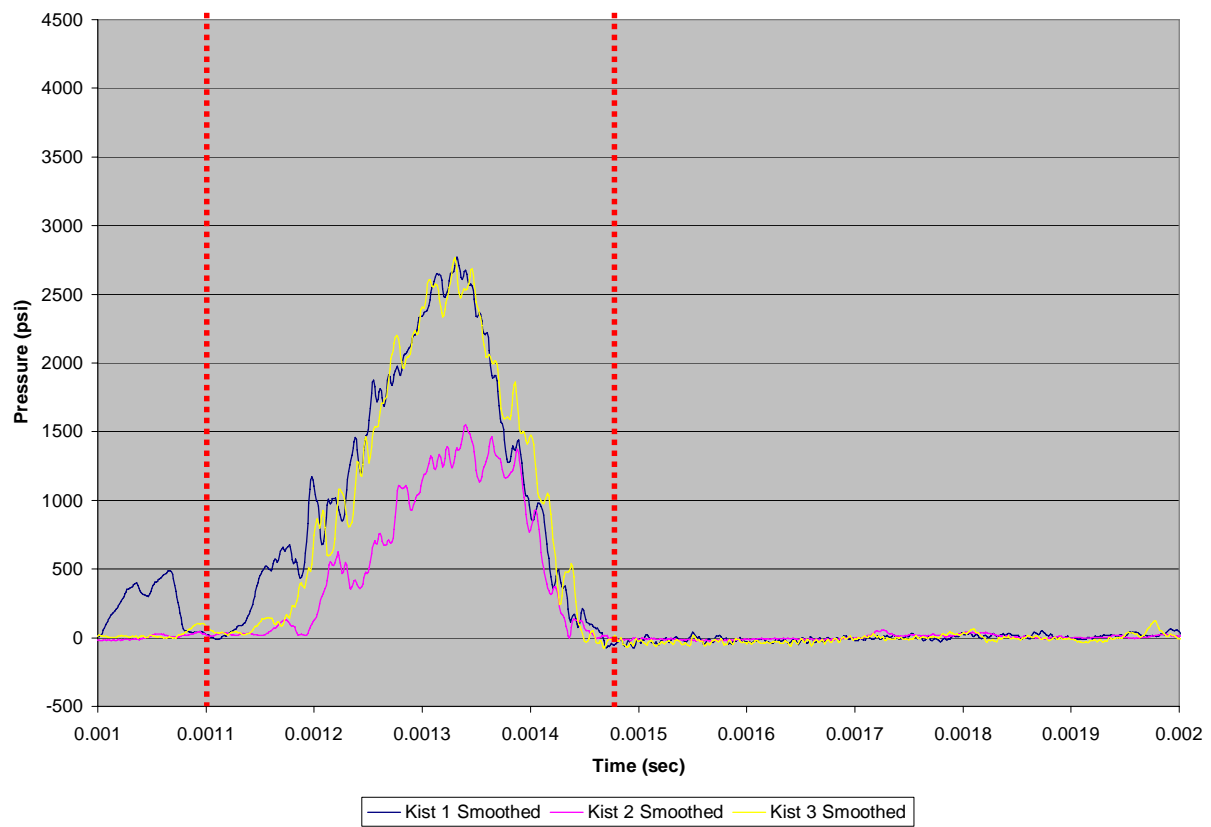


Figure C.7c.1: Kistler pressure vs. time (Specimen 7c)

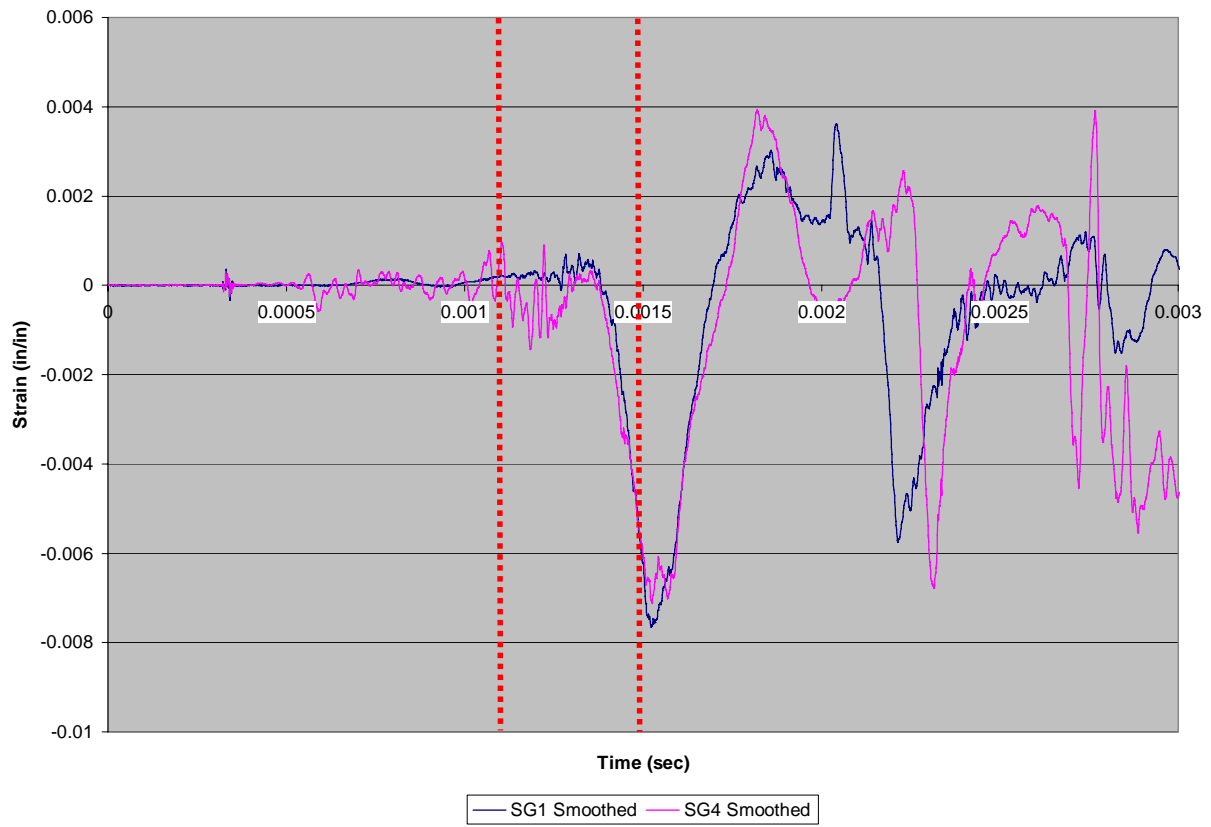


Figure C.7c.2: SG1 & SG4 skin strain vs. time (Specimen 7c)

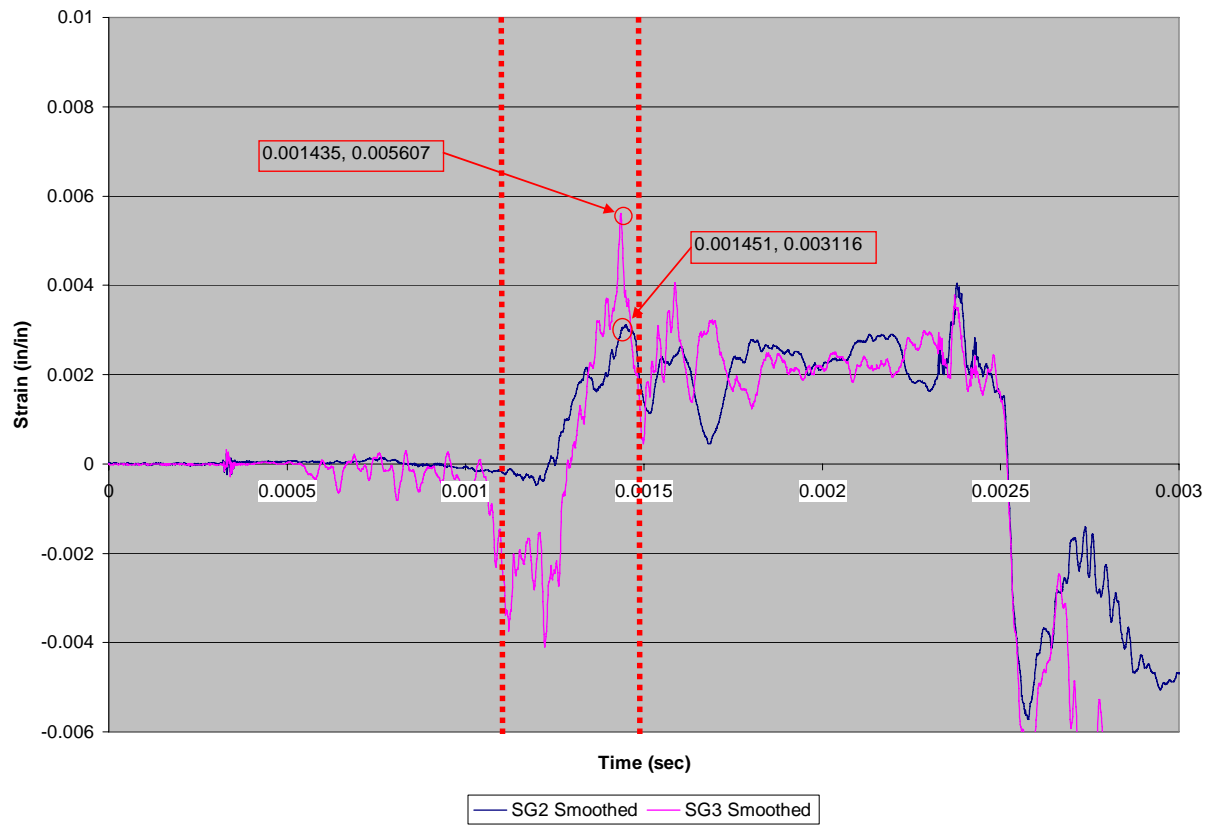


Figure C.7c.3: SG2 & SG3 spar strain vs. time (Specimen 7c)

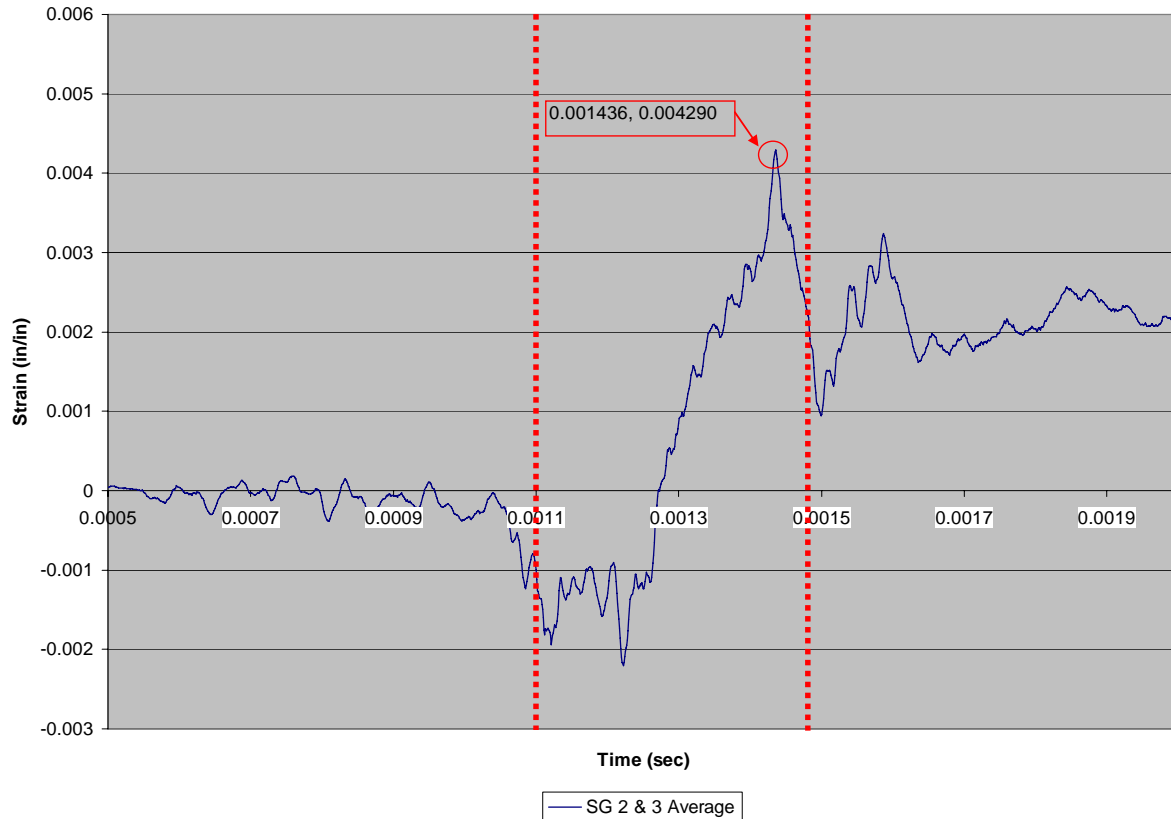


Figure C.7c.4: SG2 & SG3 average spar strain vs. time (Specimen 7c)

Specimen 7d, Test 34

For Specimen 7d, the load interval (and therefore the strain vs. time interval of interest) is approximately 1.20ms-1.50ms as shown in Figure C.7d.1. As desired, pressure sensors K1 and K3 are largely in agreement, indicating side-to-side uniformity of load on the test specimen. During the load interval, Figure C.7d.2 shows that SG1 and SG4 remain in phase. While SG2 and SG3 on the spar also appear mostly in phase, the strain amplitudes differ (as seen in Figure C.7d.3) implying asymmetric failure. Failure metrics for Specimen 7d are derived from Figure C.7d.4. Failure strain occurred at 1.466ms with a maximum strain of 0.003586 in/in.

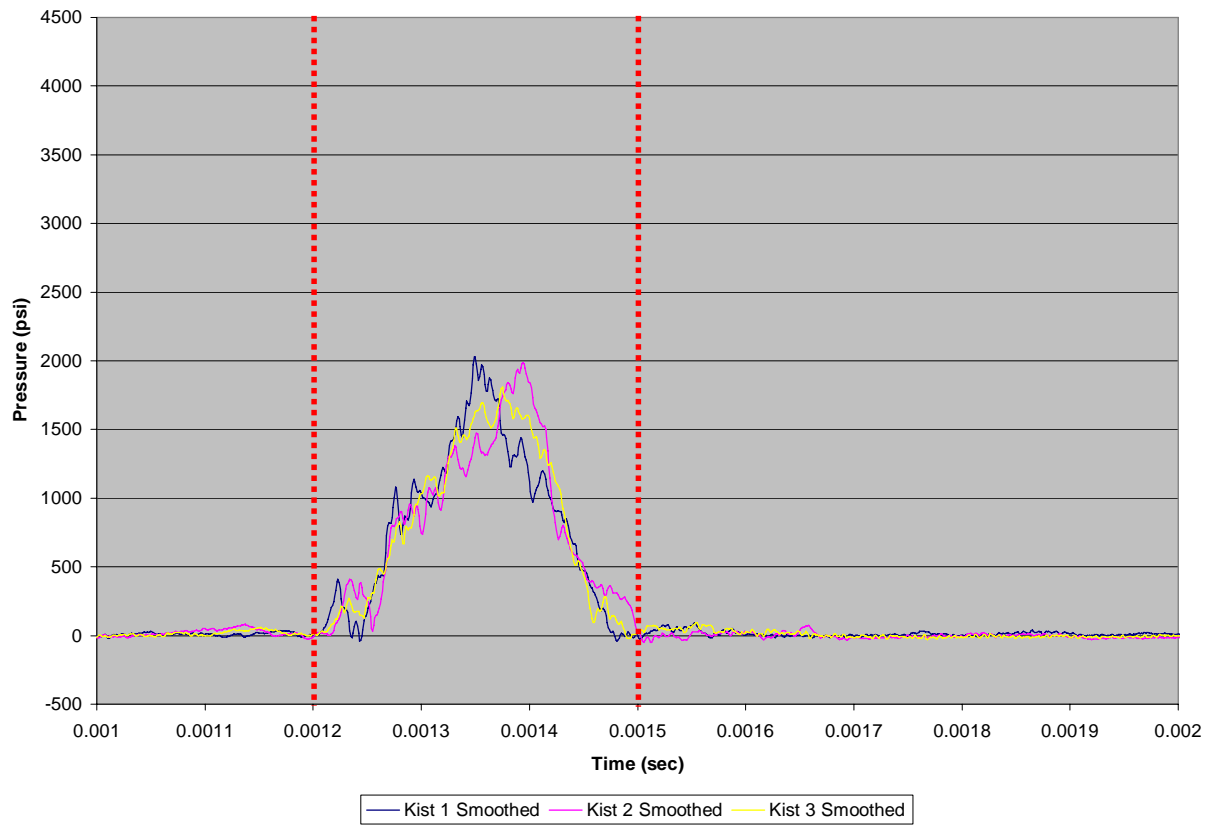


Figure C.7d.1: Kistler pressure vs. time (Specimen 7d)

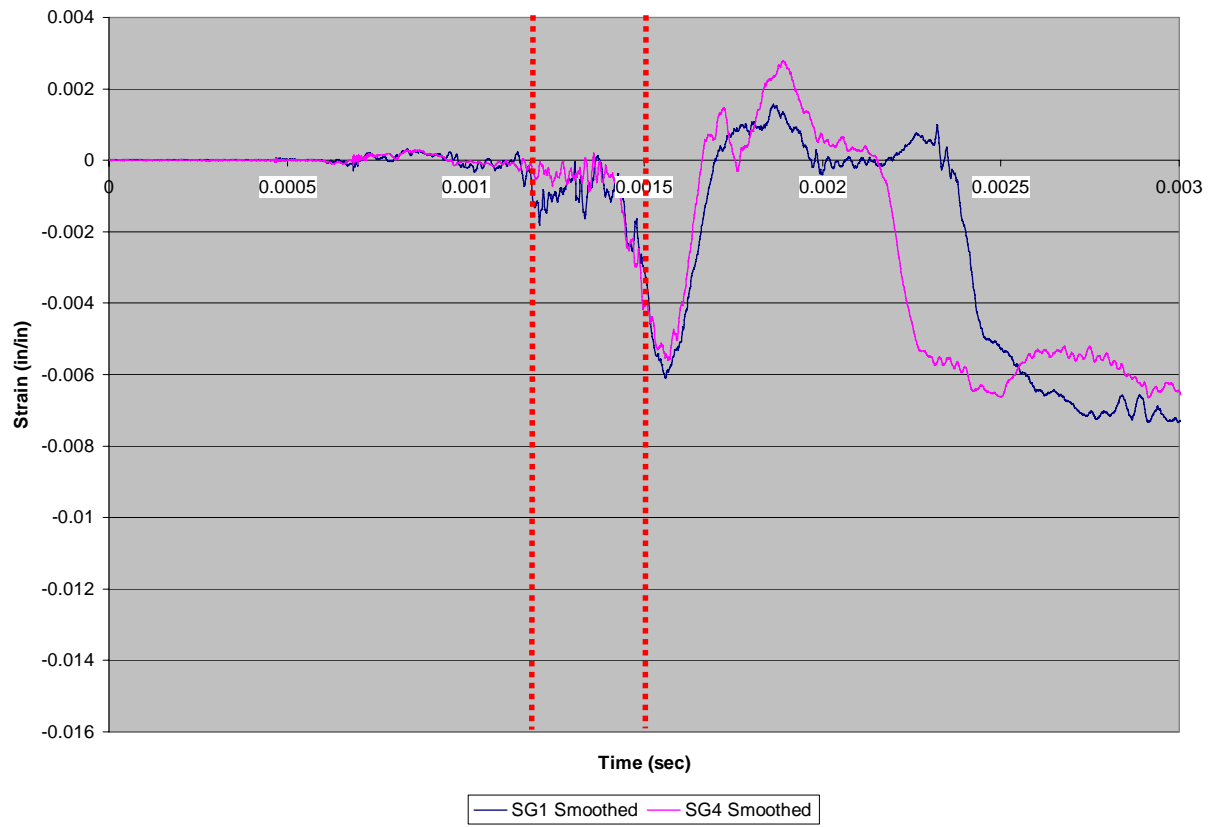


Figure C.7d.2: SG1 & SG4 skin strain vs. time (Specimen 7d)

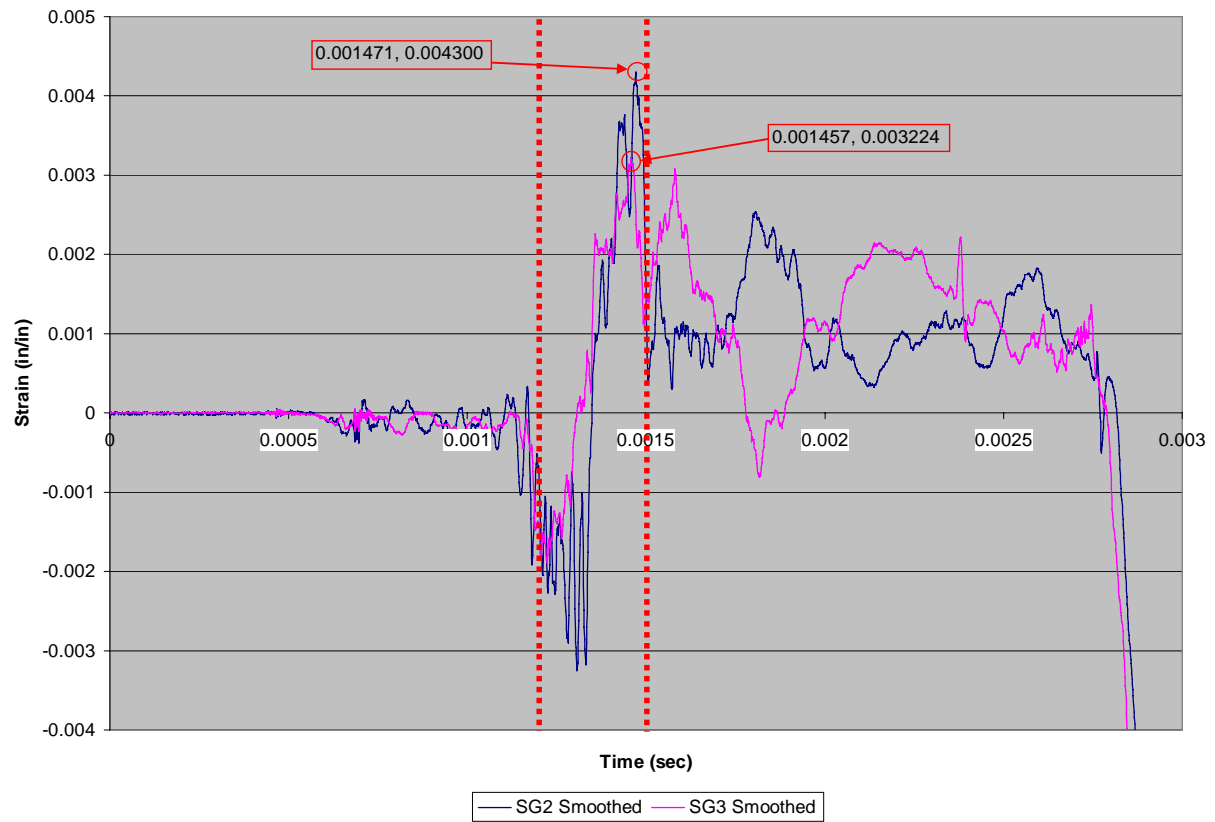


Figure C.7d.3: SG2 & SG3 spar strain vs. time (Specimen 7d)

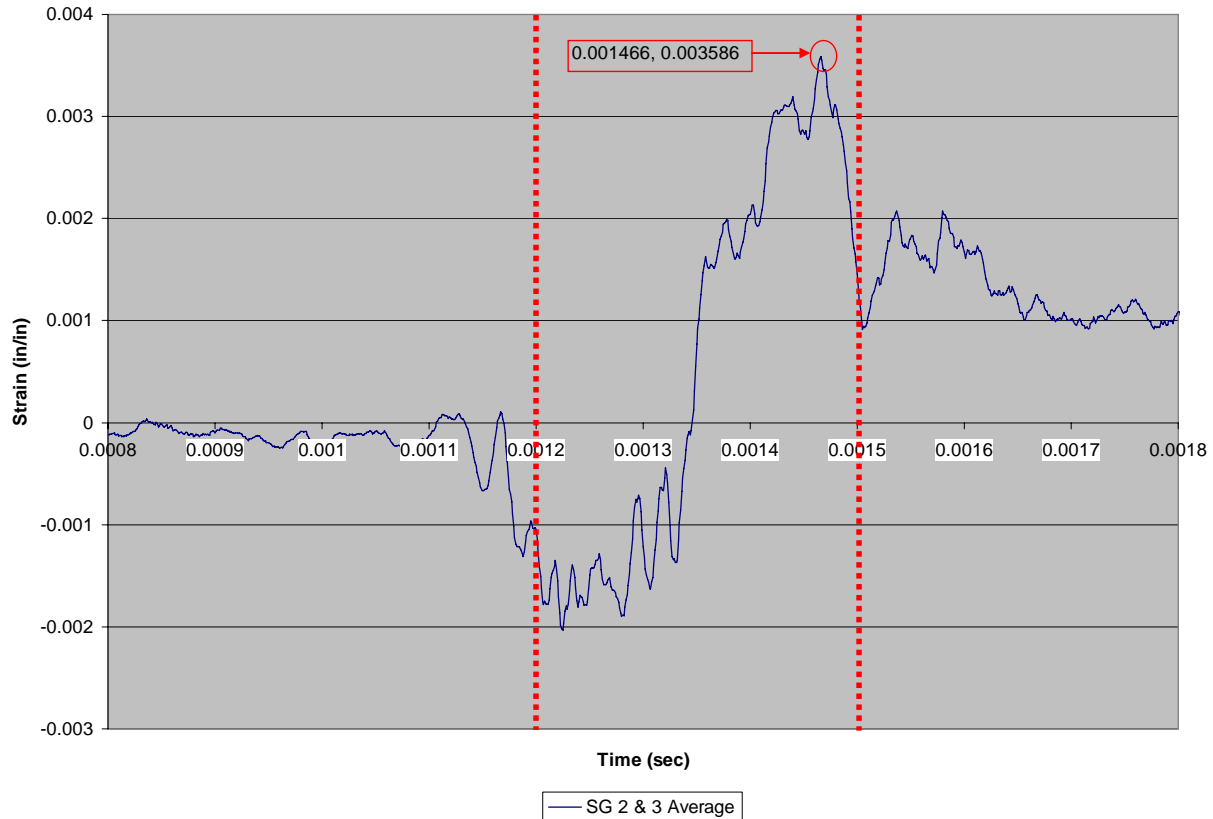


Figure C.7d.4: SG2 & SG3 average spar strain vs. time (Specimen 7d)

Specimen 7e, Test 35

For Specimen 7e, the load interval (and therefore the strain vs. time interval of interest) is approximately 1.15ms-1.50ms as shown in Figure C.7e.1. As desired, pressure sensors K1 and K3 are largely in agreement, indicating side-to-side uniformity of load on the test specimen. During the load interval, Figure C.7e.2 shows that SG1 and SG4 remain roughly in phase. While SG2 and SG3 on the spar also appear to be in phase (particularly later in the load cycle), but with strong amplitude differences (as seen in Figure C.7e.3). The failure is ruled asymmetric based on amplitude differences. Failure metrics for Specimen 7e are derived from Figure C.7e.4. Failure strain occurred at 1.421ms with a maximum strain of 0.005938 in/in.

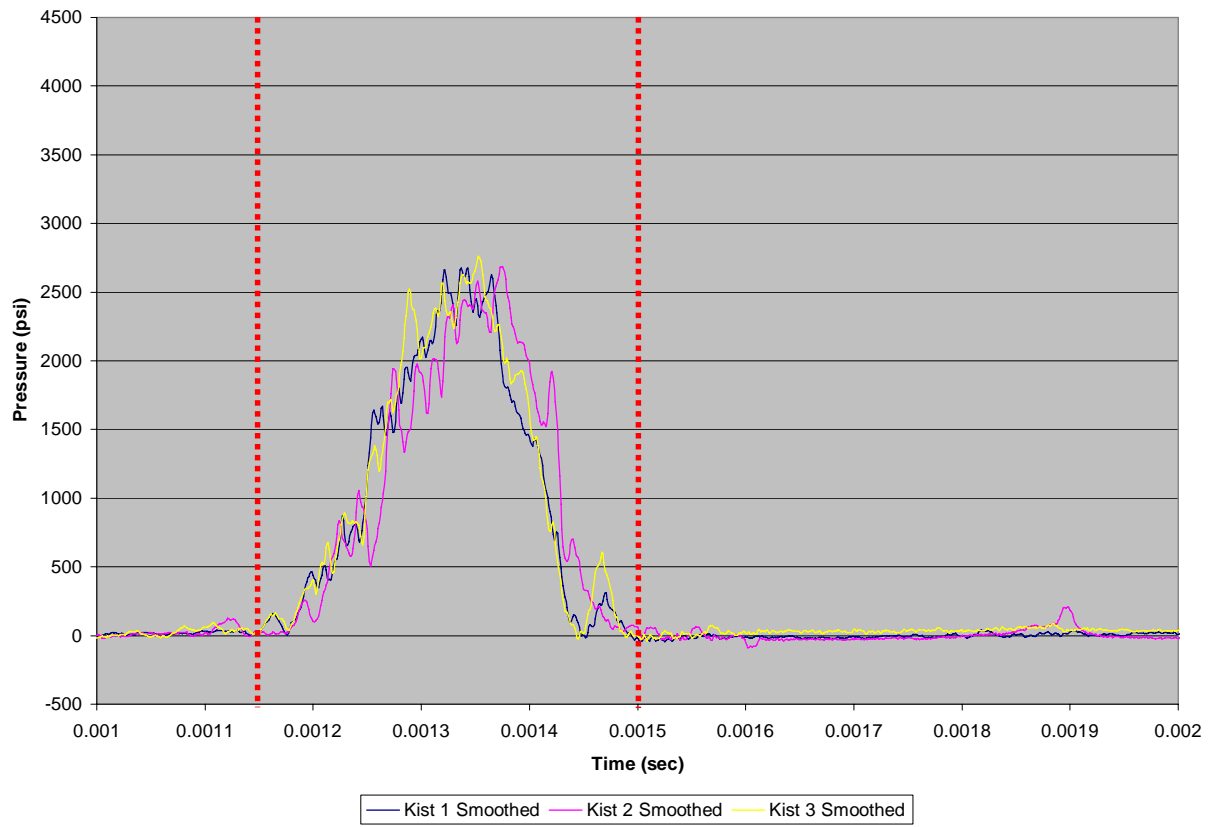


Figure C.7e.1: Kistler pressure vs. time (Specimen 7e)

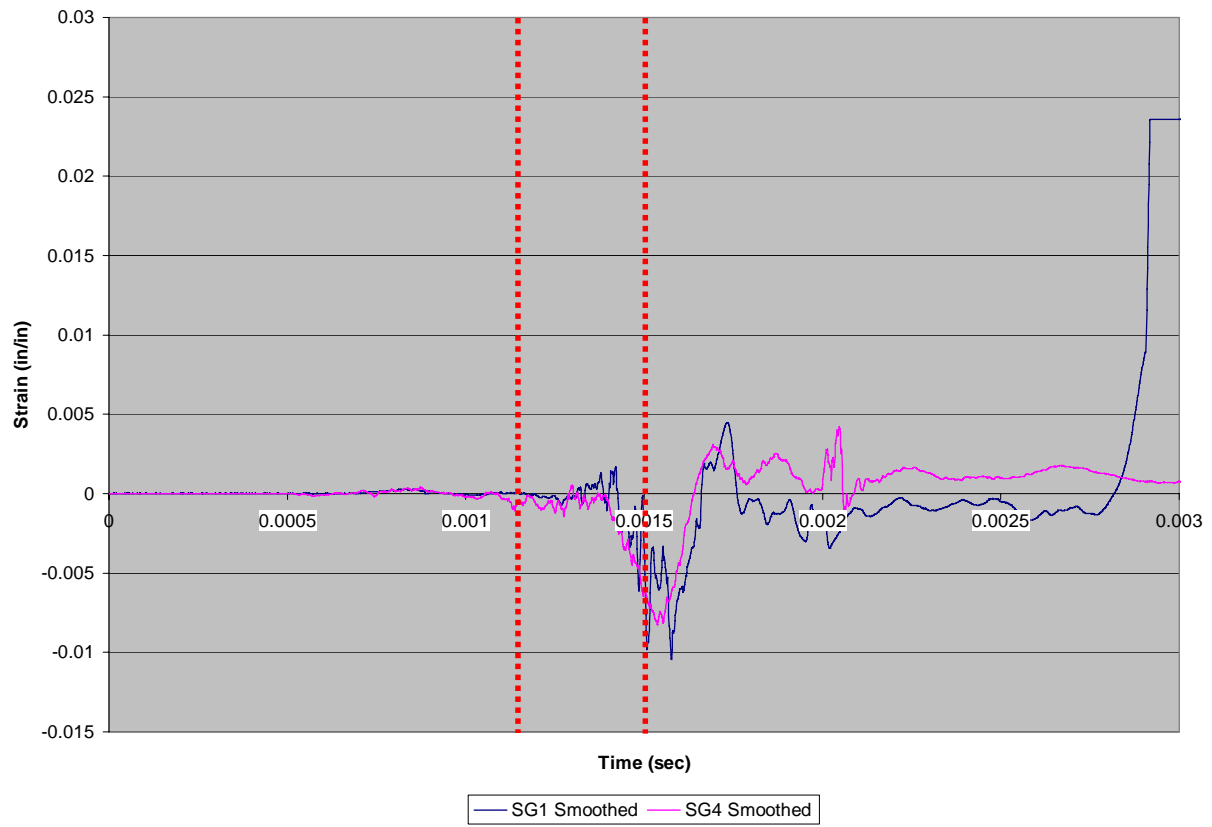


Figure C.7e.2: SG1 & SG4 skin strain vs. time (Specimen 7e)

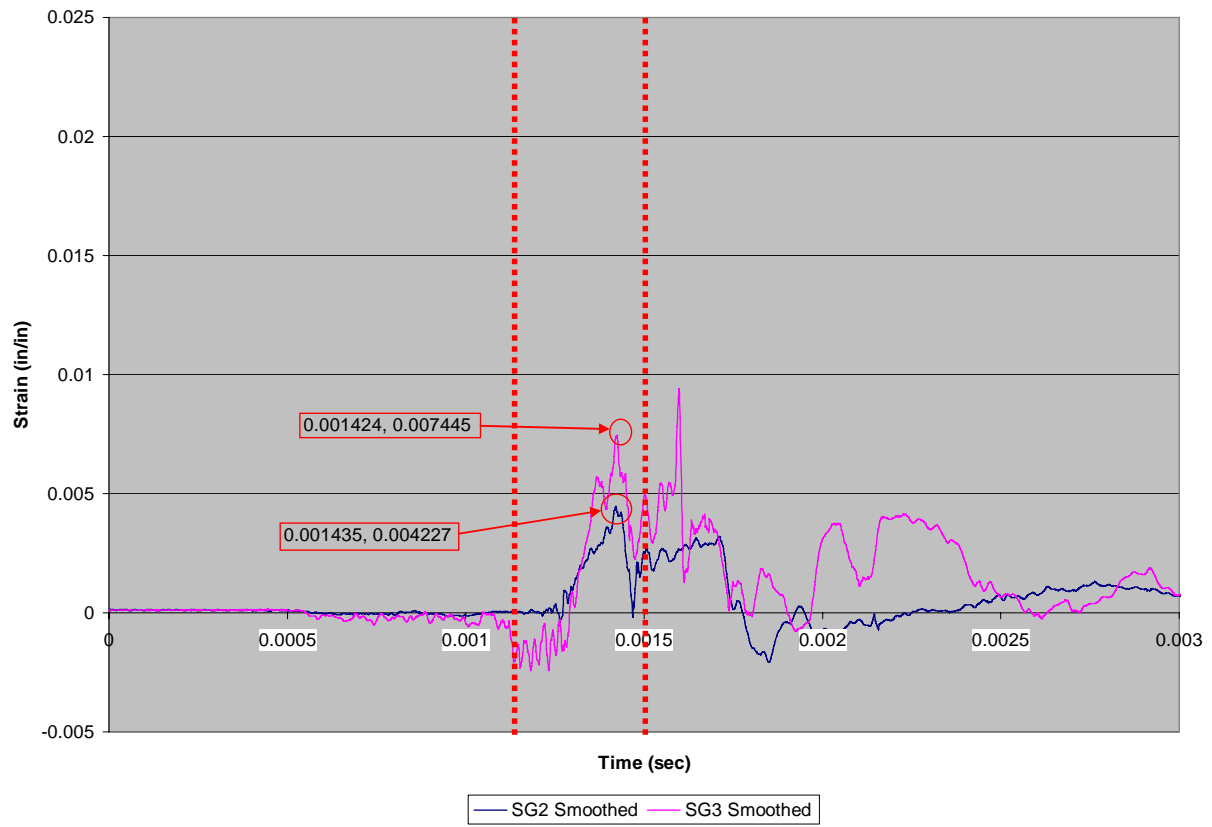


Figure C.7e.3: SG2 & SG3 spar strain vs. time (Specimen 7e)

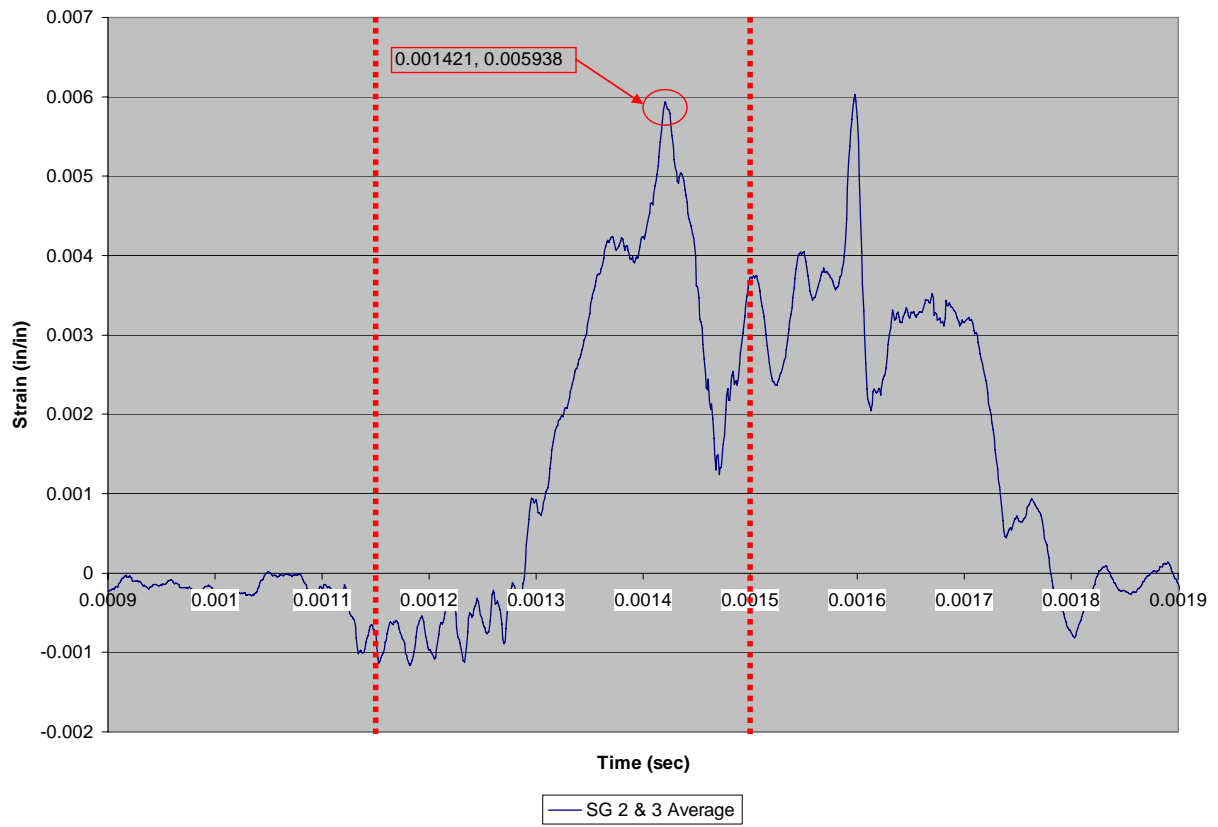


Figure C.7e.4: SG2 & SG3 average spar strain vs. time (Specimen 7e)

C.8 Specimen Set 8: Welded Aluminum

C.8.1 Dynamic Tests of Specimen Set 8

Specimen 8a, Test 22

For Specimen 8a, the load interval (and therefore the strain vs. time interval of interest) is approximately 1.10ms - 1.40ms as seen in Figure C.8a.1. As desired, pressure sensors K1 and K3 are largely in agreement, indicating side-to-side uniformity of load on the test specimen. During the load interval, Figure C.8a.2 shows that SG1 and SG4 are largely in phase and of similar amplitude, indicating the skin pulled away from the spar in a symmetric fashion. Similarly, SG2 and SG3 are in phase and of similar amplitude (as seen in Figure C.8a.3) implying symmetric failure. Failure metrics for Specimen 8a was derived from Figure C.8a.4. Failure strain occurred at 1.393ms with a maximum strain of 0.001566 in/in.

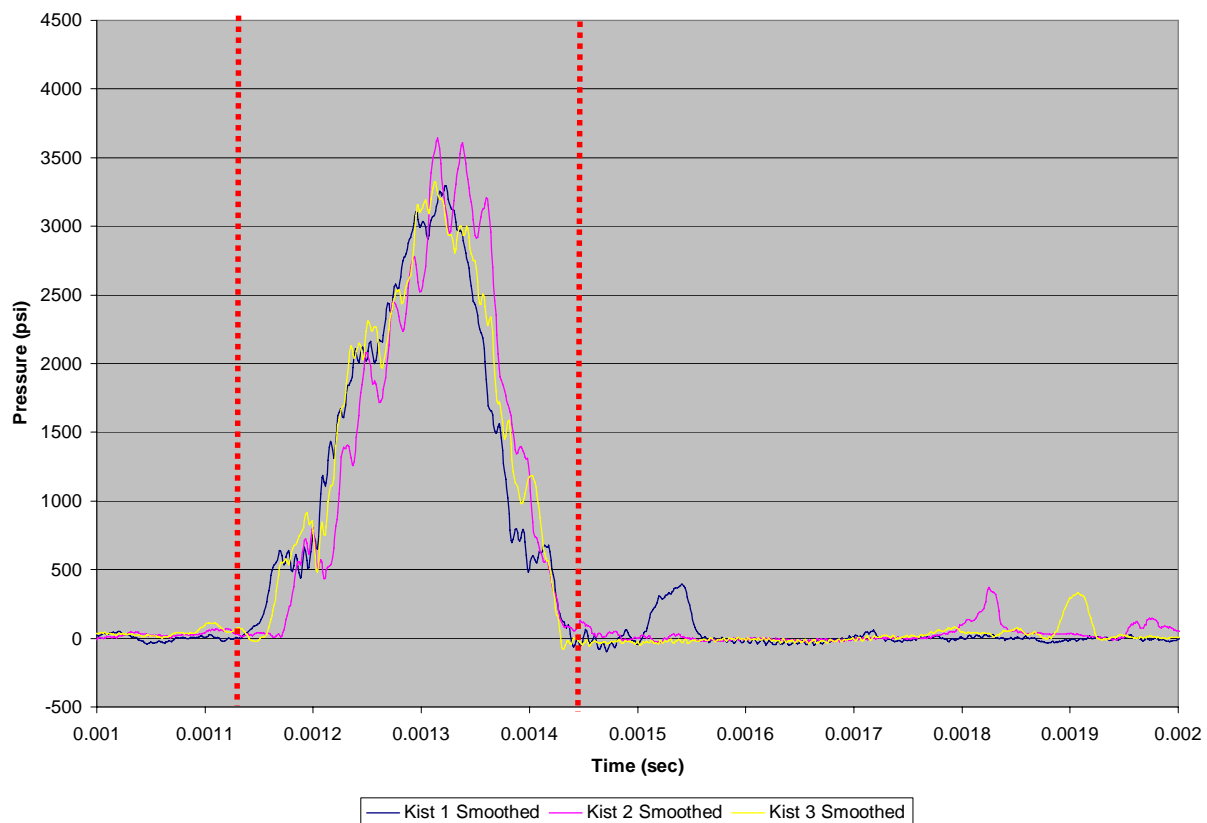


Figure C.8a.1: Kistler pressure vs. time (Specimen 8a)

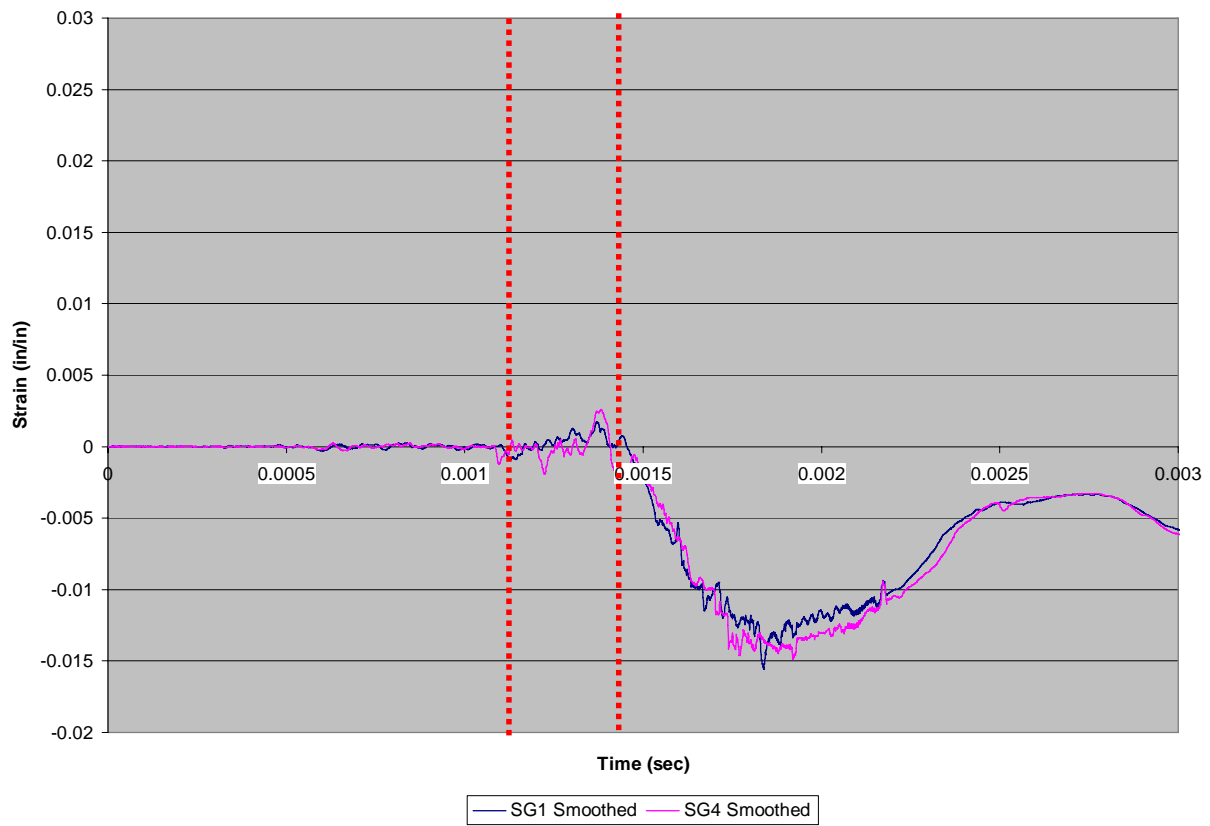


Figure C.8a.2: SG1 & SG4 skin strain vs. time (Specimen 8a)

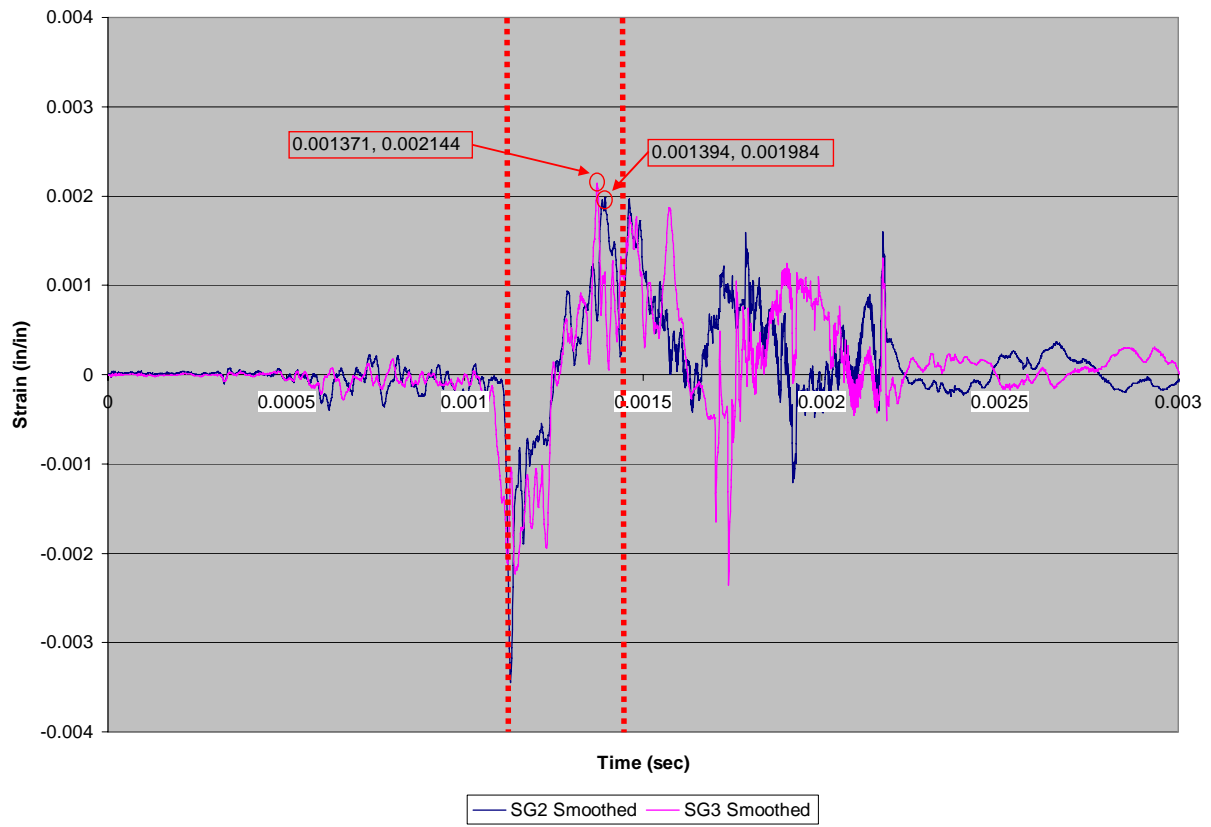


Figure C.8a.3: SG2 & SG3 spar strain vs. time (Specimen 8a)

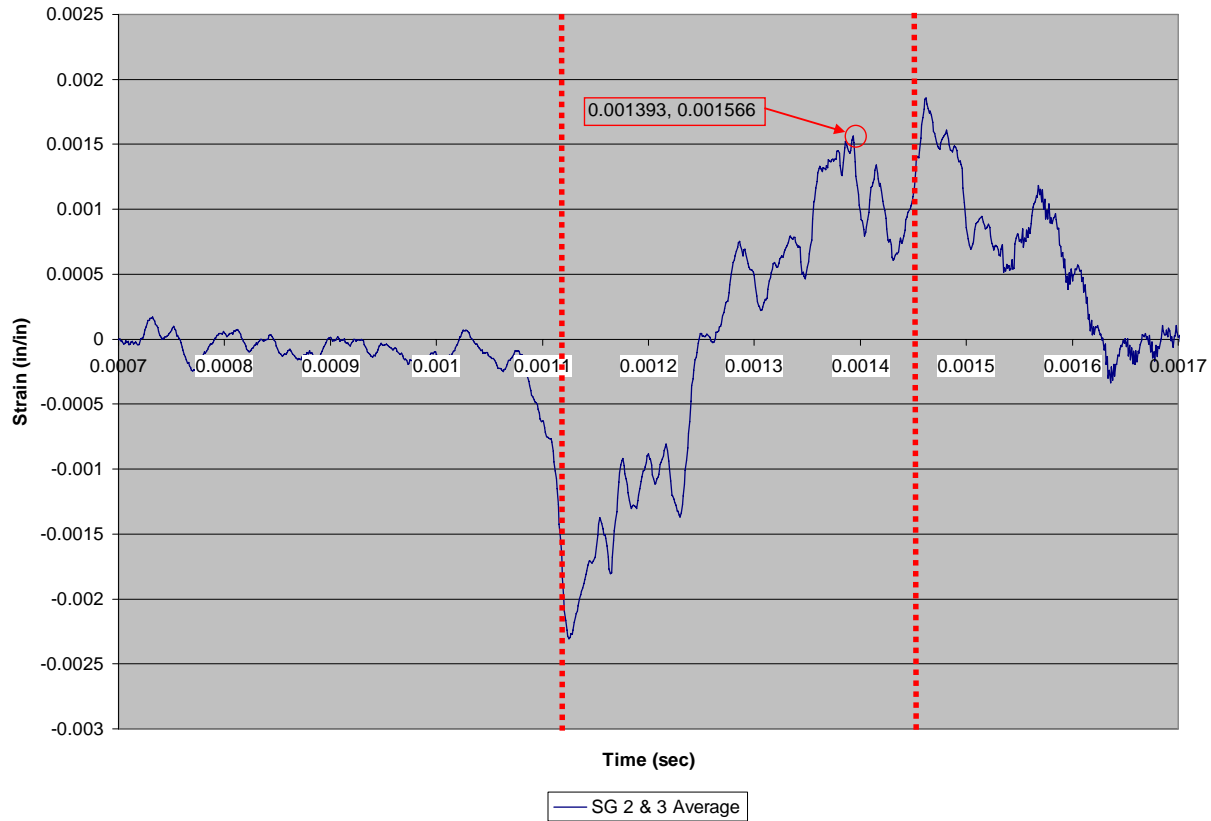


Figure C.8a.4: SG2 & SG3 average spar strain vs. time (Specimen 8a)

Specimen 8b, Test 23

For Specimen 8b, the load interval (and therefore the strain vs. time interval of interest) is approximately 1.40ms - 1.70ms as seen in Figure C.8b.1. Pressure sensor K3 was inoperative during the test, so side-to-side uniformity of the pressure load cannot be verified. During the load interval, Figure C.8b.2 shows that SG1 and SG4 are in phase and of similar amplitude, indicating the skin pulled away from the spar in a symmetric fashion. While SG2 and SG3 are in phase, strain amplitude differ (as seen in Figure C.8b.3) particularly later in the load cycle. Failure symmetry is ruled inconclusive. Failure metrics for Specimen 8b was derived from Figure C.8b.4. Failure strain occurred at 1.698ms with a maximum strain of 0.001857 in/in.

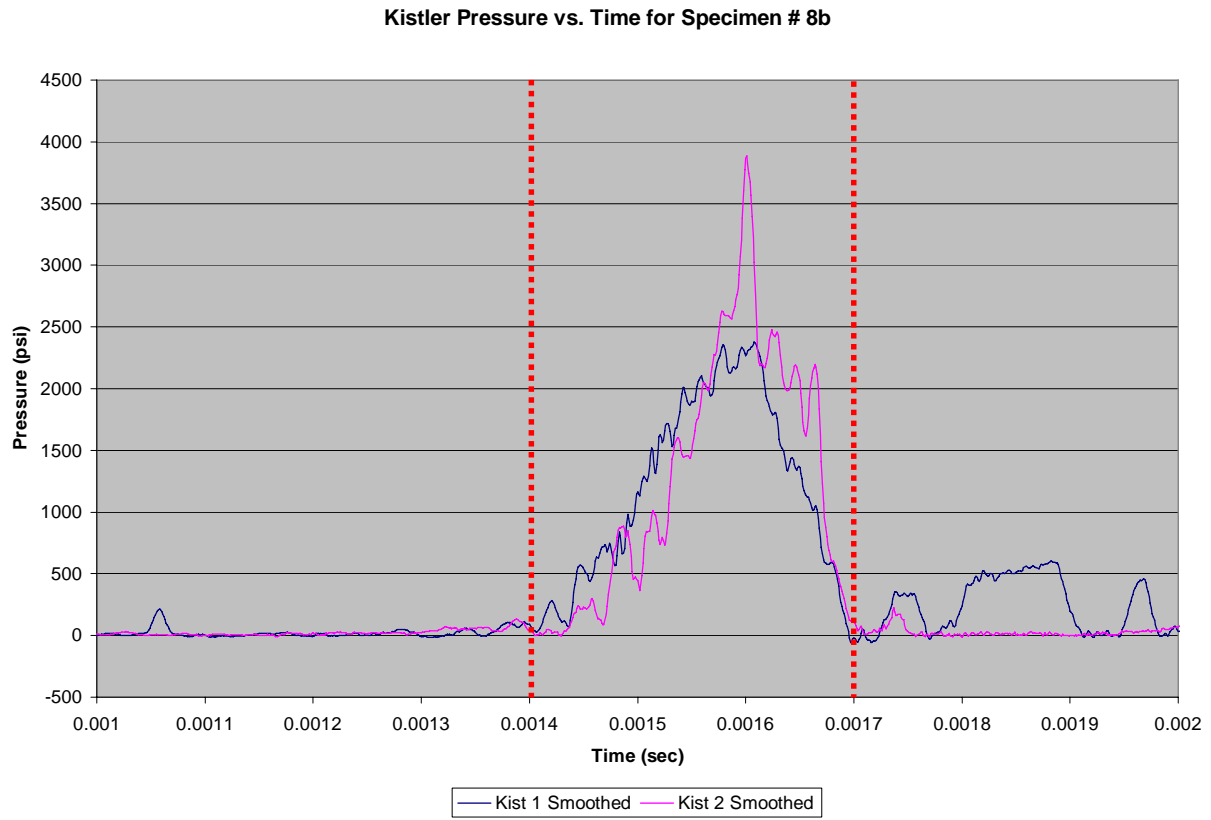


Figure C.8b.1: Kistler pressure vs. time (Specimen 8b)

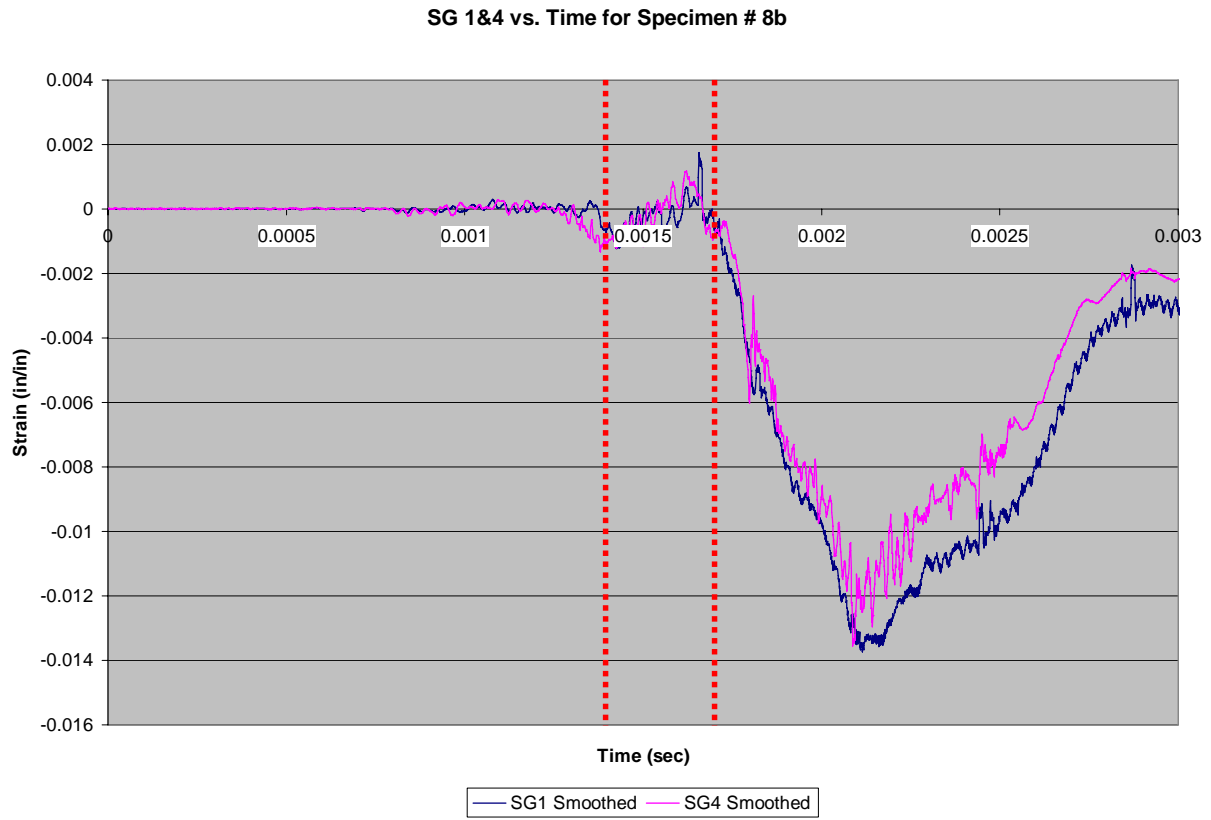


Figure C.8b.2: SG1 & SG4 skin strain vs. time (Specimen 8b)

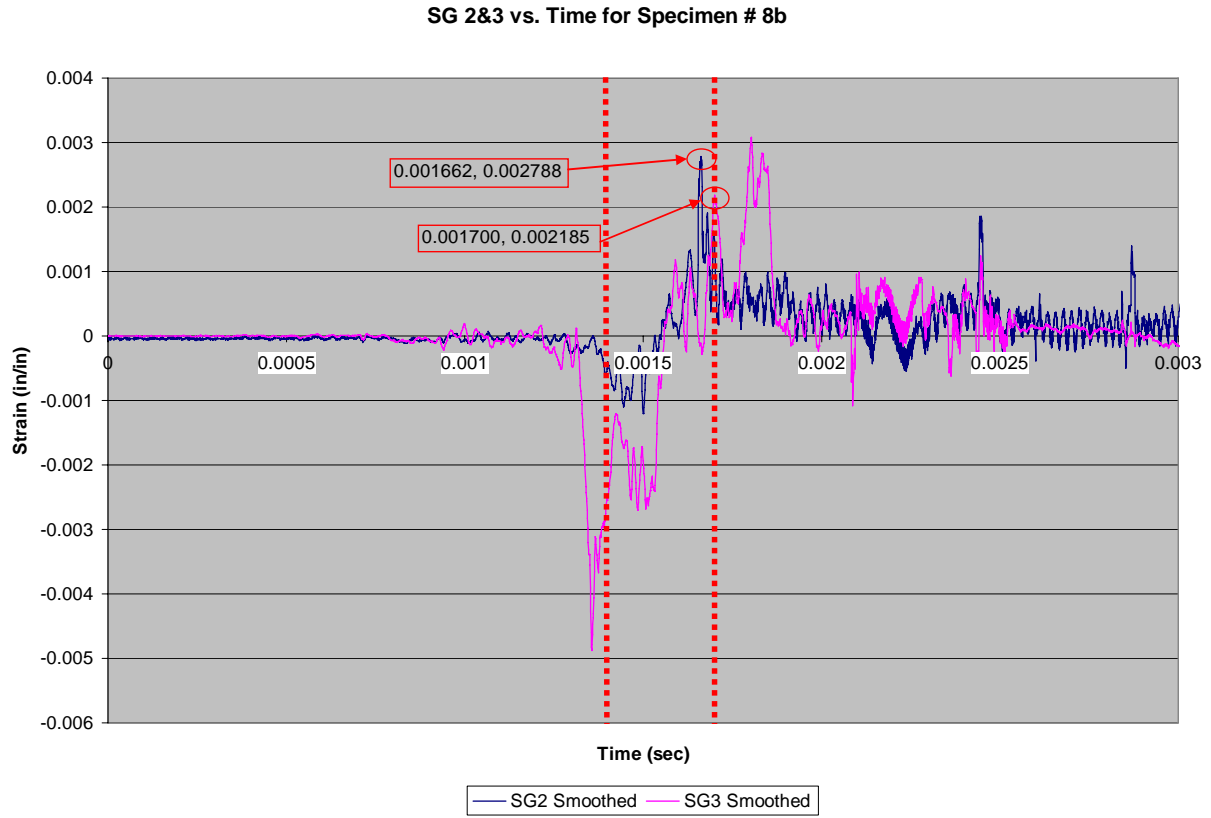


Figure C.8b.3: SG2 & SG3 spar strain vs. time (Specimen 8b)

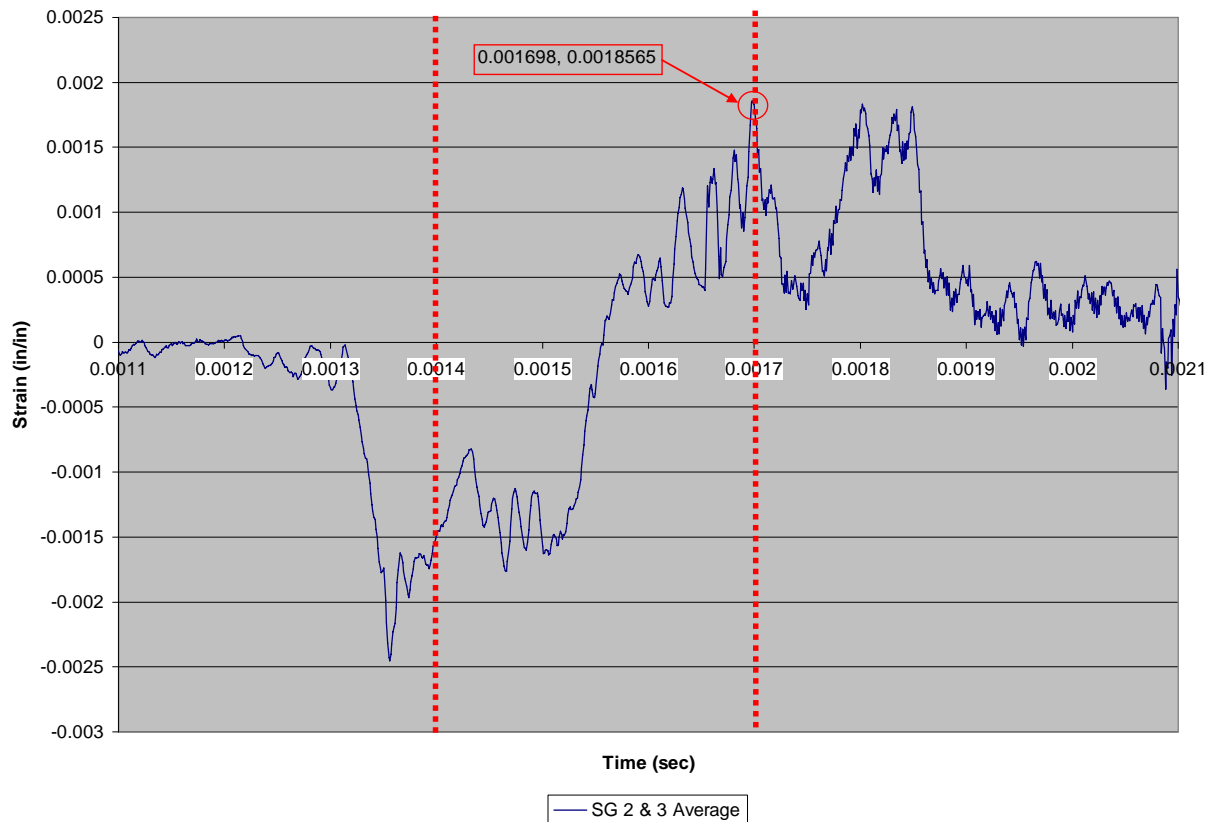


Figure C.8b.4: SG2 & SG3 average spar strain vs. time (Specimen 8b)

Specimen 8c, Test 24

For Specimen 8c, the load interval (and therefore the strain vs. time interval of interest) is approximately 1.10 ms to 1.40ms as shown in Figure C.8c.1. As desired, pressure sensors K1 and K3 are largely in agreement, indicating side-to-side uniformity of load on the test specimen. During the load interval, Figure C.8c.2 shows that SG1 and SG4 are in phase and of similar amplitude, indicating the skin pulled away from the spar in a symmetric fashion. SG2 and SG3 on the spar are also in phase, (as seen in Figure C.8c.3) but with amplitude differences indicating asymmetric failure. Failure symmetry is ruled inconclusive. Failure metrics for Specimen 8c are derived from Figure C.8c.4. Failure strain occurred at 1.351ms with a maximum strain of 0.00262 in/in.

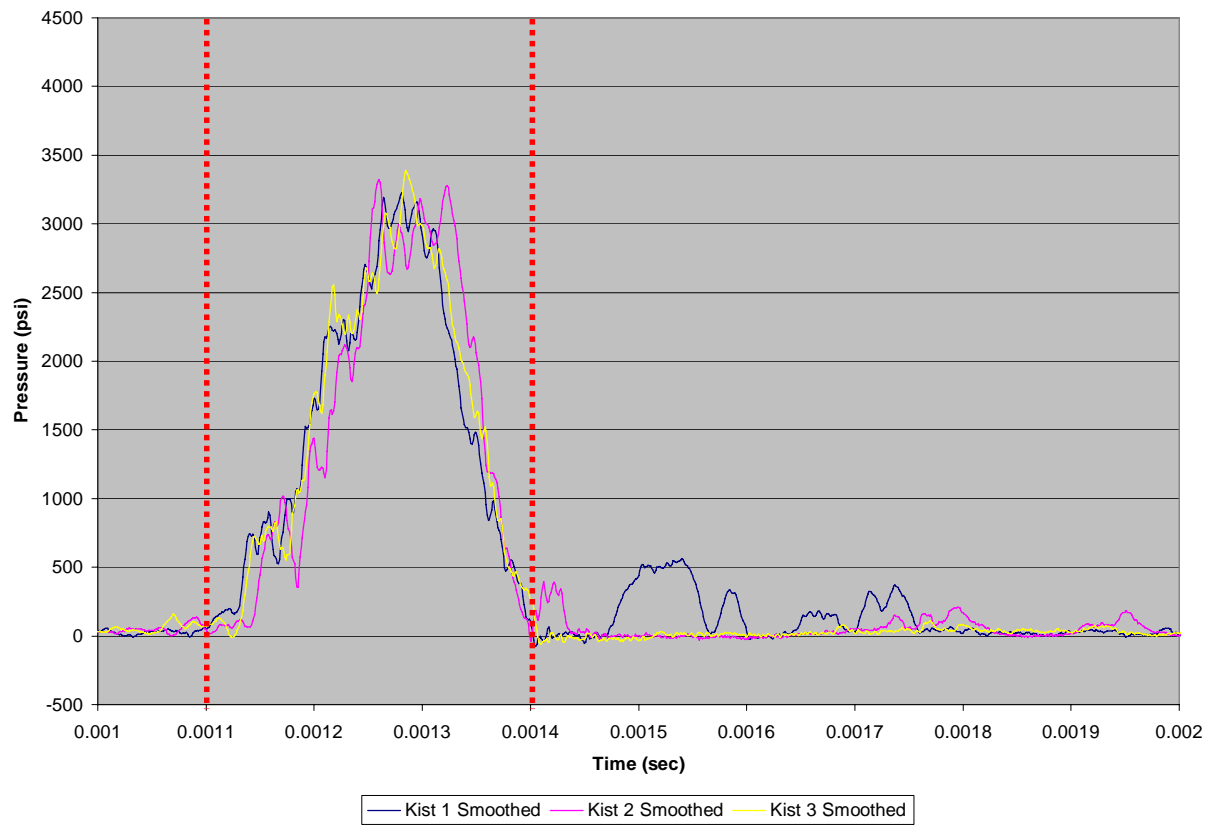


Figure C.8c.1: Kistler pressure vs. time (Specimen 8c)

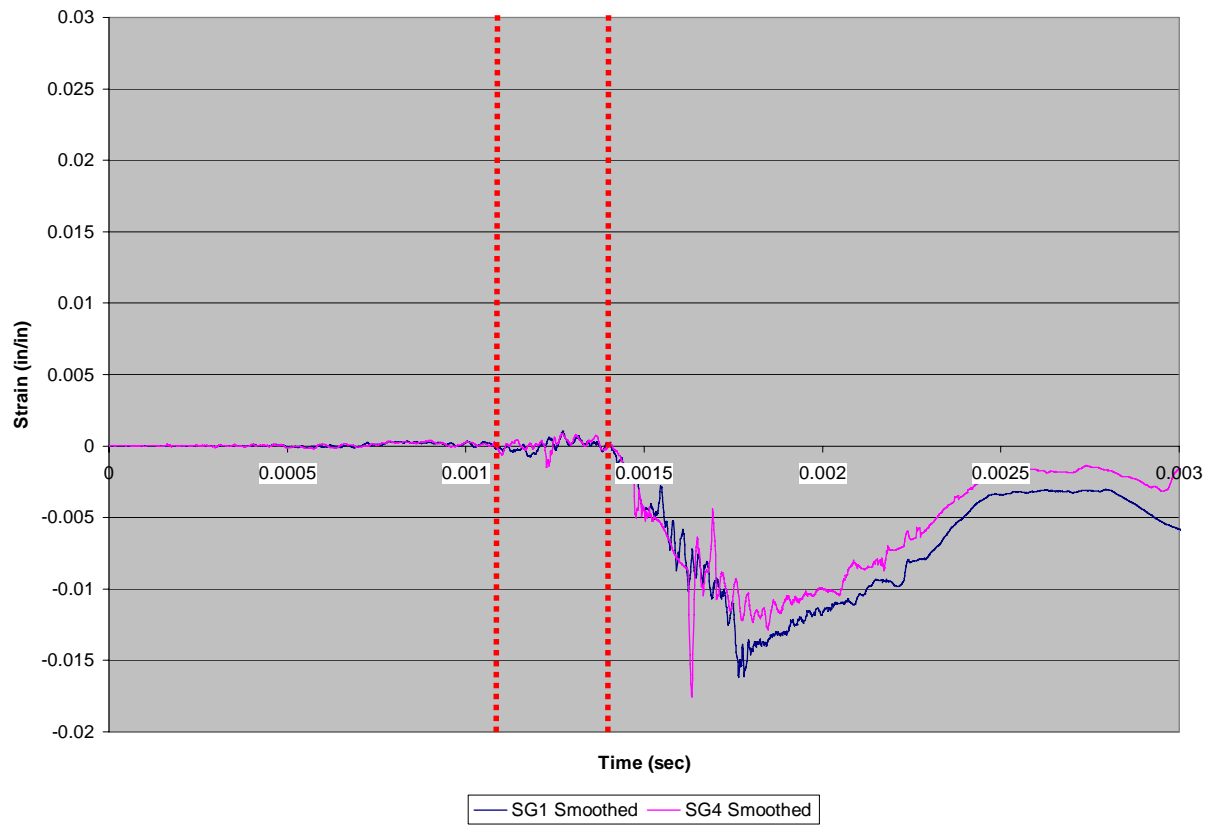


Figure C.8c.2: SG1 & SG4 skin strain vs. time (Specimen 8c)

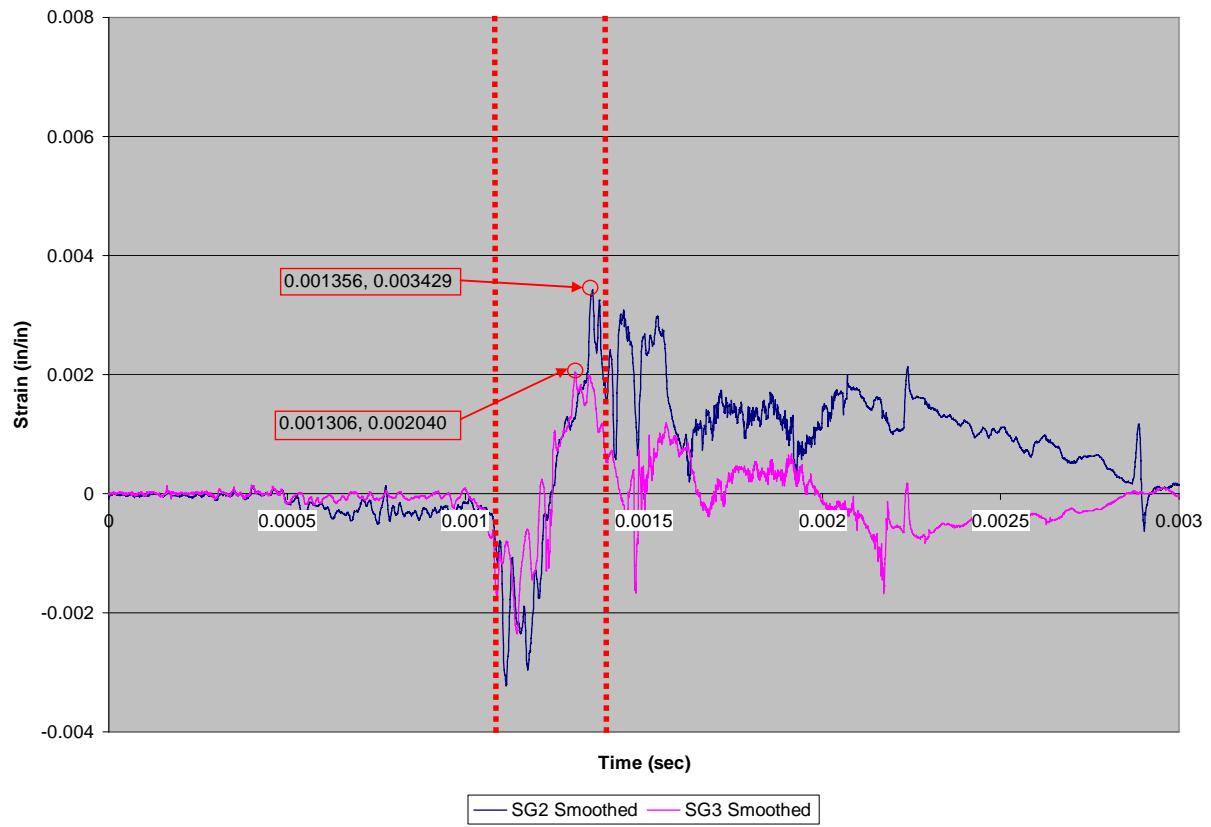


Figure C.8c.3: SG2 & SG3 spar strain vs. time (Specimen 8c)

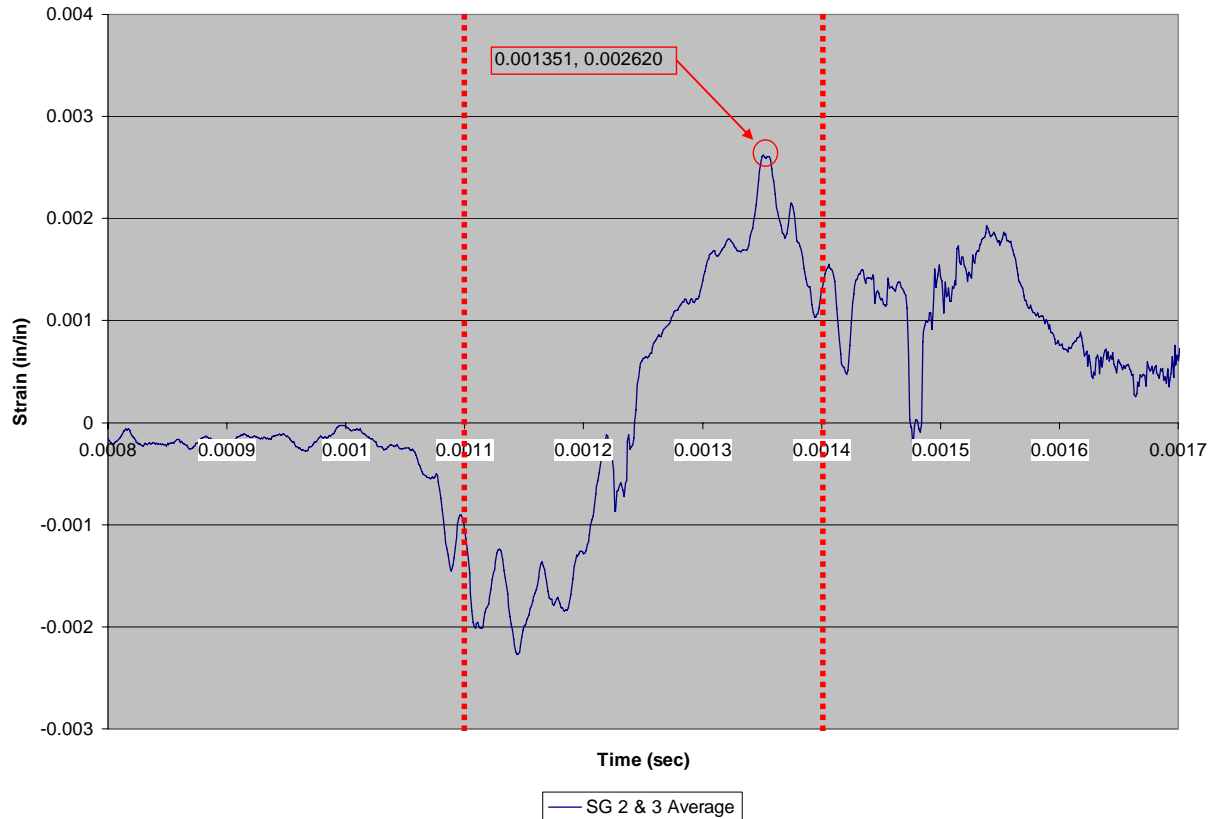


Figure C.8c.4: SG2 & SG3 average spar strain vs. time (Specimen 8c)

Specimen 8d, Test 38

For Specimen 8d, the load interval (and therefore the strain vs. time interval of interest) is approximately 1.15ms-1.50ms as shown in Figure C.8d 1. As desired, pressure sensors K1 and K3 are largely in agreement, indicating side-to-side uniformity of load on the test specimen. During the load interval, Figure C.8d 2 shows that SG1 and SG4 remain in phase and of similar amplitude. While SG2 and SG3 on the spar are in phase, their amplitudes differ (as seen in Figure C.8d 3) implying failure asymmetry. Failure symmetry is ruled inconclusive. Failure metrics for Specimen 8d are derived from Figure C.8d.4. Failure strain occurred at 1.451ms with a maximum strain of 0.002978 in/in.

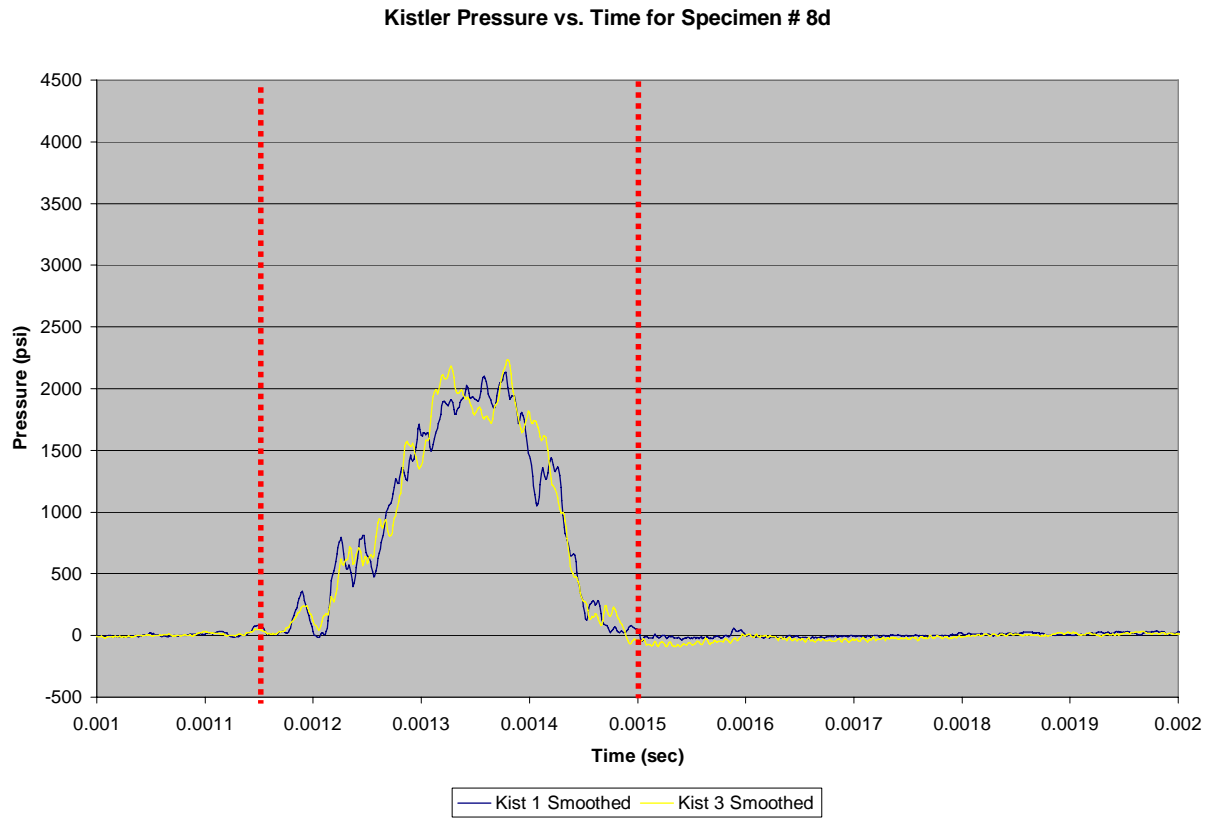


Figure C.8d.1: Kistler pressure vs. time (Specimen 8d)

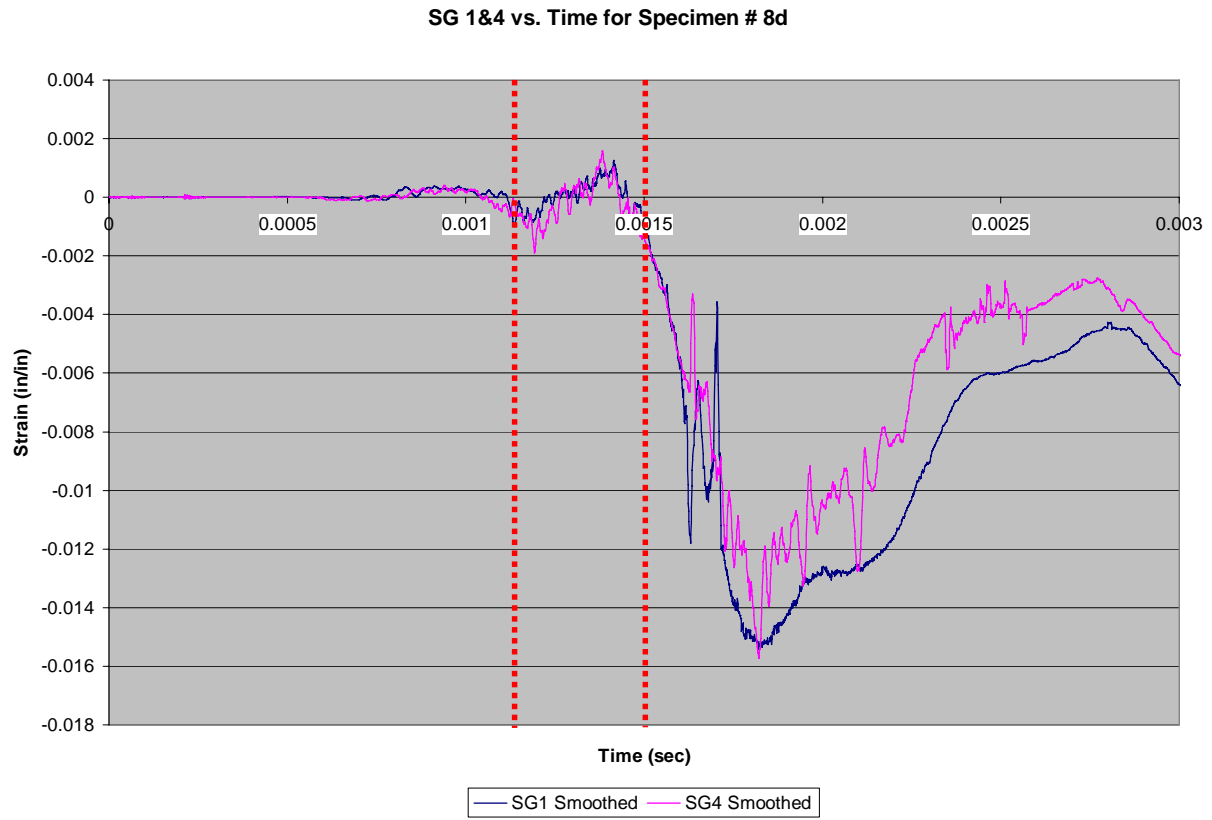


Figure C.8d.2: SG1 & SG4 skin strain vs. time (Specimen 8d)

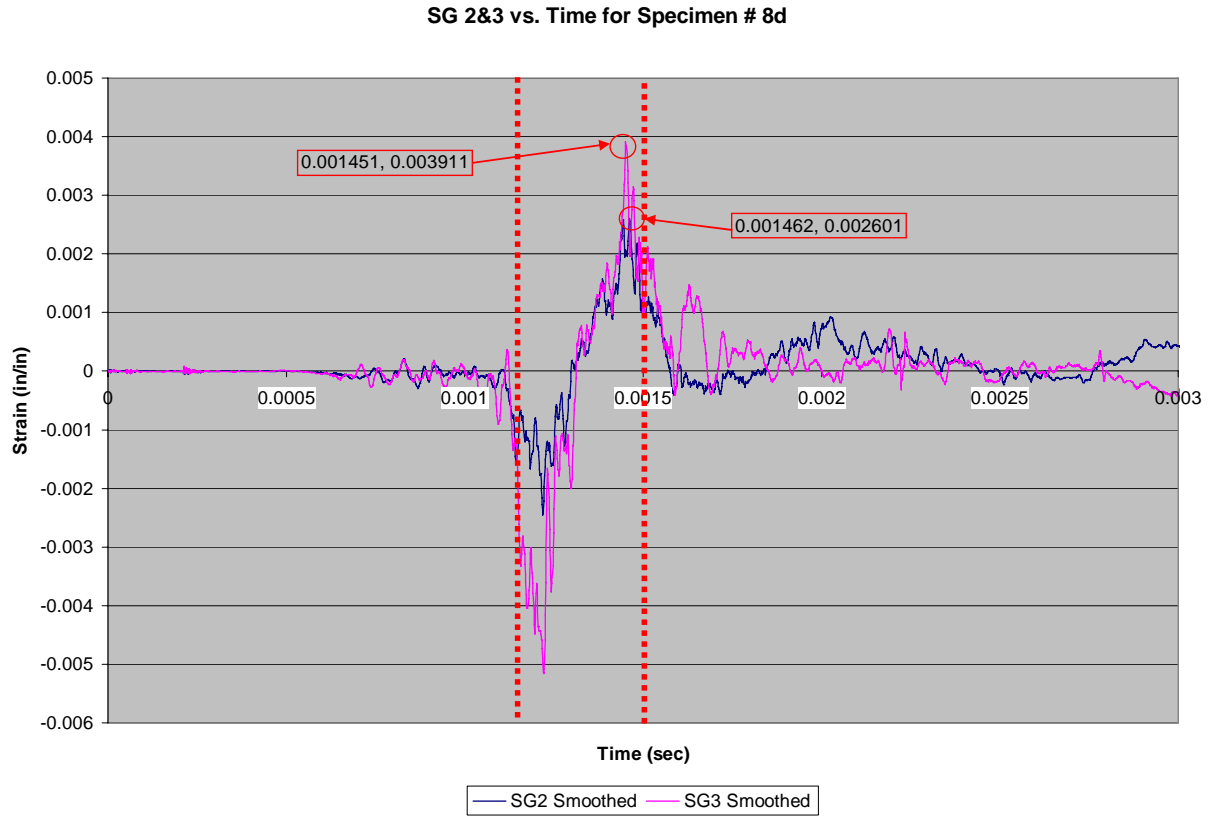


Figure C.8d.3: SG2 & SG3 spar strain vs. time (Specimen 8d)

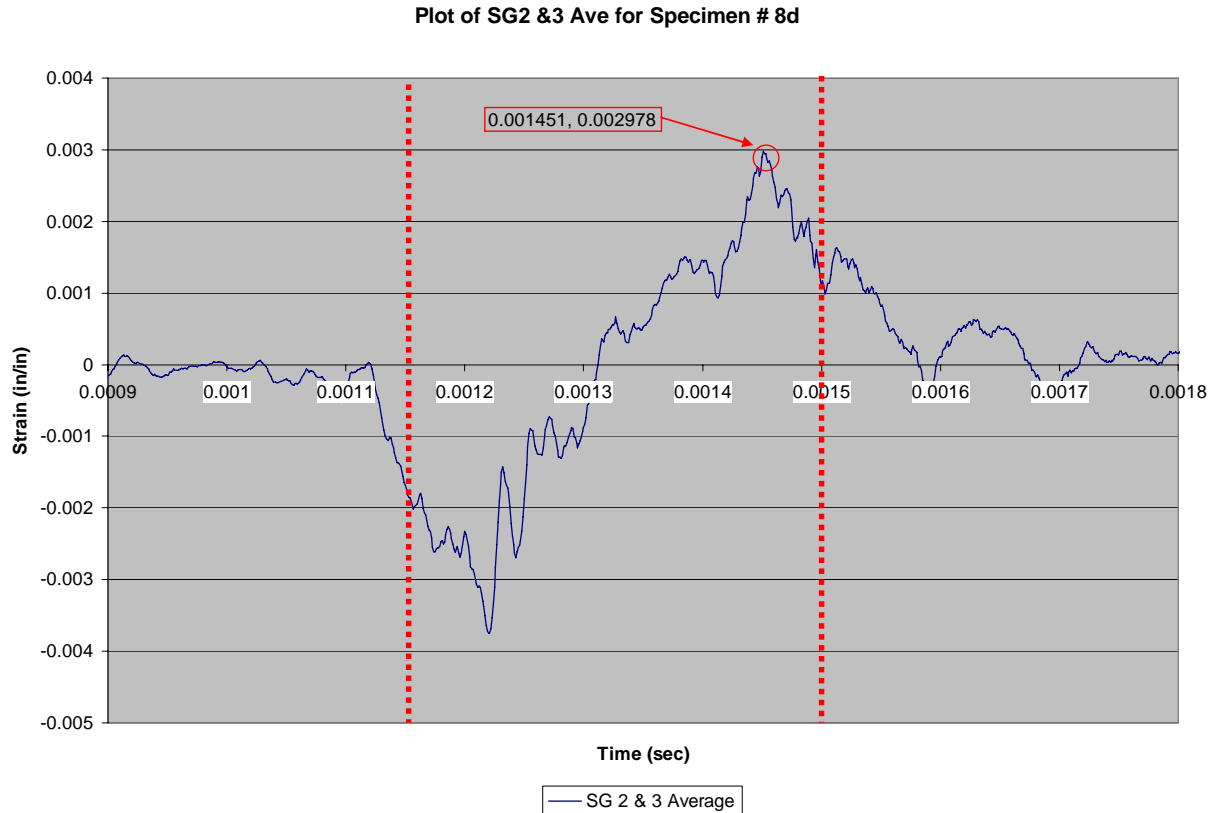


Figure C.8d.4: SG2 & SG3 average spar strain vs. time (Specimen 8d)

Specimen 8e, Test 39

For Specimen 8e, the load interval (and therefore the strain vs. time interval of interest) is approximately 1.10ms-1.50ms as shown in Figure C.8e.1. As desired, pressure sensors K1 and K3 are largely in agreement, indicating side-to-side uniformity of load on the test specimen. During the load interval, Figure C.8e.2 shows that SG1 and SG4 remain in phase and of similar amplitude. While SG2 and SG3 on the spar are in phase, their amplitudes differ (as seen in Figure C.8e.3) implying failure asymmetry. Failure symmetry is ruled inconclusive. Failure metrics for Specimen 8e are derived from Figure C.8e.4. Failure strain occurred at 1.429ms with a maximum strain of 0.002064 in/in. As such, it appears that the specimen strained in a symmetric manner up to the time of failure.

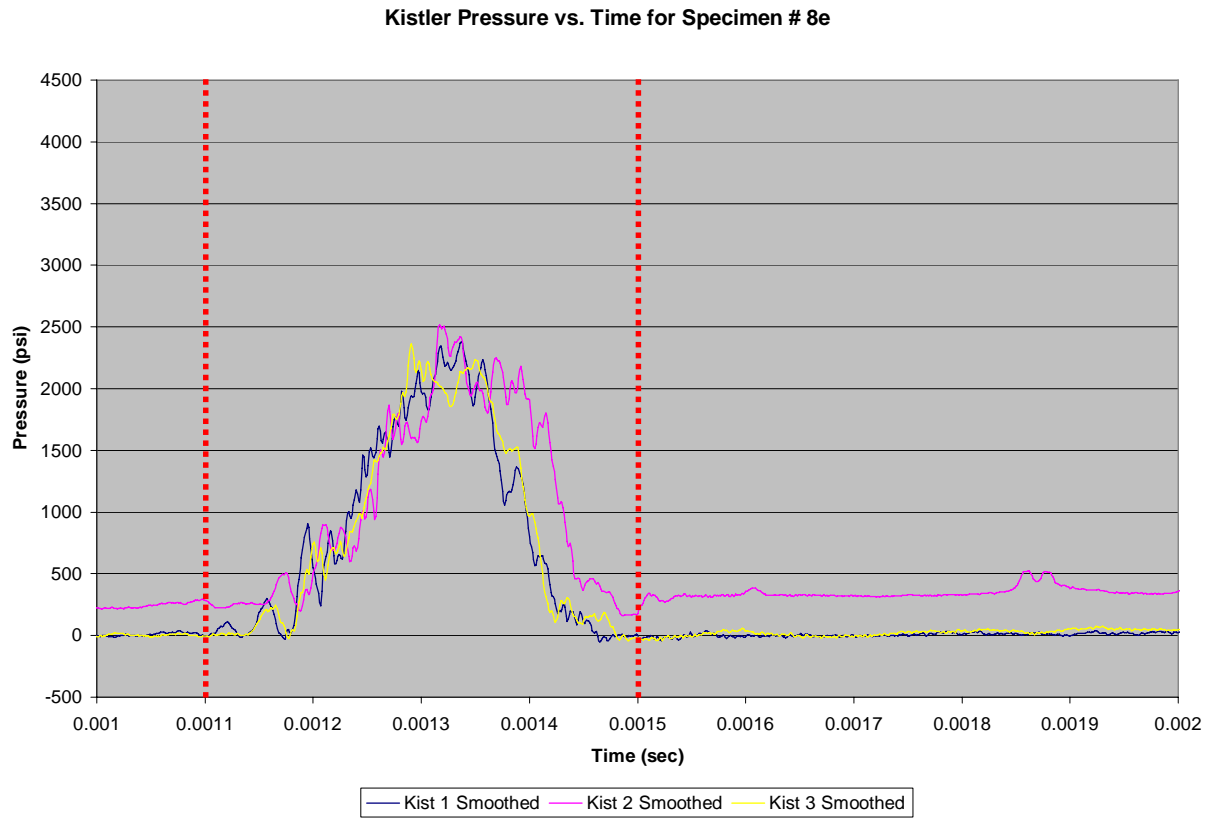


Figure C.8e.1: Kistler pressure vs. time (Specimen 8e)

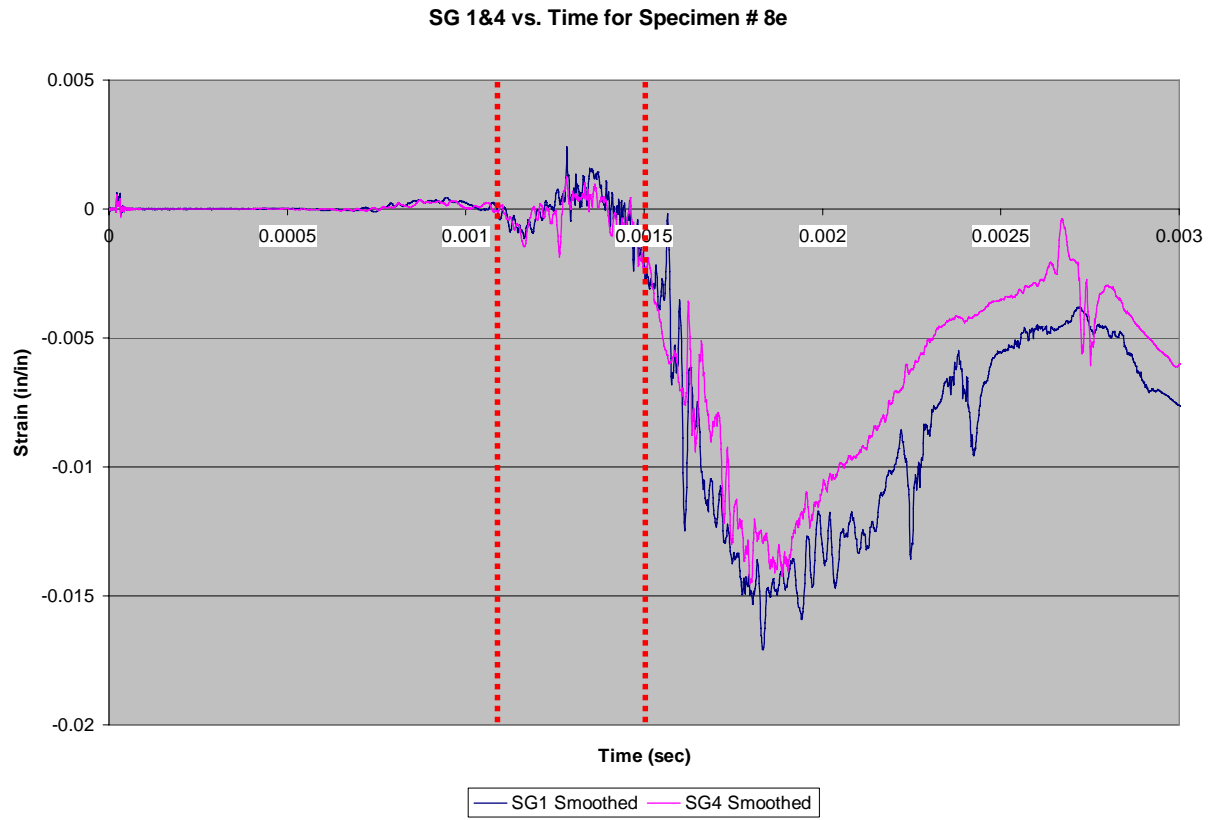


Figure C.8e.2: SG1 & SG4 skin strain vs. time (Specimen 8e)

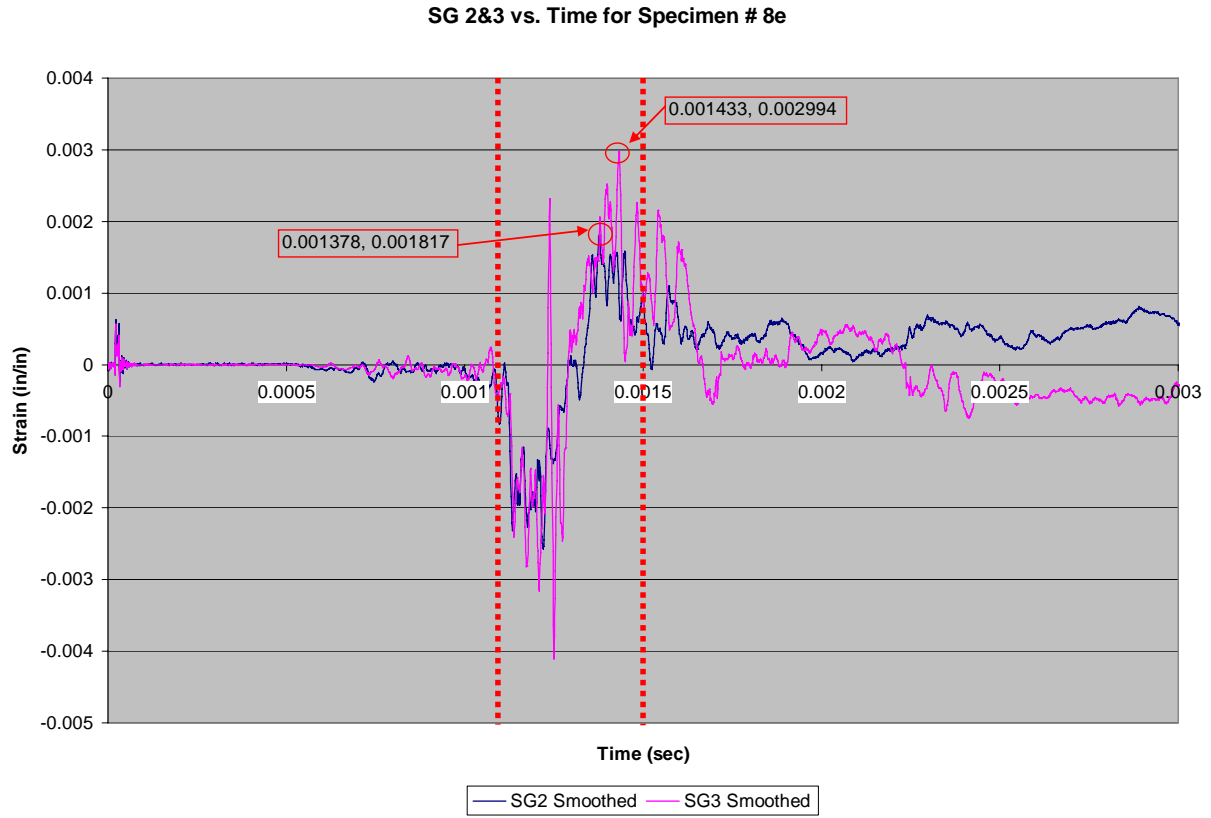


Figure C.8e.3: SG2 & SG3 spar strain vs. time (Specimen 8e)

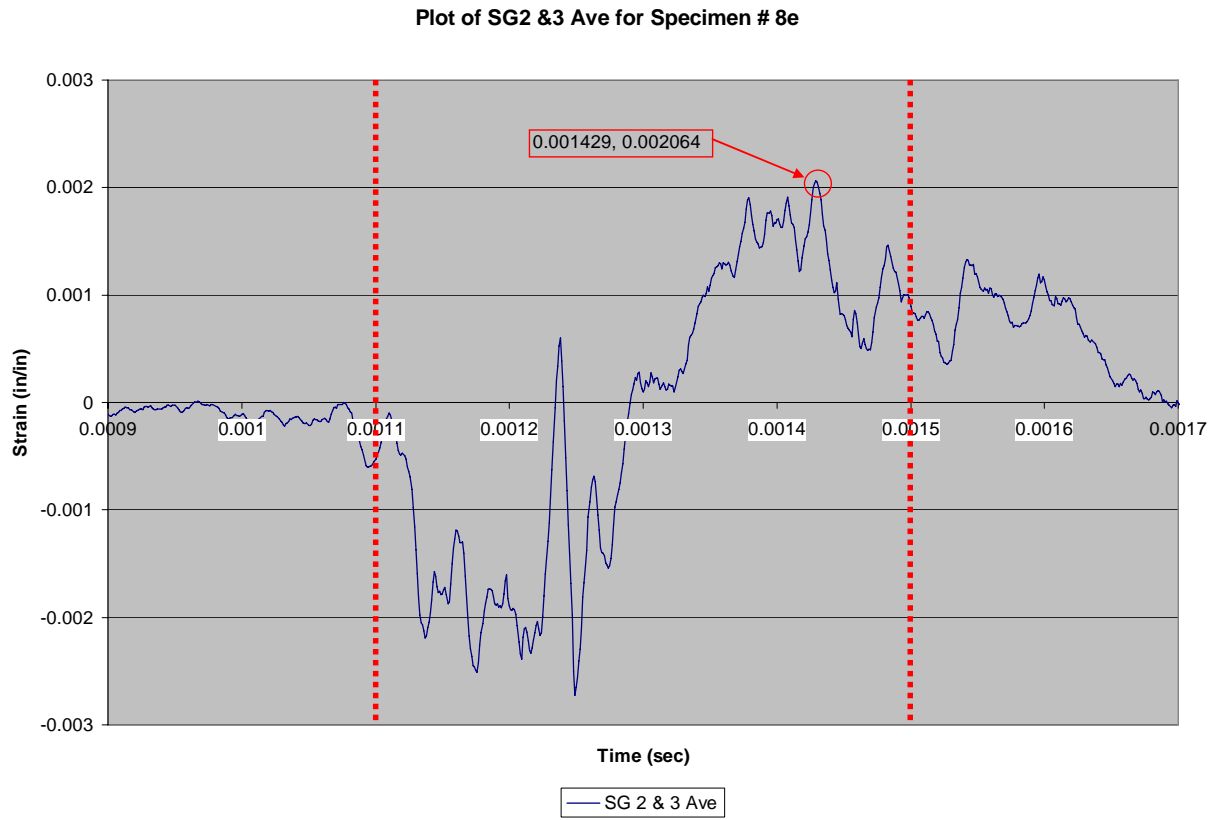


Figure C.8e.4: SG2 & SG3 average spar strain vs. time (Specimen 8e)

C.9 Specimen Set 9: Bonded

C.9.1 Dynamic Tests of Specimen Set 9

Specimen 9a, Test 40

For Specimen 9a, the load interval (and therefore the strain vs. time interval of interest) is approximately 1.15ms - 1.47ms as seen in Figure C.9a.1. As desired, pressure sensors K1 and K3 are largely in agreement, indicating side-to-side uniformity of load on the test specimen. During the load interval, Figure C.9a.2 shows that SG1 and SG4 are in phase indicating the skin pulled away from the spar in a symmetric fashion. Conversely, SG2 and SG3 appear to be out of phase (strongly so after failure) as seen in Figure C.9a.3. This implies that the spar underwent bending during testing. The lack of correlation between skin and spar gages means that failure symmetry is inconclusive. Failure metrics for Specimen 9a was derived from Figure C.9a.4. Failure strain occurred at 1.34ms with a maximum strain of 0.004206 in/in.

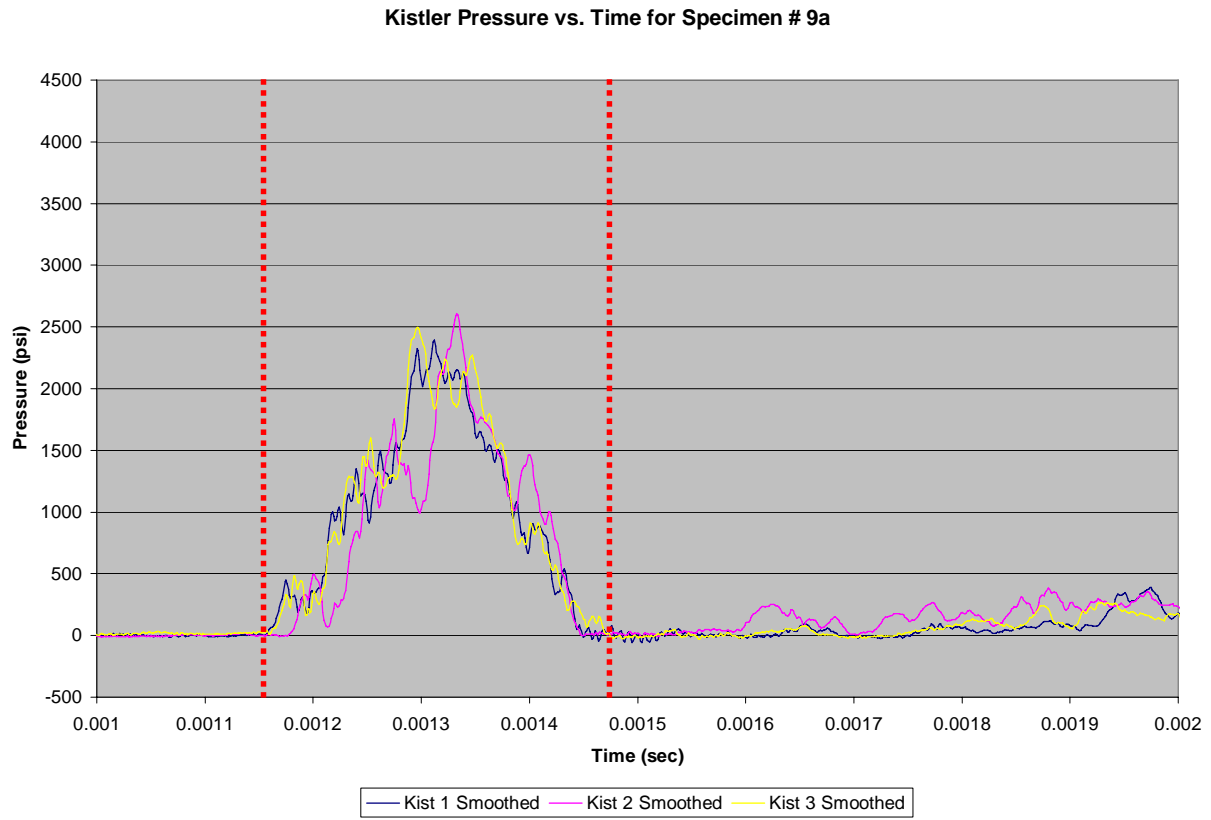


Figure C.9a.1: Kistler pressure vs. time (Specimen 9a)

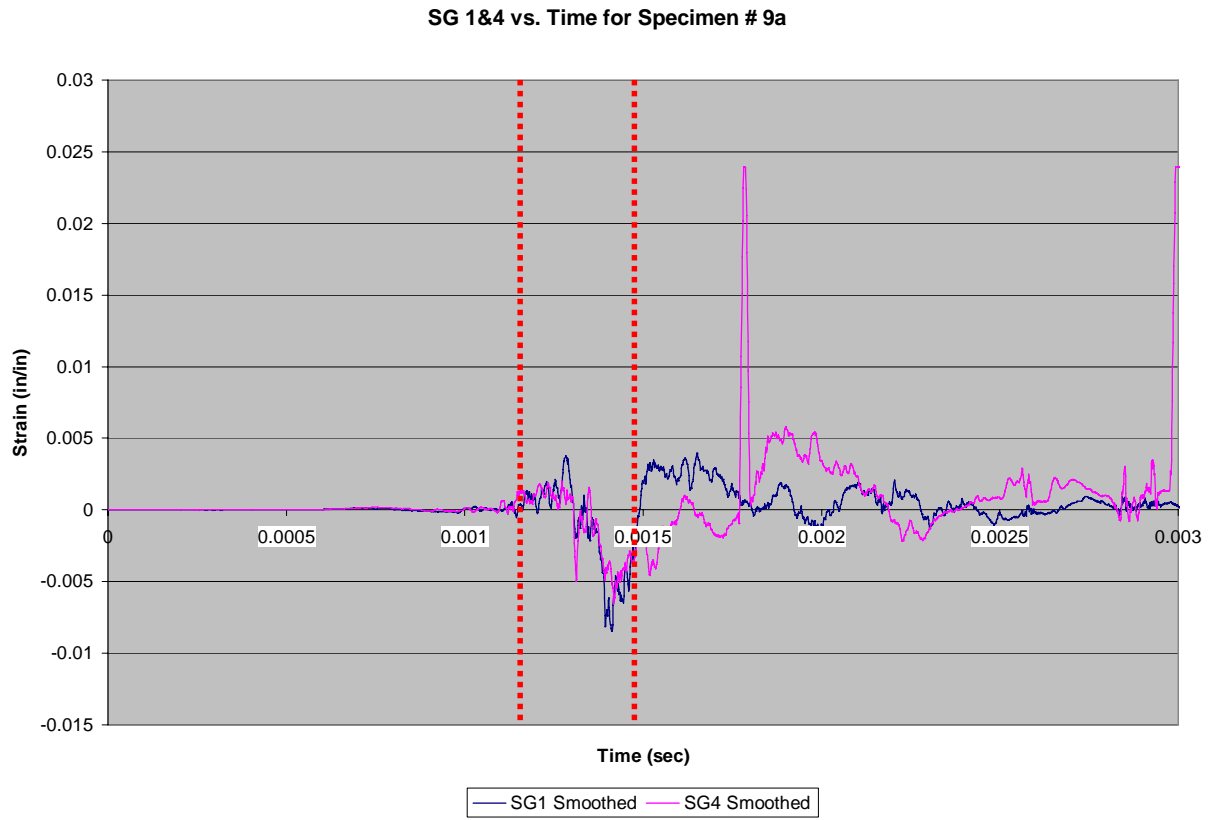


Figure C.9a.2: SG1 & SG4 skin strain vs. time (Specimen 9a)

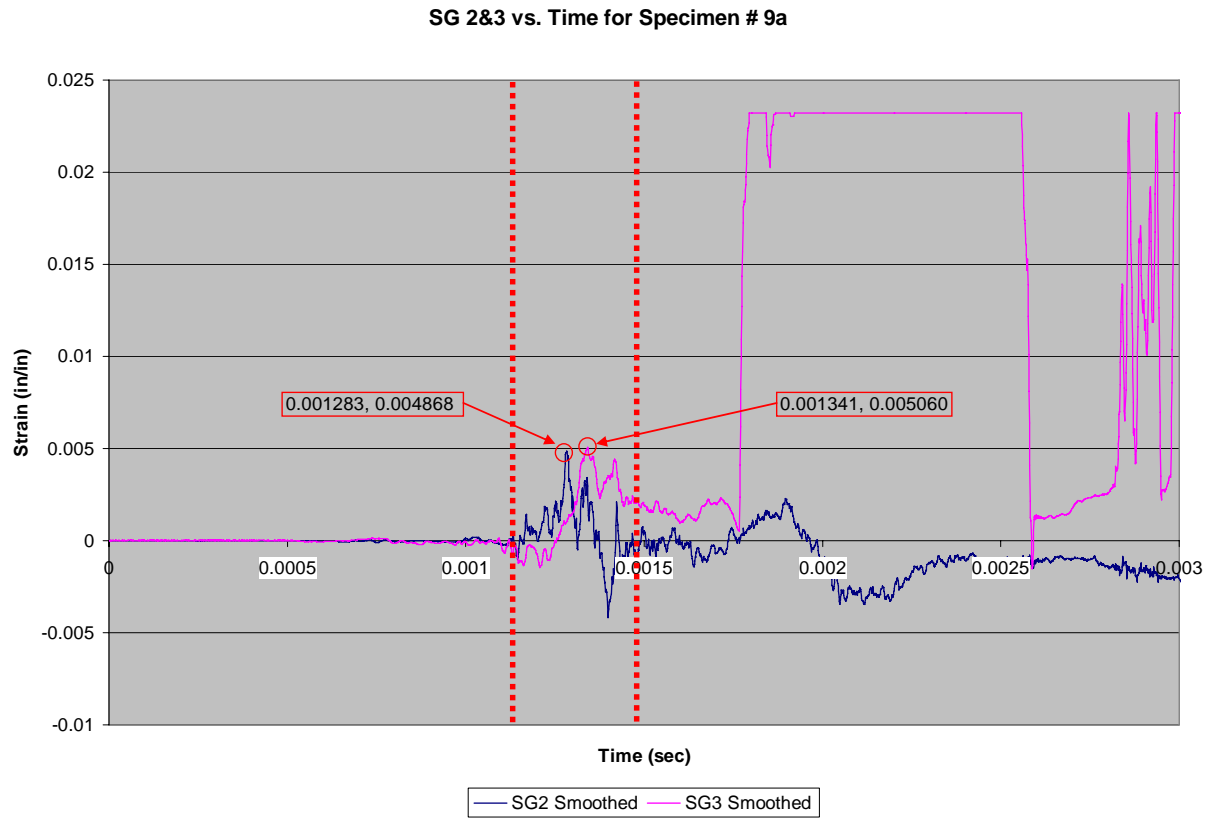


Figure C.9a.3: SG2 & SG3 spar strain vs. time (Specimen 9a)

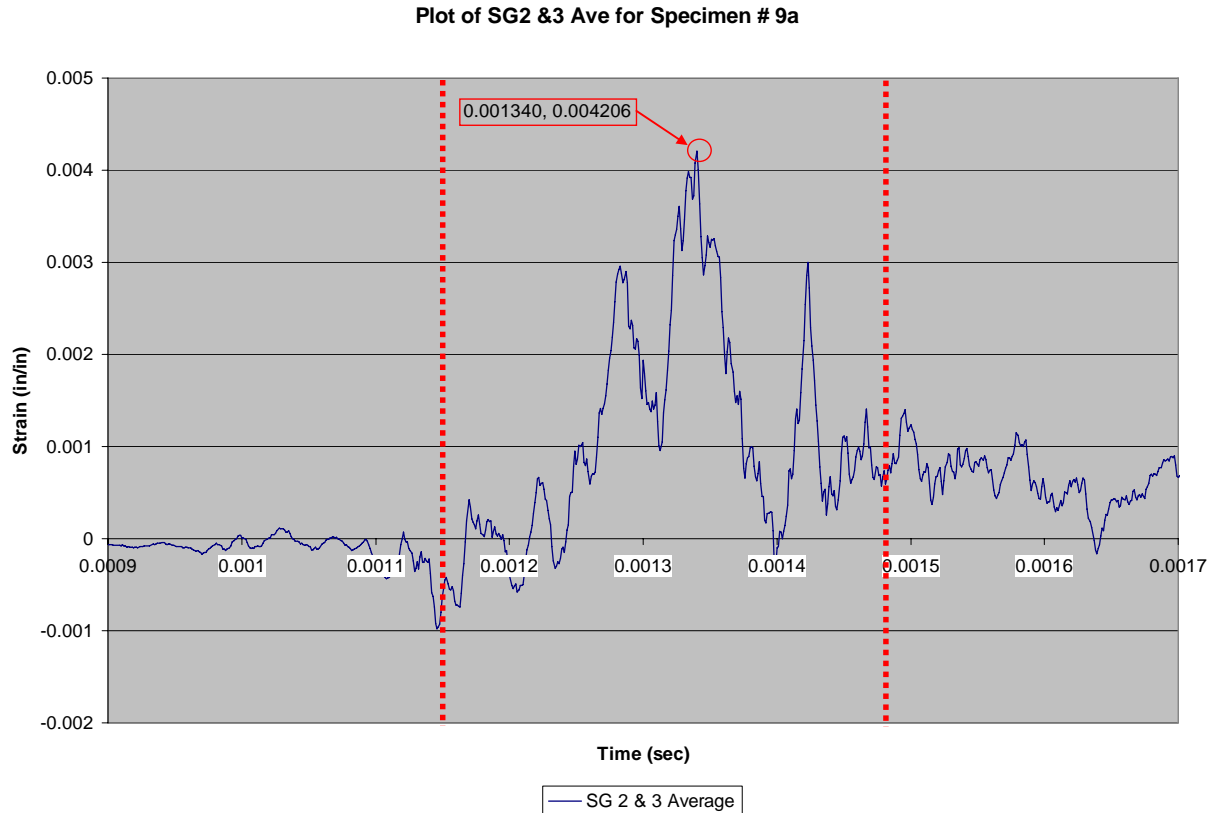


Figure C.9a.4: SG2 & SG3 average spar strain vs. time (Specimen 9a)

Specimen 9b, Test 41

For Specimen 9b, the load interval (and therefore the strain vs. time interval of interest) is approximately 1.20ms - 1.60ms as seen in Figure C.9b.1. As desired, pressure sensors K1 and K3 are largely in agreement, indicating side-to-side uniformity of load on the test specimen. During this time interval of interest, Figure C.9b.2 shows that SG1 and SG4 tend to stay in phase, but differ in amplitude, indicating the skin pulled away from the spar in an asymmetric fashion. Similarly, SG2 and SG3 appear to remain roughly in phase, but of different amplitudes (as seen in Figure C.9b.3). Failure symmetry is marginal. Failure metrics for Specimen 9b was derived from Figure C.9b.4. Failure strain occurred at 1.431ms with a maximum strain of 0.003707 in/in.

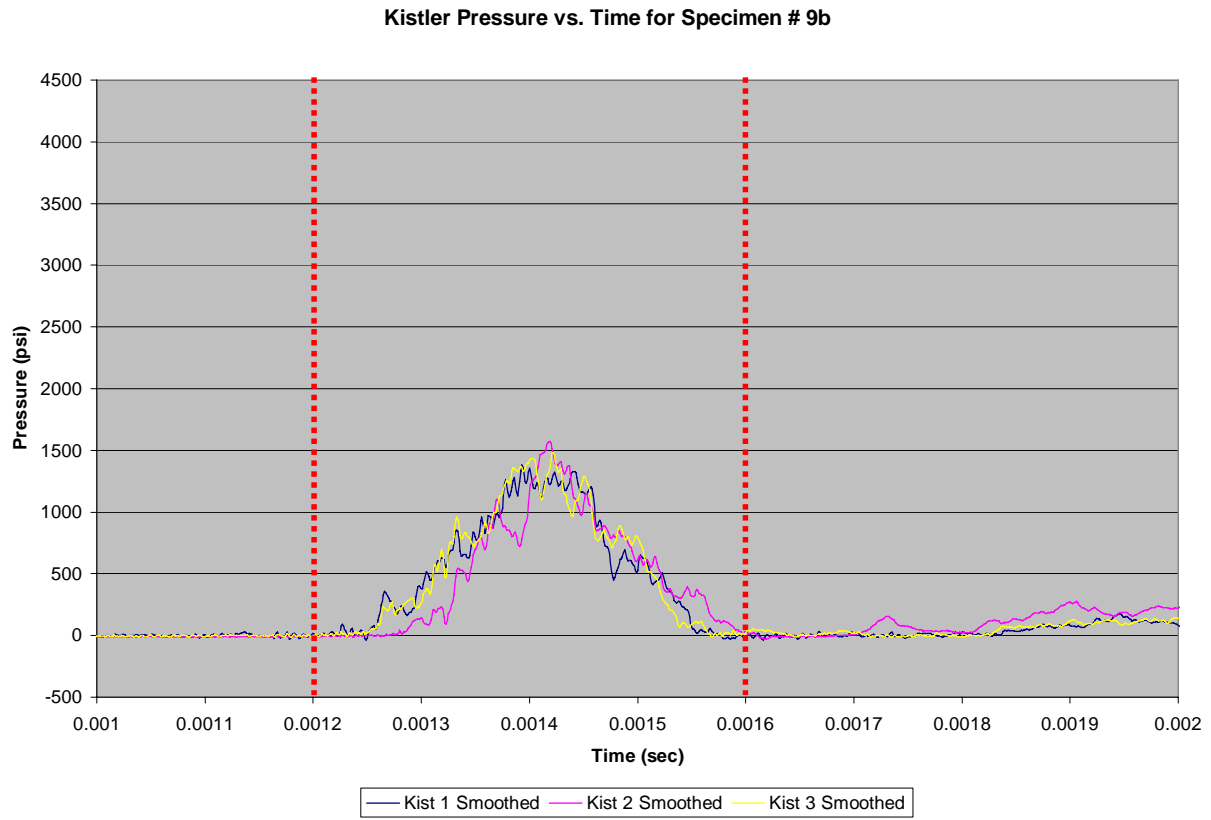


Figure C.9b.1: Kistler pressure vs. time (Specimen 9b)

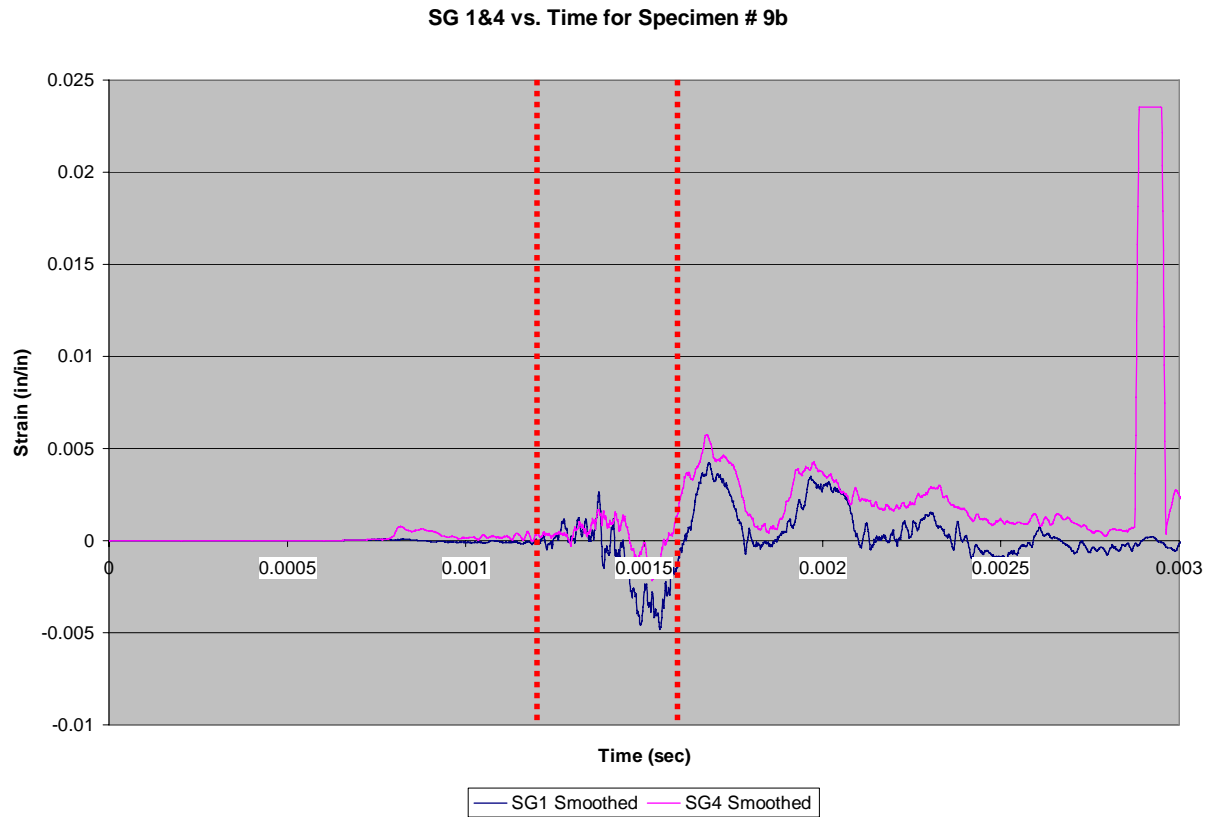


Figure C.9b.2: SG1 & SG4 skin strain vs. time (Specimen 9b)

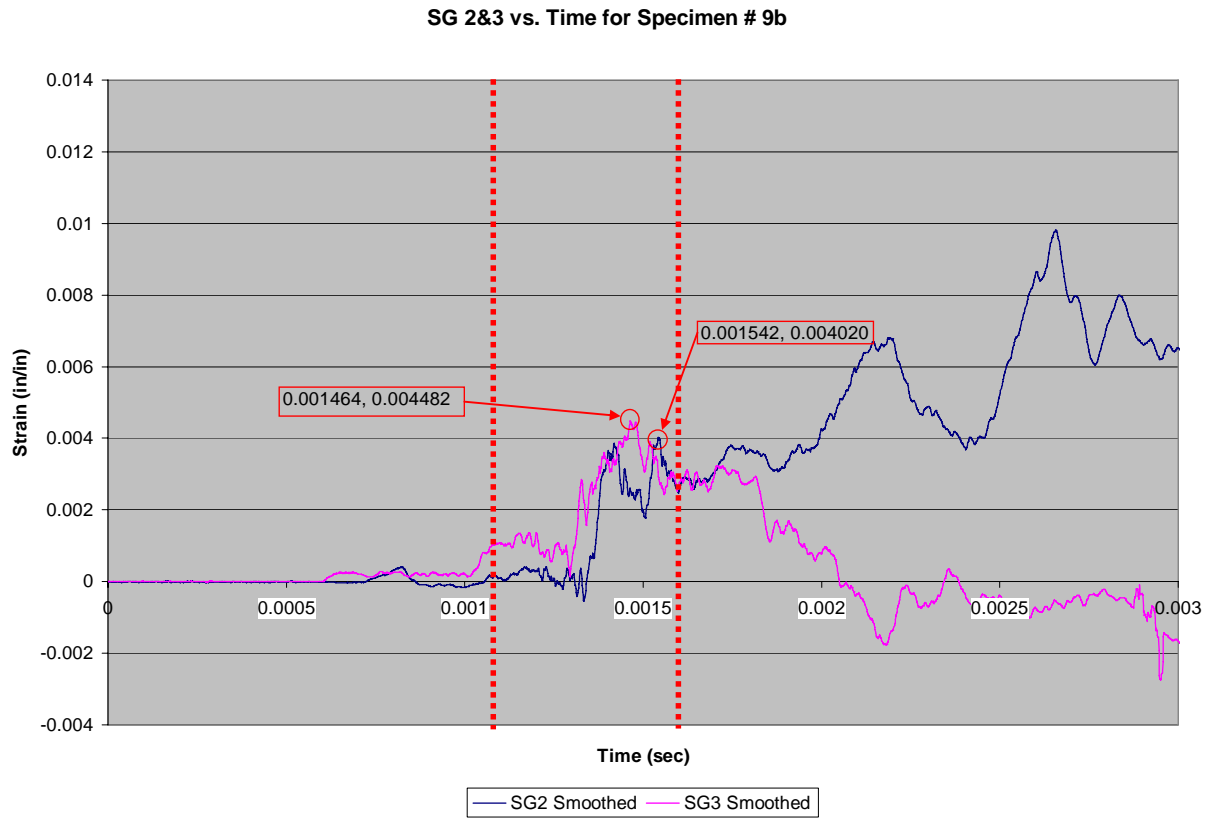


Figure C.9b.3: SG2 & SG3 spar strain vs. time (Specimen 9b)

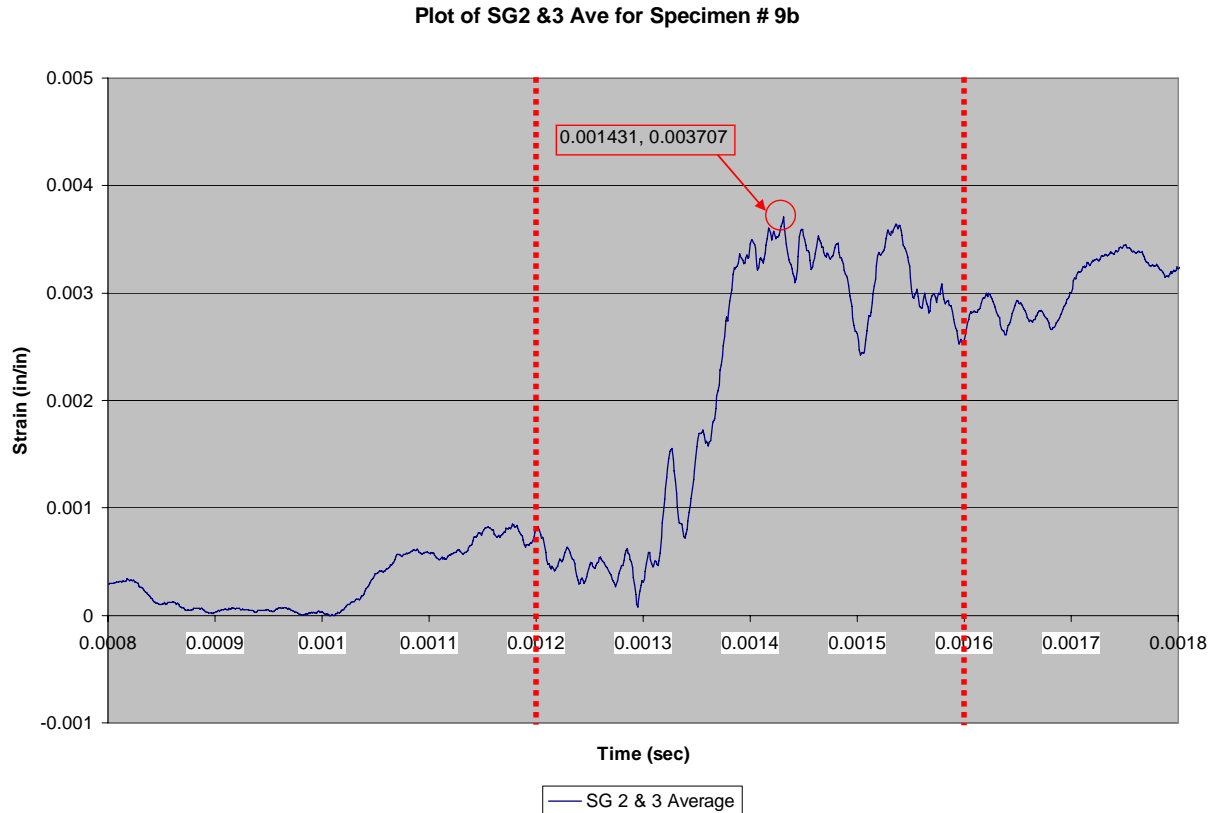


Figure C.9b.4: SG2 & SG3 average spar strain vs. time (Specimen 9b)

Specimen 9c, Test 42

For Specimen 9c, the load interval (and therefore the strain vs. time interval of interest) is approximately 1.17 ms to 1.50ms as shown in Figure C.9c.1. As desired, pressure sensors K1 and K3 are largely in agreement, indicating side-to-side uniformity of load on the test specimen. During the load interval, Figure C.9c.2 shows that SG1 and SG4 are in phase, but differ in amplitude, indicating the skin pulled away from the spar in an asymmetric fashion. SG2 and SG3 on the spar are also in phase and of differing amplitudes (as seen in Figure C.9c.3) implying failure asymmetry. Failure metrics for Specimen 9c are derived from Figure C.9c.4. Failure strain occurred at 1.314ms with a maximum strain of 0.003736 in/in.

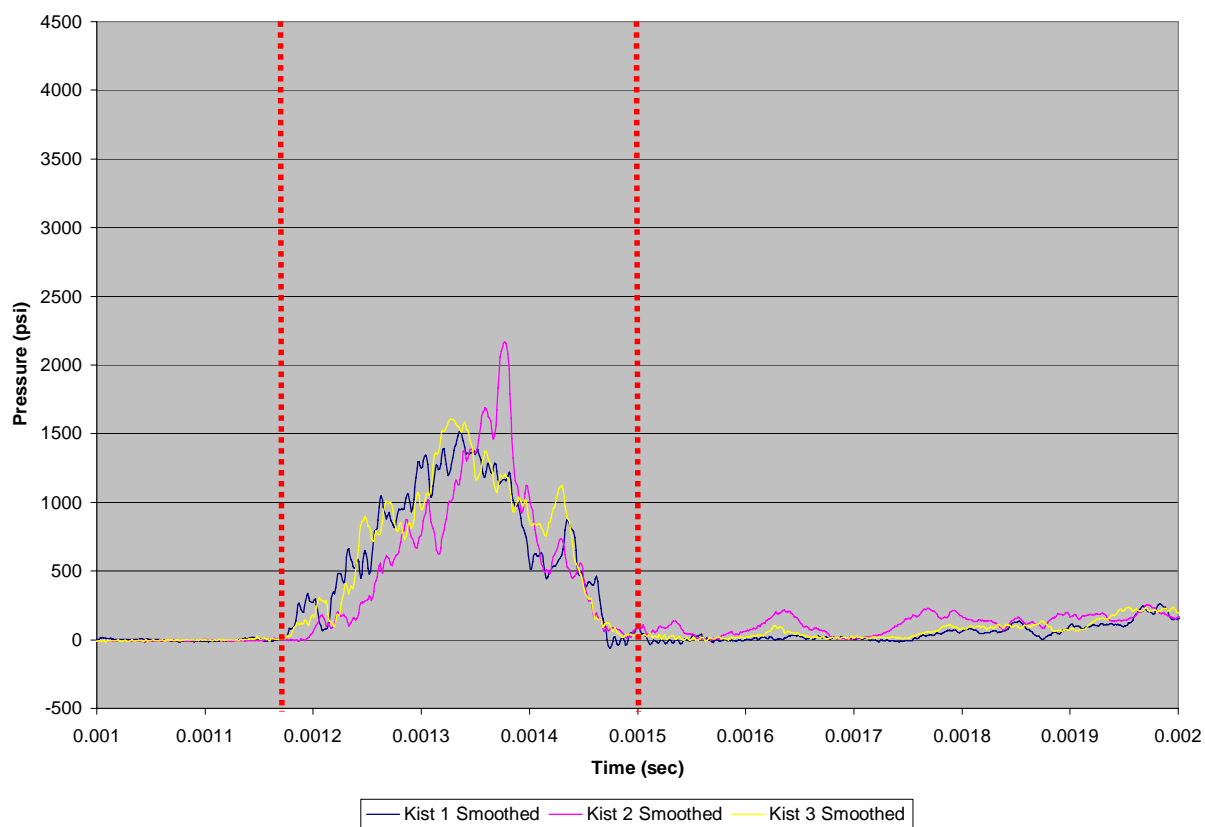


Figure C.9c.1: Kistler pressure vs. time (Specimen 9c)

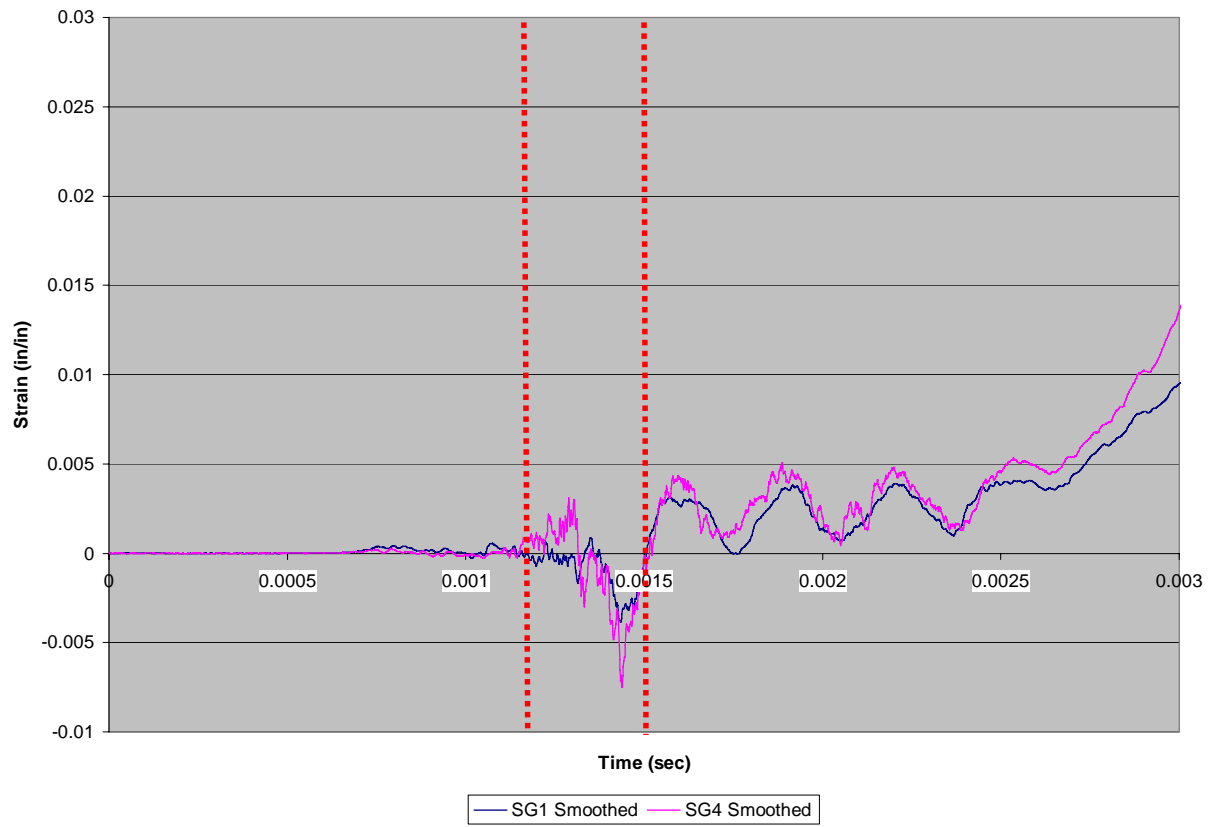


Figure C.9c.2: SG1 & SG4 skin strain vs. time (Specimen 9c)

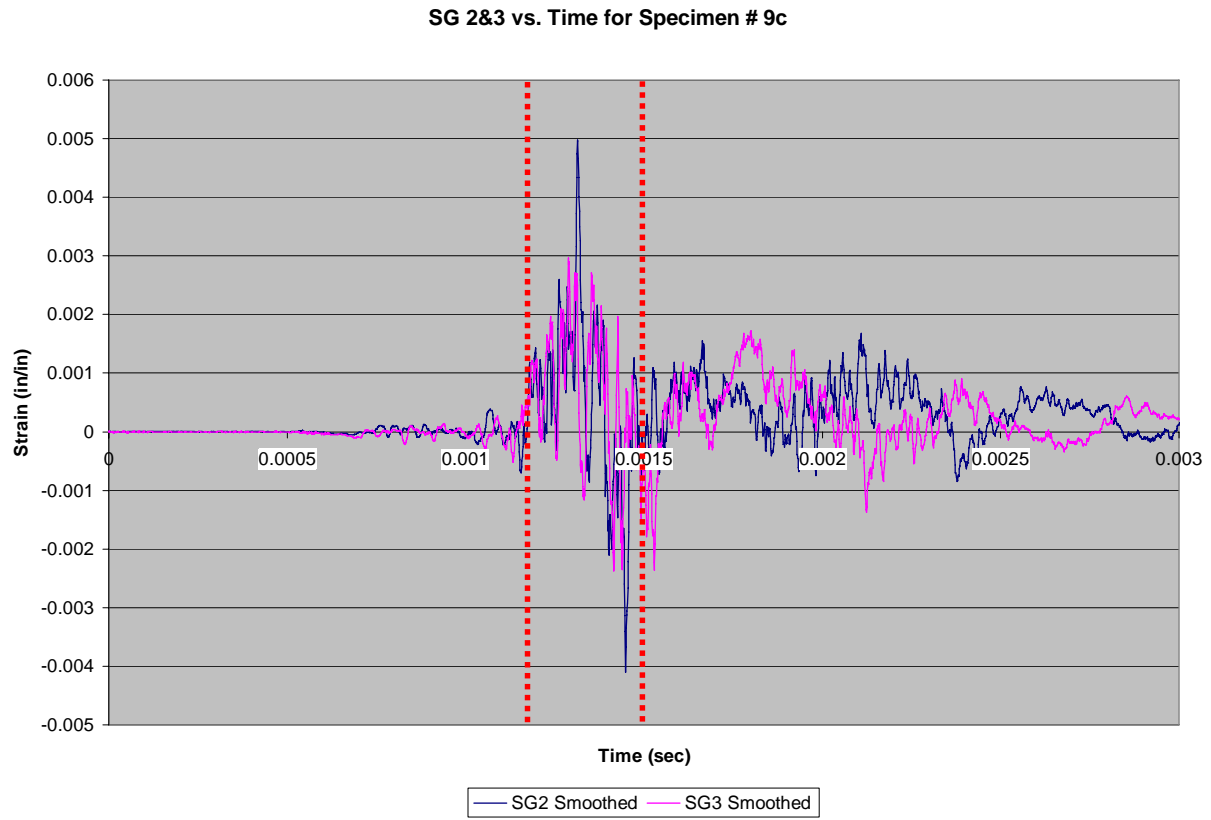


Figure C.9c.3: SG2 & SG3 spar strain vs. time (Specimen 9c)

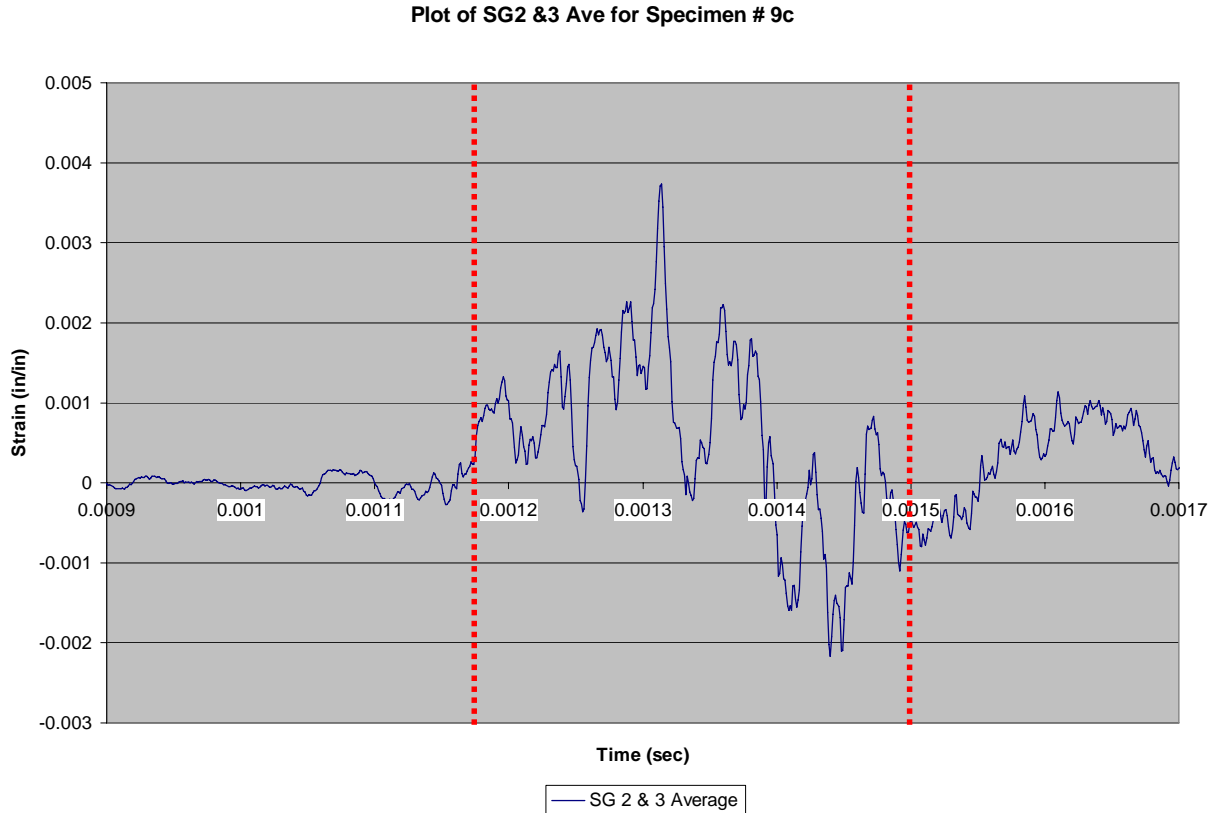


Figure C.9c.4: SG2 & SG3 average spar strain vs. time (Specimen 9c)

Specimen 9d, Test 43

For Specimen 9d, the load interval (and therefore the strain vs. time interval of interest) is approximately 1.13ms-1.47ms as shown in Figure C.9d.1. As desired, pressure sensors K1 and K3 are largely in agreement, indicating side-to-side uniformity of load on the test specimen. During the load interval, Figure C.9d.2 shows that SG1 and SG4 are strongly out of phase, indicating skin pull-off from the spar in an asymmetric fashion. Similarly, SG2 and SG3 on the spar are also out of phase (as seen in Figure C.9d.3) indicating spar bending during failure. Failure metrics for Specimen 9d are derived from Figure C.9d.4. Failure strain occurred at 1.267ms with a maximum strain of 0.002771 in/in.

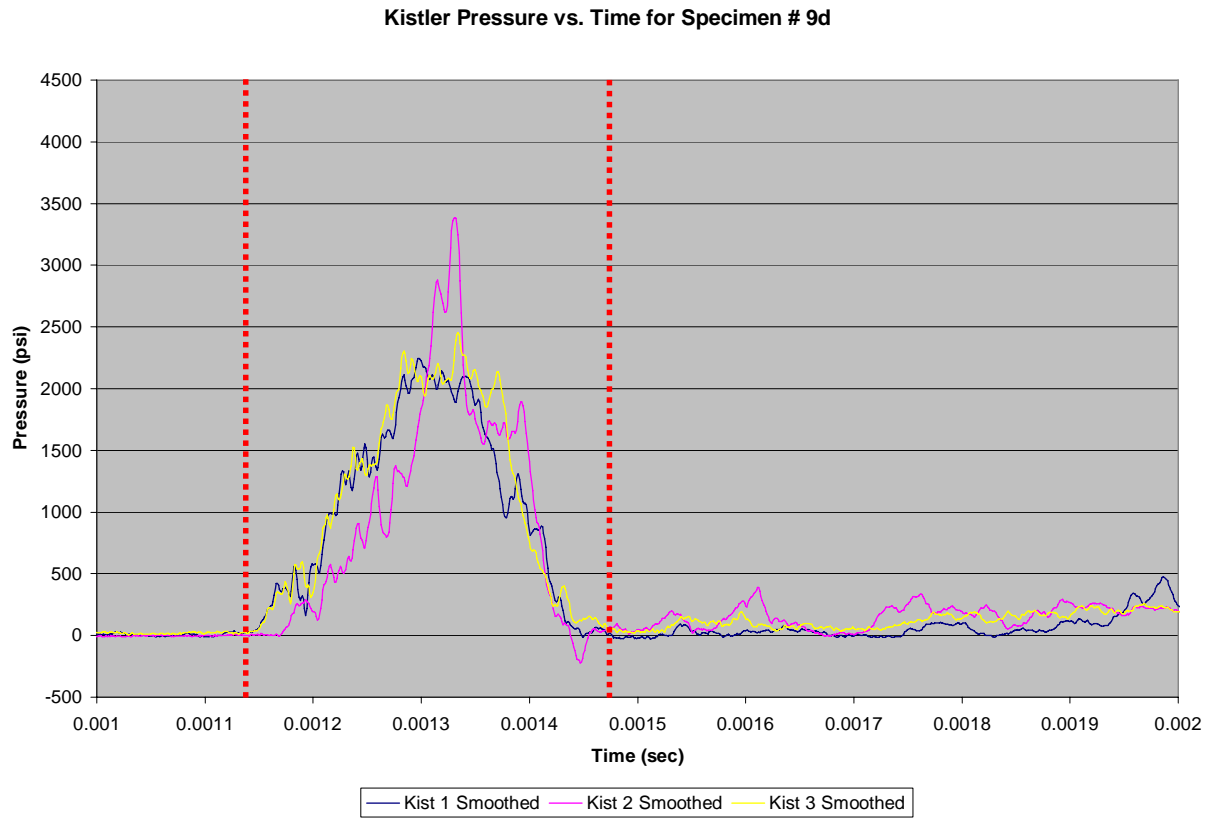


Figure C.9d.1: Kistler pressure vs. time (Specimen 9d)

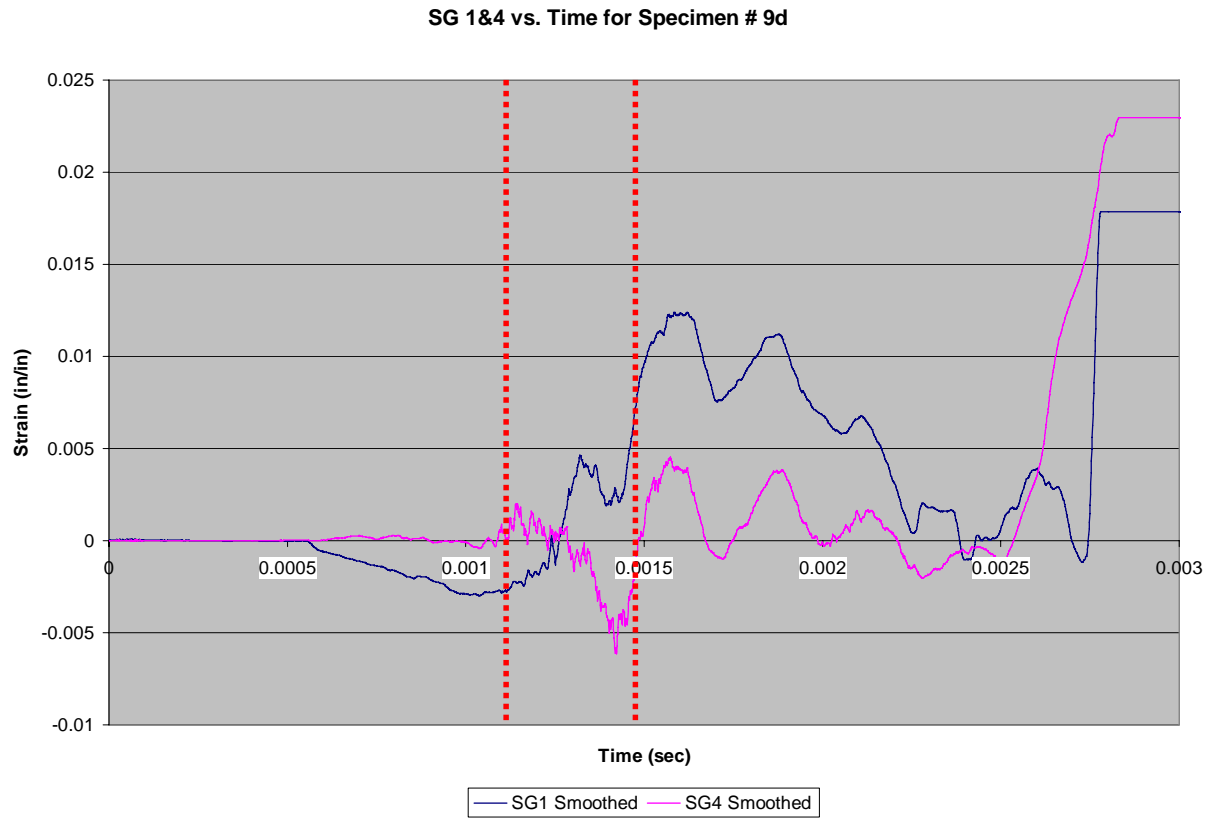


Figure C.9d.2: SG1 & SG4 skin strain vs. time (Specimen 9d)

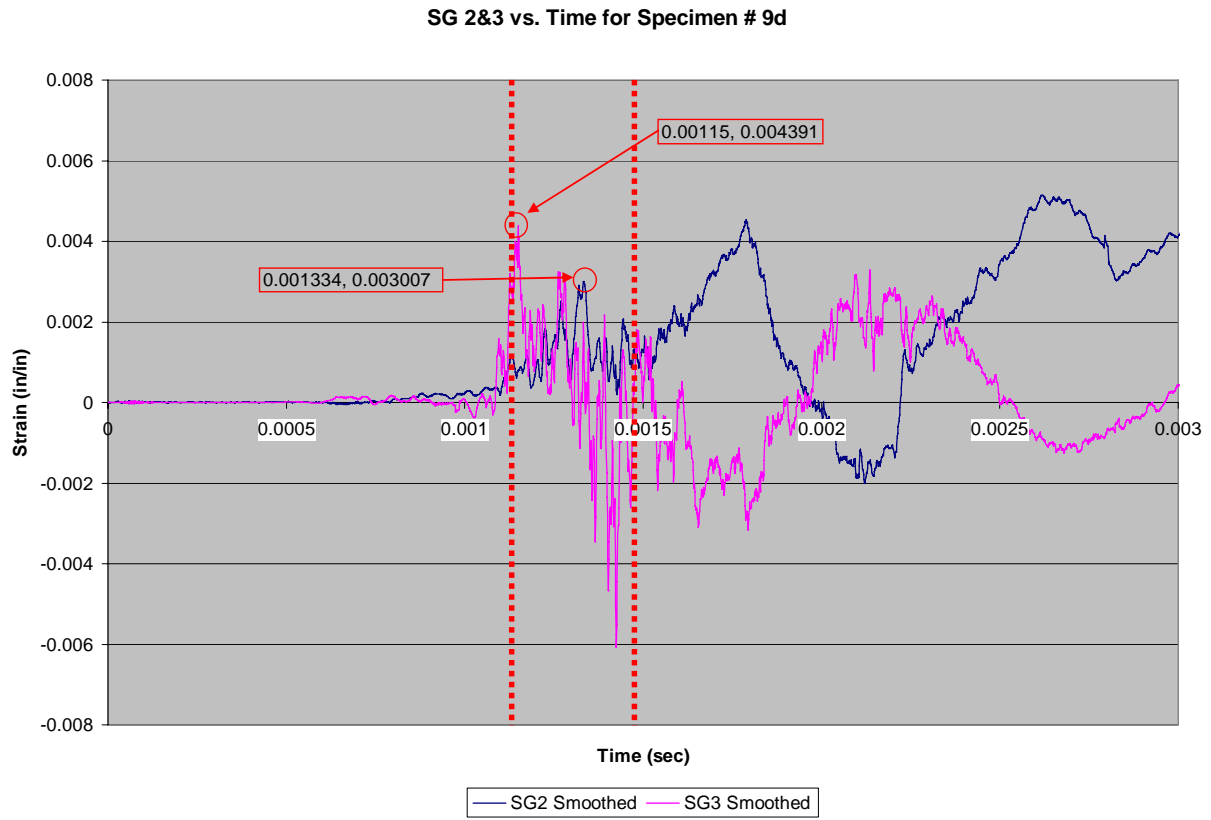


Figure C.9d.3: SG2 & SG3 spar strain vs. time (Specimen 9d)

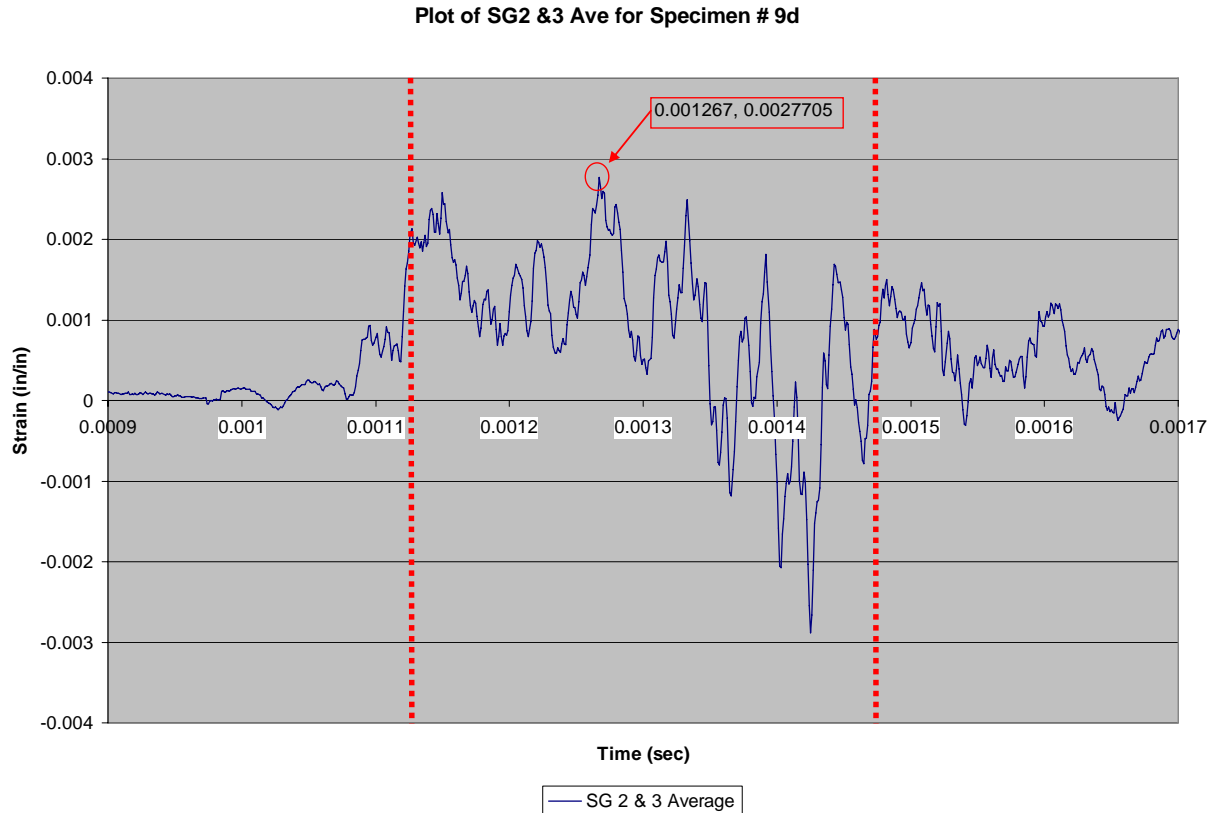


Figure C.9d.4: SG2 & SG3 average spar strain vs. time (Specimen 9d)

Specimen 9e, Test 44

For Specimen 9e, the load interval (and therefore the strain vs. time interval of interest) is approximately 1.20ms-1.52ms as shown in Figure C.9e.1. As desired, pressure sensors K1 and K3 are largely in agreement, indicating side-to-side uniformity of load on the test specimen. During this time interval of interest, Figure C.9e.2 shows that SG1 and SG4 remain in phase and of similar amplitude. Similarly, spar gages SG2 and SG3 appear roughly in phase, but the amplitudes differ (as seen in Figure C.9e.3) implying failure asymmetry. Failure symmetry is ruled inconclusive. Failure metrics for Specimen 9e are derived from Figure C.9e.4. Failure strain occurred at 1.370ms with a maximum strain of 0.002085 in/in.

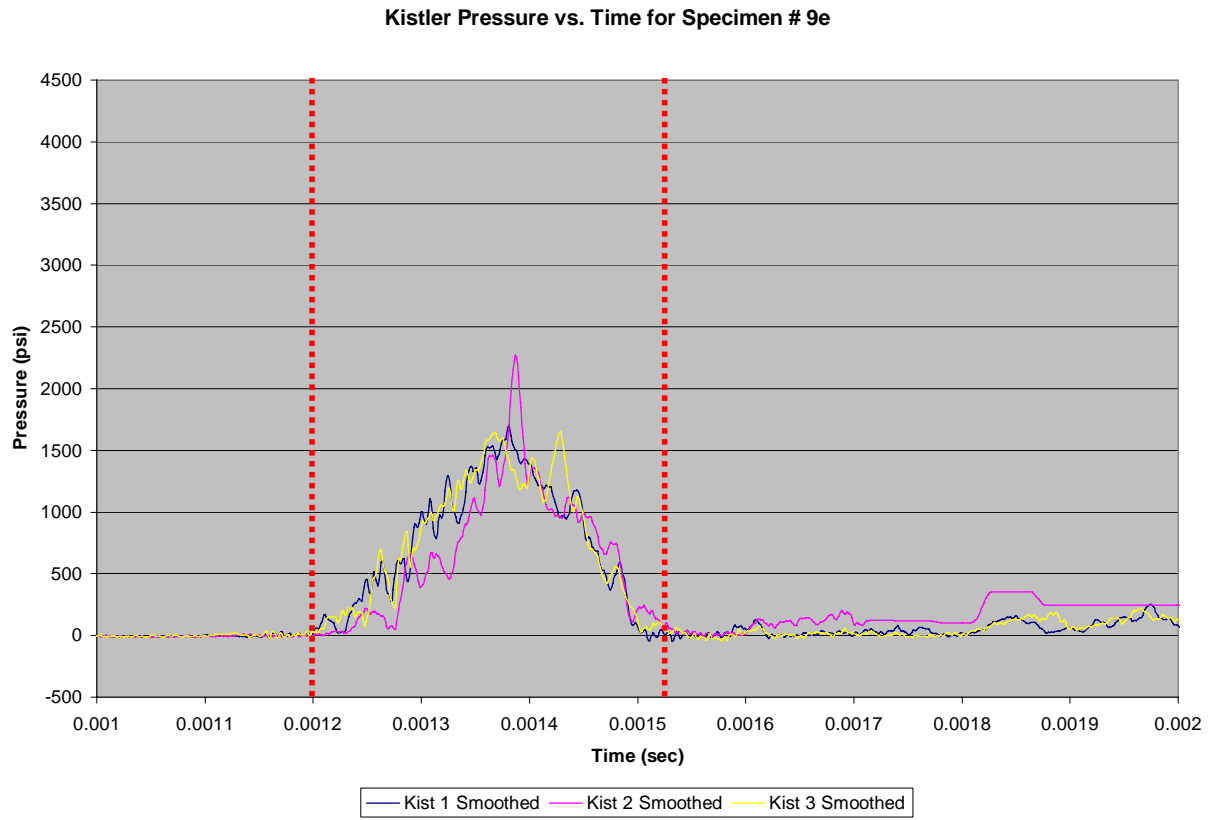


Figure C.9e.1: Kistler pressure vs. time (Specimen 9e)

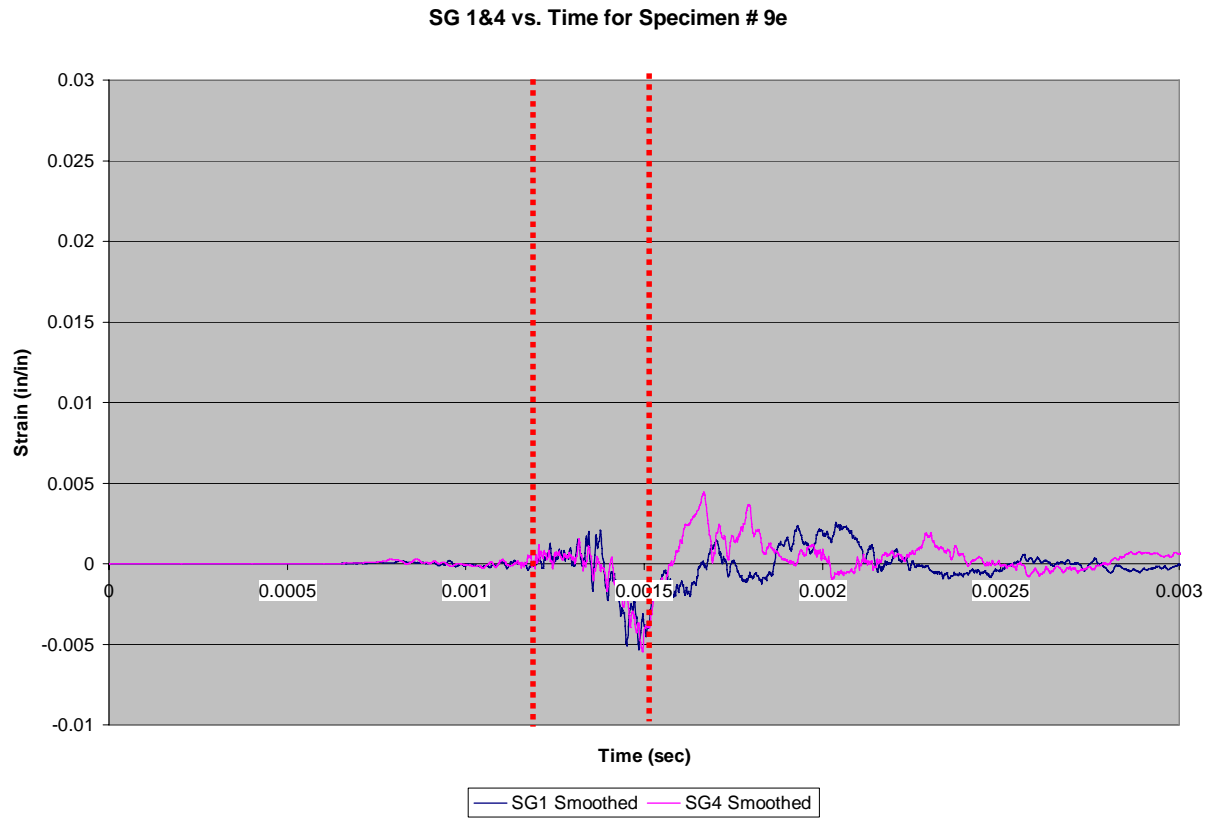


Figure C.9e.2: SG1 & SG4 skin strain vs. time (Specimen 9e)

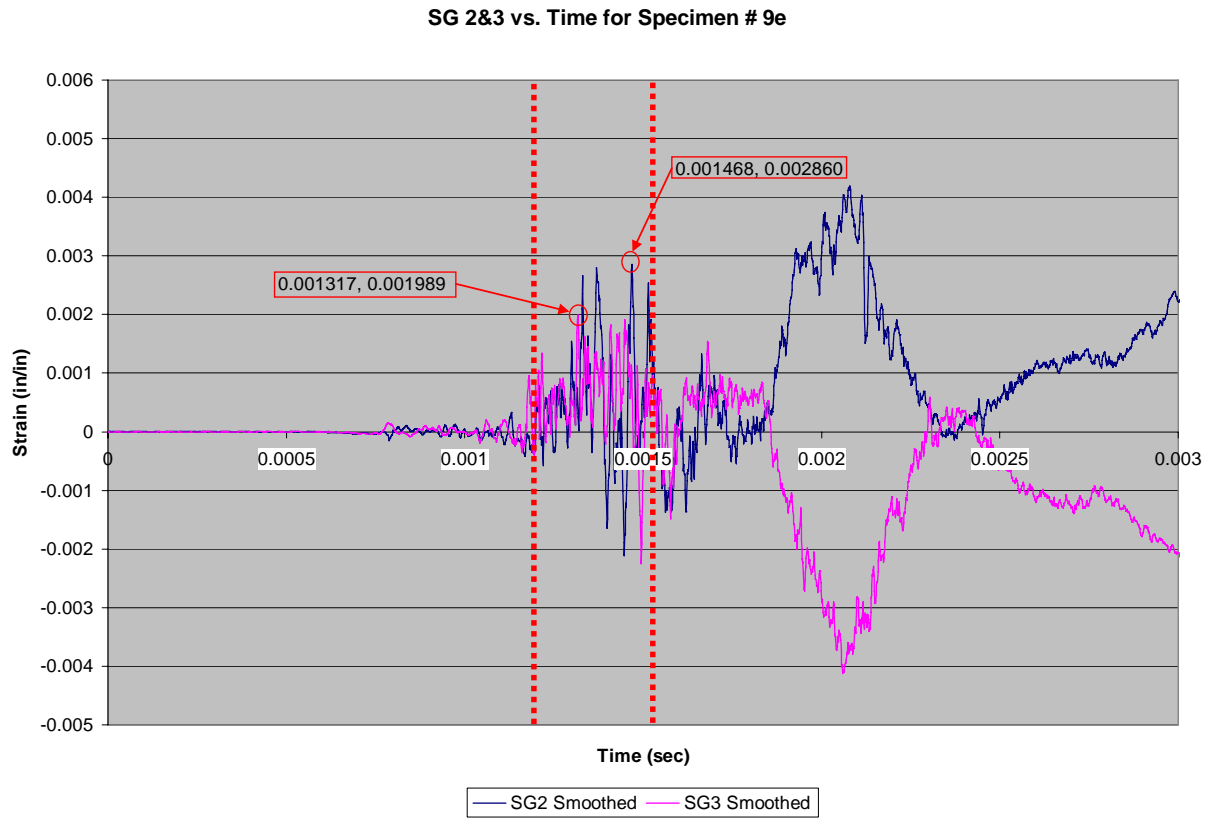


Figure C.9e.3: SG2 & SG3 spar strain vs. time (Specimen 9e)

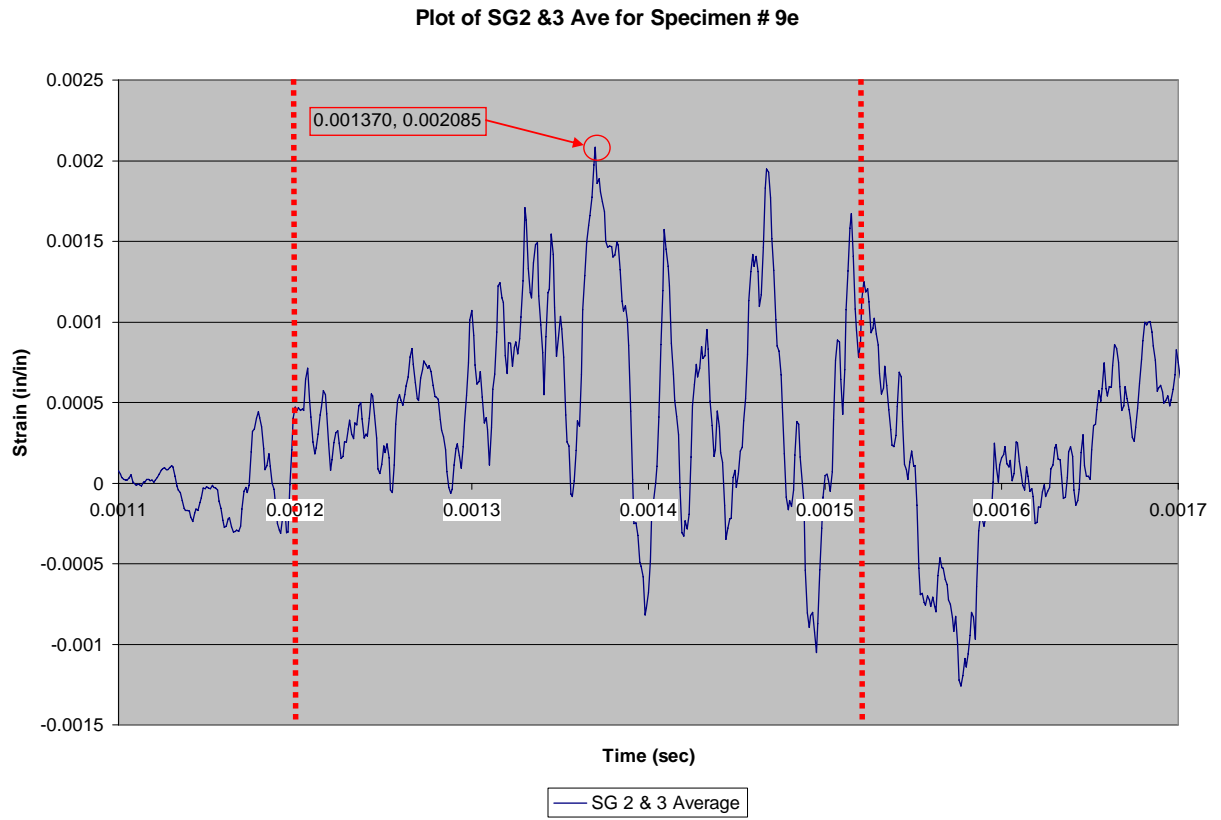


Figure C.9e.4: SG2 & SG3 average spar strain vs. time (Specimen 9e)

C.10 Specimen Set 10: Bonded (Honeycomb Core)

C.10.1 Dynamic Tests of Specimen Set 10

Specimen 10a, Test 50

For Specimen 10a, the load interval (and therefore the strain vs. time interval of interest) is approximately 1.16ms - 1.47ms as seen in Figure C.10a.1. As desired, pressure sensors K1 and K3 are largely in agreement, indicating side-to-side uniformity of load on the test specimen. During the load interval, Figure C.10a.2 shows that SG4 failed prematurely. This disallows an assessment of failure symmetry based on the skin gages. Spar gages SG2 and SG3 appear to be in phase (as seen in Figure C.10a.3) until gage failure occurs part way through the load cycle. Assessment of failure symmetry is inconclusive. Failure metrics for Specimen 10a was derived from Figure C.10a.4. Failure strain occurred at 1.369ms with a maximum strain of 0.004506 in/in.

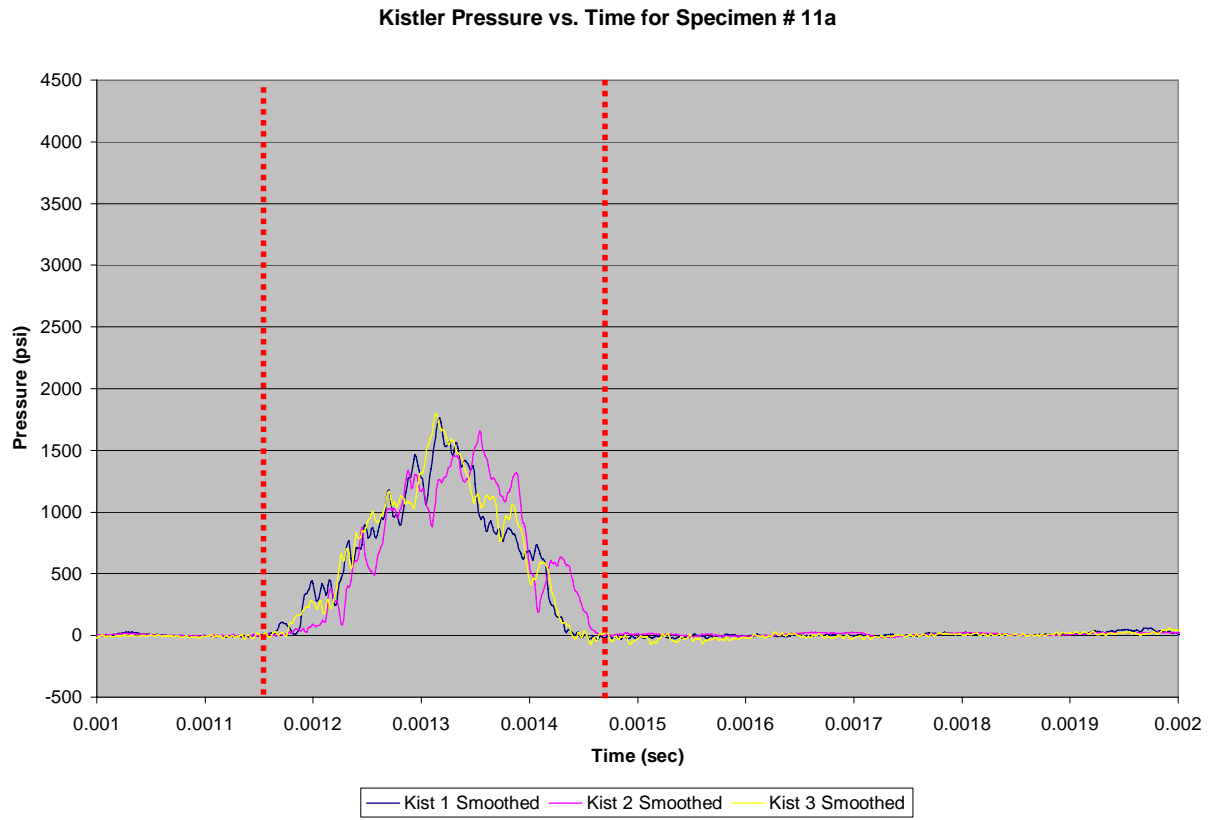


Figure C.10a.1: Kistler pressure vs. time (Specimen 10a)

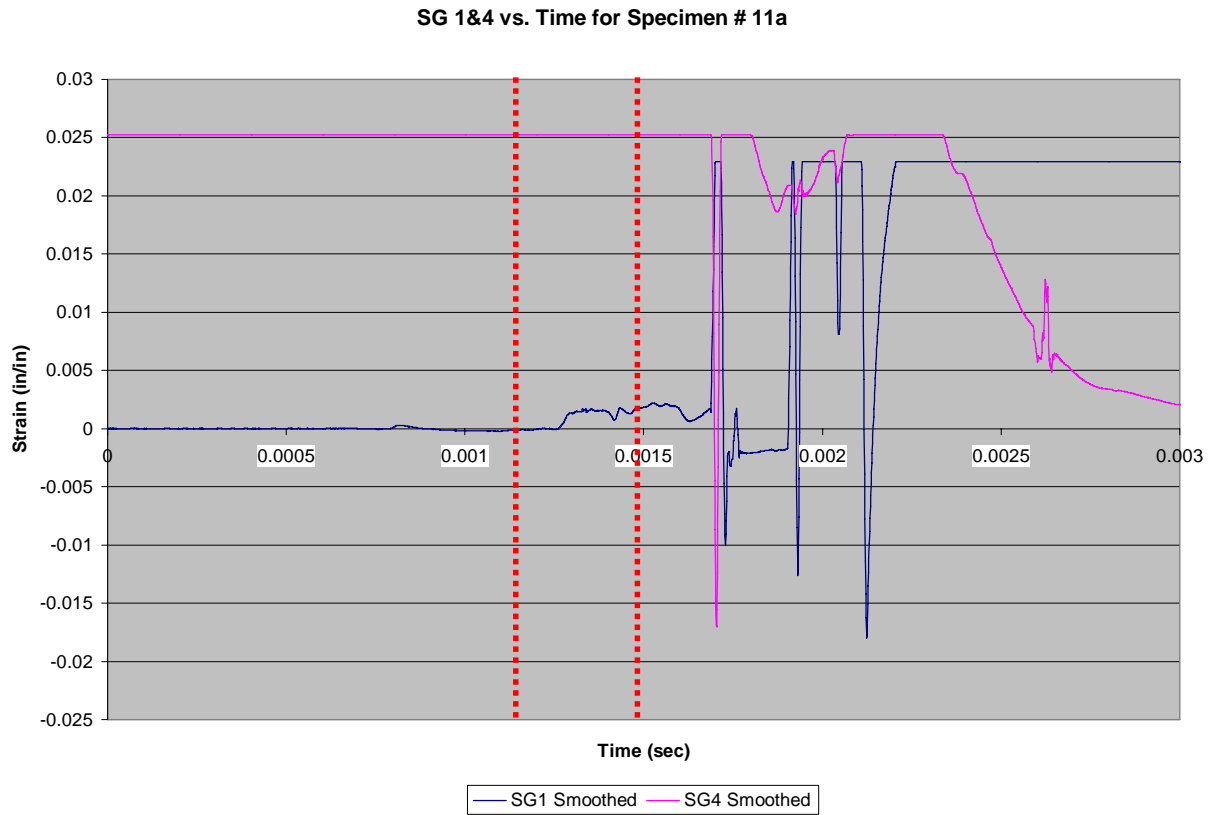


Figure C.10a.2: SG1 & SG4 skin strain vs. time (Specimen 10a)

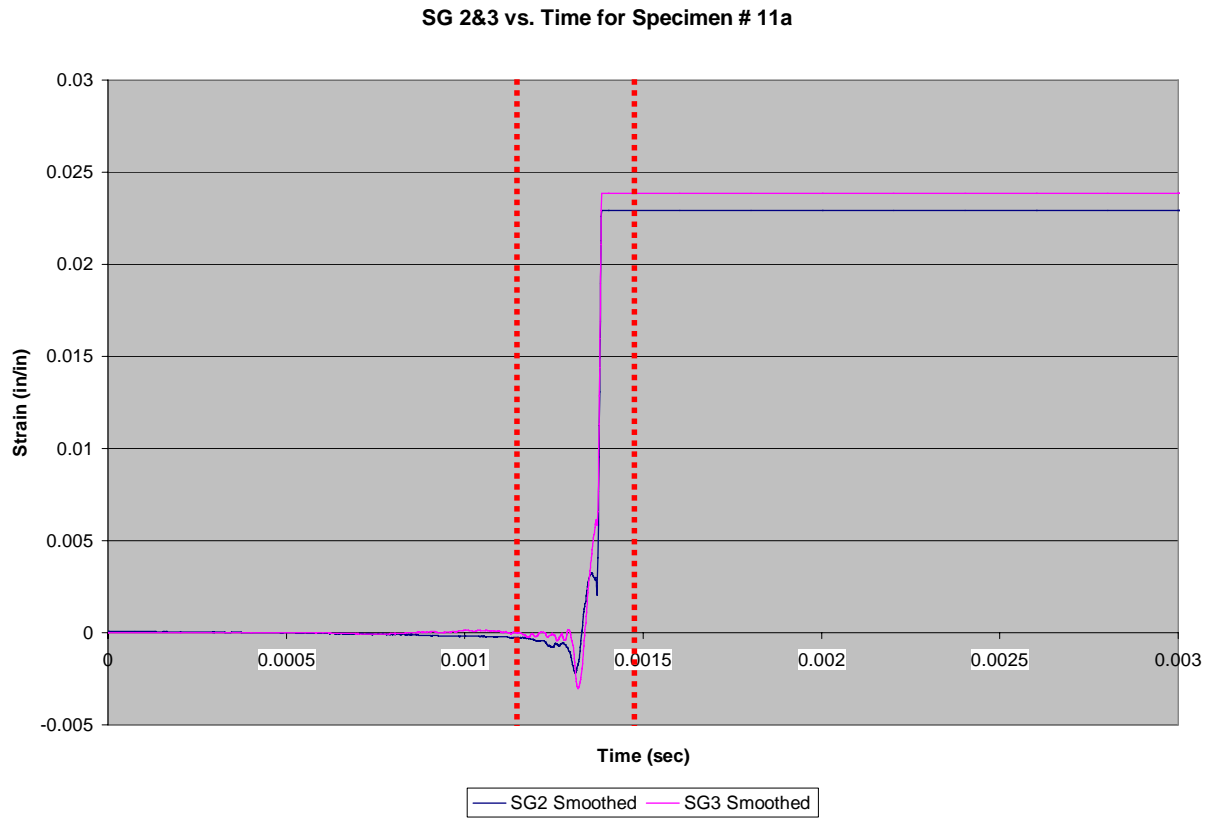


Figure C.10a.3: SG2 & SG3 spar strain vs. time (Specimen 10a)

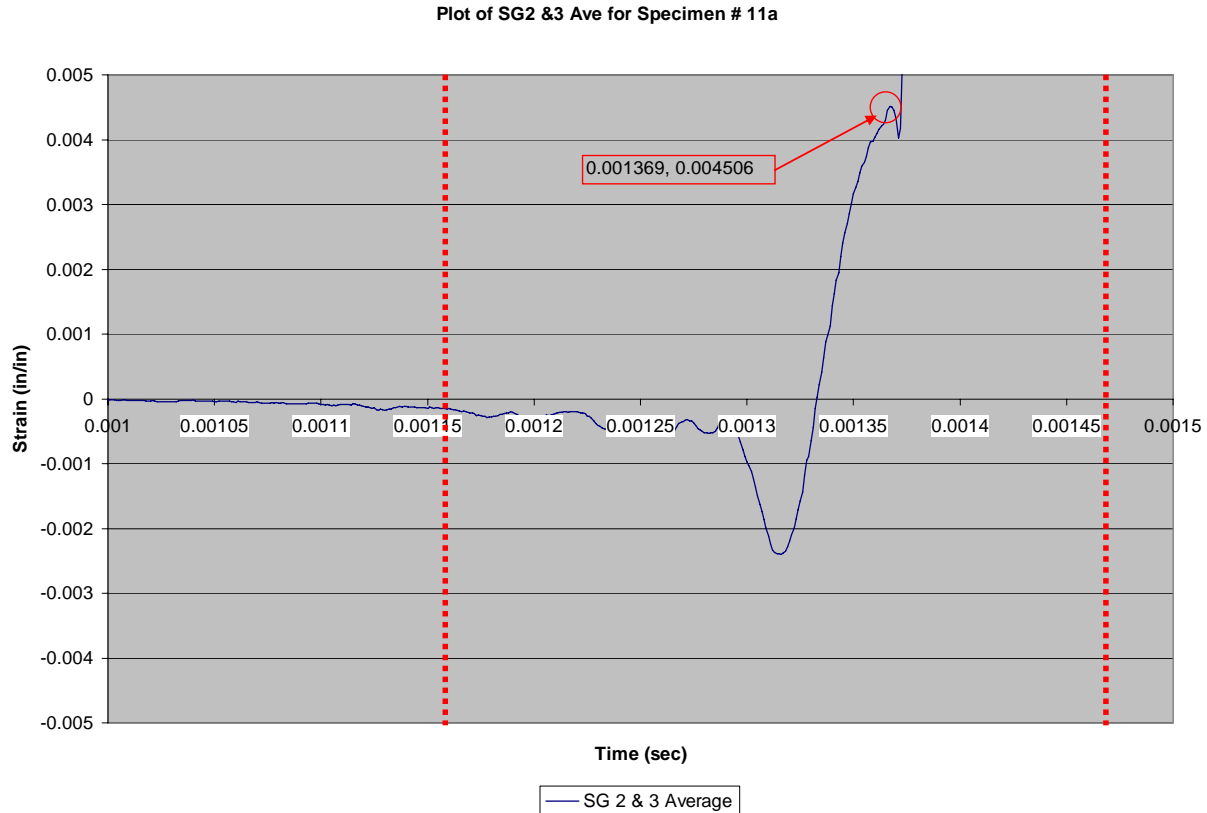


Figure C.10a.4: SG2 & SG3 average spar strain vs. time (Specimen 10a)

Specimen 10b, Test 51

For Specimen 10b, the load interval (and therefore the strain vs. time interval of interest) is approximately 1.22s - 1.51ms as seen in Figure C.10b.1. As desired, pressure sensors K1 and K3 are largely in agreement, indicating side-to-side uniformity of load on the test specimen. During the load interval, Figure C.10b.2 shows that SG1 and SG4 are out of phase, indicating the skin pulled away from the spar in an asymmetric fashion. Conversely, SG2 and SG3 appear to be in phase (as seen in Figure C.10b.3) until the moment of SG3 gage failure. The lack of correlation between skin and spar gages means that failure symmetry is inconclusive. Assessment of specimen failure is based on the valid segment of strains recorded on the spar. Failure metrics for Specimen 10b was derived from Figure C.10b.4. Failure strain occurred at 1.405ms with a maximum strain of 0.00603 in/in.

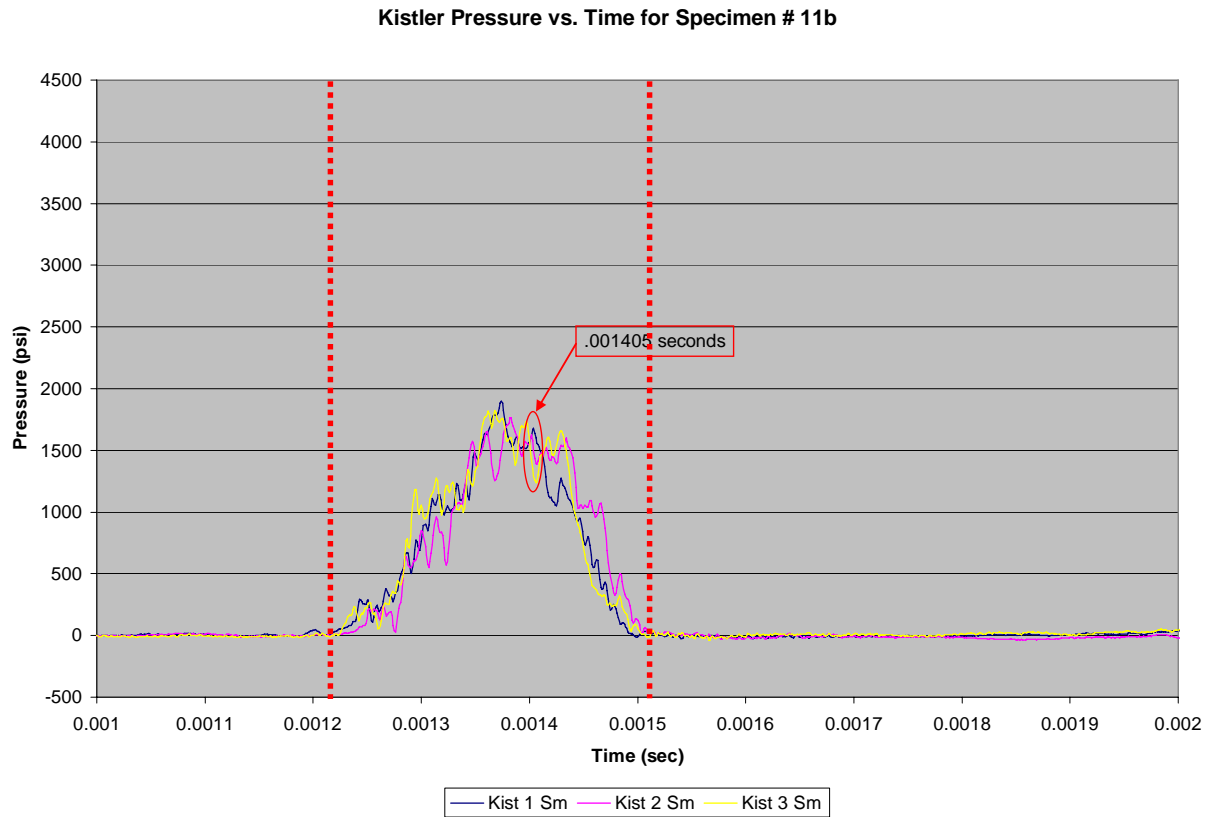


Figure C.10b.1: Kistler pressure vs. time (Specimen 10b)

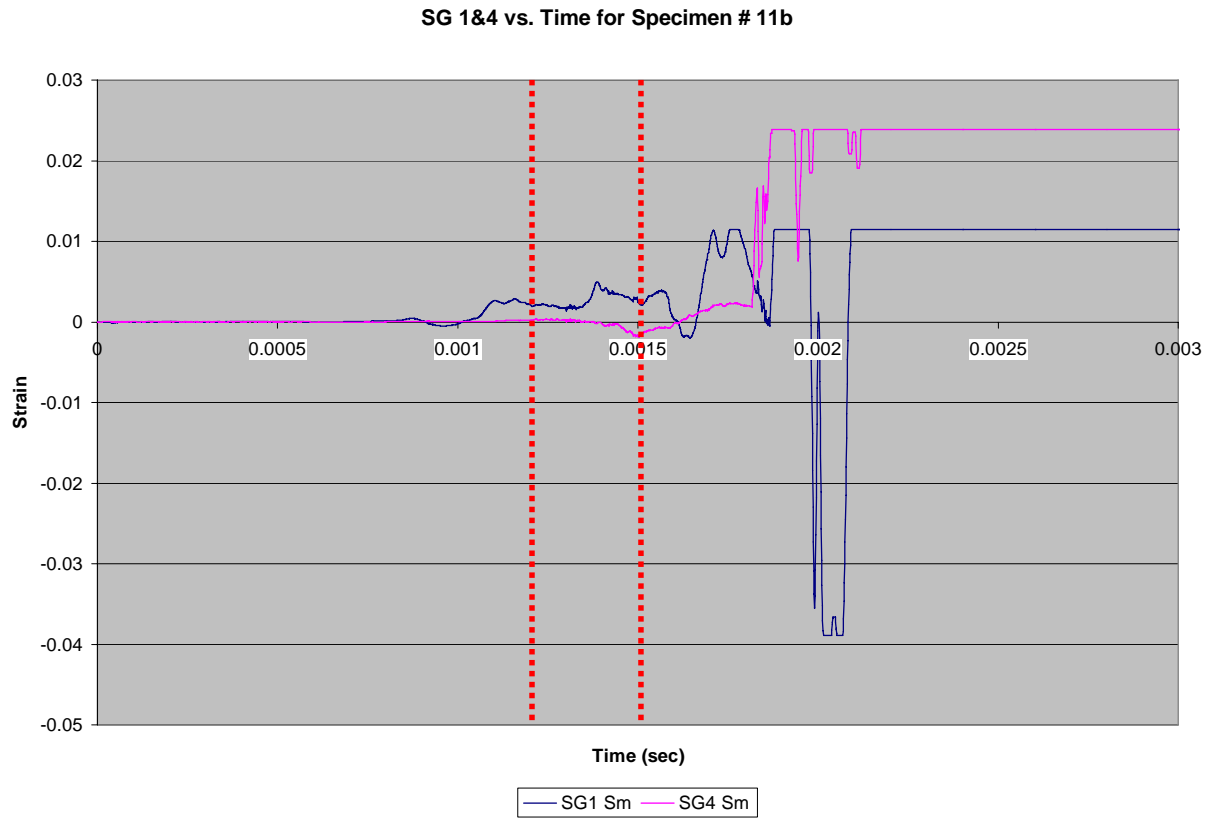


Figure C.10b.2: SG1 & SG4 skin strain vs. time (Specimen 10b)

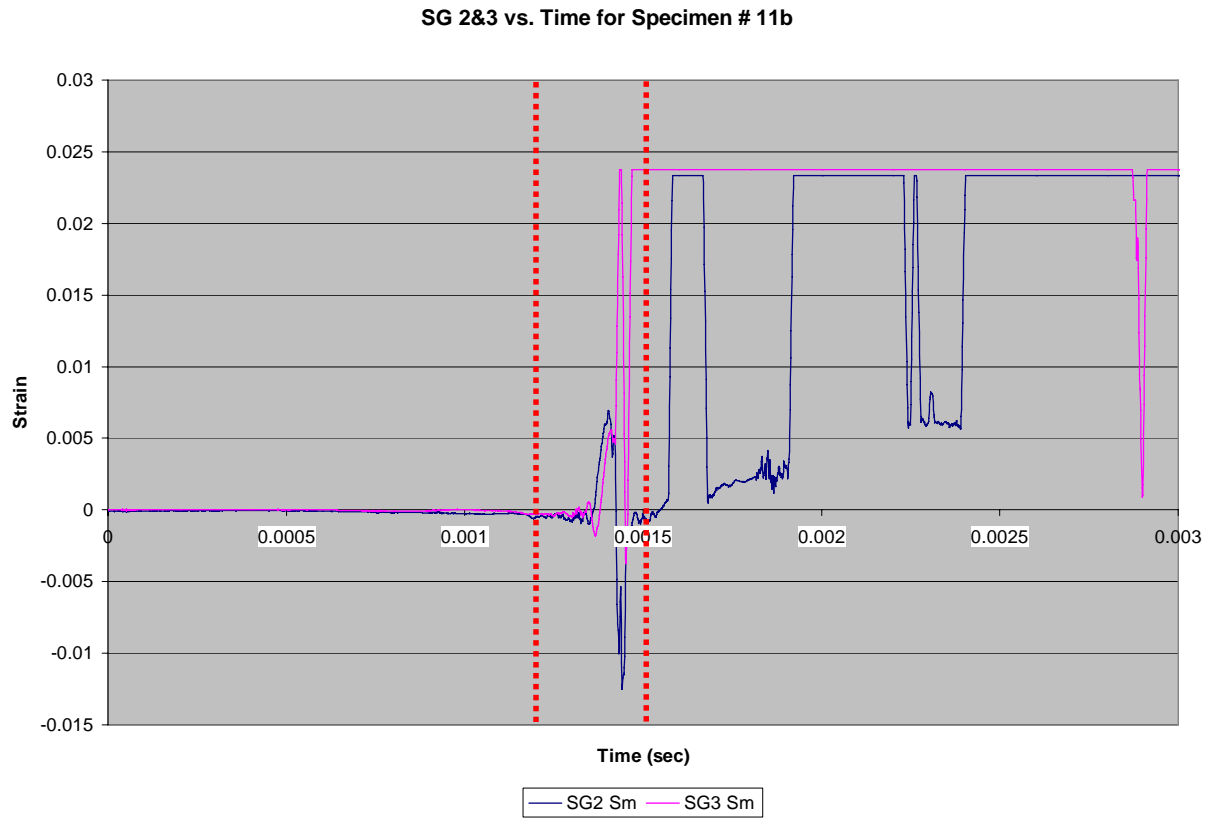


Figure C.10b.3: SG2 & SG3 spar strain vs. time (Specimen 10b)

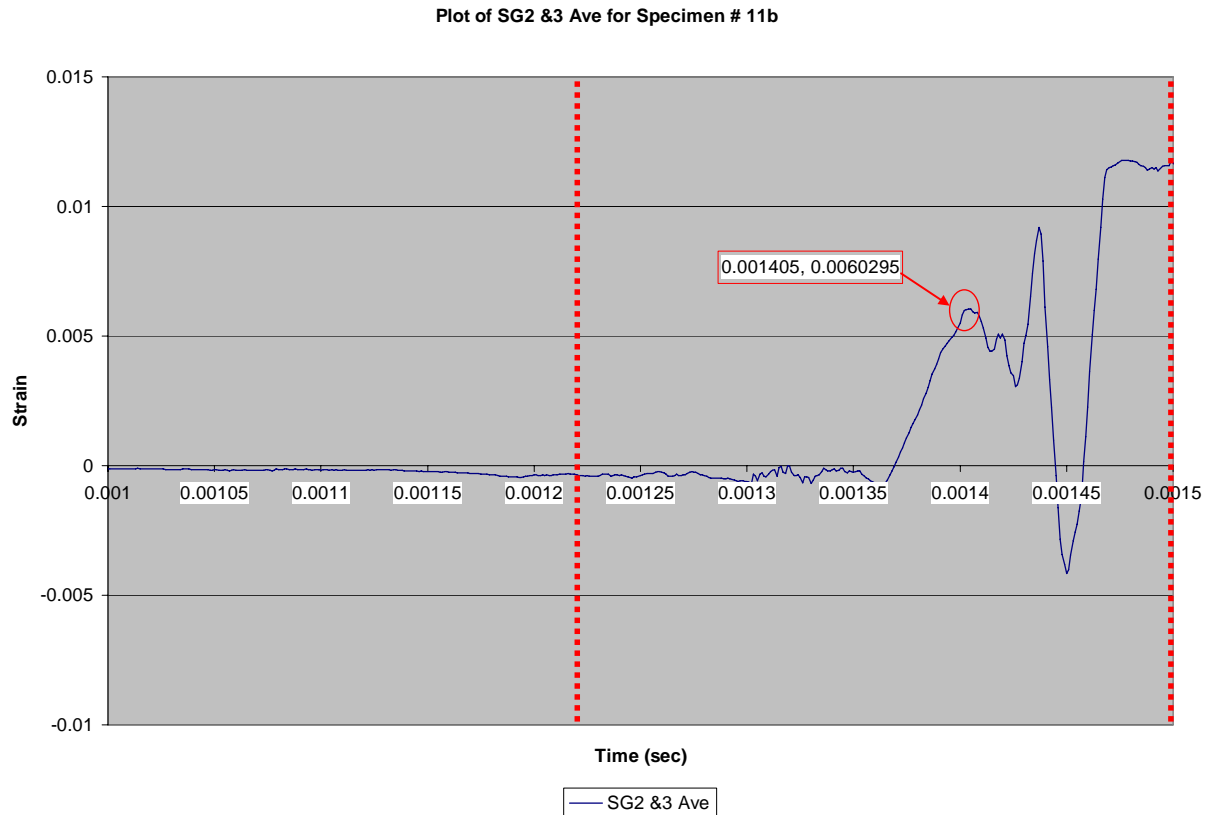


Figure C.10b.4: SG2 & SG3 average spar strain vs. time (Specimen 10b)

Specimen 10c, Test 52

For Specimen 10c, the load interval (and therefore the strain vs. time interval of interest) is approximately 1.14 ms to 1.43ms as shown in Figure C.10c.1. As desired, pressure sensors K1 and K3 are largely in agreement, indicating side-to-side uniformity of load on the test specimen. During the load interval, Figure C.10c.2 shows that SG1 and SG4 are initially in phase, but go out of phase midway through the load cycle, indicating the skin pulled away from the spar in an asymmetric fashion. Spar gages SG2 and SG3 are also out of phase (as seen in Figure C.10c.3) and remain so until the moment of SG2 gage failure. This implies that the spar underwent bending during testing and that the failure was asymmetric. Assessment of specimen failure is based on the valid segment of strains recorded on the spar. Failure metrics for Specimen 10c are derived from Figure C.10c.4. Failure strain occurred at 1.308ms with a maximum strain of 0.003477 in/in.

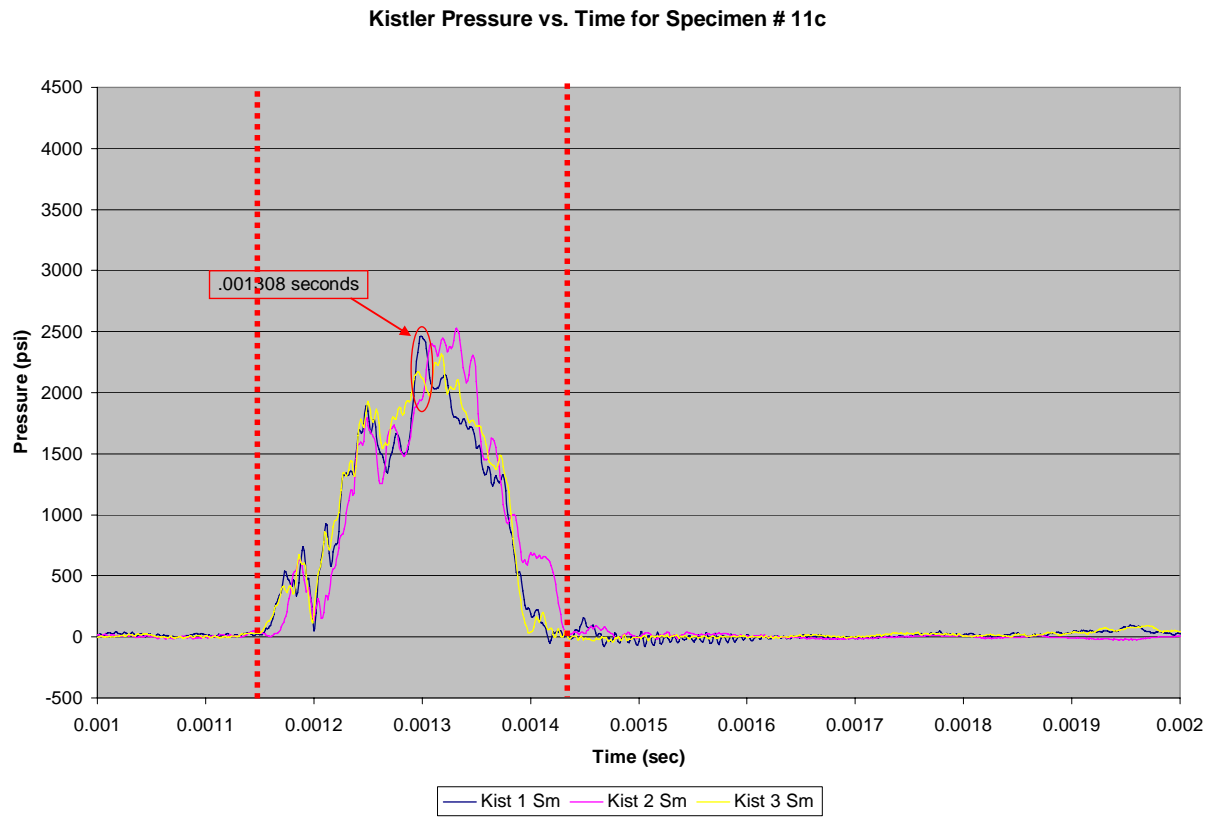


Figure C.10c.1: Kistler pressure vs. time (Specimen 10c)

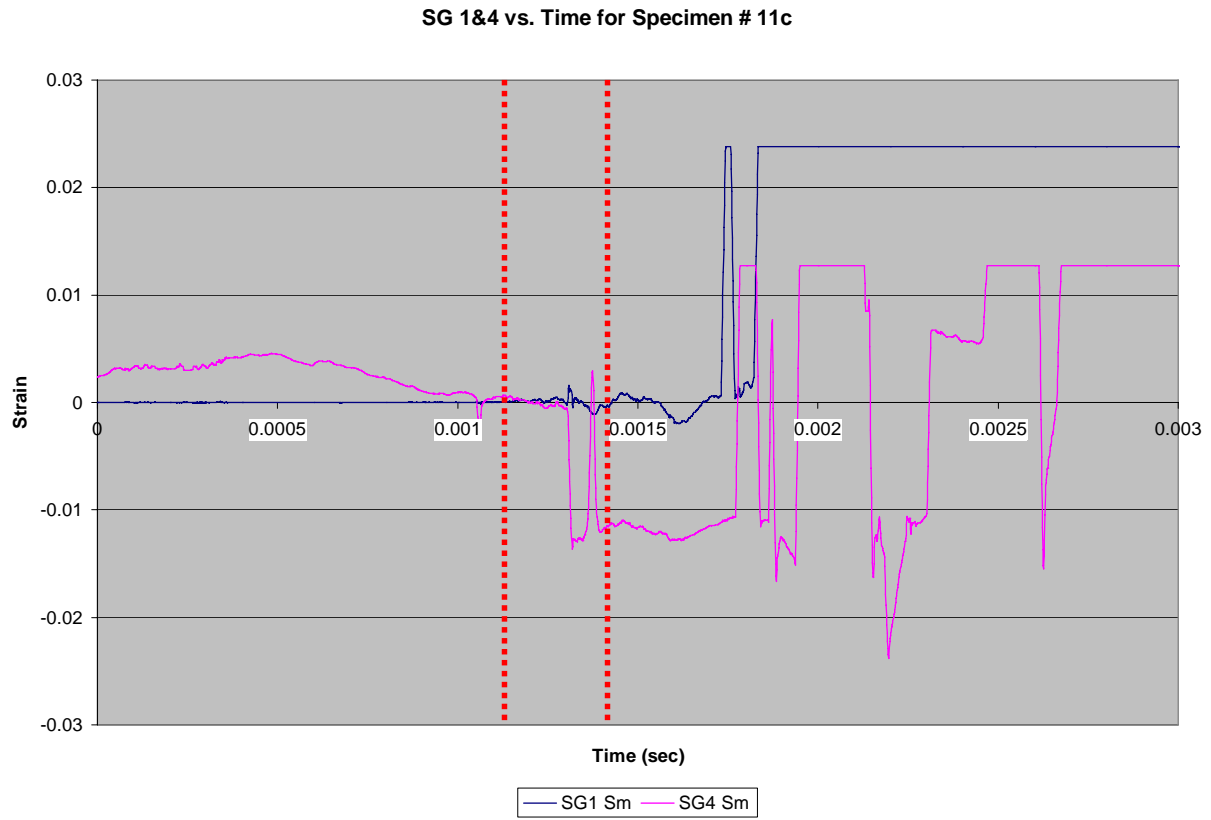


Figure C.10c.2: SG1 & SG4 skin strain vs. time (Specimen 10c)

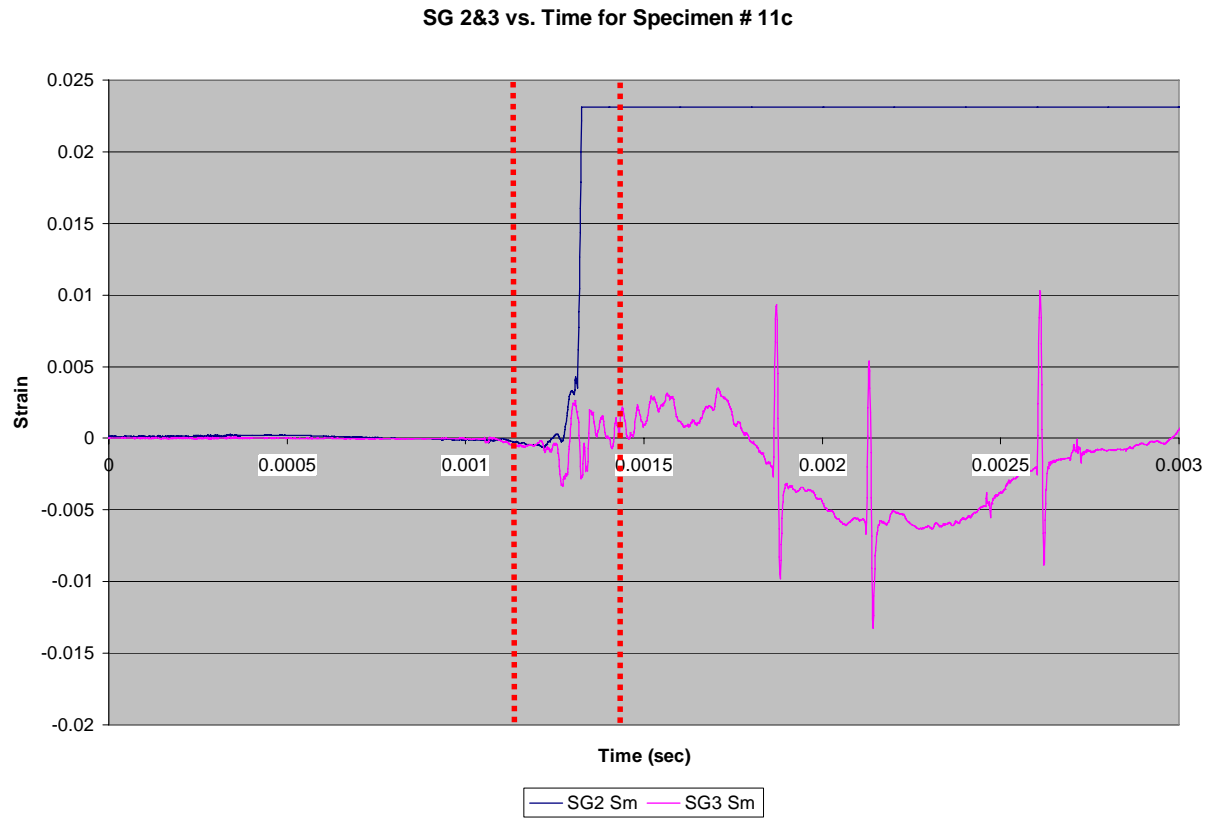


Figure C.10c.3: SG2 & SG3 spar strain vs. time (Specimen 10c)

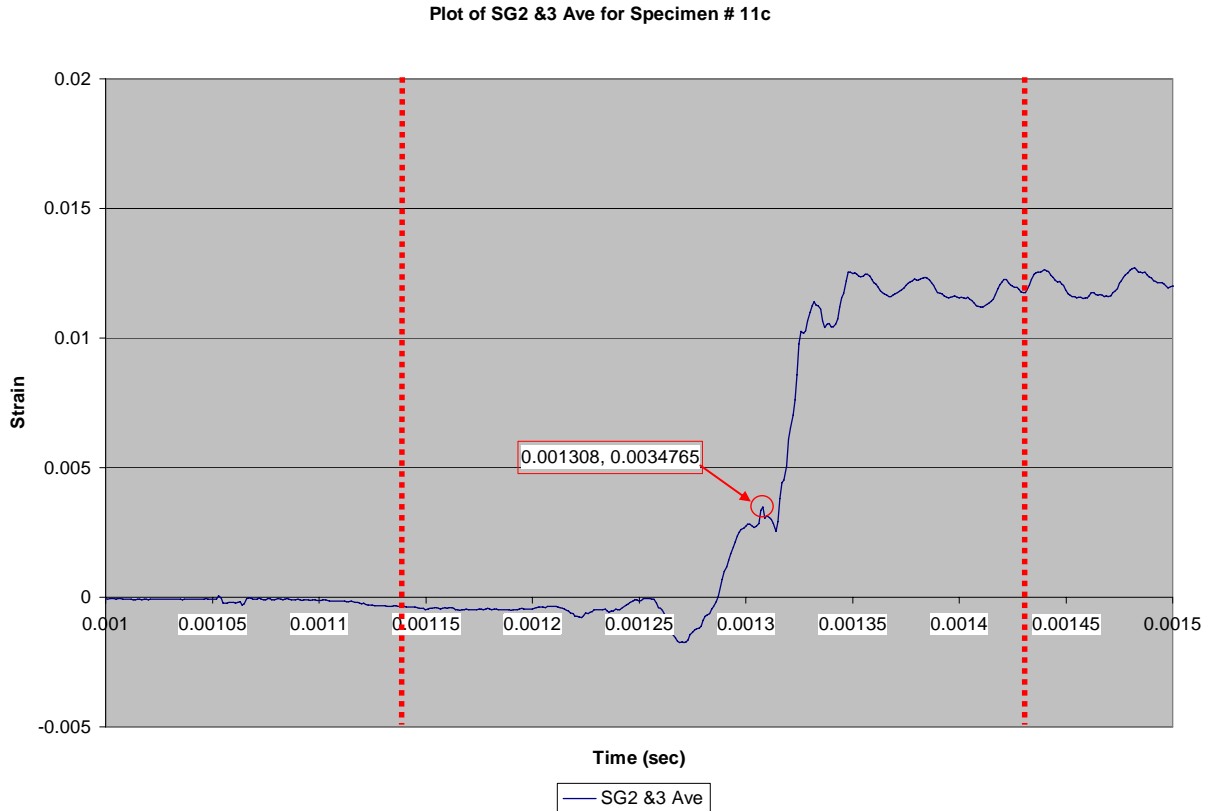


Figure C.10c.4: SG2 & SG3 average spar strain vs. time (Specimen 10c)

C.11 Specimen Set 11: Pi Bonded

C.11.1 Dynamic Tests of Specimen Set 11

Specimen 11a, Test 53

For Specimen 11a, the load interval (and therefore the strain vs. time interval of interest) is approximately 1.21ms - 1.50ms as seen in Figure C.11a.1. As desired, pressure sensors K1 and K3 are largely in agreement, indicating side-to-side uniformity of load on the test specimen. During the load interval, Figure C.11b.2 shows that SG2 and SG4 are marginally in phase. Conversely, SG5 and SG6 appear strongly out of phase (as seen in Figure C.11b.3). A lack of correlation between skin and spar gages means that failure symmetry is inconclusive. Failure metrics for Specimen 11a was derived from Figure C.11a.4. Failure strain occurred at 1.497ms with a maximum strain of 0.001063 in/in.

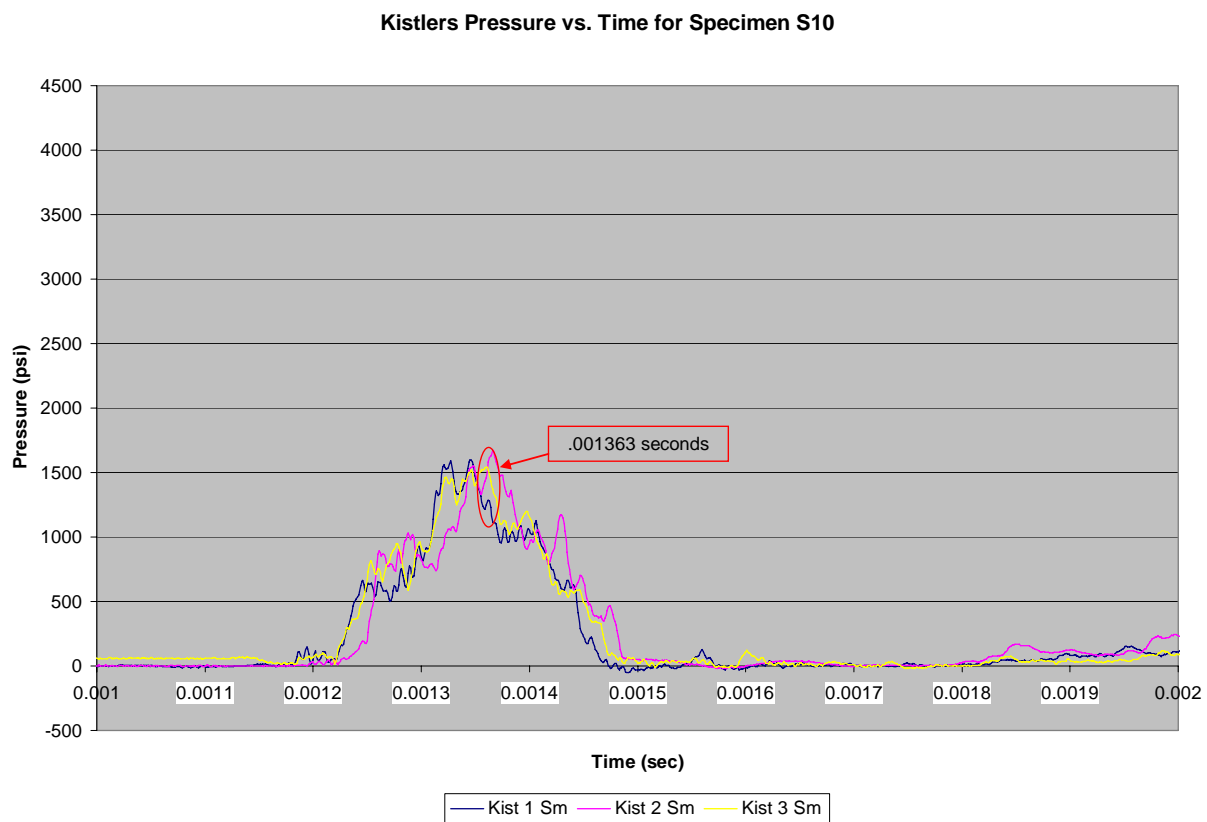


Figure C.11a.1: Kistler pressure vs. time (Specimen 11a)

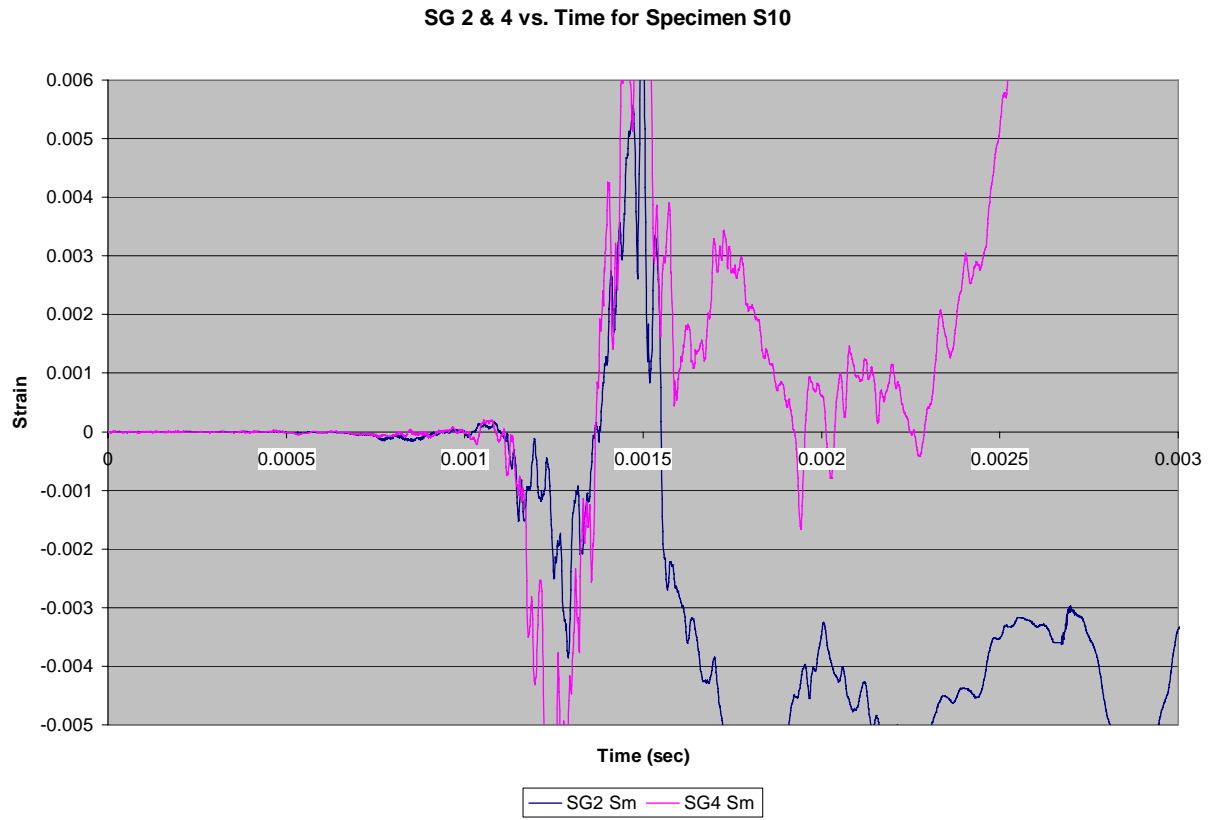


Figure C.11a.2: SG2 & SG4 skin strain vs. time (Specimen 11a)

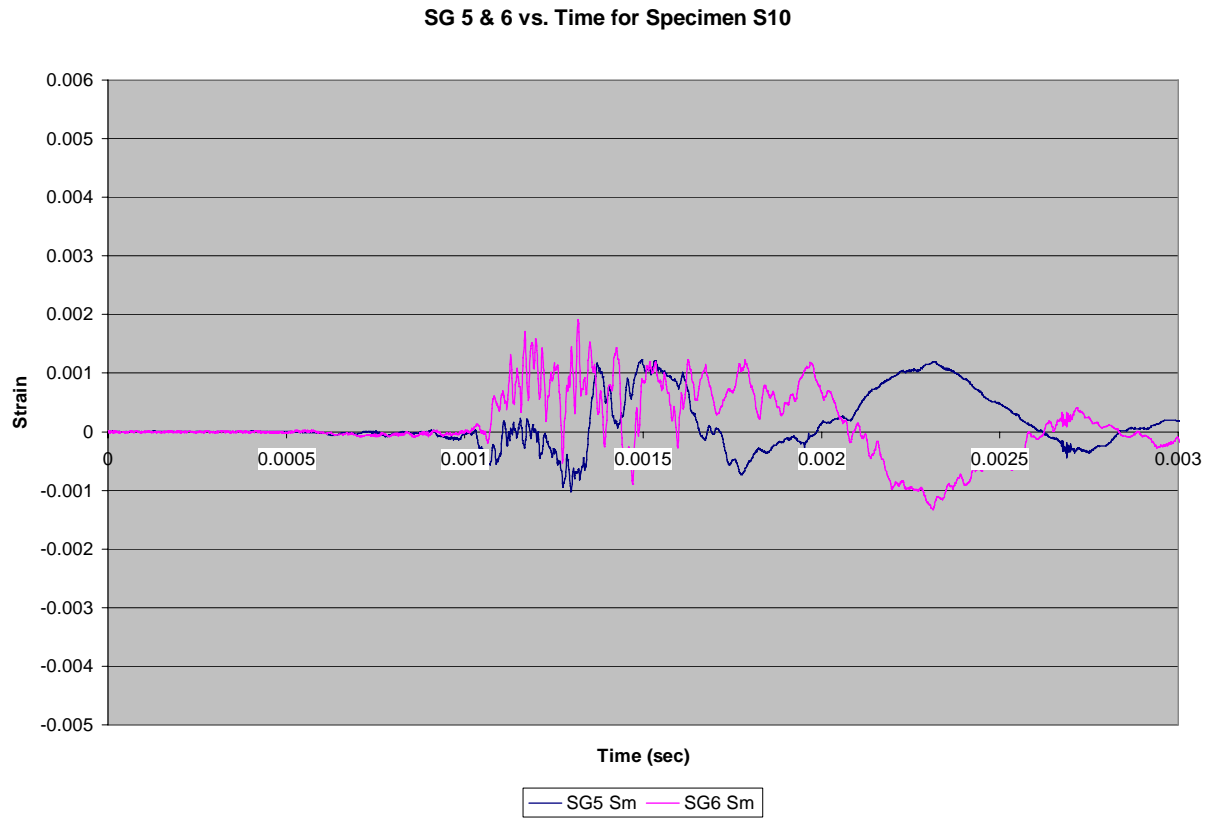


Figure C.11a.3: SG5 & SG6 spar strain vs. time (Specimen 11a)

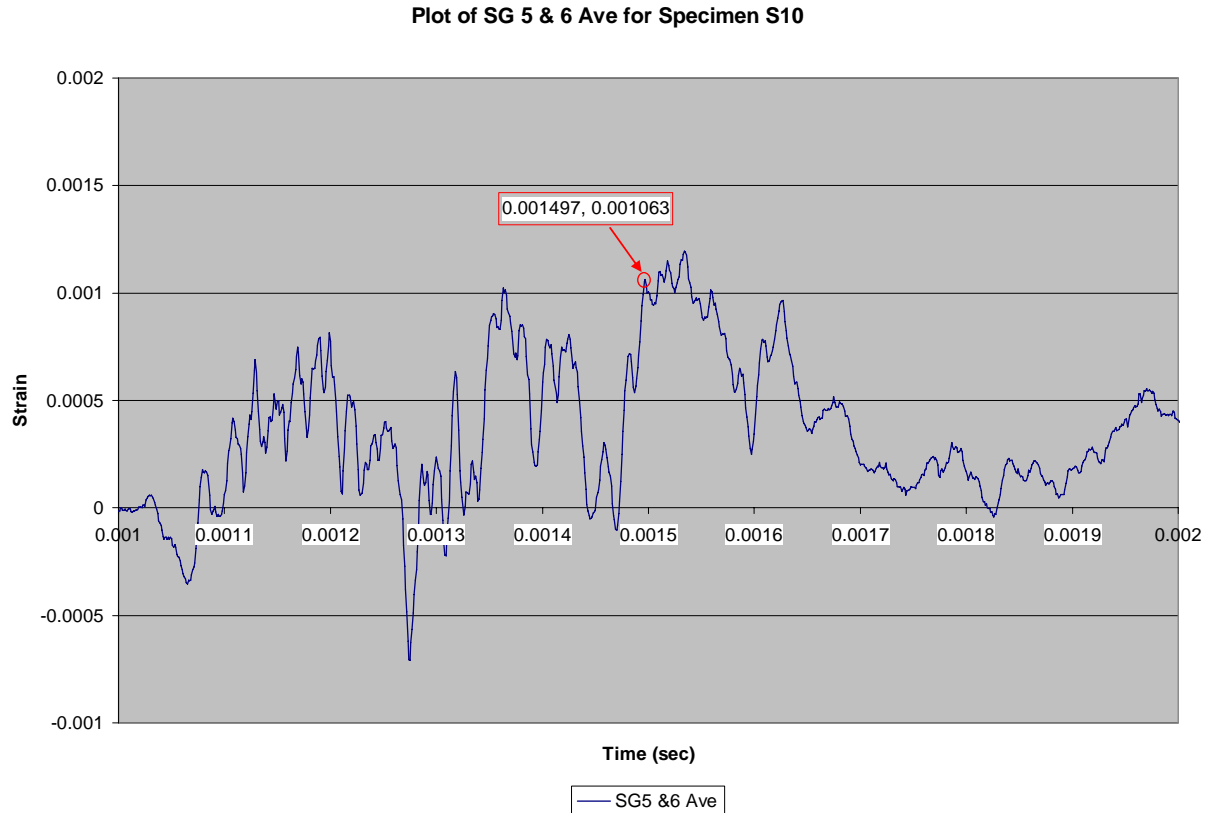


Figure C.11a.4: SG5 & SG6 average spar strain vs. time (Specimen 11a)

Specimen 11b, Test 59

For Specimen 11b, the load interval (and therefore the strain vs. time interval of interest) is approximately 1.14s - 1.44ms as seen in Figure C.11b.1. As desired, pressure sensors K1 and K3 are largely in agreement, indicating side-to-side uniformity of load on the test specimen. During the load interval, Figure C.11b.2 shows that SG2 and SG4 are in phase, indicating the skin pulled away from the spar in a symmetric fashion. Conversely, SG5 and SG6 appear somewhat out of phase by virtue of amplitude differences (as seen in Figure C.11b.3). A lack of correlation between skin and spar gages means that failure symmetry is inconclusive. Assessment of specimen failure is based on the valid segment of strains recorded on the spar. Failure metrics for Specimen 11b was derived from Figure C.11b.4. Failure strain occurred at 1.370ms with a maximum strain of 0.003241 in/in.

Kistlers Pressure vs. Time for Specimen S11

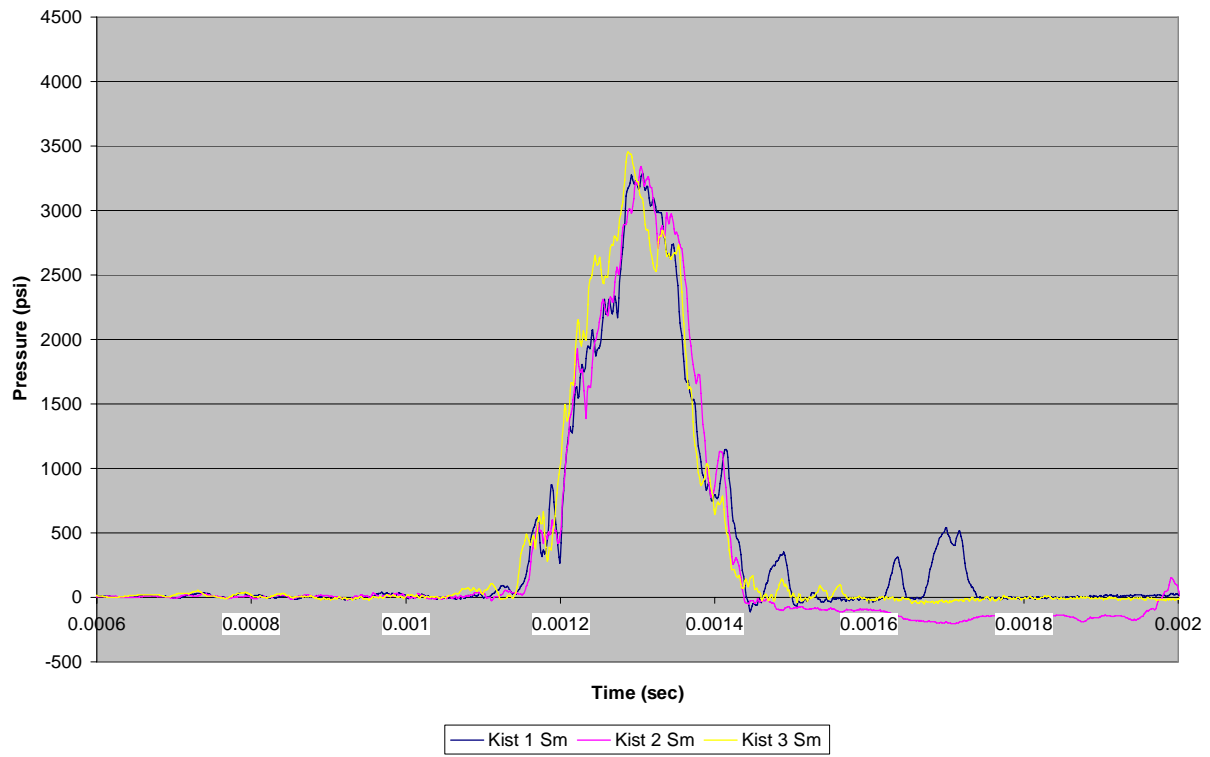


Figure C.11b.1: Kistler pressure vs. time (Specimen 11b)

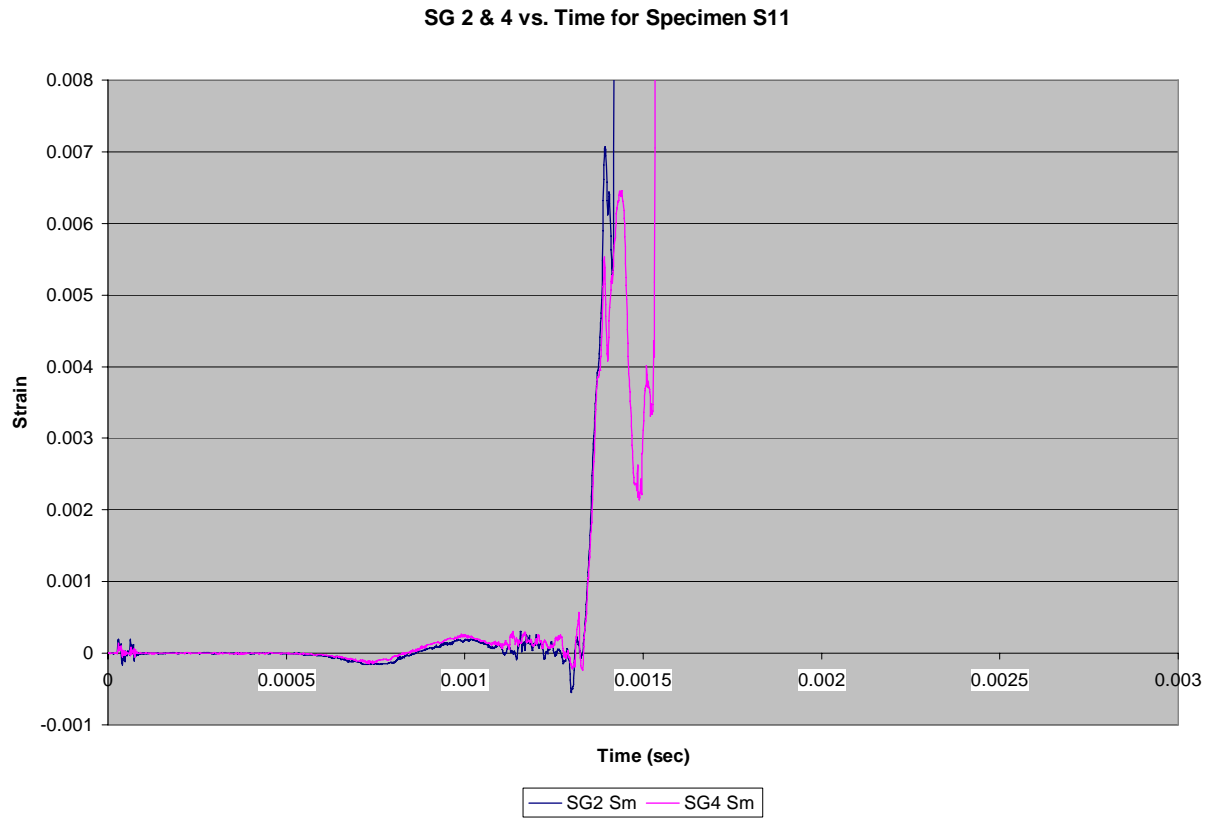


Figure C.11b.2: SG2 & SG4 skin strain vs. time (Specimen 11b)

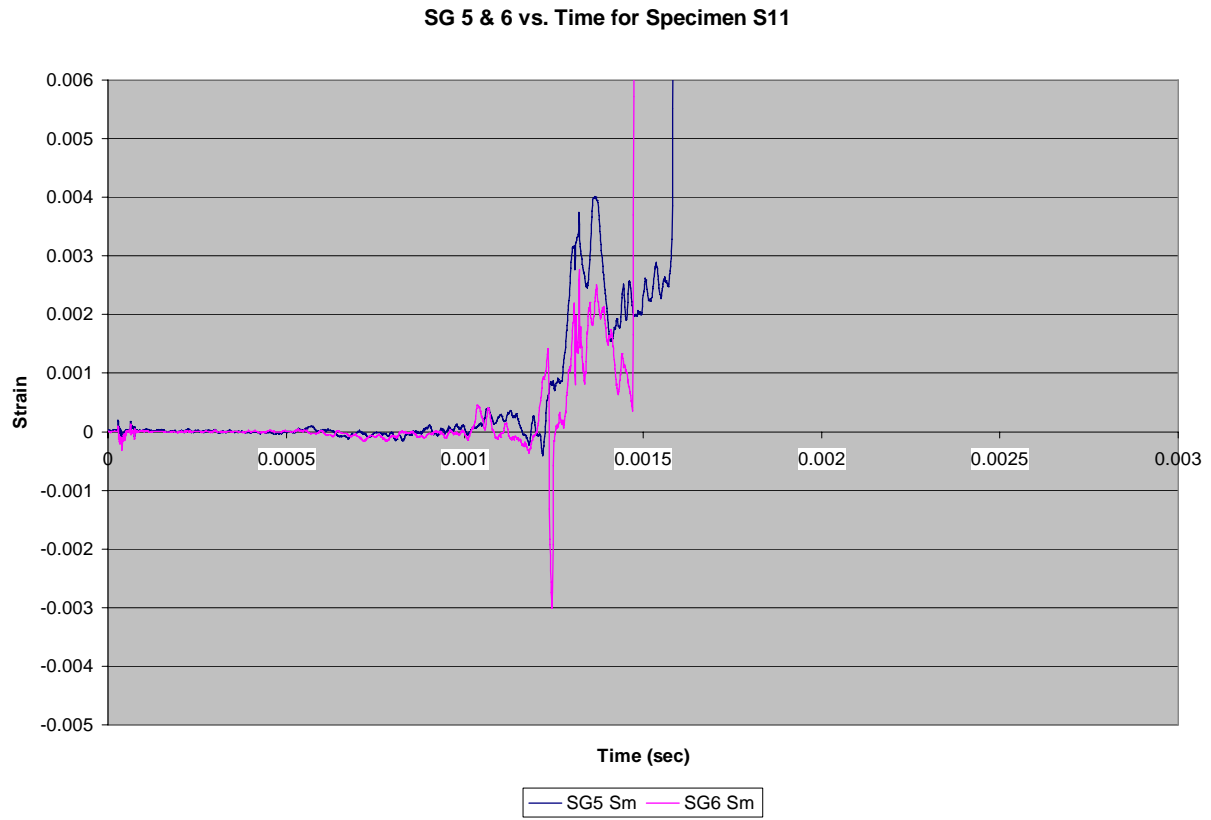


Figure C.11b.3: SG5 & SG6 spar strain vs. time (Specimen 11b)

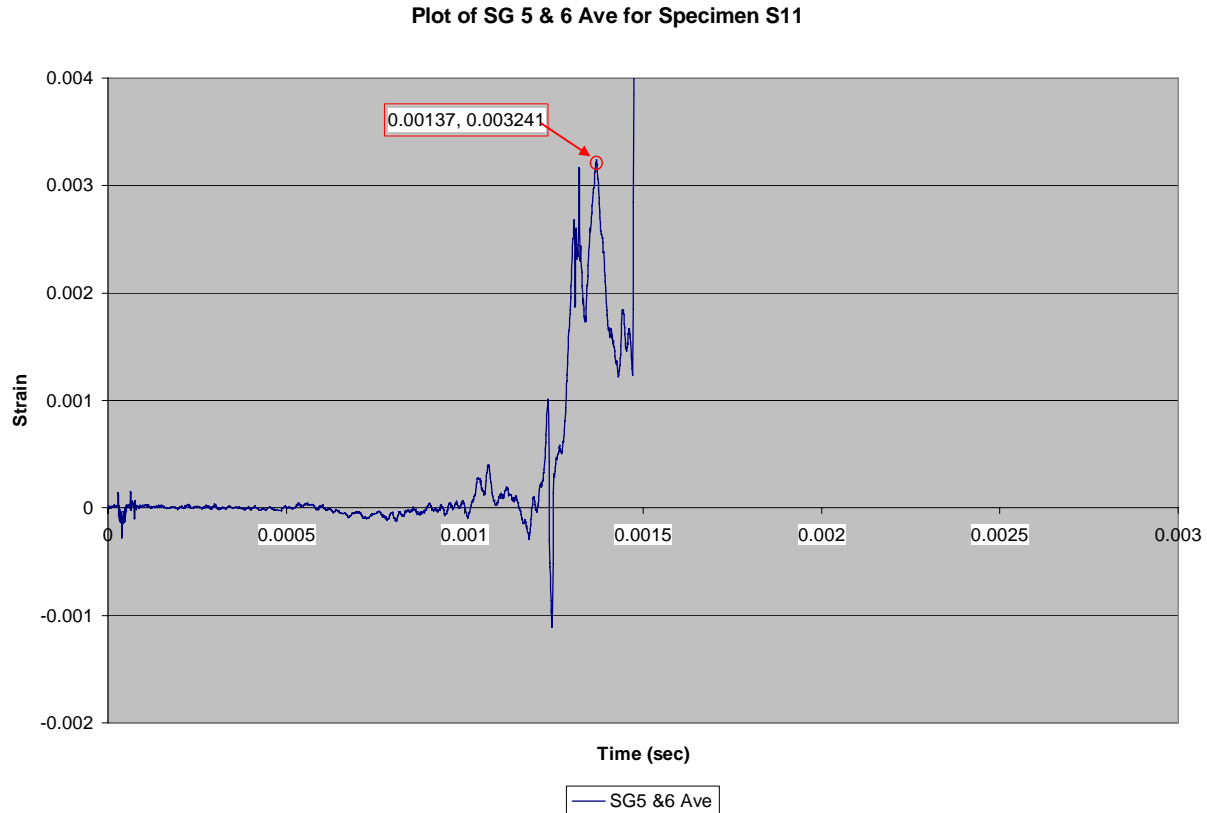


Figure C.11b.4: SG5 & SG6 average spar strain vs. time (Specimen 11b)

Specimen 11c, Test 60

For Specimen 11c, the load interval (and therefore the strain vs. time interval of interest) is approximately 1.16 ms to 1.47ms as shown in Figure C.11c.1. As desired, pressure sensors K1 and K3 are largely in agreement, indicating side-to-side uniformity of load on the test specimen. During the load interval, Figure C.11c.2 shows that SG2 and SG4 are mostly in phase throughout the load cycle, indicating the skin pulled away from the spar in a symmetric fashion. Spar gages SG5 and SG6 are also in phase (as seen in Figure C.11c.3) and remain so until the moment of failure. Failure is ruled as symmetric. Assessment of specimen failure is based on the valid segment of strains recorded on the spar. Failure metrics for Specimen 11c are derived from Figure C.11c.4. Failure strain occurred at 1.362ms with a maximum strain of 0.0027975in/in.

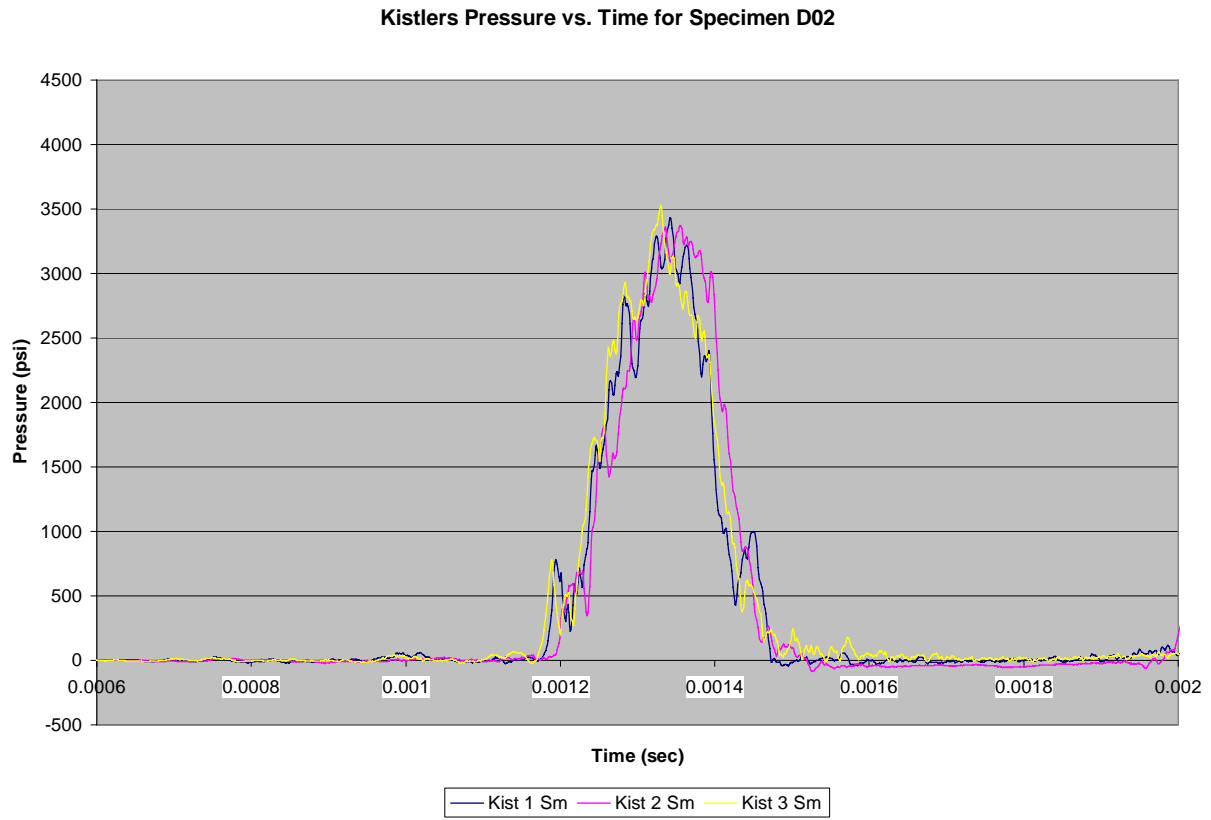


Figure C.11c.1: Kistler pressure vs. time (Specimen 11c)

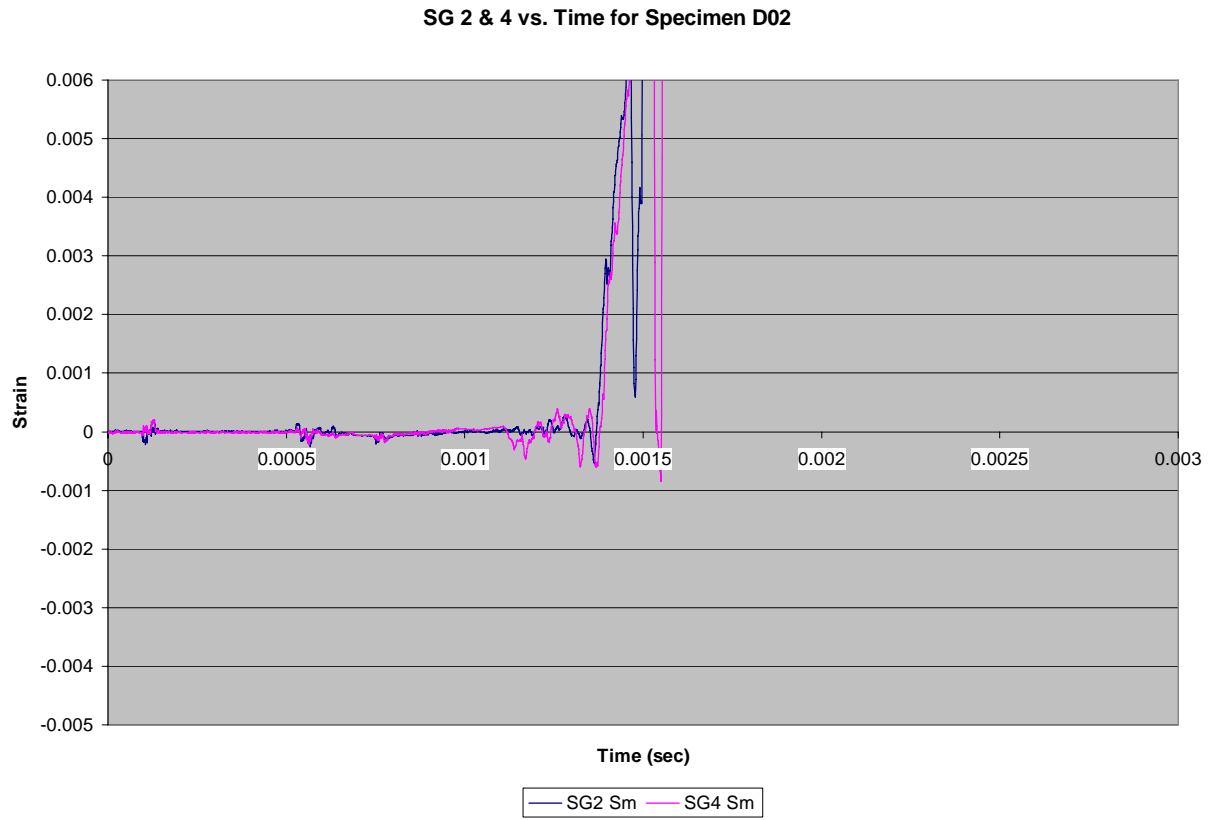


Figure C.11c.2: SG2 & SG4 skin strain vs. time (Specimen 11c)

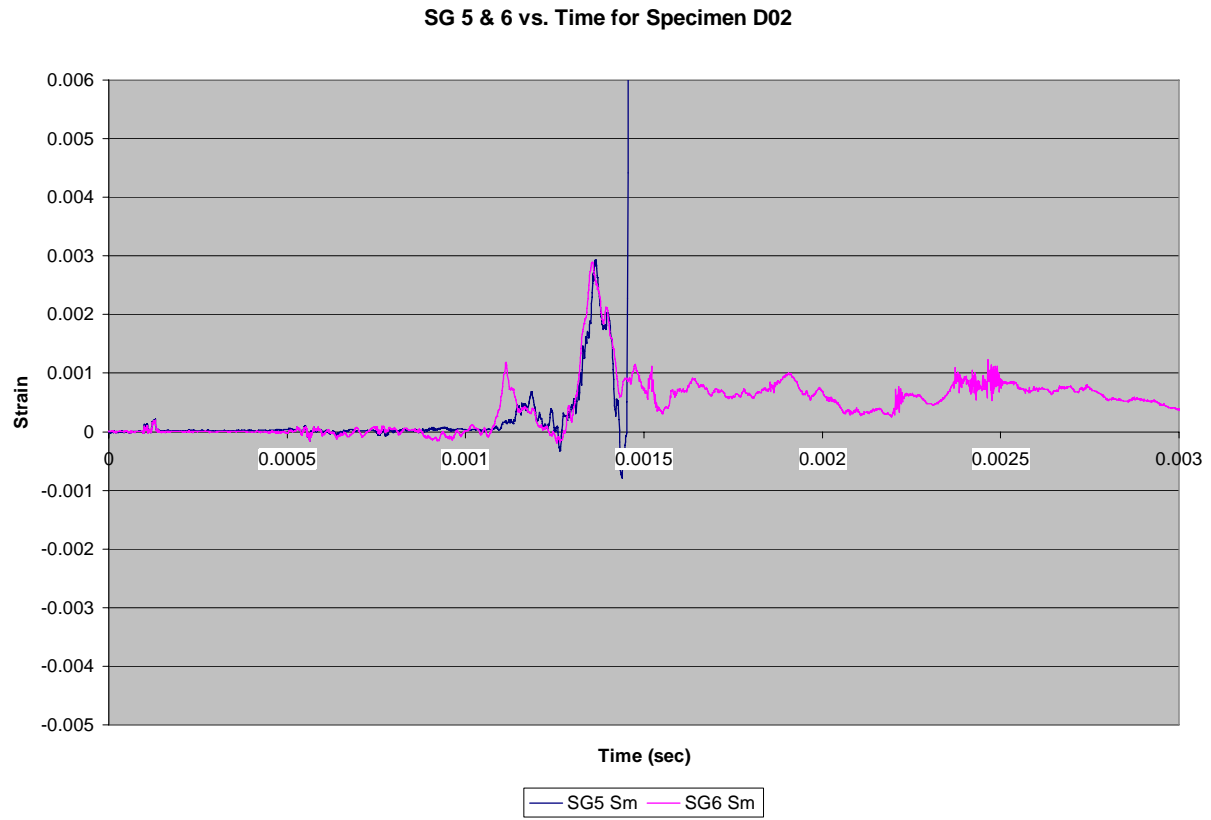


Figure C.11c.3: SG5 & SG6 spar strain vs. time (Specimen 11c)

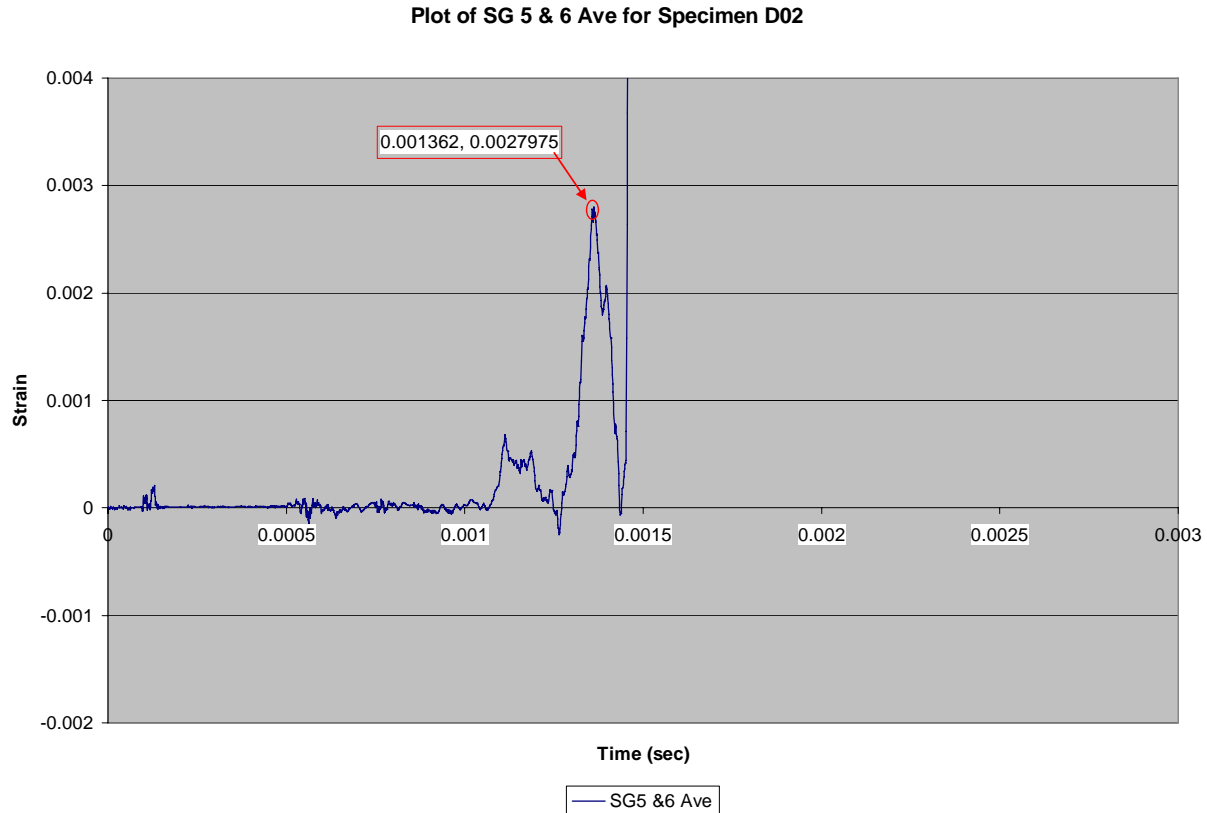


Figure C.11c.4: SG5 & SG6 average spar strain vs. time (Specimen 11c)

Specimen 11d, Test 61

For Specimen 11d, the load interval (and therefore the strain vs. time interval of interest) is approximately 1.16 ms to 1.44ms as shown in Figure C.11d.1. As desired, pressure sensors K1 and K3 are largely in agreement, indicating side-to-side uniformity of load on the test specimen. During the load interval, Figure C.11d.2 shows that skin gages SG2 and SG4 are initially out of phase. Spar gages SG5 and SG6 are mostly in phase (as seen in Figure C.11d.3), particularly at the moment of failure. This implies that the spar loading was largely symmetric. The lack of correlation between skin and spar gages means that failure symmetry is inconclusive. Assessment of specimen failure is based on the valid segment of strains recorded on the spar. Failure metrics for Specimen 11d are derived from Figure C.11d.4. Failure strain occurred at 1.343ms with a maximum strain of 0.002898 in/in.

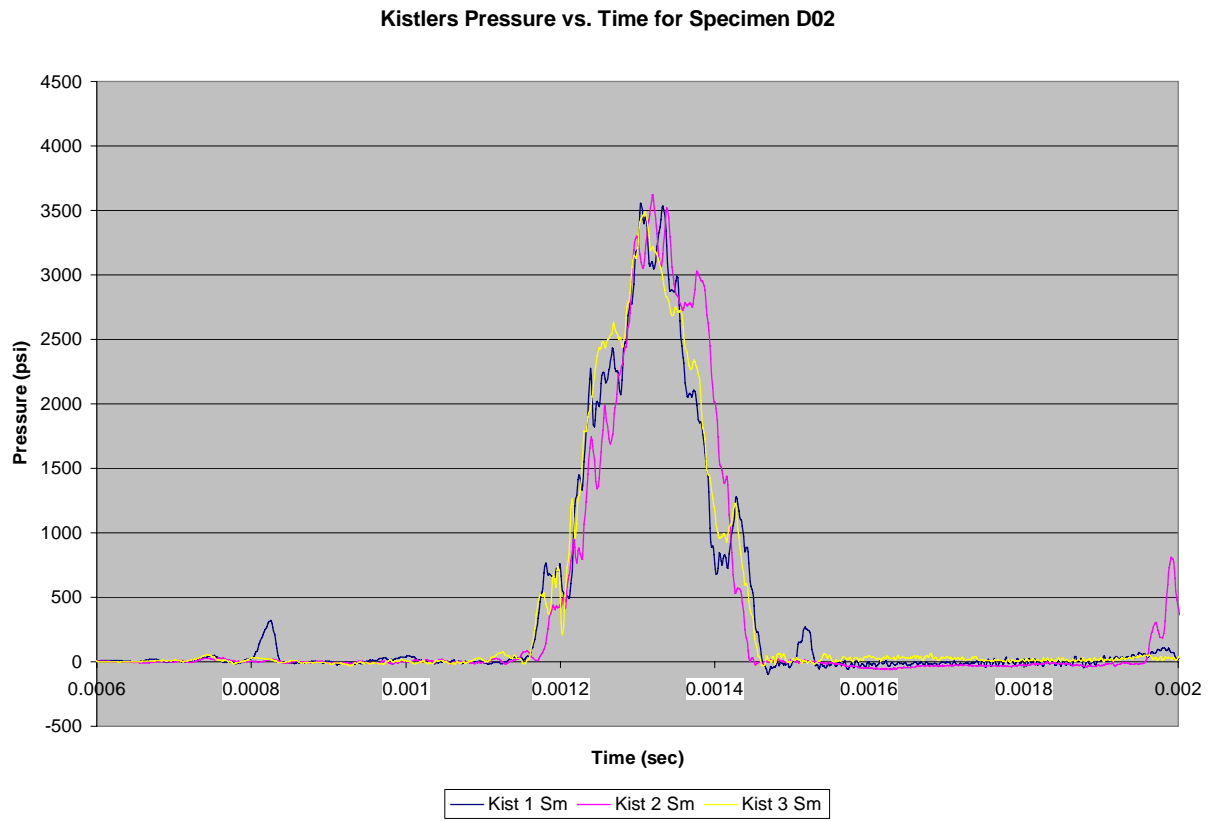


Figure C.11d.1: Kistler pressure vs. time (Specimen 11d)

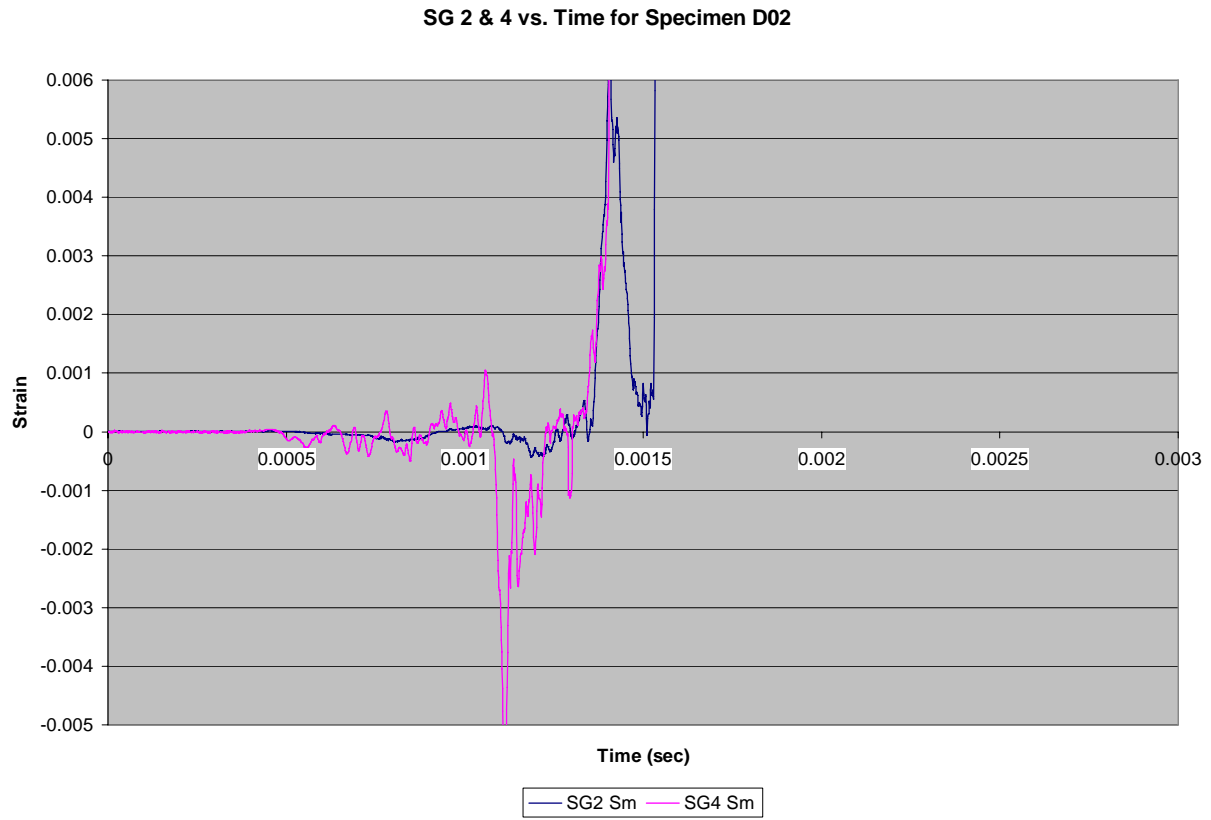


Figure C.11d.2: SG2 & SG4 skin strain vs. time (Specimen 11d)

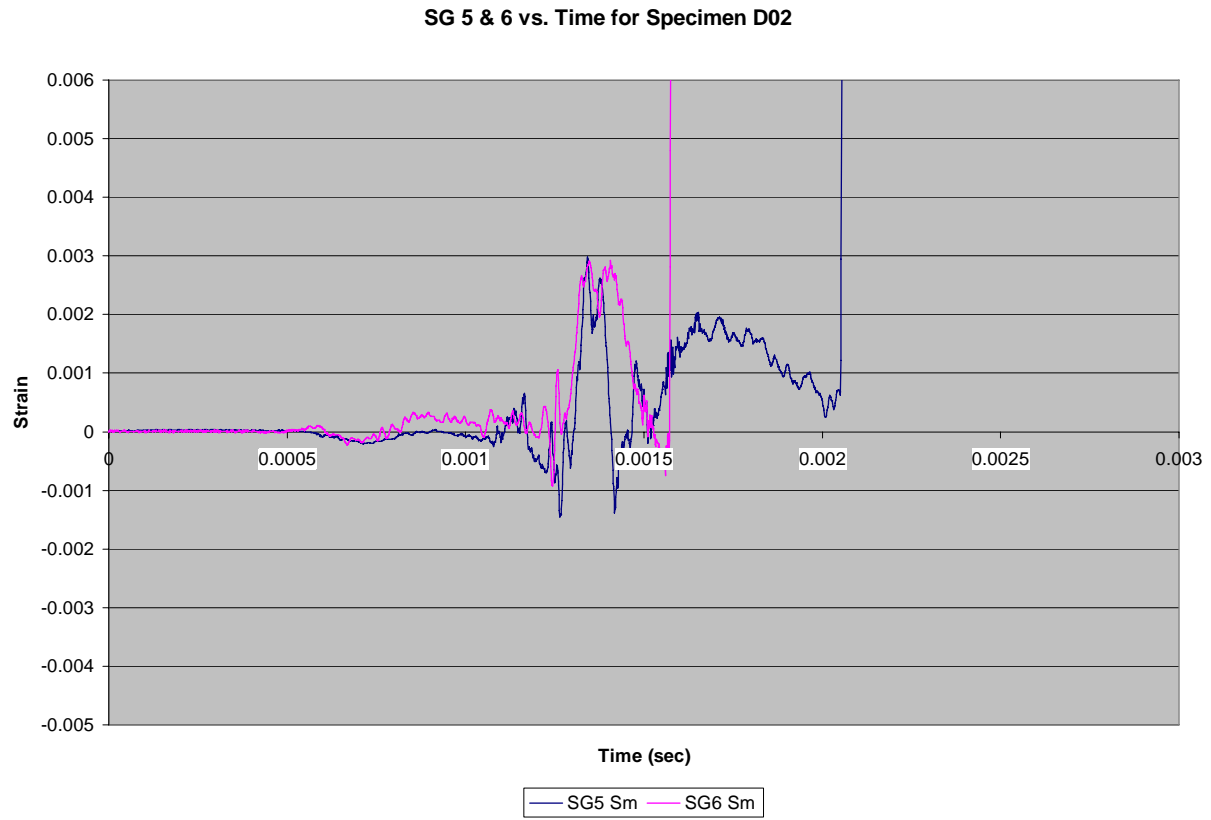


Figure C.11d.3: SG5 & SG6 spar strain vs. time (Specimen 11d)

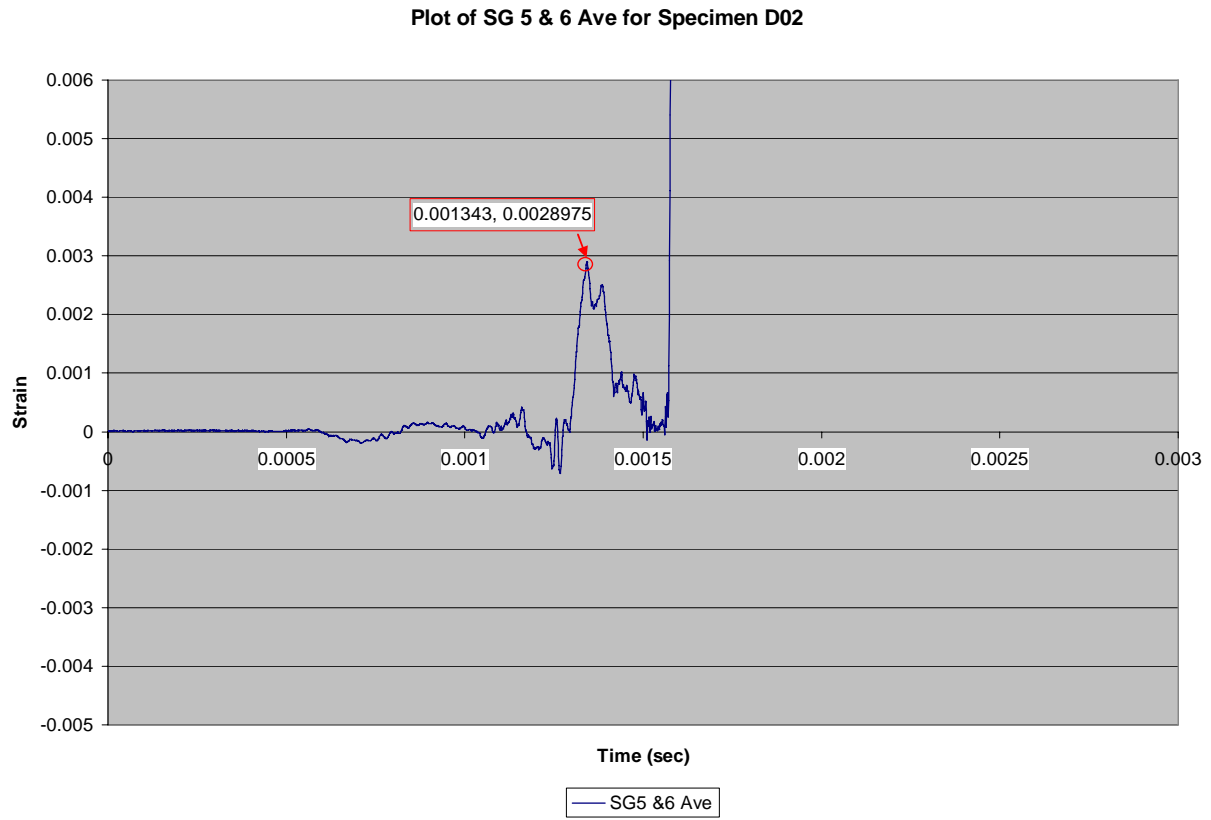


Figure C.11d.4: SG5 & SG6 average spar strain vs. time (Specimen 11d)